
universität
mainz

Novel therapeutic approaches to hypoxemia and tissue hypoxia

Habilitationsschrift

zur Erlangung der *venia legendi* für das Fach Biochemie

Vorgelegt dem Fachbereich 09 für Chemie, Pharmazie und Geowissenschaften der Johannes Gutenberg-Universität Mainz

von

Dr. Thies Schröder

Mainz, im April 2017

1 Acknowledgements

I would like to thank first and foremost my supervisors Prof. Dr. Dirk Schneider and Prof. Dr. Mark Helm at the Institute of Pharmacy and Biochemistry for their time and effort in helping the habilitation process move along, and for aiding me to acquire teaching skills at Mainz University.

I would also like to thank my former supervisor and mentor at Duke University Medical Center, Prof. Dr. Mark W. Dewhirst, for teaching me fundamentals of cancer pathophysiology and practical tumor research in animal models, and for giving me resources to help me start my own line of research.

I am very grateful to Prof. Dr. Christopher G. Willett, Chair of the Department of Radiation Oncology at the Duke University Medical Center, for allowing me to bud off my own laboratory and for providing departmental protection when needed.

I also thank Prof. Dr. Claude A. Piantadosi at the Duke Medical Center for Hyperbaric Medicine for being a wonderful mentor, and for teaching me the art of publishing in the physiology field.

I would like to thank my long-term research collaborator Prof. Dr. David C. Irwin at UC Denver Medical Center for being an excellent collaborator, and a good friend.

I also want to thank my colleagues Prof. Dr. Karyn L. Hamilton and Prof. Dr. Christopher Bell at the Department of Exercise Sciences at Colorado State University in Fort Collins, CO, as well as Prof. Dr. Robert J. Noveck at Duke Medical Center, NC, for all their helpful input with study design and manuscript writing.

I would also like to thank Dr. Timothy Bentley at the US Office of Naval Research for his continuing trust and support.

I would also like to thank my collaborator at the University of Mainz, Prof. Dr. Carsten Sönnichsen, for his help during my transition into the German academic landscape.

I also owe special gratitude to my very good friends Drs. Malte Bussiek and Jens Wiehler, who played a highly supportive and encouraging role during multiple episodes of my academic life

I am also very much obliged to my wonderful wife and children, all of whom I hope will still recognize me when I am not in front of my computer.

I will also forever be grateful to my parents, who have been endlessly supportive throughout my career.

2 Table of Contents

3 Introduction

In the blood of humans that live at sea level, the percentage of hemoglobin loading with oxygen (HbO_2, SaO_2) is carefully maintained at 95-99%, corresponding to 79-145 mmHg of oxygen partial pressure [1]. Steady-state blood oxygen concentrations differ by tissue, with highest concentrations in the brain and the heart, and lowest concentrations in organs supplied by mostly venous circulation, such as the liver and the lung [2]. Significant aberration from this status of maximal oxygenation of the systemic arterial blood is called hypoxemia and can lead to more or less serious pathophysiologies, depending on severity and duration of the oxygen shortage. Apart from decreased physical endurance, short-termed hypoxemia normally does not affect human health; however, chronic hypoxemia can cause pulmonary hypertension, right ventricular hypertrophy, and potentially cardiac stroke and death. Tissue remodeling after sustained hypoxemia is particularly problematic, exemplified by the development of arterial hypertension, insulin-resistant diabetes, and CNS degeneration in sleep apnea patients [3]. Extreme hypoxemia, such as experienced after un-acclimatized ascent to very high altitude, can lead to lethal pulmonary and brain edema [4, 5].

Hypoxemia can arise from a variety of conditions, such as “thin air” at high altitude, obstruction of the airways (asthma, obstructive sleep apnea, pneumonia, lung fibrosis), disturbances in ventilation-perfusion balance in the lung (pulmonary arterial hypertension, PAH), anemia (anatomic arteriovenous shunting, iron deficiency), and central nervous dysregulation (anesthesia, central sleep apnea). While hypoxemia is defined as less than normal oxygen in the blood and is often expressed as the percent hemoglobin saturation, the resulting lack of oxygen in the tissue is termed (tissue) hypoxia, and typically expressed as the oxygen partial pressure (mmHg).

To comprehend the pathophysiology associated with hypoxemia, it is important to understand that on a local level, hypoxemia, or tissue hypoxia, is not necessarily a pathological occurrence and develops e.g. in the exercising musculature as a consequence of increased oxidative metabolism. In the tissue, hypoxia, metabolites arising from muscular activity, and shear stress cause vasodilation in the microcirculation (the blood circulation inside the organs), leading to increased blood flow (hyperemia) to the affected area. With increasing exercise intensity, the increased demand for oxygen and nutrients is answered by a concerted action of extrinsic and intrinsic factors to meet such need, termed the “sympathetic response”: hypoxia and other metabolic signals in the muscle stimulate the afferent sympathetic nervous system. This ultimately leads to an increase in cardiac output and net vasoconstriction of resistance vessels in splanchnic organs, causing an increase in perfusion pressure on all organs.

Though the sympathetic response also causes net vasoconstriction in the skeletal muscle, local vasodilatory mechanisms synergize to translate the increased perfusion pressure into enhanced oxygen delivery to the capillary beds [6-8]. However, although many of the tissue factors, receptors, and signal transduction pathways of this finely orchestrated response are long known, their exact biological role is still insufficiently understood to create a complete picture.

Because the local oxygen level is such an important analyte to help homeostase and fine-tune blood flow in tissue, systemic hypoxemia causes significant disturbance and dysregulation: tissue factors that normally play an important role to regulate local blood flow, such as endothelin-1 (ET-1), cause major health problems, such as pulmonary hypertension and edema, when their concentration in the systemic circulation is upregulated by hypoxemia [9, 10]. Moreover, while nitric oxide (NO) and prostaglandins are important local effectors to adjust local blood flow to changing demands, their global, hypoxemia-triggered upregulation lead to vasodilation and arterial hypotension, compensatory increase of cardiac output. This is followed by increased hydrostatic pressure on the pulmonary

microvasculature, and consequentially, in combination with hypoxic pulmonary vasoconstriction, increased risk of pulmonary edema [10, 11]. Even human populations such as Andean people in Bolivia and Peru that dwell at high altitude of >4,000m for the considerable time of approximately 12,000 years, still suffer from disorders caused by hypoxia at high altitude, such as polycythemia, also known as Monge's disease or chronic mountain sickness [12, 13].

In humans, hypoxemia is classified depending on the purpose: Whereas an arterial oxygen hemoglobin saturation (HbO_2) of less than 95% may trigger the decision to equip a patient with an oxygen mask, in a more general setting, an SaO_2 of less than 90% is often classified as moderate (75-89% HbO_2) or severe hypoxemia (<75% HbO_2) [14-16]. As a first-line treatment, hypoxemia is often alleviated with supplemental oxygen, but has also been successfully improved by reversing its downstream microvascular dysregulation, such as through the employment of phosphodiesterase 5 (PDE5) inhibitors, β2 sympathomimetics, and endothelin receptor antagonists against high altitude-induced performance decrement [17, 18] or in the context of congenital PAH [19]. I have shown efficacy for several approaches that target hemodynamic downstream pathophysiologies of hypoxemia, which will be discussed in chapter 4 [20-22]. The sheer fact that hypoxemia-induced exercise performance decrement can be pharmacologically reversed raises the question whether it is oxygen availability that limits exercise performance and body function under hypoxemia, or whether hypoxemia-induced hemodynamic aberrations are more important barriers to oxygen transport to tissue than the reduced oxygen concentration itself. It is interesting that under resting conditions, less than 50% of the oxygen in the arterial blood is extracted to be metabolized, which may rise up to 80% under heavy exercise [23]. At high terrestrial altitude of 4,500 m, residual central venous oxygen saturation still approximates 60% in resting and 40% in exercising subjects [24]. Taken together, this leads to the hypothesis that under moderate hypoxemia, such as experienced during PAH, sleep apnea, and at high altitude, hypoxemia-triggered hemodynamic dysregulation has a stronger limiting impact on the bioavailability of oxygen to the parenchymatic tissues than the reduced blood concentration of oxygen itself. I therefore hypothesize that a carefully designed, pleiotropic cardiovascular treatment will be able to largely restore normoxic exercise capacity and health in hypoxemic patients. Moreover, because such treatment involves the overriding of microvascular barriers that are also present in diffusion-limited tissues, I also hypothesize that some of these treatments can be modified to improve the delivery of blood-born therapeutic agents to diffusion-limited tissue, such as solid tumors.

The following paragraphs will cover some relevant specific information about organ systems, their response to hypoxemia that is critical to my approach, and currently available treatments against the impact of hypoxemia. I will concentrate on hypoxemia and tissue hypoxia in the skeletal muscle, in the lung, and in the solid tumor, although hypoxemia strongly affects other organ systems too, such as the brain and the kidney [4, 25, 26]. I will first cover the skeletal muscle microcirculation, then summarize hypoxemic disturbances of the lung, and subsequently briefly describe the microcirculation and corresponding metabolic microenvironment of solid tumors. I will then summarize my progress so far on developing these anti-hypoxemic treatments and give an outlook as to which direction these developments will take from here.

4 State of the art

4.1 Reaction of the skeletal muscle microcirculation to hypoxemia

Skeletal muscle is involved in hypoxemia-triggered pathophysiologies in at least two ways: First, hypoxemia causes net dilation in most organs except the lung, thus leading to arterial hypovolemia, which triggers enhanced compensatory cardiac output via the sympathetic reaction [11, 17]. Because approximately 20% of cardiac output benefits the skeletal musculature, which itself is also responsible for 20% of the overall vascular resistance in the human body [27], the skeletal musculature is a major player in conducting hypoxemia-triggered peripheral vasodilation. Second, there is evidence that hypoxemia reduces capillary perfusion in the muscle, through constriction of pre-capillary sphincters and pericytes [28]. This vasoconstriction is likely caused by the systemic upregulation of endothelin-1, which is a powerful vasoconstrictor [9, 29].

4.1.1 Vascular anatomy of skeletal muscle

The vasculature of skeletal muscle is organized into three basic levels of hierarchy:

(1) Feed- or distributing arterioles connect the skeletal muscle microcirculation inside the muscle fascicle with the systemic arterial system. They serve as resistance vessels and account for approximately 50% of the total resistance to blood flow in skeletal muscle [30].

(2) Secondary arterioles branch at right angles from these feed arteries, enter the perimysium and travel perpendicular to the muscle fiber until branching into terminal arterioles.

(3) Terminal arterioles penetrate the perimysium (the connective tissue layer that groups muscle fibers into bundles) and immediately branch into capillaries, which travel parallel to the muscle fibers. Capillaries surrounding muscle fibers are interconnected (Figure 1).

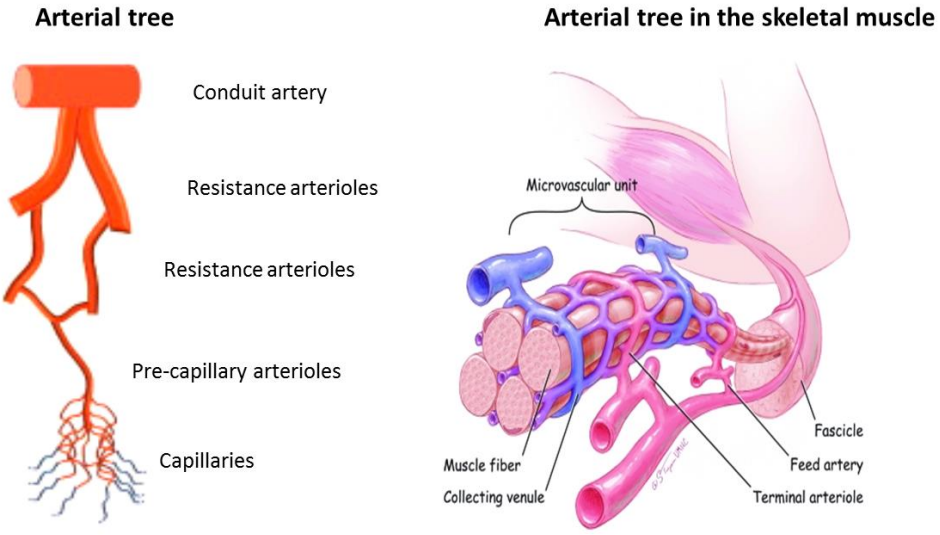

Figure 1: Anatomy of the skeletal vasculature: Resistance arterioles are regulated via different mechanisms than precapillary sphincters and pericytes. Adapted from [23, 31]

Pericytes are contractile mesenchymal cells that wrap around virtually all capillaries and venules, but are also present in the walls of larger arteries. An important biological pericyte function is the control of capillary conductivity via constriction or relaxation [32-36].

4.1.2 Vasoactive mechanisms in the skeletal muscle

Regulation of vasoactivity in the skeletal muscle serves two different purposes and is, accordingly, regulated on two different levels: **resistance vessels**, which are largely identical with feed arteries and low-order arterioles (Figure 1), **regulate systemic arterial blood pressure** [37, 38]. **Capillary perfusion** of muscle fibers on the other hand, which ultimately controls oxygen and nutrient delivery to the parenchymatic tissue, **is regulated by the tone in precapillary sphincters and in pericytes** [39, 40].

An abundance of effectors and signal transduction pathways regulate vasoactivity in the skeletal muscle and they are often located on a distinct level of the vascular tree. Among the most important mechanisms are the following:

Nitric oxide (NO) is a gaseous signaling molecule that acts downstream of multiple mechanisms of vasodilation. NO is produced from the amino acid L-arginine and molecular oxygen, via the enzymatic activity of endothelial (eNOS) and other nitric oxide synthases. NO activates soluble guanylyl cyclases in vascular smooth muscle cells (VSM), causing vasodilation via formation of cyclic guanosine monophosphate (cGMP), activation of protein kinase G (PKG), and Ca^{2+} withdrawal [41]. NO operates downstream of vasodilators such as adenosine, acetylcholine and norepinephrine, which trigger NO release through their respective receptors. eNOS is activated via increased intracellular Ca^{2+}, and can be activated by mechanical forces (shear-dependent vasodilation) [23]. Hypoxic peripheral vasodilation is mediated via the NO pathway [42-44].

Prostaglandins are a family of vasoactive signaling molecules involved in regulation of systemic and tissue blood flow. Three types of prostaglandins, PGI_2, PGE_2, and $PGF_{2\alpha}$, bind to over 10 receptors [45]. Prostaglandin receptors elicit vasodilation via production of cAMP and stimulation of protein kinase A (PKA). PKA phosphorylates myosin light chain kinase (MLCK), causing dephosphorylation of myosin light chain (MLC) and vasorelaxation [46, 47]. Prostaglandins are synthesized from arachidonic acid via cyclooxygenase (COX I and II) and peroxidase, and released from the cells by specific transporters [48]. They are strongly involved in mediating hypoxic and shear stress-induced vasodilation and play an important part in hypoxemia-induced dysregulation of circulation and microcirculation [49]. Also, blocking prostaglandin EP4 receptors greatly reduces NO-dependent pericyte vasodilation [35].

Adenosine and ATP are very important vasodilators as part of the auto-regulation of tissue blood flow. Similar to prostaglandins, adenosine and ATP are local vasomotive effectors that partially originate from increased skeletal muscle metabolism. These effectors cause vasodilation and thus hyperemia of the affected region [50]. ATP is also released by red blood cells upon hypoxia, low pH, and deformation stress [23, 51, 52]. Both adenosine and ATP bind to G-protein coupled purinergic receptors (adenosine: P1 receptors A_1, A_{2A}, A_{2B}, A_3, ATP: P2 receptors) cause vasodilation via cAMP formation, stimulation of PKA, phosphorylation of MLCK, and dephosphorylation of MLC [53]. ATP signaling on P2Y receptors also stimulates the production of NO and prostaglandins [54, 55]. ATP is released from erythrocytes and from active muscle cells, when their metabolism is increased. ATP is also degraded to adenosine, thus stimulating P1 receptors. Adenosine, ATP and NO produce further vasodilation by downregulating norepinephrine release from sympathetic nerve terminals in the vascular wall. Hypoxia, such as produced by exercise-induced metabolism, induces ATP release from RBCs, thus RBCs could be an important source of ATP during exercise hyperemia. Adenosine is increased in the interstitium of human skeletal muscle during systemic hypoxia [56].

Endothelin-1 (ET-1) is a powerful vasoconstrictive peptide hormone that is cleaved from its precursor big endothelin into the active form. ET-1 is released from endothelial cells via two mechanisms, a constitutive release mode, which contributes to the maintenance of a continuous underlying vascular

tone, and a triggered release, where ET-1 is released from endothelium-specific granules upon external stimulation [57]. ET-1 carries out its biological role by binding to two possible receptors, endothelin receptor type A (ETA) and type B (ETB). Both receptor types are coupled to G-proteins and exert their effect via inositol-triphosphate (IP3). ETA causes IP_3-triggered Ca^{2+} release from the sarcoplasmic reticulum, leading to Ca^{2+}-calmodulin interaction, phosphorylation of myosin, and vasoconstriction [58]. ETB on the other hand triggers the production and release of NO and prostaglandin (PGI_2), causing net vasodilation. In the lung, ET-1 is internalized after binding to ETB, thus providing systemic clearance by the lung [59]. Endothelin receptors in the skeletal muscle are located mostly in the terminal vasculature, i.e. on terminal arterioles and on pericytes [28, 60, 61]. ET-1 plays an important role in fine-tuning blood flow and nutrient transport to capillary beds on a local level, and its concentration in the blood is, under normal condition, very lowly concentrated in the venous and arterial blood (2-3 pg/ml). Under moderate hypoxemia, ET-1 concentration approximately doubles, with venous concentrations exceeding those in arterial blood, reflecting its pulmonary clearance and production in the capillary beds [9, 59, 62]. The detrimental role of systemically elevated ET-1 is now well accepted and its importance in the mediation of hypoxemic pathophysiologies is recognized [17, 59, 63, 64].

Angiotensin: Sympathetic stimulation also activates the renin-angiotensin system, by causing release of renin from the kidney, which then cleaves angiotensinogen, which is produced by the liver, into angiotensin I. Angiotensin I (largely inactive), is then activated to angiotensin II by angiotensin-converting enzyme (ACE). Angiotensin II can enhance the contracting force of norepinephrine in arterial VSM [65]. It exerts its vasoconstrictive effect via AT1-receptors, which are G-protein-coupled proteins that increase intracellular Ca^{2+} , activates phospholipase C and causes myosin light chain phosphorylation via myosin light chain kinase (MLCK) [66].

Potassium channels: A large variety of K^+ channels are involved in vasomotive regulation of microcircular blood flow in the skeletal muscle and other organs, as they are downstream effectors of many vasoactive mechanisms. Opening of K^+-channels leads to outward flux of K^+, thus producing a negative membrane potential. This hyperpolarization causes closing of voltage-dependent Ca^{2+} channels, thus reducing Ca^{2+} influx and leading to vasodilation. Closing of K^+-channels on the other hand leads to vasoconstriction [23]. Members of this group include **Ca^{2+} activated K^+ channels (K_{Ca} channels)** that are downstream of adenosine, NO, epinephrine, and hydrogen ions, all of which cause vasodilation. Endothelin-1 and angiotensin II inhibit K_{Ca} channels via Protein Kinase C (PKC), leading to vasoconstriction [23]. **Voltage-dependent K^+ channels (K_V channels)** are opened by depolarization, thus allowing K^+ to evacuate from the cell, reducing vasoconstriction. These channels transduce β-adrenergic stimulation by causing adenylyl kinase to produce cAMP, which phosphorylates PKA, causing relaxation [23]. **ATP-sensitive K+ channels (K_{ATP})** are sensitive to the metabolic state, as their probability to open (and thus vasodilate) increases when the ratio of ADP vs. ATP rises in vascular smooth muscle. These channels are also opened by acidosis, hypoxia, and mediators that arise from exercise activity, such as epinephrine, prostacyclin, and adenosine, and they have been described on the surface of pericytes [67]. **Transient receptor potential (TRP) K^+ channels** react to the stimuli light, temperature, chemical agents, and mechanical stimuli, and are an important part of the autonomous myogenic response to increases in perfusion pressure. TRP channels can produce both vasodilation and vasoconstriction, modulate endothelial permeability in post-capillary venules, and are involved in the sensing of hypoxia in the lung and function as redox sensors in endothelial cells [23]. Because pharmacological and otherwise-induced vasodilation can only partially be attenuated by blockade of prostaglandin and NO signaling, an **Endothelial-Derived Hyperpolarizing Factor was hypothesized (EDHF)**, which might be an epoxyeicosatrienoic acid (EETs). Additional vasoactive effectors include carbon monoxide (CO) and hydrogen sulfite (H_2S) [23].

4.1.2.1 *α- and β- adrenergic receptors and the influence of the autonomous nervous system on skeletal muscle blood flow*

Blood flow distribution in skeletal muscle is strongly influenced by the autonomous nervous system, i.e. via its parasympathetic and sympathetic outlets. While parasympathetic neurons mainly regulate the heart rate, sympathetic branches influence both heart rate and contractility, peripheral resistance to blood flow, and venous compliance [68]. In resting conditions, baseline sympathetic activity maintains arteries and arterioles in a partially constricted state, and the reduction of sympathetic outflow therefore results in vasodilation [23]. Sympathetic impulses are mediated via norepinephrine and epinephrine through their release from chromaffin cells in the adrenal medulla and via sympathetic nerve fibers that induce peripheral release of norepinephrine from the medial walls of blood vessels [23]. α- and β-adrenoceptors are located on smooth muscle cells of arteries and arterioles. Adrenoceptors are G protein-coupled receptors that conduct their signal via influencing the presence of Ca^{2+} in the cytoplasm: α1 adrenoceptors activate phospholipase C and cause Ca^{2+} influx, followed by cAMP-triggered vasoconstriction. α2 cause vasoconstriction through adenylyl cyclase inhibition, whereas in the case of $\beta_{1\text{-}3}$ adrenoceptors, production of cAMP activates PKA and causes vasodilation by Ca^{2+} withdrawal. Norepinephrine binds to α1-receptors or α2-receptors to produce vasoconstriction, and epinephrine preferentially binds to β2-receptors on VSM, causing vasodilation [23]. During exercise, less norepinephrine is released than epinephrine, causing net vasodilation. Larger resistance vessels carry mostly α1-receptors, whereas smaller and terminal arterioles mostly carry α2-receptors [69]. α2-mediated vasoconstriction is profoundly weakened by acidosis, which arises from active muscle metabolism [69]. Epinephrine binds preferentially to β-adrenoceptors, mostly inducing vasodilation. In the skeletal musculature, β2 adrenoceptors are present on resistance and small pre-capillary arterioles, and on pericytes [32]. Sympathetic nerve stimulation also produces coronary vasodilation through β1-adrenoceptor stimulation, leading to increased heart rate and contractility. This extrinsic control is the main mechanism to adjust cardiac output to increased metabolic demand. Sympathetic neural stimulation also increases vascular resistance in arterial vessels that supply visceral organs, leading to net re-distribution of blood to the skeletal muscle [23].

The appearance of adrenoceptors on terminal arterioles and pericytes indicates that they may be particularly important in regulating capillary blood flow [28, 36, 67]. Via circulating epinephrine, hypoxia influences both α and β adrenoceptors [49], but it is unclear whether this activation improves or deteriorates capillary conductivity. Interestingly however, β2-adrenoceptor stimulation recovers the work force of severely hypoxic muscle ex vivo, which suggests a potential influence of these drugs on capillary beds [65]. We have found that the β2-adrenoceptor agonist bambuterol improves hypoxemic exercise performance in rats in a way that does not require the improvement of blood oxygen concentration, which is a strong indicator that the mechanism involves the reversal of hypoxemic microvascular dysregulation (Strand et al, *in press*, appended).

4.1.2.2 *Metabolic vasodilation and exercise hyperemia*

The active skeletal muscle extracts substantially more oxygen from the blood than its resting state and thus, a regulatory cascade is initiated by the commencement of exercise that aims to homeostase oxygen and nutrient availability to the parenchymatic muscle. Metabolic products of muscle activity, such as CO_2, lactate, H_2O_2, and H^+ ions activate K^+ channels, and/or prostaglandin, adenosine and NO cause local vasodilation in and around capillary beds, thus increasing blood flow to the area. This in turn triggers extrinsic (sympathetic reaction) and intrinsic processes that lead to exercise hyperemia, i.e. an increase of blood flow to the area [70]. Blood flow enhancement occurs within one second of the onset of muscular activity. This fast vasodilator response is followed by a larger vasodilation, dependent on magnitude and duration of exercise. Sympathetic outflow is not responsible for initial

fast vasodilation but likely for most of the second phase. Up to 60% of the hyperemic response is due to muscle pumping [23].

Vasodilation of pre-capillary sphincters also increases capillary recruitment and thus increases nutrient and oxygen transport to tissue. Hypoxia also causes local vasoactivity through ET-1 on the capillary and pre-capillary level, but the exact mechanism how this important tissue factor improves oxygen transport to the parenchymal skeletal muscle in a non-pathophysiological setting remains to be described [28, 57, 59, 71]. Because continuous blood flow leads, upon cessation of muscle activity, to quick clearance of local concentrations of signaling metabolites, metabolic vasodilation is tightly controlled in time [23]. Metabolic vasodilation explains, in part, the phenomenon of exercise hyperemia, where the onset of muscle activity induces an increase in local blood flow that can even be incited in muscle that is isolated from neuronal interference [23, 72, 73].

4.1.2.3 Shear-stress induced vasodilation

Vasodilation as a reaction to increased blood flow (the opposite of the myogenic response) occurs in some larger arterioles, resistance arteries, and conduit vessels, but not in small arterioles. It serves as a mechanism to augment flow delivery to arterioles when these vessels vasodilate. Mechanistically, shear stress is sensed and induces vasodilation, mediated via eNOS, NO, and EDHF [23].

4.1.2.4 Pericytes

Pericytes are mesenchymal, contractile cells that accompany microvascular blood vessels in virtually all organs. Their functions are diverse and include vascular growth and angiogenesis, wound repair, and the regulation of vascular permeability and contractility [40]. Pericytes have a round shape and possess multiple thin projections that wrap around endothelial cells. While pericytes are present around arterioles and venules, they are particularly prominent in their function as contractile elements around blood capillaries, which otherwise lack the ability to constrict. Pericytes play a critical role in regulating capillary perfusion and thus, oxygen and nutrient transport to tissue, and waste clearance. Pericyte constriction is controlled by catecholamines, ATP, adenosine, lactate, hypoxia, ET-1, and potentially other effectors [28, 32, 67, 74-76]. However, the exact biological role of pericytes in blood flow homeostasis in skeletal muscle, and in the response to hypoxia and hypoxemia remains unclear and may in fact differ greatly between tissues and organs. But, blockade of pericyte constriction could be key to any therapeutic effort that attempts to increase oxygen, drug, or other mass transport to tissue via the blood stream.

4.1.2.5 Myogenic regulation of blood flow

When VSM are exposed to increased transmural pressure, they react with contraction, thus increasing resistance to blood flow. When transmural pressure is reduced, VSM dilate, thus increasing blood flow. Under steady flow conditions, this “myogenic response” creates a continuous, pressure-correlated tone. This mechanism is very important to prevent overshooting, thus potentially damaging, perfusion of capillary beds. On the other side, the myogenic response is also critical in maintaining tissue blood flow even when perfusion pressure to the organ is cut low. Myogenic regulation is a crucial part of tissue blood flow autoregulation in all tissues, most prominently in the brain, where this mechanism ensures relatively homogenous blood flow within perfusion pressures of approximately 60-120 mmHg of arterial blood pressure in humans [23]. Transient Receptor Potential (TRP) K^+ channels, such as TRPM4 and TRPC6, play an important role in the myogenic response [77, 78], but also endothelin-1 and angiotensin II [79, 80].

4.1.2.6 Hypoxemia-induced changes in skeletal muscle microcirculation

Hypoxemia elicits vasodilation in skeletal muscle, leading to hyperemia, which is mediated by local control mechanisms [49, 81]. β2 adrenergic-controlled nitrodilation plays the most important role in mediating hypoxic vasodilation in resting and exercising skeletal muscle, but prostaglandin- and adenosine-mediated vasodilation are important as well [43, 55, 82]. Hypoxia-triggered, locally increased levels of ET-1 may serve to limit exercise-induced hyperemia and prevent systemic hypotension [83].

It is also known that hypoxia induces a vasoconstrictive response in the skeletal muscle, which is in part due to α-adrenergic responses [23], however, it is not fully recognized which parts of the microcirculation exactly are affected by this response. Indeed, a reduction in muscular blood flow under hypoxia, and an overshooting restoration thereof under ensuing hyperoxia, has been demonstrated in mice [84]. The fact that hypoxemia-triggered ET-1 elicits strong and sometimes irreversible vasoconstriction in pericytes argues that, while hypoxic vasodilation and local hyperemia are regulated on the level of resistance vessels, pre-capillary sphincters undergo ET-1 dependent vasoconstriction, leading to hypoxemic reduction in capillary recruitment [28, 84]. Indeed, we have shown that pharmacological targeting of pericytes and precapillary sphincters using endothelin-1 blockade increases the oxygen availability of hypoxemic skeletal muscle in rats, which is strongly indicative of improved capillary recruitment and perfusion [22]. In summary, endothelin-1 plays a major role in causing hemodynamic changes, specifically a reduction in capillary blood flow, in the skeletal muscle. However, a conclusive study of the exact influence of the role in hypoxemia-triggered endothelin-1 upregulation in skeletal muscle does not yet exist.

4.1.3 Therapeutic approaches

While decreased physical exercise performance is a hallmark consequence of hypoxemia, it is predominantly believed this decrement is due to the reduced availability of oxygen in the blood, ultimately caused by increased oxygen diffusion times to the muscle cell [85], or alternatively, due to limited pulmonary throughput following pulmonary arterial hypertension [17]. While it is indeed challenging to clearly separate the influence of oxygen diffusion vs. hypoxemic microvascular dysregulation on hypoxemic exercise performance, the sheer fact that hypoxemic performance decrements can be improved in rats and humans without enhancing blood oxygen levels emphasizes the importance of microvascular dysregulation, and vascular targeting [21, 22] (Schroeder et al, *conditionally accepted, appended*).

4.2 Reaction of the pulmonary vasculature to hypoxemia

4.2.1 Functional vascular anatomy of the lung

The mammalian lung is supplied by two different circulatory systems: the **pulmonary circulation** that transports deoxygenated blood via the pulmonary artery to the zone of gas exchange and shuttles the re-oxygenated blood via the *vena pulmonalis* back to the left atrium of the heart, and the **bronchial artery**, which supplies the airways with fully oxygenated blood. In the pulmonary circulation, deoxygenated, venous blood exits the right ventricle via the *truncus pulmonalis*, which divides into the left and right pulmonary artery and then subdivides into pulmonary arteries and arterioles. The vasculature from both the pulmonary and bronchial circulation is closely attached to the airway duct, branching along closely with its ramifications (Figure 2). Terminal arterioles diverge into pulmonary capillaries which wrap around the alveoli, forming a highly interconnected microcirculatory network.

The spatial association between vasculature and airways is so tight that gas exchange in the alveoli already occurs on the pre-capillary level [86].

The pulmonary vasculature can, besides its separation into precapillary, capillary, and postcapillary vessels, be categorized by whether blood vessels are within the acini and alveoli, or outside of that compartment. The pulmonary vasculature contains vascular smooth muscle cells and other contractile elements, such as fibroblasts and pericytes, endothelium, nerve cells, mast cells, and macrophages. In terms of the structure, both the pulmonary and the bronchial circulation are attached to the airway ducts, and divide coincidental with airway branching. The broncho-vascular bundles are held together by a common adventitial sheath [87]. The human pulmonary arterial tree has approximately 17 branch orders, with diameters ranging from 30 mm in the main pulmonary artery, down to 10-15 µm in arterioles and capillaries. Vessels in the parenchyma, i.e. the region of the terminal acini where gas exchange takes place, are always under 25 µm in diameter. Endothelial cells line the inner layer of the blood vessels without fenestration, including the capillaries. The morphology of capillaries that supply the airways is long and tubular, whereas capillaries that cover the alveolar septal walls are short, densely scattered (covering usually over 80% of the alveolar surface), and interconnected, thus forming a highly redundant network. Alveolar capillaries differ from extra-alveolar vessels in their glycocalyx, and in that they contain less or no Weibel-Palate bodies. Pericytes are present around human alveolar capillaries and contain contractile elements [87, 88].

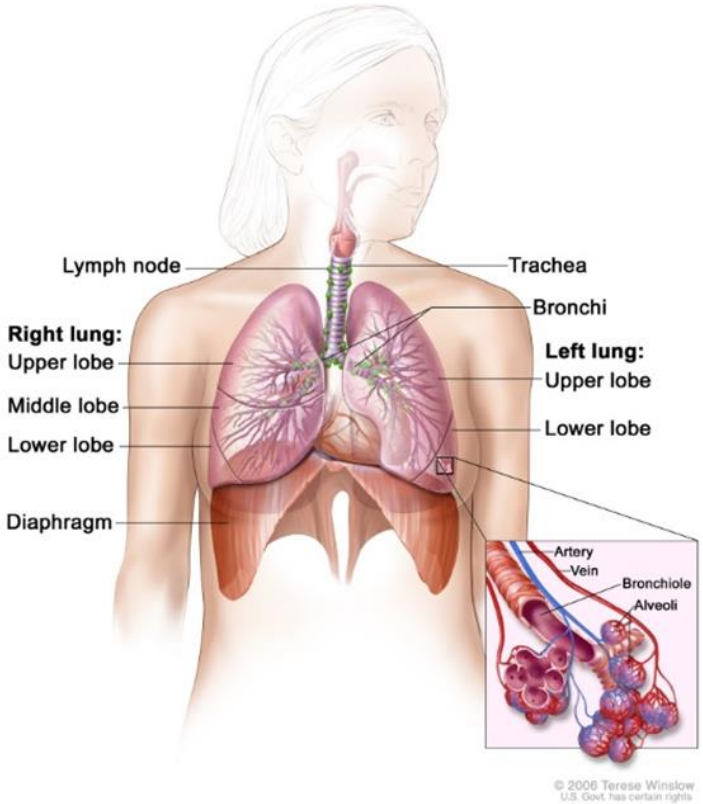

Figure 2: Terminal bronchiolar and arteriolar tree in the lung. Note that the pulmonary artery is depicted in blue, as it carries oxygen-poor blood, whereas branches of the pulmonary vein are carrying oxygen-rich blood and are therefore colored red. Branches of both pulmonary artery and pulmonary vein, as well as the branches of the bronchial artery and vein associate closely with the bronchial tree, and therefore diverge along with every branching point of the bronchi and broncheoles. Image used with permission from the artist [89].

4.2.2 Regulation of pulmonary blood pressure

The pulmonary circulation runs at lower blood pressures than the systemic circulation: whereas systolic and arterial pressure in the healthy systemic circulation is approximately 120/80 mmHg, arterial pressures in the normal pulmonary circulation range between 7 and 19 mmHg [90, 91]. Pulmonary arterial blood pressure is maintained by right ventricular pressure on one side and by the tone of the pre-capillary resistance vessels on the other side [92].

4.2.3 Vasoactive mechanisms in the pulmonary circulation

4.2.3.1 Ventilation-perfusion matching and hypoxic pulmonary vasoconstriction (HPV)

Blood flow through lung segments is strongly influenced by the respective ventilator activity in this segment in a way that less ventilated segments receive less blood flow. This mechanism, termed ventilation-perfusion matching, or V/Q-matching, which is designed to optimize oxygen loading of desaturated, venous blood, is, among mechanical factors, strongly influenced by the oxygen content of the inspired gas mixture. To a lesser degree, V/Q-matching is also affected by the oxygen concentration in the pulmonary arterial blood [93, 94]. As a consequence of this mechanism, acute exposure to hypoxic air leads to global constriction of pulmonary vessels, termed hypoxic pulmonary vasoconstriction (HPV), or the von Euler-Liljestrand reaction [95]. During embryonal development, the biological function of HPV is to drive blood away from the pulmonary circulation. In the adult lung, HPV aids to provide a local homeostatic reaction to focal hypoxia, such as during lung infection, to optimize oxygen uptake while avoiding changes to pulmonary artery pressure [94]. Under global hypoxemia, HPV causes increased hydrostatic pressure on the pulmonary microvasculature, thus increasing the chance for pulmonary edema (such as high altitude pulmonary edema, HAPE), and it also limits trans-pulmonary blood passage, thus limiting peak exercise performance [17].

Studies with artificial perfusion of animals with hypoxemic blood revealed that the effect of the oxygen content in the inspired gas mixture is much greater than that of the oxygen concentration in the venous blood [96-98]. However, these results may need revision following the discovery that systemic hypoxemia leads to the upregulation of endothelium-derived vasoactive factors such as ET-1, which strongly contribute to HPV and HAPE, and which have not been accounted for in these early experiments [10, 71, 99, 100].

The mechanism that is responsible for sensing and transducing alveolar hypoxia has been subject to intense research, but is not yet fully characterized: briefly, oxygen sensing is thought to take place in the vascular smooth muscle cells that accompany arteries and arterioles, and is hypothesized to be sensitive to changes in reactive oxygen species as by-products of mitochondrial respiration. Such radicals would then inhibit potassium channels, particularly TRPV4 and TRPV6, thus increasing cytosolic Ca^{2+}, causing vasoconstriction potentially via calcium sensitization [94, 101].

The HPV reaction to alveolar hypoxia happens within seconds and reaches a maximum within a few minutes. While continued exposure to hypoxic air breathing leads to adaptation, such exposure also causes remodeling of pulmonary resistance vessels, causing chronic pulmonary hypertension (discussed below) and polycythemia [92, 94].

4.2.3.2 Chronic pulmonary hypertension is a key pathophysiological consequence of long-term hypoxemia

Hypoxemia- or hypoxia-triggered hypoxic pulmonary vasoconstriction (HPV) fully reverses if hypoxia is transient. However, if hypoxia lasts over approximately 24h, pulmonary arterial pressure remains slightly elevated, compared to the baseline value [102, 103]. This indicates the hypoxia-induced changes to the tissue architecture that result in a sustained increase in pulmonary vascular resistance. Mechanistically, sustained hypoxia activates rho kinase and HIF-1a, reinforcing vasoconstriction, and leading to adverse pulmonary vascular remodeling and pulmonary arterial hypertension (PAH) [94]. Pulmonary hypertension is defined as pulmonary artery pressures exceeding 25 mmHg, with normal values being 8-20 mmHg [104]. PAH causes decrement in exercise capacity, but can lead to much more serious downstream pathologies, such as right ventricular maladaptation and hypertrophy, leading to high lethality due to cardiac ischemia [105]. Structurally, PAH results from to two main changes in the pulmonary arterial vasculature: (1) remodeling of pulmonary resistance vessels, which involves a decrease in arteriolar diameter due to muscularization and increases in the density of collagen and other matrix components, and (2) a total decrease in pulmonary vascularity, called rarefaction [92]. Pulmonary vascular rarefaction is one of the pathologies associated with conditions that involve hypoxemia, such as PAH and cystic fibrosis, and coincides with a reduction in the number of alveoli in the acini [106, 107]. Hypoxia-triggered PAH can result from pneumonia and other infection of the airways, asthma and chronic obstructive lung disease (COPD), diffuse parenchymal lung disease (DLPD), emphysema, lung fibrosis, and exposure to hypoxia at high altitude. Pulmonary hypertension resulting from chronic lung disease and/or hypoxia has been termed as group 3 PAH, as opposed to PAH caused by idiopathic factors, drugs, left heart disease, and other reasons, summarized in groups 1, 2, and 4 [104, 108]. PAH is an extremely grave condition, with untreated average survival margins from a few years down to only 2-3 months after diagnosis in severe cases. The cause of death is right ventricular failure (*cor pulmonale*) [104].

4.2.4 Treatment options against the effects of alveolar hypoxia and hypoxemia on the pulmonary vasculature

The myogenic tone in the resistance and pre-capillary arteries and arterioles of the healthy pulmonary vasculature is regulated by a multitude of effectors, many of which are identical to those described in chapter 3 [109, 110]. Many locally active mediators that regulate pulmonary vascular smooth muscle tone are produced in the vascular endothelium. The most important effectors are the vasodilators NO and prostacyclin (PGI2), both of which also inhibit remodeling, and the vasoconstrictor endothelin-1, which promotes vascular remodeling [111-114]. Other important mediators include prostaglandin F2α (PGF2α) and platelet-derived growth factor B (PDGFB) [5, 115, 116]. The lung also plays a major role in catabolizing vasoactive factors, such as endothelin-1 [59]. The pulmonary vascular tone is also regulated via sympathetic innervation, which is, for example, capable of causing vasodilation, and is potentially important in modulating HPV [117, 118].

Severe and acute hypoxemia, e.g. following acute respiratory distress (ARDS), carbon monoxide poisoning, or during exacerbating conditions in patients with congenital PAH, is treated with supplemental oxygen [5, 19]. Hypoxic pulmonary hypertension (HPV), i.e. the immediate response of the pulmonary vasculature to inspired hypoxic air, is strongly dependent on the inhibition of nitrodilation by endothelin-1 [119]. HPV is accordingly alleviated by phosphodiesterase type 5 (PDE5) inhibitors [18, 120], and endothelin receptor antagonists [17, 18, 63]. Calcium channel blockers like nifedipine and β2 adrenergic agonists like salmeterol are effective in preventing hypoxia-triggered high altitude edema and likely also alleviate HPV. β2 adrenergic agonists may also alleviate HPV [11]. Pulmonary arterial hypertension following the re-modeling of the pulmonary vasculature is treated

mostly with vasodilators, such as prostaglandin derivatives (prostacycline, epoprostenol, iloprost), endothelin receptor blockers (bosentan, ambrisentan, macitentan), phosphodiesterase 5 inhibitors (sildenafil, tadalafil), and activators of intracellular guanylate cyclase (riociguat) [104]. In severe cases and in non-responders, patients are receiving heart-lung transplants as a life-saving measure [121]. The diversity of treatments against pulmonary hypertension reflects, in part, the high level of redundancy of the pulmonary capillary network, where blockade on one branch can be easily circumvented by increasing the flow through another branch (Figure 2).

In summary, hypoxemia elicits a strong vasoconstrictive response of the pulmonary resistance arterioles, leading to pulmonary arterial hypertension and, after extended exposure, to vascular remodeling and chronic pulmonary hypertension. Blockade of the endothelin pathway, agonism of β2 adrenergic and prostanoid signaling, and nitrodilation all have shown efficacy to alleviate acute and chronic pulmonary hypertension.

4.3 Hypoxia and hypoxic metabolism in solid tumors

4.3.1 Insufficient microcirculatory supply causes hypoxia in solid tumors

In order to grow beyond a size of a few millimeters, tumors need to solicit their blood supply and vascular network from the surrounding vasculature. Because free oxygen in a tumor is consumed within less than 100 µm (very much depending on the local oxygen consumption rate) uncontrolled cancer cell growth leads to local hypoxia, which is the major stimulus for the neovascularization of the tumor [122]. Because tumor angiogenesis is “need-driven” and subject to continuous dynamic change, tumor vascularity and blood flow is very different from the microcirculation of normal tissues: tumor vessels are immature and disorganized, in that they do not follow normal vascular hierarchy and differentiation, and are often more fenestrated and leaky than their normal counterparts [123]. Tumor microvessels are also often dilated and saccular, and often longer than normal capillaries [124]. As a consequence, tumor blood flow is also “irregular”, i.e. often much slower or faster than blood flow in normal tissues. The tumor hemodynamics is characterized by strong heterogeneity of flow characteristics, a large fraction of deoxygenated blood, flow outside of the endothelium, arteriovenous shunting, and sluggish or oscillating blood cell movement, or even hemostasis [122, 125]. As a result, large areas of the solid tumor are poorly supplied with oxygen and nutrients, and thus characterized by perpetuated hypoxia and strong accumulation of products of the hypoxic metabolism.

4.3.2 Oxygen, lactate, and glucose follow specific gradients in solid tumors

The metabolic microenvironment of the tumor mirrors the inadequate supply situation and is characterized by oxygen depletion, i.e. hypoxia or anoxia, high levels of lactate, high acidity, low glucose and other energy-rich substrates, and cancer necrosis. ATP content in tumor cells is generally lower than in normal cells [123]. Tumor cells are reported to process glucose at much higher rates, often termed the “Warburg Effect”, but this is mostly true for dividing cells [126-128]. However, the metabolism of quiescent cancer cells, which typically constitute the majority of the cancer cell population in a given tumor, is not well investigated yet. There is a likelihood that the chronically hypoxic, quiescent cancer cell population is largely identical with the much propagated “cancer stem cells”, and these cells have distinct metabolic properties, such as high glucose consumption and comparably low lactate production [128, 129]. Because the metabolism of cancer cells differs depending on their location in the tumor, there is no direct correlation between glycolytic capacity of a given cancer cell line in vitro and its glucose consumption rate in vivo [130].

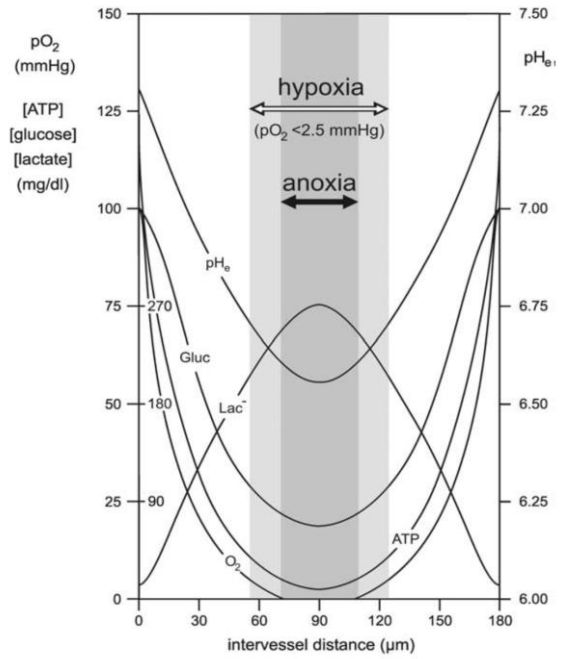

Figure 3: General profile of the key metabolites oxygen, glucose, lactate, and ATP in experimental animal tumors [123].

As these local tissue concentrations are formed by supply and clearance through the blood stream vs. demand and production by the tumor cells, they form specific geographic gradients that are determined by the presence and activity of the microvessels: in general, the steady-state tissue oxygen concentration decreases with increasing distance from the blood vessel. Likewise, a decrease from the site of the active blood vessel can be seen for the extracellular glucose, and for the intracellular ATP [123, 130, 131]. Lactate on the other hand is thought to increase with distance from active blood vessels [130, 132].

Necrosis, a feature that is highly characteristic for solid tumors, appears to occur when tumor cells experience both extremely low glucose (glucopenia), very high local concentrations of lactate, and hypoxia or anoxia [123]. Lactate in the tumor arises from sources like glucose and glutamine, following either oncogenic alterations of cell metabolism [133, 134], loss of mitochondrial function [135, 136], or production as part of anaerobic glycolysis during hypoxia [137, 138].

The metabolic microenvironment has an important influence on the cancer cells: It is known, and can be easily verified in a laboratory setting, that cancer cells under hypoxia exit their cycling activity and become quiescent. This anti-proliferative effect is further aggravated by glucopenia and lactacidosis. As a consequence, tumor regions distal to blood vessels and close to the necrotic edge are mostly quiescent, which gives them immunity to traditional cytotoxic chemotherapeutic agents [139, 140]. Importantly, both severe tumor hypoxia and high tumor lactate concentration are both correlated with tumor resistance to therapy, distant metastasis, and poor outcome [141-146].

4.3.3 Clinical implications of tumor hypoxia

Tumor hypoxia has multiple important effects on the clinical course of the disease. First, because chronic tumor hypoxia occurs in regions that are distal to active blood flow, hypoxic cancer cells are more protected from (blood-born) anticancer drugs, which may only travel some 100 µm from the active vessel [140, 147] (Figure 4).

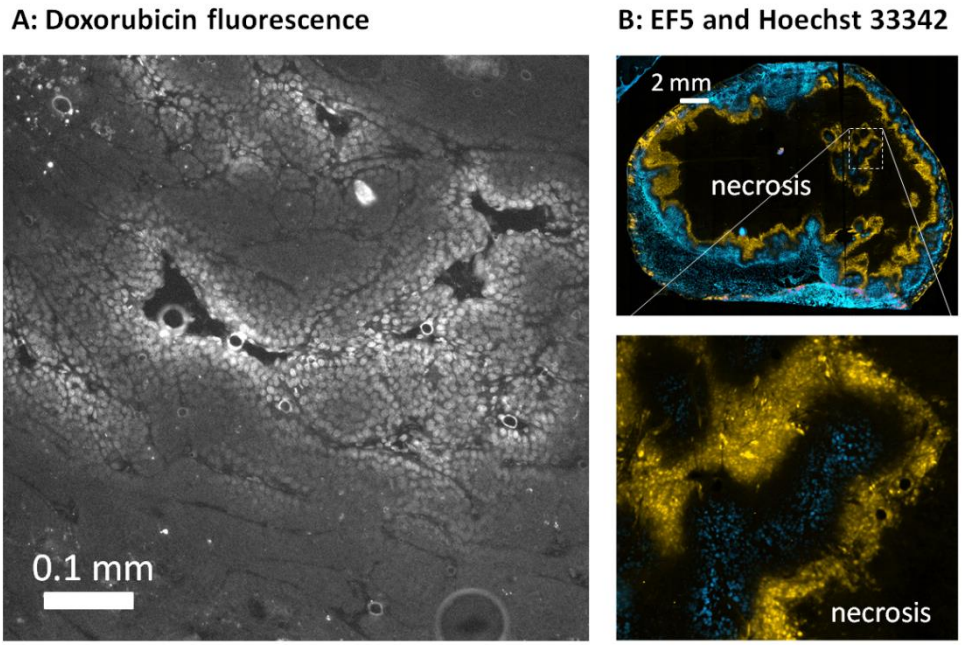

Figure 4: Hypoxic tumor cells are largely protected against intravenous chemotherapeutic drugs, because they are located in non-overlapping regions of the tumor. A: Example of doxorubicin fluorescence micrograph from a frozen histological section of an R3230 rat mammary carcinoma. Doxorubicin fluorescence can be found in the vicinity of functional blood vessels. B: example of an EF5 stained (yellow) frozen section of a FaDu human head and neck tumor cell line, grown in the flank of an athymic nude mouse. The perfusion marker Hoechst 33342 was co-injected, to label perfused cancer cells. Procedures were done as previously published [148]. Note that EF5 labeling is consistently found bordering tumor necrosis. All data: Schroeder, unpublished.

Moreover, tumor cells do not proliferate under severe hypoxia or substrate starvation [149], which leads to the surprising fact that tumors vary widely in the extent of their "growth fraction", i.e. the proportion of actively dividing vs. non-dividing cells, ranging from over 80% down to 10% and less [150-154]. Quiescent (i.e. non-dividing) cancer cells are resistant to most classic cytostatic chemotherapeutic agents that target only dividing cells [139, 155, 156]. Also, because quiescent cancer cells are much more resistant to ionizing radiation than proliferating cells, hypoxia-induced quiescence also produces a survival advantage for cancer cells under radiotherapy [157]. It has been elegantly demonstrated by Dr. Andrew Minchinton's group how hypoxic, quiescent cancer cells contribute to treatment resistance: Conventional cytotoxic chemotherapy, such as gemcitabine, will kill off cancer cells close to perfused tumor blood vessels, while not affecting chronic hypoxic cells that dwell at a distance from perfused vessels, which are quiescent following hypoxia and substrate shortage. After perivascular cancer cells are killed, oxygen, glucose and other nutrients can now diffuse further, thus causing previously starving, hypoxic, quiescent tumor cells to resume cycling activity, thus re-populating the tumor and ultimately causing chemotherapeutic failure [139, 158].

The efficacy of contemporary chemotherapy as a standalone treatment against solid primary and metastatic tumors in humans is difficult to assess, because it is ethically not feasible to run control groups (which would be untreated patients). However, blood-born anticancer drugs are in general far from able to cure solid tumors: as a first-line treatment, cytotoxic chemotherapy involving both traditional and novel treatments can control breast cancer only for 7.6 months until the tumor resumes growth, allowing patients a median survival of 21.7 months [159]. Chemotherapeutic drugs mostly target cycling, growing, or actively metabolizing cells, such as anthracyclines which block topoisomerase II, inhibitors of DNA-synthesis such as fluorouracil or methotrexate, or DNA-cross-linkers such as carboplatin. The efficacy of chemotherapy can also be assessed as an adjuvant to an existing therapeutic protocol. As such, chemotherapy is soberingly ineffective in even improving

patient survival, increasing life spans by only a few months at best, e.g. only 1-2 months in colorectal cancer [160]. More modern drugs such as EGF blockers have produced similarly disappointing results [161]. Other approaches such as the much acclaimed angiogenesis inhibitor bevacizumab adds 3-5 months to progression-free survival when supplemented to standard chemotherapeutic protocols in colorectal cancer [162] and carries no additional benefit whatsoever in breast cancer [163]. The median survival benefit of the recently introduced immune checkpoint inhibitors such as nivolumab exceeds that of traditional chemotherapeutic regimen but also ranges within only 5-8 months [164-166]. The extortionate costs connected with the development and launching of new anticancer drugs while these, at best, return only a few months of added survival to the patient are recognized and discussed in the field [167]. Moreover, while most contemporary chemotherapeutic treatments are drug combinations that consist of highly optimized, time-scheduled, fixed-dose combinations, it is still important to remember that cytostatic therapy, after causing initial cytostasis, triggers tumors to grow even faster than before treatment [168].

Since failure to target the right cell population is such a plausible explanation for the lack of success of cytotoxic and cytostatic drugs, it is even more surprising that the presence of the substantial and well-documented fraction of non-dividing cancer cells present in all solid tumors is so thoroughly ignored when financing decisions for chemotherapeutic drug development projects are made, or when new treatment combinations are assembled. Because oxygen and nutrient starvation, and cancer cell survival at distance from blood vessels, are important and well-documented causes for cancer cell quiescence and diffusion limitation, these factors should be of foremost interest when systemic cancer treatments are designed.

4.3.4 Therapeutic approaches that leverage the microcirculation and the hypoxic environment of the tumor

4.3.4.1 Antiangiogenic therapy

The idea of targeting and destroying the vascular supply of solid tumors was introduced by Judah Folkman in the 1970ies [169], and brought to life with the discovery of pro-angiogenic (VEGF, PDGF) and anti-angiogenic factors (angiostatin, endostatin) [170]. Inhibition of angiogenesis is thus mainly achieved by blocking one or more subtypes of the vascular endothelial growth factor VEGF (A-D), or placental growth factor (PLGF), or any of the VEGF receptors FLT1-3, but also the angiopoietin pathway, in particular the TIE2 receptor kinase [171]. However, antiangiogenic therapy has multiple problems: first, destruction of the tumor vasculature leads to increased hypoxia in the tumor, which triggers higher treatment resistance, activates alternative, hypoxia-driven angiogenic pathways, and might increase the likelihood of hypoxia-induced metastasis [172, 173]. Second, because not all tumors depend on VEGF to create their vascular supply, the response to anti-VEGF therapy is heterogeneous. Third, because older tumors and many metastases depend on already mature or co-opt pre-existing vasculature, antiangiogenic therapy is not efficacious in these entities, and causes tumor stasis, at best [171]. Among the tumor types that have shown sensitivity towards antiangiogenic therapy are renal cell carcinomas and ovarian and cervical cancer. However, even in these tumor entities, survival benefits due to treatment did not exceed 4 months [171, 174]. Important antiangiogenic drugs in contemporary clinical use are the VEGF blocker bevacizumab (Avastin) and the kinase inhibitors sorafenib, sunitinib, pazopanib, and imatinib [163, 171, 175-178]. Interestingly, antiangiogenic therapy leads to hypertension in about 25% of the patients, which however appears to benefit the outcome [179, 180].

4.3.4.2 Provascular therapy

The chaotic architecture and inefficiency of the tumor microcirculation produces a barrier to the delivery of blood-born cytotoxic drugs to the cancer cells. The approach to improve the delivery of therapies to the tumor via targeting the intra- or extratumoral vasculature has been termed the "pro-vascular" strategy [181]. In addition to the delivery of cytotoxic drugs, pro-vascular strategies have been exploited to improve the delivery of oxygen to the tumor to improve the outcome of radiation therapy [182, 183]. Successful utilization of the tumor vasculature is closely linked to the maturation and differentiation status of the tumor vessels. Particularly in slow-growing human tumors, blood vessels are often innervated and associated with contractile cells: colon and breast cancers show average pericyte coverage of around 70%, lung cancer displaying a broad variety between 5 and 60%, and kidney and brain cancer ranging around 5-25% [184].

The differentiation of blood vessels within the tumor determines their responsivity to vasoactive agents. However, because blood vessels in the vicinity of tumors are better differentiated and vasodilate more efficiently than tumor vessels, a given vasodilatory stimulus leads to a net outflow of blood from the tumor, a phenomenon termed "vascular steal" [185, 186]. However, increased vascular resistance due to high capillary lengths and augmented interstitial pressure in tumors also contribute to this phenomenon [124]. For the same reason, a vasoconstrictive stimulus affects peritumoral vessels more than those in the tumor, which can be leveraged to specifically improve mass delivery to tumors, as will be discussed below.

Assisted drug and oxygen delivery during radio/chemotherapy has been pursued through multiple strategies:

4.3.4.2.1 Nitrodilation

The application of NO donors via the blood stream has been attempted frequently, with the goal of specific dilation of tumor vessels and a net increase in tumor blood flow. Although a variety of NO donors were tested for this purpose, the results were mixed, likely because nitric oxide can produce systemic hypotension and thus induce vascular steal [186-190].

4.3.4.2.2 Endothelin receptor blockade

This strategy has demonstrated great potential in dilating tumor vessels. One of the hallmarks of many tumor vessels is the maintenance of an endothelin-responsive basal vasoconstrictive tone. Importantly, it has been shown that blockade of the endothelin pathway in tumor vessels abolishes the autonomous myogenic response in these vessels, thus reducing vascular resistance, improving tumor blood flow, increasing cytotoxic drug delivery and improving therapeutic success [191, 192]. Part of the basis for this important discovery is the responsiveness of pericytes to endothelin and endothelin receptor blockers [28, 34, 193], paired with their high prevalence in the tumor microvasculature [184]. We have found initial evidence that an endothelin receptor A blocker in combination with a hypertensive drug increases tumor blood flow in pulmonary metastases in rats [194]. Clearly, pharmacological targeting of the endothelin pathway has high potential of improving therapeutic success in cancer therapy.

4.3.4.2.3 Induced hypertension

This strategy has the goal to increase the systemic perfusion pressure, in order to re-distribute the blood supply towards the tumor, create local tumor hyperemia, and thus deliver more anticancer drug, or improve the outcome of radiation therapy. Another effect of vasoconstrictive substances is that blood vessels in the neighborhood of the tumor show a stronger net vasoconstriction than tumor

vessels, leading to a net relative increase in blood perfusion of the tumor [195]. Indeed, infusion of the vasoconstrictor angiotensin II has shown to increase blood flow and drug delivery to experimental tumors and produced better outcome compared to chemo- and radiotherapy alone [195-199]. Angiotensin II-mediated tumor hyperemia has shown promise in humans, too [200-202]. However, this has raised concerns, because angiotensin II is a powerful mitogen and angiogenic factor [203]. On the other hand, post-synaptic adrenergic agonism via epinephrine has also been successfully employed to improve tumor blood flow via creating hypertension [204]. From our own experience, induced hypertension, if combined with endothelin receptor type A blockade, has not only the capacity to improve microcirculatory blood flow under hypoxemia in normal tissue, but also in metastatic tumors of the lung [194]. This angle warrants in-depth investigation, as it holds solid promise to solve the problem of insufficient drug delivery to solid tumors, which is a central reason for chemotherapeutic treatment failure in cancer.

4.3.4.2.4 Nicotinamide and carbogen breathing

Nicotinamide has been found to increase the impact of radio- [205] and chemotherapy [206]. This could be due to its conversion into NAD^+, leading to increased lactate production and lactacidosis-triggered local vasodilation [207]. Carbogen, a gas mixture of up to 5% CO_2, balance O_2, has been introduced in the 1950ies for the treatment of neurological disorders in human patients [208]. In combination, carbogen and nicotinamide have been shown to increase tumor blood flow in humans, although the mechanism remains unclear [209]. A therapy based on combined nicotinamide and carbogen termed ARCON (Accelerated Radiotherapy, Carbogen, and Nicotinamide) has shown impressive improvements in treatment success of certain tumors such as head-and-neck and bladder cancer, although rectal and urinary blood loss have been dose-limiting [210-212].

4.3.4.2.5 Vascular normalization

It has been hypothesized that the inhibition of angiogenesis will lead to a more efficient perfusion of solid tumors, due to a reduction of tortuous, inefficient, and leaky microvessels, thus improving tumor blood flow and oxygenation, reversing interstitial pressure, reducing the immunosuppressive effect of the tumor microenvironment, and making chemotherapeutic drug delivery and radiation therapy more efficient, ultimately improving clinical outcome [213]. The addition of an antiangiogenic drug to a standard chemotherapeutic or radiation treatment has proven somewhat efficacious in terms of extending patient survival in *glioblastoma multiforme*, head and neck cancer, pancreatic cancer, soft tissue sarcoma, and breast cancer, improving progression-free survival within a margin of approximately 4-6 months, compared to the respective standard of care [214, 215].

4.3.4.2.6 Other approaches

Bradikinin is a vasoactive peptide hormone and natural antagonist of angiotensin II. It has a mostly vasodilatory activity and mediates pain and inflammation. The bradykinin derivative lobradimil/ cereport has been engineered to have a prolonged half-life, and for penetrating the blood-brain barrier. Cereport has shown promise in improving chemotherapeutic delivery to metastatic brain tumors in rats [216], but has not met expectations in the clinical setting [217].

Two more pro-vascular strategies will be mentioned here: intravenous hydralazine has been used to induce hypoxia by shifting blood away from the tumor, which then makes the tumor vulnerable to hypoxic cytotoxins [218, 219]. Also, hyperthermia, i.e. heating of the tumor, has shown some potential to induce tumor vasodilation and increase tumor blood flow and oxygenation [220, 221].

In summary, the diffusion/perfusion limitation of solid tumor sub-regions has been recognized as a tumor-specific, pharmaceutically targetable trait, and a great variety of approaches have been

developed against it. However, an important safety premise is that the enhancement of blood flow to the tumor must not feed its growth. It is therefore important to carefully tailor the time schedule of tumor hyperemia, to avoid growth-stimulating effects. Also, metastatic dissemination has a mechanical aspect, i.e. sudden increases in tumor blood flow may shear off cells, or clusters thereof, from the primary tumor, which then could cause hematogenous metastases [222]. Such risk needs to be carefully examined. Last, temporarily increased blood pressure could cause headaches and might constitute a challenge to the peripheral vasculature. This needs to be addressed by establishing personalized safety margins for blood pressure manipulation ahead of therapy.

4.3.4.3 Treatments that leverage the hypoxic tumor microenvironment

4.3.4.3.1 Hypoxia-activated prodrugs

The recognition of chronic hypoxic tumor cells as a major source of chemoradioresistance has led to the novel class of anticancer drugs named hypoxic cytotoxins. The most important concept in this field is that of the hypoxia-activated prodrug (HAP), or bioreductive toxin. Chemically, HAPs are cyclic nitro compounds, aromatic N-oxides, aliphatic N-oxides, and quinone derivatives [223, 224]. Structurally, HAPs include (1) a trigger, (2) a linker and (3) an effector [225]. The effector is the cytotoxic component, typically exerting its effect by interacting with DNA, such as by arresting the replication fork, or causing DNA interstrand crosslink [224]. The linker serves to uphold the effector in a deactivated state, and the trigger activates the prodrug and ensures hypoxia selectivity [225]. The most widely used trigger mechanism is the conversion of the prodrug into a prodrug radical via one-electron reduction through cellular oxidoreductases. Under hypoxic conditions, the prodrug radical cannot be detoxified via the cellular detoxification machinery and the prodrug is subjected to further reduction or fragmentation, resulting in the final cytotoxic compound [225]. The flagship compound in this field has been tirapazamine, a heterocyclic aromatic N-oxide, which under hypoxic conditions causes the formation of a DNA-damaging free radical that is responsible for its cytotoxicity [224]. Tirapazamine has shown potential to not only kill tumor cells, but also blood vessels in hypoxic regions of the tumor [226, 227]. Tirapazamine has prevailed through phase III trials, however, its clinical use is hampered by dose-limiting toxicity, such as anemia and neutropenia, nausea and vomiting, diarrhea and skin rash [228]. Additional bioreductive hypoxic cytotoxins have been brought forward through clinical tests, such as TH‑302 (evofosfamide™) or PR-104 [224]. However, it remains to be determined if these compounds can truly overcome the toxicity problems of the first generation of these drugs.

4.3.4.3.2 Autophagy inhibitors

Cells continuously recycle their content to phase out misfolded or damaged proteins, using ubiquitination/proteasomal degradation and other mechanisms. Larger overly abundant, damaged, or aging compartments such as large proteins and organelles are resolved and recycled by autophagy, consisting essentially of the incorporation into autophagosomes, followed by lysosomal degradation (autolysosomes) and recycling or metabolic breakdown of the content. This mechanism, which is maintained at a low basal level under normal conditions, can be recruited by cancer cells to withstand and endure nutrient and oxygen deprivation in the tumor, and thus resist chemoradiation therapy [229]. While stimulation of autophagy can also improve therapeutic outcome in some cancers via triggering autophagic cell death, the inhibition of autophagy, typically as an adjuvant to a secondary therapeutic regiment, is the more common route [229, 230]. With the discovery that the anti-malaria treatments chloroquine and hydroxychloroquine are efficient autophagy inhibitors, at least nineteen clinical trials are currently underway to investigate the efficacy of autophagy inhibition alone and in combination with a secondary therapeutic regimen [229].

5 Summarized achievements

Part of the work summarized here has focused on identifying novel pharmacological strategies of treating and reversing hypoxemic microvascular dysregulation in the skeletal muscle and the lung, and to test them in human candidates. An important aspect here was the potential transition of these findings to improving oxygen and drug delivery to solid primary and metastatic tumors. Important work was done in identifying the lactate consumption and lactate catabolism of cancer cells in solid tumors, with an emphasis on developing new treatment strategies to block this cancer cell survival mechanism. Third, my team and I were making strong attempts to establish innovative animal models of intravital microscopy, to fill the existing gap of methods that allow the direct visualization of organ and tissue microcirculation.

5.1 Discovery of novel drug combinations to alleviate hypoxemic dysregulation

As part of a US Defense Advanced Research Projects Agency (DARPA) sponsored multi-institutional program termed "Rapid Acclimatization to Hypoxia at High Altitude" (RAHA), my research team and I have identified several of treatments that showed promise to alleviate the detrimental effects of hypoxia on human health, and in particular improve oxygen availability to tissue. This effort, which was reviewed in a dedicated article in Nature Medicine [231] was heavily reliant on rat-based screening models under simulated high altitude or inspired hypoxia to identify promising treatments consisting mostly of already FDA-approved drugs, followed by clinical phase 1 and phase 2 testing of up-prioritized compounds and combinations in humans. The following strategies have been pursued:

Theophylline and ambrisentan: In 2012, I have published the results of an animal trial, reporting that the combination of the xanthine drug theophylline and the endothelin receptor type A antagonist ambrisentan, increased hypobaric, hypoxic exercise endurance in rats [21]. An important hallmark of this treatment was that while environmental hypoxia naturally decreased the arterial blood oxygen saturation (SpO_2) in all treatment groups, the treatment did not cause an increase in SpO_2 between any of the groups. We then proceeded to test this treatment in humans: A phase 1 study in normoxic volunteers revealed that 400mg single-dose aminophylline (a soluble formulation of theophylline) is nontoxic if combined with 5mg single-dose ambrisentan, and the drugs do not substantially interact. In a laborious placebo-controlled, randomized Phase 1/Phase 2 setup, we have tested whether these drugs would be safe to apply together at high altitude, in resting and exercising healthy human subjects (Figure 5A). Besides testing the safety of these drugs, we have also made an effort to produce initial information on the efficacy of this combination, in terms of alleviating symptoms of high altitude illness, and in regard to restoring exercise performance capacity: The onset of early altitude sickness with and without treatment on board was tested using a scoring sheet, where lead symptoms of acute mountain sickness (AMS), such as headaches, nausea, dizziness, and fatigue, were quantified. The potential alleviating effect of the treatment on hypoxic exercise decrement was compared to the decline of exercise performance between normoxia and hypoxia in treatment vs. placebo groups. We found that not only were the drugs and their combination tolerated well under hypobaric hypoxia in both, resting and exercising individuals, with adverse events mostly connected to the impact of simulated altitude (Figure 5B). But also, all treatments (aminophylline alone, ambrisentan alone, and the combination of them) led to a significant improvement in hypoxic exercise performance in virtually all treatment groups (Figure 5C). Importantly, as hypothesized, the drug combination did not systematically increase SaO_2 in resting or in exercising subjects (Figure 5D,E). A manuscript resulting from this effort has been conditionally accepted (Schroeder et al, appended).

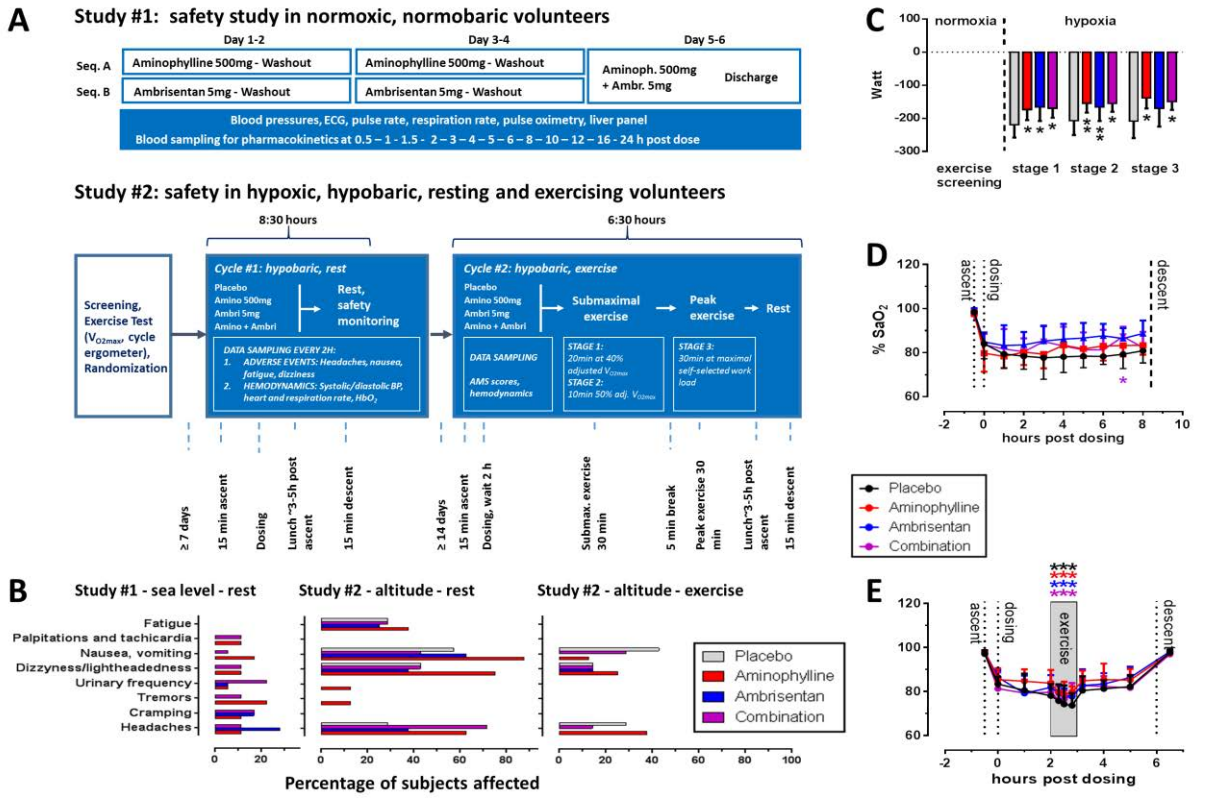

Figure 5: Testing of tolerability and efficacy of combined aminophylline and ambrisentan in human subjects. A: study design: a normoxic Phase 1 crossover trial was performed to investigate the basic tolerability, as well as potential drug interaction, of the novel combination of aminophylline (400mg) and ambrisentan (5mg) in humans. This was followed by a second trial, where the tolerability of combined aminophylline and ambrisentan was tested in resting and subsequently in exercising subjects under hypobaric hypoxia (inspired O2 and barometric pressure equivalent to 4268 m of altitude). B: Simulated high altitude, but not drug treatment, increased the percentage of subjects affected by most adverse events. The incidence, but not the severity of headaches increased with aminophylline or combination treatment. C: During all three stages of exercise (stages 1-2: submaximal exercise, stage 3: maximum exercise), treatment with aminophylline, ambrisentan, and their combination significantly improved the overall exercise performance over the placebo group, after values were normalized to the individual peak performance level during initial exercise screening. D: in resting, hypoxic subjects, combination treatment did not raise SaO2 over any of the other treatments except in time point 7h, where a significant increase over placebo-treated subjects was seen. E: in exercising, hypoxic subjects, none of the treatments increased SaO_2 over any of the other ones (modified from Schroeder et al, conditionally accepted, appended).

Ephedrine and ambrisentan: In order to test the hypothesis that a straightforward hypertensive drug could replace theophylline to improve, if combined with an endothelin inhibitor, exercise performance of rats under simulated high altitude, we have tested the influence of ephedrine and methylphenidate, respectively combined with ambrisentan, on the endurance capacity of rats under such conditions. Both ephedrine and methylphenidate significantly increased animal performance under simulated high altitude, whereas the single treatments had no such effect. Hemodynamic screening of anesthetized rats treated with ephedrine and ambrisentan revealed the ability of ephedrine and methylphenidate to increase blood flow to the muscle under both normoxia and hypoxia (Figure 6). However, only in combination with the endothelin A receptor blocker ambrisentan was this augmented flow accompanied with increased oxygen transport to the skeletal muscle under hypoxia (Figure 6C, D) [22]. Again, none of the treatments modified hemoglobin oxygen saturation under hypoxia, indicating that such increase is not the reason for the observed endurance-restoring effect. These results supported the hypothesis that a blood-pressure stabilizing compound is required to make this pharmacological strategy work.

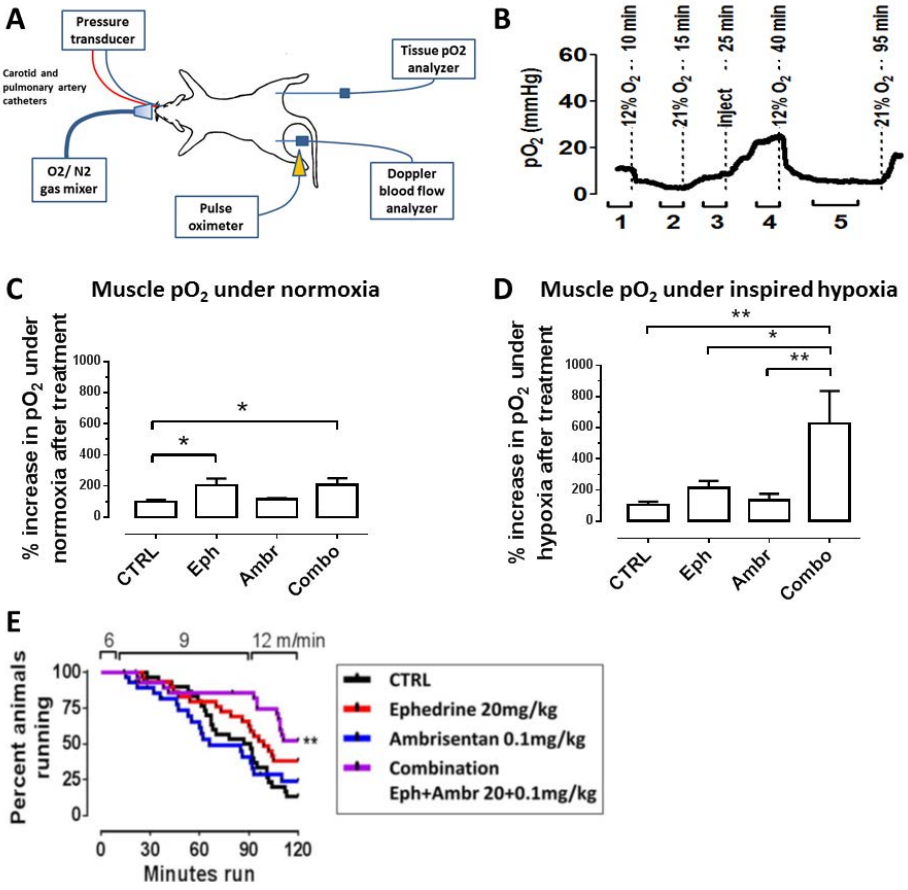

Figure 6: Hypertensive drugs synergize with endothelin receptor blockers to improve tissue blood flow under hypoxia. A: Experimental setup of measuring the influence of ephedrine and ambrisentan on skeletal muscle and oxygenation in anesthetized rats. B: Experimental time schedule and example of a muscle tissue pO2 track. Inhaled hypoxia was applied both before and after the treatment, to obtain an internal control. Numbers represent time points considered for measurements. C: Changes in pO2 relative to controls during normoxia (panel B time point 4). D: Changes in pO2 relative to controls during hypoxia (time point 5) Statistics: one-way ANOVA with Bonferroni correction, *p<0.05, **p<0.01. E: results of run-to-fatigue experiments with rats after injection of ephedrine and/or ambrisentan. N = 28–31 per treatment group. Statistics: log rank test, **p=0.0024. Data modified from [22]

Theophylline and bambuterol: We have investigated the question whether a long-acting β2 adrenergic receptor agonist (LABA) would synergize with theophylline to improve hypoxic exercise performance in rats and would be feasible in humans. We found that the LABA bambuterol increases exercise performance in hypoxic hypobaric rats by itself, and does so in combination with theophylline as well, again without changing SpO_2. In humans, the combination of theophylline and bambuterol is relatively non-toxic and drug interaction is negligible (Strand et al, *in press*, appended). These drugs were however not yet tested in hypoxic, hypobaric humans thus far.

Aminophylline and methazolamide: As part of our animal screening, we had demonstrated that theophylline has shown efficacy if combined with the carboanhydrase inhibitor and anti-glaucoma drug methazolamide in hypoxic hypobaric rats (Figure 7A).

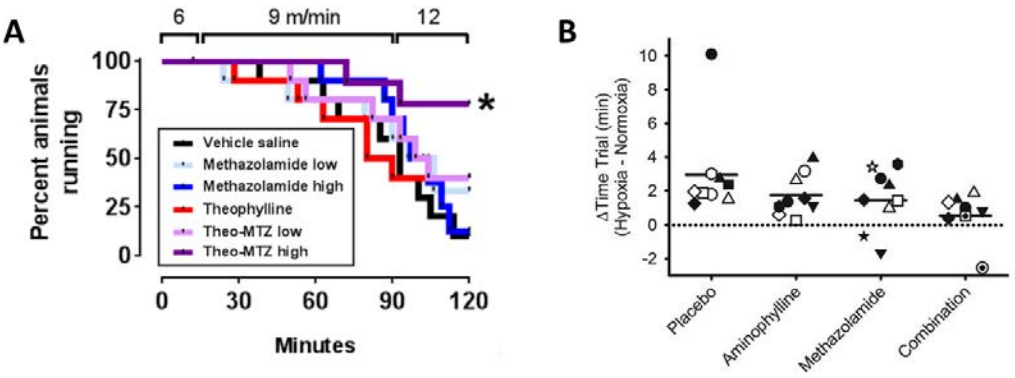

Figure 7: Combined theophylline and methazolamide improve hypoxic hypobaric performance in rats and humans. A: Rats were subjected to running in a forced exercise wheel under simulated high altitude of 4268m (14,000 ft), after receiving the study drugs i.p. Theophylline was 15 mg/kg, Methazolamide (MTZ) low/ dose was 3.5/ 7 mg/kg. Rats dosed with combined theophylline and high-dose MTZ ran significantly longer than animals that received vehicle (log rank test, $p<0.05$) (Schroeder et al, unpublished). B: In humans, the combined drugs decreased the performance decrement induced by normobaric environmental hypoxia (15% O_2), compared to placebo (two-way ANOVA with Bonferroni correction, $p=0.01$) [20].

We proceeded to test these drugs in humans: After confirming initial safety of the drug combination of aminophylline and methazolamide, we performed a placebo-controlled, randomized two-period human normoxic-hypoxic time trial. During the first period, subjects underwent a normoxic (FiO_2, i.e. inspired O_2 concentration, 21%) time trial, where subjects received the masked study drug (placebo, methazolamide 250mg, aminophylline 400mg, or the combination of the latter two) and 4:30 hours after dosing, they were subjected to an exercise trial: study subjects commenced cycling on a stationary cycle ergometer, with resistance set to a moderate 100W, for 30 minutes. After a brief 5-minute break, subjects were then asked to cycle an equivalent of 12.5 km as quickly as possible. The same trial was then repeated, only at a FiO_2 of 15%. Time trials were significantly slower in all groups under hypoxia, compared to normoxia, except with the drug combination aminophylline-methazolamide, and the hypoxia-induced decrement in the combination group was significantly less than in the placebo group (Figure 7B). Both methazolamide- and combination treated subjects had significantly higher hemoglobin concentrations under hypoxia than the placebo group [20].

Methazolamide is, in several aspects, similar to acetazolamide, which is also a carbonic anhydrase inhibitor, and a common prophylaxis against high altitude sickness. Acetazolamide prevents the excretion of hydronium ions and thus pre-empts alkalosis following increased ventilation at high altitude. Hypothetically, this leads to an augmented tolerance toward increased ventilation, leading to higher oxygen loading of the blood. However, the efficacy of acetazolamide to improve health and increase endurance at high altitude is debated [232]. Our data suggests that carboanhydrase inhibitors such as methazolamide and acetazolamide might be more efficient in combination with other drugs than as alone standing agents.

5.2 Mapping and characterization of the metabolic microenvironment in solid tumors

I have produced direct knowledge about the actual distribution of the key metabolites lactate, glucose, and oxygen in solid tumors. Figure 3 represents the general assumption of how metabolite concentrations in experimental and human clinical tumors are distributed, in relation to blood vessels [123, 131]. Using experimental rat mammary adenocarcinoma (R3230Ac) and fibrosarcoma (FSA), I have, on one hand, experimentally confirmed this basic assumption, with glucose decreasing toward chronic hypoxic regions, lactate increasing toward them, and hypoxia being the most severe at the edge of necrosis [130] (Figure 8A). However, multiple additional lessons were learned from this

descriptive study: first, lactate and glucose gradients corresponded relatively well with the concentration of these metabolites in the blood of the animals (Figure 8B). But, fibrosarcomas produced a surprising phenotype, as large areas of the tumor were apparently void of free glucose, indicating a very high rate of demand vs. supply and indicating a high resilience of these cells toward glucose starvation. Superimposed H&E histology, as well as the pattern for the exogenous hypoxia marker EF5, the uptake of which is a dynamic and hard indicator of cell viability, showed that these regions of the tumor were nonetheless viable (Figure 8A).

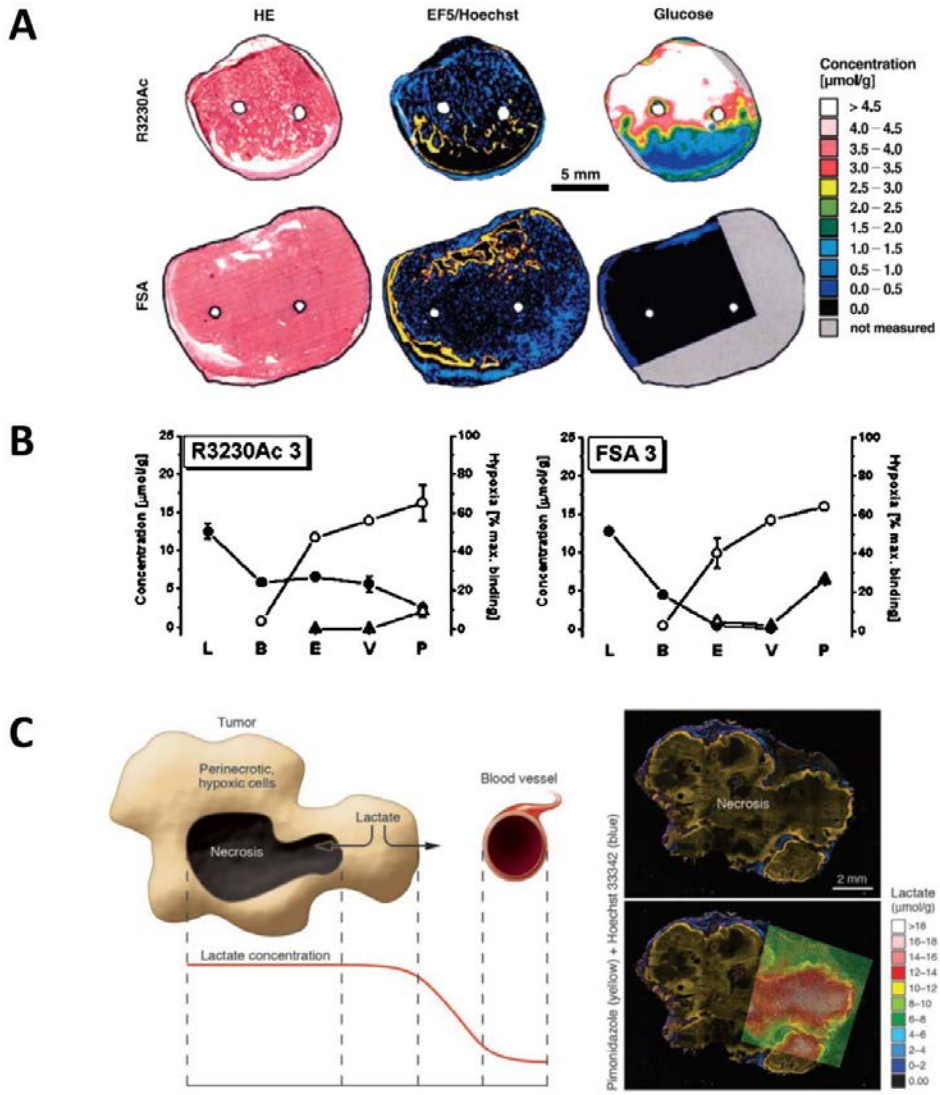

Figure 8: Distribution of chronic hypoxia (EF5, yellow), glucose, and lactate in solid tumors grown in the flank of rats and mice. A: Histological frozen sections of R3230 mammary rat adenocarcinoma and FSA rat fibrosarcoma, grown in the flank of rats, and injected pre-sacrifice with the hypoxia marker EF5 and the perfusion marker Hoechst 33342. Subsequent sections were processed for general histology (H&E), EF5/CD31 immunostaining (blood vessels and hypoxia), glucose and lactate bioluminescence enzymatic assay. B: glucose and lactate gradients in the liver (L), blood (B), tumor edge (E), viable tumor (V), and necrotic edge (P) of the animals were analyzed and plotted [130]. C: Histological sections stained for lactate, superimposed on a parallel section stained for EF5/Hoechst 33342 [132].

We have proceeded to investigate the lactate concentration in tumor necrosis, which was predicted to reach a maximum in this area, because of lack of clearance of lactate out of the necrotic basin, in combination with the "Pasteur reaction", which is the increase of glycolytic energy metabolism and lactate production of tumor cells in response to hypoxia or anoxia [138] (Figure 8C). This is important, because high extracellular lactate causes reductive stress, if combined with hypoxia or anoxia, and low

or absent glucose [233]. Based on our data, it may be hypothesized that the exceeding lactate concentration in perinecrotic cancer cells is the dominant factor causing cancer necrosis, as it forces the consumption of residual oxygen for its clearance via oxidative phosphorylation, thus causing anoxia, which is not well tolerated by many cancer cells, especially when they do not have access to glucose [138].

I am currently completing a descriptive study on metabolite concentrations in human tumors. Initial evaluations indicate that human tumors show a spatial association between hypoxia, low glucose, and high lactate. In analogy to what I observed in rat tumors, I found that some of these tumors have large areas where free glucose is virtually absent, where staining for the exogenous hypoxia marker EF5 again confirmed both the presence of hypoxia and the viability of the cancer cells (Figure 9).

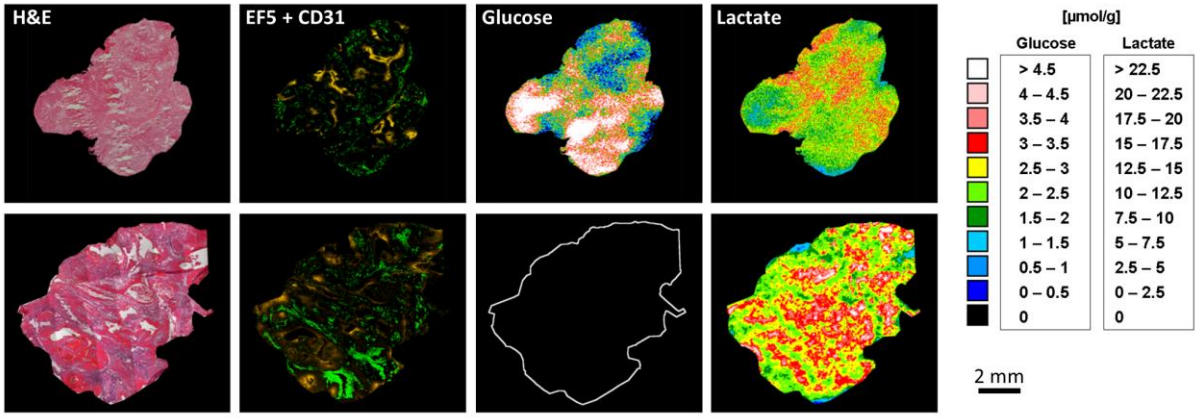

Figure 9: General histology (hematoxylin-eosin, H&E) and the distribution of chronic hypoxia (EF5, orange), blood vessels (CD31, green), glucose, and lactate, in co-registered images from serial frozen biopsy sections of human squamous cell carcinomas of the head and neck region (HNSCC). (Schroeder et al, in preparation).

In summary, these data has on one hand confirmed the current concept of metabolite distribution in solid tumors, using direct measurements. However, I have found direct evidence in both animal and human tumors that in particular the concentration of free glucose can vary considerably, even declining to zero in the viable, non-hypoxic tumor. Importantly, I have produced evidence that the necrotic cavity is filled with lactate, which accumulates largely because there is no route of clearance. Because lactate is a reductive cytotoxin, this discovery could be important, as this extremely high lactate concentration might provide a “synthetic lethal”, i.e. a combination of synergistically acting, cytotoxic factors that selectively kill chronic hypoxic tumor cells.

5.3 Discovery of lactate consumption in solid tumors

In 2008, our research team reported that cancer cells with the ability of oxidative metabolism can take up and utilize lactate as an energy substrate. In the live tumor, this can lead to a metabolic symbiont, where cells adjacent to the blood stream that have access to oxygen oxidize and metabolize lactate, thereby letting through glucose. Cells that are distant from blood vessels that are hypoxic would then use glucose for anaerobic glycolysis. This symbiont can be disabled by inhibiting lactate transport, using the monocarboxylate transport blocker α-cyano-4-hydroxycinnamate, leading to core necrosis and radiosensitization of these tumors [234] (Figure 10).

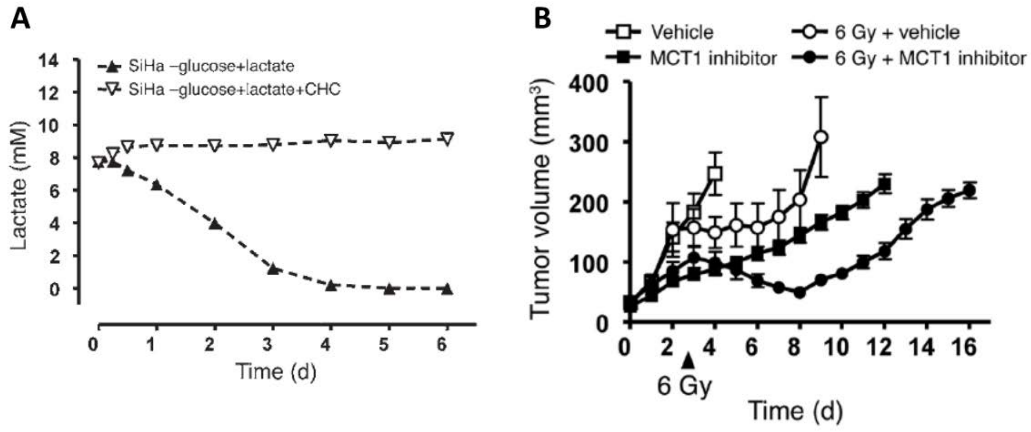

Figure 10: Lactate consumption in cancer cells. A: SiHa human uterine cervical carcinoma cells can reduce lactate concentrations in the medium. This phenotype can be inhibited by blocking lactate transporters via α-cyano-4-hydroxycinnamate (CHC). B: Applied in flank-tumor-bearing mice, CHC slows down tumor growth and delays re-growth after radiation therapy [234]

Following this discovery, we have investigated the fate of exogenous lactate when applied to tumor cells. Lactate is transported passively into the cancer cell in a concentration-dependent manner (Figure 11A), which is consistent with the concept of a passive proton co-transport, as we have reported before [234]. Because lactate is subsequently converted into pyruvate via the lactate dehydrogenase (LDH) reaction, it immediately increases the reduction potential in the cell by scavenging NAD^+ (Figure 11B). Because lactate enters the cell together with a proton via the MCT-1, MCT-4, or similar proton co-transporter, it arrives in the cytoplasm as an acid, thus reducing cytoplasmic pH (Figure 11C). Exogenous lactate also inhibits glycolysis in a concentration-dependent fashion (Figure 11D). Lactate induces its own clearance via oxidative phosphorylation (Figure 11E). In many cancer and normal cell lines, lactate is partially catabolized into alanine and glutamate, and other yet unidentified catabolites, which are then extruded from the cell (Figure 11F, G). Mechanisms exist that restrict lactate entry into the cell after continued exposure to high external lactate concentrations (Figure 11F). The lactate/pyruvate transport inhibitor α-cyano-4-hydroxycinnamate (CHC) inhibits the formation/extrusion of glutamate and alanine in R3230 cells (Figure 11G). α-cyano-4-hydroxycinnamate (CHC) also reduces cell viability in FaDu head and neck carcinoma cells specifically under glucose starvation, hypoxia, and high lactate, in a concentration-dependent fashion, whereas in R3230 cells, there is a general sensitivity of the cells to low glucose that is unaffected by CHC (Figure 11H).

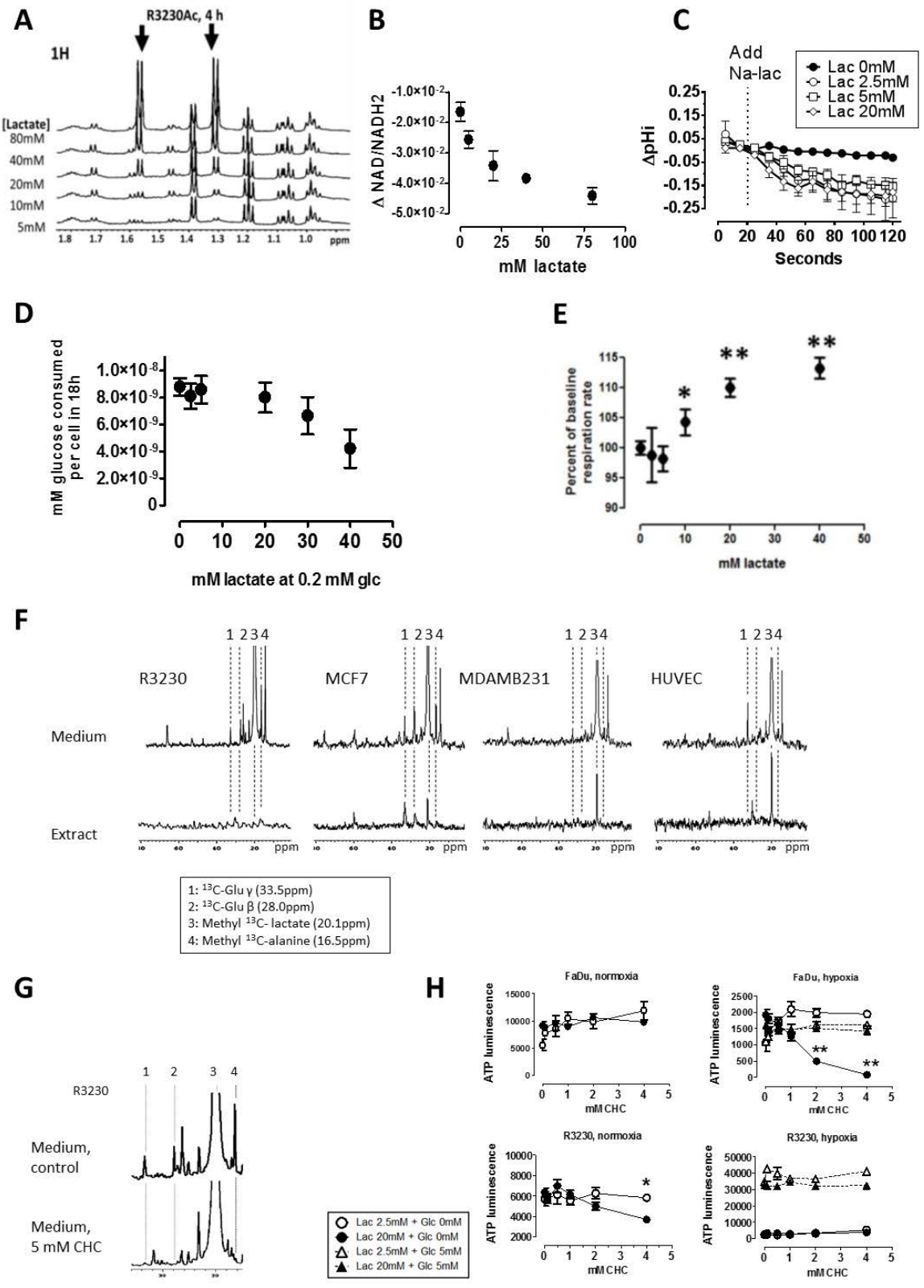

Figure 11: Processing of external lactate in normal and cancerous cells. A: exogenous lactate enters the cell in a concentration-dependent matter, seen by enrichment of ^{13}C-lactate in the cell extract. B: Inside of the cell, lactate scavenges NAD$^+$ in a concentration-dependent manner. Measured by 280 vs. 340 nm ratios in R3230 cells in suspension in a temperature-stabilized cuvette. C: Exogenous Na-lactate reduces intracellular pH upon entry, consistent with the concept of a proton-coupled co-transport. Method: Fluorescence Microscopy of R3230 cells grown on cover slides, treated with BCECF pH dye. D: lactate inhibits glycolysis in a concentration-dependent manner. Changes in glucose concentration were measured over 18 hours in serum-free DMEM medium with controlled lactate concentrations, at 21% O_2. Glucose concentrations were normalized to the number of cells counted. E: Oxygen consumption rate with increasing

concentrations of lactate, measured with a Seahorse™ oxygen consumption analyzer. F: Medium and cell extract ^{13}C NMR profiles 24 hours after addition of 40 mM ^{13}C-labeled Na-lactate to the medium. Note that lactate and its catabolites are partially or full cleared from the intracellular space, and/or prevented from entering the cell. Cells are the rat mammary carcinoma cell line R3230, the human mammary carcinoma cell lines MCF-7 and MDAMB231, and human umbilical vein endothelial cells HUVEC. G: ^{13}C NMR profile of medium with 40 mM ^{13}C Na-lactate, with or without α-cyano-4-hydroxycinnamate present. H: FaDu human head and neck cancer cells and rat R3230 mammary adenocarcinoma cells, incubated under high and low/no concentrations of Na-lactate and glucose, in hypoxia or normoxia for 18 hours, under different concentrations of α-cyano-4-hydroxycinnamate, followed by ATP quantification using a bioluminescent kit. Panels A, E, F, G are taken from Kennedy et al [233], the others are unpublished data from the author.

5.4 New method of imaging and quantification of the microcirculation in the healthy and cancerous rat lung

As has been highlighted in section 2.3., the lung is a major target site of hypoxemic microcirculatory dysregulation, which in turn affects the rest of the body, because it controls hemodynamic throughput and hemoglobin oxygen loading. However, because the lung is in constant motion, there are only few methods to follow microcirculatory processes, such as capillary blood flow, or vasoconstriction and vasodilatation, in a dynamic fashion and on a microscopic level. We have developed a novel method of intravital microscopy for this purpose, consisting of a surgically inserted window on a socket that attaches directly to the pulmonary pleura of an anesthetized rat, thus permitting the production of micrographic films through the lens of a microscope of the pulmonary circulation. The movement through breathing and heart beat were reduced by restricting vertical motility. Ventilator-controlled breathing using positive airway pressure helped to further restrict movement (Figure 12A). Third, a computer annotation algorithm was produced to re-align subsequent images in a stack that were affected by motion. Last, we developed a Matlab-based algorithm to automatically quantify microcirculatory blood flow, by the help of fluorescently labeled, re-injected red blood cells [235, 236] (Figure 12B). We proceeded to use this method for the quantification of blood flow in experimental pulmonary cancer metastases in rats, which included the demonstration that we are able to increase blood flow in these metastases using a mixture of a hypertensive drug and an endothelin receptor antagonist [194] (Figure 12C).

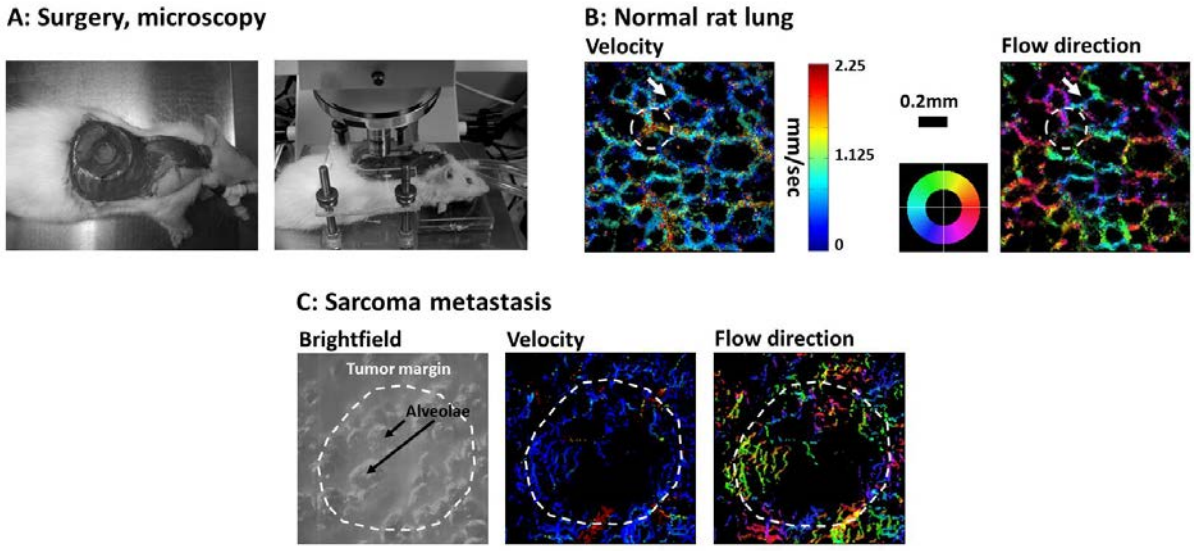

Figure 12: Pulmonary window surgery for blood flow mapping of normal lung and pulmonary metastasis, using pulmonary intravital microscopy. C: Virally induced mouse sarcoma cells were injected i.v. at 1x10^6 into the tail vein, and approximately 4 weeks later, the animal was subjected to surgery and acute microscopy. Tumor was clearly visible by GFP labeling and white color (vs. pink in non-tumorous lung, not shown). A-B from Hanna et al [236], C: Blueschke et al [194]

6 Future directions

6.1 Development of an effective combination drug therapy against solid primary and metastatic cancer

As outlined in section 4.3.3., chemotherapeutic therapy desperately lacks efficacy, extending patient lives for only weeks or months. One of the reasons for this failure is that contemporary treatment relies heavily on the targeting of proliferating, growing, normoxic cells, whereas non-proliferating, nutrient-starved, hypoxic cells are predominantly neglected as therapeutic targets, although there is solid evidence that these latter cells might be largely responsible for chemotherapeutic failure and tumor regrowth. However, quiescent cells are difficult to reach by blood-born treatments, because drugs only diffuse out some 100-500 µm from the active tumor blood vessel [147]. Hypoxic cytotoxins are a drug class that is able to kill off these cells, if the drug is able to reach the hypoxic target cells at pharmaceutically relevant concentrations. Induction of arterial hypertension by Angiotensin II, as outlined in section 3.3.4., bears potential to increase the relative concentration of chemotherapeutic drugs in the tumor, but has worrying side effects. Our research suggests that sympathomimetic drugs might be equally useful as Angiotensin II in increasing the drug exposure of the tumor, but with less cancer-promoting side effects. Moreover, as has been explained in section 4, there is overwhelming evidence that the addition of endothelin-blocking vasodilators will critically increase drug delivery to the tumor, very similar to what we have seen in the hypoxic skeletal muscle [22].

Based on these considerations, a therapeutic regimen could therefore be designed to contain three essential components: (1) a conventional cycotoxic compound (or radiation therapy) to target actively dividing and growing cells, (2) a hypoxic or reductive cytotoxin to kill off non-dividing, hypoxic cells, and (3) a compound that enhances tumor perfusion, to ensure the hypoxic cytotoxin is delivered to its target cell population at sufficient concentration. In summary, I propose to address critical weaknesses of contemporary cancer drug treatment, with the aim to make intravenous cancer chemotherapy available as a curative tool.

6.2 Development of anti-hypoxemic treatments

With our pre-clinical and clinical testing ranges, we have created a solid foundation of multiple treatments that will improve health and body function of hypoxemic individuals that we intend to expand on.

Skeletal muscle: Although there is ample evidence that hypoxemia affects skeletal muscle microcirculation, no direct evidence exists yet showing exactly how this occurs. We will employ intravital microscopy of skeletal muscle microvascular beds in rats to clarify how hypoxemia affects capillary blood flow and what the specific role of endothelin type A and type B receptors play in this. In turn, this knowledge will serve to design specific treatments to reduce hypoxemic perturbation to skeletal muscle blood flow.

Pulmonary microcirculation: my collaborating research team and I have recently found that pulmonary vasoactive substances are effective even when applied over the airways. This is remarkable, because they enter the blood on the capillary level and will either have to work their way “upstream” to exert their pharmacological effect on the arteriolar level, or alternatively, deliver their main therapeutic impact via pulmonary pericytes. I will further examine this phenomenon and design treatments based on this discovery. I am also currently pursuing the development of drug-encapsulating fluorocarbon amphiphile nanoshells, which will enable the dissolution of our drugs in

hydrofluoroalkane (HFA) type propellants, which are the drug solvents of choice in pressured metered dose inhalers (pMDI).

6.3 Development of novel intravital microscopy methods to image and quantify tumor and tissue microcirculation

Several questions raised earlier require methods to directly visualize the microcirculation in a dynamic fashion.

Long-term tumor imaging window in rats and mice: I am currently establishing a method to repeatedly visualize the microcirculation of tumors grown in the subcutaneous skin of rats and mice in long-term, longitudinal experiments. The tumor is grown in a flap of the dorsal skin that is prepared in a way that allows the repeated opening and closing of the wound, to allow repeated microscopic observation over long periods of time. Such a visualization technique will permit to obtain direct information about the reaction of the tumor vasculature to vasoactive intervention in different stages of its growth. Also, apart from permanently implanted windows, which are seriously flawed by surgical artifacts, there is no method yet that permits visualization of the microcirculation of experimental tumors.

Skeletal muscle window: I am preparing a surgical window of the rat trapezius muscle, to permit the visualization and dynamic quantification of the skeletal muscle microcirculation. This is pivotal in answering above-mentioned key questions about endothelin- and beta-adrenergic regulation of capillary blood flow in connection to hypoxemia. The surgical procedure is based on previously established techniques.

In summary, multiple assays are being developed to allow the study of the normal tissue and tumor microcirculation on the microscopic level in animal models, with the ultimate goal to identify better treatments to improve oxygen and drug delivery to parenchymatic tissue.

6.4 Drug development effort to target the perinecrotic tumor fraction

My research has revealed that the perinecrotic tumor cell fraction in solid tumors is characterized by the combination of hypoxia or anoxia, high lactate, and low to no glucose. These cells are known to be largely responsible for the resistance to radio- and chemotherapy. The lactate transport inhibitor α-cyano-4-hydroxycinnamate has potential to specifically target cancer cells in this environment, but has limited ability as an anticancer drug. However, the newly identified lactate catabolism is a pleiotropic phenomenon, where multiple protein targets, e.g. membrane transporters of alanine and glutamate, are potentially targetable through drugs. In order to screen larger substance databases for pharmacologically active transport inhibitors etc., a screening assay needs to be developed that can be standardized for high-throughput drug screening. This assay needs to include the parameters hypoxia, lactate concentration, glucose concentration, and cell quiescence, with the readout being the ability of the tumor cell to re-grow after therapy, i.e. clonogenic survival.

The tumor lactate catabolism is also far from being fully characterized. I will pursue further mechanistic research to identify (1) additional catabolic targets of lactate, which were already visible as additional peaks, (2) the effect of cell quiescence on lactate transport across the membrane and on its clearance, (3) cellular compartments and protein targets that are critical for the observed phenotype and (4) the variability of cancer and normal cell types in their response to extracellular lactate.

7 Literature

1. Zander R. The oxygen status of arterial human blood. Scandinavian journal of clinical and laboratory investigation Supplementum 1990; 203: 187-96.
2. Jiang J, Nakashima T, Liu KJ, Goda F, Shima T, Swartz HM. Measurement of PO2 in liver using EPR oximetry. Journal of applied physiology 1996; 80: 552-8.
3. Rosenzweig I, Glasser M, Polsek D, Leschziner GD, Williams SC, Morrell MJ. Sleep apnoea and the brain: a complex relationship. The Lancet Respiratory medicine 2015; 3: 404-14.
4. Wilson MH, Newman S, Imray CH. The cerebral effects of ascent to high altitudes. The Lancet Neurology 2009; 8: 175-91.
5. Maggiorini M. Prevention and treatment of high-altitude pulmonary edema. Progress in cardiovascular diseases 2010; 52: 500-6.
6. Christensen NJ, Galbo H. Sympathetic nervous activity during exercise. Annual review of physiology 1983; 45: 139-53.
7. Dietrich HH. Effect of locally applied epinephrine and norepinephrine on blood flow and diameter in capillaries of rat mesentery. Microvascular research 1989; 38: 125-35.
8. Guyenet PG. The sympathetic control of blood pressure. Nature reviews Neuroscience 2006; 7: 335-46.
9. Goerre S, Wenk M, Bartsch P, Luscher TF, Niroomand F, Hohenhaus E, Oelz O, Reinhart WH. Endothelin-1 in pulmonary hypertension associated with high-altitude exposure. Circulation 1995; 91: 359-64.
10. Scherrer U, Rexhaj E, Jayet PY, Allemann Y, Sartori C. New insights in the pathogenesis of high-altitude pulmonary edema. Progress in cardiovascular diseases 2010; 52: 485-92.
11. Bartsch P, Gibbs JS. Effect of altitude on the heart and the lungs. Circulation 2007; 116: 2191-202.
12. Rademaker K, Hodgins G, Moore K, Zarrillo S, Miller C, Bromley GR, Leach P, Reid DA, Alvarez WY, Sandweiss DH. Paleoindian settlement of the high-altitude Peruvian Andes. Science 2014; 346: 466-9.
13. Penaloza D, Arias-Stella J. The heart and pulmonary circulation at high altitudes: healthy highlanders and chronic mountain sickness. Circulation 2007; 115: 1132-46.
14. Robinson BR, Cotton BA, Pritts TA, Branson R, Holcomb JB, Muskat P, Fox EE, Wade CE, del Junco DJ, Bulger EM, Cohen MJ, Schreiber MA, Myers JG, Brasel KJ, Phelan HA, Alarcon LH, Rahbar MH, Callcut RA, group Ps. Application of the Berlin definition in PROMMTT patients: the impact of resuscitation on the incidence of hypoxemia. The journal of trauma and acute care surgery 2013; 75: S61-7.
15. Saclarides TJ, Myers JA, Millikan KW, Springer (Firm). Common surgical diseases : an algorithmic approach to problem solving. Third Edition. Editon.
16. Donahoe M. Acute respiratory distress syndrome: A clinical review. Pulmonary circulation 2011; 1: 192-211.
17. Naeije R, Huez S, Lamotte M, Retailleau K, Neupane S, Abramowicz D, Faoro V. Pulmonary artery pressure limits exercise capacity at high altitude. The European respiratory journal 2010; 36: 1049-55.
18. Olfert IM, Loeckinger A, Treml B, Faulhaber M, Flatz M, Burtscher M, Truebsbach S, Kleinsasser A. Sildenafil and bosentan improve arterial oxygenation during acute hypoxic exercise: a controlled laboratory trial. Wilderness & environmental medicine 2011; 22: 211-21.
19. Pitsiou GG, Chavouzis N, Nakou C, Boutou AK, Argyropoulou P, Stanopoulos I. Successful up-front combination therapy in a patient with idiopathic pulmonary hypertension and patent foramen ovale: an alternative to epoprostenol therapy? The Journal of heart and lung transplantation : the official publication of the International Society for Heart Transplantation 2009; 28: 651-3.
20. Scalzo RL, Binns SE, Klochak AL, Giordano GR, Paris HL, Sevits KJ, Beals JW, Biela LM, Larson DG, Luckasen GJ, Irwin D, Schroeder T, Hamilton KL, Bell C. Methazolamide Plus Aminophylline Abrogates

Hypoxia-Mediated Endurance Exercise Impairment. High altitude medicine & biology 2015; 16: 331-42.
21. Radiloff DR, Zhao Y, Boico A, Wu C, Shan S, Palmer G, Hamilton K, Irwin D, Hanna G, Piantadosi CA, Schroeder T. The combination of theophylline and endothelin receptor antagonism improves exercise performance of rats under simulated high altitude. Journal of applied physiology 2012; 113: 1243-52.
22. Radiloff D, Zhao Y, Boico A, Blueschke G, Palmer G, Fontanella A, Dewhirst M, Piantadosi CA, Noveck R, Irwin D, Hamilton K, Klitzman B, Schroeder T. Anti-hypotensive treatment and endothelin blockade synergistically antagonize exercise fatigue in rats under simulated high altitude. PloS one 2014; 9: e99309.
23. Korthuis RJ. In: Skeletal Muscle Circulation, San Rafael (CA), 2011.
24. Martin DS, Cobb A, Meale P, Mitchell K, Edsell M, Mythen MG, Grocott MP, Xtreme Alps Research G. Systemic oxygen extraction during exercise at high altitude. British journal of anaesthesia 2015; 114: 677-82.
25. Lawley JS, Alperin N, Bagci AM, Lee SH, Mullins PG, Oliver SJ, Macdonald JH. Normobaric hypoxia and symptoms of acute mountain sickness: Elevated brain volume and intracranial hypertension. Annals of neurology 2014; 75: 890-8.
26. Goldfarb-Rumyantzev AS, Alper SL. Short-term responses of the kidney to high altitude in mountain climbers. Nephrology, dialysis, transplantation : official publication of the European Dialysis and Transplant Association - European Renal Association 2014; 29: 497-506.
27. Klabunde RE. Cardiovascular physiology concepts. 2nd Editon. Philadelphia, PA: Lippincott Williams & Wilkins/Wolters Kluwer, 2012.
28. Neuhaus AA, Couch Y, Sutherland BA, Buchan AM. Novel method to study pericyte contractility and responses to ischaemia in vitro using electrical impedance. Journal of cerebral blood flow and metabolism : official journal of the International Society of Cerebral Blood Flow and Metabolism 2016.
29. Mitchell D, Bihari A, Sandig M, Tyml K. Endothelin-a receptor in rat skeletal muscle microvasculature. Microvascular research 2002; 64: 179-85.
30. Lash JM. Contribution of arterial feed vessels to skeletal muscle functional hyperemia. Journal of applied physiology 1994; 76: 1512-9.
31. Zheng C, Liu Z. Vascular function, insulin action, and exercise: an intricate interplay. Trends in endocrinology and metabolism: TEM 2015; 26: 297-304.
32. Bergers G, Song S. The role of pericytes in blood-vessel formation and maintenance. Neuro-oncology 2005; 7: 452-64.
33. Birbrair A, Zhang T, Wang ZM, Messi ML, Enikolopov GN, Mintz A, Delbono O. Role of pericytes in skeletal muscle regeneration and fat accumulation. Stem cells and development 2013; 22: 2298-314.
34. Borysova L, Wray S, Eisner DA, Burdyga T. How calcium signals in myocytes and pericytes are integrated across in situ microvascular networks and control microvascular tone. Cell calcium 2013; 54: 163-74.
35. Hall CN, Reynell C, Gesslein B, Hamilton NB, Mishra A, Sutherland BA, O'Farrell FM, Buchan AM, Lauritzen M, Attwell D. Capillary pericytes regulate cerebral blood flow in health and disease. Nature 2014; 508: 55-60.
36. Speyer CL, Steffes CP, Ram JL. Effects of vasoactive mediators on the rat lung pericyte: quantitative analysis of contraction on collagen lattice matrices. Microvascular research 1999; 57: 134-43.
37. Segal SS. Integration of blood flow control to skeletal muscle: key role of feed arteries. Acta physiologica Scandinavica 2000; 168: 511-8.
38. Segal SS, Welsh DG, Kurjiaka DT. Spread of vasodilatation and vasoconstriction along feed arteries and arterioles of hamster skeletal muscle. The Journal of physiology 1999; 516 (Pt 1): 283-91.
39. Bentzer P, Kongstad L, Grande PO. Capillary filtration coefficient is independent of number of perfused capillaries in cat skeletal muscle. American journal of physiology Heart and circulatory physiology 2001; 280: H2697-706.

40. Murray IR, Baily JE, Chen WC, Dar A, Gonzalez ZN, Jensen AR, Petrigliano FA, Deb A, Henderson NC. Skeletal and cardiac muscle pericytes: Functions and therapeutic potential. Pharmacology & therapeutics 2016.
41. Dou D, Zheng X, Ying L, Ye L, Gao Y. Sulfhydryl-dependent dimerization and cGMP-mediated vasodilatation. Journal of cardiovascular pharmacology 2013; 62: 1-5.
42. Blitzer ML, Lee SD, Creager MA. Endothelium-derived nitric oxide mediates hypoxic vasodilation of resistance vessels in humans. The American journal of physiology 1996; 271: H1182-5.
43. Crecelius AR, Kirby BS, Voyles WF, Dinenno FA. Augmented skeletal muscle hyperaemia during hypoxic exercise in humans is blunted by combined inhibition of nitric oxide and vasodilating prostaglandins. The Journal of physiology 2011; 589: 3671-83.
44. Gilligan DM, Panza JA, Kilcoyne CM, Waclawiw MA, Casino PR, Quyyumi AA. Contribution of endothelium-derived nitric oxide to exercise-induced vasodilation. Circulation 1994; 90: 2853-8.
45. Norel X. Prostanoid receptors in the human vascular wall. TheScientificWorldJournal 2007; 7: 1359-74.
46. Lopez Bernal A. Mechanisms of labour--biochemical aspects. BJOG : an international journal of obstetrics and gynaecology 2003; 110 Suppl 20: 39-45.
47. Silver PJ. Regulation of contractile activity in vascular smooth muscle by protein kinases. Reviews in clinical & basic pharmacology 1985; 5: 341-95.
48. Simmons DL, Botting RM, Hla T. Cyclooxygenase isozymes: the biology of prostaglandin synthesis and inhibition. Pharmacological reviews 2004; 56: 387-437.
49. Dinenno FA. Skeletal muscle vasodilation during systemic hypoxia in humans. Journal of applied physiology 2016; 120: 216-25.
50. Marshall JM. Adenosine and muscle vasodilatation in acute systemic hypoxia. Acta physiologica Scandinavica 2000; 168: 561-73.
51. Sikora J, Orlov SN, Furuya K, Grygorczyk R. Hemolysis is a primary ATP-release mechanism in human erythrocytes. Blood 2014; 124: 2150-7.
52. Diesen DL, Hess DT, Stamler JS. Hypoxic vasodilation by red blood cells: evidence for an s-nitrosothiol-based signal. Circulation research 2008; 103: 545-53.
53. Kunduri SS, Mustafa SJ, Ponnoth DS, Dick GM, Nayeem MA. Adenosine A1 receptors link to smooth muscle contraction via CYP4a, protein kinase C-alpha, and ERK1/2. Journal of cardiovascular pharmacology 2013; 62: 78-83.
54. Li JM, Fenton RA, Cutler BS, Dobson JG, Jr. Adenosine enhances nitric oxide production by vascular endothelial cells. The American journal of physiology 1995; 269: C519-23.
55. Casey DP, Joyner MJ. Local control of skeletal muscle blood flow during exercise: influence of available oxygen. Journal of applied physiology 2011; 111: 1527-38.
56. MacLean DA, Sinoway LI, Leuenberger U. Systemic hypoxia elevates skeletal muscle interstitial adenosine levels in humans. Circulation 1998; 98: 1990-2.
57. Davenport AP, Maguire JJ. Endothelin. Handbook of experimental pharmacology 2006: 295-329.
58. Wynne BM, Chiao CW, Webb RC. Vascular Smooth Muscle Cell Signaling Mechanisms for Contraction to Angiotensin II and Endothelin-1. Journal of the American Society of Hypertension : JASH 2009; 3: 84-95.
59. Mazzuca MQ, Khalil RA. Vascular endothelin receptor type B: structure, function and dysregulation in vascular disease. Biochemical pharmacology 2012; 84: 147-62.
60. Lougee L, Hinojosa-Laborde C, Harder DR, Lombard JH. Effect of nifedipine on endothelin induced contractions of skeletal muscle arterioles of spontaneously hypertensive rats. Microcirculation, endothelium, and lymphatics 1990; 6: 355-68.
61. Toribatake Y, Tomita K, Kawahara N, Baba H, Ohnari H, Tanaka S. Regulation of vasomotion of arterioles and capillaries in the cat spinal cord: role of alpha actin and endothelin-1. Spinal cord 1997; 35: 26-32.
62. Galie N, Manes A, Branzi A. The endothelin system in pulmonary arterial hypertension. Cardiovascular research 2004; 61: 227-37.

63. Modesti PA, Vanni S, Morabito M, Modesti A, Marchetta M, Gamberi T, Sofi F, Savia G, Mancia G, Gensini GF, Parati G. Role of endothelin-1 in exposure to high altitude: Acute Mountain Sickness and Endothelin-1 (ACME-1) study. Circulation 2006; 114: 1410-6.
64. Peacock AJ, Zamboni W, Vizza CD. Ambrisentan for the treatment of adults with pulmonary arterial hypertension: a review. Current medical research and opinion 2015; 31: 1793-807.
65. McDonald FB, Skelly JR, O'Halloran KD. The beta2 -adrenoceptor agonist terbutaline recovers rat pharyngeal dilator muscle force decline during severe hypoxia. Oral diseases 2015; 21: e121-7.
66. Kanaide H, Ichiki T, Nishimura J, Hirano K. Cellular mechanism of vasoconstriction induced by angiotensin II: it remains to be determined. Circulation research 2003; 93: 1015-7.
67. Li Q, Puro DG. Adenosine activates ATP-sensitive K(+) currents in pericytes of rat retinal microvessels: role of A1 and A2a receptors. Brain research 2001; 907: 93-9.
68. Gordan R, Gwathmey JK, Xie LH. Autonomic and endocrine control of cardiovascular function. World journal of cardiology 2015; 7: 204-14.
69. McGillivray-Anderson KM, Faber JE. Effect of reduced blood flow on alpha 1- and alpha 2-adrenoceptor constriction of rat skeletal muscle microvessels. Circulation research 1991; 69: 165-73.
70. Martin EA, Nicholson WT, Eisenach JH, Charkoudian N, Joyner MJ. Influences of adenosine receptor antagonism on vasodilator responses to adenosine and exercise in adenosine responders and nonresponders. Journal of applied physiology 2006; 101: 1678-84.
71. Cargill RI, Kiely DG, Clark RA, Lipworth BJ. Hypoxaemia and release of endothelin-1. Thorax 1995; 50: 1308-10.
72. Joyner MJ, Casey DP. Muscle blood flow, hypoxia, and hypoperfusion. Journal of applied physiology 2014; 116: 852-7.
73. Murrant CL, Sarelius IH. Coupling of muscle metabolism and muscle blood flow in capillary units during contraction. Acta physiologica Scandinavica 2000; 168: 531-41.
74. Crawford C, Wildman SS, Kelly MC, Kennedy-Lydon TM, Peppiatt-Wildman CM. Sympathetic nerve-derived ATP regulates renal medullary vasa recta diameter via pericyte cells: a role for regulating medullary blood flow? Frontiers in physiology 2013; 4: 307.
75. Lombard JH. A novel mechanism for regulation of retinal blood flow by lactate: gap junctions, hypoxia, and pericytes. American journal of physiology Heart and circulatory physiology 2006; 290: H921-2.
76. Yamanishi S, Katsumura K, Kobayashi T, Puro DG. Extracellular lactate as a dynamic vasoactive signal in the rat retinal microvasculature. American journal of physiology Heart and circulatory physiology 2006; 290: H925-34.
77. Earley S, Brayden JE. Transient receptor potential channels and vascular function. Clinical science 2010; 119: 19-36.
78. Patel A, Sharif-Naeini R, Folgering JR, Bichet D, Duprat F, Honore E. Canonical TRP channels and mechanotransduction: from physiology to disease states. Pflugers Archiv : European journal of physiology 2010; 460: 571-81.
79. Matrougui K, Levy BI, Henrion D. Tissue angiotensin II and endothelin-1 modulate differently the response to flow in mesenteric resistance arteries of normotensive and spontaneously hypertensive rats. British journal of pharmacology 2000; 130: 521-6.
80. Petersen HH, Choy J, Stauffer B, Moien-Afshari F, Aalkjaer C, Leinwand L, McManus BM, Laher I. Coronary artery myogenic response in a genetic model of hypertrophic cardiomyopathy. American journal of physiology Heart and circulatory physiology 2002; 283: H2244-9.
81. Marshall JM. Interactions between local dilator and sympathetic vasoconstrictor influences in skeletal muscle in acute and chronic hypoxia. Experimental physiology 2015; 100: 1400-11.
82. Markwald RR, Kirby BS, Crecelius AR, Carlson RE, Voyles WF, Dinenno FA. Combined inhibition of nitric oxide and vasodilating prostaglandins abolishes forearm vasodilatation to systemic hypoxia in healthy humans. The Journal of physiology 2011; 589: 1979-90.
83. Barrett-O'Keefe Z, Ives SJ, Trinity JD, Morgan G, Rossman MJ, Donato AJ, Runnels S, Morgan DE, Gmelch BS, Bledsoe AD, Richardson RS, Wray DW. Taming the "sleeping giant": the role of

endothelin-1 in the regulation of skeletal muscle blood flow and arterial blood pressure during exercise. American journal of physiology Heart and circulatory physiology 2013; 304: H162-9.
84. Jia Y, Li P, Dziennis S, Wang RK. Responses of peripheral blood flow to acute hypoxia and hyperoxia as measured by optical microangiography. PloS one 2011; 6: e26802.
85. Lundby C, Calbet JA. Why Are High-Altitude Natives So Strong at Altitude? Maximal Oxygen Transport to the Muscle Cell in Altitude Natives. Advances in experimental medicine and biology 2016; 903: 65-81.
86. Tabuchi A, Styp-Rekowska B, Slutsky AS, Wagner PD, Pries AR, Kuebler WM. Precapillary oxygenation contributes relevantly to gas exchange in the intact lung. American journal of respiratory and critical care medicine 2013; 188: 474-81.
87. Townsley MI. Structure and composition of pulmonary arteries, capillaries, and veins. Comprehensive Physiology 2012; 2: 675-709.
88. Weibel ER. On pericytes, particularly their existence on lung capillaries. Microvascular research 1974; 8: 218-35.
89. Lung Cancer Screening (PDQ(R)): Patient Version. In: PDQ Cancer Information Summaries, Bethesda (MD), 2002.
90. Maggiorini M, Melot C, Pierre S, Pfeiffer F, Greve I, Sartori C, Lepori M, Hauser M, Scherrer U, Naeije R. High-altitude pulmonary edema is initially caused by an increase in capillary pressure. Circulation 2001; 103: 2078-83.
91. Naeije R, Chesler N. Pulmonary circulation at exercise. Comprehensive Physiology 2012; 2: 711-41.
92. Hopkins N, McLoughlin P. The structural basis of pulmonary hypertension in chronic lung disease: remodelling, rarefaction or angiogenesis? Journal of anatomy 2002; 201: 335-48.
93. Arai TJ, Theilmann RJ, Sa RC, Villongco MT, Hopkins SR. The effect of lung deformation on the spatial distribution of pulmonary blood flow. The Journal of physiology 2016; 594: 6333-47.
94. Dunham-Snary KJ, Danchen W, Sykes EA, Thakrar A, Parlow LR, Mewburn JD, Parlow JL, Archer SL. Hypoxic pulmonary vasoconstriction: from molecular mechanisms to medicine. Chest 2016.
95. Sommer N, Dietrich A, Schermuly RT, Ghofrani HA, Gudermann T, Schulz R, Seeger W, Grimminger F, Weissmann N. Regulation of hypoxic pulmonary vasoconstriction: basic mechanisms. The European respiratory journal 2008; 32: 1639-51.
96. Duke HN, Killick EM. Pulmonary vasomotor responses of isolated perfused cat lungs to anoxia. The Journal of physiology 1952; 117: 303-16.
97. Pellett AA, Cairo JM, Levitzky MG. Hypoxemia and hypoxic pulmonary vasoconstriction: autonomic nervous system versus mixed venous PO2. Respiration physiology 1997; 109: 249-60.
98. Moudgil R, Michelakis ED, Archer SL. Hypoxic pulmonary vasoconstriction. Journal of applied physiology 2005; 98: 390-403.
99. Swenson ER, Bartsch P. High-altitude pulmonary edema. Comprehensive Physiology 2012; 2: 2753-73.
100. Kylhammar D, Radegran G. The principal pathways involved in the in vivo modulation of hypoxic pulmonary vasoconstriction, pulmonary arterial remodelling and pulmonary hypertension. Acta physiologica 2016.
101. Goldenberg NM, Wang L, Ranke H, Liedtke W, Tabuchi A, Kuebler WM. TRPV4 Is Required for Hypoxic Pulmonary Vasoconstriction. Anesthesiology 2015; 122: 1338-48.
102. Sime F, Penaloza D, Ruiz L. Bradycardia, increased cardiac output, and reversal of pulmonary hypertension in altitude natives living at sea level. British heart journal 1971; 33: 647-57.
103. Fried R, Meyrick B, Rabinovitch M, Reid L. Polycythemia and the acute hypoxic response in awake rats following chronic hypoxia. Journal of applied physiology: respiratory, environmental and exercise physiology 1983; 55: 1167-72.
104. Seeger W, Adir Y, Barbera JA, Champion H, Coghlan JG, Cottin V, De Marco T, Galie N, Ghio S, Gibbs S, Martinez FJ, Semigran MJ, Simonneau G, Wells AU, Vachiery JL. Pulmonary hypertension in chronic lung diseases. Journal of the American College of Cardiology 2013; 62: D109-16.

105. Vonk-Noordegraaf A, Haddad F, Chin KM, Forfia PR, Kawut SM, Lumens J, Naeije R, Newman J, Oudiz RJ, Provencher S, Torbicki A, Voelkel NF, Hassoun PM. Right heart adaptation to pulmonary arterial hypertension: physiology and pathobiology. Journal of the American College of Cardiology 2013; 62: D22-33.
106. Rabinovitch M, Gamble W, Nadas AS, Miettinen OS, Reid L. Rat pulmonary circulation after chronic hypoxia: hemodynamic and structural features. The American journal of physiology 1979; 236: H818-27.
107. Ryland D, Reid L. The pulmonary circulation in cystic fibrosis. Thorax 1975; 30: 285-92.
108. Oswald-Mammosser M, Weitzenblum E, Quoix E, Moser G, Chaouat A, Charpentier C, Kessler R. Prognostic factors in COPD patients receiving long-term oxygen therapy. Importance of pulmonary artery pressure. Chest 1995; 107: 1193-8.
109. Yang XR, Lin AH, Hughes JM, Flavahan NA, Cao YN, Liedtke W, Sham JS. Upregulation of osmo-mechanosensitive TRPV4 channel facilitates chronic hypoxia-induced myogenic tone and pulmonary hypertension. American journal of physiology Lung cellular and molecular physiology 2012; 302: L555-68.
110. Lin MJ, Leung GP, Zhang WM, Yang XR, Yip KP, Tse CM, Sham JS. Chronic hypoxia-induced upregulation of store-operated and receptor-operated Ca2+ channels in pulmonary arterial smooth muscle cells: a novel mechanism of hypoxic pulmonary hypertension. Circulation research 2004; 95: 496-505.
111. Chester AH, Yacoub MH. The role of endothelin-1 in pulmonary arterial hypertension. Global cardiology science & practice 2014; 2014: 62-78.
112. Kouyoumdjian C, Adnot S, Levame M, Eddahibi S, Bousbaa H, Raffestin B. Continuous inhalation of nitric oxide protects against development of pulmonary hypertension in chronically hypoxic rats. The Journal of clinical investigation 1994; 94: 578-84.
113. MacLean MR. Endothelin-1 and serotonin: mediators of primary and secondary pulmonary hypertension? The Journal of laboratory and clinical medicine 1999; 134: 105-14.
114. Roberts JD, Jr., Roberts CT, Jones RC, Zapol WM, Bloch KD. Continuous nitric oxide inhalation reduces pulmonary arterial structural changes, right ventricular hypertrophy, and growth retardation in the hypoxic newborn rat. Circulation research 1995; 76: 215-22.
115. Van Ly D, Burgess JK, Brock TG, Lee TH, Black JL, Oliver BG. Prostaglandins but not leukotrienes alter extracellular matrix protein deposition and cytokine release in primary human airway smooth muscle cells and fibroblasts. American journal of physiology Lung cellular and molecular physiology 2012; 303: L239-50.
116. Zhang L, Ma J, Shen T, Wang S, Ma C, Liu Y, Ran Y, Wang L, Liu L, Zhu D. Platelet-derived growth factor (PDGF) induces pulmonary vascular remodeling through 15-LO/15-HETE pathway under hypoxic condition. Cellular signalling 2012; 24: 1931-9.
117. Fitzgerald RS, Dehghani GA, Sham JS, Shirahata M, Mitzner WA. Peripheral chemoreceptor modulation of the pulmonary vasculature in the cat. Journal of applied physiology 1992; 73: 20-9.
118. Shirai M, Tsuchimochi H, Nagai H, Gray E, Pearson JT, Sonobe T, Yoshimoto M, Inagaki T, Fujii Y, Umetani K, Kuwahira I, Schwenke DO. Pulmonary vascular tone is dependent on the central modulation of sympathetic nerve activity following chronic intermittent hypoxia. Basic research in cardiology 2014; 109: 432.
119. Jernigan NL, Walker BR, Resta TC. Endothelium-derived reactive oxygen species and endothelin-1 attenuate NO-dependent pulmonary vasodilation following chronic hypoxia. American journal of physiology Lung cellular and molecular physiology 2004; 287: L801-8.
120. Ricart A, Maristany J, Fort N, Leal C, Pages T, Viscor G. Effects of sildenafil on the human response to acute hypoxia and exercise. High altitude medicine & biology 2005; 6: 43-9.
121. Roth TS, Aboulhosn JA. Pulmonary Hypertension and Congenital Heart Disease. Cardiology clinics 2016; 34: 391-400.
122. Multhoff G, Radons J, Vaupel P. Critical role of aberrant angiogenesis in the development of tumor hypoxia and associated radioresistance. Cancers 2014; 6: 813-28.

123. Vaupel P. Tumor microenvironmental physiology and its implications for radiation oncology. Seminars in radiation oncology 2004; 14: 198-206.
124. Pries AR, Hopfner M, le Noble F, Dewhirst MW, Secomb TW. The shunt problem: control of functional shunting in normal and tumour vasculature. Nature reviews Cancer 2010; 10: 587-93.
125. Wheeler RH, Ziessman HA, Medvec BR, Juni JE, Thrall JH, Keyes JW, Pitt SR, Baker SR. Tumor blood flow and systemic shunting in patients receiving intraarterial chemotherapy for head and neck cancer. Cancer research 1986; 46: 4200-4.
126. Deberardinis RJ, Sayed N, Ditsworth D, Thompson CB. Brick by brick: metabolism and tumor cell growth. Current opinion in genetics & development 2008; 18: 54-61.
127. Kroemer G, Pouyssegur J. Tumor cell metabolism: cancer's Achilles' heel. Cancer cell 2008; 13: 472-82.
128. Vlashi E, Lagadec C, Vergnes L, Reue K, Frohnen P, Chan M, Alhiyari Y, Dratver MB, Pajonk F. Metabolic differences in breast cancer stem cells and differentiated progeny. Breast cancer research and treatment 2014; 146: 525-34.
129. Ciavardelli D, Rossi C, Barcaroli D, Volpe S, Consalvo A, Zucchelli M, De Cola A, Scavo E, Carollo R, D'Agostino D, Forli F, D'Aguanno S, Todaro M, Stassi G, Di Ilio C, De Laurenzi V, Urbani A. Breast cancer stem cells rely on fermentative glycolysis and are sensitive to 2-deoxyglucose treatment. Cell death & disease 2014; 5: e1336.
130. Schroeder T, Yuan H, Viglianti BL, Peltz C, Asopa S, Vujaskovic Z, Dewhirst MW. Spatial heterogeneity and oxygen dependence of glucose consumption in R3230Ac and fibrosarcomas of the Fischer 344 rat. Cancer research 2005; 65: 5163-71.
131. Thomlinson RH, Gray LH. The histological structure of some human lung cancers and the possible implications for radiotherapy. British journal of cancer 1955; 9: 539-49.
132. Manzoor AA, Schroeder T, Dewhirst MW. One-stop-shop tumor imaging: buy hypoxia, get lactate free. The Journal of clinical investigation 2008; 118: 1616-9.
133. Altman BJ, Stine ZE, Dang CV. From Krebs to clinic: glutamine metabolism to cancer therapy. Nature reviews Cancer 2016; 16: 619-34.
134. Feron O. Pyruvate into lactate and back: from the Warburg effect to symbiotic energy fuel exchange in cancer cells. Radiotherapy and oncology : journal of the European Society for Therapeutic Radiology and Oncology 2009; 92: 329-33.
135. Calabrese C, Iommarini L, Kurelac I, Calvaruso MA, Capristo M, Lollini PL, Nanni P, Bergamini C, Nicoletti G, Giovanni CD, Ghelli A, Giorgio V, Caratozzolo MF, Marzano F, Manzari C, Betts CM, Carelli V, Ceccarelli C, Attimonelli M, Romeo G, Fato R, Rugolo M, Tullo A, Gasparre G, Porcelli AM. Respiratory complex I is essential to induce a Warburg profile in mitochondria-defective tumor cells. Cancer & metabolism 2013; 1: 11.
136. Gasparre G, Porcelli AM, Lenaz G, Romeo G. Relevance of mitochondrial genetics and metabolism in cancer development. Cold Spring Harbor perspectives in biology 2013; 5.
137. Busk M, Walenta S, Mueller-Klieser W, Steiniche T, Jakobsen S, Horsman MR, Overgaard J. Inhibition of tumor lactate oxidation: consequences for the tumor microenvironment. Radiotherapy and oncology : journal of the European Society for Therapeutic Radiology and Oncology 2011; 99: 404-11.
138. Yasuda M, Matsubara J, Yamasaki H, Fujita Y, Konishi H, Koinuma S, Taketani S, Horiuchi Y, Utsumi H, Yasuda Y. Death-resistant and nonresistant malignant human cell lines under anoxia in vitro. International journal of clinical oncology 2007; 12: 455-62.
139. Huxham LA, Kyle AH, Baker JH, Nykilchuk LK, Minchinton AI. Microregional effects of gemcitabine in HCT-116 xenografts. Cancer research 2004; 64: 6537-41.
140. Kyle AH, Huxham LA, Yeoman DM, Minchinton AI. Limited tissue penetration of taxanes: a mechanism for resistance in solid tumors. Clinical cancer research : an official journal of the American Association for Cancer Research 2007; 13: 2804-10.
141. Brizel DM, Schroeder T, Scher RL, Walenta S, Clough RW, Dewhirst MW, Mueller-Klieser W. Elevated tumor lactate concentrations predict for an increased risk of metastases in head-and-neck cancer. International journal of radiation oncology, biology, physics 2001; 51: 349-53.

142. Brizel DM, Scully SP, Harrelson JM, Layfield LJ, Bean JM, Prosnitz LR, Dewhirst MW. Tumor oxygenation predicts for the likelihood of distant metastases in human soft tissue sarcoma. Cancer research 1996; 56: 941-3.
143. Brizel DM, Sibley GS, Prosnitz LR, Scher RL, Dewhirst MW. Tumor hypoxia adversely affects the prognosis of carcinoma of the head and neck. International journal of radiation oncology, biology, physics 1997; 38: 285-9.
144. Hockel M, Vorndran B, Schlenger K, Baussmann E, Knapstein PG. Tumor oxygenation: a new predictive parameter in locally advanced cancer of the uterine cervix. Gynecologic oncology 1993; 51: 141-9.
145. Walenta S, Schroeder T, Mueller-Klieser W. Lactate in solid malignant tumors: potential basis of a metabolic classification in clinical oncology. Current medicinal chemistry 2004; 11: 2195-204.
146. Walenta S, Wetterling M, Lehrke M, Schwickert G, Sundfor K, Rofstad EK, Mueller-Klieser W. High lactate levels predict likelihood of metastases, tumor recurrence, and restricted patient survival in human cervical cancers. Cancer research 2000; 60: 916-21.
147. Minchinton AI, Tannock IF. Drug penetration in solid tumours. Nature reviews Cancer 2006; 6: 583-92.
148. Manzoor AA, Lindner LH, Landon CD, Park JY, Simnick AJ, Dreher MR, Das S, Hanna G, Park W, Chilkoti A, Koning GA, ten Hagen TL, Needham D, Dewhirst MW. Overcoming limitations in nanoparticle drug delivery: triggered, intravascular release to improve drug penetration into tumors. Cancer research 2012; 72: 5566-75.
149. Fung AS, Jonkman J, Tannock IF. Quantitative immunohistochemistry for evaluating the distribution of Ki67 and other biomarkers in tumor sections and use of the method to study repopulation in xenografts after treatment with paclitaxel. Neoplasia 2012; 14: 324-34.
150. Gerdes J, Lelle RJ, Pickartz H, Heidenreich W, Schwarting R, Kurtsiefer L, Stauch G, Stein H. Growth fractions in breast cancers determined in situ with monoclonal antibody Ki-67. Journal of clinical pathology 1986; 39: 977-80.
151. Gerdes J, Van Baarlen J, Pileri S, Schwarting R, Van Unnik JA, Stein H. Tumor cell growth fraction in Hodgkin's disease. The American journal of pathology 1987; 128: 390-3.
152. Mellor HR, Ferguson DJ, Callaghan R. A model of quiescent tumour microregions for evaluating multicellular resistance to chemotherapeutic drugs. British journal of cancer 2005; 93: 302-9.
153. Nakano T, Oka K. Differential values of Ki-67 index and mitotic index of proliferating cell population. An assessment of cell cycle and prognosis in radiation therapy for cervical cancer. Cancer 1993; 72: 2401-8.
154. Nielsen AL, Nyholm HC. The combination of p53 and age predict cancer specific death in advanced stage (FIGO Ic-IV) of endometrial carcinoma of endometrioid type. An immunohistochemical examination of growth fraction: Ki-67, MIB-1 and PC10; suppressor oncogene protein: p53; oncogene protein: p185 and age, hormone treatment, stage, and histologic grade. European journal of obstetrics, gynecology, and reproductive biology 1996; 70: 79-85.
155. Finlay GJ, Wilson WR, Baguley BC. Cytokinetic factors in drug resistance of Lewis lung carcinoma: comparison of cells freshly isolated from tumours with cells from exponential and plateau-phase cultures. British journal of cancer 1987; 56: 755-62.
156. Fryknas M, Zhang X, Bremberg U, Senkowski W, Olofsson MH, Brandt P, Persson I, D'Arcy P, Gullbo J, Nygren P, Schughart LK, Linder S, Larsson R. Iron chelators target both proliferating and quiescent cancer cells. Scientific reports 2016; 6: 38343.
157. Kangwan N, Park JM, Kim EH, Hahm KB. Chemoquiescence for ideal cancer treatment and prevention: where are we now? Journal of cancer prevention 2014; 19: 89-6.
158. Saggar JK, Tannock IF. Chemotherapy Rescues Hypoxic Tumor Cells and Induces Their Reoxygenation and Repopulation-An Effect That Is Inhibited by the Hypoxia-Activated Prodrug TH-302. Clinical cancer research : an official journal of the American Association for Cancer Research 2015; 21: 2107-14.
159. Kiely BE, Soon YY, Tattersall MH, Stockler MR. How long have I got? Estimating typical, best-case, and worst-case scenarios for patients starting first-line chemotherapy for metastatic breast

cancer: a systematic review of recent randomized trials. Journal of clinical oncology : official journal of the American Society of Clinical Oncology 2011; 29: 456-63.
160. Hind D, Tappenden P, Tumur I, Eggington S, Sutcliffe P, Ryan A. The use of irinotecan, oxaliplatin and raltitrexed for the treatment of advanced colorectal cancer: systematic review and economic evaluation. Health technology assessment 2008; 12: iii-ix, xi-162.
161. Zhang M, Guo H, Zhao S, Wang Y, Yang M, Yu J, Yan Y, Wang Y. Efficacy of epidermal growth factor receptor inhibitors in combination with chemotherapy in advanced non-small cell lung cancer: a meta-analysis of randomized controlled trials. Oncotarget 2016; 7: 39823-33.
162. Tappenden P, Jones R, Paisley S, Carroll C. Systematic review and economic evaluation of bevacizumab and cetuximab for the treatment of metastatic colorectal cancer. Health technology assessment 2007; 11: 1-128, iii-iv.
163. Kumler I, Christiansen OG, Nielsen DL. A systematic review of bevacizumab efficacy in breast cancer. Cancer treatment reviews 2014; 40: 960-73.
164. Borghaei H, Paz-Ares L, Horn L, Spigel DR, Steins M, Ready NE, Chow LQ, Vokes EE, Felip E, Holgado E, Barlesi F, Kohlhaufl M, Arrieta O, Burgio MA, Fayette J, Lena H, Poddubskaya E, Gerber DE, Gettinger SN, Rudin CM, Rizvi N, Crino L, Blumenschein GR, Jr., Antonia SJ, Dorange C, Harbison CT, Graf Finckenstein F, Brahmer JR. Nivolumab versus Docetaxel in Advanced Nonsquamous Non-Small-Cell Lung Cancer. The New England journal of medicine 2015; 373: 1627-39.
165. Ferris RL, Blumenschein G, Jr., Fayette J, Guigay J, Colevas AD, Licitra L, Harrington K, Kasper S, Vokes EE, Even C, Worden F, Saba NF, Iglesias Docampo LC, Haddad R, Rordorf T, Kiyota N, Tahara M, Monga M, Lynch M, Geese WJ, Kopit J, Shaw JW, Gillison ML. Nivolumab for Recurrent Squamous-Cell Carcinoma of the Head and Neck. The New England journal of medicine 2016; 375: 1856-67.
166. Gupta K, Tiu DY, Tiu J, Aragon-Ching JB. The promising role of nivolumab in renal cell cancers. Cancer biology & therapy 2016; 17: 123-4.
167. Siddiqui M, Rajkumar SV. The high cost of cancer drugs and what we can do about it. Mayo Clinic proceedings 2012; 87: 935-43.
168. El Sharouni SY, Kal HB, Battermann JJ. Accelerated regrowth of non-small-cell lung tumours after induction chemotherapy. British journal of cancer 2003; 89: 2184-9.
169. Folkman J. Tumor angiogenesis: therapeutic implications. The New England journal of medicine 1971; 285: 1182-6.
170. Folkman J. Role of angiogenesis in tumor growth and metastasis. Seminars in oncology 2002; 29: 15-8.
171. Jayson GC, Kerbel R, Ellis LM, Harris AL. Antiangiogenic therapy in oncology: current status and future directions. Lancet 2016; 388: 518-29.
172. Cairns RA, Hill RP. Acute hypoxia enhances spontaneous lymph node metastasis in an orthotopic murine model of human cervical carcinoma. Cancer research 2004; 64: 2054-61.
173. Cairns RA, Kalliomaki T, Hill RP. Acute (cyclic) hypoxia enhances spontaneous metastasis of KHT murine tumors. Cancer research 2001; 61: 8903-8.
174. Tewari KS, Sill MW, Long HJ, 3rd, Penson RT, Huang H, Ramondetta LM, Landrum LM, Oaknin A, Reid TJ, Leitao MM, Michael HE, Monk BJ. Improved survival with bevacizumab in advanced cervical cancer. The New England journal of medicine 2014; 370: 734-43.
175. Aravantinos G, Pectasides D. Bevacizumab in combination with chemotherapy for the treatment of advanced ovarian cancer: a systematic review. Journal of ovarian research 2014; 7: 57.
176. Bolondi L, Craxi A, Trevisani F, Daniele B, Di Costanzo GG, Fagiuoli S, Camma C, Bruzzi P, Danesi R, Spandonaro F, Boni C, Santoro A, Colombo M. Refining sorafenib therapy: lessons from clinical practice. Future oncology 2015; 11: 449-65.
177. Rutkowski P, Gronchi A. Efficacy and economic value of adjuvant imatinib for gastrointestinal stromal tumors. The oncologist 2013; 18: 689-96.
178. Santoni M, Conti A, Massari F, Arnaldi G, Iacovelli R, Rizzo M, De Giorgi U, Trementino L, Procopio G, Tortora G, Cascinu S. Treatment-related fatigue with sorafenib, sunitinib and pazopanib in patients with advanced solid tumors: an up-to-date review and meta-analysis of clinical trials. International journal of cancer 2015; 136: 1-10.

179. Burger RA, Brady MF, Bookman MA, Fleming GF, Monk BJ, Huang H, Mannel RS, Homesley HD, Fowler J, Greer BE, Boente M, Birrer MJ, Liang SX, Gynecologic Oncology G. Incorporation of bevacizumab in the primary treatment of ovarian cancer. The New England journal of medicine 2011; 365: 2473-83.
180. Hurwitz H, Fehrenbacher L, Novotny W, Cartwright T, Hainsworth J, Heim W, Berlin J, Baron A, Griffing S, Holmgren E, Ferrara N, Fyfe G, Rogers B, Ross R, Kabbinavar F. Bevacizumab plus irinotecan, fluorouracil, and leucovorin for metastatic colorectal cancer. The New England journal of medicine 2004; 350: 2335-42.
181. Sonveaux P. Provascular strategy: targeting functional adaptations of mature blood vessels in tumors to selectively influence the tumor vascular reactivity and improve cancer treatment. Radiotherapy and oncology : journal of the European Society for Therapeutic Radiology and Oncology 2008; 86: 300-13.
182. Powell ME, Hill SA, Saunders MI, Hoskin PJ, Chaplin DJ. Effect of carbogen breathing on tumour microregional blood flow in humans. Radiotherapy and oncology : journal of the European Society for Therapeutic Radiology and Oncology 1996; 41: 225-31.
183. Thomas CD, Stern S, Chaplin DJ, Guichard M. Transient perfusion and radiosensitizing effect after nicotinamide, carbogen, and perflubron emulsion administration. Radiotherapy and oncology : journal of the European Society for Therapeutic Radiology and Oncology 1996; 39: 235-41.
184. Eberhard A, Kahlert S, Goede V, Hemmerlein B, Plate KH, Augustin HG. Heterogeneity of angiogenesis and blood vessel maturation in human tumors: implications for antiangiogenic tumor therapies. Cancer research 2000; 60: 1388-93.
185. Dewhirst MW, Vinuya RZ, Ong ET, Klitzman B, Rosner G, Secomb TW, Gross JF. Effects of bradykinin on the hemodynamics of tumor and granulating normal tissue microvasculature. Radiation research 1992; 130: 345-54.
186. Shan SQ, Rosner GL, Braun RD, Hahn J, Pearce C, Dewhirst MW. Effects of diethylamine/nitric oxide on blood perfusion and oxygenation in the R3230Ac mammary carcinoma. British journal of cancer 1997; 76: 429-37.
187. Burrell JS, Walker-Samuel S, Boult JK, Baker LC, Jamin Y, Halliday J, Waterton JC, Robinson SP. Investigating the Vascular Phenotype of Subcutaneously and Orthotopically Propagated PC3 Prostate Cancer Xenografts Using Combined Carbogen Ultrasmall Superparamagnetic Iron Oxide MRI. Topics in magnetic resonance imaging : TMRI 2016; 25: 237-43.
188. Sonveaux P, Kaz AM, Snyder SA, Richardson RA, Cardenas-Navia LI, Braun RD, Pawloski JR, Tozer GM, Bonaventura J, McMahon TJ, Stamler JS, Dewhirst MW. Oxygen regulation of tumor perfusion by S-nitrosohemoglobin reveals a pressor activity of nitric oxide. Circulation research 2005; 96: 1119-26.
189. Thews O, Kelleher DK, Vaupel P. No improvement in perfusion and oxygenation of experimental tumors upon application of vasodilator drugs. International journal of oncology 2001; 19: 1243-7.
190. Wood PJ, Sansom JM, Stratford IJ, Adams GE, Szabo C, Thiemermann C, Vane JR. Changes in energy metabolism and X-ray sensitivity in murine tumours by the nitric oxide donor SIN-1. The British journal of cancer Supplement 1996; 27: S177-80.
191. Martinive P, De Wever J, Bouzin C, Baudelet C, Sonveaux P, Gregoire V, Gallez B, Feron O. Reversal of temporal and spatial heterogeneities in tumor perfusion identifies the tumor vascular tone as a tunable variable to improve drug delivery. Molecular cancer therapeutics 2006; 5: 1620-7.
192. Sonveaux P, Dessy C, Martinive P, Havaux X, Jordan BF, Gallez B, Gregoire V, Balligand JL, Feron O. Endothelin-1 is a critical mediator of myogenic tone in tumor arterioles: implications for cancer treatment. Cancer research 2004; 64: 3209-14.
193. Dore-Duffy P, Wang S, Mehedi A, Katyshev V, Cleary K, Tapper A, Reynolds C, Ding Y, Zhan P, Rafols J, Kreipke CW. Pericyte-mediated vasoconstriction underlies TBI-induced hypoperfusion. Neurological research 2011; 33: 176-86.

194. Blueschke G, Hanna G, Fontanella AN, Palmer GM, Boico A, Min H, Dewhirst MW, Irwin DC, Zhao Y, Schroeder T. Automated measurement of microcirculatory blood flow velocity in pulmonary metastases of rats. Journal of visualized experiments : JoVE 2014: e51630.
195. Burton MA, Gray BN, Self GW, Heggie JC, Townsend PS. Manipulation of experimental rat and rabbit liver tumor blood flow with angiotensin II. Cancer research 1985; 45: 5390-3.
196. Kato T, Murakami Y, Saito Y, Tomura N, Shindo M, Watarai J, Tamakawa Y. New modality of radiation therapy under increased tumor oxygen tension with angiotensin II: a pilot study. Radiation medicine 1993; 11: 86-90.
197. Ohigashi H, Ishikawa O, Yokayama S, Sasaki Y, Yamada T, Imaoka S, Nakaizumi A, Uehara H. Intra-arterial infusion chemotherapy with angiotensin-II for locally advanced and nonresectable pancreatic adenocarcinoma: further evaluation and prognostic implications. Annals of surgical oncology 2003; 10: 927-34.
198. Suzuki M, Hori K, Abe I, Saito S, Sato H. A new approach to cancer chemotherapy: selective enhancement of tumor blood flow with angiotensin II. Journal of the National Cancer Institute 1981; 67: 663-9.
199. Trotter MJ, Chaplin DJ, Olive PL. Effect of angiotensin II on intermittent tumour blood flow and acute hypoxia in the murine SCCVII carcinoma. European journal of cancer 1991; 27: 887-93.
200. Ishikawa T, Ushiki T, Kamimura H, Togashi T, Tsuchiya A, Watanabe K, Seki K, Ohta H, Yoshida T, Takeda K, Kamimura T. Angiotensin-II administration is useful for the detection of liver metastasis from pancreatic cancer during pharmacoangiographic computed tomography. World journal of gastroenterology 2007; 13: 3080-3.
201. Sasaki Y, Imaoka S, Hasegawa Y, Nakano S, Ishikawa O, Ohigashi H, Taniguchi K, Koyama H, Iwanaga T, Terasawa T. Changes in distribution of hepatic blood flow induced by intra-arterial infusion of angiotensin II in human hepatic cancer. Cancer 1985; 55: 311-6.
202. van den Hoven AF, Smits ML, Rosenbaum CE, Verkooijen HM, van den Bosch MA, Lam MG. The effect of intra-arterial angiotensin II on the hepatic tumor to non-tumor blood flow ratio for radioembolization: a systematic review. PloS one 2014; 9: e86394.
203. Ino K, Shibata K, Kajiyama H, Nawa A, Nomura S, Kikkawa F. Manipulating the angiotensin system--new approaches to the treatment of solid tumours. Expert opinion on biological therapy 2006; 6: 243-55.
204. Hafstrom L, Nobin A, Persson B, Sundqvist K. Effects of catecholamines on cardiovascular response and blood flow distribution to normal tissue and liver tumors in rats. Cancer research 1980; 40: 481-5.
205. Calcutt G, Ting SM, Preece AV. Tissue NAD levels and the response to irradiation of cytotoxic drugs. British journal of cancer 1970; 24: 380-8.
206. Masunaga S, Ono K, Akuta K, Akaboshi M, Kawai K, Takagaki M, Abe M. Enhancement of chemosensitivity of quiescent cell populations in murine solid tumors using nicotinamide. Chemotherapy 1994; 40: 418-26.
207. Kelleher DK, Vaupel PW. Possible mechanisms involved in tumor radiosensitization following nicotinamide administration. Radiotherapy and oncology : journal of the European Society for Therapeutic Radiology and Oncology 1994; 32: 47-53.
208. Meduna LJ. The carbon dioxide treatment; a review. Journal of clinical and experimental psychopathology 1954; 15: 235-54.
209. Powell ME, Hill SA, Saunders MI, Hoskin PJ, Chaplin DJ. Human tumor blood flow is enhanced by nicotinamide and carbogen breathing. Cancer research 1997; 57: 5261-4.
210. Hoskin P, Rojas A, Saunders M. Accelerated radiotherapy, carbogen, and nicotinamide (ARCON) in the treatment of advanced bladder cancer: mature results of a Phase II nonrandomized study. International journal of radiation oncology, biology, physics 2009; 73: 1425-31.
211. Janssens GO, Rademakers SE, Terhaard CH, Doornaert PA, Bijl HP, van den Ende P, Chin A, Takes RP, de Bree R, Hoogsteen IJ, Bussink J, Span PN, Kaanders JH. Improved recurrence-free survival with ARCON for anemic patients with laryngeal cancer. Clinical cancer research : an official journal of the American Association for Cancer Research 2014; 20: 1345-54.

212. Kaanders JH, Bussink J, van der Kogel AJ. ARCON: a novel biology-based approach in radiotherapy. The Lancet Oncology 2002; 3: 728-37.
213. Jain RK. Antiangiogenesis strategies revisited: from starving tumors to alleviating hypoxia. Cancer cell 2014; 26: 605-22.
214. Schmidt B, Lee HJ, Ryeom S, Yoon SS. Combining Bevacizumab with Radiation or Chemoradiation for Solid Tumors: A Review of the Scientific Rationale, and Clinical Trials. Current angiogenesis 2012; 1: 169-79.
215. Tolaney SM, Boucher Y, Duda DG, Martin JD, Seano G, Ancukiewicz M, Barry WT, Goel S, Lahdenrata J, Isakoff SJ, Yeh ED, Jain SR, Golshan M, Brock J, Snuderl M, Winer EP, Krop IE, Jain RK. Role of vascular density and normalization in response to neoadjuvant bevacizumab and chemotherapy in breast cancer patients. Proceedings of the National Academy of Sciences of the United States of America 2015; 112: 14325-30.
216. Emerich DF, Dean RL, Marsh J, Pink M, Lafreniere D, Snodgrass P, Bartus RT. Intravenous cereport (RMP-7) enhances delivery of hydrophilic chemotherapeutics and increases survival in rats with metastatic tumors in the brain. Pharmaceutical research 2000; 17: 1212-9.
217. Warren K, Jakacki R, Widemann B, Aikin A, Libucha M, Packer R, Vezina G, Reaman G, Shaw D, Krailo M, Osborne C, Cehelsky J, Caldwell D, Stanwood J, Steinberg SM, Balis FM. Phase II trial of intravenous lobradimil and carboplatin in childhood brain tumors: a report from the Children's Oncology Group. Cancer chemotherapy and pharmacology 2006; 58: 343-7.
218. Belfi CA, Paul CR, Shan S, Ngo FQ. Comparison of the effects of hydralazine on tumor and normal tissue blood perfusion by MRI. International journal of radiation oncology, biology, physics 1994; 29: 473-9.
219. Kalmus J, Okunieff P, Vaupel P. Dose-dependent effects of hydralazine on microcirculatory function and hyperthermic response of murine FSall tumors. Cancer research 1990; 50: 15-9.
220. Song CW, Park HJ, Lee CK, Griffin R. Implications of increased tumor blood flow and oxygenation caused by mild temperature hyperthermia in tumor treatment. International journal of hyperthermia : the official journal of European Society for Hyperthermic Oncology, North American Hyperthermia Group 2005; 21: 761-7.
221. Song CW, Shakil A, Osborn JL, Iwata K. Tumour oxygenation is increased by hyperthermia at mild temperatures. 1996. International journal of hyperthermia : the official journal of European Society for Hyperthermic Oncology, North American Hyperthermia Group 2009; 25: 91-5.
222. Yano HJ, Hatano K, Tsuno N, Osada T, Watanabe T, Tsuruo T, Muto T, Nagawa H. Clustered cancer cells show a distinct adhesion behavior from single cell form under physiological shear conditions. Journal of experimental & clinical cancer research : CR 2001; 20: 407-12.
223. Phillips RM. Targeting the hypoxic fraction of tumours using hypoxia-activated prodrugs. Cancer chemotherapy and pharmacology 2016; 77: 441-57.
224. Wilson WR, Hay MP. Targeting hypoxia in cancer therapy. Nature reviews Cancer 2011; 11: 393-410.
225. Denny WA, Wilson WR, Hay MP. Recent developments in the design of bioreductive drugs. The British journal of cancer Supplement 1996; 27: S32-8.
226. Huxham LA, Kyle AH, Baker JH, McNicol KL, Minchinton AI. Tirapazamine causes vascular dysfunction in HCT-116 tumour xenografts. Radiotherapy and oncology : journal of the European Society for Therapeutic Radiology and Oncology 2006; 78: 138-45.
227. Huxham LA, Kyle AH, Baker JH, McNicol KL, Minchinton AI. Exploring vascular dysfunction caused by tirapazamine. Microvascular research 2008; 75: 247-55.
228. McKeown SR, Cowen RL, Williams KJ. Bioreductive drugs: from concept to clinic. Clinical oncology 2007; 19: 427-42.
229. Swampillai AL, Salomoni P, Short SC. The role of autophagy in clinical practice. Clinical oncology 2012; 24: 387-95.
230. Fulda S, Kogel D. Cell death by autophagy: emerging molecular mechanisms and implications for cancer therapy. Oncogene 2015; 34: 5105-13.
231. Borrell B. Mountains to climb. Nature medicine 2010; 16: 1176-9.

232. Lalande S, Snyder EM, Olson TP, Hulsebus ML, Orban M, Somers VK, Johnson BD, Frantz RP. The effects of sildenafil and acetazolamide on breathing efficiency and ventilatory control during hypoxic exercise. European journal of applied physiology 2009; 106: 509-15.
233. Kennedy KM, Scarbrough PM, Ribeiro A, Richardson R, Yuan H, Sonveaux P, Landon CD, Chi JT, Pizzo S, Schroeder T, Dewhirst MW. Catabolism of exogenous lactate reveals it as a legitimate metabolic substrate in breast cancer. PloS one 2013; 8: e75154.
234. Sonveaux P, Vegran F, Schroeder T, Wergin MC, Verrax J, Rabbani ZN, De Saedeleer CJ, Kennedy KM, Diepart C, Jordan BF, Kelley MJ, Gallez B, Wahl ML, Feron O, Dewhirst MW. Targeting lactate-fueled respiration selectively kills hypoxic tumor cells in mice. The Journal of clinical investigation 2008; 118: 3930-42.
235. Fontanella AN, Schroeder T, Hochman DW, Chen RE, Hanna G, Haglund MM, Rajaram N, Frees AE, Secomb TW, Palmer GM, Dewhirst MW. Quantitative mapping of hemodynamics in the lung, brain, and dorsal window chamber-grown tumors using a novel, automated algorithm. Microcirculation 2013; 20: 724-35.
236. Hanna G, Fontanella A, Palmer G, Shan S, Radiloff DR, Zhao Y, Irwin D, Hamilton K, Boico A, Piantadosi CA, Blueschke G, Dewhirst M, McMahon T, Schroeder T. Automated measurement of blood flow velocity and direction and hemoglobin oxygen saturation in the rat lung using intravital microscopy. American journal of physiology Lung cellular and molecular physiology 2013; 304: L86-91.

8 Appendix

CURRICULUM VITAE of DR. THIES SCHROEDER

PERSONAL DATA

Date of Birth April 12, 1969
Place Herzberg/Harz, Germany
Citizen of Germany
Status Married, four children

EDUCATION

High School
Hainberg-Gymnasium, Goettingen, Germany
1988, University Entrance Permission (Abitur)

College
Christian-Albrechts-Universitaet, Kiel, Germany
1996, University Degree (Universitätsdiplom) in Zoology, Microbiology, Biochemistry

Graduate School
Johannes-Gutenberg-Universitaet Mainz, Germany
2002, PhD, Physiology – *Summa Cum Laude*

PROFESSIONAL TRAINING AND ACADEMIC CAREER

May 2002 – September 2002
Research Associate
Institute of Biochemistry
University of Mainz, Germany

September 2002 - October 2003
September 2004 – August 2009
Research Associate
Department of Radiation Oncology
Duke University Medical Center, NC, USA

September 2009 – November 2013
Assistant Professor
Department of Radiation Oncology
Duke University Medical Center, NC, USA

December 2013 – present
Research Associate
Institute of Physical Chemistry
Institute of Biochemistry
University of Mainz, Germany

Adjunct Assistant Professor of Cardiopulmonary Medicine, University of Colorado Denver Medical Center, CO, USA
(since Oct 2014)

8.2 Publications in scientific journals

I have authored 40 manuscripts in scientific journals, with an H-factor of 19. First and last authorships are marked with an asterisk (*).

40 **SCHROEDER T**, Piantadosi CA, Natoli M, Autmizguine J, Cohen-Wolkowiez M, Hamilton KL, Bell C, Klawitter J, Christians U, Irwin DC, Noveck RJ. Treating hypoxemia without supplemental oxygen: Combined aminophylline and ambrisentan are safe and improve hypoxic exercise performance. *Clin Pharm Ther, accepted with minor revisions*

39 Strand TE, Khiabani HZ, Boico A, Radiloff DR, Zhao Y,Hamilton KL, Christians U, Klawitter J, Noveck RJ, Piantadosi CA, Bell C, Irwin DC, **SCHROEDER T***. Safety of combined bambuterol and theophylline as a potential treatment of high altitude-induced fatigue in humans. *Can J Physiol Pharm 2017, in press*

38 Blatt S, Voelxen N, Sagheb K, Pabst AM, Walenta S, **SCHROEDER T**, Mueller-Klieser W, Ziebart T. Lactate as a predictive marker for tumor recurrence in patients with head and neck squamous cell carcinoma (HNSCC) post radiation: a prospective study over 15 years. *Clin Oral Invest. 2016 Jan 4*

37 Register JK, Fales AM, Wang HN, Norton SJ, Cho EH, Boico A, Pradhan S, Kim J, **SCHROEDER T**, Wisniewski NA, Klitzman B, Vo-Dinh T. In vivo detection of SERS-encoded plasmonic nanostars in human skin grafts and live animal models. *Anal Bioanal Chem. 2015 Nov;407(27):8215-24*

36 Khademi S, Frye MA, Jeckel KM, **SCHROEDER T**, Monnet E, Irwin DC, Cole PA, Bell C, Miller BF, Hamilton KL. Hypoxia mediated pulmonary edema: potential influence of oxidative stress, sympathetic activation and cerebral blood flow. *BMC Physiol. 2015 Oct 9;15:4*

35 Scalzo RL, Binns SE, Klochak AL, Giordano GR, Paris HL, Sevits KJ, Beals JW, Biela LM, Larson DG, Luckasen GJ, Irwin D, **SCHROEDER T**, Hamilton KL, Bell C. Methazolamide Plus Aminophylline Abrogates Hypoxia-Mediated Endurance Exercise Impairment. *High Alt Med Biol. 2015 Dec;16(4):331-42*

34 Fontanella EN, Boss MK, Hadsell M, Zhang J, **SCHROEDER T**, Berman KG, Dewhirst MW, Chang S, Palmer GM. Effects of High-Dose Microbeam Irradiation on Tumor Microvascular Function and Angiogenesis. *Radiat Res. 2015 Feb;183(2):147-58*

33 Scalzo RL, Binns SE, Klochak AL, Giordano GL, Paris HLR, Sevits KJ, Beals JW, Biela LA, Larson DG, Luckasen GJ, Irwin DC, **SCHROEDER T**, Hamilton KL, Bell C. The Effects of Sympathetic Inhibition on Metabolic and Cardiopulmonary Responses to Exercise in Hypoxic Conditions. *Wilderness Environ Med. 2015 Dec;26(4):520-4*

32 Eigenberger P, Faino A, Maltzahn J, Lisk C, Frank E, Frank A, Loomis Z, **SCHROEDER T**, Strand M, Irwin DC. Retrospective Study of Acute Mountain Sickness on Mt. Kilimanjaro using Trekking Company Data. *Aviat Space Environ Med. 2014 Nov;85(11):1125-9*

31 Blueschke G, Hanna G, Fontanella AN, Palmer GM, Boico A, Min H, Dewhirst MW, **SCHROEDER T***. Automated measurement of microcirculatory blood flow velocity in pulmonary metastases of rats. *J Vis Exp. 2014 Nov 30;(93)*

30 Radiloff DR, Boico A, Zhao Y, Blueschke G, Irwin D, Hamilton K, Noveck R, **SCHROEDER T***. Anti-hypotensive treatment and endothelin blockade synergistically antagonize exercise fatigue in rats under simulated high altitude . *PLoS One. 2014 Jun 24;9(6):e99309*

29 Kennedy KM, Scarbrough PM, Ribeiro A, Richardson R, Yuan H, Sonveaux P, Landon CD, Chi JT, Pizzo S, **SCHROEDER T* (co-Senior Author)**, Dewhirst MW. Catabolism of exogenous lactate reveals it as a legitimate metabolic substrate in breast cancer. *PLoS One. 2013 Sep 12;8(9)*

28 Fontanella A, **SCHROEDER T**, Palmer G, Hanna G, Secomb T, Dewhirst MW. Quantitative mapping of hemodynamics in the lung, brain, and dorsal window chamber-grown tumors using a novel, automated algorithm. *Microcirculation. 2013 Jun 19*

27 Lisk C, McCord J, Bose S, Sullivan T, Loomis Z, Nozik-Grayck E, **SCHROEDER T**, Hamilton K, Irwin DC. Nrf2 Activation: A potential strategy for the prevention of Acute Mountain Sickness: Therapeutic strategy for acute mountain sickness. *Free Radic Biol Med. 2013 May 27*

26 Hanna G, Fontanella A, Palmer G, Shan S, Zhao Y, Irwin D, Hamilton K, Boico A, Blueschke G, Piantadosi C, Dewhirst M, McMahon T, **SCHROEDER T***. Automated measurement of blood flow velocity and direction, and hemoglobin oxygen saturation in the rat lung using intravital microscopy. *Am J Physiol Lung Cell Mol Physiol. 2013 Jan; 304(2):L86-91*

25 Radiloff DR, Shan S, Zhao Y, Hanna G, Hamilton K, Irwin DR, Piantadosi CA, **SCHROEDER T***. Evidence for synergism between theophylline and endothelin receptor antagonists to improve exercise performance of rats under simulated high altitude. *J Appl Physiol 2012, Oct 15, 113:1243-1252*

24 Peltonen GL, Scalzo RL, Schweder MM, Larson DG, Luckasen GJ, Irwin D, Hamilton KL, **SCHROEDER T**, Bell C. Sympathetic inhibition attenuates hypoxia induced insulin resistance in healthy adult humans. *J Physiol. 2012 Jun 1;590(Pt 11):2801-9*.

23 Prichard HL, **SCHROEDER T**, Reichert WM, Klitzman B. Bioluminescence imaging of glucose in tissue surrounding polyurethane and glucose sensor implants. *J Diabetes Sci Technol. 2010 Sep 1;4(5):1055-62*

22 Moon E, Sonveaux P, Porporato PE, Danhier P, Gallez B, Batinic-Haberle I, Nien YC, **SCHROEDER T**, Dewhirst MW. NADPH oxidase-mediated ROS production activates HIF-1 via the ERK pathway after hyperthermia treatment. *Proc Natl Acad Sci. 2010, Nov 8*

21 Dewhirst MW, Thrall DE, Palmer G, **SCHROEDER T**, Vujaskovic Z, Cecil Charles H, Macfall J, Wong T. Utility of functional imaging in prediction or assessment of treatment response and prognosis following thermotherapy. *Int J Hyperthermia. 2010;26(3):283-93*.

20 Jones LW, Viglianti BL, Tashjian JA, Kothadia SM, Keir ST, Freedland SJ, Potter MQ, Moon EJ, **SCHROEDER T**, Herndon JE 2nd, Dewhirst MW Effect of aerobic exercise on tumor

physiology in an animal model of human breast cancer. *J Appl Physiol. 2010 Feb;108(2):343-8*

19 Vishwanath K, Klein D, Chang K, **SCHROEDER T**, Dewhirst MW, Ramanujam N. Quantitative optical spectroscopy can identify long-term local tumor control in irradiated murine head and neck xenografts. *J Biomed Opt. 2009 Sep-Oct;14(5):054051*

18 Palmer GM, Viola RJ, **SCHROEDER T**, Yarmolenko PS, Dewhirst MW, Ramanujam N. Quantitative diffuse reflectance and fluorescence spectroscopy: tool to monitor tumor physiology in vivo. *J Biomed Opt. 2009 Mar-Apr;14(2):024010*.

17 Chen JL, Lucas JE, **SCHROEDER T**, Mori S, Wu J, Nevins J, Dewhirst M, West M, Chi JT. The genomic analysis of lactic acidosis and acidosis response in human cancers. *PLoS Genet. 2008 Dec;4(12):e1000293. Epub 2008 Dec 5*

16 Sonveaux P, Végran F, **SCHROEDER T**, Wergin MC, Verrax J, Rabbani ZN, De Saedeleer CJ, Kennedy KM, Diepart C, Jordan BF, Kelley MJ, Gallez B, Wahl ML, Feron O, Dewhirst MW. Targeting lactate-fueled respiration selectively kills hypoxic tumor cells in mice. *J Clin Invest. 2008 Dec;118(12):3930-42*

15 Stein RA, Chang CY, Kazmin DA, Way J, **SCHROEDER T**, Wergin M, Dewhirst MW, McDonnell DP. Estrogen-related receptor alpha is critical for the growth of estrogen receptor-negative breast cancer. *Cancer Res. 2008 Nov 1;68(21):8805-12*

14 **SCHROEDER T***, Viglianti BL, Dewhirst MW. Low-intensity alternating electric fields: a potentially safe and effective treatment of cancer? *Onkologie. 2008 Jul;31(7):357-8*

13 Manzoor AA, **SCHROEDER T**, Dewhirst MW. One-stop-shop tumor imaging: buy hypoxia, get lactate free. *J Clin Invest. 2008 May;118(5):1616-9*

12 Davis BH, **SCHROEDER T**, Yarmolenko PS, Guilak F, Dewhirst MW, Taylor DA. An in vitro system to evaluate the effects of ischemia on survival of cells used for cell therapy. *Ann Biomed Eng. 2007 Aug;35(8):1414-24*

11 Viglianti BL, Ponce AM, Michelich CR, Yu D, Abraham SA, Sanders L, Yarmolenko PS, **SCHROEDER T**, MacFall JR, Barboriak DP, Colvin OM, Bally MB, Dewhirst MW. Chemodosimetry of in vivo tumor liposomal drug concentration using MRI. *Magn Reson Med. 2006 Nov;56(5):1011-8*

10 Yuan H, **SCHROEDER T**, Bowsher JE, Hedlund LW, Wong T, Dewhirst MW. Intertumoral differences in hypoxia selectivity of the PET imaging agent 64Cu(II)-diacetyl-bis(N4-methylthiosemicarbazone). *J Nucl Med. 2006 Jun;47(6):989-98*

09 Peltz C, **SCHROEDER T**, Dewhirst MW. Monitoring metabolite gradients in the blood, liver, and tumor after induced hyperglycemia in rats with R3230 flank tumors using microdialysis and bioluminescence imaging. *Adv Exp Med Biol. 2005;566:343-8*

08 Moeller BJ, Dreher MR, Rabbani ZN, **SCHROEDER T**, Cao Y, Li CY, Dewhirst MW. Pleiotropic effects of HIF-1 blockade on tumor radiosensitivity. *Cancer Cell 2005, Aug;8(2):99-110*

07 **SCHROEDER T***, Yuan H, Viglianti BJ, Peltz C, Asopa S, Vujaskovic Z, Dewhirst MW. Spatial heterogeneity and oxygen dependence of glucose consumption in R3230AC and fibrosarcomas (FSA) of the Fischer 344 rat. *Cancer Research 2005, 65 (12), 1-9*

06 Walenta S, **SCHROEDER T**, Mueller-Klieser W. Lactate in solid malignant tumors: potential basis of a metabolic classification in clinical oncology. *Current Medicinal Chemistry 2004, Aug;11(16):2195-204*

05 Walenta S, Chau TV, **SCHROEDER T**, Lehr HA, Kunz-Schughart L, Fuerst A, Mueller-Klieser W: Metabolic classification of human rectal adenocarcinomas: a novel guideline for clinical oncologists? *Journal of Cancer Research and Clinical Oncology 2003, 129, 321-6*

04 Walenta S, **SCHROEDER T**, Mueller-Klieser W. In regard to Tarnawski et al., IJROBP 2002;52:1271-1276. *Int J Radiat Oncol Biol Phys. 2002, Dec 1;54(5):1576*

03 Weinmann M, Thews O, **SCHROEDER T**, Vaupel P: Expression pattern of the urokinase-plasminogen activator system in rat DS-sarcoma: role of oxygenation status and tumour size. *British Journal of Cancer 2002, 86 (8), 1355-61*

02 Walenta S, **SCHROEDER T**, Mueller-Klieser W: Metabolic mapping with bioluminescence: basic and clinical relevance. *Biomolecular Engineering 2002, 18 (6), 249-62*

01 Brizel DM, **SCHROEDER T**, Scher RL, Walenta S, Clough RW, Dewhirst MW, Mueller-Klieser W: Elevated tumor lactate concentrations predict for an increased risk of metastases in head-and-neck cancer. *International Journal of Radiation Oncology *Biology*Physics 2001, 51 (2), 349-53*

Book chapters

SCHROEDER T, Shan S, Dewhirst, MW: Anesthetic Considerations for the Study of Murine Tumor Models. In: Tumor Models in Cancer Research, Humana Press, New York City, NY. Beverly A. Teicher (Editor). 2nd edition.

Patents

1. "Compositions and methods for the treatment of cancer". PCT/US2011/030953
2. "Systems and Methods for the Automatic Quantification of Flow Dynamics". Provisional patent application (Duke Ref. DU3854PROV)

Clinical studies

SCHROEDER T. The Safety Evaluation of Aminophylline and Ambrisentan When Administered Orally Alone and in Combination to Healthy Volunteers (GQ01). Sponsor: US Defense Advanced Research Projects Agency (DARPA). *www.ClinicalTrials.gov identifyer: NCT01530464*

SCHROEDER T. A Randomized, 4-Sequence, Double-Blind Study to Test the Safety of Combined Dosing with Aminophylline and Ambrisentan in Exercising Healthy Human Volunteers at Simulated High Altitude (GQ02). Sponsor: US Defense Advanced Research Projects Agency (DARPA). *www.ClinicalTrials.gov identifyer: NCT01794078*

Strand TE und **SCHROEDER T**. The Safety Evaluation of Drug Combinations Against High Altitude Pulmonary Hypertension. Institution: Institute of Aviation Medicine, Oslo University Hospital,Oslo, Norway. Sponsor: Norwegian Armed Forces Medical Service, Oslo, Norwegen. *www.ClinicalTrials.gov identifier: NCT01566565*

Invited talks

SCHROEDER T: The importance of tumor cell respiration for the formation of the tumor microenvironment. 4th International Conference on Tumor Cell Metabolism, Louisville KY, 2006

SCHROEDER T: How lactate uptake affects the tumor microenvironment. 5th International Conference on Tumor Cell Metabolism, Louisville KY, 2009

SCHROEDER T: Lactate as a potential synthetic lethal condition in Cancer. Regulation of Metabolism in Cancer, Banbury Center of Cold Spring Harbor Laboratory, Laurel Hollow, NY, May 14-17, 2012

8.3 Publications that constitute the habilitation

1 **SCHROEDER T**, Piantadosi CA, Natoli MJ, Irwin DC, Hamilton KL, Bell C, Noveck RJ: Combined aminophylline and ambrisentan are safe and potentially efficacious to restore exercise performance in hypobaric hypoxic humans. *Accepted with minor revisions at Clin Pharm Ther*

2 Strand TE, Khiabani HZ, Boico A, Radiloff DR, Zhao Y, Hamilton KL, Christians U, Klawitter J, Noveck RJ, Piantadosi CA, Bell C, Irwin DC, **SCHROEDER T**. The Novel Combination of Theophylline and Bambuterol as a Potential Treatment of Hypoxaemia in Humans. *In Press at Can J Physiol Pharm*

3 Scalzo RL, Binns SE, Klochak AL, Giordano GR, Paris HL, Sevits KJ, Beals JW, Biela LM, Larson DG, Luckasen GJ, Irwin D, **SCHROEDER T**, Hamilton KL, Bell C. Methazolamide Plus Aminophylline Abrogates Hypoxia-Mediated Endurance Exercise Impairment. *High Alt Med Biol. 2015 Dec;16(4):331-42. PMID 26680684*

My contribution: I provided substantial input into the concept of this study, including the choice and dosing of the drugs. I also planned and conducted critical animal efficacy experiments that provided grounds for performing this study.

4 Blueschke G, Hanna G, Fontanella AN, Palmer GM, Boico A, Min H, Dewhirst MW, Irwin DC, Zhao Y, **SCHROEDER T**. Automated measurement of microcirculatory blood flow velocity in pulmonary metastases of rats. *J Vis Exp. 2014 Nov 30;(93):e51630. PMID 25490280*

5 Hanna G, Fontanella A, Palmer G, Shan S, Radiloff DR, Zhao Y, Irwin D, Hamilton K, Boico A, Piantadosi CA, Blueschke G, Dewhirst M, McMahon T, **SCHROEDER T**. Automated measurement of blood flow velocity and direction and hemoglobin oxygen saturation in the rat lung using intravital microscopy. *Am J Physiol Lung Cell Mol Physiol. 2013 Jan 15;304(2):L86-91. PMID 23161885*

6 Radiloff D, Zhao Y, Boico A, Blueschke G, Palmer G, Fontanella A, Dewhirst M, Piantadosi CA, Noveck R, Irwin D, Hamilton K, Klitzman B, **SCHROEDER T**. Anti-hypotensive treatment and endothelin blockade synergistically antagonize exercise fatigue in rats under simulated high altitude. *PLoS One. 2014 Jun 24;9(6):e99309. PMID 24960187*

7 Kennedy KM, Scarbrough PM, Ribeiro A, Richardson R, Yuan H, Sonveaux P, Landon CD, Chi JT, Pizzo S, **SCHROEDER T**, Dewhirst MW **(shared senior authorship)**. Catabolism of exogenous lactate reveals it as a legitimate metabolic substrate in breast cancer. *PLoS One. 2013 Sep 12;8(9):e75154. PMID 24069390*

8 Radiloff DR, Zhao Y, Boico A, Wu C, Shan S, Palmer G, Hamilton K, Irwin D, Hanna G, Piantadosi CA, **SCHROEDER T**. The combination of theophylline and endothelin receptor antagonism improves exercise performance of rats under simulated high altitude. *J Appl Physiol (1985). 2012 Oct 15;113(8):1243-52*

9 Manzoor AA, **SCHROEDER T**, Dewhirst MW. One-stop-shop tumor imaging: buy hypoxia, get lactate free. *J Clin Invest. 2008 May;118(5):1616-9 PMID 18431517*

My contribution: This commentary contains original data, in particular measurements of hypoxia and lactate from histological tumor slices, that substantiate the claims made in the commentary. I designed the experiments and produced and interpreted the data.

10 Sonveaux P, Végran F, **SCHROEDER T**, Wergin MC, Verrax J, Rabbani ZN, De Saedeleer CJ, Kennedy KM, Diepart C, Jordan BF, Kelley MJ, Gallez B, Wahl ML, Feron O, Dewhirst MW. Targeting lactate-fueled respiration selectively kills hypoxic tumor cells in mice. *J Clin Invest. 2008 Dec;118(12):3930-42. PMID 19033663*

My contribution: The hypothesis that lactate is consumed by cancer cells for energy gains and that this ability might lead to a metabolic symbiont that may benefit cancer cell survival in vivo arose from discussions I had with Dr. Sonveaux during the time of his postdoctoral position in 2004 and 2005 in the Duke Radiation Biology Laboratories.

8.4 Hardcopies of the publications that constitute the habilitation

Treating hypoxemia without supplemental oxygen: Combined aminophylline and ambrisentan are safe and improve hypoxic exercise performance

[1]Thies Schroeder, PhD; [2]Claude A. Piantadosi, MD, PhD; [2]Michael J. Natoli, MS, [3]Julie Autmizguine, MD, [4]Michael Cohen-Wolkowiez, MD, [5]Karyn L. Hamilton, PhD, [5]Christopher Bell, PhD, [6]Jelena Klawitter, PhD, [6]Uwe Christians, PhD [7]David C. Irwin, PhD; [2]Robert J. Noveck, MD, PhD

1. Department of Biochemistry, University of Mainz, Germany
2. Hyperbaric Center, Duke University Medical Center, Durham NC, USA
3. Department of Pharmacology, University of Montreal, Montreal QC, Canada
4. Duke Early Phase Clinical Research Unit, Duke Clinical Research Institute, Durham NC, USA
5. Department of Health and Exercise Science, Colorado State University Fort Collins, CO, USA
6. iC42 Integrated Solutions in Clinical Research and Development. University of Colorado, Bioscience East, Suite 100, 1999 North Fitzsimons Parkway, Aurora, Colorado 80045-7503, USA
7. Department of Medicine, University of Colorado Denver Anschutz Campus, Aurora CO, USA

To whom reprint requests should be sent:
Thies Schroeder, Ph.D.
Department of Biochemistry, University of Mainz
Jakob Welder-Weg 11, 55128 Mainz, Germany
Phone 1: +49 6131 392 4853
Phone 2: +49 6131 392 2967
Fax: +49 6131 392 6747
Email: thschroe@uni-mainz.de

Word count (introduction through methods): 3965 words
Number of references: 50
Number of figures: 5
Number of tables: 2
Key words: Hypoxemia, hypobaric hypoxia, combination treatment, drug safety, drug efficacy, adenosine, endothelin-1

Abstract

Hypoxemia, e.g. following rapid ascent to high altitude, causes loss of exercise endurance. We hypothesized that concomitant pharmacological inhibition of the endothelin and adenosine pathway is safe and improves exercise performance in hypoxic humans, via a mechanism that does not involve augmentation of blood oxygenation. To test this hypothesis, we established safety and drug interactions for aminophylline (500mg) plus ambrisentan (5mg) in normoxic humans. Subsequently, a placebo-controlled study was employed to test the combination in healthy resting and exercising humans at simulated altitude (4,267m). No Serious Adverse Events occurred. Drug interaction was minimal or absent. Aminophylline alleviated early mountain sickness. Aminophylline, ambrisentan, and their combination all significantly improved hypoxic exercise performance (23.8, 18.0, and 23.0% >placebo). Single-dose ambrisentan increased blood oxygenation in resting, hypoxic subjects. We conclude that combined aminophylline and ambrisentan offer promise to improve health and exercise capacity in hypoxemic humans without relying on increasing blood oxygen availability.

Introduction

Although some human subpopulations have adapted to high terrestrial altitude, hominids predominantly thrived in the lowland habitats of the African plains throughout most of their evolutionary history (1, 2). Thus, it is not surprising that when exposed to high altitude, most humans encounter health problems, such as decreased exercise endurance, acute mountain sickness (AMS), high altitude pulmonary edema (HAPE), and cerebral edema (HACE) (3-5). Similar to exercise-induced hypoxemia at sea level, diminished blood oxygenation is often thought to limit endurance at high altitude (6, 7). However, since even at 4,500 m, residual central venous oxygen saturation still approximates 60% in resting and 40% in exercising subjects, the importance of oxygen as a performance-limiting substrate is probably overestimated (8). On the other hand, systemic hypoxemia causes a battery of microvascular disorders that represent a barrier to oxygen delivery to tissue, including excessive release of the peptide hormone endothelin-1 (ET-1), which causes hypoxic pulmonary hypertension (9, 10) and capillary occlusion in the skeletal musculature (11-13). Hypoxemia also triggers global vasodilation, causing relative hypotension that is compensated by increased cardiac output (14, 15). Pharmaceutical targeting can alleviate the hypoxia-induced decline of exercise endurance in rats. Specifically, endothelin receptor A antagonists (ETRA), combined with either adenosine receptor antagonists (ARA) or hypertensive sympathomimetics, improve exercise performance of rats at altitude (13, 16). Importantly, the mechanism of this performance-restoring effect did not involve any increase in blood oxygen concentrations.

We hypothesized that the combination of the ARA aminophylline and the ETRA ambrisentan (Letairis™, Gilead) is well-tolerated in resting and exercising humans at simulated high altitude (>4,000 m) and that the combination improves exercise performance without augmenting blood oxygenation. We also tested whether the treatment would interfere with early AMS in human subjects.

Results

Study population

71 (100%) subjects were screened for **Study 1**. 40 (56.3%) qualified and 31 (43.7%) did not meet inclusion criteria (Supplemental Table 1), withdrew consent, or failed to follow-up. 22 (31.06%) were admitted, 4 (5.6%) withdrew consent and 18 (25.4%) completed the study. For **Study 2**, 91 (100%) subjects were consented, of which 58 (63.7%) did not meet inclusion criteria, 30 (33%) were enrolled, and 27 (29.7%) completed the study. Demographics are summarized in Supplemental Table 2.

Adverse Events

Study 1: 70 transient AEs occurred in nine (50%) subjects; predominantly in Period 1 (91%, Figure 1A) and after aminophylline alone (38%) or with ambrisentan (47%, Table 1). No serious adverse events (SAE) occurred. Most frequent AEs were headaches, leg cramping, tremors, and increased urinary frequency. Extremity cramping occurred only during Study 1, along with palpitations/tachycardia and facial flushing. During some of the cramping episodes, serum electrolytes [Na^{+}, K^{+}, Cl^{-}, Ca^{2+}, P^{2-}, and Mg^{2+}] were evaluated for added safety, and found to be normal.

Study 2: During Period 1 (Figure 1B), most frequent AEs were nausea, headaches, and dizziness. During Period 2, most frequent AEs were headaches and nausea (Table 1). When comparing the most common AEs (headaches, cramping, tremors, urinary frequency, dizziness/ lightheadedness, nausea/ vomiting, palpitations/ tachycardia, and fatigue) between study periods, there was a significant decrease in AEs from Period 1 to Period 2 in the aminophylline group (paired T-test, $p<0.05$). Two subjects voluntarily withdrew from procedures and revoked consent, due to intolerable side effects. Symptoms resolved after supplementation of oxygen, return to ground level, and provision of fluid and Tylenol. One subject was removed by the investigator.

Hepatic tests

Study 1: AST and ALT levels were raised over normal in one subject on Day 4 and Day 6 who had received sequence B (ambrisentan - aminophylline - combination). Liver enzymes were still elevated on Day 10, but normalized by Day 22. Highest AST and ALT levels were 80 and 162 IU/L, which was less than thrice the upper normal limit (40 and 55 IU/L, respectively), our boundary of clinical significance.

Study 2: Mildly elevated hepatic parameters were found in four subjects: Subject 25 had significantly elevated AST levels at screening that were resolved on follow-up. Subject 33 (combination treatment) had elevated bilirubin after Period 2. Subject 49 (aminophylline) had elevated ALT after Period 1. Both had resolved at follow-up. Subject 81 (ambrisentan), had elevated bilirubin after Period 2, which had resolved on follow-up.

Pharmacokinetics and analysis of bioequivalence

Pharmacokinetic (PK) analyses were done during Study 1 only. 18 subjects were analyzed after single-drug dosing, and 17 after the combination.

All analytical assays had acceptable intra-day and inter-day precision, with a coefficient of variation (CV) of <10% for theophylline (≥15 ng/ml) and < 5% for ambrisentan (≥15 ng/ml). For both drugs, inter-day accuracy averaged approximately 100% of the nominal concentrations. Lower and upper limits of quantification for theophylline were 1 ng/ml and 10,000 ng/ml, and for ambrisentan 2.5 ng/ml and 5,000 ng/ml.

Drug interaction analyses and PK data are listed in Table 2 and Supplemental Table 3. The 90% lower and upper confidence limits for both aminophylline (theophylline) and ambrisentan after combined dosing were within the 80% and 125% boundaries for the area under the plasma drug concentration versus time curve from zero to infinity ($AUC_{0\text{-}inf}$) after aminophylline single dosing. The time of peak concentration (T_{max}) for theophylline was 10% lower when administered together with ambrisentan,

compared with theophylline alone. In the case of ambrisentan, T_{max} was 20% lower when administered together with aminophylline, compared to ambrisentan alone.

Hemodynamic results

Study 1: Hemodynamic results are shown in Figure 2 (C-T). Systolic pressures increased significantly in subjects after aminophylline and combination, but not with ambrisentan, and returned to baseline at 8 h. Average systolic blood pressures post aminophylline dosing were significantly higher than post ambrisentan (Figure 2C-E). Diastolic pressures were elevated in subjects receiving aminophylline and the combination over time, but returned to baseline in both groups 10 hours post-dosing. Ambrisentan-dosed subjects had lower diastolic pressures 12 hours post-dosing, compared to baseline (Figure 2F-H). Heart rates increased significantly 6h after both aminophylline and ambrisentan. After the combination, heart rates increased at 2h and remained elevated after 24h with no differences among treatment groups (Figure 2I-L). Breathing rates increased in ambrisentan-treated subjects 10, 12, and 24h with no differences between treatment groups (Figure 2 M-O). SaO_2 was significantly reduced 6-10h post dosing in ambrisentan-treated subjects. No change in SaO_2 was found in any of the other groups (Figure 2P, Q). Treatment groups did not differ in their SaO_2 (Figure 2R). QT intervals did not change after dosing in any of the treatment groups, and no difference was found between them (Figure 2S, T).

Study 2: Hemodynamic results are shown in Figure 3. Systolic blood pressures after combination treatment were significantly lower 1h post exercise and 1h post descent than pre-ascent (Figure 3C). No differences were found between groups (Figure 3C). Diastolic blood pressures were reduced after combination treatment 2h post-ascent and 2h post-exercise, compared with time 0. There were no differences between treatment groups. Heart rates increased in all groups during exercise, compared with pre ascent and time of dosing. After exercise, heart rates remained elevated, compared to time 0, in all groups except ambrisentan. Average heart rates did not differ among groups during exercise. Top heart rates seen under maximum exercise conditions were significantly lower than maximum heart rates during (normoxic) VO_2max screening (paired T-test, $p<0.0005$). SaO_2 decreased in all

treatment groups post-ascent to altitude (Figure 3K) and continued to decline until 2h post-ascent. Hemoglobin saturation in the combination group 7 h post dosing was higher than placebo. Comparing averaged SaO_2 values between groups, blood oxygen was higher in ambrisentan-treated than in placebo subjects (Figure 3L). SaO_2 declined further during exercise in all groups (Figure 3M). Breathing rates did not change during the resting phases of Period 2, except with combination treatment, where rates increased 2h post dosing and post exercise, compared to the time of dosing (Figure 3P). When data was normalized to the time of dosing, ambrisentan post exercise had significantly lower breathing rates than both placebo and combination post exercise (Figure 3P).

Hypoxic exercise tolerance

Screening

Mean VO_2max was 49.1 ± 6.4 ml/kg/min, with values ranging from 41.8 to 64.1 ml/kg/min. Average maximum heart rate (HR_{max}) was 182.9 ± 11.8 bpm, with values ranging from 157.0 to 205.0 bpm. Mean power achieved during exercise was 241.0 ± 41.9 W, with values ranging between 145.0 and 302.2 W. Individual work rate averages were 272.1 ± 40.7 W (placebo), 231.2 ± 43.0 W (aminophylline), 234.4 ± 32.3 W (ambrisentan) and 228.6 ± 44.4 W (combination).

Hypoxic exercise

During exercise stage 1, mean power (± SD) was 73.9 ± 7.1 W (placebo), 57.6 ± 13.2 W (aminophylline), 62.1 ± 10.1 W (ambrisentan), and 59.3 ±17.1 W (combination). During stage 2, mean power was 91.1 ± 6.2 W, 76.8 ± 15.1 W, 78.6 ± 37.1 W, and 79.0 ± 36.5 W, respectively. During stage 3, mean power was 88.6 ± 27.6 W, 83.3 ± 40.7 W, 73.3 ± 37.1 W, and 79.0 ± 36.5 W. Comparing absolute individual power levels, there was no significant difference between treatment groups during any of the stages. However, when power was normalized to the individual work rate during screening, all treatment groups performed significantly better than placebo during stage 1 and stage 2, and both aminophylline and combination subjects performed better than placebo during stage 3 (Figure 5C). There was no significant difference in exercise performance among aminophylline,

ambrisentan, or the combination. A significant increase in wattage was observed between stage 1 and 2 in all groups including placebo, but no further increase between stage 2 and 3 (repeated measures ANOVA, $p<0.05$).

Acute Mountain Sickness (AMS) scores

Cumulative AMS scores increased in the placebo group at 8h, and in the aminophylline group at 4h, compared with baseline (Figure 4A). **Headaches** increased significantly during Period 1 in the placebo group (6h and 8h, vs. zero), and in the ambrisentan and combination group (8h vs. baseline, Figure 4B). Headaches did not increase after aminophylline, and headache severity was less than in the placebo group at 8h. During Period 2, headaches were generally less severe than in resting subjects, and severity did not differ between groups (Figure 4B). **Fatigue** did not change significantly during Period 1. **Dizziness**: In Period 1, aminophylline produced dizziness at 4h, followed by reversal. **Nausea**: In Period 1, aminophylline-treated subjects experienced nausea that resolved two hours later.

Discussion

Combined treatment with aminophylline and ambrisentan was tolerated relatively well by human subjects with no SAE. Drug interaction was minimal or absent. The combination improved hypoxic exercise performance without inducing a change in SaO_2.

ET-1 and hypoxemia

Alveolar hypoxia causes local constriction of pulmonary resistance arterioles (hypoxic pulmonary vasoconstriction, HPV), as part of the autonomous response that matches blood flow to ventilation (17, 18). However, extended systemic hypoxemia triggers excessive release of the powerful vasoconstrictor ET-1 by endothelial cells, which escalates pulmonary vasoconstriction pathologically (9, 10, 19-22). ET-1 binds to two main receptors ETRA and ETRB that are distributed throughout the body, and although ETRB can mediate vasodilation, the net effect of ET-1 is vasoconstriction (23, 24). Under normal conditions, constitutive release of ET-1 maintains a ubiquitous basic vascular tone,

whereas acute release antagonizes excessive vasodilation during exercise hyperemia (25-27). The importance of ET-1 as a mediator of hypoxemic dysregulation is highlighted by the observation that altitude-induced reduction of peak performance can be partially reversed by blockade of ET-1 signaling (28, 29), also supported by our findings.

ET-1 acts predominantly on vascular elements near the end of the arterial tree, including pericytes. Thus ET-1 accumulation reduces capillary filtration and oxygen transport to the parenchymatic skeletal muscle, and other organs (11, 12, 30, 31). Combined with augmented perfusion pressure, ET-1 inhibition strongly enhances tissue oxygenation under hypoxemia (13).

Hypoxemic peripheral vasodilation

In addition to ET-1 dependent vasoconstriction, hypoxemia also triggers vasodilation of extra-pulmonary resistance arteries located proximal to the central circulation, which are often identical with feed arteries (32, 33). Hypoxic vasodilation decreases systemic blood pressure, which is promptly antagonized by increased cardiac output (14, 15). Hypoxic vasodilation is part of the normal hyperemic reaction of skeletal muscle to local exercise-induced hypoxia and is partially mediated by adenosine (34). Inhibition of adenosine signaling may thus stabilize arterial perfusion pressure under hypoxemia and improve tissue perfusion (34-36).

Feasibility of combined blockade of ET and adenosine signaling in hypoxic humans

Theoretically, stabilized perfusion pressure synergizes with ETRAs to improve capillary conductance under hypoxemia. Indeed, adenosine blockade increases hypoxic exercise endurance in rats, if combined with an ETRA (16). This concept contrasts to other treatments that increase oxygen levels in the blood (37).

ET receptor type A blockade was achieved by Ambrisentan, which has low hepatotoxicity (38, 39), and worked well with theophylline in rats (16). Hepatic enzyme elevations in Study 1 were likely not caused by ambrisentan, because the elevation was stable 10 days after treatment, bilirubin was unchanged, and no other hepatotoxic events occurred. During Study 2, all four cases with elevated

liver enzymes resolved quickly, and cases were spread across treatment groups. This argues against drug treatment as a cause.

Aminophylline (theophylline) does not only block adenosine receptors, but is also an unspecific phosphodiesterase (PDE) inhibitor (40). However, PDE inhibition is only at half maximum when plasma theophylline reaches 100 µmol/l (18,016.4 ng/ml) (41). Because the mean peak drug concentration (C_{max}) for theophylline in our study approximated 7,000 ng/ml (38.9 µmol theophylline), with only one value exceeding 10,000 ng/ml, PDE inhibition was probably negligible.

An important concern was the interaction of the side effect profile of theophylline, which includes hypokalemia, hypotension, nausea, and headaches (40), with adverse effects of ambrisentan, simulated altitude, and exercise. However, there was no evidence of additive toxicity, even under heavy exercise at altitude.

Comparison of T_{max} of the drug plasma profiles did not fully rule out mutual drug interaction, however, AUC comparison suggested it was minimal or absent. The absence of drug interaction is consistent with the fact that the route of elimination of each drug is different (40, 42).

Increased blood pressures seen after aminophylline dosing in Study 1 are probably caused by adenosine blockade (43). These effects were lost in hypoxic individuals, likely because of hypoxic peripheral vasodilation.

Increased heart rates observed well after the plasma peak in resting normoxic subjects are probably unrelated to the study drugs. However, heart rates increases in Study 2/ Period 2 may be caused by environmental hypoxia (14). Although heart rates during hypoxic exercise peaked close to 200 bpm, individual peak heart rates never exceeded maximum heart rates obtained during VO_2max testing.

Average SaO_2 during hypoxia was adequate to the chosen altitude level (44). Values around 55%, as seen during exercise episodes, are not unusual during heavy activity at high altitude (45). The augmenting effect of ET-1 blockade on SaO_2 under hypoxia is known (29) and could reflect improved

ventilation-perfusion matching in the lung. Importantly, no such effect was seen with the drug combination.

Although the increase in nausea and dizziness found 4h post dosing in subjects treated with aminophylline could potentially be caused by peak plasma concentrations of the study medication, the fact that these changes were not significantly different from placebo argues against this explanation. Remarkably, aminophylline reduced AMS-associated headaches, and indeed, theophylline has shown efficacy in this respect in the past (46). However, longer observation periods are required for conclusive information about drug efficacy on AMS. Chronological assessment of AEs will be important during dose finding, to distinguish different sources of side effects.

Our data suggests that all three treatments offer a reversal of hypoxemic performance decrement in humans by approximately 18-24%, compared to placebo. It could be argued that the improved exercise performance in Study 2 might not be caused the drugs, but could be explained by a particularly weak placebo group. However, since the placebo group showed (non-significantly) better average performance during VO_2max screening than the treatment groups, this scenario is unlikely.

As part of a study in laboratory rats, which will be published separately, we found that aminophylline and the combination of aminophylline and ambrisentan, but not ambrisentan alone, improve hypoxic exercise performance. Interestingly, the combination offers a significant advantage over both single drugs during submaximal exercise burden, whereas under heavy hypoxic exercise, although both treatments remain efficacious, the synergistic advantage of the combination over aminophylline alone vanished. These results emphasize the need for dedicated efficacy studies in humans, to produce more precise information about the potential synergism between aminophylline and ambrisentan. It will be also important to further establish whether the proposed mechanism of this drug combination, i.e. concomitant stabilization of perfusion pressure and improved delivery of oxygen and nutrients to the muscle parenchyma, holds true in humans.

Conclusion

Concomitant inhibition of the adenosine and endothelin pathway is feasible and potentially efficacious to improve exercise performance in hypoxemic humans. Dose finding efforts may reveal drug synergism. This might represent a novel treatment option of hypoxemic pathologies that does not rely on increasing oxygen levels in the blood.

Methods

Clinical study protocol overview

Study 1 tested safety and drug interaction of combined, single-dose aminophylline and ambrisentan in healthy, normoxic subjects. **Study 2** investigated safety and efficacy of this combination in resting (Period 1) and exercising (Period 2) hypoxic, hypobaric subjects. Both studies were conducted at Duke University Medical Center under the FDA investigational new drug program (IND). All clinical procedures followed the principles of the Helsinki Declaration of 1975 (revised 1983) and were pre-approved by Duke University IRB. All subjects consented in writing after full explanation of study procedures. Both studies were registered with ClinicalTrials.gov (Study 1: NCT01530464, Study 2: NCT01794078).

Study 1: Assessment of the safety of aminophylline and ambrisentan co-administration at rest and under normoxic conditions

Study design

This was a Phase I, three period, two sequence, open-label, randomized crossover study. Periods 1 and 2 included oral administration of single-dose aminophylline (500mg) or ambrisentan (5mg) alone, followed by 48 hour wash out. Period 3 included the simultaneous ingestion of both drugs. Subjects were confined in the Duke Early Phase Clinical Research Unit (DEPRU) throughout study procedures. Recruitment goals were to consent enough subjects to enroll 24 and complete 16. Primary outcome measures were safety and PK alterations. Safety outcome measures were (1) AEs

(2) vital signs (respiration rate, pulse, systolic and diastolic pressure), (3) clinical blood chemistry panel, and (4) hepatic safety (AST, ALT, total bilirubin) at day 2, 4, and 6. Subjects were screened for medical history and underwent physical examination, vital signs, ECG, and blood and urine safety panels. Admission criteria were designed to ensure mental and physical ability to participate in the study, to preclude subjects that use drugs or abuse alcohol, to ensure abstinence from xanthines or other substances that may alter blood levels of the drugs, and, because ambrisentan is a suspected teratogen, to exclude pregnancy or fatherhood during the study (47). Admission criteria are listed in Supplemental Table 1.

Randomization to sequences A or B occurred on study day one. Sequence A involved ingestion of 500mg aminophylline followed by washout, then 5mg ambrisentan and washout, then their combination. Sequence B involved 5 mg ambrisentan, then 500 mg aminophylline, then combination (Figure 1A). Blood samples for PK were drawn pre-dose, and at 0.5, 1, 1.5, 2, 3, 4, 5, 6, 8, 10, 12, 16, and 24 hours post dose. Subjects had a follow-up visit 3-7 days after discharge, for physical examination, vital signs, and assessment of unresolved events (Figure 1A).

Blood processing for pharmacokinetic analyses

Two 5 mL venous blood samples were collected in pre-chilled 5 mL heparinized polypropylene vacutainer tubes. Tubes were gently agitated and placed on ice. Samples were centrifuged at 1,500 g for at least 10 minutes at 4°C, aliquoted, and stored at – 70°C or less.

Analytical procedures for theophylline and ambrisentan from human plasma

Plasma analysis for theophylline and ambrisentan followed Good Laboratory Practice standards in the facilities of iC42 Integrated Solutions (Aurora, CO USA). Drug analysis methodology is detailed in the Methods Supplement.

Plasma PK

PK parameters were computed from drug concentration-time data using non-compartmental methods within WinNonLin Phoenix Version 6.3 (Pharsight Corporation). Details are explained in the Methods Supplement.

Tests for drug interaction

Bioequivalence was analyzed to compare log (ln)-transformed plasma-time concentration results of each drug given alone and in combination. Nondifference was assumed when 90% confidence intervals of C_{max} and $AUC_{0\text{-}inf}$ after combined dosing were within 80-125% of C_{max} and $AUC_{0\text{-}inf}$ after single dosing (48).

Study 2: Assessment of the safety and efficacy of combined aminophylline and ambrisentan in resting and exercising subjects under hypobaric hypoxia

We conducted a phase 1, two-period, randomized, placebo-controlled, double-blinded, parallel study to test the safety of aminophylline and ambrisentan in resting and exercising subjects under simulated moderate high altitude. We also compared the efficacy of these compounds to reverse altitude-induced performance loss and their interference with early AMS symptoms. Subjects were screened for medical history, general health, pregnancy, drug or alcohol abuse, and adherence to admission criteria (Supplemental Table 1), followed by a test for maximum oxygen uptake capacity on a bicycle ergometer (Methods Supplement). In order to be admitted, participants had to meet at least 42 ml/kg/min VO_2max, or were admitted at the discretion of the investigator, if their VO_2max was slightly below the cut-off. Subjects were then randomized to receive either placebo, 500 mg aminophylline, 5 mg ambrisentan, or the combination of 500 mg aminophylline and 5 mg ambrisentan, with treatments remaining the same throughout period 1 and 2 (Figure 1B). Drugs and placebo were de-identified by over-encapsulation.

Period 1: Hypoxia - rest

After verification of compliance with admission criteria, urine collection, safety labs, physical examination, EKG, and vital signs assessments, subjects were brought to a pressure chamber in the Duke Hyperbaric Facility, for ascent to an equivalent of 4,267 m within approximately 15 minutes. Drugs were ingested on arrival, controlled via attending personnel. Subjects remained in the chamber for approximately 8 hours, being allowed to sit, stand, or lay down, and offered a small lunch approx. 4 hours after ascent. AEs were assessed non-systematically, initiated by study attendants or subject, and systematically, using a customized version of a standardized test of acute mountain sickness (AMS) (49). This involved hourly assessment of the severity of AMS key symptoms, such as headaches, fatigue, dizziness, and nausea, on a scale from 0 to 3. Subjects were subsequently descended and discharged (Figure 1B).

Period 2: Hypoxia - exercise

Subjects entered Period 2 no earlier than 14 days after Period 1, to avoid acclimatization. Subjects underwent verification of continued adherence to admission criteria, safety labs, urine tests for pregnancy and drugs of abuse, alcohol breathalyzer test, physical examination, ECG, and vital signs assessment. Subjects were then ascended to simulated 4,267 m and ingested study medication on arrival. AEs and AMS criteria were assessed as before. Approximately 2 hours after drug dosing, subjects performed submaximal exercise on a cycle ergometer for 20 minutes, cycling at an exercise burden of 40% of the calculated maximal exercise capacity at this altitude, based on VO_2max at screening (50). This was followed by cycling for 10 minutes at 50% of the altitude-adjusted maximal exercise capacity (Methods Supplement). After a break of approx. 5 minutes, 30 minutes cycling at self-chosen, maximal level of exercise burden ensued. Individual power output for the duration of each exercise period was expressed in Watt. After exercising, subjects were allowed to rest until an overall exposure time of 6 hours was reached and were then descended and discharged. Hepatic safety labs were done 2-4 days after discharge from each of the study periods. If anything significant emerged, follow-up labs were done 7 ± 3 Days after the test, and repeated if deemed necessary.

Statistical methods

Statistical analyses were done with GraphPad Prism (GraphPad Software, Inc., La Jolla, CA, USA). Paired ANOVA with Bonferroni correction for multiple comparisons served to analyze changes from baseline. Differences between treatment groups at the same time point, or differences between treatment groups from pooled data, were done with non-paired ANOVA w/Bonferroni correction.

Study Highlights

What is the current knowledge on the topic?

Hypoxemia, caused by high altitude, pulmonary obstruction and other conditions, reduces exercise capacity and causes serious health problems. It is often assumed that reduced oxygen concentration in the systemic blood directly translates into reduced oxygen bioavailability to tissue. However, hypoxemia also causes microcirculatory disturbance, such as pulmonary vasoconstriction, concealed hypotension, and precapillary vasoconstriction, each obstructing oxygen delivery to tissue. Hypoxemia should therefore be treatable by targeting microvascular disorder, without augmenting blood oxygen loading.

What question did this study address?

We investigated whether it is safe and efficacious to combine the adenosine receptor inhibitor aminophylline and the endothelin blocker ambrisentan in healthy resting and exercising volunteers under hypobaric hypoxia.

What this study adds to our knowledge

We demonstrate safety of combined aminophylline and ambrisentan in hypoxemic, resting and exercising healthy volunteers, and efficacy to alleviate hypoxemic exercise decrement without augmenting blood oxygenation.

How this might change clinical pharmacology and therapeutics

Besides affecting altitude medicine, this pharmacological concept could improve clinical treatment of hypoxemia, when oxygen supplementation is insufficient or unfeasible.

Acknowledgements

This work was supported by grants from the US Defense Advanced Research Projects Agency (DARPA), prime Award Number N66001-10-C-2134, and by the US Office of Naval Research, prime award number N0014-14-0699 (Irwin, Schroeder). The research was also supported by the National Center for Advancing Translational Sciences (NCATS) of the National Institutes of Health (NIH) under Award Number UL1TR001117 (Noveck, Cohen-Wolkowiez). Ambrisentan (Letairis™) was graciously supplied by Gilead, as part of a research collaboration.

Conflict of Interest/Disclosure

The authors have nothing to declare

Author Contributions

T.S. and R.J.N wrote the manuscript; T.S., C.A.P., M.J.N., K.L.H., C.B., D.C.I and R.J.N. designed the research; T.S., C.A.P., M.J.N., and R.J.N. performed the research; and T.S., M.J.N., J.A., M.C.W., J.K., U.C., and R.J.N. analyzed the data.

Literature

(1) Petousi, N. & Robbins, P.A. Human adaptation to the hypoxia of high altitude: the Tibetan paradigm from the pregenomic to the postgenomic era. *Journal of applied physiology* **116**, 875-84 (2014).
(2) Jeong, C. & Di Rienzo, A. Adaptations to local environments in modern human populations. *Current opinion in genetics & development* **29**, 1-8 (2014).
(3) Luks, A.M. *et al.* Wilderness Medical Society consensus guidelines for the prevention and treatment of acute altitude illness. *Wilderness & environmental medicine* **21**, 146-55 (2010).
(4) Maggiorini, M. Prevention and treatment of high-altitude pulmonary edema. *Progress in cardiovascular diseases* **52**, 500-6 (2010).
(5) Zafren, K. Prevention of high altitude illness. *Travel medicine and infectious disease* **12**, 29-39 (2014).

(6) Gaston, A.F., Durand, F., Roca, E., Doucende, G., Hapkova, I. & Subirats, E. Exercise-Induced Hypoxaemia Developed at Sea-Level Influences Responses to Exercise at Moderate Altitude. *PloS one* **11**, e0161819 (2016).
(7) West, J.B. Limiting factors for exercise at extreme altitudes. *Clinical physiology* **10**, 265-72 (1990).
(8) Martin, D.S. *et al.* Systemic oxygen extraction during exercise at high altitude. *British journal of anaesthesia* **114**, 677-82 (2015).
(9) Goerre, S. *et al.* Endothelin-1 in pulmonary hypertension associated with high-altitude exposure. *Circulation* **91**, 359-64 (1995).
(10) Scherrer, U., Rexhaj, E., Jayet, P.Y., Allemann, Y. & Sartori, C. New insights in the pathogenesis of high-altitude pulmonary edema. *Progress in cardiovascular diseases* **52**, 485-92 (2010).
(11) Mitchell, D., Bihari, A., Sandig, M. & Tyml, K. Endothelin-a receptor in rat skeletal muscle microvasculature. *Microvascular research* **64**, 179-85 (2002).
(12) Neuhaus, A.A., Couch, Y., Sutherland, B.A. & Buchan, A.M. Novel method to study pericyte contractility and responses to ischaemia in vitro using electrical impedance. *Journal of cerebral blood flow and metabolism : official journal of the International Society of Cerebral Blood Flow and Metabolism*, (2016).
(13) Radiloff, D. *et al.* Anti-hypotensive treatment and endothelin blockade synergistically antagonize exercise fatigue in rats under simulated high altitude. *PloS one* **9**, e99309 (2014).
(14) Bartsch, P. & Gibbs, J.S. Effect of altitude on the heart and the lungs. *Circulation* **116**, 2191-202 (2007).
(15) Naeije, R. Physiological adaptation of the cardiovascular system to high altitude. *Progress in cardiovascular diseases* **52**, 456-66 (2010).
(16) Radiloff, D.R. *et al.* The combination of theophylline and endothelin receptor antagonism improves exercise performance of rats under simulated high altitude. *Journal of applied physiology* **113**, 1243-52 (2012).
(17) Dunham-Snary, K.J. *et al.* Hypoxic pulmonary vasoconstriction: from molecular mechanisms to medicine. *Chest*, (2016).
(18) Sommer, N. *et al.* Regulation of hypoxic pulmonary vasoconstriction: basic mechanisms. *The European respiratory journal* **32**, 1639-51 (2008).
(19) Cargill, R.I., Kiely, D.G., Clark, R.A. & Lipworth, B.J. Hypoxaemia and release of endothelin-1. *Thorax* **50**, 1308-10 (1995).
(20) Morganti, A. *et al.* Effects of exposure to high altitude on plasma endothelin-1 levels in normal subjects. *Journal of hypertension* **13**, 859-65 (1995).
(21) Takahashi, H., Soma, S., Muramatsu, M., Oka, M. & Fukuchi, Y. Upregulation of ET-1 and its receptors and remodeling in small pulmonary veins under hypoxic conditions. *American journal of physiology Lung cellular and molecular physiology* **280**, L1104-14 (2001).
(22) Kylhammar, D. & Radegran, G. The principal pathways involved in the in vivo modulation of hypoxic pulmonary vasoconstriction, pulmonary arterial remodelling and pulmonary hypertension. *Acta physiologica*, (2016).
(23) Davenport, A.P. & Maguire, J.J. Endothelin. *Handbook of experimental pharmacology*, 295-329 (2006).
(24) Mazzuca, M.Q. & Khalil, R.A. Vascular endothelin receptor type B: structure, function and dysregulation in vascular disease. *Biochemical pharmacology* **84**, 147-62 (2012).
(25) Barrett-O'Keefe, Z. *et al.* Taming the "sleeping giant": the role of endothelin-1 in the regulation of skeletal muscle blood flow and arterial blood pressure during exercise. *American journal of physiology Heart and circulatory physiology* **304**, H162-9 (2013).
(26) Nishiyama, S.K., Zhao, J., Wray, D.W. & Richardson, R.S. Vascular function and Endothelin-1: Tipping the Balance between Vasodilation and Vasoconstriction. *Journal of applied physiology*, jap 00772 2016 (2016).

(27) Wray, D.W., Nishiyama, S.K., Donato, A.J., Sander, M., Wagner, P.D. & Richardson, R.S. Endothelin-1-mediated vasoconstriction at rest and during dynamic exercise in healthy humans. *American journal of physiology Heart and circulatory physiology* **293**, H2550-6 (2007).
(28) Naeije, R. *et al.* Pulmonary artery pressure limits exercise capacity at high altitude. *The European respiratory journal* **36**, 1049-55 (2010).
(29) Olfert, I.M. *et al.* Sildenafil and bosentan improve arterial oxygenation during acute hypoxic exercise: a controlled laboratory trial. *Wilderness & environmental medicine* **22**, 211-21 (2011).
(30) Lougee, L., Hinojosa-Laborde, C., Harder, D.R. & Lombard, J.H. Effect of nifedipine on endothelin induced contractions of skeletal muscle arterioles of spontaneously hypertensive rats. *Microcirculation, endothelium, and lymphatics* **6**, 355-68 (1990).
(31) Toribatake, Y., Tomita, K., Kawahara, N., Baba, H., Ohnari, H. & Tanaka, S. Regulation of vasomotion of arterioles and capillaries in the cat spinal cord: role of alpha actin and endothelin-1. *Spinal cord* **35**, 26-32 (1997).
(32) Ives, S.J. *et al.* Human skeletal muscle feed arteries studied in vitro: the effect of temperature on alpha(1)-adrenergic responsiveness. *Experimental physiology* **96**, 907-18 (2011).
(33) Lash, J.M. Contribution of arterial feed vessels to skeletal muscle functional hyperemia. *Journal of applied physiology* **76**, 1512-9 (1994).
(34) Dinenno, F.A. Skeletal muscle vasodilation during systemic hypoxia in humans. *Journal of applied physiology* **120**, 216-25 (2016).
(35) Casey, D.P. *et al.* Adenosine receptor antagonist and augmented vasodilation during hypoxic exercise. *Journal of applied physiology* **107**, 1128-37 (2009).
(36) Martin, E.A., Nicholson, W.T., Eisenach, J.H., Charkoudian, N. & Joyner, M.J. Influences of adenosine receptor antagonism on vasodilator responses to adenosine and exercise in adenosine responders and nonresponders. *Journal of applied physiology* **101**, 1678-84 (2006).
(37) Scalzo, R.L. *et al.* Methazolamide Plus Aminophylline Abrogates Hypoxia-Mediated Endurance Exercise Impairment. *High altitude medicine & biology* **16**, 331-42 (2015).
(38) McGoon, M.D. *et al.* Ambrisentan therapy in patients with pulmonary arterial hypertension who discontinued bosentan or sitaxsentan due to liver function test abnormalities. *Chest* **135**, 122-9 (2009).
(39) Kenna, J.G. *et al.* Multiple compound-related adverse properties contribute to liver injury caused by endothelin receptor antagonists. *The Journal of pharmacology and experimental therapeutics* **352**, 281-90 (2015).
(40) Barnes, P.J. Theophylline. *American journal of respiratory and critical care medicine* **188**, 901-6 (2013).
(41) Rabe, K.F., Magnussen, H. & Dent, G. Theophylline and selective PDE inhibitors as bronchodilators and smooth muscle relaxants. *The European respiratory journal* **8**, 637-42 (1995).
(42) Buckley, M.S. *et al.* Pharmacokinetic evaluation of ambrisentan. *Expert opinion on drug metabolism & toxicology* **7**, 371-80 (2011).
(43) Shen, F.M. & Su, D.F. The effect of adenosine on blood pressure variability in sinoaortic denervated rats is mediated by adenosine A2a-Receptor. *Journal of cardiovascular pharmacology* **36**, 681-6 (2000).
(44) Hittinger, E.A. *et al.* Ischemic preconditioning does not improve peak exercise capacity at sea level or simulated high altitude in trained male cyclists. *Applied physiology, nutrition, and metabolism = Physiologie appliquee, nutrition et metabolisme* **40**, 65-71 (2015).
(45) Cymerman, A. *et al.* Operation Everest II: maximal oxygen uptake at extreme altitude. *Journal of applied physiology* **66**, 2446-53 (1989).
(46) Fischer, R. *et al.* Theophylline improves acute mountain sickness. *The European respiratory journal* **15**, 123-7 (2000).

(47) Spence, R., Mandagere, A., Walker, G., Dufton, C. & Boinpally, R. Effect of steady-state ambrisentan on the pharmacokinetics of a single dose of the oral contraceptive norethindrone (norethisterone) 1 mg/ethinylestradiol 35 microg in healthy subjects: an open-label, single-sequence, single-centre study. *Clinical drug investigation* **30**, 313-24 (2010).
(48) ACDER, F.D.A.-. Bioavailability and Bioequivalence Studies for Orally Administered Drug Products — General Considerations. (ed. FDA-CDER) (Division of Drug Information, HFD-240, Center for Drug Evaluation and Research, Food and Drug Administration, Rockville, MD, 2003).
(49) Savourey, G., Guinet, A., Besnard, Y., Garcia, N., Hanniquet, A.M. & Bittel, J. Evaluation of the Lake Louise acute mountain sickness scoring system in a hypobaric chamber. *Aviation, space, and environmental medicine* **66**, 963-7 (1995).
(50) Castellani, J.W. *et al.* Effect of hypohydration and altitude exposure on aerobic exercise performance and acute mountain sickness. *Journal of applied physiology* **109**, 1792-800 (2010).

Figure legends

Figure 1

Diagram of treatment interventions

Figure 2

Hemodynamic parameters during Study 1, alongside with the respective plasma concentration of the study drugs, given alone and combined. In column three, averaged values of the treatments are compared. Asterisks indicate statistically significant differences to the value at the time of dosing (ANOVA on paired values, *$p<0.05$). A, B: theophylline and ambrisentan plasma concentrations, when given alone and in combination. C-E: systolic blood pressure. F-H: diastolic blood pressure. I-L: heart rate. M-O: breathing rate. P-R: hemoglobin oxygen saturation (SaO_2). S-U: time intervals between Q and T spikes during EKGs.

Figure 3

Hemodynamic parameters during the hypoxic studies: Column 1 contains parameters from the hypoxic study in resting subjects (Period 1). Column 2 provides averaged parameters from Period 1, excluding pre-ascent data. Column 3 contains hemodynamic parameters from the hypoxic exercising

study part, i.e. Period 2. Asterisks above the data points indicate significant differences of the respective treatment group, compared to the time of dosing (paired ANOVA). Asterisks below the data points indicate a significant difference of this data point to the placebo group (unpaired ANOVA of unpaired values). A-C: systolic blood pressure, D-F: diastolic blood pressure, G-I: heart rate, K-M: hemoglobin oxygen saturation (SaO_2), N-P: breathing rate.

Figure 4

Means and standard deviation of symptoms of acute mountain sickness, AMS, in Period 1 and B, using an abbreviated Lake Louise Score: An asterisk indicates a significant change compared to the time of dosing (ANOVA on paired values, *p<0.05, **p<0.01). A: Average cumulative score, aminophylline at 4h and placebo at 8h significantly higher than baseline. B: Average score of headaches. Placebo at 4h and all groups except aminophylline at 8h was significantly higher than at time of dosing. C: Average score of fatigue. D: Average score of dizziness. Aminophylline at 4h was significantly higher than during time of dosing. E: Average score of nausea. Aminophylline at 4h significantly higher than at time of dosing

Figure 5

Results of hypoxic exercise testing during Period 2. A: average maximum heart rates normalized to the individual maximum heart rate measured during (normoxic) screening. B: average SaO2 values normalized to the individual SaO2 right before ascent to hypobaric hypoxia. C: average power level achieved during stage 1-3 of hypoxic exercise, normalized to the power achieved during VO_{2max} testing at screening. Asterisks indicate significant difference of the treatment groups to placebo (ANOVA, p<0.05).

Table 1: Adverse Events

Study	Type of AE	Absolute no. of subjects affected by treatment					Percentage of subjects affected			
		Plac	Amino	Ambri	Combo	Mean	Plac	Amino	Ambri	Combo
#1	Headaches	N/A	2	5	2	3	N/A	11.1	27.8	11.1
	Cramping	N/A	2	3	3	3	N/A	11.1	16.7	16.7
	Tremors	N/A	4	0	2	2	N/A	22.2	0.0	11.1
	Urinary frequency	N/A	1	1	4	2	N/A	5.6	5.6	22.2
	Dizziness/light-headedness	N/A	2	0	2	1	N/A	11.1	0.0	11.1
	Nausea. vomiting	N/A	3	0	1	1	N/A	16.7	0.0	5.6
	Palpitations and tachycardia	N/A	2	0	2	1	N/A	11.1	0.0	11.1
	Fatigue	N/A	0	0	0	0	N/A	0.0	0.0	0.0
	Facial flushing & hot flashes	N/A	0	0	1	0	N/A	0.0	0.0	5.6
	Sweaty clammy hands & feet	N/A	0	0	2	1	N/A	0.0	0.0	11.1
	Feeling different & increased energy	N/A	0	0	2	1	N/A	0.0	0.0	11.1
	Anxiety & restlessness	N/A	1	0	1	1	N/A	5.6	0.0	5.6
	Hiccups	N/A	1	0	0	0	N/A	5.6	0.0	0.0
	Nasal congestion	N/A	0	1	0	0	N/A	0.0	5.6	0.0
	Contact dermatitis	N/A	0	0	1	0	N/A	0.0	0.0	5.6
	Erythema at injection site	N/A	0	0	1	0	N/A	0.0	0.0	5.6
	Number of subjects		18	18	18					
	Overall sum		25	13	29					
#2 Period 1	Headache	2	5	3	5	4	28.6	62.5	37.5	71.4
	Cramping	0	0	0	0	0	0.0	0.0	0.0	0.0
	Tremors/ Shakiness	0	1	0	0	0	0.0	12.5	0.0	0.0
	Urinary frequency	0	1	0	0	0	0.0	12.5	0.0	0.0
	Dizzy/ Lightheaded	3	6	3	3	4	42.9	75.0	37.5	42.9
	Nausea, vomiting	4	7	5	3	5	57.1	87.5	62.5	42.9
	Palpitations and tachycardia	0	0	0	0	0	0.0	0.0	0.0	0.0
	Fatigue	2	3	2	2	2	28.6	37.5	25.0	28.6

	Drowsiness	0	2	0	0	1	0.0	0.0	0.0	0.0
	Stomach ache. stomach cramping	0	0	0	1	0	0.0	0.0	0.0	0.0
	Paresthesia (Buttock. fingers/toes	0	1	0	0	0	0.0	0.0	0.0	0.0
	Number of subjects	7	8	8	7					
	Overall sum	11	26	13	14					
#2 Period 2	Headache	2	3	0	1	2	28.6	37.5	0	14.3
	Cramping	0	0	0	0	0	0	0	0	0
	Tremors/Shakiness	0	0	0	0	0	0	0	0	0
	Urinary frequency	0	0	0	0	0	0	0	0	0
	Dizzy/ Lightheaded	1	2	1	1	1	14.3	25	14.3	14.3
	Nausea, vomiting	3	1	0	2	2	42.9	12.5	0	28.6
	Palpitations and tachycardia	0	0	0	0	0	0	0	0	0
	Fatigue	0	0	0	0	0	0	0	0	0
	Drowsiness	0	0	0	0	0	0	0	0	0
	Stomach ache, stomach cramping	0	0	0	1	0	0	0	0	14.3
	Paresthesia (Buttock, fingers/toes	0	1	0	0	0	0	12.5	0	0
	Number of subjects	7	8	7	7					
	Overall	6	7	1	5					

Table 2: Drug interaction analysis

	Theophylline					**Ambrisentan**			
	AUCINF (h*ng/ml)		Tmax (min)			AUCINF (h*ng/ml)		Tmax (min)	
Subj. ID	alone	combined	alone	combined	Subj. ID	alone	combined	alone	combined
26	123955	81585	120	90	26	3208	3518	60	180
28	99967	105435	120	180	28	4893	5113	90	120
31	72291	88545	60	120	31	2454	2533	180	180
33	162993	155978	60	60	33	4266	4973	180	60
35	121526	123523	30	60	35	4433	5136	180	60
36	81773	71805	240	30	36	2327	2759	90	60
38	106825	114898	90	90	38	5175	4435	120	60
39	89363	96786	60	60	39	2921	3757	90	60
41	99631	70648	120	120	41	4198	5449	120	180
43	82068	79742	90	120	43	3715	3779	300	180
46	70088	63069	90	240	46	2819	2597	90	180
47	79839	88001	120	120	47	3691	4611	180	120
51	115582	-	180	-	51	4141	-	90	-
52	100582	95265	90	60	52	3945	4468	120	90
54	72250	63494	120	60	54	2440	2416	240	60
59	132991	144972	120	30	59	2726	3530	120	120
60	149112	173843	120	120	60	3253	3536	240	90
62	67874	63327	180	180	62	4138	4268	120	180
Geomean	98164.7	94069.6	100.9	87.8		3495.9	3812.2	132.6	104.8
SD	28062.8	33678.3	50.2	57.2		866.3	977.9	65.3	52.9
90%CI_U	109044.5	107505.1	120.4	110.6		3831.7	4202.3	157.9	125.9
90%CI_L	87284.9	80634.1	81.5	65		3160	3422.1	107.3	83.7
80% LBL	78531.8	75255.7	80.8	70.2		2796.7	3049.8	106.1	83.8
125% UBL	122705.9	117587	126.2	109.8		4369.9	4765.3	165.7	131

CI_L = lower confidence interval, CI_U = upper confidence interval, LBL = lower boundary limit, UBL = upper boundary limit

A

Study #1: Drug safety in normoxic, normobaric volunteers

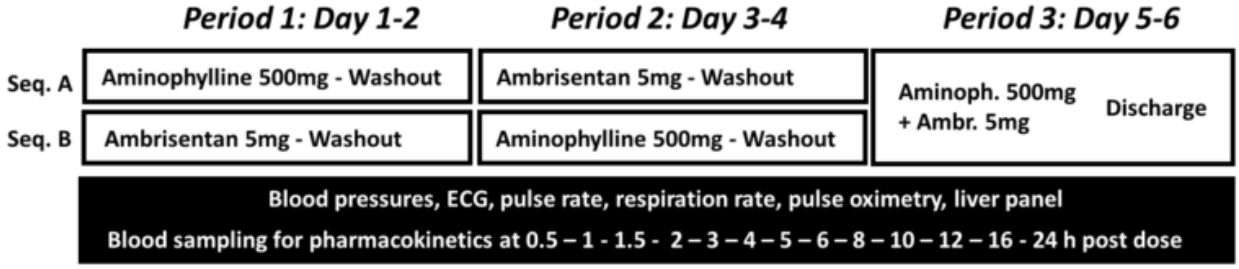

B

Study #2: Drug safety in hypoxic, hypobaric volunteers

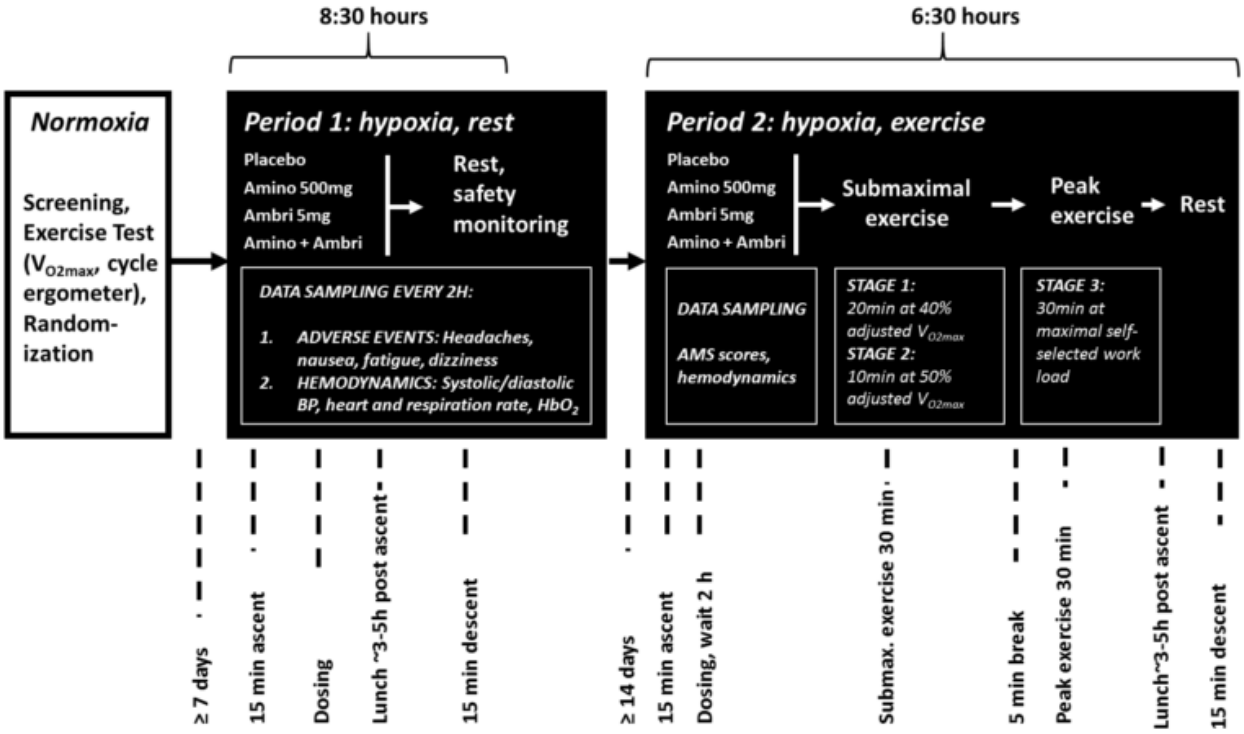

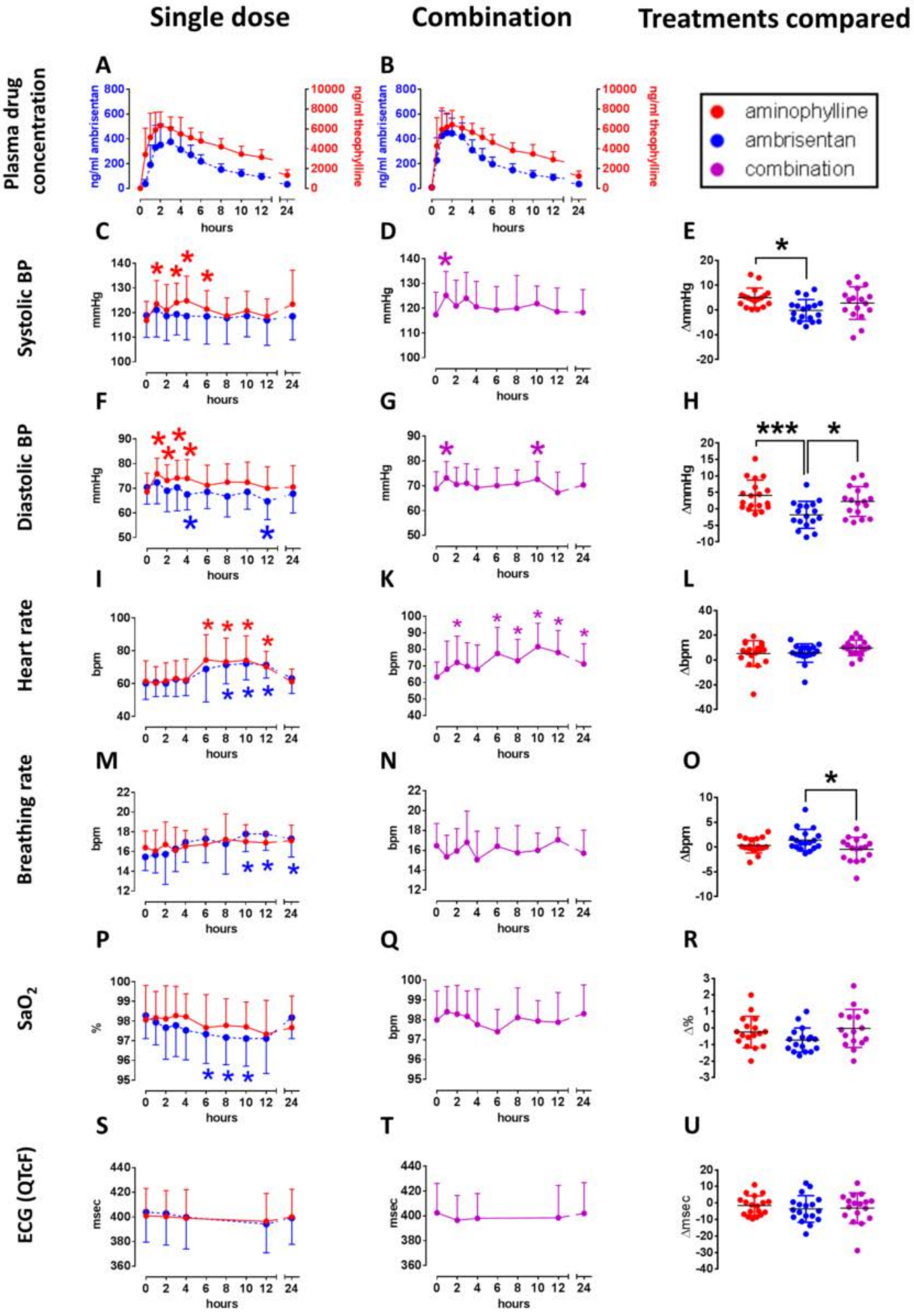
Single dose
Combination
Treatments compared
Plasma drug concentration
A
B
ng/ml ambrisentan
ng/ml theophylline
hours
aminophylline
ambrisentan
combination
Systolic BP
C
D
E
mmHg
ΔmmHg
Diastolic BP
F
G
H
Heart rate
I
K
L
bpm
Δbpm
Breathing rate
M
N
O
SaO2
P
Q
R
%
Δ%
ECG (QTcF)
S
T
U
msec
Δmsec

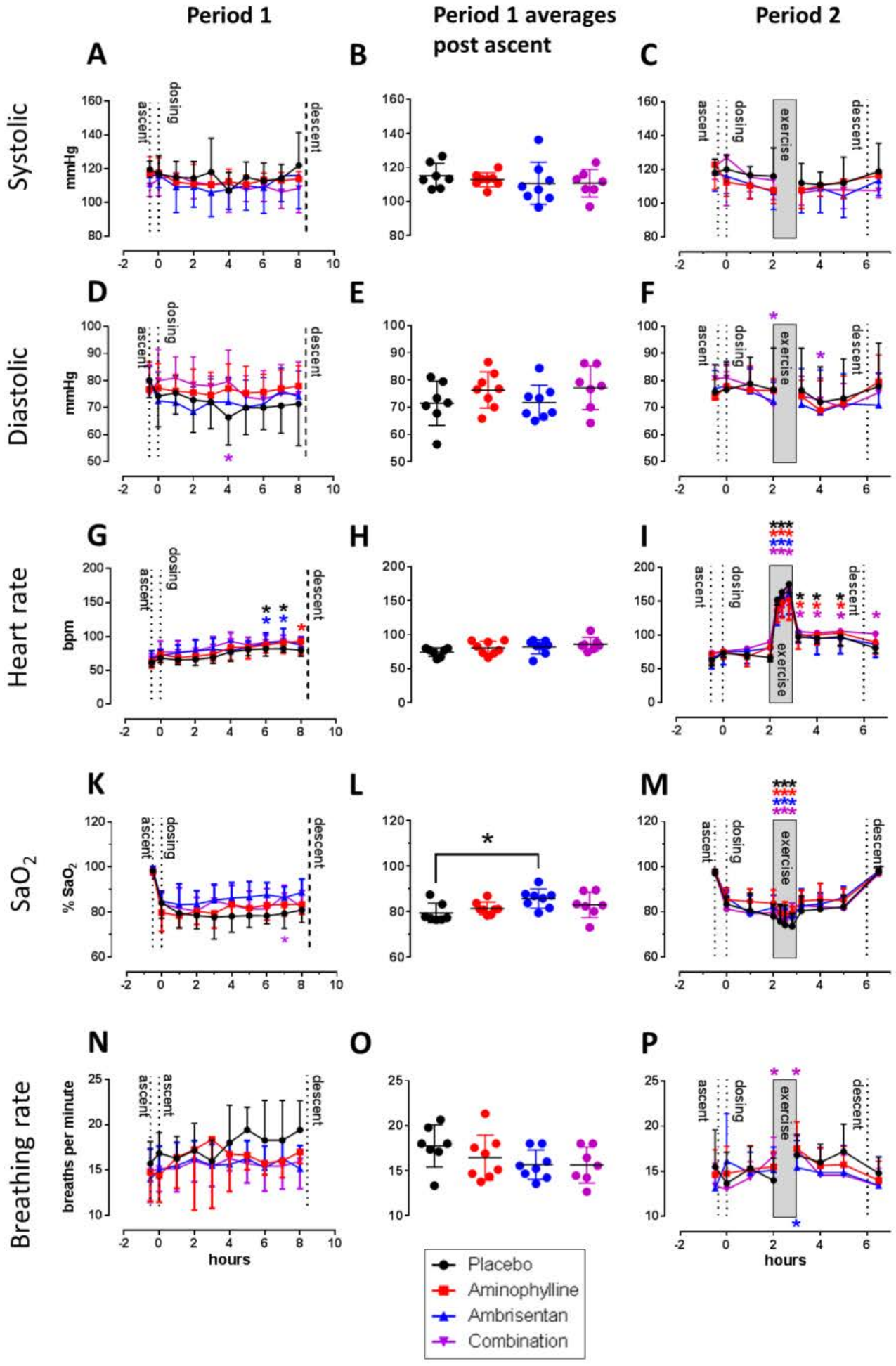
Period 1
Period 1 averages post ascent
Period 2
A
B
C
D
E
F
G
H
I
K
L
M
N
O
P
Systolic
Diastolic
Heart rate
SaO2
Breathing rate
mmHg
bpm
% SaO2
breaths per minute
ascent
dosing
descent
exercise
hours
Placebo
Aminophylline
Ambrisentan
Combination

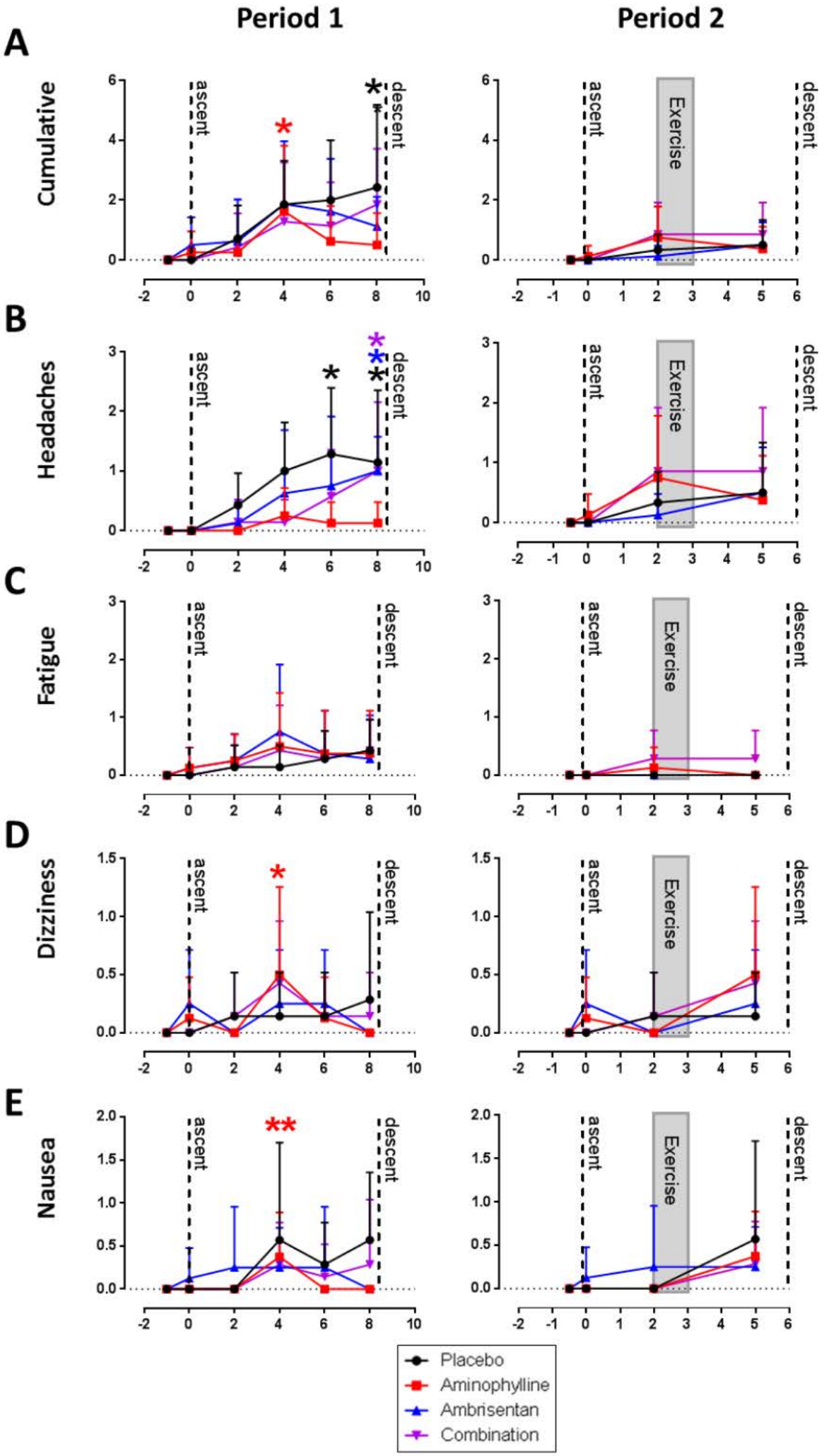
Period 1
Period 2
A
Cumulative
B
Headaches
C
Fatigue
D
Dizziness
E
Nausea
ascent
descent
Exercise
Placebo
Aminophylline
Ambrisentan
Combination

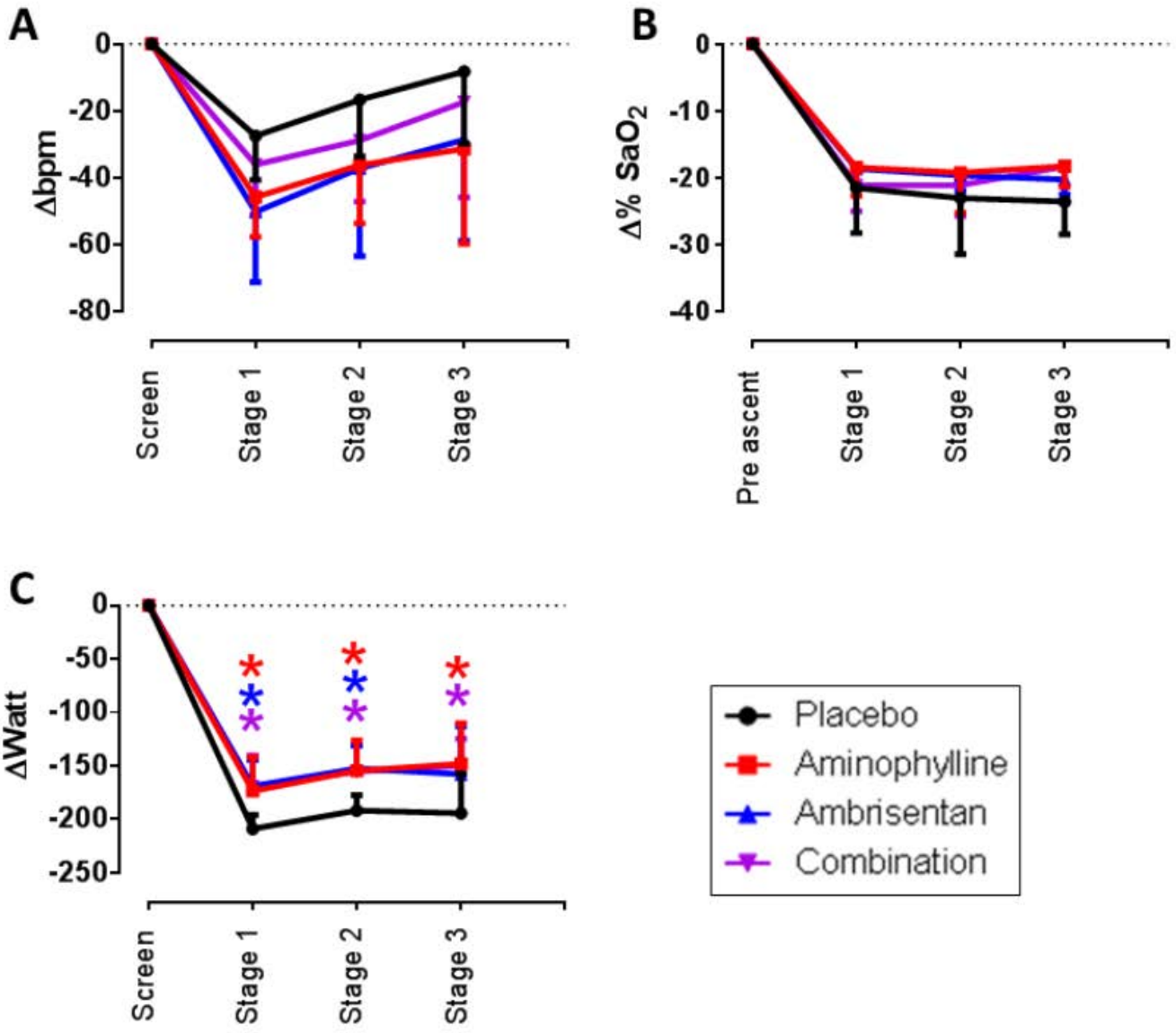
A
0
-20
-40
-60
-80
Δbpm
Screen
Stage 1
Stage 2
Stage 3
B
0
-10
-20
-30
-40
Δ% SaO2
Pre ascent
Stage 1
Stage 2
Stage 3
C
0
-50
-100
-150
-200
-250
ΔWatt
Screen
Stage 1
Stage 2
Stage 3
Placebo
Aminophylline
Ambrisentan
Combination

Methods Supplement

Analytical procedures for theophylline and ambrisentan from human plasma

Theophylline was quantified using a validated LC/MS-MS assay: Briefly, 800 µL methanol and 0.2 mmol/L $ZnSO_4$ (70/30, v/v; protein precipitation solution) were added to 200 µL plasma subject sample. Theophylline-d6 (500 ng/mL, Toronto Research Chemicals, Toronto, Canada) was added as an internal standard for theophylline (Sigma-Aldrich, St Louis, MO) to the protein precipitation solution. After centrifugation (13,000*g*, 10 min, 4˚C), 20 µL of the supernatant were injected onto the analytical column of the LC-MS/MS system (Synergi 4u Hydro-RP-80A, 250 x 3.0 mm, 4µm, Phenomenex, Torrance, CA). The mobile phases consisted of A: 0.1% formic acid and B: methanol. The column was kept at 65ºC. The HPLC system was interfaced with a triple quadrupole MS (API4000, Applied Biosystems, Foster City, CA), run in positive multiple reaction monitoring (MRM) mode. Peak area ratios obtained from MRM mode of the mass transition for theophylline (181.1→124.1 (quantifier transition; declustering potential (DP): 75V; entrance potential (EP): 10V; collision energy (CE): 29V; collision cell exit potential (CXP): 10V)) and 181.1→96.1 (qualifier transition; DP: 75V; EP: 8V; CE: 24V; CXP: 10V)) and its internal standard d6-theophylline (187.2→127.1; DP: 75V; EP: 10V; CE: 29V; CXP: 10V) were used for quantification. Following mass spectrometer parameters were used: collision gas (ultra-high pure (UHP) nitrogen): 8 L/min, curtain gas (UHP nitrogen): 20 L/min, ion source gases 1 and 2 (UHP nitrogen): 35 L/min, ion spray voltage: 4200V, temperature: 450˚C. Quality assessment involved the determination of the lower limit of quantification in 1% human serum albumin, which was found to be 1 ng/ml (LLQ) and 10 µg/ml (ULQ). Intra-day precision and accuracy was determined for the assay. Also, extraction recovery and freeze-thaw stability was tested.

Ambrisentan was quantified using a validated LC-LC/MS-MS assay. Briefly, 800 µL methanol and 0.2 mmol/L $ZnSO_4$ (70/30, v/v; protein precipitation solution) were added to 200 µL plasma subject sample. Ambrisentan-d5 (500 ng/mL, Toronto Research Chemicals, Toronto, Canada) was added as

an internal standard for ambrisentan (Toronto Research Chemicals, Toronto, Canada) to the protein precipitation solution. After centrifugation (13,000*g*, 10 min, 4˚C), 30 µL of the supernatant were injected onto the online extraction column (Eclipse XDB-C8, 4.6x12.5mm, 5µm, Agilent Technologies, Palo Alto, CA). After 0.5 minutes sample loading time onto the extraction column the sample was back-flushed onto the analytical column of the LC-LC-MS/MS system (Synergi 2.5 Hydro-RP 100A 50 x 3.00mm, 2.5 µm, Phenomenex, Torrance, CA). The mobile phases consisted of A: 0.1% formic acid and B: methanol. The column was kept at 60ºC. After 3.5 minutes, the switching valve was returned back to loading position. The HPLC system was interfaced with a triple quadrupole MS (API4000, Applied Biosystems, Foster City, CA), run in negative multiple reaction monitoring (MRM) mode. Peak area ratios obtained from MRM mode of the mass transition for theophylline (376.8→301.1 (quantifier transition; declustering potential (DP): -45V; entrance potential (EP): -10V; collision energy (CE): -30V; collision cell exit potential (CXP): -15V) and 376.8→195.1 (qualifier transition; DP: -45V; EP: -10V; CE: -20V; CXP: -15V) and its internal standard d5-ambrisentan (382.3→306.1; DP: -40V; EP: -8V; CE: -20V; CXP: -15V) were used for quantification. Following mass spectrometer parameters were used: collision gas (ultra-high pure (UHP) nitrogen): 10 L/min, curtain gas (UHP nitrogen): 20 L/min, ion source gases 1 and 2 (UHP nitrogen): 25 L/min, ion spray voltage: -4200V, temperature: 550˚C.

Plasma pharmacokinetics

It was assumed that ambrisentan concentrations were zero at the time of the first dose. The peak drug concentration (C_{max}) and time of peak concentration (T_{max}) were obtained directly from the observed data, with time zero being the time of oral administration. The disposition rate constant (λ_z) was determined as the slope of a log-linear least squares of at least 3 concentration-time points judged, by visual inspection, to be in the apparent terminal elimination phase (Tables 1-4 in appendix A and B). Half-life was calculated as $t_{1/2} = \ln 2/\lambda_z$. Partial area under the drug concentration curve (AUC_{24}) was calculated from 0-24 hours using the linear up log down trapezoidal method. The area

under the plasma drug concentration versus time curve from zero to infinity (AUC_{inf}) was obtained from $AUC_{0\text{-}last} + C_t/ \lambda_z$ where $AUC_{0\text{-}last}$ is the partial AUC from time 0 to the time of the last measured concentration and C_t is the last measurable concentration. The AUC_{inf} % extrapolated was obtained from $[(AUC_{inf} - AUC_{24})/ AUC_{inf}]*100$. Apparent oral clearance (CL/F) was calculated as CL/F = $dose/AUC_{inf}$. Apparent volume of distribution V/F was calculated as $V/F = (CL/F)/ \lambda_z$.

The single-dose pharmacokinetic (PK) parameters for theophylline and ambrisentan were computed from the drug concentration-time data after a single oral dose of aminophylline or ambrisentan and single oral dose of the same drugs in combination. Analyses were performed using non-compartmental methods within WinNonLin Phoenix Version 6.3 (Pharsight Corporation, Sunnyvale, CA, USA). It was assumed that ambrisentan concentrations were zero at the time of the first dose. The peak drug concentration (C_{max}) and time of peak concentration (T_{max}) were obtained directly from the observed data, with time zero being the time of oral administration. The disposition rate constant (λ_z) was determined as the slope of a log-linear least squares of at least 3 concentration-time points judged, by visual inspection, to be in the apparent terminal elimination phase. Half-life was calculated as $t_{1/2} = \ln 2/\lambda_z$. Partial area under the drug concentration curve (AUC_{24}) was calculated from 0-24 hours using the linear up log down trapezoidal method. The area under the plasma drug concentration versus time curve from zero to infinity (AUC_{inf}) was obtained from $AUC_{0\text{-}last}$ + Ct¬/ λ_z where $AUC_{0\text{-}last}$ is the partial AUC from time 0 to the time of the last measured concentration and Ct is the last measurable concentration. The AUC_{inf} % extrapolated was obtained from $[(AUC_{inf} - AUC_{24})/ AUC_{inf}]*100$. Apparent oral clearance (CL/F) was calculated as CL/F = $dose/AUC_{inf}$. Apparent volume of distribution V/F was calculated as $V/F=(CL/F)/ \lambda_z$. The single-dose pharmacokinetic (PK) parameters for theophylline and ambrisentan were computed from the drug concentration-time data after a single oral dose of aminophylline or ambrisentan and single oral dose of the same drugs in combination. Analyses were performed using non-compartmental methods within WinNonLin Phoenix Version 6.3 (Pharsight Corporation). It was assumed that ambrisentan concentrations were zero at the time of the first dose. The peak drug concentration (C_{max}) and time of peak concentration

(T_{max}) were obtained directly from the observed data, with time zero being the time of oral administration. The disposition rate constant (λ_z) was determined as the slope of a log-linear least squares of at least 3 concentration-time points judged, by visual inspection, to be in the apparent terminal elimination phase (Tables 1-4 in appendix A and B). Half-life was calculated as $t_{1/2} = \ln 2/\lambda_z$. Partial area under the drug concentration curve (AUC_{24}) was calculated from 0-24 hours using the linear up log down trapezoidal method. The area under the plasma drug concentration versus time curve from zero to infinity (AUC_{inf}) was obtained from $AUC_{0\text{-}last}$ + Ct¬/ λ_z where $AUC_{0\text{-}last}$ is the partial AUC from time 0 to the time of the last measured concentration and C_t is the last measurable concentration. The AUC_{inf} % extrapolated was obtained from [(AUC_{inf} - AUC_{24})/ AUC_{inf}]*100. Apparent oral clearance (CL/F) was calculated as CL/F = dose/AUC_{inf}. Apparent volume of distribution V/F was calculated as V/F=(CL/F)/ λ_z. The single-dose pharmacokinetic (PK) parameters for theophylline and ambrisentan were computed from the drug concentration-time data after a single oral dose of aminophylline or ambrisentan and single oral dose of the same drugs in combination. Analyses were performed using non-compartmental methods within WinNonLin Phoenix Version 6.3 (Pharsight Corporation). It was assumed that ambrisentan concentrations were zero at the time of the first dose. The peak drug concentration (C_{max}) and time of peak concentration (T_{max}) were obtained directly from the observed data, with time zero being the time of oral administration. The disposition rate constant (λ_z) was determined as the slope of a log-linear least squares of at least 3 concentration-time points judged, by visual inspection, to be in the apparent terminal elimination phase (Tables 1-4 in appendix A and B). Half-life was calculated as $t_{1/2} = \ln 2/\lambda_z$. Partial area under the drug concentration curve (AUC_{24}) was calculated from 0-24 hours using the linear up log down trapezoidal method. The area under the plasma drug concentration versus time curve from zero to infinity (AUC_{inf}) was obtained from $AUC_{0\text{-}last}$ + C_t/ λ_z where $AUC_{0\text{-}last}$ is the partial AUC from time 0 to the time of the last measured concentration and C_t is the last measurable concentration. The AUC_{inf} % extrapolated was obtained from [(AUC_{inf} - AUC_{24})/ AUC_{inf}]*100. Apparent oral clearance (CL/F) was

calculated as CL/F = dose/AUC_{inf}. Apparent volume of distribution V/F was calculated as V/F = (CL/F)/ λ_z.

Fitness screening and VO_2max determination

In order to minimize potential health hazards, an at least moderate level of physical fitness was required for participation in this study, i.e. the ability to take up at least 42 ml/kg/min in a heavy exercise situation, as part of the screening procedures. Subjects were first weighed and height was measured. On a cycle ergometer that was equipped with a cycle rate counter and adjustable workload, subjects were connected with a spirometer and O_2/ CO_2 gas analyzer via mouthpiece and a face mask, and a nose clamp was attached to prevent respiration through the nose. During exercise, subjects were required to maintain a constant number of rounds per minute. The following exercise protocol was applied:

Stage	Time (min)	Rounds per minute	Total Workload (watts)	Leg Load (kilopond)
1	0 - 3	75	50	0.68
2	3 - 6	75	100	1.36
3	6 – 9	75	150	2.04
4	9 – 10	75	175	2.38
5	10 – 11	75	200	2.72
6	11 – 12	75	225	3.06
7	12 – 13	75	250	3.4
8	13 – 14	75	275	3.74
9	14 – 15	75	300	4.08
10	15 – 16	75	325	4.42
11	16 – 17	75	350	4.76
12	17 – 18	75	375	5.10

13	18 – 19	75	400	5.44
14	19 – 20	75	425	5.78
15	20 – 21	75	450	6.12

To help the investigator verify whether exhaustion was truly reached, subjects were asked during every stage to describe the perceived severity of the exercise on the following scale:

Description	Rank
	6
Very, very light	7
	8
Very light	9
	10
Somewhat light	11
	12
Somewhat hard	13
	14
Hard	15
	16
Very hard	17
	18
Very, very hard	19
	20

Results for VO_2 max measurements were displayed in milliliters per kilogram per minute, representing the volume of oxygen consumed each minute per kilogram of body mass. VO_2 was calculated using the following equation:

VO_2 = [VI x %O2VI] - [VE x $\%O_2VE$]

VI = Volume of Inspired Air
$\%O_2VI$ = Percent Oxygen in Inspired Air
VE = Volume of Expired Air
$\%O_2VE$ = Percent Oxygen in Expired Air (Plowman SA, Smith DL (1997) Exercise physiology for health, fitness, and performance. Boston: Allyn & Bacon)

A VO_2 max of at least 42 ml/kg/min was required to pass screening. This value represents an educated estimate based on expert input and published data (*Mier CM, Gibson AL (2004) Occup Med (Lond) 54(6): 373-8)*, and was subject to change at the discretion of the PI, if new information became available.

Adjustment of VO_2 max from sea level to simulated high altitude of 4,267 meters

At an altitude of 4,267 m (=14,000 ft), human VO_2 max is decreased by approximately 30% (*Fulco CS, Rock PB, Cymerman A (1998) Aviat Space Environ Med 69(8): 793-801*). Therefore, a VO_2 max of 42 mL/kg/min would equate a VO_2 max $_{(altitude)}$ of 29.4 mL/kg/min. Work load during stage 1 and 2 was adjusted accordingly.

Supplemental Table 1: Admission criteria

Study 1	
Inclusion criteria	**Exclusion criteria**
Subjects must be compliant with all inclusion and meet none of the exclusion criteria	
Subjects must give written informed consent to participation in the study prior to screening. Consent will be documented by the subject's dated signature that will be counter-signed and dated by a witness. The appropriate HIPAA authorization forms must be signed and dated by the subject.	Subjects with laboratory results outside the normal range, if considered clinically significant by the Investigator. In addition, subjects must have a normal hematocrit and hemoglobin concentration and be ≥ 36% and ≥ 12.0 g/dL, respectively.
Subjects must be healthy non-smoking adult male and female volunteers between the ages of 18 and 40 years, with a BMI of 18-30 kg/m^2 and weighing at least 150 lbs. Subjects health status will be determined by the medical history, physical examination, vital signs, electrocardiogram, blood chemistry, hematology, and urinalysis performed at screening.	A mental capacity that is limited to the extent that the subject cannot provide legal consent or understand information regarding the side effects of the study drug.
Subjects must be willing to fast a minimum of 8 hours prior to screening.	Currently abusing drugs or alcohol or with a history of drug or alcohol abuse within the past two years.
Subjects must be willing to abstain from alcohol and xanthine-containing food and beverages from the time of admission to the clinical research inpatient unit through at least 48 hours following discharge.	Unwillingness or lack of ability to comply with the protocol, or to reside in the inpatient unit during the required time period, or to cooperate fully with the Principle Investigator and site personnel.
Subjects must be willing to remain in the clinical research unit continuously for the inpatient portion of the study from admission to discharge.	Use of any of the following: Any concomitant medication including oral contraceptive hormones. Subjects who have received any prescribed or non-prescribed (over-the-counter [OTC]) systemic medication, topical medications, or herbal supplements within 14 days from Day 1. St. John's Wort (hypericin) must not have been taken for at least 30 days prior to Period 1, Day 1. Any drugs, foods or substances known to be strong inhibitors or strong inducers of CYP enzymes (also known as cytochrome P450 enzymes); especially CYP 1A2, or Pgp within 30 days prior to Period 1, Day 1
Women who are of non-childbearing potential, must be: **Surgically sterile (removal of both ovaries and/ or uterus at least 12 months prior to dosing)** **Naturally postmenopausal (spontaneous cessation of menses) for at least 24 consecutive months prior to dosing on Day -1, with an FSH level at screening of ≥ 40 mIU/mL.**	Clinically significant ECG abnormality in the opinion of the Investigator.
Women of child-bearing potential must have a negative serum pregnancy test within 48 hours of receiving study drug and must agree to avoid pregnancy during study and for one month after the last dose of study drug	Vital signs or clinically significant laboratory values at the screening visit that in the opinion of the Investigator would make the subject an inappropriate candidate for the study.

Male subjects of child-bearing potential must agree to avoid pregnancy during study and for three months after the last dose of study drug.	Has taken any other investigational drug during the 30 days prior to the screening visit or is currently participating in another investigational clinical trial.
Subjects must agree not to donate blood, plasma, platelets, or any other blood components during the study and for 4 weeks after the last dose.	Made any significant donation (including plasma) or have had a significant loss of blood within 30 or 90 days prior to Period 1, Day 1.
Male subjects must agree not to donate sperm during the study and for 12 weeks after the last dose.	History or manifestation of clinically significant neurological, gastrointestinal, renal, hepatic, cardiovascular, psychological, pulmonary, metabolic, endocrine, hematologic or other medical disorders.
	Subjects who are carriers of the Hepatitis B surface antigen (HbsAg), Hepatitis C antibody, or HIV antibody
	Serious mental or physical illness within the past year.
	Male subjects who consume more than 28 units of alcohol per week and female subjects who consume more than 21 units of alcohol per week (one unit of alcohol equals 250 mL of beer, 100 mL or a medium glass of wine, or 25 mL of spirits) or those subjects who have a significant history of alcoholism or drug/ chemical abuse within the last 2 years
	Failure to agree to abstain from alcohol, cola, tea, coffee, chocolate and other caffeinated drink/ food from 2 days before dosing and throughout confinement
	Positive results on screening tests for drugs of abuse, cotinine or alcohol at screening or the pre-dose assessment at check-in
	Subjects who have used tobacco products or nicotine-containing products (including smoking cessation aids, such as gums or patches) within 12 months prior to Period 1, Day 1
	Women of childbearing potential who are pregnant (as based on test results) or are breast feeding
	Subjects who have a history of hypersensitivity or idiosyncratic reaction to any of the products administered during the study.
	Subjects who, in the opinion of the Investigator, should not participate in the study.
	Subjects who are employed by the DCRU
	Subjects who have a history of unexplained syncope; i.e., autonomic dysfunction.
	Subjects who have a history of hypotension, including orthostatic hypotension
	A positive test for hepatitis B surface antigen, hepatitis C antibody, or HIV antibody at screening.

	Lack of ability to understand verbal and/ or written English
	History of severe hypersensitivity or allergic reaction to study medication
	Failure to agree to abstain from grapefruit and grapefruit juice as well as oranges and orange juice from 10 days before the first dose and throughout the study
	History of clinically significant illness within 4 weeks prior to Day 1
	Receipt of a transfusion or any blood products within 90 days prior to Period 1, Day 1
	History of participation in another investigational study or who have participated in an investigational study within the past 30 days prior to Period 1, Day 1.

Study 2	
Inclusion criteria	**Exclusion criteria**
Subjects must be compliant with all inclusion and meet none of the exclusion criteria	
Subjects must give written Informed Consent to participate in the study prior to undergoing any screening procedures. The subject will be given a signed and dated copy of the Informed Consent.	Subjects with laboratory results outside the normal range, if considered clinically significant (CS) by the PI or delegate. In addition, subjects must have a hemoglobin concentration of ≥ 12.0 g/dL.
Subjects must be healthy non-smoking (for 6 months or greater at commencement of Period 1) adult male and female volunteers; at least 18 through 50 years at screening, with a BMI of 18-33 kg/m^2 and weighing at least 143 lbs. (65 kg). Subjects' health status will be determined by the medical history, physical examination, vital signs, ECG, blood chemistry, hematology, and urinalysis performed at screening.	A mental capacity that is limited to the extent that the subject cannot provide legal consent or understand information regarding the side effects of the study drug.
Subjects must be willing to fast a minimum of 2 hours prior to screening.	Currently abusing drugs or alcohol or with a history of drug or alcohol abuse within the past two years.
Subjects must be willing to abstain from alcohol and xanthine-containing food and beverages from 48 hours before check-in for each study day,	Unwillingness or lack of ability to comply with the protocol, or to cooperate fully with the PI and site personnel.
Women who are of non-childbearing potential, must be: **Surgically sterile (removal of both ovaries and/ or uterus at least 12 months prior to dosing) and with an FSH level at screening of ≥ 40 mIU/mL.** **Naturally postmenopausal (spontaneous cessation of menses) for at least 24 consecutive months prior to dosing on Day -1, and with an FSH level at screening of ≥ 40 mIU/mL.**	Use of any of the following: Any concomitant medication including oral contraceptive hormones. Subjects who have received any prescribed or non-prescribed (over-the-counter [OTC]) systemic medication, topical medications, or herbal supplements within 14 days from Day 1. St. John's Wort (hypericin) must not have been taken for at least 30 days prior to *Period 1*, Day 1. Any drugs, foods or substances known to be strong inhibitors or strong inducers of CYP enzymes (also known as cytochrome P450 enzymes); especially CYP 1A2, or Pgp within 7 days prior to *Period 1*, Day 1.
Women of child-bearing potential must have a negative serum or urine pregnancy test at screening, during the study, and must agree to avoid pregnancy during study and for three months after the last dose of study drug. Pregnancy is tested at screening, during check-in of each testing cycle, during the follow-up visit, and at any given point if deemed necessary to the PI or designate. During treatment, women of child-bearing potential must use two acceptable methods of contraception at the same time unless the subject has had a documented tubal sterilization or chooses to use a Copper T 380A IUD or LNG 20 IUS, in which case no additional contraception is required. Abstinence is not considered a form of contraception. Medically acceptable contraceptives include: (1) documented surgical sterilization (such as a hysterectomy), (2) barrier methods (such as a condom or diaphragm) used with a spermicide, or (3) an intrauterine device (IUD) or intrauterine system (IUS).	Clinically significant ECG abnormality in the opinion of the PI or delegate.
Male subjects must agree to take all necessary measures to avoid causing pregnancy in their sexual partners during the study and for three months after the last dose of study drug. Medically acceptable contraceptives include: (1) surgical sterilization (such as a vasectomy), or (2) a condom used with a spermicidal.	Vital signs or clinically significant laboratory values at the screening visit that in the opinion of the PI or delegate would make the subject an inappropriate candidate for the study.

Contraceptive measures such as Plan B (TM), sold for emergency use after unprotected sex, are not acceptable methods for routine use.	
Subjects must agree not to donate blood, platelets, or any other blood components 30 days, or plasma 90 days, prior to consenting and for 1 month after the last dose.	A VO_2 max value of less than 42 mL/kg/min, as determined during exercise testing at screening. This value represents an educated estimate, and may be changed, to include new information, at the discretion of the PI.
Male subjects must agree not to donate sperm during the study and for 12 weeks after the last dose.	A history of, or otherwise indicated predisposition for, claustrophobia, i.e. the fear of closed, narrow spaces (because of the limited size of the high altitude chamber).
	Has taken any other investigational drug during the 30 days prior to the screening visit or is currently participating in another investigational drug clinical trial.
	Made any significant donation or have had a significant loss of blood within 30, or donated plasma within 90 days of consenting.
	Receipt of a transfusion or any blood products within 90 days prior to commencement of *Period 1*
	History or manifestation of clinically significant neurological, gastrointestinal, renal, hepatic, cardiovascular, psychological, pulmonary, metabolic, endocrine, hematologic or other medical disorders. For the purpose of the study, individual fitness and health are more important than family history of disease burden as a criterion for participation. For example, an individual may have significant family history of cardiovascular disease; however, the individual subject's active lifestyle makes a manifestation of such disease at young ages unlikely. To account for such expected variation, the ultimate decision whether to exclude or include an individual based on family history or manifestation of disease will be made by the PI. The PI may choose to use physiological assessments, such as e.g. ECG, blood pressure, and VO_2 max fitness level as an aid for decision making.
	Any condition that might interfere with the absorption of the study medications or influence the interpretation of the results of the study.
	Subjects who are carriers of the Hepatitis B surface antigen (HbsAg), Hepatitis C antibody, or HIV antibody.
	Serious mental or physical illness within the past year.
	Male subjects who consume more than 28 units of alcohol per week and female subjects who consume more than 21 units of alcohol per week (one unit of alcohol equals 250 mL of beer, 100 mL of a medium glass of wine, or 25 mL of spirits) or those subjects who have a significant history of alcoholism or drug/ chemical abuse within the last 2 years.
	Failure to agree to abstain from alcohol, cola, tea, coffee, chocolate and other caffeinated drink/ food from 48 h before check-in for *Cycles 1 & 2*.
	Subjects who have used tobacco products or nicotine-containing products (including smoking cessation aids, such as gums or patches) within 6 months prior to commencement of *Period 1*
	Women of childbearing potential who are pregnant (as based on test results) or are breast feeding
	Subjects who have a history of hypersensitivity or idiosyncratic reaction to any of the products administered during the study.
	Subjects who, in the opinion of the PI (or delegate), should not participate in the study.
	Subjects who are employed by the Duke Clinical Research Unit and/or the Duke Hypobaric/ Hyperbaric Center

	Subjects who have a history of unexplained syncope or fainting from the collection of blood; i.e., autonomic dysfunction.
	Subjects who have a history of hypotension, including orthostatic hypotension. The ultimate decision about exclusion or inclusion of a potential subject is made by the PI.
	Lack of ability to understand verbal and/ or written English.
	History of clinically significant illness within 4 weeks prior to commencement of *Period 1*. In case a subject develops an illness between any of the study activities (Screening, *Period 1*, and Period 2), the subject may be removed from the study, if it deems appropriate and/ or necessary to the PI.

Supplemental Table 2: Demographics

Study 1				
	Age (yrs)	Sex	Weight (kg)	BMI (kg/m^2)
Mean	28.67		86.67	27.43
SD	6.51		13.28	3.31
Median	26.50	15M/3F	85.80	26.95
Min	18.00		62.20	21.90
Max	41.00		109.40	33.00

Study 2					
	Age (yrs)	Sex	Weight (kg)	BMI (kg/m^2)	Max V_{O2} (ml*kg^{-1}*min^{-1})
Mean	29.80		76.60	24.20	48.70
SD	8.40		7.00	2.50	6.20
Median	28.00	25M/2F	77.30	24.10	47.00
Min	19.00		65.80	20.40	41.80
Max	45.00		89.90	31.30	64.10

Supplemental Table 3: Pharmacokinetic parameters

Pharmacokinetic parameters for theophylline monotherapy									
Subject_ID	**Day**	**Lambda_z (1/h)**	**Half-life (h)**	**Tmax (h)**	**Cmax (ng/mL)**	**AUC_0-24 (h*ng/mL)**	**AUCinf (h*ng/mL)**	**Vz/F (mL)**	**Cl/F (mL/h)**
26	1	0.06	11.03	2	7860	97023	123955	50723.28	3186.63
28	3	0.06	11.68	2	6440	75845	99967	66561.06	3951.29
31	3	0.07	10.28	1	5560	60035	72291	81068.99	5464.06
33	1	0.06	12.03	1	8780	120314	162993	42044.49	2423.42
35	3	0.06	12.1	0.5	11420	92624	121526	56728.45	3250.34
36	1	0.08	8.71	4	5300	67746	81773	60715.94	4830.43
38	3	0.06	11.41	1.5	7260	82585	106825	60890.84	3697.62
39	1	0.13	5.26	1	9320	84215	89363	33559.53	4420.17
41	1	0.1	7.15	2	8560	89178	99631	40871.46	3964.63
43	1	0.07	9.41	1.5	5500	67522	82068	65308.48	4813.08
46	3	0.06	11.19	1.5	4800	57566	70088	90942.69	5635.77
47	3	0.07	10.24	2	5580	63504	79839	73070.53	4947.44
51	1	0.04	16.71	3	5340	73577	115582	82405.28	3417.49
52	1	0.06	12.21	1.5	6300	76097	100582	69178.6	3927.14
54	3	0.1	7.11	2	6740	65229	72250	56113.98	5467.13
59	1	0.05	13.6	2	7120	92962	132991	58279.92	2970.12
60	3	0.04	17.73	2	6740	92311	149112	67777.11	2649.02
62	1	0.09	8.08	3	5580	59967	67874	67870.63	5819.59
N		**18**	**18**	**18**	**18**	**18**	**18**	**18**	**18**
Mean		**0.07**	**10.89**	**1.9**	**6900**	**78794.47**	**101595.04**	**62450.63**	**4157.52**
SD		**0.02**	**3.15**	**0.8**	**1731.09**	**16537.85**	**28062.69**	**14847.3**	**1065.38**
Min		**0.04**	**5.26**	**0.5**	**4800**	**57565.98**	**67874.23**	**33559.53**	**2423.42**
Median		**0.06**	**11.11**	**2**	**6590**	**75970.66**	**99799.27**	**63099.66**	**3957.96**
Max		**0.13**	**17.73**	**4**	**11420**	**120313.65**	**162992.76**	**90942.69**	**5819.59**
Geometric Mean		**0.07**	**10.45**	**1.7**	**6717.04**	**77249.45**	**98164.77**	**60647.59**	**4023.85**
CV% Geometric Mean		**30.76**	**30.76**	**51.3**	**23.66**	**20.49**	**27.2**	**26.07**	**27.2**

Pharmacokinetic parameters for theophylline in combination with ambrisentan									
Subject_ID	**Day**	**Lambda_z (1/h)**	**Half-life (h)**	**Tmax (h)**	**Cmax (ng/mL)**	**AUC_0-24 (h*ng/mL)**	**AUCinf (h*ng/mL)**	**Vz/F (mL)**	**Cl/F (mL/h)**
26	5	0.1	6.78	1.5	7620	74451	81585	47378.36	4841.56
28	5	0.07	10.39	3	6720	82870	105435	56132.57	3746.39
31	5	0.05	13.17	2	5640	65740	88545	84777.31	4461
33	5	0.05	13.5	1	9840	112351	155978	49322.14	2532.41
35	5	0.06	12.53	1	8140	92498	123523	57815.83	3197.79
36	5	0.09	7.38	0.5	6000	63591	71805	58532.31	5501.01
38	5	0.07	9.96	1.5	7620	93009	114898	49377.49	3437.83
39	5	0.11	6.45	1	9720	88387	96786	38002.68	4081.16
41	5	0.12	5.99	2	8040	66555	70648	48278.82	5591.11
43	5	0.07	9.67	2	5460	65311	79742	69129.02	4953.51

46	5	0.08	8.17	4	4600	37625	63069	73775.77	6262.96
47	5	0.06	11.1	2	5440	68142	88001	71885.91	4488.58
52	5	0.06	10.8	1	6780	75036	95265	64620.09	4146.32
54	5	0.09	7.6	1	5840	56935	63494	68232.81	6221.08
59	5	0.05	15.19	0.5	8080	98499	144972	59727.62	2724.67
60	5	0.04	18.11	2	7500	105404	173843	59352.88	2272.16
62	5	0.09	7.91	3	5580	55655	63327	71215.91	6237.46
N		**17**	**17**	**17**	**17**	**17**	**17**	**17**	**17**
Mean		**0.07**	**10.28**	**1.71**	**6977.65**	**76591.71**	**98877.39**	**60444.56**	**4393.94**
SD		**0.02**	**3.37**	**0.95**	**1519.16**	**19726.55**	**33678.29**	**11910.25**	**1301.28**
Min		**0.04**	**5.99**	**0.5**	**4600**	**37625.05**	**63069.18**	**38002.68**	**2272.16**
Median		**0.07**	**9.96**	**1.5**	**6780**	**74451.38**	**88545.08**	**59352.88**	**4461**
Max		**0.12**	**18.11**	**4**	**9840**	**112350.7**	**173843.46**	**84777.31**	**6262.96**
Geometric Mean		**0.07**	**9.79**	**1.46**	**6824.82**	**74056.93**	**94069.57**	**59312.06**	**4199.02**
CV% Geometric Mean		**32.7**	**32.7**	**64.48**	**21.96**	**27.98**	**32.74**	**20.5**	**32.74**

Pharmacokinetic parameters for ambrisentan monotherapy

Subject_ID	Day	Lambda_z (1/h)	Half-life (h)	Tmax (h)	Cmax (ng/mL)	AUC_0-24 (h*ng/mL)	AUCinf (h*ng/mL)	Vz/F (mL)	Cl/F (mL/h)
26	3	0.09	8.03	1	701	2912	3208	18055.08	1558.66
28	1	0.07	10.12	1.5	436	4104	4893	14921.23	1021.97
31	1	0.12	5.69	3	456	2354	2454	16710.15	2037.1
33	3	0.11	6.26	3	589	3979	4266	10584.43	1172.1
35	1	0.08	8.36	3	615	3872	4433	13600.85	1128.03
36	3	0.09	7.52	1.5	452	2147	2327	23308.91	2148.57
38	1	0.06	11.92	2	600	4114	5175	16611.08	966.24
39	3	0.07	9.78	1.5	473	2512	2921	24147.67	1711.78
41	3	0.1	6.66	2	512	3872	4198	11434.95	1190.91
43	3	0.09	7.63	5	408	3323	3715	14814.78	1345.85
46	1	0.06	11.6	1.5	306	2293	2819	29691.36	1773.9
47	1	0.08	8.77	3	445	3128	3691	17145.07	1354.69
51	3	0.08	8.39	1.5	495	3603	4141	14605.52	1207.34
52	3	0.08	9.05	2	560	3405	3945	16537.88	1267.34
54	1	0.11	6.35	4	254	2248	2440	18777.02	2049.25
59	3	0.08	8.47	2	437	2487	2726	22402.41	1834.08
60	1	0.1	7.05	4	383	2981	3253	15621.01	1536.83
62	3	0.08	8.18	2	585	3759	4138	14261.88	1208.33
N		**18**	**18**	**18**	**18**	**18**	**18**	**18**	**18**
Mean		**0.09**	**8.32**	**2.42**	**483.72**	**3171.88**	**3596.85**	**17401.74**	**1472.94**
SD		**0.02**	**1.72**	**1.09**	**112.23**	**700.84**	**866.21**	**4795.2**	**372.47**
Min		**0.06**	**5.69**	**1**	**254**	**2147.04**	**2327.13**	**10584.43**	**966.24**
Median		**0.08**	**8.27**	**2**	**464.5**	**3225.47**	**3703.01**	**16574.48**	**1350.27**
Max		**0.12**	**11.92**	**5**	**701**	**4114**	**5174.72**	**29691.36**	**2148.57**
Geometric Mean		**0.08**	**8.16**	**2.21**	**470.36**	**3095.84**	**3495.92**	**16837.33**	**1430.24**
CV% Geometric Mean		**20.55**	**20.55**	**45.31**	**25.52**	**23.27**	**25.21**	**26.48**	**25.21**

Pharmacokinetic parameters for ambrisentan in combination therapy									
Subject_ID	**Day**	**Lambda_z (1/h)**	**Half-life (h)**	**Tmax (h)**	**Cmax (ng/mL)**	**AUC_0-24 (h*ng/mL)**	**AUCinf (h*ng/mL)**	**Vz/F (mL)**	**Cl/F (mL/h)**
26	5	0.1	6.64	3	582	3273	3518	13611.09	1421.45
28	5	0.09	7.97	2	558	4532	5113	11243.77	977.91
31	5	0.09	7.72	3	454	2352	2533	21998.19	1974.18
33	5	0.08	8.76	1	762	4522	4973	12702.04	1005.42
35	5	0.05	12.8	1	700	4139	5136	17977.24	973.44
36	5	0.07	10.02	1	462	2402	2759	26185.68	1812.15
38	5	0.07	9.25	1	528	3811	4435	15039.31	1127.43
39	5	0.07	9.74	1	705	3289	3757	18694.99	1330.85
41	5	0.08	9.12	3	665	4814	5449	12078.75	917.64
43	5	0.1	7.24	3	431	3428	3779	13815.98	1323.03
46	5	0.15	4.61	3	365	2077	2597	12795	1925.45
47	5	0.06	11.84	2	482	3668	4611	18520.14	1084.33
52	5	0.07	9.65	1.5	587	3853	4468	15577.48	1119.08
54	5	0.09	8.12	1	570	2240	2416	24229.29	2069.17
59	5	0.04	18.63	2	562	2732	3530	38063.17	1416.4
60	5	0.1	7.08	1.5	642	3313	3536	14447.96	1414.05
62	5	0.05	14.82	3	443	3338	4268	25053.04	1171.38
N		**17**	**17**	**17**	**17**	**17**	**17**	**17**	**17**
Mean		**0.08**	**9.65**	**1.94**	**558.71**	**3399.1**	**3934.03**	**18354.89**	**1356.67**
SD		**0.03**	**3.35**	**0.88**	**110.9**	**837.03**	**977.93**	**6948.8**	**375.56**
Min		**0.04**	**4.61**	**1**	**365**	**2077.14**	**2416.43**	**11243.77**	**917.64**
Median		**0.08**	**9.12**	**2**	**562**	**3338.09**	**3779.21**	**15577.48**	**1323.03**
Max		**0.15**	**18.63**	**3**	**762**	**4814.32**	**5448.77**	**38063.17**	**2069.17**
Geometric Mean		**0.08**	**9.17**	**1.75**	**548.2**	**3297.63**	**3812.24**	**17344.86**	**1311.57**
CV% Geometric Mean		**33.39**	**33.39**	**51.19**	**20.46**	**26.26**	**26.87**	**34.37**	**26.87**

λ_z: elimination rate. T_{max}: time to maximum concentration. C_{max}:maximum concentration. AUC_{0-24}: AUC from 0 to 24h. AUC_{inf}: AUC from 0 to infinity. Vz/F: apparent volume of distribution. CL/F: apparent oral clearance. SD: standard deviation. CV: coefficient variation

The Novel Combination of Theophylline and Bambuterol as a Potential Treatment of Hypoxemia in Humans

Trond-Eirik Strand (M.D., Ph.D.)[1], Hasse Z Khiabani (M.D., Ph.D.) [2], Alina Boico (B.S.)[3], Daniel Radiloff (Ph.D.)[4], Yulin Zhao (M.D.)[3], Karyn L. Hamilton (Ph.D.)[5], Uwe Christians (Ph.D.)[6], Jelena Klawitter (Ph.D.)[6], Robert J. Noveck (M.D., Ph.D.)[7], Claude A. Piantadosi (M.D.)[8], Christopher Bell (Ph.D.)[5], David Irwin (Ph.D.)[9] , Thies Schroeder (Ph.D.)[9,10]

1. Norwegian Armed Forces Medical Services, Institute of Aviation Medicine, Oslo, Norway
2. Department of Pharmacology, Oslo University Hospital, Rikshospitalet, Oslo, Norway
3. Department of Radiation Oncology, Duke University Medical Center, Durham NC, USA
4. Taconic Biosciences, Hudson NY, USA
5. Department of Health and Exercise Science, Colorado State University, Fort Collins CO, USA
6. iC42 Integrated Solutions in Clinical Research and Development, University of Colorado Denver, Anschutz Medical Campus, Aurora CO, USA
7. Department of Medicine, Duke University Medical Center, Durham NC, USA
8. Hyperbaric Center, Duke University Medical Center, Durham NC, USA
9. Department of Medicine, University of Colorado Denver, Anschutz Medical Campus, Aurora CO, USA
10. Department of Biochemistry and Pharmacology, University of Mainz, Germany

To whom communication should be directed:
Thies Schroeder, PhD
Department of Biochemistry
University of Mainz
Jakob Welder-Weg 11
55128 Mainz, Germany
Phone 1: +49 +6131 39-22967
Phone 2: +49 +6131 39-24853
Fax: +49 6131 39-26747
Email: thschroe@uni.mainz.de

Short running title: Drug combination to alleviate hypoxemia

Abstract

Hypoxemia can be life-threatening both, acutely and chronically. Because hypoxemia causes vascular dysregulation that further restricts oxygen availability to tissue, it can be pharmacologically addressed. We hypothesized that theophylline can be safely combined with the β2 adrenergic vasodilator bambuterol to improve oxygen availability in hypoxemic patients. Ergogenicity and hemodynamic effects of bambuterol and theophylline were measured in rats under hypobaric and normobaric hypoxia (12% O_2). Feasibility in humans was assessed using randomized, double-blind testing of the influence of combined slow-release theophylline (300 mg) and bambuterol (20mg) on adverse events (AEs), plasma K^+, pulse, blood pressure, and drug interaction. Both drugs and their combination significantly improved hypoxic endurance in rats. In humans, common AEs were low K^+ (<3.5mmol/L, bambuterol: 12, theophylline: 4, combination: 13 episodes) and tremors (10, 0, 14 episodes). No exacerbation or SAE occurred when drugs were combined. A drop in plasma K^+ coincided with peak bambuterol plasma concentrations. Bambuterol increased heart rate by approx. 13 bpm. Drug interaction was present but small. We report promise, feasibility and relative safety of combined theophylline and bambuterol as a treatment of hypoxemia in humans. Cardiac safety and blood K^+ will be important safety endpoints when testing these drugs in hypoxemic subjects.

Key words: Hypoxemia, hypoxia, combination therapy, xanthine drugs, beta adrenergic receptor agonist, drug safety, bioequivalence, human study, animal study

Clinical trials: This study contains results from a human clinical trial. The description of the trial lists under the following URL: https://clinicaltrials.gov/ct2/show/NCT01566565

Introduction

Lack of oxygen in the blood, hypoxemia, can be caused by various conditions, such as environmental shortage of oxygen ("thin air" at high altitude), obstruction of air flow (chronic obstructive pulmonary disease, pneumonia, pulmonary fibrosis), inefficient oxygen loading of the blood (anatomic shunting, anemia) and central nervous dysregulation (anesthesia, central sleep apnea). While severe hypoxemia (<75% SaO_2) requires immediate intervention, moderate hypoxemia (75-89%) leads, in the short term, to decreased physical endurance. However, long-term consequences of chronic hypoxemia can be much more serious, involving digital clubbing, progressive pulmonary remodeling and pulmonary arterial hypertension (PAH), and right ventricular failure (Kim et al. 2015; Nakamura et al. 2002; H. Zhang et al. 2015). Hypoxemia is usually treated with supplemental oxygen (Fromm et al. 1994), however, when oxygen supplementation is insufficient or difficult to achieve, such as during severe PAH or at high altitude, a pharmacological relief of hypoxemia would be a useful alternative.

Hypoxemia can be pharmacologically targeted by inhibiting its downstream dysregulation that further reduces oxygen availability to tissue: for example, hypoxemia triggers the release of the vasoconstrictive protein hormone endothelin-1, which contributes to reduced uptake of oxygen by causing ventilation-perfusion mismatching in the lung (Kylhammar et al. 2016). Endothelin-1 can also lead to vasoconstriction of terminal elements of the arterial tree, thus negatively affecting capillary blood flow in the terminal circulation and further reducing transport and availability of oxygen to tissue (Barrett-O'Keefe et al. 2013; Borysova et al. 2013; Hall et al. 2014; Murray et al. 2016; Neuhaus et al. 2016). Consequently, anti-vasoconstrictive therapy with endothelin-1 blockade demonstrates efficacy to relieve oxygen shortage to tissue by inhibiting these known dysregulations (Kawano et al. 2007; Naeije et al. 2010; Pitsiou et al. 2009). Since additional factors, such as prostaglandins and adenosine, are involved in hypoxemic dysregulation of tissue hemodynamics, combination treatment might be more effective than monotherapy in improving the supply of oxygen to tissue during hypoxemia (Dayan et al. 2016; Dubrey et al. 2016; Gouyon et al. 1988). We recently demonstrated

that the combination of the xanthine drug theophylline and an endothelin-blocking vasodilator improves exercise performance capacity of hypoxemic rats (Radiloff et al. 2012). This treatment, which we have recently tested for safety in humans (ClinicalTrials.gov, NCT01530464 and NCT01794078), has the advantage that it does not rely on increasing SaO_2, but rather accelerates the rate of oxygen transport to the skeletal muscle. However, not all hypoxemic patients respond equally well to endothelin receptor antagonism (Jain et al. 2016) and thus, alternative treatment options would be useful. Because β-adrenergic receptors are also strongly involved in pulmonary and peripheral blood flow regulation (Blauw et al. 1995; Leblais et al. 2008; Nagai et al. 2014), we hypothesize that the combination of theophylline with a β-adrenergic receptor agonist has also beneficial effects. We further hypothesize that this combination is, in principle, feasible in humans. To test this hypothesis, we have chosen the long-acting β-agonist bambuterol as a combination partner for theophylline, which is orally available and has a plasma half-life comparable to theophylline.

Methods

Measurement of exercise capacity of theophylline- and bambuterol-treated rats under hypobaric hypoxia

These animal procedures were pre-approved by Duke University Institutional Animal Care and Use Committee (DUIACUC) and were carried out in accordance with the *Guide for the Care and Use of Laboratory Animals* (1996, published by National Academy Press, 2101 Constitution Ave. NW, Washington, DC 20055, USA). Bambuterol and theophylline were administered intraperitoneally (IP). Theophylline was dosed at 15 mg/kg and bambuterol at either 0.05 mg/kg (high dose) or 0.01 mg/kg (low dose). Only the low dose was tested in combination with theophylline. Female Sprague Dawley rats were consistently used for all exercise experiments as reported (Radiloff et al. 2012). Procedures to measure exercise performance capacity at simulated high altitude in rats have also been published (Radiloff et al. 2012). In brief, rats were habituated to running in motorized wheels (Figure 1A,

Lafayette Instruments, Lafayette, IN) at a slow pace for approximately 10 days, to teach them to run in a motorized wheel while avoiding physical training effects. On days of drug efficacy testing, the animals were injected i.p. with the study drug or control treatment and then transferred to individual running wheels inside a hypobaric chamber accompanied by an investigator (Figure 1A). The air was then evacuated from the chamber until an atmospheric equivalent of 4,267 m (approx. 0.6 atm) was reached. Wheel motion was started 30 minutes post injection of the study drugs, at 3 meters per minute, was then increased to 9 m/min, and finally to 12 m/min (Figure 1B). Signs of exhaustion caused the removal of individual animals from the wheel, followed by a short test to confirm fatigue (Radiloff et al. 2012). After the run, all animals were returned to sea level and euthanized using CO_2, as determined by the protocol.

Hemodynamic studies in awake, theophylline- and bambuterol-treated rats in normoxia and hypoxia

In order to address safety concerns ahead of combining theophylline and bambuterol in hypoxemic humans, we have employed a rat model to monitor mean arterial pressures, heart rates, and plasma concentrations of K^+. These animal procedures were pre-approved by the UC Denver Institutional Animal Care and Use Committee (IACUC) and were carried out in accordance with the *Guide for the Care and Use of Laboratory Animals* (1996, published by National Academy Press, 2101 Constitution Ave. NW, Washington, DC 20055, USA). An awake hypoxic rat model was used to study changes in hemodynamics and blood chemistry, as described previously (Irwin et al. 2008). Briefly, male Sprague Dawley rats of 280-350 g were anesthetized and equipped with chronic indwelling catheters into the carotid and pulmonary artery, and vena cava for hemodynamic and cardiac output measurements. Treatments were administered through the jugular catheter. Rats were randomized into four treatment groups (vehicle, theophylline, bambuterol and the combination of theophylline and bambuterol) and placed into a gas-controlled Plexiglas chamber with a portal for catheter access. Breathing gas was normal (21% O_2) and hypoxic air (12% O_2, Figure 1C). Blood pressures and heart

rates were measured through pressure transducers, and blood chemistries were measured from samples collected from arterial and venous catheters, as described previously (Irwin et al. 2008).

Criteria for human study participation

Candidates were recruited in Oslo, Norway, and the human study was conducted at the Oslo University Hospital, Rikshospitalet. Healthy, non-smoking adults between 18 and 40 years old (both genders) were eligible for study participation if they were willing to fast 8 hours prior to screening, abstain from alcohol or xanthine-containing food or beverages for at least 48 hours before admission to meeting all of the inclusion and none of the exclusion criteria, which are listed in Supplementary Table 1.

Clinical study design

This was an open-label, two-sequence, three-period, randomized crossover study. Study subjects (n=20 at study start, 3 withdrew during the study) were randomized into one of two sequences to receive either a single dose of theophylline slow release (Theo-Dur, 300 mg) or bambuterol (Bambec, 20 mg, period 1). After a washout time of 96 hours, dosing schedules were crossed over to receive the second study drug (period 2). After a second washout period of 96 hours, all subjects received both drugs concomitantly (period 3). Subjects were discharged following another washout of 96 hours (Figure 1D). The study was conducted in compliance with the Declaration of Helsinki and with international guidelines of Good Clinical Practice (GCP). All procedures were approved by the appropriate regulatory bodies, which include Norwegian Medicines Agency and local Ethics Committee. All study subjects gave informed written consent before commencement of study procedures.

Pharmacokinetic evaluations

Whole blood samples for analysis of drug metabolites and plasma K^+ concentrations were collected at the following time points: 0.5, 1, 2, 3, 4, 5, 6, 8, 10, 12, 24 hr using a small indwelling venous catheter. Sodium heparin (20-30 U/ml) was used to maintain catheter patency prior to and/or during

the collection periods. A 5-7 ml venous blood sample was collected at the specified times in pre-chilled polypropylene Vacutainer tubes containing sodium heparin for the preparation of plasma. The tube containing blood was gently inverted at about 6-8 times to ensure thorough mixing of anticoagulant with blood and placed into an ice-water bath until centrifuged. The samples were centrifuged at 1500 g for at least 10 minutes at 4°C. Immediately after centrifugation, the plasma was separated into aliquots of at least 2-3 mL. All aliquoted samples for pharmacokinetics analysis were stored at -80°C until shipment.

Theophylline was analyzed at the Department of Biochemistry, Oslo University Hospital, following the procedure outlined for the Cobas 8000 C502 analyzer (Roche/Hitachi). The analysis was based on the kinetic interaction of micro particles in solution (KIMS). Theophylline antibody is bound covalently to micro particles and drug derivatives are linked to a macromolecule. The kinetic interaction of micro particle in resolutions induced by the drug derivatives bind to the antibody on the micro particles and is inhibited by the presence of theophylline. There is a competitive reaction between the substance conjugate and theophylline to bind to theophylline antibody on micro particles. The subsequent kinetic interaction of micro particles is indirectly proportional to the amount of substance in the sample. The method was linear from 0.8-40.0 µg/mL (4.4-222 µmol/L) for theophylline and the lower limit of quantification was 0.8 µg/mL. Samples having higher drug concentrations were diluted with Preciset TDM I diluent (0 µg/mL) (1 + 1) and re-assayed. The lower detection limit representing the lowest measurable analyte level that could be distinguished from zero was calculated as the value lying two standard deviations above that of the 0 µg/mL calibrator (standard 1 + 2 SD, repeatability, *n* = 21).

After shipment of blood samples on dry ice, bambuterol and its active metabolite terbutaline were analyzed by iC42 Integrated Solutions in Clinical Research and Development (Aurora, CO, USA) using high-performance liquid chromatography- tandem mass spectrometry (LC-MS/MS). In brief, for quantification of bambuterol and terbutaline in EDTA plasma, 800 µL methanol and 0.2 mmol/L ZnSO4 (70/30, v/v; protein precipitation solution) were added to 200 µL sample. Terbutaline-d9

(Toronto Research Chemicals (TRC), Toronto, Canada) was added as an internal standard to the protein precipitation solution. After centrifugation (13,000g, 10 min, 4˚C), 50 µL of the supernatant were injected onto the analytical column of the LC-MS/MS system (SB-C18, 250 x 4.6 mm, 5 µm, Agilent Technologies, Santa Clara, CA). The HPLC mobile phases consisted of either 0.1% formic acid or methanol/acetonitrile (1:1, v/v). Calibrators and quality control samples were run with each study sample batch. Calibration curves were linear with $r^2 > 0.99$, accuracy of the quality control samples was within 85-115% of the nominal concentrations and imprecision was <15%.

Safety evaluation in the human trial

Safety was determined by recording adverse events, laboratory endpoints (in particular plasma K^+), and vital signs. K^+ was measured using an ABL 825 Flex blood gas analyser (Radiometer, Copenhagen, DK). All parameters were accredited for ISO 15189 and 22870 (POCT) by the Norwegian Accreditation authorities. Cardiac safety was assessed by comparing 12-lead electrocardiograms collected at pre-dose with those collected at 2, 4, and 12 hours post dose.

Statistics

Rats study: assessment of ergogenicity under hypobaric hypoxia

Individual endurance data for each animal was plotted using the Kaplan-Meyer method. Treatment effects were determined by comparison with the vehicle control using Log Rank Test and GraphPad Prism as statistics software. *P* values of less than 0.05 were considered statistically significant.

Rat study: hemodynamic analysis in awake rat under normoxia and hypoxia

Differences in longitudinal parameters, i.e. between baseline, post drug injection, post hypoxia, and return to normoxia, were assessed using two-tailed, paired T-test. Analysis of variance (Kwon et al. 2015) was not used for this part of the analysis, to permit matched comparison if a parameter was missing. Cross-sectional differences between treatment groups were analyzed using ANOVA. Statistical software was GraphPad Prism (GraphPad Software, San Diego, CA, USA).

Human study: pharmacokinetic analysis

The pharmacokinetics of both study drugs alone and in combination was estimated using a non-compartment model. Pharmacokinetics and bioequivalence analyses were carried out using the WinNonlin software (Phoenix, version 6.4., Pharsight/Certara, Princeton, NJ, USA).

The presence of pharmacokinetic drug-drug interactions was assessed using bioequivalence metrics as recommended by the 2012 FDA-CDER guidelines "Guidance for Industry. Drug Interaction Studies — Study Design, Data Analysis, Implications for Dosing, and Labeling Recommendations", whereas no pharmacokinetic drug-drug interaction is assumed if the 90% confidence intervals of the geometric mean test/reference ratios of C_{max} and AUC_{0-T} fall entirely within the 80-125% equivalence limits. The bioequivalence analysis was based on ln-transformed drug concentrations and included mixed effect model, sequence, period, and treatment as fixed effects and subject with sequence as a random effect.

Human study: power consideration for bioequivalence testing

The standard bioequivalence acceptance limits of 80-125% were used to demonstrate that exposure to the test drug (co-administration of bambuterol and theophylline) was bioequivalent to the reference drug (bambuterol or theophylline alone). The within-subject coefficient of variation (CV) was expected to be approximately 20% and the mean ratio was expected to be unity ($\mu_{GT}/\mu_{RT} = 1.0$). Although this study was a three-period design, sample size was estimated based on an AB/BA two period crossover design. For a type I error rate of 5%, 16 subjects resulted in >80% statistical power (Julious 2004).

Statistics: side-by-side comparisons between treatment parameters at all time points were carried out to investigate whether the drug combination would change vital signs, compared to the single drugs. This analysis was done from raw values, using ANOVA with correction for multiple comparisons.

Human study: hemodynamic assessments

Significance in changes in hemodynamic parameters over time within a treatment group was assessed using paired ANOVA. Significant difference between treatment groups were analyzed using ANOVA on data that was normalized to the respective value at the time of dosing.

Results

Assessment of ergogenic effects of theophylline and bambuterol on hypoxic exercise performance of rats

Rats that were treated with bambuterol (0.05 mg/kg, i.p.) ran significantly longer under simulated high altitude at 4267 m than the control-treated group (Figure 2A). Treatment with theophylline (15 mg/kg, i.p.) also significantly increased exercise performance in hypoxic hypobaric rats (Figure 2B). When given at a lower dose (0.01 mg/kg), bambuterol in combination with theophylline (15 mg/kg) increased the time run to fatigue, whereas the single treatments did not (Figure 2C). Animal numbers were 43-45 per treatment group in Figure 2A-B, and 10 per group in Figure 2C.

Pre-clinical safety assessment of combined theophylline and bambuterol in awake normoxic and hypoxic rats

Treatment with theophylline and bambuterol significantly decreased Mean Arterial Pressure (MAP) compared with control and combination: MAP dropped in all groups from an average of 132 ± 13 mmHg at baseline (1) to 129 ± 13 mmHg post injection (2), then to 114 ± 14 mmHg during hypoxia (3), and 126 ± 12 mmHg after return to normoxia (4) (Figure 2D). While hypoxia itself did not have an effect on heart rates, treatment with theophylline, both alone and in combination with bambuterol, increased heart rates under hypoxia (Figure 2E). None of the treatments altered plasma K^+, compared to controls. Hypoxia significantly reduced plasma K^+ stores in all treatment groups and controls (time point #1: 74 ± 0.4, #2: 3.4 ± 0.2, #3: 2.8 ± 0.2, #4: 2.7 ± 0.2 meq/L) and levels did not recover after return to normoxia (Figure 2F). Hemoglobin saturation decreased in all groups with

onset of hypoxia, but not significantly different in any single treatment group, compared with the other (Figure 2G).

Clinical study population

Of 37 candidates that responded to invitation, 26 were screened and 20 were included into the study. Of these, 19 (17 male, 2 female) subjects presented for study procedures (Table 1). Subjects were between 19 and 31 years of age, 169 to 195 cm tall, weighed 69.3 to 98.2 kg, were non-smokers and had an alcohol consumption of 0-23 units per week, with one unit equaling 250 mL of beer, 100 mL or a medium glass of wine, or 25 mL of spirits.

Safety outcomes and adverse events

Adverse events are listed in Table 2. The most common adverse event was low plasma K^+ and tremors both associated with bambuterol treatment. Although two subjects terminated early following the occurrence of adverse events, no hospitalization was necessary and no SAEs were recorded during the study. An inverted T-wave was observed for one subject, respectively, with both theophylline and bambuterol, but not with the combination. No other abnormal ECG-values were observed as part of any of the scans, pre- and post-dose.

Clinical hemodynamics and blood chemistry outcomes

Hemodynamic measurements and measurements of plasma K^+ concentrations in human subjects are shown in Figure 3, alongside with the respective average plasma drug concentration (Figure 3A, B). A significant drop in plasma K^+ concentration was found after treatment with bambuterol, alone and in combination with theophylline, whereas no significant drop in plasma K^+ was found after treatment with theophylline alone. The drop in plasma K^+ concentrations after bambuterol treatment roughly coincided with the peak terbutaline concentration in plasma after 4 hours (Figure 3C). The addition of theophylline to bambuterol did not aggravate plasma K^+ concentrations: side-by side comparison revealed no significantly reduced plasma K^+ concentration in combination-treated vs. bambuterol-treated subjects in any time point, although both were significantly lower than in theophylline-

treated subjects at time points 6-10 (Figure 3D). Systolic blood pressures did not change in response to any treatment, and did also not differ between any of the treatments, when compared side-by side (Figure 3E, F). Diastolic blood pressures experienced a significant drop 8 hours after treatment with bambuterol alone, but neither did so with theophylline, nor with combined treatment. No differences were found in diastolic blood pressures between treatments in any of the time points (Figure 3G, H). Heart rates increased significantly approx. 3 hours after treatment with bambuterol, alone and in combination with theophylline, and remained elevated even after 24 hours, compared to baseline (Figure 3I, K). Heart rates did not increase after theophylline alone, and while both bambuterol and combination caused significantly higher heart rates compared to theophylline alone (time points 2, 4-12), they did not increase significantly with the combination, compared to bambuterol alone (Figure 3I).

Pharmacokinetic evaluation and bioequivalence testing outcomes

In human study samples, bambuterol concentrations in plasma were only sporadically found above the lower limit of quantification of 0.05 ng/mL and therefore, no pharmacokinetic analysis of bambuterol was possible. Drug plasma concentrations of the bambuterol catabolite terbutaline and theophylline, alone and in combination, are shown in Figure 4. Results of pharmacokinetic evaluations are in Table 3. When bambuterol was given alone, the geometric mean of the terbutaline C_{max} and AUC_{0-T} was 7.9 ng/ml and 107.8 h*ng/ml, respectively. When bambuterol was given together with theophylline, the geometric mean of terbutaline C_{max} and AUC_{0-T} was 6.7 ng/ml and 85.0 h*ng/ml. The 90% CI limits for the C_{max} test/reference ratios were 61.1 % and 100.9 %, and for the AUC_{0-T} test/reference ratios 70.9% and 103.6%. A two-sided T-test failed to confirm inclusion of the 90% CI within the 80-125% limit for both C_{max} and AUC_{0-T} (Table 3). The power of the test was 42.6% and 62.1%, respectively.

When theophylline was given alone, the geometric mean of C_{max} and AUC_{0-T} was 25.8 ng/ml and 407.8 h*ng/ml, respectively. When theophylline was given together with bambuterol, the geometric mean of C_{max} and AUC_{0-T} was 24.3 ng/ml and 360.9 h*ng/ml, respectively. The 90% CI limits for the

individual test/reference ratios C_{max} were 87.2% and 101%, and for AUC_{0-T} 77.1% and 95.9%. For AUC_{0-T}, the two-sided T-test failed to confirm inclusion of the 90% CI limits within the 80-125% acceptance interval, whereas in case of C_{max}, the 90% CI limits were confined within the 80-125% interval. The power of the test was 95.6% and 99.8%, respectively.

Discussion

The main findings are that theophylline, bambuterol, and their combination, all improve exercise performance in rats under hypobaric hypoxia and that the combination of Theo-Dur (300mg) and bambuterol (20mg) is relatively safe in normoxic, healthy human volunteers, with no serious AEs recorded. The AEs that were noted consisted mainly of low plasma K^+ and tremor following bambuterol treatment. Bambuterol caused an increase in heart rate that was present when given alone or in combination with Theo-Dur and persisted 24h after dosing. Drug interaction was present, but low.

Theophylline is a pleiotropic drug which, besides its long-term use to treat severe asthma, has potential value to improve health and endurance in hypoxemic individuals: although not known for any performance-enhancing effects at sea-level, theophylline, if combined with a carbonic anhydrase inhibitor, improves exercise performance capacity in hypoxemic human subjects (Scalzo et al. 2015). If combined with an endothelin-blocking vasodilator, theophylline increases hypoxic exercise performance in rats, while the single compounds are ineffective, or far less efficient (Radiloff et al. 2012). However, theophylline reportedly challenges plasma K^+ stores (Crane et al. 1987), although we did not observe this effect in human subjects. Since hypoxemia itself aggravates K^+ plasma stores (Malhotra et al. 1975), which we have confirmed in rats, this parameter will require careful monitoring when theophylline is tested in hypoxemic humans.

The mechanism of action of theophylline potentially relies on its two major effects on the cardiovascular system: nonspecific phosphodiesterase inhibition produces bronchial and vascular smooth muscle dilatation, and adenosine A1 and A2 receptor antagonism is responsible for its

vasoconstrictive effect (Barnes 2013; Casey et al. 2009). The latter mechanism is of particular importance: adenosine is a hypoxia-triggered vasodilatory tissue factor that serves to direct local blood flow to the site of demand (Marshall 2000). Under acute hypoxemia, excessive dilatation of peripheral resistance vessels, partially caused by adenosine, causes initial systemic hypotension which is then quickly compensated for by increased cardiac output (Naeije 2010). This cardiac effect of theophylline, which is likely present in humans too, is known to be specific to hypoxia and is rooted in the inhibition of sympathetic outflow by adenosine. Adenosine receptor inhibition thus increases sympathetic nerve activity and adrenaline levels in the blood under hypoxia (Marshall 2000). Theophylline might therefore partially relieve the heart from its compensatory duty, by reducing or preventing hypoxemia-induced, adenosine-triggered vasodilatation (Radiloff et al. 2012).

Bambuterol, an orally available, long-acting β2- adrenergic receptor agonist (Dorfmuller et al. 2003), was chosen as a pairing vasodilator, to improve oxygen availability by increasing capillary conductivity in skeletal muscle and other tissues. Bambuterol is a carbamate prodrug of the β2AR agonist terbutaline, and the kinetics of its conversion permits for single daily oral dosing (D'Alonzo et al. 1995; Sitar et al. 1993).

Typical adverse effects of bambuterol include tachycardia, palpitations, hypokalemia, and associated tremor (Cazzola et al. 2013). Pharmacokinetic parameters of terbutaline are the expected range, compared to previous work: In previous studies, the mean plasma half-life for bambuterol was 12 and 14 h, individually ranging over 20 hours (Bang et al. 1998; Nyberg et al. 1998), which agrees well with our finding of 15.3h. Bambuterol clearly challenged plasma K^+ stores, with average values undercutting 3.5 mM and the lowest value being 2.9 mM. While no effect was found on systolic blood pressure, the slight decrease in diastolic blood pressure observed with bambuterol alone is best explained by decreased vascular resistance following vasodilatation. The increase in heart rates with bambuterol present is a known side effect of β2AR agonists and can be partially assigned to the decreased K^+ plasma concentration.

As beta-adrenergic stimulation is almost exclusively linked to vasodilatation, such effect in the lung and the periphery is most likely part of the efficacy of bambuterol that we have seen in rats and that we would also expect in humans (Maggiorini 2010). Although bambuterol increases heart rates in human subjects by approximately 10 beats per minute 3 hours after ingestion, an effect that was reported before in humans (D'Alonzo et al. 1995), it is interesting that we did not observe this in rats in our study at given dose. With systolic pressure remaining relatively stable in humans, such rise in cardiac activity could translate into increased perfusion pressure to tissue, potentially resulting in increased rates of oxygen and nutrient transport to skeletal muscle, with appropriate peripheral vasodilatation in place. Net vasodilatation also probably underlies the hypotensive effect of bambuterol observed in rats under hypoxia, while cardiac stimulation was absent (Figure 2D, CE). Because β2- adrenergic vasodilatation plays a dominant role in maintaining normal tissue blood flow (Blauw et al. 1995; Marshall 2000; Weisbrod et al. 2001), the stimulation of β2 adrenoceptors could indeed improve oxygen transport to tissues by acting locally: terbutaline, the active metabolite of bambuterol, has reported abilities to restore the contractile force of isolated hypoxic skeletal muscle in vitro, highlighting its potential efficacy in hypoxic peripheral tissues in vivo (McDonald et al. 2015). Whether such increased transport to peripheral tissue after bambuterol treatment is actually happening in hypoxic/ hypoxemic humans will be the subject of future studies.

Combination of theophylline and bambuterol: Initial data on the combination of theophylline and bambuterol were acquired in awake rats, to better understand the cardiovascular effect of this drug combination and to identify any potential unexpected acute toxicity. The run-to-fatigue trials demonstrated that the combination of theophylline increased hypoxic exercise endurance in the animals over the single compounds, suggesting the absence of immediate negative health effects and indicating potential efficacy of the combination. The drug combination also had no detrimental effects on the mean arterial blood pressure and heart rates of the animals. It is interesting that hypoxia decreased mean arterial pressure in all treatment groups, which has only been reported in anesthetized, but not in awake rats (Duong 2007; Gao et al. 2001). This might be partially connected

to the absence of a hypoxia-induced augmentation of heart rates (except in theophylline-treated rats), which would be part of the normal response to hypoxemic peripheral vasodilation (Bartsch et al. 2007). Also, the combination did not challenge plasma K^+ pools beyond the single compounds. The observed overall decrease in plasma K^+ is a known consequence of hypoxia (Vats et al. 2001). The absence of drug (in particular bambuterol) effects on plasma K^+ in rats could have various reasons, among them the possibility that the drug dose in rats was smaller than the corresponding dose given to humans. Blood oxygenation (SaO_2) was not increased in any treatment group either, indicating that augmentation of blood oxygen levels was not the mechanism by which hypoxic exercise endurance was improved in these animals. In summary, the data acquired in rats provided strong motivation to move forward with testing the combination of theophylline and bambuterol in humans.

None of the human subjects dosed with the combination of theophylline and bambuterol experienced adverse events that led to injury and/or required subsequent hospitalization, i.e. Serious Adverse Events (SAE). The largest change in any of the AE parameters occurred when the incidents of tremor increased from 10 to 14 from single-dose bambuterol to the combined dose. None of the vital parameters, including heart rates, were exacerbated when the drugs were given together, compared to the single drug situation.

Because theophylline as a single drug did not aggravate plasma K^+ and because of the similarity of the plasma K^+ curves of bambuterol during single and combined dosing, we assume that bambuterol was the dominant factor influencing plasma K^+ during combined treatment in humans. In other studies, patients with theophylline intoxication that led to hypokalemia (plasma K^+ less than 3.5 mmol/L) had average theophylline concentrations of 0.331 mmol/L, which more than doubles the highest average measured in our study (24.7ng/ml at time points 10 during theophylline single dose, eq. 0.137 mmol/L (Shannon et al. 1989). Thus, although we dosed theophylline at the higher end of the therapeutic range, blood levels of the drug were insufficient to aggravate K^+ stores significantly. In a previous safety study that combined inhaled salbutamol and intravenous aminophylline (a

soluble formulation of theophylline), both drugs caused significant hypokalemic effects, along with alterations in ECG profiles, such as increased QT-interval, depressed T-wave amplitude, and decreased PR interval (Crane et al. 1987).

The known stimulatory effects of theophylline on the heart are thought to be mainly caused by its inhibitory effects on phosphodiesterases (PDE) 3 and 4 (Eschenhagen 2013). PDE inhibition will initiate at concentrations beyond 2 µg/ml and reach a half maximum at approximately 18 µg/ml (Rabe et al. 1995). Since the average C_{max} of theophylline was 24.3 and 25.8 µg/ml in this study, PDE inhibition was, although likely present, still insufficient to translate into increased heart rates around the plasma peak time.

Our finding that the drug combination, dosed at therapeutically relevant levels, does not negatively affect plasma K^+ and heart rates and does not cause arrhythmia, is important enabling information for future studies in hypoxemic subjects, although these parameters will require close monitoring.

Drug interaction: Theophylline is vulnerable to drug interaction, since it is cleared to 90% via metabolism (Upton 1991). It is not known whether terbutaline directly affects the hepatic microsomal p450 enzyme CYP1A2, which is mainly responsible for theophylline hydroxylation (Nahata 1996; Upton 1991; Z. Y. Zhang et al. 1995). Terbutaline however, the active compound of bambuterol, is mainly metabolized via sulphation, which takes place both in the liver and the intestinal wall (Pacifici et al. 1993).

We found that the clearance of theophylline is slightly decelerated in the presence of bambuterol. Our results also indicate that co-administration of theophylline and bambuterol result in lower systemic exposure and C_{max} of both terbutaline and theophylline. While no evidence of interaction has been found in a previous study involving terbutaline (Jonkman et al. 1988), such discrepancy can be explained by the fact that our study has, in comparison, produced higher plasma concentrations of terbutaline, thus its potential impact on theophylline metabolism was also higher. Pharmacokinetic parameters such as plasma half-lives of theophylline that were measured in our

study are similar to those found previously, with Theo-Dur showing a slightly longer half-life than what was reported before (Hayashi et al. 2007; Hendeles et al. 1985; Nyberg et al. 1998).

Application of the drug combination to improve human performance during hypoxemia: In the light of our findings, we expect that the combination of theophylline and bambuterol will improve oxygen availability and exercise capacity in hypoxemic humans, through improvement of blood flow in the lung and in other tissues. However, combining these drugs in hypoxemic subjects has distinct potential risks: hypoxia itself decreases plasma K^+ in rats and humans, and increases heart rate and cardiac output (Bartsch et al. 2007; Malhotra et al. 1975), all of which may interfere with the effects of the drugs. In addition, hypoxemia may decrease the expression of liver enzymes, thus decreasing theophylline clearance (Li et al. 2014). In particular the potential of hypoxemia to interfere with cardiac activity and plasma K^+ in humans are grounds for careful dosing considerations, and for close monitoring of cardiac activity and ionic profiles when testing β2AR agonists and theophylline in hypoxemic subjects. This drug combination could be efficacious in restoring health and exercise capacity under environmental hypoxia, as well as in individuals suffering from PAH and lung fibrosis. The long half-life of the components would enable dosing schedules of only once per day.

Conclusions

We demonstrate that sustained-release theophylline and bambuterol can be safely combined in human subjects, evidenced by a lack of any observed additive effects or adverse events, changes in K^+ stores, and alterations in cardiac function. The drugs appear to influence each other's clearance to a small extent. Yet, we believe this can be resolved after dose optimization studies. Key parameters to monitor when performing testing and dose finding of combined theophylline and β2 adrenoceptor agonists in hypoxic/ hypoxaemic volunteers are heart rates, ECG, and plasma K^+ concentration. In summary, the combination of bambuterol and theophylline is a promising and potentially feasible treatment of hypoxemia-related complications and hypoxemia-induced fatigue in humans.

Acknowledgements

This work was supported by grants from the Norwegian Armed Forces Medical Service, Institute of Aviation Medicine, the US Defense Advanced Research Projects Agency (DARPA), prime Award Number N66001-10-C-2134, and by the US Office of Naval Research, prime award number N0014-14-0699 (Irwin, Schroeder).

Figure captions

Figure 1

Experimental setup. A: Rat in a motorized running wheel in a hypobaric tank. B: Common experimental protocol for run-to-fatigue measurements. C: Common experimental protocol for hemodynamic measurements in awake rats. Animals were injected through an intraperitoneal catheter with the study drug(s) (0.05 mg/kg bambuterol, 15 mg/kg theophylline, or both) or pH-adjusted saline, while breathing normoxic air (21% oxygen). 15 minutes post injection, oxygen was reduced to 10%, and normoxia was re-instated 60 minutes after drug injection. D: Treatment schedule of the human trial.

Figure 2

Results from animal studies: A: High-dose bambuterol (0.05 mg/kg, i.p.) increases the time run to fatigue in female Sprague Dawley rats under simulated high altitude (4267m, log rank test, $p<0.05$, n=24 per group). The exercise tests were carried out in motorized wheels using pre-habituated rats (Radiloff et al. 2012). B: Theophylline alone (15 mg/kg, i.p.) increases the time run to fatigue in female Sprague Dawley rats under simulated 4267m of altitude. C: The combination of theophylline and bambuterol significantly increases exercise capacity under simulated altitude (n=10 per group). All statistics were done with log rank test. D-G: results from hemodynamic studies on awake rats equipped with fluid-filled catheters, in a hypoxic box. 1: baseline, 2: 15 min post i.p. injection, 3: 30 min post onset of hypoxia, 4: 15 min post return to normoxia. Upper panels: absolute, longitudinal

data; lower panels: values at time points, normalized to individual baselines. Significant differences between time points or treatment groups are indicated by asterisks: $p<0.05$*, $p<0.01$**, $p<0.005$***, $p<0.001$****.

Figure 3

Time course of hemodynamic data after single and combined dosing. A, B: plasma concentrations of theophylline and terbutaline. C, D: plasma K^+ concentration. E, F: systolic blood pressure. G, H: diastolic blood pressure. I, K: heart rate. Error bars represent the standard deviation from the mean. Longitudinal differences from the baseline value are indicated with an asterisk (*). Statistics were done with ANOVA plus Bonferroni correction for multiple comparisons.

Figure 4

Pharmacokinetics of bambuterol (terbutaline) and theophylline, given alone and in combination with each other to human subjects. Error bars represent the standard deviation from the mean.

References

Bang, U., Nyberg, L., Rosenborg, J., and Viby-Mogensen, J. 1998. Pharmacokinetics of bambuterol in subjects homozygous for the atypical gene for plasma cholinesterase. Br. J. Clin. Pharmacol., 45(5), 479-484.

Barnes, P. J. 2013. Theophylline. Am. J. Respir. Crit. Care Med., 188(8), 901-906.

Barrett-O'Keefe, Z., Ives, S. J., Trinity, J. D., Morgan, G., Rossman, M. J., Donato, A. J., et al. 2013. Taming the "sleeping giant": the role of endothelin-1 in the regulation of skeletal muscle blood flow and arterial blood pressure during exercise. Am. J. Physiol. Heart. Circ. Physiol., 304(1), H162-169.

Bartsch, P., and Gibbs, J. S. 2007. Effect of altitude on the heart and the lungs. Circulation, 116(19), 2191-2202.

Blauw, G. J., Westendorp, R. G., Simons, M., Chang, P. C., Frolich, M., and Meinders, A. E. 1995. beta-Adrenergic receptors contribute to hypoxaemia induced vasodilation in man. Br. J. Clin. Pharmacol., 40(5), 453-458.

Borysova, L., Wray, S., Eisner, D. A., and Burdyga, T. 2013. How calcium signals in myocytes and pericytes are integrated across in situ microvascular networks and control microvascular tone. Cell Calcium, 54(3), 163-174.

Casey, D. P., Madery, B. D., Pike, T. L., Eisenach, J. H., Dietz, N. M., Joyner, M. J., et al. 2009. Adenosine receptor antagonist and augmented vasodilation during hypoxic exercise. J. Appl. Physiol. (1985), 107(4), 1128-1137.

Cazzola, M., Page, C. P., Rogliani, P., and Matera, M. G. 2013. beta2-agonist therapy in lung disease. Am. J. Respir. Crit. Care. Med., 187(7), 690-696.

Crane, J., Burgess, C. D., Graham, A. N., and Maling, T. J. 1987. Hypokalaemic and electrocardiographic effects of aminophylline and salbutamol in obstructive airways disease. N. Z. Med. J., 100(824), 309-311.
D'Alonzo, G. E., Smolensky, M. H., Feldman, S., Gnosspelius, Y., and Karlsson, K. 1995. Bambuterol in the treatment of asthma. A placebo-controlled comparison of once-daily morning vs evening administration. Chest, 107(2), 406-412.
Dayan, L., Brill, S., Hochberg, U., and Jacob, G. 2016. Is adenosine a modulator of peripheral vasoconstrictor responses? Clin. Auton. Res.
Dorfmuller, P., Perros, F., Balabanian, K., and Humbert, M. 2003. Inflammation in pulmonary arterial hypertension. Eur. Respir. J., 22(2), 358-363.
Dubrey, S., Pal, S., Singh, S., and Karagiannis, G. 2016. Digital clubbing: forms, associations and pathophysiology. Br. J. Hosp. Med. (Lond), 77(7), 403-408.
Duong, T. Q. 2007. Cerebral blood flow and BOLD fMRI responses to hypoxia in awake and anesthetized rats. Brain Res., 1135(1), 186-194.
Eschenhagen, T. 2013. PDE4 in the human heart - major player or little helper? Br. J. Pharmacol., 169(3), 524-527.
Fromm, R. E., Jr., and Varon, J. 1994. Acute exacerbations of obstructive lung disease. What to do when immediate care is crucial. Postgrad. Med., 95(8), 101-106.
Gao, E., Kaplan, J. L., Shi, Y., Victain, M., Dalsey, W. C., and de Garavilla, L. 2001. Adenosine A1 receptor antagonist prolongs survival in the hypoxic rat. J. Cardiovasc. Pharmacol., 38(3), 384-394.
Gouyon, J. B., and Guignard, J. P. 1988. Theophylline prevents the hypoxemia-induced renal hemodynamic changes in rabbits. Kidney Int., 33(6), 1078-1083.
Hall, C. N., Reynell, C., Gesslein, B., Hamilton, N. B., Mishra, A., Sutherland, B. A., et al. 2014. Capillary pericytes regulate cerebral blood flow in health and disease. Nature, 508(7494), 55-60.
Hayashi, T., Kanbe, H., Okada, M., Kawase, I., Ikeda, Y., Onuki, Y., et al. 2007. In vitro and in vivo sustained-release characteristics of theophylline matrix tablets and novel cluster tablets. Int. J. Pharm., 341(1-2), 105-113.
Hendeles, L., Massanari, M., and Weinberger, M. 1985. Update on the pharmacodynamics and pharmacokinetics of theophylline. Chest, 88(2 Suppl), 103S-111S.
Irwin, D. C., Foreman, B., Morris, K., White, M., Sullivan, T., Jacobs, R., et al. 2008. Polymerized bovine hemoglobin decreases oxygen delivery during normoxia and acute hypoxia in the rat. Am. J. Physiol. Heart Circ. Physiol., 295(3), H1090-H1099.
Jain, S., Khera, R., Girotra, S., Badesch, D., Wang, Z., Murad, M. H., et al. 2016. Comparative Effectiveness of Pharmacological Interventions for Pulmonary Arterial Hypertension: A Systematic Review and Network Meta-Analysis. Chest.
Jonkman, J. H., Borgstrom, L., van der Boon, W. J., and de Noord, O. E. 1988. Theophylline-terbutaline, a steady state study on possible pharmacokinetic interactions with special reference to chronopharmacokinetic aspects. Br. J. Clin. Pharmacol., 26(3), 285-293.
Julious, S. A. 2004. Sample sizes for clinical trials with normal data. Stat. Med., 23(12), 1921-1986.
Kawano, H., Sengyoku, H., Satoh, O., Urabe, S., Koide, Y., and Yano, K. 2007. Marked improvement with sildenafil in a patient with idiopathic pulmonary arterial hypertension unresponsive to beraprost and sarpogrelate. Intern. Med., 46(12), 893-898.
Kim, K. J., Baek, I. W., Yoon, C. H., Kim, W. U., and Cho, C. S. 2015. Association of Anemic Hypoxia and Increased Pulmonary Artery Systolic Pressure in Patients With Systemic Lupus Erythematosus. Arthritis Care. Res. (Hoboken), 67(12), 1702-1711.
Kwon, M. S., Woo, S. K., Kurland, D. B., Yoon, S. H., Palmer, A. F., Banerjee, U., et al. 2015. Methemoglobin is an endogenous toll-like receptor 4 ligand-relevance to subarachnoid hemorrhage. Int. J. Mol. Sci., 16(3), 5028-5046.
Kylhammar, D., and Radegran, G. 2016. The principal pathways involved in the in vivo modulation of hypoxic pulmonary vasoconstriction, pulmonary arterial remodelling and pulmonary hypertension. Acta Physiol. (Oxf).

Leblais, V., Delannoy, E., Fresquet, F., Begueret, H., Bellance, N., Banquet, S., et al. 2008. beta-adrenergic relaxation in pulmonary arteries: preservation of the endothelial nitric oxide-dependent beta2 component in pulmonary hypertension. Cardiovasc. Res., 77(1), 202-210.

Li, X., Wang, X., Li, Y., Yuan, M., Zhu, J., Su, X., et al. 2014. Effect of exposure to acute and chronic high-altitude hypoxia on the activity and expression of CYP1A2, CYP2D6, CYP2C9, CYP2C19 and NAT2 in rats. Pharmacology, 93(1-2), 76-83.

Maggiorini, M. 2010. Prevention and treatment of high-altitude pulmonary edema. Prog. Cardiovasc. Dis., 52(6), 500-506.

Malhotra, M. S., Brahmachari, H. D., Sridharan, K., Purshottam, T., Ramachandran, K., and Radhakrishnan, U. 1975. Electrolyte changes at 3500 m in males with and without high-altitude pulmonary edema. Aviat. Space Environ. Med., 46(4 Sec 1), 409-412.

Marshall, J. M. 2000. Adenosine and muscle vasodilatation in acute systemic hypoxia. Acta. Physiol. Scand., 168(4), 561-573.

McDonald, F. B., Skelly, J. R., and O'Halloran, K. D. 2015. The beta2 -adrenoceptor agonist terbutaline recovers rat pharyngeal dilator muscle force decline during severe hypoxia. Oral Dis., 21(1), e121-127.

Murray, I. R., Baily, J. E., Chen, W. C., Dar, A., Gonzalez, Z. N., Jensen, A. R., et al. 2016. Skeletal and cardiac muscle pericytes: Functions and therapeutic potential. Pharmacol. Ther., 65-74.

Naeije, R. 2010. Physiological adaptation of the cardiovascular system to high altitude. Prog. Cardiovasc. Dis., 52(6), 456-466.

Naeije, R., Huez, S., Lamotte, M., Retailleau, K., Neupane, S., Abramowicz, D., et al. 2010. Pulmonary artery pressure limits exercise capacity at high altitude. Eur. Respir. J., 36(5), 1049-1055.

Nagai, H., Kuwahira, I., Schwenke, D. O., Tsuchimochi, H., Nara, A., Inagaki, T., et al. 2014. beta2-Adrenergic receptor-dependent attenuation of hypoxic pulmonary vasoconstriction prevents progression of pulmonary arterial hypertension in intermittent hypoxic rats. PLoS One, 9(10), e110693.

Nahata, M. 1996. Drug interactions with azithromycin and the macrolides: an overview. J. Antimicrob. Chemother., 37 Suppl. C, 133-142.

Nakamura, C. T., Ng, G. Y., Paton, J. Y., Keens, T. G., Witmer, J. C., Bautista-Bolduc, D., et al. 2002. Correlation between digital clubbing and pulmonary function in cystic fibrosis. Pediatr. Pulmonol., 33(5), 332-338.

Neuhaus, A. A., Couch, Y., Sutherland, B. A., and Buchan, A. M. 2016. Novel method to study pericyte contractility and responses to ischaemia in vitro using electrical impedance. J. Cereb. Blood Flow Metab., 1-12.

Nyberg, L., Rosenborg, J., Weibull, E., Jonsson, S., Kennedy, B. M., and Nilsson, M. 1998. Pharmacokinetics of bambuterol in healthy subjects. Br. J. Clin. Pharmacol., 45(5), 471-478.

Pacifici, G. M., Eligi, M., and Giuliani, L. 1993. (+) and (-) terbutaline are sulphated at a higher rate in human intestine than in liver. Eur. J. Clin. Pharmacol., 45(5), 483-487.

Pitsiou, G. G., Chavouzis, N., Nakou, C., Boutou, A. K., Argyropoulou, P., and Stanopoulos, I. 2009. Successful up-front combination therapy in a patient with idiopathic pulmonary hypertension and patent foramen ovale: an alternative to epoprostenol therapy? J. Heart Lung Transplant., 28(6), 651-653.

Rabe, K. F., Magnussen, H., and Dent, G. 1995. Theophylline and selective PDE inhibitors as bronchodilators and smooth muscle relaxants. Eur. Respir. J., 8(4), 637-642.

Radiloff, D. R., Zhao, Y., Boico, A., Wu, C., Shan, S., Palmer, G., et al. 2012. The combination of theophylline and endothelin receptor antagonism improves exercise performance of rats under simulated high altitude. J. Appl. Physiol. (1985), 113(8), 1243-1252.

Scalzo, R. L., Binns, S. E., Klochak, A. L., Giordano, G. R., Paris, H. L., Sevits, K. J., et al. 2015. Methazolamide Plus Aminophylline Abrogates Hypoxia-Mediated Endurance Exercise Impairment. High. Alt. Med. Biol., 16(4), 331-342.

Shannon, M., and Lovejoy, F. H., Jr. 1989. Hypokalemia after theophylline intoxication. The effects of acute vs chronic poisoning. Arch. Intern. Med., 149(12), 2725-2729.

Sitar, D. S., Aoki, F. Y., Warren, C. P., Knight, A., Grossman, R. F., Alexander, M., et al. 1993. A placebo-controlled dose-finding study with bambuterol in elderly patients with asthma. Chest, 103(3), 771-776.

Upton, R. A. 1991. Pharmacokinetic interactions between theophylline and other medication (Part I). Clin. Pharmacokinet., 20(1), 66-80.

Vats, P., Singh, S. N., Kumria, M. M., Ranganathan, S., Arora, M. P., Jain, C. L., et al. 2001. Effect of hypoxia on the circulating levels of essential mineral elements in rats. J. Environ. Biol., 22(4), 277-282.

Weisbrod, C. J., Minson, C. T., Joyner, M. J., and Halliwill, J. R. 2001. Effects of regional phentolamine on hypoxic vasodilatation in healthy humans. J. Physiol., 537(Pt 2), 613-621.

Zhang, H., Feng, L., Wan, Q. L., Hong, Y., Li, Y. M., Cheng, G. C., et al. 2015. Sleep-disordered breathing is associated with depletion of circulating endothelial progenitor cells and elevation in pulmonary arterial pressure in patients with decompensated systolic heart failure. J. Geriatr. Cardiol., 12(4), 424-430.

Zhang, Z. Y., and Kaminsky, L. S. 1995. Characterization of human cytochromes P450 involved in theophylline 8-hydroxylation. Biochem. Pharmacol., 50(2), 205-211.

Table 1: Demographics

Sex	Female	Male
Number	2	17
Age (yrs)	23.7 (19-27)	23.6 (20-31)
Height (cm)	175.3 (169-183)	181.2 (171-195)
Weight (kg)	78.7 (72.4-83.4)	81.4 (69.3-98.2)

Table 2: Summary of adverse events

	Bambuterol	Theophylline	Combination
K^+<3.5mM	12	4	13
Tremor	10	0	14
Dizziness	0	1	0
Palpitations	4	1	4
Nausea	3	1	2
Chest pain and inspirational discomfort	1	0	1
Reduced appetite	0	1	0
Upper respiratory tract infection	0	1	0
Sleeping disturbances	0	0	1
Mucosal gum bleeding	0	1	0
Tachycardia	1	0	1
Inverted T-wave in ECG	1	1	0
Fatigue	1	0	0
Extrasystole in ECG	0	0	1
Headache	0	1	0
Increased diuresis	0	1	0
Lower extremity fasciculation	0	1	0
Overall number of adverse events	***33***	***14***	***37***

Table 3: Pharmacokinetic results from the human trial of terbutaline and theophylline after dosing of bambuterol and theophylline alone and in combination

Parameter		Bambuterol alone (Terbutaline)			Bambuterol (Terbutaline), theophylline present			Theophylline alone			Theophylline (bambuterol present)		
		Geomean	SD	*N*	Geomean	SD	*N*	Geomean	SD	*N*	Geomean	SD	*N*
K_{el}	1/*h*	0.0452	0.0228	16	0.0493	0.1223	16	0.0640	0.0129	6	0.0666	0.0048	3
$t_{1/2}$	*h*	15.3	14.4	16	14.1	22.0	16	10.8	2.1	6	10.4	0.7	3
T_{max}	*h*	5.0	2.1	18	4.2	1.8	16	9.7	3.8	19	10.2	4.0	17
C_{max}	µg/mL	7.9	2.2	18	6.7	2.4	16	25.8	3.6	19	24.3	4.9	17
T_{last}	*h*	23.1	2.8	18	21.8	4.5	16	23.1	2.8	19	22.1	4.0	17
C_{last}	µg/mL	2.7	0.8	18	2.1	1.0	16	12.8	5.6	19	12.8	4.7	17
$AUC_{0\text{-}T}$	*h*·ng/mL_{Bam} *h*·µg/mL_{Theo}	107.8	31.3	18	85.0	37.7	16	407.8	86.4	19	360.9	95.9	17
$AUC_{0\text{-}INF}$	*h*·ng/mL_{Bam} *h*·µg/mL_{Theo}	177.5	56.4	16	146.0	133.8	16	552.3	93.3	6	455.9	60.6	3
Vz/F	*L*	2491.2	1155.4	16	2816.2	1319.6	16	8.5	1.9	6	9.9	0.7	3
CL/F	mL/min	1878.3	467.4	16	2314.3	3815.5	16	9.1	1.9	6	11.0	1.5	3
MRT_{last}	*h*	10.1	1.1	18	9.6	2.0	16	11.6	1.5	19	11.5	2.0	17

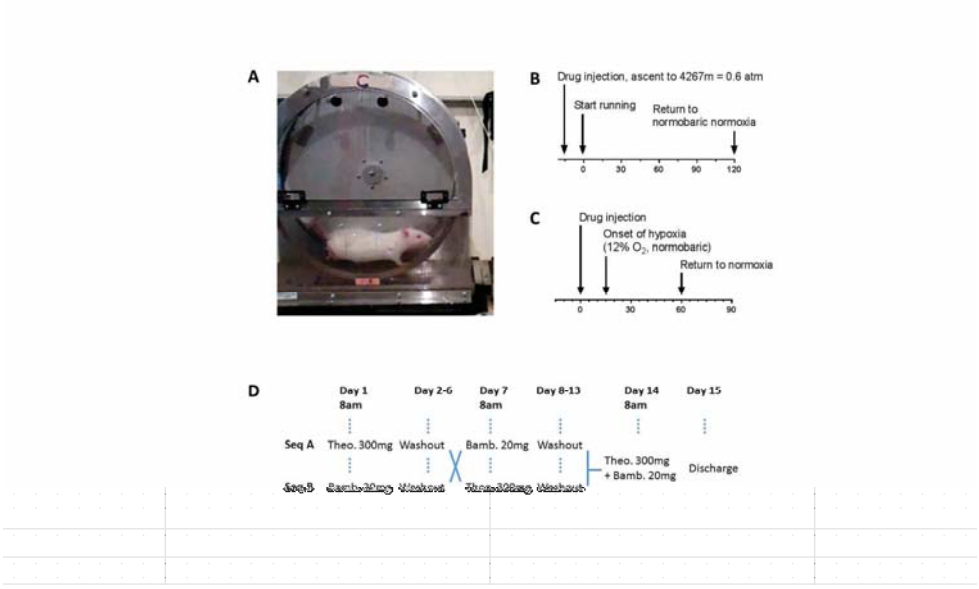

Experimental setup. A: Rat in a motorized running wheel in a hypobaric tank. B: Common experimental protocol for run-to-fatigue measurements. C: Common experimental protocol for hemodynamic measurements in awake rats. Animals were injected through an intraperitoneal catheter with the study drug(s) (0.05 mg/kg bambuterol, 15 mg/kg theophylline, or both) or pH-adjusted saline, while breathing normoxic air (21% oxygen). 15 minutes post injection, oxygen was reduced to 10%, and normoxia was re-instated 60 minutes after drug injection. D: Treatment schedule of the human trial.

500x400mm (300 x 300 DPI)

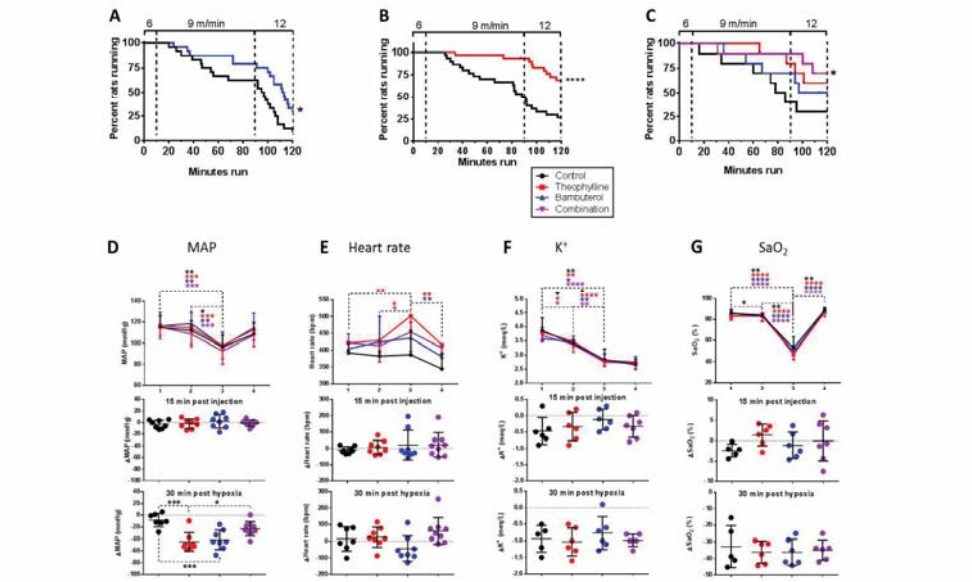

Results from animal studies: A: High-dose bambuterol (0.05 mg/kg, i.p.) increases the time run to fatigue in female Sprague Dawley rats under simulated high altitude (4267m, log rank test, $p<0.05$, n=24 per group). The exercise tests were carried out in motorized wheels using pre-habituated rats (Radiloff et al. 2012). B: Theophylline alone (15 mg/kg, i.p.) increases the time run to fatigue in female Sprague Dawley rats under simulated 4267m of altitude. C: The combination of theophylline and bambuterol significantly increases exercise capacity under simulated altitude (n=10 per group). All statistics were done with log rank test. D-G: results from hemodynamic studies on awake rats equipped with fluid-filled catheters, in a hypoxic box. 1: baseline, 2: 15 min post i.p. injection, 3: 30 min post onset of hypoxia, 4: 15 min post return to normoxia. Upper panels: absolute, longitudinal data; lower panels: values at time points, normalized to individual baselines. Significant differences between time points or treatment groups are indicated by asterisks: $p<0.05$*, $p<0.01$**, $p<0.005$***, $p<0.001$****.

500x400mm (300 x 300 DPI)

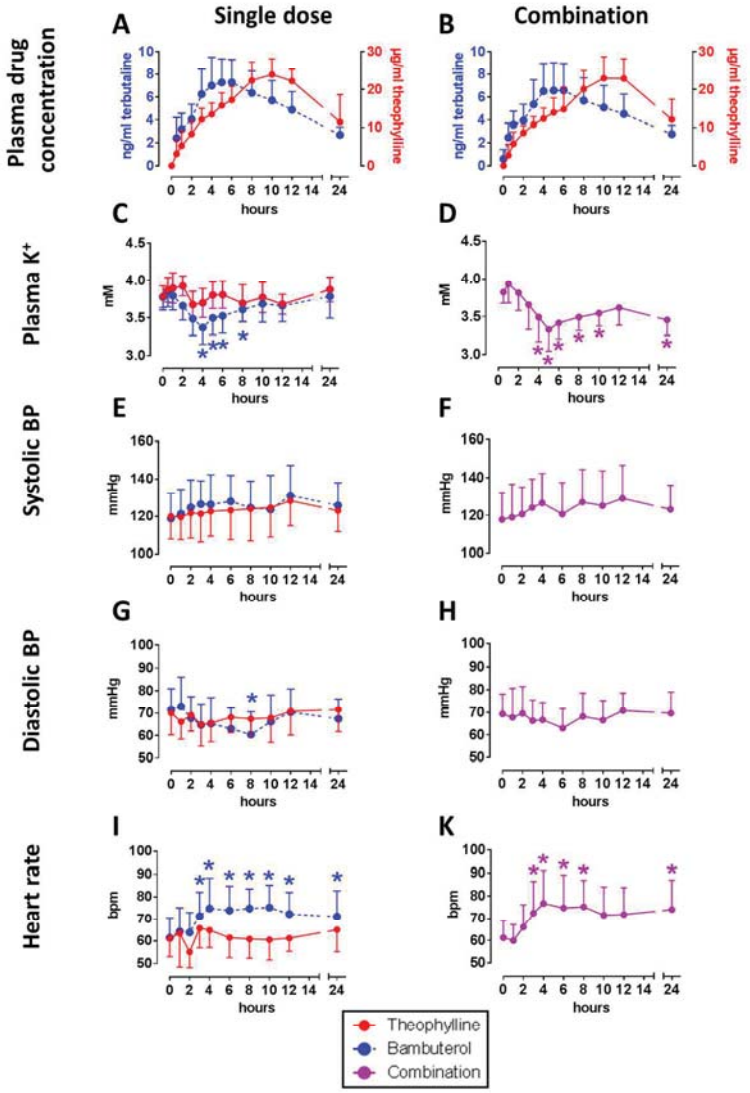

Time course of hemodynamic data after single and combined dosing. A, B: plasma concentrations of theophylline and terbutaline. C, D: plasma K+ concentration. E, F: systolic blood pressure. G, H: diastolic blood pressure. I, K: heart rate. Error bars represent the standard deviation from the mean. Longitudinal differences from the baseline value are indicated with an asterisk (*). Statistics were done with ANOVA plus Bonferroni correction for multiple comparisons.

500x650mm (250 x 250 DPI)

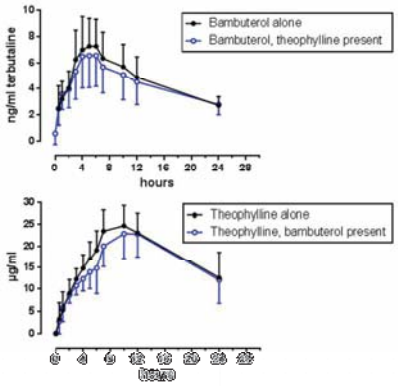

Pharmacokinetics of bambuterol (terbutaline) and theophylline, given alone and in combination with each other to human subjects. Error bars represent the standard deviation from the mean.

190x107mm (300 x 300 DPI)

Supplementary Table 1: Inclusion and Exclusion Criteria

	Inclusion criteria	Exclusion criteria
	Subjects will be admitted only if they meet ALL of the following criteria	***Individuals meeting ANY ONE of the following criteria will be excluded from the study:***
1.	Subjects must give written informed consent to participation in the study prior to screening.	Subjects with laboratory results outside the normal range, if considered clinically significant by the Investigator. In addition, subjects must have a normal hematocrit and hemoglobin concentration and be ≥ 36% and ≥ 12.0 g/dL, respectively.
2.	Subjects must be healthy non-smoking adult male and female volunteers between the ages of 18 and 40 years, with a BMI of 18-30 kg/m2 and weighing at least 68 kg.	A mental capacity that is limited to the extent that the subject cannot provide legal consent or understand information regarding the side effects of the study drug.
3.	Subjects must be willing to fast a minimum of 8 hours prior to screening.	Currently abusing drugs or alcohol or with a history of drug or alcohol abuse within the past two years.
4.	Subjects must be willing to abstain from alcohol and xanthine-containing food and beverages from the time of admission to the clinical research inpatient unit through at least 48 hours following discharge.	Unwillingness or lack of ability to comply with the protocol, or to reside in the inpatient unit during the required time period, or to cooperate fully with the Principle Investigator and site personnel.
5.	Subjects must be willing to remain in the clinical research unit continuously for the inpatient portion of the study from admission to discharge.	Use of any of the following: (a) Any concomitant medication including oral contraceptive hormones. Subjects who have received any prescribed or non-prescribed (over-the-counter [OTC]) systemic medication, topical medications, or herbal supplements within 14 days from Day 1. St. John's Wort (hypericin) must not have been taken for at least 30 days prior to Period 1, Day 1. (b) Any drugs, foods or substances known to be strong inhibitors or strong inducers of CYP enzymes (also known as cytochrome P450 enzymes); especially CYP 1A2, or Pgp within 30 days prior to Period 1, Day 1
6.	Women who are of non-childbearing potential, must be: (a) Surgically sterile (removal of both ovaries and/ or uterus at least 12 months prior to dosing), or (b) Naturally postmenopausal (spontaneous cessation of menses) for at least 24 consecutive months prior to dosing on Day -1, with an FSH level at screening of >= 40 mIU/mL.	Clinically significant ECG abnormality in the opinion of the Investigator.

	Inclusion criteria	Exclusion criteria
	Subjects will be admitted only if they meet ALL of the following criteria	***Individuals meeting ANY ONE of the following criteria will be excluded from the study:***
7.	Women of child-bearing potential must have a negative serum pregnancy test within 48 hours of receiving study drug and must agree to avoid pregnancy during study and for one month after the last dose of study drug	Vital signs or clinically significant laboratory values at the screening visit that in the opinion of the Investigator would make the subject an inappropriate candidate for the study.
8.	Female subjects of child-bearing potential must agree to avoid pregnancy during study and for three months after the last dose of study drug.	Has taken any other investigational drug during the 30 days prior to the screening visit or is currently participating in another investigational clinical trial.
9.	Subjects must agree not to donate blood, plasma, platelets, or any other blood components during the study and for 4 weeks after the last dose.	Made any significant donation (including plasma) or have had a significant loss of blood within 30 or 90 days prior to Period 1, Day 1.
10.	Male subjects must agree not to donate sperm during the study and for 12 weeks after the last dose.	History or manifestation of clinically significant neurological, gastrointestinal, renal, hepatic, cardiovascular, psychological, pulmonary, metabolic, endocrine, hematologic or other medical disorders.
11.		Subjects who are carriers of the Hepatitis B surface antigen (HbsAg), Hepatitis C antibody, or HIV antibody
12.		Serious mental or physical illness within the past year.
13.		Male subjects who consume more than 28 units of alcohol per week and female subjects who consume more than 21 units of alcohol per week (one unit of alcohol equals 250 mL of beer, 100 mL or a medium glass of wine, or 25 mL of spirits) or those subjects who have a significant history of alcoholism or drug/ chemical abuse within the last 2 years
14.		Failure to agree to abstain from alcohol, cola, tea, coffee, chocolate and other caffeinated drink/ food from 2 days before dosing and throughout confinement
15.		Positive results on screening tests for drugs of abuse, cotinine or alcohol at screening or the pre-dose assessment at check-in
16.		Subjects who have used tobacco products or nicotine-containing products (including smoking cessation aids, such as gums or patches) within 12 months prior to Period 1, Day 1
17.		Women of childbearing potential who are pregnant (as based on test results) or are breast feeding

Inclusion criteria	Exclusion criteria
Subjects will be admitted only if they meet ALL of the following criteria	***Individuals meeting ANY ONE of the following criteria will be excluded from the study:***
18.	Subjects who have a history of hypersensitivity or idiosyncratic reaction to any of the products administered during the study.
19.	Subjects who, in the opinion of the Investigator, should not participate in the study.
20.	Subjects who have a history of unexplained syncope; i.e., autonomic dysfunction.
21.	Subjects who have a history of hypotension, including orthostatic hypotension
22.	A positive test for hepatitis B surface antigen, hepatitis C antibody, or HIV antibody at screening.
23.	Lack of ability to understand verbal and/ or written Norwegian
24.	History of severe hypersensitivity or allergic reaction to study medication
25.	Failure to agree to abstain from grapefruit and grapefruit juice as well as oranges and orange juice from 10 days before the first dose and throughout the study
26.	History of clinically significant illness within 4 weeks prior to Day 1
27.	Receipt of a transfusion or any blood products within 90 days prior to Period 1, Day 1
28.	History of participation in another investigational study or who have participated in an investigational study within the past 30 days prior to Period 1, Day 1.

HIGH ALTITUDE MEDICINE & BIOLOGY
Volume 16, Number 4, 2015

DOI: 10.1089/ham.2015.0066

Methazolamide Plus Aminophylline Abrogates Hypoxia-Mediated Endurance Exercise Impairment

Rebecca L. Scalzo,[1] Scott E. Binns,[1] Anna L. Klochak,[1] Gregory R. Giordano,[1] Hunter L.R. Paris,[1] Kyle J. Sevits,[1] Joseph W. Beals,[1] Laurie M. Biela,[1] Dennis G. Larson,[2] Gary J. Luckasen,[2] David Irwin,[3] Thies Schroeder,[4] Karyn L. Hamilton,[1] and Christopher Bell[1]

Abstract

Scalzo, Rebecca L., Scott E. Binns, Anna L. Klochak, Gregory R. Giordano, Hunter L.R. Paris, Kyle J. Sevits, Joseph W. Beals, Laurie M. Biela, Dennis G. Larson, Gary J. Luckasen, David Irwin, Thies Schroeder, Karyn L. Hamilton, and Christopher Bell. Methazolamide plus aminophylline abrogates hypoxia-mediated endurance exercise impairment. *High Alt Med Biol* 16:331–342, 2015.—In hypoxia, endurance exercise performance is diminished; pharmacotherapy may abrogate this performance deficit. Based on positive outcomes in preclinical trials, we hypothesized that oral administration of methazolamide, a carbonic anhydrase inhibitor, aminophylline, a nonselective adenosine receptor antagonist and phosphodiesterase inhibitor, and/or methazolamide combined with aminophylline would attenuate hypoxia-mediated decrements in endurance exercise performance in humans. Fifteen healthy males (26 ± 5 years, body–mass index: $24.9 \pm 1.6\,kg/m^2$; mean ± SD) were randomly assigned to one of four treatments: placebo ($n = 9$), methazolamide (250 mg; $n = 10$), aminophylline (400 mg; $n = 9$), or methazolamide (250 mg) with aminophylline (400 mg; $n = 8$). On two separate occasions, the first in normoxia ($FIO_2 = 0.21$) and the second in hypoxia ($FIO_2 = 0.15$), participants sat for 4.5 hours before completing a standardized exercise bout (30 minutes, stationary cycling, 100 W), followed by a 12.5-km time trial. The magnitude of time trial performance decrement in hypoxia versus normoxia did not differ between placebo ($+3.0 \pm 2.7$ minutes), methazolamide ($+1.4 \pm 1.7$ minutes), and aminophylline ($+1.8 \pm 1.2$ minutes), all with $p > 0.09$; however, the performance decrement in hypoxia versus normoxia with methazolamide combined with aminophylline was less than placebo ($+0.6 \pm 1.5$ minutes; $p = 0.01$). This improvement may have been partially mediated by increased SpO_2 in hypoxia with methazolamide combined with aminophylline compared with placebo ($73\% \pm 3\%$ vs. $79\% \pm 6\%$; $p < 0.02$). In conclusion, coadministration of methazolamide and aminophylline may promote endurance exercise performance during a sojourn at high altitude.

Key Words: high-altitude; methazolamide; theophylline

Introduction

Rapid transition from sea level to high altitude is accompanied by impaired physiological function; impairments that may have important health implications for both professional (such as the military) and recreational travelers. Documented responses to high altitude and/or simulated high altitude (hypoxia) include compromised cognitive ability (Li et al., 2012), sleep disturbances (Stadelmann et al., 2014), decreased insulin sensitivity (Peltonen et al., 2012), and reduced exercise capacity/performance (Lawler et al., 1988; Martin and O'Kroy, 1993; Ferretti et al., 1997; Chapman et al., 1999). With regard to the latter, performance decrements at high altitude range from 0 to ~30% depending on the duration of the activity and/or the severity of hypobaria (Fulco et al., 1998). For example, in a recent review of marathon performance and high altitude, marathon completion times were reported to increase by ~10%–12% per 1000 m gain in altitude (Lara et al., 2014).

Several nutraceutical and pharmacological strategies, including administration of acetazolamide, sildenafil, and caffeine (Bradwell et al., 1986; Stager et al., 1990; Fulco et al.,

[1]Department of Health and Exercise Science, Colorado State University, Fort Collins, Colorado.
[2]Heart Center of the Rockies, University of Colorado Health, Fort Collins, Colorado.
[3]University of Colorado–Denver, Denver, Colorado.
[4]Department of Physical Chemistry, University of Mainz, Mainz, Germany.

1994; Hsu et al., 2006; Kressler et al., 2011), have been explored to prevent the hypoxia/hypobaria-mediated decline in function. Some of these strategies have focused on alleviating nausea and acute mountain sickness (Fischer et al., 2000; Kupper et al., 2008; Ritchie et al., 2012), while others have targeted improved oxygen delivery (Fulco et al., 1994; Hsu et al., 2006; Kressler et al., 2011). Recent published studies (Radiloff et al., 2012) and unpublished preliminary data demonstrate the success in a rodent model of the asthma medication, theophylline, when combined with either a pulmonary hypertension medication, such as sitaxsentan and ambrisentan, or the glaucoma medication, methazolamide.

The purpose of this investigation was to determine, in humans, the efficacy of aminophylline (active ingredient: theophylline), methazolamide, and aminophylline combined with methazolamide to attenuate hypoxia-mediated decrements in endurance exercise performance. Aminophylline comprises theophylline and ethylenediamine, a compound that serves to increase the solubility of theophylline. The pharmacokinetics of theophylline in circulation is similar (Aslaksen et al., 1981) or augmented (Schulz et al., 1984) when theophylline is administered with ethylenediamine (aminophylline) compared with theophylline alone. Methazolamide differs from its more common carbonic anhydrase inhibitor family member, acetazolamide, by being more soluble in water and lipids and having a greater tissue diffusion capacity (Maren et al., 1977). These characteristics make aminophylline and methazolamide attractive, potential, fast-acting ergogenic aids during an acute exposure to hypoxia. Identification of an effective pharmacological strategy to abrogate the deleterious effects of short-term exposure to hypoxia would be of benefit to professional and recreational travelers during sojourns at high altitude. We hypothesized that aminophylline, methazolamide, and/or the combination of aminophylline and methazolamide would attenuate the hypoxia-mediated decrement in endurance exercise performance in humans.

Materials and Methods

Drug safety

Before the initiation of the current investigation, an inpatient study was undertaken by our collaborators at the University of Colorado Health (formerly Poudre Valley Health System) to determine the safety of aminophylline and methazolamide when consumed independently and in combination, and also to provide insight into the pharmacokinetics of the drug combination. This safety study was registered as a clinical trial (ClinicalTrials.gov Identifier: NCT01587027). Sixteen healthy adults participated in a 5-day study protocol comprising single-dose administration of aminophylline (500 mg), methazolamide (250 mg), and aminophylline (500 mg) combined with methazolamide (250 mg), with a 24-hour washout period between each dosing. The order of individual administration of aminophylline and methazolamide was randomized; the combined administration was always the third/final treatment. The studied doses were based on recommended clinical dosing for asthma (aminophylline) and glaucoma (methazolamide). Vital signs were monitored and venous blood sampled before and during absorption. The primary findings of the study were (1) when consumed during rest, the drugs, either independently or in combination, were well tolerated at the administered doses (no serious adverse events were reported, although some participants reported headaches and/or jitteriness; full details are available at ClinicalTrials.gov Identifier: NCT01587027); (2) the time to peak circulating concentrations of the primary active agents of each drug (i.e., theophylline for aminophylline) was 2–3 hours following administration; coadministration did not affect these time to peak concentration values; and (3) consistent with previous literature, the half-lives of the drugs were 8 and 14 hours for aminophylline (Weinberger and Hendeles, 1996) and methazolamide (Maren et al., 1977), respectively. Based on these observations and on the advice of our physician collaborators (D.G.L. and G.J.L.), to decrease the incidence of headaches and reports of jitteriness, in the current study, the administered dose of aminophylline was decreased from 500 to 400 mg.

Participants

From June 2012 through December 2012, 15 young healthy men were recruited and they participated in the current investigation. The experimental protocol conformed to the standards set by the Declaration of Helsinki of 1975, as revised in 1983, and was approved by the Institutional Review Board at Colorado State University. The nature, purpose, and risks of the study were explained to each research participant before written informed consent was obtained. The study was also registered as a clinical trial (ClinicalTrials.gov Identifier: NCT01702025).

Inclusion criteria consisted of age within the range 18–40 years, body–mass index within the range 18.5–30 kg/m^2, body mass >68.2 kg, free from overt disease as determined through medical history and assessment of blood pressure and heart rate (via 12-lead electrocardiogram) at rest and during incremental exercise to volitional exhaustion, and approval from a supervising cardiologist (D.G.L or G.J.L). Exclusion criteria included current use of tobacco products or any prescribed medications, unwillingness to abstain from caffeinated or theophylline-containing food or beverages 48 hours before each study visit, history of acute mountain sickness, history of allergic reaction, hypersensitivity or idiosyncratic reaction to methazolamide and/or theophylline, or an allergy to any sulfa or sulfonamide derivatives, asthma, or any other type of lung/pulmonary dysfunction, and/or contraindications to vigorous exercise. Consequently, research participants demonstrated physiological attributes typical of fit and healthy, recreationally active young men. It is noteworthy that all listed cycling as a component of their habitual physical activity.

Following screening procedures, research participants completed additional assessment that included measurement of body composition (via dual-energy x-ray absorptiometry: DEXA-IQ, software v. 4.1; Lunar Radiation Corp., Madison, WI) and determination of maximal oxygen uptake (VO_{2max}) during incremental stationary cycle ergometer exercise (via indirect calorimetry) as previously described (Richards et al., 2010).

Protocol overview

Research participants were randomly assigned utilizing a double coin flip randomization scheme by the study coordinator, in a double-blind manner, to one of four treatments (Fig. 1): placebo (200 mg of white cornmeal packaged in gel capsules), methazolamide (250 mg), aminophylline (400 mg),

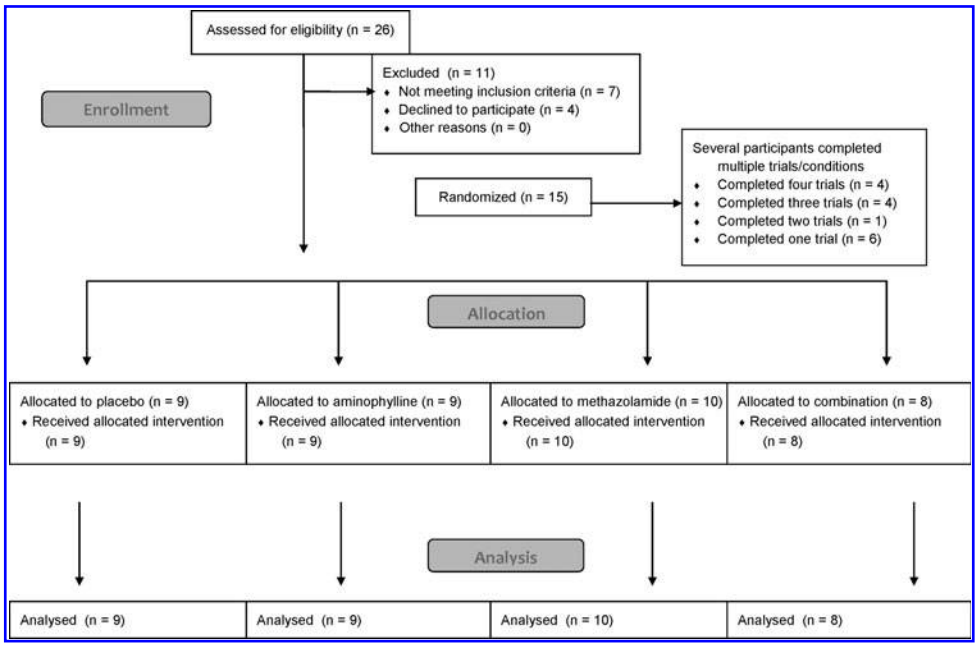

FIG. 1. Participant flow diagram. Data from all participants allocated to a treatment were included in analysis. No participants allocated to the treatment discontinued the study or were lost to follow-up.

or methazolamide (250 mg) combined with aminophylline (400 mg). The size of each individual capsule was 25 and 100 mg for methazolamide and aminophylline, respectively. Consequently, each participant was required to ingest multiple capsules for a single drug assignment. A favorable consequence of this method of drug administration was the facilitation and maintenance of the double-blind experimental design. That is, irrespective of whether participants were ingesting a single or combination drug treatment, they always consumed multiple capsules. Participants reported to the laboratory on two separate occasions, separated by 7–28 days, to be studied during normoxia and hypoxia. In light of the half-lives of aminophylline (Weinberger and Hendeles, 1996) and methazolamide (Maren et al., 1977) (8 and 14 hours, respectively), this duration of separation between visits was sufficient for drug clearance. During each visit, following oral administration of the drug(s), participants were studied at rest, during standardized exercise, and during performance of an exercise time trial. To further minimize potential health risks associated with administering this novel drug combination to exercising adults in a laboratory environment, the normoxic trials always preceded the hypoxic trials; thus, this design represented a controlled incremental risk (i.e., study of treatments in normoxia at rest, during standardized moderate-intensity exercise, and during vigorous exercise, and then, after a minimum of 7 days, study of treatments in hypoxia during rest, during standardized moderate-intensity exercise, and during vigorous exercise). Neither participants, nor research staff, were naïve as to the environmental condition. To familiarize participants with procedures before the treatment visits, standardized exercise and habituation time trials were completed in normoxia without drug intervention.

Colorado State University (Fort Collins campus) is situated at an altitude of 1525 m ($\sim$5000 ft) above sea level, thus the normoxic conditions may be considered mildly hypobaric (typical barometric pressure $\sim$640 mmHg). All research participants had been residents of Fort Collins for a minimum of 12 months and refrained from travel to sea level destinations before and during study participation.

Protocol

Following a 12-hour fast and 24-hour abstention from vigorous physical activity, research participants arrived at the laboratory and were instrumented for measurement of heart rate (3-lead ECG), blood pressure, and peripheral oxygen saturation (SpO_2, pulse oximeter, physiological monitor, Cardiocap 5; GE Datex-Ohmeda, Madison, WI). An intravenous catheter was inserted into an antecubital vein for subsequent and repeated blood sampling. The venous catheter was kept patent through a saline drip. After recording of baseline vital signs, participants were transferred to a clinical laboratory or to an environmental chamber within which the inspired oxygen concentration could be manipulated (Colorado Altitude Training, Louisville, CO). During the first visit, in the clinical laboratory, the inspired oxygen concentration was normoxic ($FIO_2 = 0.21$), and during the second, it was hypoxic ($FIO_2 = 0.15$) for the entire duration of the trial. Participants rested in a seated position for 15 minutes before oral consumption of placebo, methazolamide, aminophylline, or methazolamide combined with aminophylline. Participants remained resting in the seated position for 4.5 hours. Heart rate, blood pressure, and SpO_2 were recorded every 15 minutes. Fifteen and 120 minutes postdrug administration, standardized nutrition was provided: a liquid meal (250 kcal: 57% carbohydrate, 28% fat, and 15% protein; Ensure, Ross Laboratories, Abbott Park, IL) and an energy-dense sports bar (220 kcal, 58% carbohydrate, 25% fat, and 17% protein; PowerBar Triple Threat, Fremont, MI). Water was consumed ad libitum.

Four and a half hours after drug administration, participants began 30 minutes of standardized exercise on a computer-controlled, electrically braked, stationary cycle ergometer (Dynafit Velotron; Racermate, Inc., Seattle, WA); resistance was set to 100 W. Based on the physiological characteristics

and habitual physical activity of the research participants, this workload represented low- to moderate-intensity exercise that could easily be completed in both normoxia and hypoxia. On completion, participants were permitted a brief (up to 5 minutes) break before beginning an exercise time trial, the goal of which was to perform stationary cycle ergometer exercise equivalent to a distance of 12.5 km (7.75 miles) as quickly as possible. During the time trial, all time cues were hidden from the participants, but feedback regarding distance cycled was provided continuously. Measurements of heart rate, blood pressure, and oxyhemoglobin saturation were made every 5 minutes, and ratings of perceived exertion (Borg, 1982) were made every 10 minutes during both the standardized exercise bout and the time trial.

Blood sampling and analysis

During rest, blood ($\sim$10 mL into a chilled tube and preserved with ethylenediaminetetraacetic acid) was sampled before drug administration and again at times 0, 60, 120, 180, 240, and 270 minutes. During exercise, blood was sampled immediately following completion of the standardized exercise and the time trial. Plasma and red blood cells were separated through chilled (4°C) centrifugation from resting and exercise samples and stored at −80°C for subsequent determination of circulating concentrations of theophylline (the active ingredient of aminophylline) and methazolamide. Approximately 1 mL of each sample collected before and during exercise was also analyzed immediately for lactate concentration using an automated device (2300 STAT Plus Glucose Lactate Analyzer; YSI, Inc., Yellow Springs, OH).

To quantify theophylline concentrations, 800 μL of methanol and 0.2 mmol/L ZnSO4 (70/30, v/v; protein precipitation solution) were added to 200 μL of plasma. Theophylline-d6 (at 500 ng/mL; Toronto Research Chemicals [TRC], Toronto, Canada) was added as an internal standard (Sigma-Aldrich, St Louis, MO) to the protein precipitation solution. After centrifugation (13,000 *g*, 10 minutes, 4°C), 20 μL of the supernatant was injected onto the analytical column of an LC-MS system (Synergi 4u Hydro-RP-80A, 250 × 3.0 mm, 4 μm; Phenomenex, Torrance, CA). The mobile phases consisted of A: 0.1% formic acid and B: methanol. The following gradient was run: 0 to 2.7 minutes with 60% B, 2.7 to 4 minutes with 99% B, and finally the column was re-equilibrated until 5 minutes with 60% B. The flow rate was 0.6 mL/min and the column was kept at 65°C.

Circulating methazolamide concentration was analyzed using a validated and fully automated inline extraction–tandem mass spectrometry assay. Briefly, 800 μL of protein precipitation solution (vide supra) containing d6-methazolamide (at 100 ng/mL, TRC) was added to 200 μL of red blood cell or plasma sample. After centrifugation (13,000 *g*, 10 minutes, 4°C), 50 μL of the supernatant was injected into the HPLC system and loaded onto an extraction column (12.5 × 4.6 mm, Zorbax XDB C8; Agilent Technologies, Palo Alto, CA). Samples were washed with a mobile phase of 70% methanol (B) and 30% 0.1% formic acid (A) with a flow of 3 mL/min. After 1 minute, the switching valve was activated and the analytes were eluted in the back-flush mode from the extraction column onto an analytical column kept at 60°C (Zorbax XDB C8, 150 × 4.6 mm, 5 μm; Agilent Technologies). The mobile phase consisted of B: methanol and A: 0.1% formic acid. The following gradient was run: 0–1 minute: 70% B, 1.1–3.5 minutes: 99% B, and 3.6–4 minutes: 70% B. The flow rate was 1 mL/min throughout the assay.

The HPLC system was interfaced with a triple quadrupole MS (API4000; Applied Biosystems, Foster City, CA). For theophylline, MS was run in positive multiple reaction monitoring (MRM) mode. Peak area ratios obtained from MRM mode of the mass transition for theophylline (181.1 → 124.1 [quantifier transition; declustering potential (DP): 75 V; entrance potential (EP): 10 V; collision energy (CE): 29 V; collision cell exit potential (CXP): 10 V] and 181.1 → 96.1 [qualifier transition; DP: 75 V; EP: 8 V; CE: 24 V; CXP: 10 V]) and its internal standard d6-theophylline (187.2 → 127.1; DP: 75 V; EP: 10 V; CE: 29 V; CXP: 10 V) were used for quantification.

For methazolamide, peak area ratios obtained from negative MRM mode of the mass transition (235.2 → 78.1 [quantifier transition; DP: −52 V; EP: −12 V; CE: −29 V; CXP: −5 V] and 235.2 → 129.1 [qualifier transition; DP: −52 V; EP: −12 V; CE: −19 V; CXP: −9 V]) and its internal standard d6-methazolamide (241.2 → 78.1; DP: −58 V; EP: −12 V; CE: −30 V; CXP: −5 V) were used for quantification.

Statistical analysis

As stated, the purpose of this investigation was to determine the efficacy of aminophylline, methazolamide, and aminophylline combined with methazolamide to attenuate hypoxia-mediated decrements in endurance exercise performance. The overarching goal was to identify an intervention to promote exercise performance in hypoxia, and not to compare the efficacy of three treatments against each other. Accordingly, the influence of the treatments was investigated using a planned comparisons approach where each intervention was compared with placebo. This was accomplished through *post-hoc* investigation of two-way analysis of variance (placebo vs. treatment) with repeated measures on one factor (normoxia vs. hypoxia), and also comparison of the magnitude of hypoxia-mediated decline in time trial performance (i.e., hypoxia time trial–normoxia time trial). The level of statistical significance was set at $p < 0.05$. Correction for multiple comparisons was made using the modified Bonferroni technique. To address potential drug/FIO_2 interactions and drug combination/FIO_2 interactions, differences in circulating concentrations of theophylline (the active ingredient of aminophylline) and methazolamide over time were examined with three-way analyses of variance (normoxia vs. hypoxia) and treatment (individual drug administration vs. combination), with repeated measures on one factor (time). Throughout the manuscript, data are expressed as mean and standard deviation.

Results

Participants

Fifteen research participants were randomly assigned to one of four treatments (Fig. 1). Completing a normoxic and hypoxic visit for one randomly assigned treatment constituted completion of the study. All participants were given the opportunity to re-enroll in the study and complete multiple trials/conditions. If they chose to participate in additional trials, a 7-day washout period separated the hypoxic visit of the previous trial and the normoxic visit of the next, and the new treatment group was selected by the same randomization

procedure. If during the randomization procedure a treatment was selected that the participant had already completed, the double-coin flip process was repeated until a novel treatment for that participant was assigned. Several participants completed multiple trials/conditions: four completed all treatments (placebo, methazolamide, and/or aminophylline), four completed three treatments, one completed two, and six completed one treatment. Each trial completion (normoxic and hypoxic visit for one treatment) was treated as an individual data set. Selected physiological characteristics of the research participants are presented in Table 1. During the trials, one participant reported facial tingling after consuming methazolamide in combination with aminophylline; another reported mild, brief double vision after consuming methazolamide alone. Both participants completed the study. Aside from these two incidents, methazolamide and/or aminophylline were well tolerated.

Resting data

Resting heart rate, blood pressure, and oxyhemoglobin saturation during normoxia and hypoxia with and without methazolamide and/or aminophylline are presented in Table 2. In all treatments, hypoxia increased resting heart rate ($p < 0.012$); compared with placebo, methazolamide and/or aminophylline did not influence the effect of hypoxia on heart rate ($p > 0.60$).

Hypoxia did not influence resting blood pressure (systolic or diastolic; $p > 0.27$). Compared with placebo, systolic blood pressure was lower with the combination of methazolamide and aminophylline; however, this difference did not attain statistical significance ($p = 0.061$).

Hypoxia decreased resting oxyhemoglobin saturation ($p < 0.001$); compared with placebo, methazolamide, aminophylline, or the combination did not influence the effect of hypoxia on oxyhemoglobin saturation ($p > 0.15$).

Standardized exercise

Specific to our participants, the absolute standardized exercise bout (100 W) represented low–moderate-intensity exercise ($\sim$30% of maximal work rate, an estimated metabolic response of $\sim$40% of VO_{2max}, and ratings of perceived exertion between 9 and 12). There was no difference in the relative intensity of the standardized exercise between treatment groups ($p = 0.939$). In all treatments, hypoxia increased the heart rate during standardized exercise (Table 2; $p < 0.048$); compared with placebo, methazolamide and/or aminophylline did not influence the effect of hypoxia on exercising heart rate ($p > 0.56$).

Blood pressure during standardized exercise was unaffected by hypoxia for all treatments (Table 2; $p > 0.10$).

Hypoxia decreased oxyhemoglobin saturation during standardized exercise in all treatments (Table 2; $p < 0.001$). Compared with placebo, methazolamide and methazolamide combined with aminophylline increased oxyhemoglobin saturation ($p < 0.001$). Aminophylline alone did not influence oxyhemoglobin saturation ($p = 0.269$).

Rating of perceived exertion was increased with hypoxia in the aminophylline and methazolamide treatments compared with placebo (Table 2; $p < 0.018$). Methazolamide combined with aminophylline removed the effect of hypoxia compared with placebo ($p = 0.27$).

Time trial

Normoxic time trial performance was not different from the habituation trials for any treatment group (all $p \geq 0.205$). Methazolamide, aminophylline, or methazolamide combined with aminophylline did not affect the time to cycle 12.5 km in normoxia ($p > 0.10$). Time trial performance was slower in hypoxia compared with normoxia with placebo (22.3 ± 2.1 vs. 25.2 ± 5.7 minutes, $p < 0.001$), aminophylline (22.2 ± 1.5 vs. 23.9 ± 2.1 minutes, $p = 0.009$), and methazolamide (23.2 ± 1.6 vs. 24.6 ± 1.6 minutes, $p = 0.023$), but not with methazolamide combined with aminophylline (24.0 ± 1.7 vs. 24.5 ± 1.7 minutes, $p = 0.376$). Examination of the delta values (magnitude of hypoxia-mediated performance decrement) revealed that neither methazolamide nor aminophylline was different from placebo (Fig. 2; $p > 0.09$); the hypoxia-mediated performance decrement with methazolamide combined with aminophylline was less than placebo ($p = 0.01$). It is noteworthy that inspection of Figure 2 reveals two research participants who appear to be outliers (one participant who was considerably slower in hypoxia in the placebo condition and one participant who appeared to be appreciably faster in hypoxia in the combined aminophylline/methazolamide condition). Neither of the participants was a statistical outlier, and removal of either or both participants from the final analyses did not change the overall conclusion pertaining to the ergogenic effect of aminophylline combined with methazolamide in hypoxia.

Hypoxia did not affect the heart rate or systolic and diastolic blood pressures during the time trial (the means of these variables during the entire time trial are presented in Table 2; $p > 0.41$). Hypoxia decreased oxyhemoglobin saturation (Table 2; $p < 0.001$). Compared with placebo, methazolamide and methazolamide and aminophylline increased oxyhemoglobin saturation ($p < 0.02$) in hypoxia. Rating of perceived

Table 1. Select Participant Characteristics

	Placebo	*Aminophylline*	*Methazolamide*	*Combination*
n	9	9	10	8
Age (years)	28 ± 6	27 ± 6	27 ± 6	26 ± 6
BMI (kg/m^2)	24.9 ± 1.8	25.2 ± 1.8	25.1 ± 4.7	24.9 ± 2.0
Body fat %	20.2 ± 2.7	19.3 ± 2.7	20.6 ± 2.2	19.4 ± 2.3
Fat mass (kg)	15.4 ± 2.1	15.0 ± 2.1	16.1 ± 1.9	15.4 ± 2.3
Fat-free mass (kg)	58.4 ± 5.7	59.7 ± 6.6	58.9 ± 7.0	60.8 ± 6.5
VO_{2max} (mL/kg/min)	48.8 ± 8.1	51.4 ± 8.4	49.8 ± 8.2	48.3 ± 7.4
Work rate$_{max}$ (W)	358 ± 57	378 ± 66	371 ± 63	360 ± 59

Data are mean ± SD.
BMI, body–mass index; VO_{2max}, maximal oxygen consumption; *n*, No. of participants.

TABLE 2. AVERAGE HEMODYNAMIC RESPONSES IN NORMOXIA AND HYPOXIA DURING REST, STANDARDIZED EXERCISE (30 MINUTES AT 100 W), AND A 12.5-KM TIME TRIAL

	Placebo, n = *9*		*Aminophylline,* n = *9*		*Methazolamide,* n = *10*		*Combination,* n = *8*	
	N	*H*	N	*H*	N	*H*	N	*H*
HR_{rest}	64 ± 6	72 ± 9*	65 ± 6	74 ± 9*	62 ± 6	68 ± 10*	66 ± 9	72 ± 11*
$HR_{100\,W}$	117 ± 12	132 ± 18*	117 ± 12	134 ± 15*	115 ± 16	126 ± 19*	118 ± 26	130 ± 20*
HR_{TT}	156 ± 12	159 ± 12	162 ± 12	162 ± 9	150 ± 13	152 ± 13	155 ± 14	162 ± 11
SBP_{rest}	121 ± 6	125 ± 12	128 ± 12	120 ± 6	125 ± 6	119 ± 6	123 ± 14	117 ± 6
$SBP_{100\,W}$	139 ± 12	148 ± 15	140 ± 15	142 ± 15	140 ± 10	141 ± 10	138 ± 9	140 ± 11
SBP_{TT}	156 ± 15	157 ± 12	152 ± 15	156 ± 12	148 ± 13	151 ± 16	152 ± 11	150 ± 14
DBP_{rest}	70 ± 6	72 ± 6	71 ± 9	71 ± 6	69 ± 3	71 ± 6	73 ± 9	68 ± 6
$DBP_{100\,W}$	70 ± 9	71 ± 9	73 ± 12	73 ± 9	70 ± 10	68 ± 6	73 ± 9	75 ± 6
DBP_{TT}	71 ± 9	69 ± 9	71 ± 9	73 ± 9	72 ± 13	67 ± 10	74 ± 9	72 ± 6
SpO_{2rest}	95 ± 1	84 ± 3*	96 ± 1	83 ± 3*	96 ± 1	85 ± 3*	97 ± 1	83 ± 6*
$SpO_{2100\,w}$	94 ± 1	75 ± 3*	94 ± 1	78 ± 6*	95 ± 3	83 ± 3*,†	94 ± 3	84 ± 6*,†
SpO_{2TT}	91 ± 3	75 ± 3*	92 ± 3	78 ± 3*	93 ± 3	81 ± 3*,†	93 ± 3	80 ± 6*,†
$RPE_{100\,W}$	10 ± 1	11 ± 1	10 ± 1	12 ± 1	10 ± 1	12 ± 1	11 ± 1	12 ± 1
RPE_{TT}	15 ± 1	16 ± 1	16 ± 1	16 ± 1	16 ± 1	16 ± 1	16 ± 1	16 ± 1

Data are mean ± SD.
*Different than normoxia ($p < 0.05$).
†Different than placebo in hypoxia ($p < 0.05$).
100 W, average values during 30 minutes of standardized exercise at 100 W; DBP, diastolic blood pressure; H, hypoxia; HR, heart rate; N, normoxia; Rest, average resting values; RPE, rating of perceived exertion; SBP, systolic blood pressure; SpO_2, oxyhemoglobin saturation; TT, average values during a 12.5-km time trial.

exertion was unaffected by hypoxia (Table 2; $p > 0.39$). To better describe the dynamic nature of these variables during the 12.5-km time trial, the heart rate (Fig. 3), blood pressure (Fig. 4), oxyhemoglobin saturation (Fig. 5), and rating of perceived exertion (Fig. 6) are also illustrated at 5-minute intervals during the first 15 minutes. Data collected after 20 minutes have been omitted to keep the number of observations (number of subjects) constant. That is, if a participant completed one trial in 19 minutes and another in 21 minutes, only the data up to 15 minutes are presented.

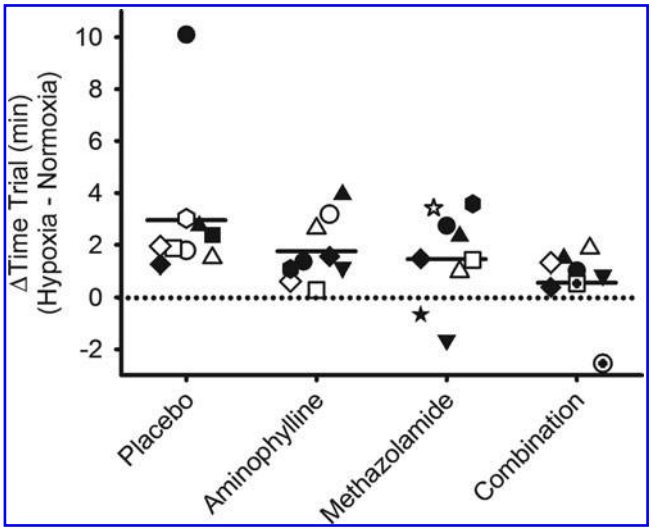

FIG. 2. Change in 12.5-km time trial performance from normoxia to hypoxia following oral administration of placebo, methazolamide, aminophylline, or methazolamide with aminophylline. *Symbols* represent individual research participants. *Heavy line* represents group mean. *Dotted line* represents no change from normoxia; symbols above the *dotted line* represent slower time trial performance in hypoxia, and symbols below the line are time trial performances that are faster in hypoxia compared with normoxia.

Blood data—methazolamide and theophylline concentrations

The active drug components of methazolamide and aminophylline are methazolamide and theophylline, respectively; the concentrations of these components in plasma (both methazolamide and theophylline) and red blood cells (methazolamide only) were measured over the course of each condition (Fig. 7). Hypoxia did not affect plasma theophylline concentrations whether aminophylline was taken alone or with methazolamide ($p > 0.80$). When aminophylline was administered alone or in combination with methazolamide, theophylline concentrations peaked at 180 minutes in normoxia and hypoxia. In plasma, hypoxia increased methazolamide concentrations when methazolamide was taken alone ($p = 0.01$) and with aminophylline ($p = 0.04$). Plasma methazolamide concentrations peaked at 240 minutes in normoxia and hypoxia. Hypoxia also augmented the rate of increase of red blood cell concentration of methazolamide such that it was greater at 60 minutes (normoxia: 22.3 ± 25.0 μg/mL; hypoxia: 30.1 ± 30.0 μg/mL; $p = 0.001$). However, when methazolamide was taken with aminophylline, the influence of hypoxia on red blood cell concentration of methazolamide was removed ($p = 0.08$). Red blood cell concentrations of methazolamide peaked at 180 minutes when methazolamide was given alone in both normoxia and hypoxia. When aminophylline was given in combination with methazolamide, the red blood cell concentration of methazolamide peaked at 240 minutes in normoxia and 120 minutes in hypoxia.

Blood lactate following exercise

Blood lactate concentration was unaffected by the standardized exercise bout regardless of hypoxia and treatment

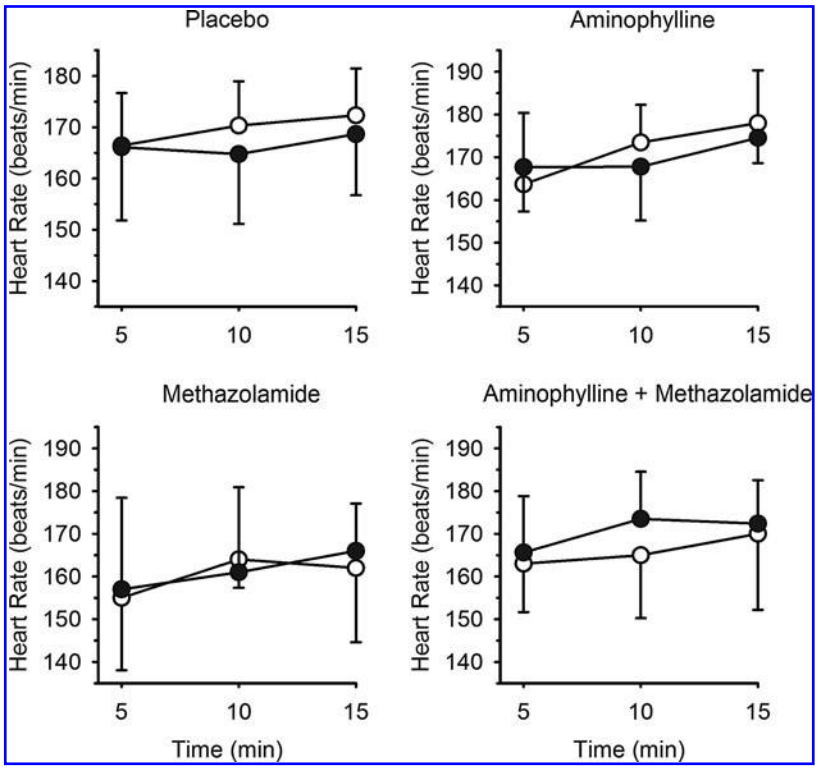

FIG. 3. Heart rate response during the 12.5-km time trial in normoxia and hypoxia following oral administration of placebo, methazolamide, and/or aminophylline. The *open circles* represent normoxia, and the *closed circles* represent hypoxia. Data are mean ± SD.

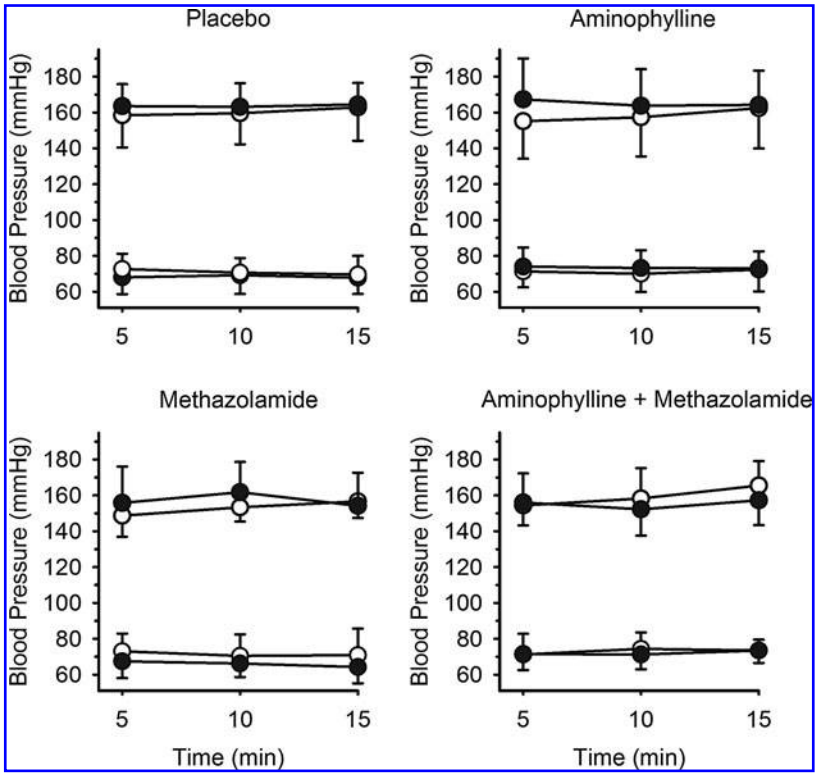

FIG. 4. Systolic and diastolic blood pressure response during the 12.5-km time trial in normoxia and hypoxia following oral administration of placebo, methazolamide, and/or aminophylline. The *open circles* represent normoxia, and the *closed circles* represent hypoxia. Data are mean ± SD.

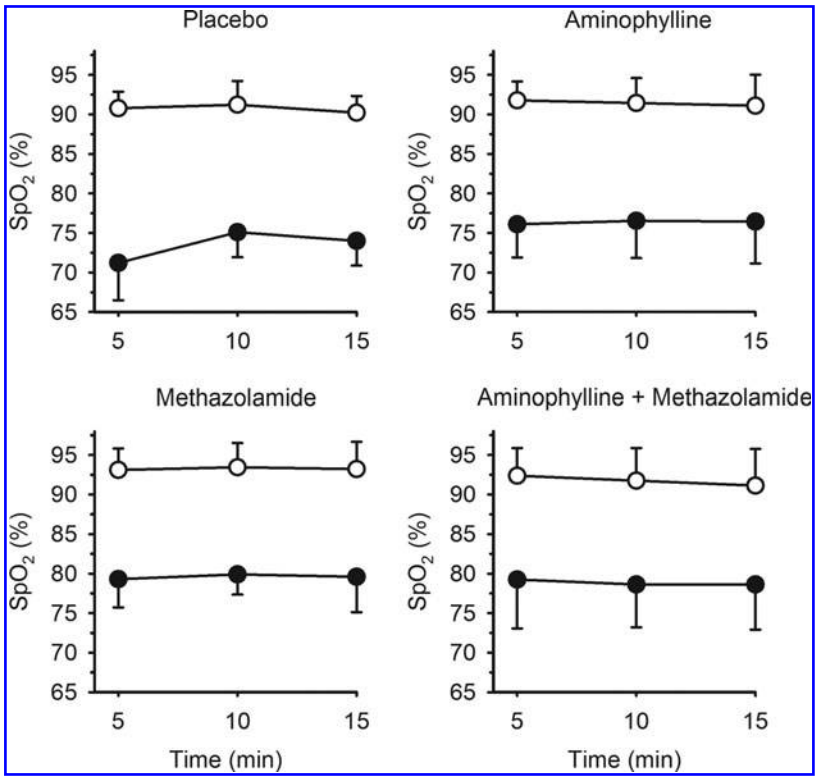

FIG. 5. Oxyhemoglobin saturation response during the 12.5-km time trial in normoxia and hypoxia following oral administration of placebo, methazolamide, and/or aminophylline. The *open circles* represent normoxia, and the *closed circles* represent hypoxia. Data are mean ± SD.

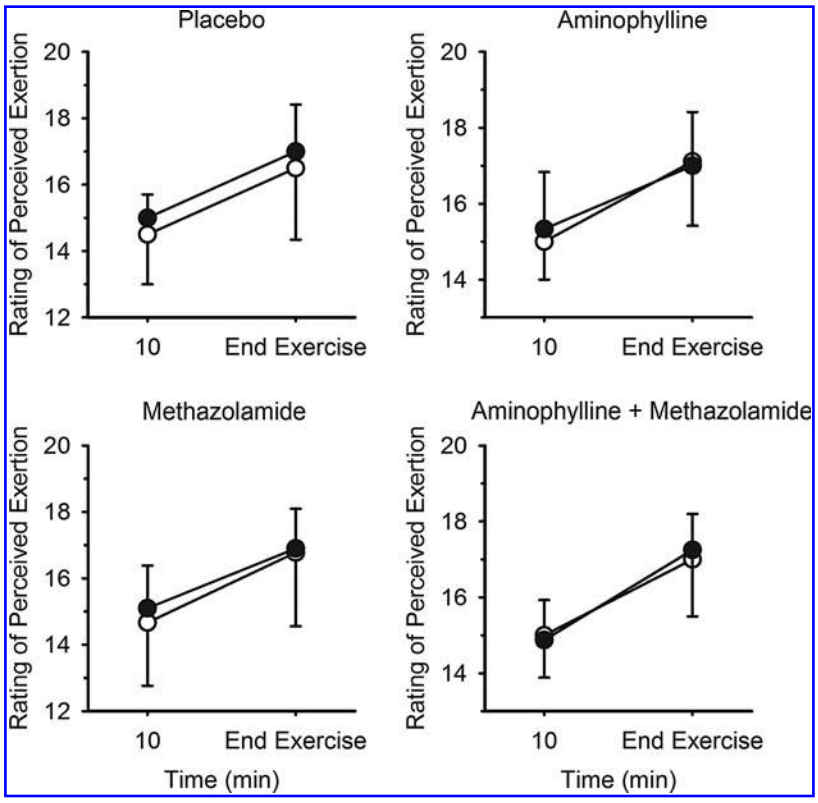

FIG. 6. Rating of perceived exertion response during the 12.5-km time trial in normoxia and hypoxia following oral administration of placebo, methazolamide, and/or aminophylline. The *open circles* represent normoxia, and the *closed circles* represent hypoxia. Data are mean ± SD.

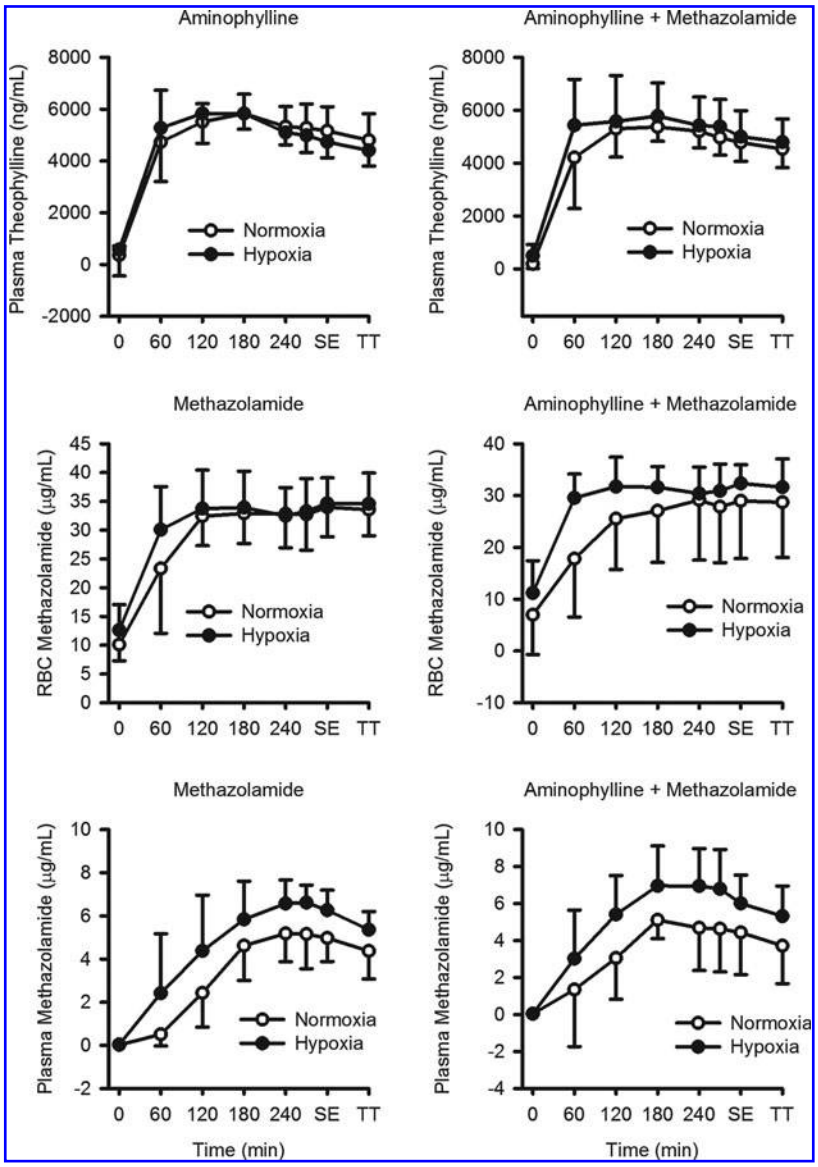

FIG. 7. Plasma concentrations of theophylline and methazolamide and red blood cell concentrations of methazolamide in normoxia and hypoxia following oral administration of methazolamide and/or aminophylline (theophylline). Data are mean ± SD. Hypoxia did not affect plasma theophylline concentrations, whether aminophylline was taken alone or with methazolamide ($p > 0.80$), but did increase plasma methazolamide concentrations when methazolamide was taken alone ($p = 0.01$) or with aminophylline ($p = 0.04$). Red blood cell concentrations of methazolamide were greater at 60 minutes in hypoxia when methazolamide was taken alone ($p = 0.001$), but not when methazolamide was taken with aminophylline ($p = 0.08$). SE, standardized exercise; TT, time trial.

(Table 3; $p > 0.188$) and was always greater at completion of the time trial compared with any other point for all treatments ($p < 0.001$). Hypoxia did not affect blood lactate ($p > 0.42$). Blood lactate was lower at the completion of the time trial with both methazolamide alone and in combination with aminophylline ($p < 0.021$).

Discussion

The novel finding of this study was that compared with placebo, methazolamide combined with aminophylline abrogated the hypoxia-mediated decrement in endurance exercise performance. This beneficial effect may have been mediated, in part, through a smaller magnitude of decrease in oxyhemoglobin saturation during exposure to the simulated high-altitude environment. When administered alone, neither methazolamide nor aminophylline influenced endurance exercise performance in hypoxia compared with placebo. These data imply that coadministration of methazolamide and aminophylline may promote endurance exercise performance during a brief sojourn to high altitude.

While it was not the purpose of the current study to provide a mechanism of ergogenic action of the drug combination, a brief discussion is warranted. The favorable effects of methazolamide combined with aminophylline in hypoxia represent a novel off-target application of two established drugs. Methazolamide is indicated for the lowering of intraocular pressure before and during treatment for glaucoma. Its primary mechanism of action is through inhibition of carbonic anhydrase. Indications for the use of aminophylline are

Table 3. Blood Lactate Concentration in Normoxia and Hypoxia

	Placebo, n = *9*		*Aminophylline,* n = *9*		*Methazolamide,* n = *10*		*Combination,* n = *8*	
	N	*H*	N	*H*	N	*H*	N	*H*
$[La^-]_{rest}$	0.8 ± 0.3	0.9 ± 0.1	0.8 ± 0.1	1.0 ± 0.3	0.7 ± 0.3	0.7 ± 0.3	0.8 ± 0.3	0.9 ± 0.3
$[La^-]_{100W}$	0.9 ± 0.3	1.3 ± 0.9	0.9 ± 0.3	1.3 ± 0.6	0.7 ± 0.3	0.9 ± 0.6	1.2 ± 1.1	1.5 ± 0.8
$[La^-]_{TT}$†	6.3 ± 1.8	5.1 ± 2.1	6.1 ± 1.5	5.3 ± 1.5	3.8 ± 1.9*	3.2 ± 1.3*	3.8 ± 1.4*	3.3 ± 1.1*

Data are mean ± SD.
*Different than placebo ($p < 0.05$).
†Different than rest and 100 W ($p < 0.001$).
100 W, at completion of 30 minutes of standardized exercise; H, hypoxia; [La⁻], blood lactate concentration; N, normoxia; TT, at completion of 12.5-km time trial.

usually related to relief from symptoms of asthma and other chronic pulmonary diseases. Its actions are mediated through nonselective inhibition of phosphodiesterase and adenosine receptor antagonism. When administered in combination, the separate mechanism(s) of action of each of these drugs may have proved complimentary. That is, it is plausible that methazolamide may have augmented ventilation to increase oxyhemoglobin saturation and increased renal secretion of bicarbonate, leading to metabolic acidosis, thus attenuating the leftward shift in the oxyhemoglobin dissociation curve usually observed during immediate exposure to hypoxia (Lahiri, 1977). Additionally, methazolamide may have attenuated the increase in mean pulmonary arterial pressure often observed when breathing hypoxic gases (Pickerodt et al., 2014). The inhibition of phosphodiesterase, plus the antagonism of adenosine receptors, associated with aminophylline use may have increased cardiac output and augmented systemic circulation (Vestal et al., 1983; Goirand et al., 2001; Lopez et al., 2012) while potentially preventing hypoxia-mediated pulmonary vasoconstriction (Naeije and Dedobbeleer, 2013). Thus, in combination, methazolamide and aminophylline may have promoted oxygen delivery to exercising tissue in hypoxia. It is noteworthy that based on observations during habituation, the combination of methazolamide and aminophylline did not improve time trial performance in normoxia. While we acknowledge the limitations of comparing habituation trials with the normoxic drug conditions, these comparisons imply that under normal conditions (i.e., normoxia), the drug combination is not ergogenic. Furthermore, the mechanism by which methazolamide may have increased ventilation during exercise is not clear. Carbonic anhydrase inhibition through acetazolamide is known to increase ventilation during cycle ergometer exercise while breathing normoxic and hypoxic gases (Schoene et al., 1983); we are unable to implicitly attribute any possible change in ventilation with methazolamide in the current study to carbonic anhydrase inhibition and recognize that other differences exist between the physiological effects of acetazolamide and methazolamide (Teppema et al., 2006).

Compared with placebo, methazolamide combined with aminophylline abrogated the decrement in endurance exercise performance during brief (~5 hours) exposure to simulated high altitude. One important limitation of the current investigation is the data do not provide any insight as to the beneficial effects of this drug combination over longer durations (hours/days). Presumably the ergogenic benefits over longer duration visits would require additional doses of the drug combination, potentially increasing the risk of unfavorable reactions (side effects) of the drugs. Another important consideration pertains to the gradual acclimation to high altitude as the duration of the visit increases. The influence of methazolamide combined with aminophylline on the rate of acclimation to high altitude is unknown; it is possible that the short-term benefits of the drug combination may interfere with some of the physiological processes required for high-altitude acclimation. Consistent with this, administration of the carbonic anhydrase inhibitor, acetazolamide, over two weeks at 4120 m attenuates the improvement of oxyhemoglobin saturation during exercise in hypoxia (Lafleur et al., 2010), implying that pharmaceutical strategies to promote rapid acclimation to hypoxia may be better suited for brief exposures rather than longer-term visits. It may be that repeated drug dosing negates the need for acclimatization over extended high-altitude exposure.

Many nutraceutical and pharmacological strategies have been explored to prevent hypoxia/hypobaria-mediated decline in physiological function. Some of these strategies have focused primarily on alleviating nausea and acute mountain sickness (Fischer et al., 2000; Kupper et al., 2008; Ritchie et al., 2012). In this regard, acetazolamide, commonly administered as Diamox, is widely accepted as an effective prophylaxis, reducing nausea symptoms by half (Ritchie et al., 2012) and even improving periodic sleep-disordered breathing in hypoxia (Hackett et al., 1987; Fischer et al., 2004). In the current investigation, we did not record symptoms of acute mountain sickness and therefore have no direct observations pertinent to how aminophylline and/or methazolamide might influence this disorder. However, previous studies have reported on the beneficial effects of theophylline administration, including reduced acute mountain sickness and apneic episodes during sleep (Fischer et al., 2000; Fischer et al., 2004; Kupper et al., 2008). Additionally, methazolamide has been reported to be as effective as acetazolamide in reducing acute mountain sickness symptoms (Wright et al., 1983). Collectively, these observations imply that in addition to an ergogenic effect, the combination of aminophylline and methazolamide may also alleviate acute mountain sickness.

In the current study, methazolamide, presumably through carbonic anhydrase inhibition, lowered circulating lactate concentration at the completion of the time trial (both methazolamide and methazolamide combined with aminophylline). This observation is consistent with previous reports (Davies et al., 1986; Scheuermann et al., 2000) and may be attributed to increased clearance of lactate by nonexercising tissues (Scheuermann et al., 2000) or a decrease in lactate efflux from exercising skeletal muscle (Kowalchuk et al., 2000).

Several other considerations pertaining to the current study and outcomes are worthy of mention: (1) A repeated-measures crossover design, in which the same research participants completed the placebo and all of the drug treatments

(individual and combination), would have strengthened our conclusions; however, the required number and duration of laboratory visits for each participant ($\sim$45 hours over 10 visits) in addition to the cost–benefit and potential safety concerns of repeated exposures to hypoxia and/or drug treatments made such an approach unfeasible. (2) Research participants completed only one habituation protocol before normoxic time trial performance with one of the treatments. It is plausible that one habituation protocol may have been insufficient, thus when combined with the standardized order of normoxic and then hypoxic time trials, the hypoxia-mediated performance decrement may have been underexaggerated. We do not believe this to be the case given the lack of appreciable difference between the habituation and normoxic time trials, and also based on previous reports of high consistency and reproducibility across self-paced laboratory tests (Stone et al., 2011; Thomas et al., 2012; Gee et al., 2013). (3) The active ingredient in aminophylline, theophylline, has a narrow therapeutic window. A small dose may prove to be ineffective, while a larger dose may increase the risk of overdose and/or toxicity. In the current study, all research participants were administered the same absolute dose. To decrease the chances of overdose, a body mass >68 kg was adopted as an inclusion criterion. Adults with a body mass <68 kg may need to consider a smaller dose. It is noteworthy that the data collected during the standardized exercise (100 W; Table 2) suggest that the drug treatments do not evoke abnormal or exaggerated responses to low–moderate-intensity exercise in either normoxia or hypoxia. (4) Finally, all of the research participants in the current investigation were male. While we have no reason to suspect drug tolerance and the beneficial effects in hypoxia would be different in females, we have no direct evidence to support or refute this.

In summary, rapid transition from sea level to high altitude is accompanied by impaired physiological function and decreased capacity for physical work. Based on experimental animal data, we have examined, in humans, the efficacy of aminophylline, methazolamide, and aminophylline combined with methazolamide to promote exercise performance in simulated high altitude (hypoxia). Compared with placebo, methazolamide combined with aminophylline abrogated the hypoxia-mediated decrement in endurance exercise performance. This novel off-target application of two established drugs may be of ergogenic benefit to professional and recreational travelers during sojourns at high altitude.

Acknowledgment

The Defense Advanced Research Projects Agency (DARPA) supported this study (N66001-10-c-2134). Trial Registration ClinicalTrials.gov Identifier: NCT01702025.

Author Disclosure Statement

No competing financial interests exist.

References

Aslaksen A, Bakke OM, and Vigander T. (1981). Comparative pharmacokinetics of theophylline and aminophylline in man. Br J Clin Pharmacol 11:269–273.

Borg GA. (1982). Psychophysical bases of perceived exertion. Med Sci Sports Exerc 14:377–381.

Bradwell AR, Dykes PW, Coote JH, Forster PJ, Milles JJ, Chesner I, and Richardson NV. (1986). Effect of acetazolamide on exercise performance and muscle mass at high altitude. Lancet 1:1001–1005.

Chapman RF, Emery M, and Stager JM. (1999). Degree of arterial desaturation in normoxia influences VO2max decline in mild hypoxia. Med Sci Sports Exerc 31:658–663.

Davies SF, Iber C, Keene SA, McArthur CD, and Path MJ. (1986). Effect of respiratory alkalosis during exercise on blood lactate. J Appl Physiol (1985) 61:948–952.

Ferretti G, Moia C, Thomet JM, and Kayser B. (1997). The decrease of maximal oxygen consumption during hypoxia in man: a mirror image of the oxygen equilibrium curve. J Physiol 498 (Pt 1):231–237.

Fischer R, Lang SM, Leitl M, Thiere M, Steiner U, and Huber RM. (2004). Theophylline and acetazolamide reduce sleep-disordered breathing at high altitude. Eur Respir J 23: 47–52.

Fischer R, Lang SM, Steiner U, Toepfer M, Hautmann H, Pongratz H, and Huber RM. (2000). Theophylline improves acute mountain sickness. Eur Respir J 15:123–127.

Fulco CS, Rock PB, and Cymerman A. (1998). Maximal and submaximal exercise performance at altitude. Aviat Space Environ Med 69:793–801.

Fulco CS, Rock PB, Trad LA, Rose MS, Forte VA, Jr., Young PM, and Cymerman A. (1994). Effect of caffeine on submaximal exercise performance at altitude. Aviat Space Environ Med 65:539–545.

Gee TI, French DN, Gibbon KC, and Thompson KG. (2013). Consistency of pacing and metabolic responses during 2000-m rowing ergometry. Int J Sports Physiol Perform 8: 70–76.

Goirand F, Bardou M, Dumas J, Rochette L, and Dumas M. (2001). Effects of phosphodiesterase inhibitors on hypoxic pulmonary vasoconstriction. Influence of K(+) channels and nitric oxide. Eur J Pharmacol 417:141–148.

Hackett PH, Roach RC, Harrison GL, Schoene RB, and Mills WJ, Jr. (1987). Respiratory stimulants and sleep periodic breathing at high altitude. Almitrine versus acetazolamide. Am Rev Respir Dis 135:896–898.

Hsu AR, Barnholt KE, Grundmann NK, Lin JH, McCallum SW, and Friedlander AL. (2006). Sildenafil improves cardiac output and exercise performance during acute hypoxia, but not normoxia. J Appl Physiol (1985) 100:2031–2040.

Kowalchuk JM, Smith SA, Weening BS, Marsh GD, and Paterson DH. (2000). Forearm muscle metabolism studied using (31)P-MRS during progressive exercise to fatigue after Acz administration. J Appl Physiol (1985) 89:200–209.

Kressler J, Stoutenberg M, Roos BA, Friedlander AL, Perry AC, Signorile JF, and Jacobs KA. (2011). Sildenafil does not improve steady state cardiovascular hemodynamics, peak power, or 15-km time trial cycling performance at simulated moderate or high altitudes in men and women. Eur J Appl Physiol 111: 3031–3040.

Kupper TE, Strohl KP, Hoefer M, Gieseler U, Netzer CM, and Netzer NC. (2008). Low-dose theophylline reduces symptoms of acute mountain sickness. J Travel Med 15:307–314.

Lafleur JE, Bartniczuk D, Collier A, Griffin N, and Swenson ER. (2010). Acetazolamide and exercise hypoxia. Int J Sports Med 31:372–376.

Lahiri S. (1977). Physiological responses and adaptations to high altitude. Int Rev Physiol 15:217–251.

Lara B, Salinero JJ, and Del Coso J. (2014). Altitude is positively correlated to race time during the marathon. High Alt Med Biol 15:64–69.

Lawler J, Powers SK, and Thompson D. (1988). Linear relationship between VO2max and VO2max decrement during exposure to acute hypoxia. J Appl Physiol (1985) 64:1486–1492.

Li P, Zhang G, You HY, Zheng R, and Gao YQ. (2012). Training-dependent cognitive advantage is suppressed at high altitude. Physiol Behav 106:439–445.

Lopez MG, Silva BM, Joyner MJ, and Casey DP. (2012). Ischemic exercise hyperemia in the human forearm: reproducibility and roles of adenosine and nitric oxide. Eur J Appl Physiol 112:2065–2072.

Maren TH, Haywood JR, Chapman SK, and Zimmerman TJ. (1977). The pharmacology of methazolamide in relation to the treatment of glaucoma. Invest Ophthalmol Vis Sci 16:730–742.

Martin D, and O'Kroy J. (1993). Effects of acute hypoxia on the VO2 max of trained and untrained subjects. J Sports Sci 11: 37–42.

Naeije R, and Dedobbeleer C. (2013). Pulmonary hypertension and the right ventricle in hypoxia. Exp Physiol 98:1247–1256.

Peltonen GL, Scalzo RL, Schweder MM, Larson DG, Luckasen GJ, Irwin D, Hamilton KL, Schroeder T, and Bell C. (2012). Sympathetic inhibition attenuates hypoxia induced insulin resistance in healthy adult humans. J Physiol 590:2801–2809.

Pickerodt PA, Francis RC, Hohne C, Neubert F, Telalbasic S, Boemke W, and Swenson ER. (2014). Pulmonary vasodilation by acetazolamide during hypoxia: impact of methyl-group substitutions and administration route in conscious, spontaneously breathing dogs. J Appl Physiol (1985) 116:715–723.

Radiloff DR, Zhao Y, Boico A, Wu C, Shan S, Palmer G, Hamilton K, Irwin D, Hanna G, Piantadosi CA, et al. (2012). The combination of theophylline and endothelin receptor antagonism improves exercise performance of rats under simulated high altitude. J Appl Physiol (1985) 113:1243–1252.

Richards JC, Johnson TK, Kuzma JN, Lonac MC, Schweder MM, Voyles WF, and Bell C. (2010). Short-Term Sprint Interval Training Increases Insulin Sensitivity In Healthy Adults But Does Not Affect The Thermogenic Response to Beta-Adrenergic Stimulation. J Physiol 588:2961–2972.

Ritchie ND, Baggott AV, and Andrew Todd WT. (2012). Acetazolamide for the prevention of acute mountain sickness—a systematic review and meta-analysis. J Travel Med 19:298–307.

Scheuermann BW, Kowalchuk JM, Paterson DH, Taylor AW, and Green HJ. (2000). Muscle metabolism during heavy-intensity exercise after acute acetazolamide administration. J Appl Physiol (1985) 88:722–729.

Schoene RB, Bates PW, Larson EB, and Pierson DJ. (1983). Effect of acetazolamide on normoxic and hypoxic exercise in humans at sea level. J Appl Physiol Respir Environ Exerc Physiol 55:1772–1776.

Schulz HU, Steinijans VW, and Gabel H. (1984). Differences in steady-state plasma levels between aminophylline and theophylline sustained-release micropellets after repeated circadian dosing. Int J Clin Pharmacol Ther Toxicol 22: 621–625.

Stadelmann K, Latshang TD, Tarokh L, Lo Cascio CM, Tesler N, Stoewhas AC, Kohler M, Bloch KE, Huber R, and Achermann P. (2014). Sleep respiratory disturbances and arousals at moderate altitude have overlapping electroencephalogram spectral signatures. J Sleep Res 23:463–468.

Stager JM, Tucker A, Cordain L, Engebretsen BJ, Brechue WF, and Matulich CC. (1990). Normoxic and acute hypoxic exercise tolerance in man following acetazolamide. Med Sci Sports Exerc 22:178–184.

Stone MR, Thomas K, Wilkinson M, St Clair Gibson A, and Thompson KG. (2011). Consistency of perceptual and metabolic responses to a laboratory-based simulated 4,000-m cycling time trial. Eur J Appl Physiol 111:1807–1813.

Teppema LJ, Bijl H, Mousavi Gourabi B, and Dahan A. (2006). The carbonic anhydrase inhibitors methazolamide and acetazolamide have different effects on the hypoxic ventilatory response in the anaesthetized cat. J Physiol 574:565–572.

Thomas K, Stone MR, Thompson KG, St Clair Gibson A, and Ansley L. (2012). Reproducibility of pacing strategy during simulated 20-km cycling time trials in well-trained cyclists. Eur J Appl Physiol 112:223–229.

Vestal RE, Eiriksson CE, Jr., Musser B, Ozaki LK, and Halter JB. (1983). Effect of intravenous aminophylline on plasma levels of catecholamines and related cardiovascular and metabolic responses in man. Circulation 67:162–171.

Weinberger M, and Hendeles L. (1996). Theophylline in asthma. N Engl J Med 334:1380–1388.

Wright AD, Bradwell AR, and Fletcher RF. (1983). Methazolamide and acetazolamide in acute mountain sickness. Aviat Space Environ Med 54:619–621.

Address correspondence to:
Christopher Bell, PhD
Department of Health and Exercise Science
Colorado State University
205E Moby B Complex
Fort Collins, CO 80523-1582

E-mail: christopher.bell@colostate.edu

Received June 11, 2015;
accepted in final form September 13, 2015.

Video Article

Automated Measurement of Microcirculatory Blood Flow Velocity in Pulmonary Metastases of Rats

Gert Blueschke*[1], Gabi Hanna*[2], Andrew N. Fontanella[2], Gregory M. Palmer[2], Alina Boico[2], Hooney Min[2], Mark W. Dewhirst[2], David C. Irwin[3], Yulin Zhao[2], Thies Schroeder[4]

[1]Division of Plastic, Maxillofacial, and Oral Surgery, Duke University Medical Center

[2]Department of Radiation Oncology, Duke University Medical Center

[3]Department of Cardiology, University of Colorado Denver

[4]Department of Physical Chemistry, University of Mainz

*These authors contributed equally

Correspondence to: Thies Schroeder at thschroe@uni-mainz.de

URL: http://www.jove.com/video/51630
DOI: doi:10.3791/51630

Keywords: Cancer Biology, Issue 93, Lung metastases, intravital microscopy, tumor blood flow, tumor vasculature, blood flow velocity, sarcoma metastasis, breast cancer metastasis

Date Published: 11/30/2014

Citation: Blueschke, G., Hanna, G., Fontanella, A.N., Palmer, G.M., Boico, A., Min, H., Dewhirst, M.W., Irwin, D.C., Zhao, Y., Schroeder, T. Automated Measurement of Microcirculatory Blood Flow Velocity in Pulmonary Metastases of Rats. *J. Vis. Exp.* (93), e51630, doi:10.3791/51630 (2014).

Abstract

Because the lung is a major target organ of metastatic disease, animal models to study the physiology of pulmonary metastases are of great importance. However, very few methods exist to date to investigate lung metastases in a dynamic fashion at the microcirculatory level, due to the difficulty to access the lung with a microscope. Here, an intravital microscopy method is presented to functionally image and quantify the microcirculation of superficial pulmonary metastases in rats, using a closed-chest pulmonary window and automated analysis of blood flow velocity and direction. The utility of this method is demonstrated to measure increases in blood flow velocity in response to pharmacological intervention, and to image the well-known tortuous vasculature of solid tumors. This is the first demonstration of intravital microscopy on pulmonary metastases in a closed-chest model. Because of its minimized invasiveness, as well as due to its relative ease and practicality, this technology has the potential to experience widespread use in laboratories that specialize on pulmonary tumor research.

Video Link

The video component of this article can be found at http://www.jove.com/video/51630/

Introduction

The lung is one of the most important target organs of metastatic disease, and because this condition is difficult to treat successfully with chemo- and radiation therapy, a cure is still rare[1,2]. Specific pathophysiological and microcirculatory features of solid primary and metastatic tumors, such as microregional hypoxia, diffusion limitation and inefficient tumor vasculature, greatly contribute to their resistance to anticancer treatment[3,4]. Due to the microscopic scale and dynamic nature of parameters such as microvascular blood flow, intravital microscopy of the tumor in the living animal has become a very important research tool in the field[5]. While intravital microscopy models have been applied to tumors in different organ sites, including the metastatic lung within an open rib cage, no protocol has been developed yet for the research of pulmonary metastases in a physiologically preserving, closed-chest environment[6,7]. Such an endeavor is particularly hampered by the necessity to surgically access the rib cage without affecting the overall function of the lung[7-9]. Recently, a method was introduced to image pulmonary microcirculatory blood flow in a close-chest setting in live rats, using fluorescence intravital microscopy[10]. This protocol enables the systematic quantification of blood flow velocity from injected, fluorescently labeled red blood cells, using computerized analysis, while keeping the animal physiologically stable and preserving the integrity of the lung[11]. In this present study, it is shown how this technology can be modified to image and quantify microcirculatory blood flow in tail vein-inoculated pulmonary metastases on the pleural surface in the immunocompromised rat. This model is also the first one to study metastatic lung tumors in a closed-chest intravital microscopy setting.

Protocol

NOTE: All animal related procedures described in this protocol have been previously approved by the Duke University Institutional Animal Care and Use Committee (DUIACUC).

1. Cancer Cell Culture and Injection

1. Cultivate fluorescently labeled metastatic cancer cells (*e.g.* human MDAMB231-GFP breast cancer cells, gift from Dr. Patricia Steeg, NCI, and YFP-labeled mouse sarcoma cells, gift from Dr. David Kirsch, Duke University Medical Center, Department of Radiation Oncology) in appropriate culture medium (*e.g.* Dulbecco's Modified Eagle Medium (DMEM) with 10% fetal bovine serum and 1% penicillin/streptavidin) at 37 °C until approximately 90% confluent.
2. Trypsinize cells, wash them 2 times with PBS, count, and then inject them into the tail veins of isoflurane-anesthetized 10 weeks old female nude rats at 5 million cells per animal, using a syringe with a 27 G needle. Surgical level anesthesia is verified by the lack of reaction to toe pinch.

2. Monitoring of Metastases Using MicroCT

1. Examine rats once a week using a micro-CT/micro-Irradiator, to detect the presence of metastases above approximately 2 mm in diameter in diameter. The micro-CT is commissioned as previously described[12].
    1. Subject rats to 3% isoflurane anesthesia prior to imaging. Confirm deep anesthesia by toe pinch.
    2. After onset of anesthesia, quickly transfer rats to the imaging cradle in the imaging chamber and connect via a nose-cone to an isoflurane-air mixture at 2.5-3%. Adjust the position of the rat in the cradle in a way that its thorax is positioned in the photon beam of the MicroCT scanner, using the external position controls and laser delimiter on the imaging cradle. Ensure the door to the imaging chamber is closed, to shield the investigator from the gamma rays.
    3. Control the position of the animal again using the color video camera. Perform a low-resolution CT imaging test run, and use the resulting image to adjust the field of view to the xyz dimensions of the thoracic cavity.
    4. Image the rat thorax using a 2 mm Al filter at 40 kVp, 2.5 mA, and 0.008 voxel at 7 FPS and return the animal to its cage. Imaging of one animal should take not more than 15 or 20 min. Do not return an animal that has undergone surgery to the company of other animals until fully recovered. Do not leave an animal unattended until it has regained sufficient consciousness to maintain sternal recumbency.
    5. Confirm metastases by the appearance of relatively radio-opaque objects that cannot be explained by intrathoracic blood vessels (**Figure 1A**)

3. Window Chamber Surgery

1. Anesthesia, vital signs and tail vein catheterization
    1. Select animals with presence of metastatic disease. Inject animal with an intraperitoneal dose of 50 mg/kg pentobarbital. Confirm surgical-level anesthesia by toe pinch before proceeding.
    Note: Anesthesia protocols should be matched to the respective experimental setup. Pentobarbital was chosen here as a long-acting anesthetic, in order to induce deep anesthesia for lengthy procedures, while offering the option of facile re-dosing. However, loss of animals to overdosing is a common problem with pentobarbital anesthesia. Another option that preserves autonomic reflexes to a larger degree than pentobarbital is ketamine in combination with sedatives such as xylazine or medetomidine, which however permits only for a single re-dosing cycle.
    2. Shave animals on the side of the body that has the metastatic disease, and in the neck area, using a clipper. Wipe off all remaining loose hair from the skin. After loose hair is removed, apply veterinary ointment to the eyes, to prevent them from drying out.
    NOTE: Athymic nude rats may have residual hair that requires removal before proceeding with surgical procedures. It is very important to remove all hair thoroughly, as it may interfere with surgical procedures and imaging.
    3. Fix the animal in a supine position on a metal plate that is placed on a 37 °C water circulated heating pad. The front and hind extremities are fixed on the plate with tape.
    NOTE: It is useful to control and record vital signs, such as heart rates and arterial blood oxygenation by using a pulse oximeter, throughout surgical and experimental procedures.

2. Tracheal intubation
    1. In order to place a catheter for ventilation of the animal, first make a transversal cervical skin incision, followed by the median separation of the longitudinal musculature ventral to the trachea.
    2. Use repeated opening-to-closing action with a sharp forceps to create a passage for the suture through the dorsal side of the trachea.
    3. Make a small incision into the trachea on the ventral side, not more than semi-circular, approximately between the second and third tracheal ring. Leave a sufficiently long portion of the trachea exposed on the dorsal surface, to enable fixation of the tracheal catheter.
    4. Insert a 2.5 to 3.0 mm "Y" tracheal cannula into the trachea, and tighten with a 4-0 monofilament suture. Ensure the cannula is connected to a pressure cycled ventilator with a bottle connected to the expiration duct that is filled with 6 cm of water, to maintain positive pulmonary pressure. Inflowing gas should be 100% oxygen, unless experimentally desired otherwise.
    5. Insert a catheter with a 25-27 G needle, and filled with heparinized saline into one of the tail veins of the rat, and fix in place with tape.
    NOTE: Ensure patency of the tail vein catheter throughout the procedure by repeatedly injecting a small amount of heparinized saline into the tail vein. Also, oro-tracheal intubation, i.e. the guidance of a tracheal tube via the mouth of the anesthetized animal and past the larynx into the trachea, is a possible alternative to the tracheotomy procedure that is described here. However,this method requires special training and experience, to avoid damage to the trachea, and also to preclude the accidental cannulation of the esophagus.

3. Application of pulmonary window
    1. Remove the skin from the side of the chest where the metastatic disease is located, by creating an incision, and then detaching the skin using blunt dissection.
    Note: The skin can be excised and removed subsequent to detachment

2. Proceed by dissecting the two layers of overlaying musculature (pectoralis, serratus, and latissimus dorsi), but leaving the intercostal muscles intact. Create a perforation in the chest cavity of approximately 1.5 cm in diameter, by removing portions of typically two adjacent ribs. Ideally, locate the perforation in of the region of the sixth and seventh ribs.
3. Osteotomy:
    1. To minimize bleeding and damage to the lung surface, tightly hold the rib to be cut with a toothed surgical forceps during cutting. Using surgical scissors, cut the medial side of the rib first, at an angle of approximately 45°, leaving the pointed side of the remaining rib bone pointing outside.
    2. Subsequently, cut the lateral side of the rib bone in a similar manner, again leaving the pointed side of the rib bone pointing outwards, to prevent damage to the lung surface.
    3. Repeat the procedure for the adjacent rib, then cut the intercostal muscles and remove the excised piece. During this procedure, maintain lung pressure in a way that mechanical interaction between the lung surface and the rib cage is minimized. Do this by appropriately regulating inspiration pressure on the ventilator.

4. Insertion of the window:
    1. Insert a custom made lung window, consisting of a coverglass that is attached to a Plexiglas socket (**Figure 1B**). Attach the window to the socket by gluing, or by applying a very small amount of vacuum grease. Insert the window in a way that surface metastases are located close to the center of the window. If necessary, adjust the inserted hole to bring the micrometastasis to the center of the window by enlarging the hole slightly to the respective side.
    NOTE: Metastatic disease on the pleural surface can be identified as clearly recognizable white dots or areas within the otherwise pink-to-salmon colored healthy parts of the lung surface that appear predominantly along the fissures. While micrometastases can occur on other areas of the pleural exterior, the investigated cell lines almost always display surfacing micrometastases in the perforated area, once metastatic disease can be radiologically detected.
    2. After inserting the socket into the perforation, and creating direct contact with the visceral pleura of the lung, suture the edges of the window frame to the surrounding intercostal muscle, using 4.0 monofilament suture (**Figure 1C**). Use a slight increase of inspiration pressure on the ventilator to help residual air to escape and to create a seal.
    Note: The respiration rate of rats can vary greatly, depending on the status of anesthesia, status of excitement or anxiety, oxygen concentration of inspired air (FiO_2), etc. It is recommendable to adjust the respiration rate between 70 and 90 bpm. The inspiration pressure should be adjusted with caution and not be set to more than approx. 8 cm H_2O (0.6 mmHg), to avoid damage to the lung surface.

5. Position the animal in a custom designed restrainer that is designed to eliminate Z-directional movement (**Figure 1D**) on a steel plate that is positioned on a thermostatic (electrical) heating blanket, under a fluorescence microscope. Control the animal's body temperature using a rectal thermistor. Adjust the screws of the animal restrainer, and the inspiration pressure on the ventilator to achieve optimal control of lateral movement.
Note: Natural breathing in mammals involves all three directions of lung movement and chest extension: bilateral, dorso-ventral, and cranio-caudal. In order to preserve the natural breathing movement as much as possible, it is important to minimize Z-directional compression to the necessary extent. Because the Z-dimensional restraint has the potential to introduce artifacts that may affect blood flow and other parameters, it is advisable to keep conditions constant during series of repeated measurements in the same animal.

4. Imaging and Measurement of Microcirculatory Blood Flow

1. Collect red blood cells via cardiac puncture and label them with DiI (1,1=-dioctadecyl-3,3,3=,3=-tetramethyl-indocarbocyanine perchlorate), as described previously [10].
2. Inject 300 µl of labeled red blood cells into the tail vein of the rat before the window chamber surgery is done, to avoid first pass adhesion effects to the glass window. Eliminate any air bubbles in the syringe or catheter, as introduction of air into the vein will inhibit any further injections.
3. Image blood flow with a microscope CCD camera at -40 °C chip cooling temperature, and approximately 100X overall resolution (*i.e.* with a 10X microscope objective, and 10X pre-camera ocular). Use standard Rhodamine/ TRITC filter sets (excitation 450-490 nm, emission >515 nm). Record the actual frame rate and pixel resolution of the resulting image sequences. Record at least 200 (ideally around 300) images per stack, to ensure successful analysis of flow velocity.
4. Replenish fluid loss in the animal by injecting approximately 1 ml of saline i.p. every hr.
NOTE: Experimental settings that involve an intervention, *e.g.* a drug that modifies the blood flow velocity in a pulmonary cancer metastasis, requires repeated measurements of blood flow velocity in pulmonary metastatic cancer. For these extended experiments, it is important to replenish the animal with sufficient fluid.
5. Euthanize the animals by infusion of 3 ml of 3N KCl into the tail vein
6. Evaluate the image stacks using a published, publically available Matlab-based computer algorithm that will create flow velocity grayscale and color encoded maps for all blood flow traces [10,11]. Subsequently evaluate the resulting grayscale images by using commercial or publicly available image analysis software, such as Image J, after thresholding off values that indicate no movement of blood cells, *i.e.* no active vasculature.

Representative Results

The vasculature in solid tumors is known to differ significantly from normal blood supply, showing greater degrees of tortuosity, and higher intervascular distances[13]. Accordingly, blood flow tracks in experimental pulmonary breast cancer and sarcoma metastases have irregular shapes and large intervascular gaps (**Figure 2A**, lower two panels) when compared to the normal pulmonary microcirculation (**Figure 2A**, upper panel). In a previous study, the ability of the pulmonary window method was demonstrated to perform automated measurements of changes in the blood flow velocity in normal lungs[10]. In order to investigate whether the pulmonary window method can also measure an increase in blood flow velocity in pulmonary metastases, the drug combination of the sympathomimetic drug ephedrine and the endothelin

blocker ambrisentan that has recently been found to increase the microvascular circulation in healthy lungs, was applied here (data under review elsewhere). In this study, the ability of the method is shown to detect an increase in blood flow velocity in pulmonary metastases of mouse sarcoma, caused by dosing with the combination of ephedrine (20 mg/kg) and the endothelin receptor antagonist ambrisentan (0.5 mg/kg, both drugs intraperitoneally, **Figure 2B**). Every data point represents the pooled individual averages of three measurements with five minute intervals, averaged over the data acquired in five animals. The first injection significantly ($p < 0.01$) increased blood flow velocity in the tumor area from 0.61 ± 0.12 mm/sec to 0.74 ± 0.19, whereas the second injection maintained the elevated flow velocity at 0.74 ± 0.19 mm/sec (). The second injection did not elicit any further increase in blood flow velocity. N = 5, all statistics: repeated measures ANOVA.

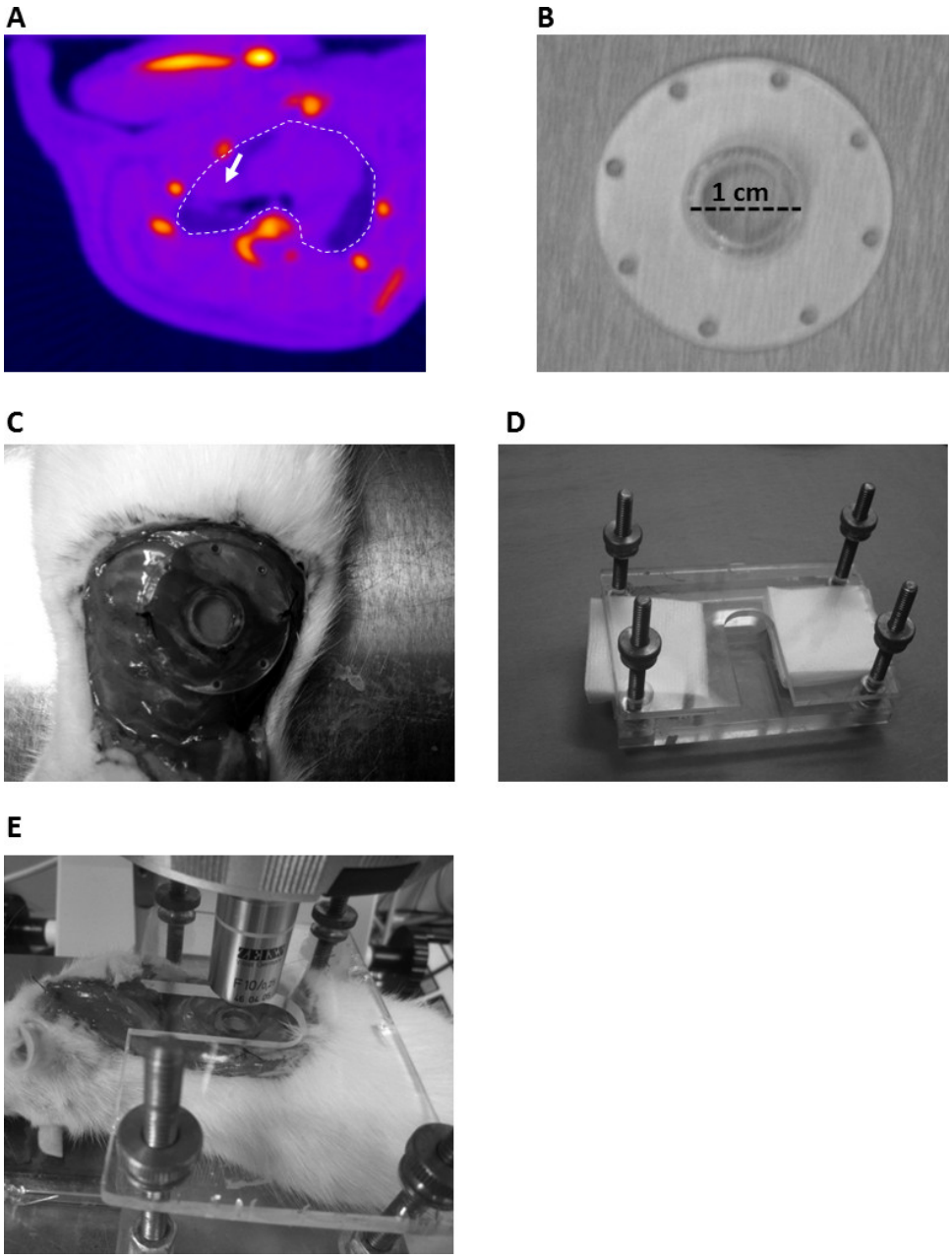

Figure 1: Procedure to prepare a lung metastases-bearing rat for live microscopy imaging. (A) MicroCT image of a rat bearing lung metastases (arrow). **(B)** Pulmonary window frame. **(C)** Rat with chest wall perforation and pulmonary window attached. **(D)** Restraining device to limit Z-directional chest movement. **(E)** Rat with window chamber and restraining device under the fluorescence microscope. Note: panel C and E show hair bearing Sprague Dawley rats, not athymic nude rats.

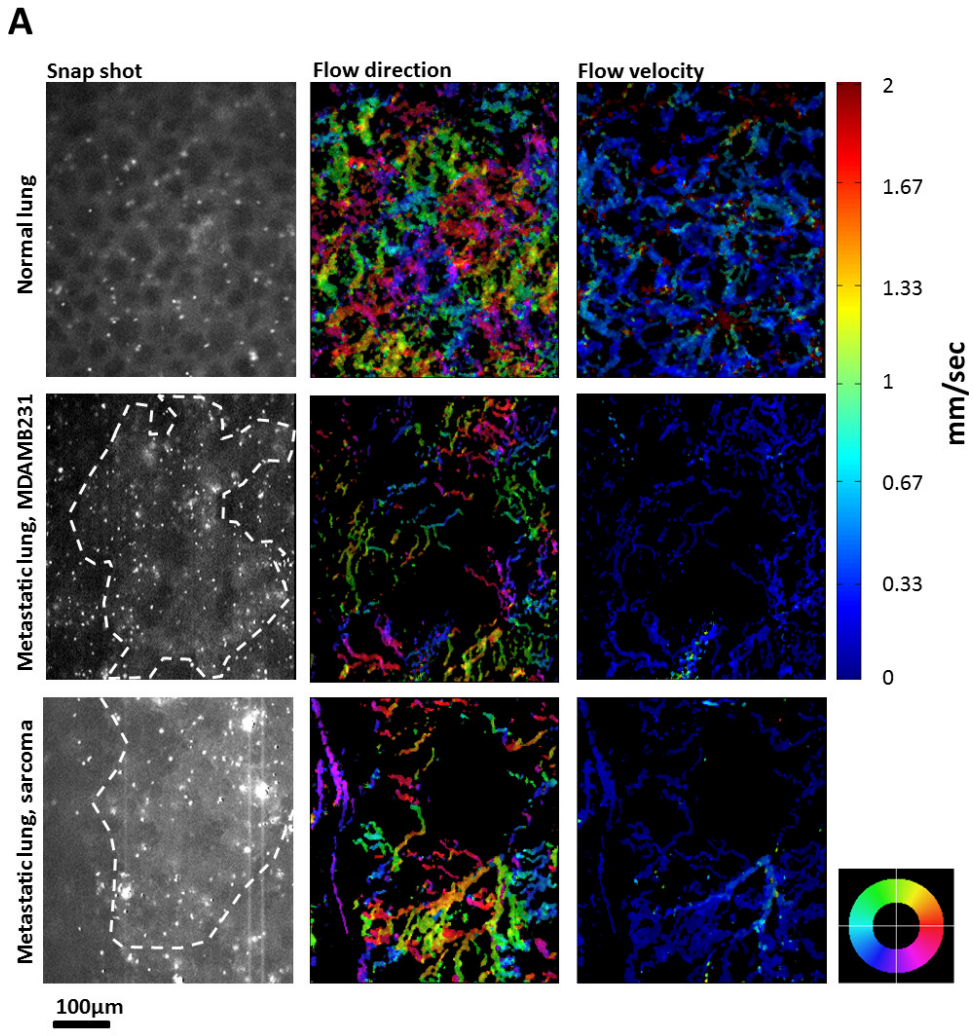

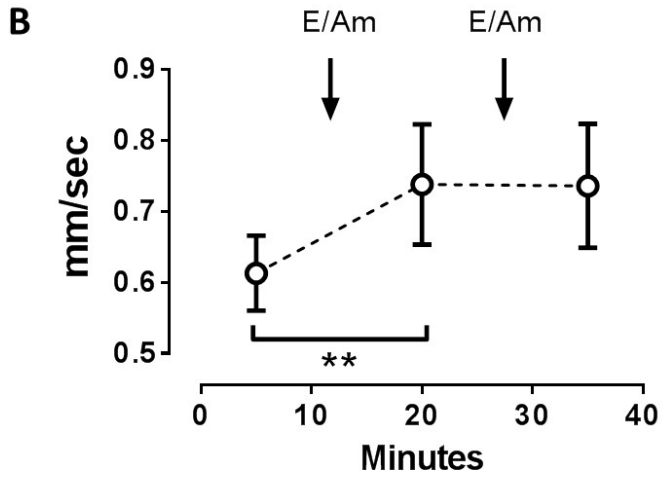

Figure 2: Quantification of increases in blood flow of pulmonary metastases. (A) blood flow direction and velocity in a normal lung, and a cancer metastasis from MDAMB-231 and mouse sarcoma. The column on the left side contains snap shots from image series of fluorescence micrographs. Alveolae can be identified as part of the background fluorescence pattern in normal lungs (upper panel). Metastases could be located by the fluorescence caused by endogenous fluorescing proteins of the injected cancer cells (dashed line). Columns to the right: color-encoded maps of blood flow direction (color indicator wheel marks the direction towards which cells flow) and flow velocity, measured in mm/second. **(B)** Changes in microcirculatory blood flow after repeated injection of combined ephedrine and ambrisentan (20 and 0.1 mg/kg per injection). A significant increase in overall flow velocity (repeated measures ANOVA, $p < 0.01$) was observed after the first injection, but not after the second (N = 5).

Discussion

A model is presented that is feasible to image changes in microcirculatory blood flow and other dynamic processes in pulmonary metastases of rats, using intravital microscopy and computational blood flow analysis. While other methods exist to perform microscopy on exposed lungs in open ribcages of rodents, this model is also the first to image pulmonary metastases through a chest wall perforation in a closed-chest setting. Using this method, the feasibility is shown to measure pharmacologically induced changes in microcirculatory blood flow of pulmonary metastases.

Two basic methods exist to image the lungs of living rodents that are perfused by spontaneous blood flow, with direct contact to the lung surface: open chest models eliminate the problem of constant motion of the lung due to respiratory and cardiac activity by applying a suction window to the surface of the lung, while allowing the rest of the cardiopulmonary complex to expand and contract within an open chest cavity [7,14]. While this method provides excellent experimental access, the open chest conditions and suction window introduce artifacts when compared to conditions of an intact lung[8]. Alternatively, closed-chest procedures that leave the rib cage largely intact bear the promise of preserving the original conditions in the intact chest cavity, such as the mutual influence of cardiac and pulmonary motion on each other's blood flow dynamic. These models typically involve a frame with a window that is sutured to the chest wall[15], or a transparent membrane that is brought in direct contact with the lung surface to prevent drying of the tissue[9]. The difficulty of negotiating the cardiopulmonary motion to accommodate and enable microscopy imaging is a major technical challenge of closed-chest procedures, and probably responsible for the low overall spread of this technique. In our case, the combination of a solid window-holding frame and a Z-directional restraining device has proven efficacious to sufficiently eliminate lateral movement of the lung to allow automated blood flow measurements of the pulmonary circulation in a closed-chest window[10].

A common method to measure blood flow velocity from intravital microscopy image stacks is the use of spatial matching of blood flow patterns in consecutive images of a given vascular segment[14]. In order to reduce the time effort associated with the analysis of single blood vessels, a blood flow imaging algorithm has been introduced that produces blood flow velocity maps of the entire optical field[11]. Besides the time advantage, this method also allows simultaneous spatial analysis of blood flow in the whole optical field, irrespective of vascular morphology or branching points. This is particularly important when studying the tumor microenvironment, where multiple blood vessels contribute to the supply status of a given tumor area[13,16,17]. Indeed, the known tortuosity of tumor vasculature and the existence of large intervascular gaps can be clearly seen in both metastatic cancer types that have been investigated, (**Figure 2A**). The pulmonary window method has also been tested for its ability to report changes in blood flow velocity in the metastatic lesion, by measuring the effect of a pharmacological treatment that has recently been found to increase blood flow velocity in the pulmonary circulation: the hypertensive drug ephedrine increases cardiac output, whereas the endothelin receptor blocker ambrisentan reduces the pre-capillary arteriolar tone, which results, when the drugs are given in combination, in increased blood flow velocity in pulmonary capillaries. While these data are currently under review elsewhere, the ability of the combination of a hypertensive drug and an endothelin receptor antagonist to increase peripheral muscular perfusion has been published independently [18]. While under normal conditions, a dose-dependent increase of blood flow velocity can be observed after both injections, the fact that the second injection does not lead to a further increase of flow velocity in sarcoma metastases might result from the fact that maximal tumor vessels vasodilation has already been reached after the first combined injection of ephedrine and ambrisentan.

The following limitations apply to the technique presented here: This protocol is applicable to rats (and theoretically, similar sized mammals) from approximately 180 to 300 g or more. Smaller mammals such as mice will require special modification to accommodate the more fragile anatomy and physiology of the rib cage. The maximum spatial resolution that can be achieved with the presented technique is theoretically only limited by the numerical aperture of the objective and the thickness of the cover slide that is used (~0.08-0.1 µm in standard brands), to 100X objectives, with the use of oil immersion. In practice however, the remaining movement of the lung might limit the use of high resolution objectives beyond 20X. If all autonomous motion of the lung is eliminated, the temporal resolution of the technique is only limited by the frame rate of the camera, and the signal strength of the fluorescent label, which determines the exposure time, to approximately 100 frames per sec. The following additional limitations apply to the presented technique: on one hand, the current microscopic and computational setting allows only the analysis of the surface of a given metastasis. The use of depth-penetrating microscopy, such as advanced confocal microscopy imaging strategies, may in the future enable measurement of blood flow velocity in 3 dimensions. Also, the presented technique cannot, in its current form, be used to visualize lesions further inside the lung parenchyma. Third, the insertion of a glass window in direct contact with active blood vessels has some potential to perturb the microvascular flow by itself, via spatial compression of blood vessels, or by impacting locoregional temperature. Fourth, the use of an external ventilator and positive pressure in the lung also has potential to alter pulmonary microcirculatory blood flow. Moreover, only limited areas of the rib cage are practically accessible for the described, relatively uncomplicated surgical procedures. Other areas of the lung surface, such as medial-ventral or dorsal access would require more elaborate surgical techniques, along with profound perturbations of the biomechanics of the rib cage. Because of the lack of alternatives to microscopy imaging to study microcirculatory blood flow, major developments can be expected in the near future to overcome these hurdles and study malignancies at high temporal-spatial resolution in all parts of the rodent lung.

In summary, a method is presented to measure patterns of, and changes in, microvascular blood flow velocity in surface metastases of the rat lung. Combining an acute closed-chest surgical model with an automated method of measuring blood flow velocity in the entire microscopic optical field, this technique offers relative preservation of the physiological environment of the lung, is capable of detecting changes in overall microcirculatory blood flow velocity and direction, and is relatively easy to use. It can be expected that this technique will be of great use to all groups that study the microcirculation of pulmonary metastases and other dynamic processes in this disease setting in rodent models.

Disclosures

The authors have nothing to disclose.

Acknowledgements

The scientific advice of Drs. Timothy McMahon and Siqing Shan is appreciated. The presenters thank Drs. David Kirsch and Patricia Steeg for the generous gift of the fluorescently labeled Mouse Sarcoma and metastatic MDAMB-231 cells, respectively. This work was funded in part by the U.S. Defense Advanced Research Projects Agency (DARPA) Prime Award Number N66001-10-C-2134, and in part by the Department of Radiation Oncology, Duke University Medical Center.

References

1. Billingsley, K. G. *et al.* Pulmonary metastases from soft tissue sarcoma: analysis of patterns of diseases and postmetastasis survival. *Ann Surg.* **229**, 602-610; discussion 610-602 (1999).
2. Rashid, O. M., & Takabe, K. The evolution of the role of surgery in the management of breast cancer lung metastasis. *J Thorac Dis.* **4**, 420-424, doi:10.3978/j.issn.2072-1439.2012.07.16jtd-04-04-420 [pii] (2012).
3. Mayer, A., & Vaupel, P. Hypoxia, lactate accumulation, and acidosis: siblings or accomplices driving tumor progression and resistance to therapy. *Advances in experimental medicine and biology.* **789**, 203-209, doi:10.1007/978-1-4614-7411-1_28 (2013).
4. Okunieff, P., O'Dell, W., Zhang, M., Zhang, L., & Maguire, D. Tumor oxygen measurements and personalized medicine. *Advances in experimental medicine and biology.* **765**, 195-201, doi:10.1007/978-1-4614-4989-8_27 (2013).
5. Palmer, G. M. *et al.* In vivo optical molecular imaging and analysis in mice using dorsal window chamber models applied to hypoxia, vasculature and fluorescent reporters. *Nature protocols.* **6**, 1355-1366, doi:10.1038/nprot.2011.349 (2011).
6. Palmer, G. M. *et al.* Optical imaging of tumor hypoxia dynamics. *Journal of biomedical optics.* **15**, 066021, doi:10.1117/1.3523363 (2010).
7. Funakoshi, N. *et al.* A new model of lung metastasis for intravital studies. *Microvasc Res.* **59**, 361-367, doi:10.1006/mvre.2000.2238S0026-2862(00)92238-6 [pii] (2000).
8. Kuebler, W. M. Real-time imaging assessment of pulmonary vascular responses. *Proc Am Thorac Soc.* **8**, 458-465, doi:8/6/458 [pii]10.1513/pats.201101-005MW (2011).
9. Tabuchi, A. *et al.* Precapillary oxygenation contributes relevantly to gas exchange in the intact lung. *Am J Respir Crit Care Med.* **188**, 474-481, doi:10.1164/rccm.201212-2177OC (2013).
10. Hanna, G. *et al.* Automated measurement of blood flow velocity and direction and hemoglobin oxygen saturation in the rat lung using intravital microscopy. *American journal of physiology. Lung cellular and molecular physiology.* **304**, L86-91, doi:10.1152/ajplung.00178.2012 (2013).
11. Fontanella, A. N. *et al.* Quantitative mapping of hemodynamics in the lung, brain, and dorsal window chamber-grown tumors using a novel, automated algorithm. *Microcirculation*, doi:10.1111/micc.12072 (2013).
12. Newton, J. *et al.* Commissioning a small-field biological irradiator using point, 2D, and 3D dosimetry techniques. *Medical physics.* **38**, 6754-6762, doi:10.1118/1.3663675 (2011).
13. Vaupel, P. Tumor microenvironmental physiology and its implications for radiation oncology. *Seminars in radiation oncology.* **14**, 198-206, doi:10.1016/j.semradonc.2004.04.008 (2004).
14. Tabuchi, A., Mertens, M., Kuppe, H., Pries, A. R., & Kuebler, W. M. Intravital microscopy of the murine pulmonary microcirculation. *J Appl Physiol.* **104**, 338-346, doi:00348.2007 [pii]10.1152/japplphysiol.00348.2007 (2008).
15. Fingar, V. H., Taber, S. W., & Wieman, T. J. A new model for the study of pulmonary microcirculation: determination of pulmonary edema in rats. *J Surg Res.* **57**, 385-393, doi:S0022-4804(84)71159-0 [pii]10.1006/jsre.1994.1159 (1994).
16. Manzoor, A. A., Schroeder, T., & Dewhirst, M. W. One-stop-shop tumor imaging: buy hypoxia, get lactate free. *The Journal of clinical investigation.* **118**, 1616-1619, doi:10.1172/JCI35543 (2008).
17. Evans, S. M. *et al.* Imaging and analytical methods as applied to the evaluation of vasculature and hypoxia in human brain tumors. *Radiation research.* **170**, 677-690, doi:10.1667/RR1207.1 (2008).
18. Radiloff, D. R. *et al.* The combination of theophylline and endothelin receptor antagonism improves exercise performance of rats under simulated high altitude. *Journal of applied physiology.* **113**, 1243-1252, doi:10.1152/japplphysiol.01622.2011 (2012).

Materials List for:

Automated Measurement of Microcirculatory Blood Flow Velocity in Pulmonary Metastases of Rats

Gert Blueschke*[1], Gabi Hanna*[2], Andrew N. Fontanella[2], Gregory M. Palmer[2], Alina Boico[2], Hooney Min[2], Mark W. Dewhirst[2], David C. Irwin[3], Yulin Zhao[2], Thies Schroeder[4]

[1]Division of Plastic, Maxillofacial, and Oral Surgery, Duke University Medical Center

[2]Department of Radiation Oncology, Duke University Medical Center

[3]Department of Cardiology, University of Colorado Denver

[4]Department of Physical Chemistry, University of Mainz

*These authors contributed equally

Correspondence to: Thies Schroeder at thschroe@uni-mainz.de

URL: http://www.jove.com/video/51630
DOI: doi:10.3791/51630

Materials

Name	Company	Catalog Number	Comments
Athymic nude rats	Charles River	Strain code 316	Female 10 week-old athymic nude rats
micro-CT/micro-Irradiator	Precision X-ray Inc.	Xrad 225Cx	Use MicroCT to detect metastases
DiI (1,1=-dioctadecyl-3,3,3=,3=-tetramethyl-indocarbocyanine perchlorate)	Sigma Aldrich	468495-100MG	Mix 100 ul packed red blood cells with 100 ul of 0.5 mg/ml DiI in 200 proof ethanol, 2 ml of 5% dextrose solution in water, and fill up to a 10-ml final volume with saline
Rodent ventilator	Kent Scientific	TOPO Small Animal Ventilator	Device is important to maintain positive lung pressure after application of pneumothorax
Zeiss Axioskop fluorescence microscope upright	Zeiss	Axioskop	Microscope for intravital imaging
Andor CCD camera	Andor	iXonEM 885	CCD camera for live imaging of blood flow
Pulse oximeter	StarrLife	MouseOx	Pulse oximeter
Fluorescence microscope	Zeiss	Axioskop	Fluorescence microscope

Am J Physiol Lung Cell Mol Physiol 304: L86–L91, 2013.
First published November 16, 2012; doi:10.1152/ajplung.00178.2012.

Automated measurement of blood flow velocity and direction and hemoglobin oxygen saturation in the rat lung using intravital microscopy

Gabi Hanna,[1] Andrew Fontanella,[1] Gregory Palmer,[1] Siqing Shan,[1] Daniel R. Radiloff,[1] Yulin Zhao,[1] David Irwin,[3] Karyn Hamilton,[4] Alina Boico,[1] Claude A. Piantadosi,[5] Gert Blueschke,[6] Mark Dewhirst,[1] Timothy McMahon,[2] and Thies Schroeder[1]

[1]*Department of Radiation Oncology, Duke University Medical Center, Durham, North Carolina;* [2]*Department of Medicine, Duke University Medical Center, Durham, North Carolina;* [3]*Department of Cardiology, University of Colorado Denver, Denver, Colorado;* [4]*Department of Health and Exercise Sciences, Colorado State University, Fort Collins, Colorado,* [5]*Department of Anesthesiology, Duke University Medical Center, Durham, North Carolina; and* [6]*Department of Surgery, Duke University Medical Center, Durham, North Carolina*

Submitted 31 May 2012; accepted in final form 13 November 2012

Hanna G, Fontanella A, Palmer G, Shan S, Radiloff DR, Zhao Y, Irwin D, Hamilton K, Boico A, Piantadosi CA, Blueschke G, Dewhirst M, McMahon T, Schroeder T. Automated measurement of blood flow velocity and direction and hemoglobin oxygen saturation in the rat lung using intravital microscopy. *Am J Physiol Lung Cell Mol Physiol* 304: L86–L91, 2013. First published November 16, 2012; doi:10.1152/ajplung.00178.2012.—Intravital microscopy of the pulmonary microcirculation in research animals is of great scientific interest for its utility in identifying regional changes in pulmonary microcirculatory blood flow. Although feasibility studies have been reported, the pulmonary window can be further refined into a practical tool for pharmaceutical research and drug development. We have established a method to visualize and quantify dynamic changes in three key features of lung function: microvascular red blood cell velocity, flow direction, and hemoglobin saturation. These physiological parameters were measured in an acute closed-chest pulmonary window, which allows real-time images to be captured by fluorescence and multispectral absorption microscopy; images were subsequently quantified using computerized analysis. We validated the model by quantifying changes in microcirculatory blood flow and hemoglobin saturation in two ways: *1*) after changes in inspired oxygen content and *2*) after pharmacological reduction of pulmonary blood flow via treatment with the β1 adrenergic receptor blocker metoprolol. This robust and relatively simple system facilitates pulmonary intravital microscopy in laboratory rats for pharmacological and physiological research.

thoracic window in rats; pulmonary intravital microscopy in rats; red blood cell flux; hemoglobin saturation

THE LUNG IS OF MAJOR INTEREST for pathophysiological research and drug development, and, therefore, methods to accurately analyze its physiology in preclinical models are in high demand. Intravital microscopy holds promise for measuring and subsequently understanding dynamic changes in the pulmonary microcirculation (2). However, pulmonary microcirculation is difficult to image without compromising its overall function. The importance of maintaining intrapleural negative pressure is paramount. Furthermore, the lung surface is fragile and easily damaged in the process of creating a window. In addition, functional microscopy requires a lengthy period of immobilization, which can interfere with the continuous movement during breathing of a healthy lung. Two main strategies have been employed to overcome these technical hurdles: *1*) a window has been inserted into, and anchored to, the chest wall via surgical suture or glue to permit visualization of the thoracic cavity; *2*) more recently, a position-stabilized window has been inserted where local negative pressure was used to eliminate motion of the lung surface in relation to the window (5, 6, 12). Although this advanced technique allows for cell tracking and quantification of particle movement, it is difficult to determine how the application of a local vacuum will alter natural capillary blood flow, and how it may stimulate arteriovenous shunting. In addition, manual cell tracking, which is the principal method to analyze blood cell movement, limits assessment of changes in network hemodynamics. Thus, although progress has been made, functional intravital microscopy in the rodent lung is not yet at a development level that allows its widespread use in preclinical research.

Here, we aimed to develop a simplified surgical approach to facilitate measurement of rat pulmonary microcirculation, and to test its reproducibility under control and manipulated conditions. We have independently established an approach to measure red blood cell flow and capillary blood oxygenation in the rat lung, using automated blood cell tracking, and multispectral absorption imaging. We have investigated the utility of this method to serially measure physiological changes in the pulmonary microcirculation in response to two conditions: *1*) inspired hypoxia, which alters hemoglobin saturation, and *2*) treatment with cardiovascular drugs that decrease pulmonary perfusion.

MATERIALS AND METHODS

Surgery and pulmonary window implantation. All surgical procedures were performed in accordance with Duke University Medical Center Institutional Animal Care and Use Committee (IACUC) protocols. Rats were anesthetized using an intraperitoneal injection of 50 mg/kg pentobarbital to achieve surgical-level anesthesia. Anesthetized animals were shaved on the right chest and neck areas and fixed in the supine position on a metal plate placed on a 37°C heating pad. Vital signs were monitored using pulse oximetry (MouseOx, Starr Life Sciences, Oakmont, PA), with blood oxygenation and heart rate recorded. A cervical skin incision was made horizontally above the jugular notch of the manubrium, and the cervical trachea was exposed by vertical separation of the sternohyoid and sternocleidomastoid muscles. The trachea was dissected and separated from surrounding muscle and connective tissue; a transverse incision was made on the anterior tracheal wall between the second and third tracheal rings. A 2.5- to 3.0-mm "Y" tracheal cannula (Kent Scientific, Torrington, CT) was inserted into the trachea and secured with a suture. The animal was then repositioned in left lateral recumbancy. The tracheal can-

Address for reprint requests and other correspondence: T. Schroeder, Dept. of Radiation Oncology, Duke Univ. Medical Center, Durham, NC 27710 (e-mail: thies.schroeder@duke.edu).

nula was connected to a pressure-cycled ventilator (Kent Scientific) to maintain positive pulmonary pressure. The ventilator was connected in line with an OxyDial oxygen blender (Starr Life Sciences). O_2 (100%) was delivered during the surgical procedure. Once connected to the ventilator, the superficial and serratus anterior muscles were dissected from the right lateral chest wall. The intercostal muscles were left intact until the next step, which involved removal of a portion of the sixth and seventh ribs. Both ribs were cut dorsally and ventrally to isolate a length of 1.2 cm. These ribs were removed as follows. To minimize damage to the lung surface by the edge of the ribs and minimize the bleeding of the intercostal vessels, the middle of the rib was held tightly with forceps. The medial side of the rib was cut first, with the rib lifted gently with the forceps. The lateral side of the same rib was then separated. After removal of the rib segments and intercostal muscles, the parietal pleura was excised to create a 1.5-cm-diameter chest wall perforation. This procedure exposed the lung surface. Positive pressure in the lung was maintained by the ventilator with expiration tube connected with a water bottle (the tube merged in water ~6 cm). A custom-fabricated lung window, consisting of a 1-cm-diameter cover glass glued to a Plexiglas socket (Fig. 1*A*) was placed in the resulting perforation in the chest wall to maintain direct contact with the visceral pleura of the lung. The window frame was then sutured via perforations at its edge to intercostal muscle using 4.0 monofilament synthetic thread. As it was sutured, residual air was allowed to escape until a seal was created (Fig. 1*B*). Following surgery and stabilization of vital signs, the animal was moved to a microscope stage covered with a thermostatic heating blanket set at 37°C. The animal was positioned in a custom-designed frame to reduce *z*-directional movement (Fig. 1, *B* and *C*).

Preparation of fluorescently labeled red blood cells. Donor rats (female Sprague-Dawley) were deeply anesthetized with pentobarbital (50 mg/kg ip). Rats were exsanguinated using cardiac puncture, and 10–14 ml of blood was collected in heparin. The blood was then centrifuged at 3,000 *g* for 3 min at 4°C. Plasma was removed and replaced with sterile saline, and the blood cell pellet was centrifuged and washed three times. Packed red blood cells (100 μl) were mixed with 100 μl of 0.5 mg/ml DiI (1,1′-dioctadecyl-3,3,3′,3′-tetramethylindocarbocyanine perchlorate) solution (Sigma Aldrich, St. Louis, MO), 2 ml of 5% dextrose solution in water, and brought up to a 10-ml final volume with saline. DiI labels cells by integrating into the plasma membrane and moving laterally until the whole cell is labeled (10). The solution was incubated at room temperature in the dark for 30 min and then centrifuged and washed three times with saline. Before injection, the red blood cells were suspended in saline to achieve a hematocrit of ~30%. Then 500 μl of this red cell suspension was infused into the jugular vein of the anesthetized rat over ~30 s.

Blood flow measurements. Animals were anesthetized with 60 mg/kg of pentobarbital. Redosing with 10 mg/kg pentobarbital was done at least 15 min before starting the experiment for measurements of red blood cell velocity. Animals were injected with the labeled red blood cells after the surgery was complete and at least 15 min before imaging began. Depth of anesthesia was such that redosing of anesthetics was not required during the imaging cycle. There were nine image sequences (65–100 images/sequence, frame rate of 16.4–23.6 Hz, frame rate and stack size kept constant throughout each experiment) taken, with 5-min intervals between each consecutive image set. After three imaging cycles, 10 mg/kg metoprolol was injected intravenously, and three cycles later the injection was repeated. For both flow and HbO_2 measurements, mechanical ventilation was deliberately paused for a maximum of 15 s. The animals were ventilated with 100% O_2, and arterial hemoglobin oxygen saturation was maintained above 99%.

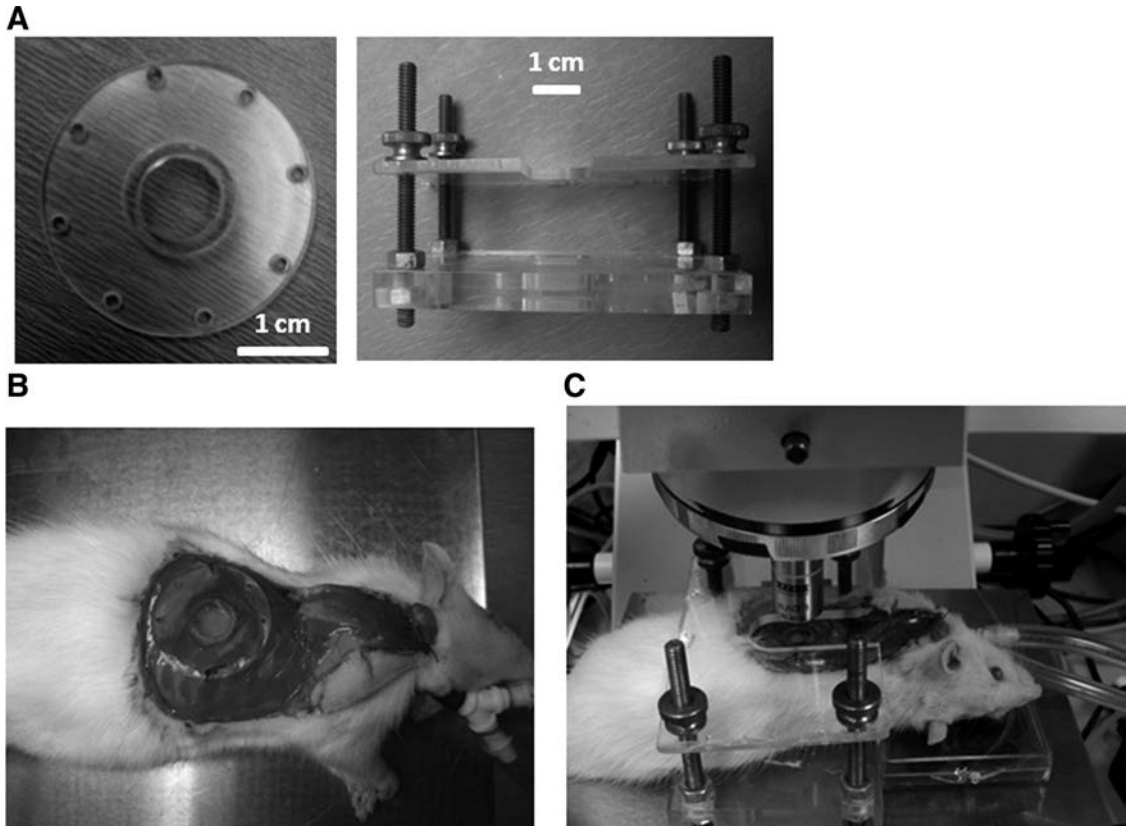

Fig. 1. Surgical procedures for pulmonary window fenestration. *A*: Plexiglas window holder with socket and window glued to it, and rat restrainer to eliminate *z*-directional movement. *B*: anesthetized intubated rat with implanted pulmonary window. *C*: rat with window in a restrainer, placed on a heating pad under a fluorescence upright microscope.

Measurement of hemoglobin saturation using hyperspectral microscopy. Anesthesia procedures, surgery, intubation, and ventilation were as described in the previous section. The level of inspired oxygen was maintained at 100% for at least three images, 12% or 16% for three consecutive images, and then 100% for the remaining three images. The 100% inspired oxygen typically yields 99% arterial hemoglobin oxygen saturation. Images were acquired during a short period of apnea, as described above. Optical microscopy was performed using an upright Zeiss fluorescence microscope (Axioscop, Carl Zeiss, Thornwood, NY). The imaging techniques and analyses have been described in detail previously (14) but are briefly outlined here. The rat, on the ventilator, was placed under the microscope objective. To enable bright field imaging, a separate optical fiber lamp was used to illuminate the window from a position adjacent to the objective (Techniquip, Roseville, CA). The illuminated lung surface was imaged at a series of discrete wavelengths using a liquid crystal tunable filter that spectrally filtered the light before incidence upon the camera (VariSpec, CRi). Reflectance images were acquired at wavelengths from 500 to 590 nm, in 10-nm increments. Before processing, the spectral profile of the imaging system was acquired using a 99% reflectance standard (Labsphere, SRS-99-010). The ratio of the reflectance standard to the tissue intensity was taken as a function of wavelength and the logarithm of this ratio describes the spectral absorption of the tissue according to the equation:

$$A(\lambda) = \log\left(\frac{I_{cal}(\lambda)}{I_{tissue}(\lambda)}\right) = b_0 + b_1\mu_{eff}(\lambda) + \sum_i \varepsilon_i(\lambda)C_i$$

where I_{cal} is the calibrated reflectance standard intensity and I_{tissue} is the tissue reflected intensity at the same wavelength (after the dark signal offset is subtracted from each term). These values were normalized to exposure time. The total absorption term (A) can be broken down into constitutive components: b_0 is a constant offset term, and μ_{eff} is the effective attenuation coefficient calculated for representative skin optical properties at each wavelength (http://omlc.ogi.edu/news/jan98/skinoptics.html) and accounting for attenuation due to non-hemoglobin absorption and scattering. b_1 is a free parameter modulating the magnitude of this term. $\varepsilon_i(\lambda)$ gives the extinction coefficient of the i^{th} absorber of interest and is a fixed parameter. In this case, oxygenated and deoxygenated hemoglobin are the absorbers of interest, and their extinction coefficients are known (http://omlc.ogi.edu/spectra/hemoglobin/). A linear, nonnegative least squares-fitting algorithm is used to extract the terms b_0, b_1, and C_i on a pixel-by-pixel basis. C_i is a composite term that represents the product of the concentration and path length of light attenuated by each absorber. This model, within which only a single composite path length is used to represent the distribution of path lengths present within each pixel region, is simplified to facilitate processing of the large number of pixels on a given image. Under this assumption, the hemoglobin oxygen saturation can be calculated as $C_{oxyHb}/(C_{deoxyHb} + C_{oxyHb}) \times 100\%$.

Analysis of red blood cell velocity and automated red blood cell tracking. Flow speed and direction maps were calculated using an algorithm developed by our laboratory, which will be published as part of a separate paper but is explained in the following. Briefly, video sequences of 65–100 images were collected using a charge-coupled device microscope camera (Andor Technology, Belfast, Northern Ireland) and converted into three-dimensional matrices for processing in MATLAB. Movement of the background (e.g., due to heartbeat or respiration) was corrected for, using a custom algorithm that repositioned adjacent images based on maximizing structural similarity.

To enable the reconstruction of red blood cell moving patterns, the stack was filtered to consist only of grayscale patterns that reflect moving blood cells. This was done by excluding all grayscale information that did not fluctuate throughout the *z* direction within a set degree of synchronization with its neighboring pixels.

Blood cell movement was tracked by performing cross-correlation analysis of the *z*-directional temporal grayscale profiles of every pixel with that of every other pixel in its set local area. In this analysis, the *z*-directional, linear profiles of the two compared pixels are aligned with each other in multiple positions, and grayscale values of corresponding pixels are multiplied with each other. Corresponding *Z*-profiles result in the highest sums of products, whereas non-corresponding profiles yield low product sums. The relative distance of the matched profiles on the *XY* map are used to calculate the flow velocity at any given point, or pixel, whereas the relative position of pixels with matching *Z*-profiles to each other enables determination of flow direction. This strategy of analysis is based, in principle, on the dual-slit technique, introduced by Baker and Wayland in 1974 (1), and has here been applied to analyze flow velocity in two-dimensional arrays rather than up- and downstream of a single vessel.

To reduce computational expense, cross-correlation operations were performed in the Fourier domain by employing the convolution theorem, which states that the Fourier transform of two convolved signals is equivalent to the product of their individual transforms. Since it was our goal to calculate the cross-correlation of the signals rather than their convolution, one signal was reversed at a time. This time reversal was performed in the Fourier domain by taking the complex conjugate of one of the transformed signals. Thus, by finding the transform of the zero-mean matrix wherein the one-dimensional Fourier transform along the temporal dimension is calculated at every spatial coordinate, the computationally intensive cross-correlation operation was simplified to an inner product operation. The Fourier transform matrix was calculated in the initial stage of the algorithm, and as two temporal signals were compared, their corresponding Fourier signals were extracted from the matrix and multiplied (after taking the complex conjugate of one signal), and the inverse Fourier transform of this product yielded the cross-correlated signal. From this vector, the maximum value was found, with its index representing the best correlated temporal offset. This process was performed for every coordinate in the local region, generating a two-dimensional temporal-offset matrix for the particular pixel of interest.

Image analysis of the velocity maps was done on 16-bit grayscale maps in Image J by evaluation of regions of interest and cancellation of areas with no flow, using appropriate thresholding.

Blood gas analysis from pulmonary arterial and carotid arterial blood. Rats were anesthetized with ketamine/xylazine mixture at 80/8 mg/kg and placed on their back onto a water-circulated heating pad. Indwelling catheters filled with heparinized saline were placed in the carotid (PE-50) and pulmonary (PE-10) artery as previously described (8). A pulse oximetry foot clip was attached to the left hindlimb of the animal (MouseOx, Starr Life Sciences) for computerized recording of arterial hemoglobin oxygen saturation (HbO_2) and heart rate. The oxygen content of the breathing air was controlled with a gas blender (Oxydial, StarrLife Sciences), which allowed for adjustment of different gas mixtures at constant flow rates. After 5 min of 100% oxygen breathing, a concentration of 12% oxygen was gradually dialed in and was maintained through the time of blood sampling. A sample of 1 ml was then collected through each catheter into a gas-tight syringe (GE Healthcare, Pittsburgh, PA), sealed, placed on ice, and then analyzed for hemoglobin oxygen content using a clinical blood gas analyzer (Instrumentation Laboratory, Bedford, MA).

RESULTS

Hemoglobin saturation and blood gas analyses. A study was conducted to investigate changes in pulmonary capillary and arterial HbO_2 under hypoxia using 12% and 16% of inspired oxygen. Under baseline conditions [100% inspired oxygen fraction (F_{IO_2})], average arterial HbO_2 was 98.9 ± 0.9% (SD). Under 16% F_{IO_2}, the average arterial saturation was 76.5 ± 7.5%, and under 12% it was 70.8 ± 12.0%. Average pulmo-

nary capillary oxygen saturation under baseline conditions was 74.8 ± 3.6%. Under 16% F_{IO_2}, average pulmonary capillary saturation was 49.2 ± 8.8%, and under 12% it was 40.6 ± 10.6% (Fig. 1, *A* and *B*). To evaluate the stability of the method over time, we have calculated the coefficient of variation of the respective baseline measurements that were acquired before the onset of hypoxia. During oxygen breathing in (four experiments over three measurement time points), the coefficients of variation across subsequent imaging time points were 3.3%, 14.2%, 14.0%, and 3.3%.

To validate the HbO_2 data calculated from the intravital microscopy experiments, blood gas analyses were done on blood samples from (nonsurgically fenestrated) anesthetized rats breathing 12% hypoxic air. Blood was sampled from the pulmonary artery (deoxygenated) and from the carotid artery (fully oxygenated) in four animals. The mean HbO_2 in pulmonary arterial blood was 25.4 ± 10.7%, and the mean HbO_2 in carotid arterial blood was 63.9 ± 3.3%.

Red blood cell blood flow. On a microscopic level, patterns of precapillary, capillary, and postcapillary blood flow were distinguishable from each other by a combination of structural and functional criteria. Precapillary blood flow manifested as appearance of cells approaching from the depth, or *z*-direction, of the image in a "source" or "fountain-type" fashion, and then diverging into several different directions. As blood cells diverged into multiple vessel branches, their flow velocity markedly decreased. Capillary blood flow could be distinguished as cells flowing at low velocity in a curved path, accurately outlining the alveolar walls, which could be identified from the nonspecific background fluorescence. Postcapillary blood flow was characterized by noticeable acceleration of blood cell movement, convergent blood flow into collecting vessels, and followed by traveling of blood cells at high velocity for some distance in a direction parallel to the image plane, before they would turn toward the depth of the image and disappear. These flow patterns were reflected by the blood flow/direction mapping algorithm, with low-speed capillary flow tracks outlining alveolar walls and collecting venules manifesting as areas of high blood flow velocity (Fig. 2*C*; see supplemental video available at the Journal website). Differential recruitment of pulmonary capillaries, which has been described in the past (11), could be observed as spontaneous cessation of blood flow through particular capillaries after subsequent imaging events (Fig. 2*C*).

We then tested whether our model would be sensitive to agents that are capable of modifying pulmonary blood flow. Metoprolol is a selective beta-1 adrenergic receptor agonist and a negative chronotrope (4, 7). In our experiments, the average blood cell velocity before treatment was 368.1 ± 14.1 μm/s at an average heart rate of 225.1 ± 18.9 beats/min. Intravenous injection of 10 mg/kg metoprolol significantly reduced the heart rate of the animals to 195.8 ± 26.7 beats/min (first injection) and 185.5 ± 31.9 beats/min (second injection). Concomitantly, pulmonary blood flow velocity was decreased to 314.3 ± 6.9 μm/s (first injection) and 279.1 ± 17.3 μm/s (second injection) (paired *t*-test, $P < 0.05$; $n = 3$; Fig. 2*D*).

The coefficient of variation between the average velocity of single image sequences was determined by performing triplicate measurements in three rats. The coefficients of variation between the average of three sequential baseline measurements of red blood cell velocity, measured in three animals, were 2.6%, 2.4%, and 6.6% of the mean.

DISCUSSION

Several approaches have been made in the past to image the pulmonary microcirculation of laboratory animals, including the manual assessment of blood flow velocity (3, 5, 16) and hemoglobin saturation (9). However, to improve the ability of this method to measure kinetic changes of the pulmonary physiology and advance its availability to a broader range of laboratories, it is necessary to automate and facilitate data acquisition and analysis procedures. In this publication, we demonstrate, for the first time, an intravital pulmonary microscopy system that permits an automated evaluation of blood flow and oxygen saturation in the pulmonary microcirculation.

The most important obstacle in establishing intravital microscopy of the lung is the movement of the lung due to respiratory and cardiac activity. One possible solution to this problem has been the application of negative pressure where vertical movement of the lung is eliminated by completely opening the rib cage, and the field of view is maintained stationary by applying a gentle vacuum between the cover glass and the lung surface (9). Although this method has shown great promise for imaging immune cell movement in mouse lungs, several aspects of it, such as the local vacuum, the continuous contact with the open air, the removal of the mechanical influence of the heart, and the lack of direct contact of the lung with the pleural wall, may change the characteristics of the pulmonary microcirculation. We have chosen a model based on an earlier study by Fingar et al. (5) using a socketed window that seals the thoracic wall. This maintains contact of the lung surface with the pleura, which in principle would better preserve the characteristics of an unperturbed microcirculation. Such a model has the additional advantage to be potentially further developed for long-term implantation as part of a survival surgery procedure.

Hemoglobin saturation. Using previously published computational tools (14) to image vascular hemoglobin saturation, we investigated the utility of our surgical model to enable the measurement of microvascular hemoglobin saturation and blood oxygen loading under maximum oxygen loading, i.e., 100% F_{IO_2}, and under two levels of hypoxia, i.e., 12% and 16%. Expectedly, the oxygen saturation in the pulmonary vascular network was consistently lower than the arterial saturation because pulmonary capillary blood consists of mixed venous (partially deoxygenated) blood and blood that is freshly loaded with oxygen. It is known, for instance, that under normoxia in humans, mixed venous blood has a P_{O_2} of ~40 Torr, equivalent to 75% HbO_2 (13, 18). The O_2 saturation values we measured in the rat's pulmonary microvasculature are therefore in the range of what would be predicted. To validate the oxygen saturation we measured in the pulmonary capillaries, we performed blood gas analyses in mixed venous and in arterial blood of rats breathing hypoxic air. We found that the HbO_2 saturation in mixed venous blood at 12% F_{IO_2} was appreciably lower than the values measured in the pulmonary capillaries, and the difference between the mixed venous and the arterial hemoglobin saturation values bracketed our intravital measurements, therefore serving as confirmation of the validity of our measurements in the pulmonary microvas-

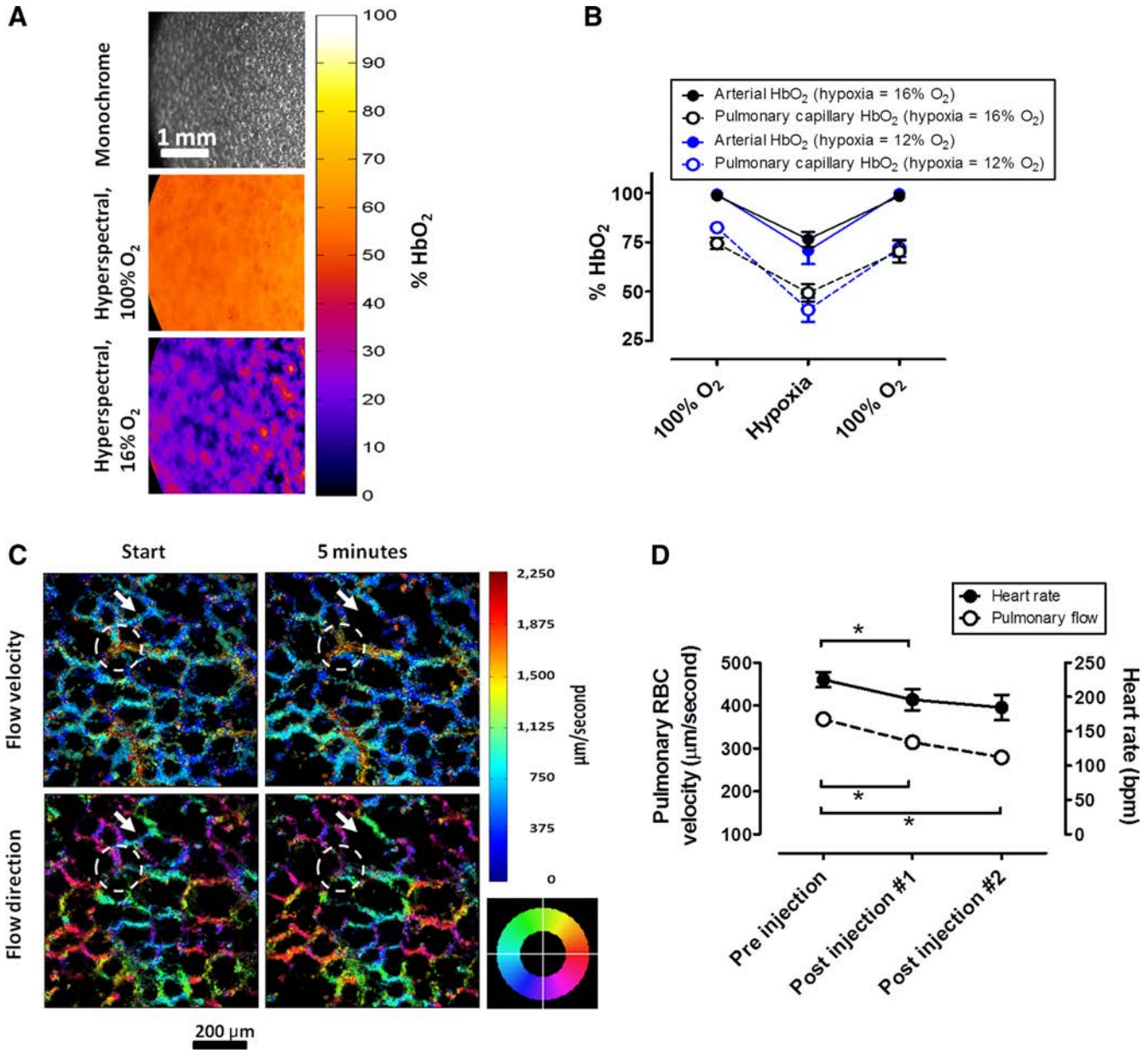

Fig. 2. Hemodynamic and microcirculatory measurements using pulmonary intravital microscopy. *A*: brightfield reflectance image at 590 nm (*top*), color-encoded hemoglobin oxygen saturation maps under 100% O_2 (*middle*), and 16% O_2 (*botom*). *B*: time course of concomitant measurements of HbO_2 in the lung using pulmonary intravital microscopy and in the arteries of the hindlimb using pulse oximetry after 15 min at 100% O_2, 15 min of hypoxia, and 15 min at 100% O_2. Hypoxia was 12% and 16% O_2. Each data point represents an average from three sequential measurements per animal, and an average between three (12% O_2) and four (16% O_2) animals. *C*: color encoded maps of red blood cell velocity (*top*) and directionality (*bottom*) in the pulmonary microcirculation. Image pairs were acquired in 5-min intervals. The arrow marks what is likely a single vessel where blood flow has stalled in between imaging events. The dashed line marks an area of venous blood flow, as visible by converging movement of blood cells. The colored compass wheel is the legend for the directionality map, with colors indicating the direction in which the blood flows. *D*: changes in heart rate and red blood cell velocity in the pulmonary microcirculation after repeated injection of metoprolol (10 mg/kg). For each individual rat, three measurements were made, before/after injections, separated by 5-min intervals. Sequential measurements from each pre-/posttreatment period were averaged per animal, and each data point on the graph represents an average from all three rats for the respective period. Significant changes in heart rates and flow are indicated with a star (paired *t*-test, $P < 0.05$, $n = 3$).

culature. The finding that pulmonary microvascular hemoglobin oxygen saturation was higher under 16% than under 12% oxygen further supports the accuracy of our model to measure microcirculatory HbO_2 at different percentages of inspired oxygen.

Blood flow velocity. We provided an automated method to quantify blood flow in the pulmonary microcirculation using a newly created computer algorithm that converted the tracks of fluorescently labeled red blood cells into velocity and directionality maps. We selected DiI as a labeling dye for the blood cells because the extraordinary stability of the labeled blood cells reported in previous studies indicates that they do not appreciably alter the rheology, i.e., membrane stiffness and flow behavior, of the blood cells (17). The resulting color maps showed the expected patterns of blood flow, mostly outlining alveolar walls, as shown in Fig. 2*C* and in the supplemental

video. Most of the blood flow tracks were between ~5 and 30 μm thick. Although it is difficult to reconstruct precisely from the thickness of the flow tracks on the diameter and hierarchical position of vessels, this range is indicative for capillaries (≤20 μm) and small venules and arterioles (20–30 μm) (16). As has been described in previous work, red blood cells accelerated in collecting venules (9). The average velocity values in untreated animals of ~370 μm/s are in excellent agreement with previous work in other mammalian lungs, acquired by offline manual tracking, reporting velocity values of ~400 μm/s in rabbits (6), and 160–1,420 μm/s in canine pulmonary capillaries (12, 15). To test the ability of our method to detect changes in pulmonary blood flow, we have investigated whether pharmacological reduction of the heart rate would lead to a detectable decrease in pulmonary blood flow rate. Indeed, after injection of the negative chronotrope metoprolol, a beta-1-specific adrenergic receptor blocker (4), at an appropriate dose (7), we found a significant reduction of pulmonary blood flow in our animals, arguing that our model is indeed capable of measuring pharmacologically induced changes in blood flow velocity.

Potential limitations to our method. Some limitations apply to our model: the field of view is restricted to the peripheral microvasculature of the caudal areas of the lung, limiting measurements to local rather than global changes. Also, functional imaging on a closed window requires a short period of apnea, which by itself might change the microcirculation. This could be improved by abbreviating imaging periods or by gating the image acquisition. Third, inflation of the lung in our model is maintained by positive pressure via a ventilator instead of the naturally occurring negative pressure in the chest. This would also impact on the physiology of the pulmonary circulation.

Although our method allows for a considerably easier acquisition of microvascular flow data than manual tracking, it also permits acquisition of much more data in a shorter time. Importantly, our method enables for the analysis of whole vascular networks instead of single, individual vessels. The relatively low coefficients of variation of both hemoglobin oxygen saturation and blood flow measurements argue that, given natural variation between time points, our method is robust and precise.

In summary, we present a refined method to precisely quantify changes in hemoglobin saturation, blood flow velocity, and directionality in the pulmonary microcirculation in the rat lung. Using this integrated technology, we have demonstrated the feasibility of measuring changes in capillary hemoglobin oxygen saturation over time. Due to its technological robustness, ease of application, and relatively low costs, this model has the potential to turn intravital microscopy of the rodent lung, facilitated through the thoracic window model presented here, into a workhorse application for pharmaceutical and physiological research in the pulmonology field.

ACKNOWLEDGMENTS

We thank Kenneth Young for excellent technical support, Dr. W. Michael Foster (Duke Department of Medicine) for reviewing the manuscript, and Dr. Jahar Bhattacharya (Department of Physiology and Cellular Biophysics, Columbia University Medical Center) for advice in developing the model.

GRANTS

This work was funded by a grant from the Defense Advanced Research Projects Agency (DARPA), Prime Award No. N66001-10-C-2134, and by Department of Defense Fellowship Grant No. BC083195.

DISCLOSURES

No conflicts of interest, financial or otherwise are declared by the author(s).

AUTHOR CONTRIBUTIONS

Author contributions: G.H., G.P., S.S., D.R.R., D.C.I., A.B., C.A.P., G.B., M.W.D., T.J.M., and T.S. conception and design of research; G.H., S.S., Y.Z., A.B., G.B., and T.S. performed experiments; G.H., A.F., G.P., G.B., and T.S. analyzed data; G.H., G.P., S.S., C.A.P., G.B., and T.S. interpreted results of experiments; G.H. and T.S. prepared figures; G.H. and T.S. drafted manuscript; G.H., A.F., G.P., S.S., D.R.R., D.C.I., K.L.H., A.B., C.A.P., G.B., M.W.D., T.J.M., and T.S. edited and revised manuscript; G.H., A.F., G.P., S.S., D.R.R., Y.Z., D.C.I., K.L.H., A.B., C.A.P., G.B., M.W.D., T.J.M., and T.S. approved final version of manuscript.

REFERENCES

1. **Baker M, Wayland H.** On-line volume flow rate and velocity profile measurement for blood in microvessels. *Microvasc Res* 7: 131–143, 1974.
2. **Bhattacharya J.** Seeing is believing. *Nat Methods* 8: 57–58, 2011.
3. **Bickenbach J, Dembinski R, Czaplik M, Meissner S, Tabuchi A, Mertens M, Knels L, Schroeder W, Pelosi P, Koch E, Kuebler WM, Rossaint R, Kuhlen R.** Comparison of two in vivo microscopy techniques to visualize alveolar mechanics. *J Clin Monit Comput* 23: 323–332, 2009.
4. **Cucherat M, Borer JS.** Reduction of resting heart rate with antianginal drugs: review and meta-analysis. *Am J Ther* 19: 269–280, 2012.
5. **Fingar VH, Taber SW, Wieman TJ.** A new model for the study of pulmonary microcirculation: determination of pulmonary edema in rats. *J Surg Res* 57: 385–393, 1994.
6. **Groh J, Kuhnle GE, Sckell A, Ney L, Goetz AE.** Isoflurane inhibits hypoxic pulmonary vasoconstriction. An in vivo fluorescence microscopic study in rabbits. *Anesthesiology* 81: 1436–1444, 1994.
7. **Hocht C, Di Verniero C, Opezzo JA, Taira CA.** Pharmacokinetic-pharmacodynamic properties of metoprolol in chronic aortic coarctated rats. *Naunyn Schmiedebergs Arch Pharmacol* 370: 1–8, 2004.
8. **Irwin DC, Foreman B, Morris K, White M, Sullivan T, Jacobs R, Monnet E, Hackett T, TissotvanPatot MC, Hamilton KL, Gotshall RW.** Polymerized bovine hemoglobin decreases oxygen delivery during normoxia and acute hypoxia in the rat. *Am J Physiol Heart Circ Physiol* 295: H1090–H1099, 2008.
9. **Kuebler WM.** Real-time imaging assessment of pulmonary vascular responses. *Proc Am Thorac Soc* 8: 458–465, 2011.
10. **Lassailly F, Griessinger E, Bonnet D.** "Microenvironmental contaminations" induced by fluorescent lipophilic dyes used for noninvasive in vitro and in vivo cell tracking. *Blood* 115: 5347–5354, 2010.
11. **Okada O, Presson RG Jr, Kirk KR, Godbey PS, Capen RL, Wagner WW Jr.** Capillary perfusion patterns in single alveolar walls. *J Appl Physiol* 72: 1838–1844, 1992.
12. **Presson RG Jr, Graham JA, Hanger CC, Godbey PS, Gebb SA, Sidner RA, Glenny RW, Wagner WW Jr.** Distribution of pulmonary capillary red blood cell transit times. *J Appl Physiol* 79: 382–388, 1995.
13. **Severinghaus JW.** Simple, accurate equations for human blood O_2 dissociation computations. *J Appl Physiol* 46: 599–602, 1979.
14. **Sorg BS, Moeller BJ, Donovan O, Cao Y, Dewhirst MW.** Hyperspectral imaging of hemoglobin saturation in tumor microvasculature and tumor hypoxia development. *J Biomed Opt* 10: 44004, 2005.
15. **Staub NC, Schultz EL.** Pulmonary capillary length in dogs, cat and rabbit. *Respir Physiol* 5: 371–378, 1968.
16. **Tabuchi A, Mertens M, Kuppe H, Pries AR, Kuebler WM.** Intravital microscopy of the murine pulmonary microcirculation. *J Appl Physiol* 104: 338–346, 2008.
17. **Unthank JL, Lash JM, Nixon JC, Sidner RA, Bohlen HG.** Evaluation of carbocyanine-labeled erythrocytes for microvascular measurements. *Microvasc Res* 45: 193–210, 1993.
18. **Wagner PD, West JB.** Effects of diffusion impairment on O_2 and CO_2 time courses in pulmonary capillaries. *J Appl Physiol* 33: 62–71, 1972.

OPEN ACCESS Freely available online

PLOS ONE

Anti-Hypotensive Treatment and Endothelin Blockade Synergistically Antagonize Exercise Fatigue in Rats under Simulated High Altitude

Daniel Radiloff[1], Yulin Zhao[1], Alina Boico[1], Gert Blueschke[2], Gregory Palmer[1], Andrew Fontanella[1], Mark Dewhirst[1], Claude A. Piantadosi[3], Robert Noveck[4], David Irwin[5], Karyn Hamilton[6], Bruce Klitzman[2], Thies Schroeder[7]*

1 Department of Radiation Oncology, Duke University Medical Center, Durham, North Carolina, United States of America, **2** Department of Surgery, Duke University Medical Center, Durham, North Carolina, United States of America, **3** Department of Medicine-Pulmonary, Duke University Medical Center, Durham, North Carolina, United States of America, **4** Department of Medicine-Clinical Pharmacology, Duke University Medical Center, Durham, North Carolina, United States of America, **5** Department of Cardiology, University of Colorado Denver, Aurora, Colorado, United States of America, **6** Department of Health and Exercise Science, Colorado State University, Fort Collins, Colorado, United States of America, **7** Department of Physical Chemistry, University of Mainz, Mainz, Germany

Abstract

Rapid ascent to high altitude causes illness and fatigue, and there is a demand for effective acute treatments to alleviate such effects. We hypothesized that increased oxygen delivery to the tissue using a combination of a hypertensive agent and an endothelin receptor A antagonist drugs would limit exercise-induced fatigue at simulated high altitude. Our data showed that the combination of 0.1 mg/kg ambrisentan with either 20 mg/kg ephedrine or 10 mg/kg methylphenidate significantly improved exercise duration in rats at simulated altitude of 4,267 m, whereas the individual compounds did not. In normoxic, anesthetized rats, ephedrine alone and in combination with ambrisentan increased heart rate, peripheral blood flow, carotid and pulmonary arterial pressures, breathing rate, and vastus lateralis muscle oxygenation, but under inspired hypoxia, only the combination treatment significantly enhanced muscle oxygenation. Our results suggest that sympathomimetic agents combined with endothelin-A receptor blockers offset altitude-induced fatigue in rats by synergistically increasing the delivery rate of oxygen to hypoxic muscle by concomitantly augmenting perfusion pressure and improving capillary conductance in the skeletal muscle. Our findings might therefore serve as a basis to develop an effective treatment to prevent high-altitude illness and fatigue in humans.

Citation: Radiloff D, Zhao Y, Boico A, Blueschke G, Palmer G, et al. (2014) Anti-Hypotensive Treatment and Endothelin Blockade Synergistically Antagonize Exercise Fatigue in Rats under Simulated High Altitude. PLoS ONE 9(6): e99309. doi:10.1371/journal.pone.0099309

Editor: Guillermo López Lluch, Universidad Pablo de Olavide, Centro Andaluz de Biología del Desarrollo-CSIC, Spain

Received August 13, 2013; **Accepted** May 12, 2014; **Published** June 24, 2014

Funding: This work was funded by the U.S. Defense Advanced Research Projects Agency (DARPA) Prime Award Number N66001-10-C-2134. The funders had no role in study design, data collection and analysis, decision to publish, or preparation of the manuscript.

Competing Interests: The authors have declared that no competing interests exist.

* Email: tschroeder28@gmail.com

Introduction

A reduction in physical performance capacity and untimely fatigue are among the deleterious acute effects of rapid ascent to high altitudes. The most important factor underlying altitude-induced fatigue is thought to be the decreased availability of oxygen in arterial blood [1,2]. Abundant experimental work has been conducted to identify mechanisms to augment arterial oxygen content (C_{aO2}) by inducing hematopoiesis and increasing the hematocrit to improve exercise capacity at high altitude, but with variable success [3–5]. A more promising approach to improve maximum exercise capacity has been to target the pulmonary circulation, e.g. using dexamethasone, sildenafil, or endothelin blockers. The beneficial effects observed for these drugs have been attributed to a reduction in pulmonary arterial pressure, and/or an improved ventilation-perfusion-matching (V/Q) [6–9].

Because high altitude compromises function in multiple organs rather than impacting only the lung, we have hypothesized that a combination of targeting agents, rather than monotherapy approach, has the highest potential to effectively counteract altitude-induced fatigue. Indeed, our group showed previously that the combined dosing with theophylline and the endothelin receptor blocker sitaxsentan significantly increased exercise capacity of rats under simulated high altitude, whereas the single compounds did not [10]. The underlying mechanism appeared to be increased muscle tissue oxygenation via an increased rate of oxygen delivery, rather than by means of increased arterial oxygen content. Our data indicated that the mechanism of action involved a theophylline-induced increase in perfusion pressure on the skeletal muscle, caused by an increase in arterial blood pressure. However, theophylline is a highly pleiotropic drug with both cardiostimulatory and vasodilatory properties, and it has remained unclear whether augmentation of arterial blood pressure was essential for the observed ergogenic effects of the combination treatment.

Vasodilation, particularly of pulmonary vasculature, is a favored drug effect in altitude medicine, mostly because pulmonary vasoconstriction is thought to contribute to high altitude induced pulmonary edema (HAPE) [11]. It is however important to note that systemic hypoxia also produces peripheral arterial vasodila-

tion, which has a profound impact on heart rate, peripheral blood flow, and the ability to compensate for orthostatic challenges [12–14]. Thus, some degree of localized vasoconstriction and increased blood pressure may be desirable under these conditions. Because hypertensive treatment heightens pulmonary arterial pressure, and thus potentially increases the risk of HAPE, such interventions would be viewed skeptically by researchers in the field [11,15]. In the light of the potential benefit of cardiostimulatory treatment, and with respect to our previous work, it is thus important to know whether distinctly hypertensive drug effects as part of a drug combination carry utility to alleviate altitude-induced performance loss.

This study was designed to understand whether the hypertensive drugs ephedrine and methylphenidate would synergize with an endothelin receptor blocker to increase exercise capacity in rats under simulated high altitude. Ephedrine is a natural compound that together with its stereoisomer pseudoephedrine, has seen widespread use as a decongestant and cough suppressant, antihypotensive agent, and as a weight-loss supplement [16–18]. Methylphenidate is a synthetic amphetamine derivative that has been used to treat hyperactivity and attention deficit disorders [19]. Hypertension is a known effect of both of these drugs, and neither has been previously reported for their potential to mitigate altitude-related performance decrements. We hypothesized that the hypertensive drugs ephedrine or methylphenidate, when combined with an endothelin-1 blocking agent, would increase exercise performance under simulated high altitude in a rat model, whereas the single compounds would not. The proposed mechanism would involve an increased perfusion pressure in peripheral organs such as skeletal muscle, synergizing with a reduction of endothelin-mediated pre-capillary arteriolar vasoconstriction and leading to improved capillary flow and oxygen transport.

Materials and Methods

Drug and dosing regimen

All animal procedures were pre-approved by Duke University Institutional Animal Care and Use Committee (DUIACUC). All drugs were administered intraperitoneally (IP). Individual sympathomimetic treatments were [low dose ephedrine (2 mg/kg body wt.); high dose ephedrine (20 mg/kg)], [low dose methylphenidate (4 mg/kg); and high dose methylphenidate (10 mg/kg)]. Combination treatments were ambrisentan 0.1 mg/kg with (1) ephedrine 2 mg/kg (combination ephedrine low), (2) ephedrine 20 mg/kg (combination ephedrine high), (3) methylphenidate 4 mg/kg (combination methylphenidate low), (4) methylphenidate 10 mg/kg (combination methylphenidate high). Normal saline (0.9% NaCl) served as a control.

Run to fatigue measurements

The protocol to measure the influence of intraperitoneally administered drugs on the exercise capacity of hypoxic rats in a forced rodent exercise wheel system has been published in detail [10]. Briefly, rats were habituated to running in a motorized wheel system (Lafayette Instruments, Lafayette, IN) at 10 min/day for approximately 10 days, and then subjected to exercise testing in the same wheels in a hypobaric chamber at the Duke University Center for Hyperbaric Medicine and Environmental Physiology. The chosen level of simulated high altitude of 4267 m has been shown to strongly decrease voluntary performance in the rat [10]. Treatment agents were injected at near sea level altitude (119 m) 30 minutes before starting the exercise protocol, and the rats were taken to altitude 15 minutes before starting the run to allow for 5–10 minutes of equilibration time at altitude before exercise. An investigator accompanied the rats in the chamber to monitor their performance. The exercise protocol consisted of 10 minutes running at 6 meters per minute (m/min), 80 min running at 9 m/min, and 30 min running at 12 m/min. Up to 15 rats were exercised at the same time in individual wheels. Rats showing signs of fatigue were removed and tested for exhaustion by observing self-locomotion on a flat surface for 30 seconds. Rats that continued to show failure to run on the wheel, or acquired injuries during the run were immediately removed from the experiment, and treated as "censored" in log-rank tests.

Hemodynamic measurements on anesthetized animals

Experiments for the measurements of heart rates, mean arterial pressure, pulmonary arterial pressure, and arterial hemoglobin saturation were designed so that the dosing schedules would mirror the sequence of events and timing of the run-to-fatigue trials. Rats were anesthetized with ketamine/xylazine (80 mg/kg/8 mg/kg), and placed in lateral recumbency on a heating pad, to maintain body temperature. Indwelling PE-50 catheters were placed in the carotid artery for measurements of mean arterial blood pressure and PV-1 catheters were inserted into the pulmonary artery, via the jugular vein, to measure pulmonary arterial pressure as described [10,20]. Collection of arterial pressure data via a fluid-filled pressure transducer as was described [10]. The experimental protocol consisted of 15 min at normoxia (oxygen/nitrogen mixture to maintain 93–96% arterial HbO_2, typically 30%), followed by drug injection and after another 15 min, by inspired hypoxia (12%, balance nitrogen) for at least 30 min more. Gas mixtures were administered at constant flow rate of 2.5 l/min using a manual adjustment system (Oxydial, StarrLife Sciences, Oakmont, PA) Breathing rates were measured by counting chest movements over successive time periods from video sequences: directly before drug injection (min 10–15), directly before onset of hypoxia (min 25–30), and under hypoxia (min 50–55). Heart rates and arterial hemoglobin saturation were measured using pulse oximetry on the hind paw (MouseOx, StarrLife Sciences, Oakmont, PA).

Laser Doppler blood flow measurements

Continuous hind-limb blood flow measurements were performed on ketamine/xylazine anesthetized rats using laser Doppler probes (Oxyflow, Oxford Optronix, UK) placed directly on the vastus lateralis muscle with the overlying skin removed.

Tissue pO_2 measurements

Tissue pO_2 measurements were performed using invasive needle-encased probes (Oxylite, Oxford Optronix, UK) inserted into the vastus lateralis muscle parallel to the muscle fibers, with overlying skin removed. Because the amplitude of response of inserted probes to changes in inspired oxygen is partially dependent on the placement of the probe, we added a pre-treatment cycle of hypoxia/normoxia, as outlined previously, to control for differences in probe placement [10]. In brief, animals were subjected to baseline normoxia (sufficient oxygen to yield 93–96% HbO_2) for at least 10 min, then hypoxia (12%) for 15 min, then normoxia for 10 min, followed by the treatment drug, followed by the above schedule for anesthetized rats, i.e. 15 min normoxia, and 30 min hypoxia. Because the experiment required that the needle probe be placed in a way that it responds to physiological changes in tissue O_2 delivery, experiments where pre-treatment muscle pO_2 recordings did not respond to inspired hypoxia were eliminated from the study.

Pulmonary flow measurements

Blood flow velocity in the pulmonary microcirculation was measured via intravital microscopy on pentobarbital-anesthetized, ventilated rats (50 mg/kg), after injection of fluorescently labeled blood cells, using a thoracic window as described [21]. A different anesthesia regimen was necessary for this experiment in order to eliminate autonomous breathing. Measurements were performed with a CCD camera (Andor, Belfast, UK), and blood flow velocity was quantified using a Matlab-based computer algorithm. [21]. The experimental schedule was the following: 15 min baseline, first injection of ephedrine/ambrisentan at 20/0.1 mg/kg, after 15 min injection of a second dose of ephedrine/ambrisentan (same dose), end of experiment 15 min thereafter. Imaging under apnea was performed every 5 minutes. Animals were ventilated on a mechanical ventilator via a tracheal catheter and received sufficient oxygen to maintain HbO_2 at 93–96% HbO_2 (typically 30% FiO_2).

Statistics

Comparisons between run-to-fatigue curves were performed using log rank tests, and correction for multiple comparisons was conducted by multiplying the resulting p values by the number of comparisons. Animals that had to be removed from the exercise trials prior to fatigue, e.g. because of injury, were treated as "censored", i.e. their running history was only considered in the analysis until the time the injury became apparent. Comparisons between multiple data sets were conducted using one-way ANOVA for independent variables, and repeated-measures ANOVA for linked variables. All ANOVA analyses were corrected for multiple comparisons by the Bonferroni method. Continuous variables between two groups were compared using either T-test, or nonparametric Mann Whitney U-test, depending on whether the data was assumed to follow a normal Gaussian distribution, or not. GraphPad Prism software was used throughout to analyze the data sets (Graphpad, San Diego, CA). In the figures, single asterisks (*) represent p-values of less than 0.05, whereas double asterisks (**) represent p-values of less than 0.01. All error bars and parameters of variation in the text represent the standard deviation.

Results

Run to fatigue

In our escalating exercise protocol under simulated high altitude, only rats treated with a combination of a high dose sympathomimetic (ephedrine 20 mg/kg or methylphenidate 10 mg/kg), and ambrisentan (0.1 mg/kg), ran significantly longer than control rats. Use of single compounds or low dose sympathomimetics (ephedrine 2 mg/k and methylphenidate 4 mg/kg, Figure 1A, B) did not improve exercise performance beyond that of controls.

Heart rates

Mean heart rates from pooled data from all treatment groups at baseline were 283.2±47.8 beats per minute (BPM). Heart rates increased significantly after treatment with ephedrine or combination, and remained elevated under hypoxia (comparison between time points for each treatment: repeated measures ANOVA with Bonferroni correction, all $p<0.01$. Comparison between treatment groups by one-way ANOVA with Bonferroni correction, all $p<0.01$, Figure 2A).

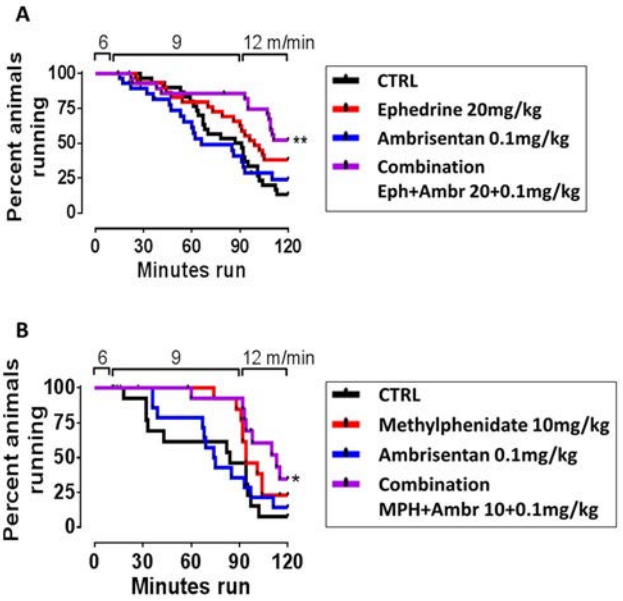

Figure 1. A: The combination of ephedrine (20 mg/kg) and ambrisentan (0.1 mg/kg), but not the single compounds, significantly increase the time run to fatigue of rats under simulated high altitude (Log rank test $p=0.0024$ after correction for multiple comparison). Lower concentrations of ephedrine (2 mg/kg) were not ergogenic, neither alone nor if combined with ambrisentan (not shown). N = 28–31 per treatment group. B: Methylphenidate (10 mg/kg) combined with ambrisentan, but not the single compounds, enhanced time run to fatigue under simulated high altitude (Log Rank test $p=0.044$ after correction for multiple comparison). Lower dose methylphenidate (4 mg/kg) did not have ergogenic effects, alone or in combination with ambrisentan (not shown). N = 14–15 per treatment group. N = 10–11 per treatment group. All drugs were injected IP.
doi:10.1371/journal.pone.0099309.g001

Blood flow in hind leg muscle

Under hypoxia, both ephedrine and combination-treated animals displayed significant increased blood flow in the vastus lateralis muscle in the hind leg, compared to control and ambrisentan only treated animals (Figure 2B). Hypoxia triggered an immediate increase in the muscle blood flow tracings in most animals in treatment groups; however, when comparing flow 1 min pre- vs. 1 min post-injection of treatment, no significance was found in any of the groups (Wilcoxon Rank test for repeated measures).

Pulmonary capillary blood flow

Treatments with combined ephedrine and ambrisentan sequentially increased blood flow velocity through the pulmonary capillary system, measured with pulmonary intravital microscopy. This increase was due mainly to an increase in heart rates (Figure 2C). Treatment with saline did not lead to a comparable change (data not shown).

Breathing rates

Treatment with ephedrine (20 mg/kg), alone and in combination, significantly increased breathing rates compared to groups without ephedrine. Hypoxia further increased breathing rates in all groups (Figure 2D).

Arterial blood oxygenation

Mean hemoglobin oxygen saturation (HbO_2) from pooled data of all treatment groups at baseline was 97.3±4%. All treatment

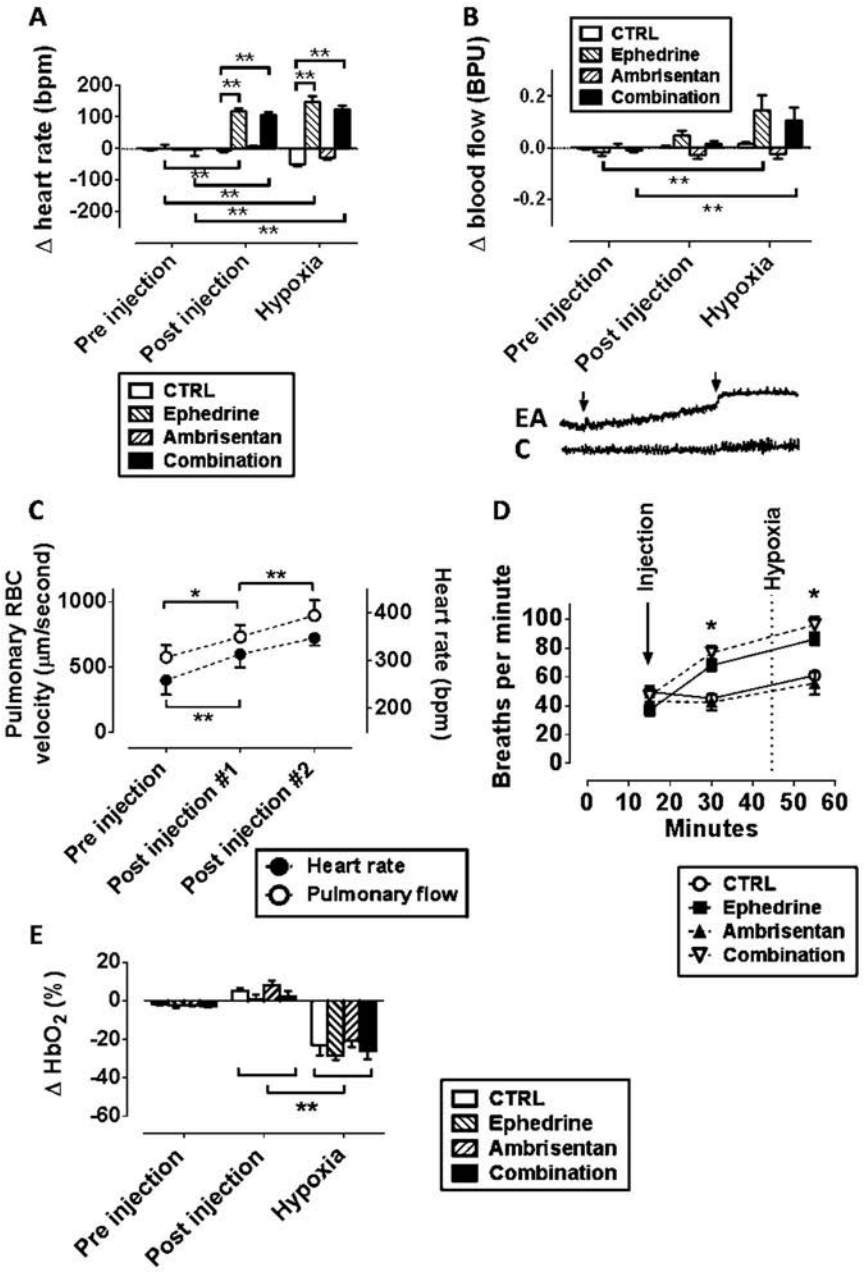

Figure 2. Hemodynamic effects of high-dose ephedrine in anesthetized rats. "Pre-injection" were averaged data −5 to 0 minutes pre injection, "post injection" was averaged −5 to 0 minutes before onset of hypoxia, and "hypoxia" was averaged 30–40 minutes post injection. A: Changes in heart rates, normalized to the time of injection. The addition of ephedrine at 20 mg/kg IP significantly increased heart rates, alone and combined with ambrisentan. Heart rates remained significantly elevated under hypoxia in ephedrine treated groups (one-way ANOVA/Bonferroni, $p<0.01$, N = 7–13). B: Changes in blood perfusion velocity in hind leg muscle after treatment, measured directly on the muscle, using a laser Doppler probe. Both ephedrine and the combination significantly enhanced muscle blood flow under hypoxia (N = 6–9). The onset of hypoxia triggered a distinct increase in muscle flow in all groups containing ephedrine, and to a lesser degree in control treated animals (example laser Doppler tracings from rat leg muscle; EA = ephedrine and ambrisentan; C = combination; first arrow: injection, second: hypoxia). C: Repeated injection of combined ephedrine (20 mg/kg) and ambrisentan (0.1 mg/kg) significantly enhances heart rates, and concomitantly, pulmonary blood flow, measured by pulmonary window blood flow measurements, and pulse oximetry (paired T-test, corrected for multiple comparison, $p<0.05$, N = 5). D: injection of ephedrine, alone or in combination with ambrisentan, caused a significant increase of breathing rates (one-sided ANOVA with Bonferroni correction, $p<0.001$, N = 5–13/group). Hypoxia further increased breathing rates in all groups (repeated measures ANOVA/Bonferroni, $p<0.001$). E: Changes in blood oxygenation after treatment: HbO_2 decreased significantly in all treatment groups after onset of inspired hypoxia (repeated measure ANOVA/Bonferroni, $p<0.001$), but there was no difference in this parameter between treatment groups (one-way ANOVA/Bonferroni, N = 5–9).
doi:10.1371/journal.pone.0099309.g002

groups experienced a significant decrease in HbO_2 after onset of hypoxia, but no differences in HbO_2 were detected among the treatment groups (Figure 2E).

Mean arterial pressure (MAP)

Mean MAP in pooled data of all treatment groups at baseline was 90.5±15.2 mmHg. Increases in MAP after treatment and

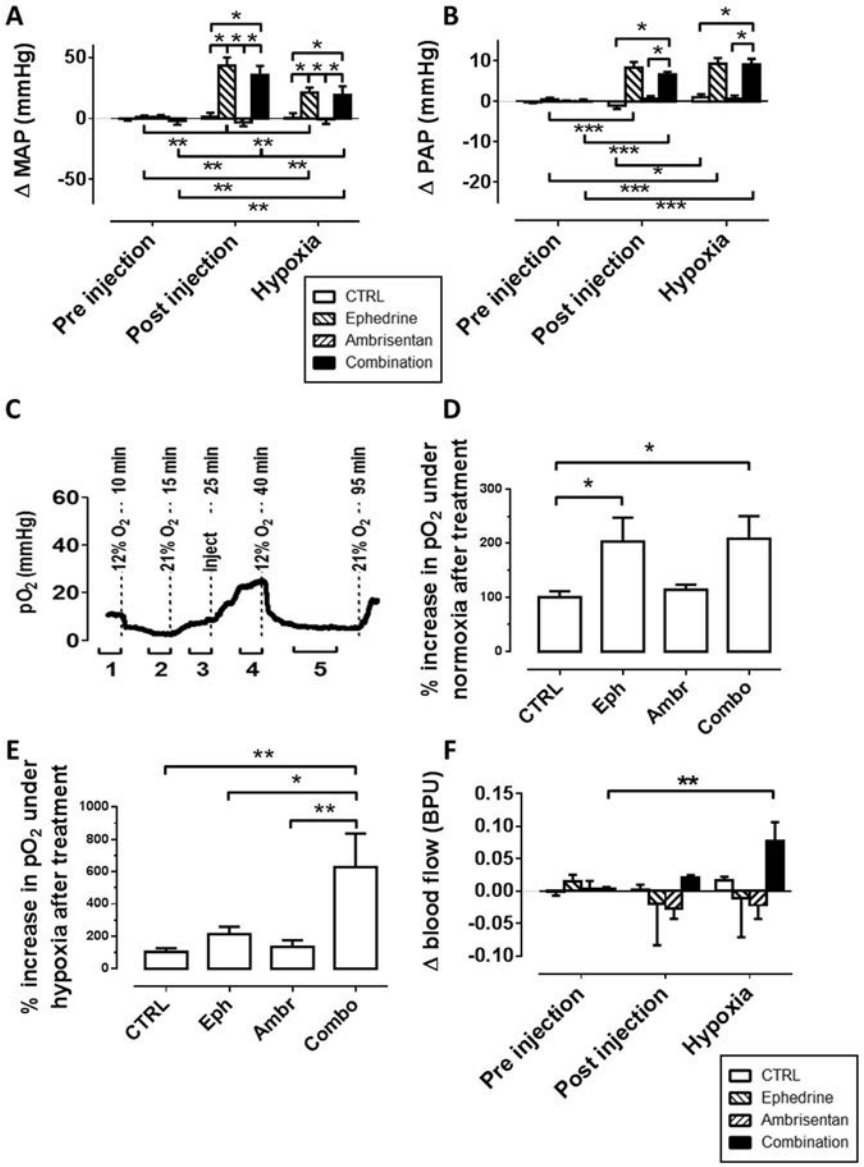

Figure 3. Blood pressure effects of ephedrine treatment. "Pre-injection" were averaged data −5 to 0 minutes pre injection, "post injection" was averaged −5 to 0 minutes before onset of hypoxia, and "hypoxia" was averaged 30–40 minutes post injection. A, B: Treatment with high dose ephedrine (20 mg/kg), alone and combination with ambrisentan, significantly increased MAP and PAP, under normoxia and hypoxia, compared to baseline (repeated measures ANOVA with Bonferroni correction, $p<0.05$), and compared to the other treatment groups (one-way ANOVA/Bonferroni, $p<0.001$). Onset of hypoxia significantly decreased MAP in these groups (repeated measures ANOVA with Bonferroni correction, $p<0.05$). In the control group, PAP increased significantly after onset of hypoxia (N = 7–14). C: Experimental schedule to measure the influence of treatment on oxygen concentration in the hind muscle. Tissue hypoxia was measured by pO_2 needle electrode tracings during inspired normoxia (1) and hypoxia at baseline (2), before (3) and after injection under normoxia (4), and during post-injection hypoxia (5). D: under post-treatment normoxia (panel D time point #4), ephedrine alone and in combination with ambrisentan significantly increased muscle oxygenation, compared to pre-treatment pO_2 (one-way ANOVA with Bonferroni correction, N = 4–8, $p<0.05$). E: Under post-treatment hypoxia (panel D #5), only the combination of high ephedrine and ambrisentan significantly increased muscle oxygen tension. Re-oxygenation after combo treatment was significantly higher than in all other treatment groups (one-way ANOVA/Bonferroni, N = 4–8, $p<0.05$ * or 0.01**). F: Low dose ephedrine (2 mg/kg) significantly increases blood flow in the hind leg muscle when combined with ambrisentan, but not alone.
doi:10.1371/journal.pone.0099309.g003

under hypoxia, compared to baseline, were significant in all groups containing ephedrine. Blood pressures in ephedrine and combination treated groups were significantly higher than controls and ambrisentan only, respectively, at each time point post treatment (Figure 3A).

Pulmonary arterial pressure (PAP)

Mean PAP in pooled data of all treatment groups at baseline was 12.3±5.3 mmHg. Increases in PAP after ephedrine containing treatments were significant both after treatment, and under subsequent hypoxia, compared to baseline. Also, PAP was significantly elevated compared to both controls and ambrisentan at all post treatment time points (Figure 3B).

Tissue oxygenation

The influence of treatment with ephedrine, ambrisentan, and the combinations was tested by comparing tissue pO_2 in the rat hind leg vastus lateralis muscle under inspired hypoxia (12% O_2) before and after injection. The pO_2 measurements were integrated over (1) the last 5 min before onset of initial hypoxia, (2) the last 5 min before restoration of normoxia, (3) the last 5 min before injection of treatment, (4) the last 5 min before onset of hypoxia, and (5) min 30–40 post injection, i.e. during hypoxia (Figure 3C, example pO_2 tracing). Average pO_2 values ± standard deviation for time points 1–5 are given in Table 1. Treatment effects on the tissue oxygen levels under (pre-hypoxic) normoxia were measured as the percentage increase in pO_2 from time point (3) to time point (4). The ability of the treatment to increase tissue pO_2 under hypoxia was measured as the percentage increase from time point (2) to time point (5). Under post-treatment normoxia, both ephedrine and ephedrine combined with ambrisentan significantly increased muscle tissue oxygenation, when compared with control treatments (Figure 3D). Under post-treatment hypoxia, only the combination of high dose ephedrine significantly increased muscle oxygenation over all other treatment groups (Figure 3E).

Hemodynamic effects of low-dose ephedrine

Experiments were repeated in the ephedrine treatment groups at a 10-fold lower dose of ephedrine, i.e. 2 mg/kg. Both treatments, ephedrine alone and in combination with ambrisentan, significantly increased the heart rate by approximately 45 bpm, compared to baseline (repeated-measures ANOVA/Bonferroni, $p<0.05$). Blood flow in hind leg muscle was significantly elevated under hypoxia following treatment with the combination, but not with the single compounds (Figure 3F). Breathing rates, HbO_2, MAP and PAP were unaffected by treatment with the reduced ephedrine dose, alone and in combination with ambrisentan (data not shown).

Discussion

We tested the novel hypothesis that combined dosing with a chronotropic, hypertensive drug and the endothelin receptor antagonist ambrisentan, under simulated high altitude, would produce a more distinct ergogenic effect than the single compounds alone. Indeed, rats that were dosed with the combination of ephedrine or methylphenidate and the endothelin receptor antagonist (ERA) ambrisentan ran significantly longer than controls under simulated high altitude, whereas those treated with single drugs did not. In anesthetized rats, both ephedrine and ephedrine combined with ambrisentan increased heart rates, MAP, PAP, breathing rates, blood flow to the hind limb musculature, and normoxic oxygenation, but only the drug combination significantly increased muscle oxygenation in hypoxic air.

Several compounds have been suggested for the potential alleviation of altitude-induced fatigue, including inhibitors of phosphodiesterase type 5 (PDE5), dexamethasone, endothelin receptor antagonists, and erythropoietin (EPO) pre-treatment [3,6–8]. Of note, increasing hematocrit by "blood doping" has not been demonstrated to enhance performance capacity at high altitude [5]. We recently reported that the combination of theophylline and the endothelin receptor antagonist (ERA) sitaxsentan synergized to improve exercise performance of rats under hypobaric hypoxia, exceeding the effects of theophylline or sitaxsentan given alone [10]. In addition, we showed that the improved exercise performance was due to increased blood flow (thus, oxygen transport rate) to peripheral tissue, potentially driven and powered by the augmenting effect of theophylline on heart rate and arterial blood pressures [10]. Subsequently, we have here investigated the effects of pharmacologically-induced hypertension in combination with endothelin blockade, using a rodent exercise model under simulated high altitude.

Study drugs

Ephedrine is a naturally-occurring sympathomimetic amine that shares structural and functional similarity with amphetamine, as well as with the neurotransmitter epinephrine [22]. Ephedrine directly activates alpha- and beta-adrenergic receptors, triggers catecholamine release, and inhibits norepinephrine reuptake [23,24]. Physiologically, ephedrine increases heart rate, peripheral resistance and arterial pressure, and may cause hallucinogenic side effects [25]. In addition to its medical use, ephedrine has been tried for many years as a performance-enhancing agent; however, consistent ergogenic effects are only achieved if combined with agents such as caffeine [26]. At high doses, ephedrine can produce cardiotoxicity, especially when taken together with caffeine [23,27,28]. In rats, ephedrine doses of 20 mg/kg i.p. (12.1% of the intraperitoneal LD_{50} of ephedrine in rats) increases locomotion, which provided the basis for the dosage used in this study [29,30].

Methylphenidate (MPH) is a benzylpiperidine derivative, structurally related to amphetamine, used for treating attention deficit disorder and depression [19]. Its CNS stimulant activity is

Table 1. Averaged tissue pO_2 values in mmHg (means ± SD), acquired with Oxylite probes.

	Tissue pO_2 (mmHg)				
Time points	**1**	**2**	**3**	**4**	**5**
Control	14.7±10.3	6.1±5.7	10.5±7.6	10.5±11	5.2±6.3
Ephedrine low (2 mg/kg)	20.5±9.5	7.1±4.3	17.6±12.2	19.2±11.7	9.6±5.6
Ephedrine high (20 mg/kg)	16±12.8	7±7	21.5±9.5	30.2±19.7	10.8±9.5
Ambrisentan (0.1 mg/kg)	19.1±9.4	3.9±1.7	8.1±4.1	9.6±6.3	4.2±2
Combination Ambr.+Eph. Low	14.7±4.3	3.5±1.4	8.4±2.7	17.8±10.6	8.7±4.5
Combination Ambr.+Eph. High	14±11.3	4±3.7	17.9±10.1	35.3±23.1	15.7±10.9

Time point 1: averaged over last 5 min before onset of 1st cycle of hypoxia; time point 2: averaged over last 5 min before return to normoxia; time point 3: averaged over last 5 min before injection; time point 4: averaged over last 5 min before onset of 2nd cycle of hypoxia; time point 3: averaged over 30–40 minutes post injection, i.e. during post-treatment hypoxia; Ambr = Ambrisentan, Eph = Ephedrine.

doi:10.1371/journal.pone.0099309.t001

mediated through re-uptake inhibition of norepinephrine and dopamine. Methylphenidate also increases norepinephrine levels in the blood, and thus raises heart rate and blood pressure [31]. MPH has shown efficacy as a single-drug performance enhancing agent in normobaric human subjects [32].

Ambrisentan is a competitive antagonist of type A receptors (Et_A) of the vasoconstrictive peptide hormone endothelin-1 [33]. Endothelin-1 is a dominant factor in tissue blood flow regulation and particularly important in regulating pre-capillary arteriolar tone [34–37]. Endothelin receptor antagonists (ERAs), such as ambrisentan, are used to treat pulmonary arterial hypertension in humans [33,38]. Drug class toxicity of ERAs include liver injury and birth defects, however, ambrisentan has been shown to be relatively safe [38,39]. More recent research has shown that blockade of endothelin-1 receptors may improve maximum exercise performance at altitude in humans [8,40]. The dose of ambrisentan selected here was based on our previous research and is lower than that of most other studies in rats [41]. After oral dosing, ambrisentan has a plasma peak at approximately two hours and an elimination half-life of approximately 15 hours [33,42]. Because ambrisentan has little effect on hepatic cytochrome P_{450} enzymes, its potential to interact with the other drugs given here is modest [33].

Exercise model and environmental conditions

We utilized an established model of escalated exercise performance in rats at altitude based on motorized rodent wheels [10]. The chosen simulated altitude level of 4267 m is sufficient to decrease voluntary exercise performance by over 60% in rats [10]. While this model is well-suited to read out exercise performance capacity under the given altitude conditions, it is technically not feasible to use it to quantify exercise performance under normoxia, because of the excessive time necessary to produce fatigue in normoxic rats, which causes early termination due to injury before fatigue (data not shown).

The use of anesthetized animals for mechanistic studies

Although it is possible to perform hemodynamic measurements on conscious rats, reliable needle-based pO_2 measurements in tissues, which are essential for this study, are not feasible in those models. We have selected anesthetic regimen that are known, and confirmed by our data, to have a comparably small effect on the cardiovascular system, as ketamine/xylazine does not affect the heart rate and only slightly reduce mean arterial pressure at higher doses [43–45]. While it is clear that cardiovascular differences between anesthetized resting and awake exercising animals are drastic, effects of hypoxia on the organism, such as hypoxemia, and hypoxic pulmonary vasoconstriction, and sympathetic activation are found in both states [10,45]. This is demonstrated e.g. by the expected increase of PAP after onset of hypoxia in control animals (Figure 3B).

Synergism between hypertensive drugs and endothelin blockade under hypoxia

The combination of ephedrine (20 mg/kg) and ambrisentan, as well as ephedrine alone, increased arterial blood pressure in anesthetized rats, both treatments also increased muscle blood flow under hypoxia. Our results obtained in the pulmonary window showed that the drug combination can, in principle, lead to increased pulmonary blood flow, driven by augmented cardiac output. Thus, our data support that the known ability of ephedrine to increase peripheral muscle blood flow is not impaired by the addition of ambrisentan and that the treatment also has the potential to improve pulmonary blood flow.

In agreement with the finding of peripheral blood flow enhancement in anesthetized rats, both ephedrine and its combination with ambrisentan enhanced oxygen delivery to the vastus lateralis muscle under normoxia. Importantly, only the combination, and not ephedrine alone, increased muscle oxygenation under inspired hypoxia. This is in remarkable conformity with the finding that only the combination, but not any of the single compounds, was ergogenic in exercising hypoxic rats.

In mammalian skeletal muscle, autoregulation of blood flow is critically important to the efficient distribution of blood supplied by the systemic vasculature to the region of demand [46,47]. For example, in resting rats, red skeletal muscle fibers are typically better perfused than white glycolytic fibers, but regional blood supplies are progressively shifted towards glycolytic fibers as maximum exercise intensity is approached [46]. Factors that are known to play a role in the autoregulation of muscle blood flow are e.g. flow/pressure-related effects such as the myogenic response, metabolic vasodilators such as adenosine [48], and local hypoxia [49,50]. Local hypoxia appears to function as a regional second messenger to redirect organ-specific blood flow to the area of greatest need, and thus, systemic hypoxia drives the fine-tuned local flow regulation in peripheral organs and the brain out of balance [51–53]. One of the well-known extrapulmonary cardiovascular effects of hypoxia is NO-mediated peripheral vasodilation, which, after rapid ascension to high altitude, leads to systemic arterial hypotension, and subsequently, to compensatory increases in heart rates [14,54,55]. However, hypoxia is also capable of causing peripheral vasoconstriction in resistance arterioles, by triggering the release of the vasoconstrictor endothelin-1 from endothelial cells [56–58]. Importantly though, while NO exerts its vasodilatory effect predominantly on 1st and 2nd order arterioles [59], endothelin-1 vasoconstricts only pre-capillary (3rd or higher order) arterioles [37,60], and, via pericytes, also directly controls capillary diameter [61,62]. Via endothelin-1 release, hypoxia is therefore capable of directly controlling capillary conductance.

The importance of maintaining perfusion pressure during hypoxic vasodilation to enable efficient capillary blood flow has been recently addressed [49,50]. In our study, ephedrine and ambrisentan exerted ergogenic effects only when ephedrine concentrations were used at doses that were sufficient to raise pulmonary and mean arterial blood pressure in anesthetized rats. Sympathetic activation, such as triggered by ephedrine or methylphenidate, specifically constricts larger, low-order peripheral arterioles [63]. It is therefore plausible that the sympathomimetic treatment used in this study directly counteracted hypoxia-triggered, NO-mediated vasodilation, thereby reversing arterial hypotension and preserving perfusion pressure on the skeletal muscle. Sympathetic activation and endothelin blockade should therefore synergize to improve capillary perfusion and thus, increase oxygen transport to the hypoxic muscle. Indeed, the observed increase in muscle blood flow and oxygenation in anesthetized rats, in the absence of changes to HbO_2 suggests that the observed enhancement of exercise performance in awake animals is mediated by changes in flow, rather than by arterial oxygen content (CaO_2).

The observed increase in ventilation rate after treatment with ephedrine has been reported, but since it had no apparent impact on blood oxygen concentrations, this effect may not carry ergogenic significance.

It is well known that the mammalian cardiovascular system responds to hypoxemia with increased cardiac output, which can, to some degree, be succeeded by increased muscle blood flow

[54,64–69]. This mechanism is probably responsible for the immediate, steep increase in muscle blood flow that was seen in many animals, following the onset of hypoxia shown in Figure 2B. Both the apparent extrapulmonary effect of ambrisentan on muscle, and the interaction between pharmaceutically-induced and hypoxia-stimulated increases in peripheral blood flow, will be important future topics for investigation, to further elucidate and leverage this cooperative drug effect.

While we focused on exercise performance as a readout for the detrimental effects of altitude on animals, the combined sympathomimetic/endothelin blocking treatment may also improve other symptoms of altitude sickness. Endothelin-1 has a role in the cerebral microcirculation that is remarkably similar to the muscle, with pre-capillary arterioles being particularly responsive to endothelin-1-mediated vasoconstriction [70,71]. Endothelin-mediated vasoconstriction in the brain, in principle, can be pharmacologically reversed [72]. It is also known that cerebral blood flow is responsive to hypoxia [52,73], and that systemic arterial hypotension, as e.g. elicited by hypoxia, will compromise cerebral blood flow if it falls below a critical threshold [74]. While we did not investigate whether endothelin-1 release plays a major role in cerebral pathophysiology at high altitude, it seems possible that combined sympathomimetic/endothelin-1 blockade may also counteract altitude-related central nervous system effects, such as acute mountain sickness (AMS).

Given the toxicity of high-dose ephedrine, it is important to ask whether the effective dose in our study is clinically feasible in humans. While detailed pharmacokinetic data on rats is not available in the literature, there is enough information for a rough prediction of the human equivalent dose (HED) to what we have found to be efficacious in rats. By extrapolation, ephedrine at 20 mg/kg intraperitoneally equals approximately 0.81 mg/kg intravenously [75]. This approximates a plasma concentration of 58.7 ng/ml [76]. Because this is only about one fifth of the human C_{max} of approximately 290 ng/ml measured after ingestion of a moderate single dose of 75 mg [77], the HED of ephedrine is probably in the clinically relevant range. However, cardioactive drugs should be used with great caution under high altitude, especially in the elderly and/or those with cardiopulmonary disease [78,79]. In addition, the increase of pulmonary arterial pressure caused by ephedrine has the potential to augment pulmonary leak in humans, thus potentially increasing the risk of developing HAPE [80]. However, among the factors known to predispose to HAPE, the exaggerated production of endothelin-1 leads to impaired plasticity and adaptability of the pulmonary vasculature [81]. It must be carefully tested whether the combined use of sympathomimetics and endothelin blockers increases or decreases the risk of HAPE.

In summary, we have presented evidence that the combination of the hypertensive drugs ephedrine or methylphenidate with the endothelin A receptor antagonist ambrisentan increase the exercise capacity of rats under simulated high altitude. The underlying mechanism probably involves a specific increase in capillary blood flow in skeletal muscle, and an elevated arterial blood pressure appears to be critical for this effect. Our data indicate that while ephedrine alone increases muscle oxygenation under normoxia, the combination with ambrisentan specifically re-oxygenates hypoxic muscle, whereas ambrisentan has little or no effect on normoxic muscle. Other hypertensive drugs, such as methylphenidate, demonstrate effects similar to ephedrine when combined with ambrisentan. These data suggest that hypertensive and endothelin-blocking drug combinations could effectively mitigate performance loss during rapid ascent to high altitudes in humans.

Acknowledgments

The authors thank Dr. Terry Opgenorth and Joseph DeAngelo for their helpful advice and Kenneth Young of Duke Radiation Oncology for his technical support. Dr. Barry Allen's (Duke Hyperbaric Medicine) scientific advice on writing the manuscript is highly appreciated. We thank Dr. David Gooden from the Duke Small Molecule Synthesis Facility for producing ambrisentan for the study. We also thank the personnel of the Duke Hyperbaric Facility for their help with the pressure chamber experiments.

Author Contributions

Conceived and designed the experiments: DR GB GP AF MD CAP RN DI KH TS. Performed the experiments: DR YZ AB GB GP AF TS. Analyzed the data: DR AB GB GP AF TS. Contributed reagents/materials/analysis tools: GP AF MD CAP RN DI KH BK TS. Wrote the paper: DR AB GP AF MD CAP RN DI KH BK TS.

References

1. Fulco CS, Rock PB, Cymerman A (1998) Maximal and submaximal exercise performance at altitude. Aviat Space Environ Med 69: 793–801.
2. Amann M, Romer LM, Pegelow DF, Jacques AJ, Hess CJ, et al. (2006) Effects of arterial oxygen content on peripheral locomotor muscle fatigue. J Appl Physiol 101: 119–127.
3. Lundby C, Robach P, Boushel R, Thomsen JJ, Rasmussen P, et al. (2008) Does recombinant human Epo increase exercise capacity by means other than augmenting oxygen transport? J Appl Physiol 105: 581–587.
4. Pace N, Consolazio WV, Lozner EL (1945) The Effect of Transfusions of Red Blood Cells on the Hypoxia Tolerance of Normal Men. Science 102: 589–591.
5. Young AJ, Sawka MN, Muza SR, Boushel R, Lyons T, et al. (1996) Effects of erythrocyte infusion on VO2max at high altitude. J Appl Physiol 81: 252–259.
6. Richalet JP, Gratadour P, Robach P, Pham I, Dechaux M, et al. (2005) Sildenafil inhibits altitude-induced hypoxemia and pulmonary hypertension. Am J Respir Crit Care Med 171: 275–281.
7. Siebenmann C, Bloch KE, Lundby C, Nussbamer-Ochsner Y, Schoeb M, et al. (2011) Dexamethasone improves maximal exercise capacity of individuals susceptible to high altitude pulmonary edema at 4559 m. High Alt Med Biol 12: 169–177.
8. Naeije R, Huez S, Lamotte M, Retailleau K, Neupane S, et al. (2010) Pulmonary artery pressure limits exercise capacity at high altitude. Eur Respir J 36: 1049–1055.
9. Ghofrani HA, Reichenberger F, Kohstall MG, Mrosek EH, Seeger T, et al. (2004) Sildenafil increased exercise capacity during hypoxia at low altitudes and at Mount Everest base camp: a randomized, double-blind, placebo-controlled crossover trial. Ann Intern Med 141: 169–177.
10. Radiloff DR, Zhao Y, Boico A, Wu C, Shan S, et al. (2012) The combination of theophylline and endothelin receptor antagonism improves exercise performance of rats under simulated high altitude. J Appl Physiol.
11. Maggiorini M (2010) Prevention and treatment of high-altitude pulmonary edema. Prog Cardiovasc Dis 52: 500–506.
12. Lundby C, Boushel R, Robach P, Moller K, Saltin B, et al. (2008) During hypoxic exercise some vasoconstriction is needed to match O2 delivery with O2 demand at the microcirculatory level. J Physiol 586: 123–130.
13. Bada AA, Svendsen JH, Secher NH, Saltin B, Mortensen SP (2012) Peripheral vasodilatation determines cardiac output in exercising humans: insight from atrial pacing. J Physiol 590: 2051–2060.
14. Thomas KN, Burgess KR, Basnyat R, Lucas SJ, Cotter JD, et al. (2010) Initial orthostatic hypotension at high altitude. High Alt Med Biol 11: 163–167.
15. Pitman JT, Harris NS (2012) Possible association with amphetamine usage and development of high altitude pulmonary edema. Wilderness Environ Med 23: 374–376.
16. Eccles R (2007) Substitution of phenylephrine for pseudoephedrine as a nasal decongeststant. An illogical way to control methamphetamine abuse. Br J Clin Pharmacol 63: 10–14.
17. Daly PA, Krieger DR, Dulloo AG, Young JB, Landsberg L (1993) Ephedrine, caffeine and aspirin: safety and efficacy for treatment of human obesity. Int J Obes Relat Metab Disord 17 Suppl 1: S73–78.
18. Shekelle P, Hardy ML, Morton SC, Maglione M, Suttorp M, et al. (2003) Ephedra and ephedrine for weight loss and athletic performance enhancement: clinical efficacy and side effects. Evid Rep Technol Assess (Summ): 1–4.
19. Prommer E (2012) Methylphenidate: established and expanding roles in symptom management. Am J Hosp Palliat Care 29: 483–490.

20. Buehler PW, Baek JH, Lisk C, Connor I, Sullivan T, et al. (2012) Free hemoglobin induction of pulmonary vascular disease: evidence for an inflammatory mechanism. Am J Physiol Lung Cell Mol Physiol 303: L312–326.
21. Hanna G, Fontanella A, Palmer G, Shan S, Radiloff DR, et al. (2013) Automated measurement of blood flow velocity and direction and hemoglobin oxygen saturation in the rat lung using intravital microscopy. Am J Physiol Lung Cell Mol Physiol 304: L86–91.
22. Avois L, Robinson N, Saudan C, Baume N, Mangin P, et al. (2006) Central nervous system stimulants and sport practice. Br J Sports Med 40 Suppl 1: i16–20.
23. Powers ME (2001) Ephedra and its application to sport performance: another concern for the athletic trainer? J Athl Train 36: 420–424.
24. Liles JT, Dabisch PA, Hude KE, Pradhan L, Varner KJ, et al. (2006) Pressor responses to ephedrine are mediated by a direct mechanism in the rat. J Pharmacol Exp Ther 316: 95–105.
25. McMahon LR, Cunningham KA (2003) Discriminative stimulus effects of (-)-ephedrine in rats: analysis with catecholamine transporter and receptor ligands. Drug Alcohol Depend 70: 255–264.
26. Magkos F, Kavouras SA (2004) Caffeine and ephedrine: physiological, metabolic and performance-enhancing effects. Sports Med 34: 871–889.
27. Pentel P (1984) Toxicity of over-the-counter stimulants. JAMA 252: 1898–1903.
28. Dunnick JK, Kissling G, Gerken DK, Vallant MA, Nyska A (2007) Cardiotoxicity of Ma Huang/caffeine or ephedrine/caffeine in a rodent model system. Toxicol Pathol 35: 657–664.
29. Wellman PJ, Miller DK, Livermore CL, Green TA, McMahon LR, et al. (1998) Effects of (−)-ephedrine on locomotion, feeding, and nucleus accumbens dopamine in rats. Psychopharmacology (Berl) 135: 133–140.
30. Miller DK, McMahon LR, Green TA, Nation JR, Wellman PJ (1998) Repeated administration of ephedrine induces behavioral sensitization in rats. Psychopharmacology (Berl) 140: 52–56.
31. Cho SC, Kim BN, Cummins TD, Kim JW, Bellgrove MA (2012) Norepinephrine transporter -3081(A/T) and alpha-2A-adrenergic receptor MspI polymorphisms are associated with cardiovascular side effects of OROS-methylphenidate treatment. J Psychopharmacol 26: 380–389.
32. Roelands B, Hasegawa H, Watson P, Piacentini MF, Buyse L, et al. (2008) The effects of acute dopamine reuptake inhibition on performance. Med Sci Sports Exerc 40: 879–885.
33. Barst RJ (2007) A review of pulmonary arterial hypertension: role of ambrisentan. Vasc Health Risk Manag 3: 11–22.
34. Spratt JC, Goddard J, Patel N, Strachan FE, Rankin AJ, et al. (2001) Systemic ETA receptor antagonism with BQ-123 blocks ET-1 induced forearm vasoconstriction and decreases peripheral vascular resistance in healthy men. Br J Pharmacol 134: 648–654.
35. Kelly JJ, Whitworth JA (1999) Endothelin-1 as a mediator in cardiovascular disease. Clin Exp Pharmacol Physiol 26: 158–161.
36. Hassoun PM, Thappa V, Landman MJ, Fanburg BL (1992) Endothelin 1: mitogenic activity on pulmonary artery smooth muscle cells and release from hypoxic endothelial cells. Proc Soc Exp Biol Med 199: 165–170.
37. Lougee L, Hinojosa-Laborde C, Harder DR, Lombard JH (1990) Effect of nifedipine on endothelin induced contractions of skeletal muscle arterioles of spontaneously hypertensive rats. Microcirc Endothelium Lymphatics 6: 355–368.
38. Rubin LJ (2012) Endothelin receptor antagonists for the treatment of pulmonary artery hypertension. Life Sci 91: 517–521.
39. McGoon MD, Frost AE, Oudiz RJ, Badesch DB, Galie N, et al. (2009) Ambrisentan therapy in patients with pulmonary arterial hypertension who discontinued bosentan or sitaxsentan due to liver function test abnormalities. Chest 135: 122–129.
40. de Bisschop C, Martinot JB, Leurquin-Sterk G, Faoro V, Guenard H, et al. (2012) Improvement in lung diffusion by endothelin A receptor blockade at high altitude. J Appl Physiol 112: 20–25.
41. Wagenaar GT, Laghmani EH, de Visser YP, Sengers RM, Steendijk P, et al. (2013) Ambrisentan reduces pulmonary arterial hypertension, but does not stimulate alveolar and vascular development in neonatal rats with hyperoxic lung injury. Am J Physiol Lung Cell Mol Physiol.
42. Spence R, Mandagere A, Dufton C, Venitz J (2008) Pharmacokinetics and safety of ambrisentan in combination with sildenafil in healthy volunteers. J Clin Pharmacol 48: 1451–1459.
43. Wixson SK, White WJ, Hughes HC Jr, Lang CM, Marshall WK (1987) The effects of pentobarbital, fentanyl-droperidol, ketamine-xylazine and ketamine-diazepam on arterial blood pH, blood gases, mean arterial blood pressure and heart rate in adult male rats. Lab Anim Sci 37: 736–742.
44. Kuwahira I, Moue Y, Ohta Y, Mori H, Gonzalez NC (1994) Distribution of pulmonary blood flow in conscious resting rats. Respir Physiol 97: 309–321.
45. Irwin DC, Foreman B, Morris K, White M, Sullivan T, et al. (2008) Polymerized bovine hemoglobin decreases oxygen delivery during normoxia and acute hypoxia in the rat. Am J Physiol Heart Circ Physiol 295: H1090–H1099.
46. Laughlin MH, Armstrong RB (1985) Muscle blood flow during locomotory exercise. Exerc Sport Sci Rev 13: 95–136.
47. Laughlin MH, Korthuis RJ, Sexton WL, Armstrong RB (1988) Regional muscle blood flow capacity and exercise hyperemia in high-intensity trained rats. J Appl Physiol 64: 2420–2427.
48. Mortensen SP, Nyberg M, Thaning P, Saltin B, Hellsten Y (2009) Adenosine contributes to blood flow regulation in the exercising human leg by increasing prostaglandin and nitric oxide formation. Hypertension 53: 993–999.
49. Joyner MJ, Casey DP (2013) Muscle Blood Flow, Hypoxia and Hypoperfusion. J Appl Physiol (1985).
50. Casey DP, Joyner MJ (2011) Local control of skeletal muscle blood flow during exercise: influence of available oxygen. J Appl Physiol (1985) 111: 1527–1538.
51. Spilk S, Herr MD, Sinoway LI, Leuenberger UA (2013) Endothelium-derived hyperpolarizing factor contributes to hypoxia-induced skeletal muscle vasodilation in humans. Am J Physiol Heart Circ Physiol 305: H1639–1645.
52. Ainslie PN, Barach A, Murrell C, Hamlin M, Hellemans J, et al. (2007) Alterations in cerebral autoregulation and cerebral blood flow velocity during acute hypoxia: rest and exercise. Am J Physiol Heart Circ Physiol 292: H976–983.
53. Hopkins SR, Kleinsasser A, Bernard S, Loeckinger A, Falor E, et al. (2007) Hypoxia has a greater effect than exercise on the redistribution of pulmonary blood flow in swine. J Appl Physiol 103: 2112–2119.
54. Naeije R (2010) Physiological adaptation of the cardiovascular system to high altitude. Prog Cardiovasc Dis 52: 456–466.
55. Umbrello M, Dyson A, Bollen Pinto B, Fernandez BO, Simon V, et al. (2014) Short-term hypoxic vasodilation in vivo is mediated by bioactive nitric oxide metabolites, rather than free nitric oxide derived from haemoglobin-mediated nitrite reduction. J Physiol.
56. Doi Y, Kudo H, Nishino T, Yamamoto O, Nagata T, et al. (2002) Enhanced expression of endothelin-1 and endothelin-converting enzyme-1 in acute hypoxic rat aorta. Histol Histopathol 17: 97–105.
57. Goerge T, Niemeyer A, Rogge P, Ossig R, Oberleithner H, et al. (2002) Secretion pores in human endothelial cells during acute hypoxia. J Membr Biol 187: 203–211.
58. Osmond JM, Gonzalez Bosc LV, Walker BR, Kanagy NL (2014) Endothelin-1-induced Vasoconstriction does not Require Intracellular Calcium Waves in Arteries from Rats Exposed to Intermittent Hypoxia. Am J Physiol Heart Circ Physiol.
59. Hester RL, Eraslan A, Saito Y (1993) Differences in EDNO contribution to arteriolar diameters at rest and during functional dilation in striated muscle. Am J Physiol 265: H146–151.
60. Hergenroder S, Munter K, Kirchengast M (1998) Effects of endothelin and endothelin receptor antagonism in arteriolar and venolar microcirculation. Vasa 27: 216–219.
61. Mitchell D, Bihari A, Sandig M, Tyml K (2002) Endothelin-a receptor in rat skeletal muscle microvasculature. Microvasc Res 64: 179–185.
62. Hamilton NB, Attwell D, Hall CN (2010) Pericyte-mediated regulation of capillary diameter: a component of neurovascular coupling in health and disease. Front Neuroenergetics 2.
63. Ping P, Johnson PC (1992) Role of myogenic response in enhancing autoregulation of flow during sympathetic nerve stimulation. Am J Physiol 263: H1177–1184.
64. Naeije R (2011) Pro: Hypoxic pulmonary vasoconstriction is a limiting factor of exercise at high altitude. High Alt Med Biol 12: 309–312.
65. Anholm JD, Foster GP (2011) Con: Hypoxic pulmonary vasoconstriction is not a limiting factor of exercise at high altitude. High Alt Med Biol 12: 313–317.
66. Anholm JD, Foster GP (2011) Con: Rebuttal. High Alt Med Biol 12: 321.
67. Naeije R (2011) Pro: Rebuttal. High Alt Med Biol 12: 319.
68. Cunningham WL, Becker EJ, Kreuzer F (1965) Catecholamines in plasma and urine at high altitude. J Appl Physiol 20: 607–610.
69. Bartsch P, Gibbs JS (2007) Effect of altitude on the heart and the lungs. Circulation 116: 2191–2202.
70. Patel TR, McAuley MA, McCulloch J (1996) Endothelin receptor mediated constriction and dilatation in feline cerebral resistance arterioles in vivo. Eur J Pharmacol 307: 41–48.
71. Touzani O, Galbraith S, Siegl P, McCulloch J (1997) Endothelin-B receptors in cerebral resistance arterioles and their functional significance after focal cerebral ischemia in cats. J Cereb Blood Flow Metab 17: 1157–1165.
72. Fernandez N, Monge L, Garcia JL, Garcia-Villalon AL, Gomez B, et al. (1998) In vivo and in vitro action of endothelin-1 on goat cerebrovascular bed. Eur J Pharmacol 348: 199–211.
73. Querido JS, Ainslie PN, Foster GE, Henderson WR, Halliwill JR, et al. (2013) Dynamic cerebral autoregulation during and following acute hypoxia: role of carbon dioxide. J Appl Physiol (1985) 114: 1183–1190.
74. Varsos GV, Richards HK, Kasprowicz M, Reinhard M, Smielewski P, et al. (2014) Cessation of diastolic cerebral blood flow velocity: the role of critical closing pressure. Neurocrit Care 20: 40–48.
75. Kobayashi S, Endou M, Sakuraya F, Matsuda N, Zhang XH, et al. (2003) The sympathomimetic actions of l-ephedrine and d-pseudoephedrine: direct receptor activation or norepinephrine release? Anesth Analg 97: 1239–1245.
76. Zheng Z, Yan T, Chen W, Ye L, Tang L, et al. (2012) Pharmacokinetic determination of ephedrine in Herba Ephedrae and Wu Tou Tang decoctions in rats using ultra performance liquid chromatography tandem mass spectrometry. Xenobiotica 42: 775–783.
77. Bordeleau R, Bell DG, Jacobs I, Zamecnik J (1999) Caffeine, ephedrine and their combination: effects on blood pressure and heart rate. Canadian Defence and Civil Institute of Environmental Medicine. 1–14 p.

78. Luks AM, Stout K, Swenson ER (2010) Evaluating the safety of high-altitude travel in patients with adult congenital heart disease. Congenit Heart Dis 5: 220–232.
79. Levine BD, Zuckerman JH, deFilippi CR (1997) Effect of high-altitude exposure in the elderly: the Tenth Mountain Division study. Circulation 96: 1224–1232.
80. Bartsch P, Mairbaurl H, Maggiorini M, Swenson ER (2005) Physiological aspects of high-altitude pulmonary edema. J Appl Physiol 98: 1101–1110.
81. Scherrer U, Rexhaj E, Jayet PY, Allemann Y, Sartori C (2010) New insights in the pathogenesis of high-altitude pulmonary edema. Prog Cardiovasc Dis 52: 485–492.

OPEN ACCESS Freely available online

PLOS ONE

Catabolism of Exogenous Lactate Reveals It as a Legitimate Metabolic Substrate in Breast Cancer

Kelly M. Kennedy[1], Peter M. Scarbrough[3], Anthony Ribeiro[4], Rachel Richardson[2], Hong Yuan[7], Pierre Sonveaux[8], Chelsea D. Landon[1], Jen-Tsan Chi[5,6], Salvatore Pizzo[1], Thies Schroeder[2☯], Mark W. Dewhirst[1,2*☯]

1 Department of Pathology, Duke University Medical Center, Durham, North Carolina, United States of America, **2** Department of Radiation Oncology, Duke University Medical Center, Durham, North Carolina, United States of America, **3** Duke Cancer Institute, Duke University Medical Center, Durham, North Carolina, United States of America, **4** Duke University Shared Resources NMR Facility, Duke University, Durham, North Carolina, United States of America, **5** Institute of Genome Sciences and Policy, Duke University Medical Center, Durham, North Carolina, United States of America, **6** Department of Molecular Genetics and Microbiology, Duke University Medical Center, Durham, North Carolina, United States of America, **7** Department of Radiology, University of North Carolina, Chapel Hill, North Carolina, United States of America, **8** Pole of Pharmacology, Institut de Recherches Expérimentales et Cliniques (IREC), Université catholique de Louvain (UCL), Brussels, Belgium

Abstract

Lactate accumulation in tumors has been associated with metastases and poor overall survival in cancer patients. Lactate promotes angiogenesis and metastasis, providing rationale for understanding how it is processed by cells. The concentration of lactate in tumors is a balance between the amount produced, amount carried away by vasculature and if/how it is catabolized by aerobic tumor or stromal cells. We examined lactate metabolism in human normal and breast tumor cell lines and rat breast cancer: 1. at relevant concentrations, 2. under aerobic vs. hypoxic conditions, 3. under conditions of normo vs. hypoglucosis. We also compared the avidity of tumors for lactate vs. glucose and identified key lactate catabolites to reveal how breast cancer cells process it. Lactate was non-toxic at clinically relevant concentrations. It was taken up and catabolized to alanine and glutamate by all cell lines. Kinetic uptake rates of lactate *in vivo* surpassed that of glucose in R3230Ac mammary carcinomas. The uptake appeared specific to aerobic tumor regions, consistent with the proposed "metabolic symbiont" model; here lactate produced by hypoxic cells is used by aerobic cells. We investigated whether treatment with alpha-cyano-4-hydroxycinnamate (CHC), a MCT1 inhibitor, would kill cells in the presence of high lactate. Both 0.1 mM and 5 mM CHC prevented lactate uptake in R3230Ac cells at lactate concentrations at $\leq$20 mM but not at 40 mM. 0.1 mM CHC was well-tolerated by R3230Ac and MCF7 cells, but 5 mM CHC killed both cell lines $\pm$ lactate, indicating off-target effects. This study showed that breast cancer cells tolerate and use lactate at clinically relevant concentrations *in vitro* ($\pm$ glucose) and *in vivo*. We provided additional support for the metabolic symbiont model and discovered that breast cells prevailingly take up and catabolize lactate, providing rationale for future studies on manipulation of lactate catabolism pathways for therapy.

Citation: Kennedy KM, Scarbrough PM, Ribeiro A, Richardson R, Yuan H, et al. (2013) Catabolism of Exogenous Lactate Reveals It as a Legitimate Metabolic Substrate in Breast Cancer. PLoS ONE 8(9): e75154. doi:10.1371/journal.pone.0075154

Editor: Rafael Moreno-Sanchez, Instituto Nacional de Cardiologia, Mexico

Received October 12, 2012; **Accepted** August 9, 2013; **Published** September 12, 2013

Funding: The work was funded through the following grants: NIH-NCI CA40355 (covering the majority of the work, P.I. Mark Dewhirst), BCRP BC083154 (Postdoctoral grant, US Department of Defense, supporting Kelly Kennedy), ERC Starting Grant 243188 TUMETABO (Pierre Sonveaux). The funders had no role in study design, data collection and analysis, decision to publish, or preparation of the manuscript.

Competing Interests: The authors have the following interests: The 14C scintillation probe was provided to us by Robert Black PhD of Sicel Technologies Inc. This does not alter the authors' adherence to all the PLOS ONE policies on sharing data and materials, as detailed online in the guide for authors.

* E-mail: mark.dewhirst@duke.edu

☯ These authors contributed equally to this work.

Introduction

Normal physiologic range of lactate concentration in the blood is $\sim$ 0.5–2 mM [1]; in contrast, pathophysiologic lactate concentrations in tumors range from normal lactate levels to concentrations as high as 40 mM [2]. In the 1920s Otto Warburg was the first to discover that tumors accumulate excess lactate [3–5]. In the last hundred years, the importance of this metabolic switch in tumor tissue has become increasingly evident, and, recently, elevated lactate levels in tumors has been coined as a hallmark of cancer by Hanahan and Weinberg [6].

Lactate accumulation within tumor tissue is mainly due to the increased glycolytic rate of cancer cells. This increase in glycolysis is in response to a number of factors: hypoxia (Pasteur Effect), proliferative demand, increased oxidative stress and altered genetic programming [7–9]. Increases in lactic acid in tumors combined with lack of buffering capacity contribute to localized areas of low pH in tumors [7,8]. It has been observed that lactate accumulation is correlated with hypoxia in some tumor types [10] (Pasteur Effect), and, clinically, hypoxia is correlated with poor patient prognosis and survival [11,12]. However, high lactate is not a surrogate marker of hypoxia. Studies of genomic regulation by hypoxia vs. lactate vs. acidosis in cancer cells showed that lactate regulated a different set of genes than hypoxia [13]. The consequences of downstream lactate signaling in normal mammary epithelial cells exposed to high lactate showed repression of glycolytic genes. In several large breast cancer clinical series where

gene expression data were available, the "lactic acidosis" genomic signature with repressed glycolysis was associated with significantly increased patient survival rates [13]. This indicates that the response of the tumor to high lactate is important to patient outcome and that lactate utilization and catabolism by the tumor warrants investigation in order to understand how cancer cells cope with high lactate concentrations.

Monocarboxylate transporters (MCTs) facilitate movement of lactate in and out of the cell. There are 14 different subtypes, four of which are relatively well-characterized: MCT1, MCT2, MCT3 and MCT4 [14,15]. Of these, MCT1 is the most ubiquitously expressed subtype. MCT1 inhibition has been receiving attention as a potential anti-cancer treatment option [16,17]. We previously reported that lactate can serve as an energy source for aerobic cells and proposed a "metabolic symbiont" model within the tumor microenvironment. In this model, lactate produced by hypoxic cells can provide an additional substrate for aerobic cells. With the aerobic cells utilizing the lactate for energy, they will utilize less glucose, thereby allowing some glucose to reach the hypoxic cells [17]. We found that SiHa (cervical cancer) cells, which expressed higher levels of MCT1 but lower levels of MCT4, consumed significantly more lactate and less glucose than WiDr (colorectal cancer) cells. Conversely, WiDr cells, which expressed higher levels of MCT4 and lower levels of MCT1, consumed less lactate and more glucose than SiHa cells [17]. Recently, MCT subtype and LDH isoform expression has been characterized in HMEC, MCF7 and MDA-MB-231 cells [18]. HMEC display the greatest amount of MCT1 expression on the cell membrane and express both LDHA and LDHB. MCF7 cells display MCT1 expression on the cell membrane in lower levels than HMEC and express both LDHA and LDHB. MCF7 cells exhibit higher LDHB expression than MDA-MB-231 cells. MDA-MB-231 cells do not express MCT1. They express both LDHA and LDHB, with higher LDHA than MCF7 cells. This suggests that there is a connection between MCT subtype expression and a lactate-consuming ability in cancer cells. Given these differences of expression of MCT subtypes [18] and our previous findings of lactate consumption in connection with MCT subtype expression [17], we hypothesized that lactate uptake and catabolism would be different between the breast cells.

Lactate transport can be manipulated by MCT-inhibitors [17]. The small molecule MCT-inhibitor α-cyano-4-hydroxycinnamate (CHC) is >10 fold more selective for inhibition of MCT1 than for inhibition of MCT4 [19]. It was proposed that inhibition of MCT1 by CHC or knockdown of MCT1 using siRNA would prevent lactate uptake in the aerobic cells, forcing them to utilize glucose, thereby starving the more treatment-resistant hypoxic cells [17]. In cell-based assays it was shown that CHC decreases lactate-fueled respiration and ATP production in both SiHa and WiDr cells [17]. It was also shown that treatment with CHC significantly decreased tumor growth similar to siMCT1 in xenograft models [17]. These results warrant further investigation of MCT1 inhibition as an anti-tumor treatment option. It has already been reported that MCT1 inhibition can lead to cancer cell death via a lethal decline in pH_i with blockade of endogenous lactic acid exportation [20]. We hypothesized that pharmacological inhibition of exogenous lactate metabolism with CHC could elicit cell death by preventing exogenous lactate entry and utilization in glucose-deprived conditions.

Our cell-based studies focused on four cell lines: Human mammary epithelial cells (HMEC), MCF7 (human mammary adenocarcinoma), MDA-MB-231 (human mammary adenocarcinoma), and R3230Ac (rat mammary carcinoma) cells. HMEC cells were included to compare a normal cell response to exogenous lactate with cancer cell responses to lactate. Catabolism studies were also conducted on HUVEC cells as a second normal tissue line. The R3230Ac rat mammary carcinoma was used as our *in vivo* model, because we have studied glucose uptake and its conversion to lactate previously in this model previously [21,22]. Both MCF7 and MDA-MB-231 cells were included as breast cancer models for two primary reasons. First, we wanted to represent a luminal (MCF7) and a basal-like (MDA-MB-231) breast cancer subtype [23], as these subtypes are known to be considerably different clinically and pathologically [23-25]. Second, it has previously been reported that MCT1 is silenced in MDA-MB-231 cells [18,26]. By including both MDA-MB-231 and MCF7 cells in our experiments, we could compare lactate uptake and metabolism in breast cancer cells lacking and expressing MCT1. Though our studies did not focus on p53 signaling and lactate metabolism, it is important to mention that the p53 status in each of these cell lines differ considerably: R3230Ac and MCF7 cells are p53 WT [27–29] while MDA-MB-231 cells are p53 null [30,31]. This may be an important avenue for future investigation because p53 influences many metabolic pathways including glycolysis, oxidative phosphorylation and mTOR signaling [32,33].

In this study, we expanded on our prior work on lactate metabolism, focusing on breast cancer. The main goals were: 1) to establish the tolerance of breast cancer cells to a range of lactate concentrations typical of that seen in human breast cancer, 2) to investigate lactate catabolism *in vitro* and *in vivo* and 3) to examine whether treatment with CHC elicits cell death in a lactate-dependent manner. We used two doses of CHC sufficient to inhibit MCT1; one concentration chosen (5 mM) was based on previous studies, and the other concentration chosen was based on reported K_i values for the compound [14,17]. To investigate lactate metabolism *in vivo*, we employed the R3230Ac tumor model, which has been shown to exhibit regions of high lactate in the absence of measureable glucose [10].

Results

Lactate accumulation occurs in locally advanced breast cancer (LABC) with a median concentration range of 0.6 – 8.0 μmol/g, and lactate accumulation shows high intra-tumoral variation

Lactate concentrations have been measured in human head and neck [34], cervical [2] and colorectal [35] cancers by bioluminescent technology. Lactate levels in breast cancer have not previously been measured. We sought to define the range of lactate concentrations found in LABC, to guide our cell-based assays. Twenty-three frozen breast-core biopsies from 21 patients with locally advanced breast cancer (LABC) (two biopsies were from the same patient, different sites of the tumor) were made available to us from an Institutional Review Board (IRB)-approved phase I/II clinical trial conducted at Duke University (Table 1).

Lactate concentrations were measured with bioluminescence imaging [10,36,37] (Fig 1A). The median lactate concentration for the entire sample set was 4.4 μmol/g. Samples could be divided into low v. high lactate groups based on this median (Table 1). The range of median lactate values for LABC biopsies was 0.6 to 8.0 μmol/g, and the median range for benign breast tissue ("bb") was 0.8 – 1.9 μmol/g (Fig 1B). The quartile range and 95% confidence intervals demonstrated a wide range of lactate values; the 95th percentile showed lactate levels greater than12 μmol/g (Fig 1B). These results illustrate the heterogeneity in lactate accumulation within individual tumors and between tumors. However, these concentrations were considerably lower than seen in other tumor types. For example, in head and neck cancer,

Table 1. Patient clinical parameters and lactate levels in LABC biopsies.

Group	Sample #	% Invasive cancer	Outcome	TMN	Distant Mets.	Relapse	Age	[La] 5PMin	[La] 25P	[La] 50PMed.	[La] 75P	[La] 95PMax
Lo [L]	bb1	0	alive	2	n	n	39	0.0	0.0	0.8	1.5	2.6
	LABC1	70	alive	2	n	n	62	0.0	0.0	0.6	1.3	2.5
	bb3	0	alive	3	n	n	54	0.6	1.7	2.5	3.9	4.8
	LABC2	30	alive	3	n	n	62	0.3	1.5	2.6	3.5	5.2
	LABC3	70	alive	3	n	n	55	0.6	1.8	2.9	3.8	5.4
	LABC4	95	alive	**4**	**y**	n	32	0.4	1.8	3.3	3.7	5.4
	LABC6	80	**dead**	**4**	**y**	n	63	1.1	2.5	3.8	4.9	7.0
	LABC7	75	**dead**	**4**	**y**	**y**	58	1.2	2.7	4.0	5.2	7.2
	LABC8	75	alive	3	n	n	55	1.4	2.9	4.2	5.3	7.5
	LABC9	70	alive	3	n	n	43	1.4	3.0	4.2	5.5	7.7
	LABC710(d)	65	alive (d)	2 (d)	n (d)	n (d)	62 (d)	1.7	3.1	4.3	5.3	7.1
	bb4	0	alive	2	n	n	35	0.7	2.5	4.4	5.5	7.8
Hi [L]	LABC11	70	**dead**	**4**	**y**	**y**	75	1.6	3.1	4.5	5.7	7.8
	LABC12	75	**dead**	**4**	**y**	?	66	0.9	2.6	4.5	5.1	7.2
	LABC13	80	alive	2	n	n	44	1.5	3.2	4.6	5.7	7.8
	LABC14	60	alive	?	?	?	?	1.5	3.3	5.0	6.3	8.9
	LABC15	95	alive	3	n	n	35	1.0	2.9	5.1	5.7	8.6
	LABC16	80	**dead**	3	n	y	32	1.6	3.1	5.2	6.0	8.2
	LABC17	80	alive	3	n	y	49	2.0	3.7	5.2	6.6	8.9
	LABC18	80	**dead**	2	n	n	27	1.8	3.8	5.6	7.0	9.4
	LABC19	75	alive	**4**	**y**	n	52	2.9	4.9	6.6	8.1	10.9
	LABC20	80	alive	3	n	n	43	3.3	5.3	7.2	8.8	12.3
	LABC21(d)	90	alive (d)	3 (d)	n (d)	n (d)	35 (d)	4.0	6.0	8.0	9.4	12.2

Specimens are named based on presence of benign breast tissue (bb) or presence of invasive cancer (LABC). Duplicate specimens are indicated (d). Measured lactate concentrations (μmol/g of tissue) are displayed in the last five columns. These values correspond to the lactate concentration range ([L]) seen in microregions in each specimen: fifth percentile/minimum (5P), twenty-fifth percentile (25P), fiftieth percentile/median (50P), seventy-fifth percentile (75P) and ninety-fifth percentile/maximum (95P). Samples are arranged in ascending order of median lactate concentrations. High and low lactate groups were determined based on median lactate concentrations >4.4 μmol/g. LABC5 and bb2 specimens are missing due to unavailable clinical information on these patients.

doi:10.1371/journal.pone.0075154.t001

median values were in the range of 7 μmol/g with microregional variation extending as high as 40 μmol/g [2,34]. Two of three biopsies that did not have any invasive cancer (''bb'') showed lower lactate accumulation than the majority of biopsies with invasive cancer (Fig 1B).

The two specimens that represented second biopsy site from the same patient (stars, Fig 1B) fell into the same high or low lactate group as the first biopsy site (Table 1). Specimens LABC1 and LABC10 are biopsies from the same patient and are in the low lactate group, while specimens LABC15 and LABC21 (Fig 1B) are from another patient and are in the high lactate group (second site indicated by ''d'' in Table 1). The median lactate concentrations measured in LABC1 and LABC10 (0.6 and 4.3 μmol/g) were significantly different (Student's T-test, $p < 0.05$), while the median lactate concentrations measured in LABC15 and LABC21 (5.1 and 8.0 μmol/g, respectively) were not (Fig 1B, Table 1). From these dual biopsy sites from one tumor, the intra-tumor metabolic heterogeneity is illustrated, indicating that lactate levels can vary significantly among different areas of the same tumor.

Lactate uptake and metabolism occurs *in vitro* in R3230Ac cells

Before studying lactate metabolism in cells it was important to assess cell viability after lactate treatment to ensure that the metabolic results would not be skewed by dying cells. The range of lactate concentrations tested *in vitro* was defined by our experimental findings in LABC (Fig 1) and the literature on lactate accumulation in tumors [2,22,34,35,38–40]. Concentrations of 5 and 10 mM lactate reflect the concentrations found in the LABC biopsies and the median lactate concentration found in other solid tumors, such as head and neck and cervical cancer [2,34,38]. It was previously published that microregions of some tumors can reach up to 40 mM lactate [2], which we defined as our upper limit. 20 mM lactate was included in some experiments as an intermediary concentration between the low and high limits; however, this concentration was still higher than what was found in the clinical LABC specimens. The acute effects of lactate toxicity were examined using Annexin V and 7-aminoactinomycin D (7-AAD) to assess apoptosis and membrane integrity, respectively, in cells exposed to lactate (0, 10, 20 and 40 mM) for 24 h (Fig S1 and S2). These studies were conducted in the presence (Fig S1) and absence of glucose (Fig S2) because it has been reported that lactate accumulation can occur in the presence or absence of glucose *in vivo* [10]. Additionally, we chose to use glucose-free media for a majority of our NMR studies in order to acquire higher signals for lactate and lactate-generated metabolites. When exogenous sodium lactate was supplemented in cell culture media containing glucose, none of the cells showed any decrease in cell

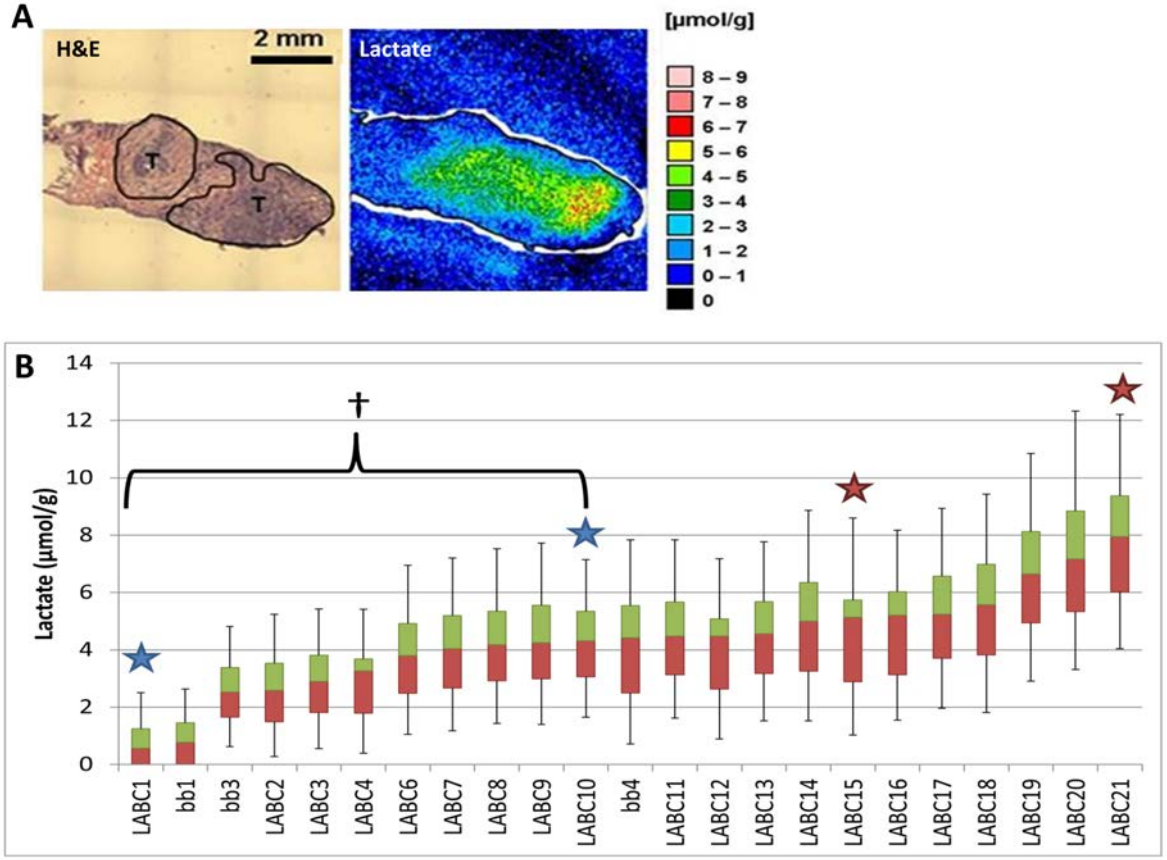

Figure 1. Human tumor samples measured for lactate with bioluminescence *ex vivo* show lactate concentrations vary considerably between samples. Bioluminescence color map for lactate concentrations measured in a LABC patient biopsy (A). Tumor regions are outlined and marked (T). Waterfall Box & Whisker plot for lactate concentrations (μmol/g) measured in benign breast tissue (bb) and LABC patient biopsies (B). Stars indicate separate biopsies from the same patient. LABC1 and LABC10 samples show a significant difference in lactate concentrations (†$p<0.05$, Student's T-test). First quartile values represented in red; third quartile values are represented in green. Median values represented at the interface of red and green boxes. Error bars represent the 5th and 95th percentile lactate concentrations. All biopsies n = 3–4.
doi:10.1371/journal.pone.0075154.g001

viability or increase in cell death responses (Fig S1). Likewise, all cell lines treated with 0 –20 mM in glucose-deprived conditions survived (Fig S2). Only at 40 mM lactate (- glucose) did MCF7 and MDA-MB-231 cells show significant cell death responses (FigS2F&G). Glucose deprivation usually elicits cell stress responses, such as activation of JNK1 and increased oxidative stress [41–45]. This may suggest that very high lactate concentrations can augment the cellular stress elicited by glucose deprivation, but 40 mM lactate has been reported very infrequently in solid tumors and concentrations this high were not found in any of the breast tumor biopsies evaluated in this study [2,10,34,38,39,46,47]. Thus, we conclude that cell viability is not appreciably affected over the range of physiologically relevant lactate concentrations observed in breast cancer (Fig 1) with or without glucose.

We hypothesized that normal breast cells and breast cancer cells could utilize exogenous lactate for metabolic purposes. We used NMR with ^{13}C-labeled lactate to track uptake; we first focused on the lactate metabolism in R3230Ac cells. *In vitro*, R3230Ac cells took up lactate in a concentration-dependent manner after 4 h of treatment (Fig 2A; lactate peaks indicated by arrows). In glucose-deprived conditions, R3230Ac cells were treated with 5 mM 3-^{13}C-lactate for 12 h. The ^{13}C spectra of the cell lysate show peaks corresponding to ^{13}C-lactate, ^{13}C-alanine and ^{13}C-glutamate (Fig 2B). When these metabolites were normalized to protein levels, glutamate was the most abundant (Figure 2C). To determine if lactate would be metabolized in the presence of glucose, 5 mM concentrations of U-^{13}C-lactate and 1-^{13}C-glucuose were infused in tumor-bearing rats. The utilization of universally labeled lactate allows one to distinguish the uptake and metabolism of lactate from the blood as opposed to lactate and other metabolites produced from glucose. In Figure 2D, the first three peaks are for lactate, and the next three peaks are for alanine. Due to the different position of ^{13}C, the lactate metabolized from 1-^{13}C-glucose is separated from universally labeled lactate; a similar pattern emerges with alanine metabolized from lactate or glucose. The ratio of universally labeled lactate taken up by the tumor versus lactate produced from glucose was 0.36. Additionally, alanine is produced from both glucose and lactate. The results indicate that the tumor takes up lactate even in the presence of glucose. This is the first time a breast tumor has been shown to simultaneously take up lactate and glucose and metabolize both substrates *in vivo*.

Lactate transport is dependent upon expression of proton-coupled, lactate-specific transporters of the monocarboxylate transporter (MCT) family. MCTs are passive, bidirectional transporters with different K_m constants for lactate(MCT1 = ~3–5 mM, MCT2 = ~0.7 mM and MCT4 = ~28 mM) [14]. MCT1 has ubiquitous tissue distribution but is found to be upregulated in cancer [48–51]. MCT4 has a more specific tissue distribution; it is associated primarily with glycolytic cells/tissues

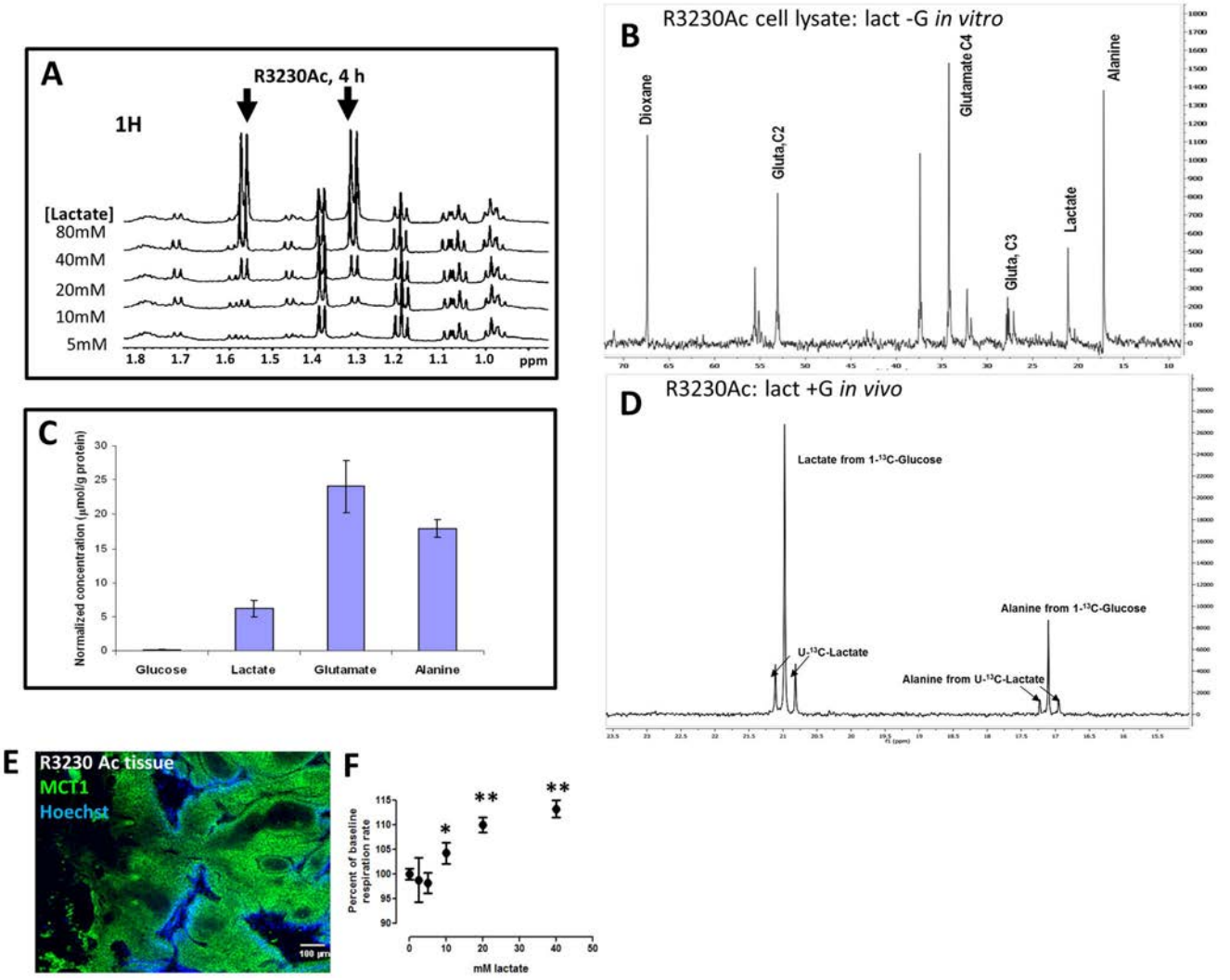

Figure 2. R3230Ac cells take up and metabolize lactate to alanine and glutamate *in vitro* and *in vivo*. ^{1}H NMR of R3230Ac cell lysates exposed to various concentrations of lactate for 4 h (glucose absent) showed a concentration-dependent lactate uptake (arrows, ~1.3 and ~1.6 ppm, **A**). ^{13}C NMR plot for R3230Ac cell lysate after 12 h treatment with 5 mM 3-^{13}C-lactate (no glucose) showing generation of ^{13}C-labeled glutamate and alanine species (**B**). Dioxane was included as an internal standard which allowed quantification of labeled metabolites (**C**). ^{13}C NMR plot from R3230Ac tumor after infusion with equimolar concentrations of universally labeled U-^{13}C-lactate and 1-^{13}C-glucose showing uptake of U-^{13}C-lactate (~20.75 and ~21.25 ppm) and generation of U-^{13}C-alanine species (~16.9 and 17.2 ppm) in the presence of labeled glucose and during production of glycolytically-derived lactate (~21 ppm) and alanine (~17.1 ppm) (**D**). Tissue staining of R3230Ac tumor shows positive expression of MCT1 (green); areas of perfusion are indicated by Hoechst 33342 (blue) (**E**). Glucose-deprived R3230Ac cells show significantly increased oxygen consumption (n = 3, Student's T-test, $p < 0.05$) with increasing concentrations of exogenous lactate compared to the untreated control (**F**).
doi:10.1371/journal.pone.0075154.g002

and is regulated by the hypoxia inducible transcription factor, HIF-1 [52–54]. Previously, we have shown that cancer cell lines with high MCT1/low MCT4 expression consume more lactate than cancer cell lines with low MCT1/high MCT4 expression [17].

Although it is well-documented that most normal cells and cancer cells typically express MCT1 [14,48–51], MCT1 expression in R3230Ac cells has not been tested previously. R3230Ac tumor shows abundant membrane expression of MCT1 (Fig 2E), while MCT4 was undetectable (Fig S3B), consistent with a lactate-consuming phenotype. It has previously been reported that R3230Ac cells utilize oxidative phosphorylation as well as glycolysis [55]. Glutamate was found to be the predominant lactate-derived metabolite produced in R3230Ac cells *in vitro* (Fig 2B). Glutamate is a TCA cycle by-product, formed from α-ketoglutarate. This indicates that one pathway of lactate metabolism is respiration. In addition to glutamate formation indicating cellular respiration of lactate, R3230Ac cells were treated with increasing concentrations of lactate (-glucose) *in vitro*, and oxygen consumption rate was measured. All concentrations of lactate ≥ 10 mM tested showed a significant increase in oxygen consumption rate in the cells (Fig 2F), providing further evidence that lactate is consumed via respiration.

Kinetic uptake of glucose and lactate *in vivo* show lactate uptake in R3230Ac tumors occurs more rapidly than glucose uptake

Kinetics of glucose and lactate uptake, retention, and clearance were measured using a novel scintillation probe following i.v. administration of either ^{14}C-glucose (n = 9) or ^{14}C-lactate (n = 3).

A three-compartment pharmacokinetic model was formed from the data to determine rate constants for glucose and lactate uptake by the tumor and subcutaneous (SQ) tissue (Fig S4). Rate constants for ^{14}C-glucose and ^{14}C-lactate are summarized in Table 2, and the time activity curves were shown in Figure 3A and 3B. Lactate was cleared much faster from plasma than glucose. Furthermore, the rate constant for the transfer of lactate from blood compartment into the tumor was higher than that of glucose (0.238 vs. 0.038), indicating much faster uptake of lactate than glucose. The back flux rate (from tissue back to blood) was higher in lactate compared to that of glucose (0.062 vs. 0.049). As the scintillation probe only detects ^{14}C signal, it was not possible to determine if the back flux signal came from free glucose/lactate or their metabolites. The uptake of both glucose and lactate was higher in tumor compared to subcutaneous compartment indicating higher tumor metabolism. The PK analysis shows that R3230Ac tumor tissue takes up lactate faster than glucose.

^{14}C-lactate autoradiography was compared in hypoxic (indicated by pimonidazole staining) v. perfused (indicated by Hoechst staining) regions of R3230Ac tumor. We found that the labeled lactate was taken up primarily in well-perfused tumor regions where hypoxia was absent (Fig 3C&D). In one small tumor that did not exhibit appreciable hypoxia, ^{14}C-lactate was evenly distributed throughout the whole section (Fig 3E&F). This data is consistent with the proposed metabolic symbiont model [17], in which lactate is preferentially taken-up by better oxygenated tumor regions.

To test if the same metabolites would be generated *in vivo* as *in vitro*, ^{13}C-lactate was infused into R3230Ac tumor-bearing rats. Tumor, liver, brain and other organs were collected and snap-frozen at time of sacrifice (15, 30, or 60 min). After 15 minutes, labeled lactate was present in the tumor at 0.5 mM/g of tissue (Fig 3G). Glucose was not significantly produced from lactate. This concentration was lower after 30 and 60 min, indicating metabolism or clearance from the tumor tissue. Both glutamate and alanine concentrations were increased in tumor after lactate infusion, with alanine reaching the highest concentration at 30 minutes (Fig 3G). This shows that the R3230Ac tumor utilizes lactate for metabolite generation. Brain and liver tissue also showed an increase in lactate uptake compared to baseline (Fig 3H&I), but the concentrations seen were not as high as lactate uptake in the tumor. As expected, liver produced glucose from the infused lactate (Cori Cycle).

Taken together, the kinetic results clearly showed: 1. lactate uptake occurs in a rat mammary carcinoma model *in vivo*, 2. Tumor tissue has a higher uptake of lactate than SQ tissue, 3. R3230Ac tumors take up lactate more rapidly than glucose, 4. Lactate uptake occurs in aerobic regions of the tumor, and 5. Glutamate and alanine are generated from lactate *in vivo*. Previous studies have shown that lactate uptake occurs in hepatoma [56], sarcoma [57], and pancreatic cancer [58], and that lactate acts as preferred substrate compared to glucose in gliomas [59,60]. Here, we have shown for the first time that lactate is also preferentially taken up in a breast cancer model with higher transfer rates than glucose. Further studies with other tumor models would be required to verify whether the preferential uptake of lactate is a class effect in breast cancer. But at the very least, we show that lactate can be taken up and metabolized in vivo, in the presence of glucose.

Table 2. Kinetic Transfer Rates for ^{14}C-glucose and ^{14}C-lactatein R3230Ac Tumors.

K_{trans}	Description	*^{14}C-glucose*	*^{14}C-lactate*	*p*
k_1	Blood to tumor transfer rate	0.038±0.008	0.238±0.055	<0.001
k_2	Tumor to blood transfer rate	0.049±0.006	0.062±0.001	0.006
k_3	Blood to SQ transfer rate	0.0016±0.0001	0.0014±0.0002	0.077
K_4	SQ to blood transfer rate	0.066±0.008	0.0744±0.009	0.166

Transfer rate constants were calculated from ^{14}C-glucose (n = 9) and ^{14}C-lactate (n = 3) kinetic data using the compartmental model explained in the Methods and Fig S3. Kinetic transfer rates of ^{14}C-glucose were evaluated against the transfer rates of ^{14}C-lactate with a two-tailed Student's T-test.

doi:10.1371/journal.pone.0075154.t002

Human breast cells metabolize lactate to alanine and glutamate

We questioned if human breast cells could also take up and metabolize lactate. First, we screened the human breast lines (HMEC, MCF7 and MDA-MB-231) for MCT1 and MCT4 expression (Fig S3). MCT1 was expressed in MCF7 and HMEC cells but not MDA-MB-231 cells (Fig S3A), consistent with the literature [18,26]. MDA-MB-231 was the only cell line that expressed abundant MCT4 (Fig S3B). HMEC showed very little MCT4 expression in the whole cell lysate, and MCT4 was undetectable for MCF7 cells (Fig S3B). Hussien and Brooks provide a more complete characterization of MCT subtype expression in these same cell lines, as they investigated mitochondrial and membrane expression in addition to using whole cell lysates.[18]. Briefly, their studies found MCT1 expression on the plasma membrane of MCF7 and HMEC cells but not MDA-MB-231 cells. MCT4 and MCT2 were found to be expressed in all three cell lines, localizing to the plasma and mitochondrial membranes [18]. Given these differences in MCT subtype expression in cell lines, we hypothesized that lactate metabolism among the breast lines would be different. Specifically, we expected relatively little lactate uptake and metabolism in MDA-MB-231 cells due to their lack of MCT1 expression.

Both malignant and nonmalignant human breast cell lines showed evidence of intracellular ^{13}C-lactate after 24 h treatment (Fig 4A, arrows). This indicates that: 1. lactate uptake occurs in both normal and cancer cells (Fig 4A). 2. lactate uptake is not MCT1-dependent in MDA-MB-231 cells. MDA-MB-231 cells have been documented to express MCT2 [18], which has a higher affinity for lactate than MCT1 [14]. We then sought to compare the rates of lactate uptake between human breast cancer cell lines. We determined lactate concentrations in glucose-free cell media from MCF7 or MDA-MB-231 cells incubated with supplemented lactate (20 mM) over 5 days. The media was not replenished over this time period. Because the lactate used was unlabeled, glucose-free media was chosen so glycolytically-derived lactate would not interfere with the measurement of lactate consumption. Figure 3B illustrates the mean lactate concentration measurements for each time point. Over 5 days, the decline in mean lactate concentrations in the cell media was significantly greater for MCF7 cells (18.3 mM drop) than for MDA-MB-231 cells (5.5 mM drop, $p < 0.0001$, Fig 4B). When the individual time point measurements of lactate concentration was applied to a linear regression analysis, the rate coefficients of lactate consumption were significantly different between MCF7 (4.01) and MDA-MB-231 (0.71) cells ($p < 0.0001$). Cell counts at the beginning and end of lactate treatment are displayed in Figure 4C; the increase in cell numbers was not significantly different for MCF7 and MDA-MB-231 cells. However, when cells were plated at equal densities and allowed to grow in high-glucose complete media or treated with 20 mM lactate (no glucose) for 5 days, MCF7 cell numbers showed no difference between treatments. Conversely MDA-MB-231 cells showed a significant increase in cell numbers when cultured in the glucose-containing lactate-supplemented media (Fig S5). These results show that MCF7 cells utilize lactate more effectively than

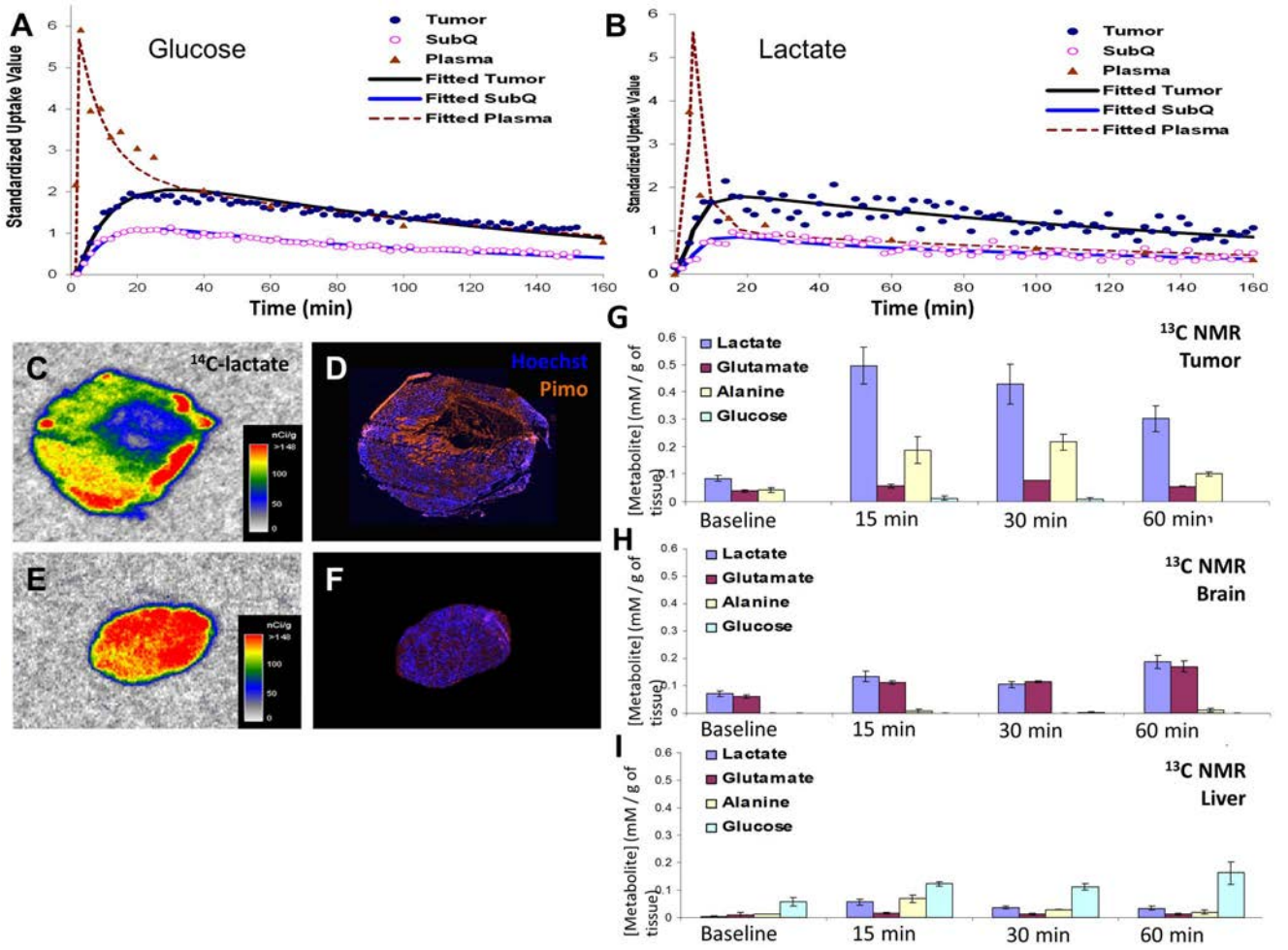

Figure 3. Kinetic analyses of metabolites with radioactive probes show fast plasma clearance of lactate and lactate uptake in perfused regions of R3230Ac tumors. Plots of individual metabolite and fitted pharmacokinetic standard uptake values (SUV) of ^{14}C-labeled glucose (100 μCi, A) and lactate (50 μCi, B) infused at a rate of 0.1 mL/min data for plasma, subcutaneous tissue (SQ) and R3230Ac tumor tissue over 160 minutes. R3230Ac tumors, grown in the flanks of Fischer 344 rats, show clearance of ^{14}C labeled glucose (n = 6) from plasma from 6 SUV to 2 SUV over 40 mins and maximum uptake of ^{14}C labeled glucose in the tumor after 16 mins (A). ^{14}C labeled lactate (n = 3) was cleared from the plasma (from 6 SUV to 2 SUV) in 14 mins and showed maximum uptake in the tumor after 14 mins (B). SUV = standard uptake rates. Autoradiography images (D-F) of ^{14}C-lactate uptake in R3230 Ac tumors show high lactate uptake (C&E) in well-perfused areas, as indicated by positive Hoechst 33342 staining (blue, D&F), compared to hypoxic tumor regions, as indicated by positive pimonidazole staining (orange, D&F). R3230Ac tumors (G) show presence of ^{13}C-lactate, ^{13}C-alanine and ^{13}C-glutamate at 15, 30 and 60 minutes after ^{13}C-lactate infusion. All ^{13}C metabolites are increased compared to baseline levels (prior to infusion). ^{13}C-lactate uptake and ^{13}C-metabolite generation in brain (H) and liver (I) after ^{13}C-lactate infusion show a slight increase in metabolites compared to baseline but do not reach concentrations found in R3230Ac tumors.
doi:10.1371/journal.pone.0075154.g003

MDA-MB-231 cells and have less of a dependence on glucose for cell growth than MDA-MB-231 cells. These results reinforce the findings in our previous study [17] that cell lines with high MCT1/low MCT4 consume more lactate than cell lines expressing high MCT4/low MCT1.

HMQC plots generated from human breast cell lysates showed evidence of ^{13}C-labeled alanine, glutamate and pyruvate in human normal breast cell lysates (Fig 4D) and human breast cancer cell lysates (Fig 4E&F) after 24 h incubation with 10 mM 3-^{13}C-lactate, indicating that lactate can be catabolized in these cell lines and that the metabolites generated are the same as those seen in R3203 Ac cells. Taken together, these data show that MCF7 and MDA-MB-231 cells consume lactate at significantly different rates but produce similar catabolites. Our original hypothesis that normal breast and breast cancer cells would metabolize lactate differently was incorrect, as HMEC cells showed the same metabolites generated from exogenous lactate as breast cancer cell lines; however, the relative rates of lactate utilization and catabolism for each cell line are different.

Lactate-derived metabolites are exported from cells

Since lactate was not toxic to cells in the physiologically relevant range, we hypothesized that lactate-generated metabolites could be released from cells after 24 h as a means to reduce levels within the cells. Media and cell lysates from each breast cancer cell line were collected after 24 h treatment with 5 mM ^{13}C-lactate (-glucose). Each of the cell lines showed ^{13}C-labeled alanine and glutamate in the media (Fig 4G). R3230Ac cells showed very little lactate, alanine and glutamate in cell lysates after 24 h, indicating that lactate metabolism is more rapid in these cells compared to MCF7 or MDA-MB-231 cells, which both retained some ^{13}C-lactate in the lysate(Fig 4G). Additionally, there is evidence of a greater amount of glutamate (peaks "1" and "2") in both the

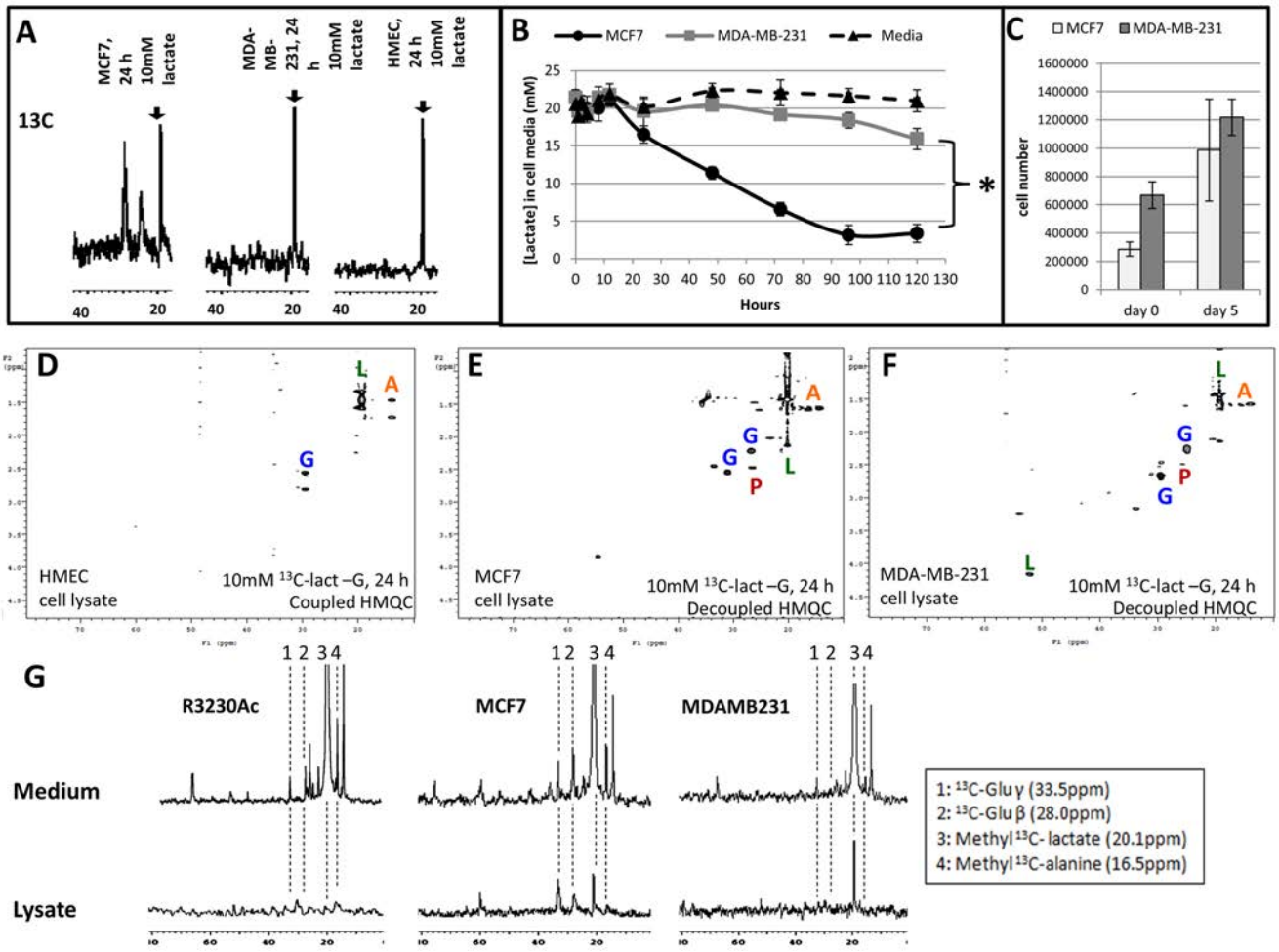

Figure 4. Lactate uptake and metabolism in human breast cells and metabolite excretion. ^{13}C NMR spectra of human breast lines indicated evidence of ^{13}C-lactate (arrow, 19 ppm) uptake after 24 h exposure to 10 mM ^{13}C-3-lactate (**A**). Lactate measurements of cell media after 5 day incubation with 20 mM unlabeled sodium lactate in glucose-free media showed a significant difference in lactate consumption between MCF7 and MDA-MB-231 cells (mean overall decrease in lactate concentrations were 0.4 mM for the no-cell media control plate, 5.5 mM for MDA-MB-231 media and 18.3 mM for MCF7 media, n = 5, *$p < 0.001$ compared to MDA-MB-231 and media control, Student's T-test, **B**). The increase in cell number of MCF7 and MDA-MB-231 cells at the beginning (day 0) and end (day 5) of lactate treatment show no significant difference (**C**). Heteronuclear multiple quantum coherence (HMQC) NMR plots of cell lysates treated for 24 h (n = 2) with 10 mM 3-^{13}C-lactate (no glucose) showed ^{13}C-lactate (dark green "**L**") uptake and ^{13}C-glutamate (blue "**G**"), ^{13}C-alanine (orange "**A**"), and ^{13}C-pyruvate (red "**P**") generation in HMEC (**D**), MCF7 (**E**), and MDA-MB-231 cells (**F**). ^{13}C NMR spectra of R3230Ac, MCF7 and MDA-MB-231 cell lysates (bottom) and media (top) show evidence of ^{13}C-metabolites in the media of each cell line and in the lysate of MCF7 and MDA-MB-231 cells after 24 h incubation with 40 mM lactate (**G**). Numeric labels: 1 = ^{13}C-Glu γ, 2 = ^{13}C-Glu β, 3 = methyl ^{13}C- lactate, 4 = methyl ^{13}C-Ala
doi:10.1371/journal.pone.0075154.g004

R3230Ac and MCF7 cells compared to MDA-MB-231 cells (Fig 4G). Although lack of MCT1 expression in MDA-MB-231 cells did not prevent lactate uptake, the lactate catabolism of these cells was considerably less efficient than the R3230Ac or MCF7 cells. Studies in normal cell lines (HMEC and HUVEC) also showed lactate uptake and metabolite release into the media after treatment with 10 mM lactate for 4.5 h (HMEC, Fig S6A&B) or 5 mM lactate for 24 h (HUVEC, Fig S6C). These results show that excretion of lactate catabolites appears to be a universal trait, shared between normal and tumor cells.

CHC prevents lactate uptake at lactate concentrations ≤20 mM; CHC prevents lactate catabolism at lactate concentrations of 40 mM

Alpha-cyano-4-hydroxycinnamate (CHC) is a small molecule inhibitor of MCTs, with a ten-fold selectivity for MCT1 compared to MCT4 [61]. Previously, we have shown that 5 mM CHC will inhibit lactate uptake, decrease cellular ATP in SiHa and WiDr cells and decrease tumorigenicity [17]; however, this study was not conducted with breast cancer cell lines, and 5 mM CHC is a rather high concentration [62]. It has been reported that concentrations of CHC between 50-500 μM will inhibit MCT1, and that the mitochondrial pyruvate carrier (MPC) is inhibited with concentrations ≤ 5 μM [14,63]. To span the range of pharmacologically effective doses, we tested the effects of 5 and 0.1 mM CHC on cell viability and lactate metabolism. The concentration of 5 mM CHC was included based on previous studies [17,64]. The lower concentration (0.1 mM) was chosen based on previous commentary [62] and evidence that 5 mM CHC may elicit nonspecific cell death responses [65].

Using ^{13}C-lactate (-glucose), we investigated the ability of 5 mM CHC to prevent lactate uptake with low (5 mM) and high

(40 mM) lactate concentrations (Fig 5A-C). Cell lysates from R3230Ac cells show metabolism of 5 mM ^{13}C-lactate to alanine and glutamate after 4 h in the absence of CHC (Fig 5A, top). When 5 mM CHC was added to the cell media with 5 mM ^{13}C-lactate (-glucose), the cell lysate did not show evidence of ^{13}C-lactate after 4 h (Fig 5A, bottom). When R3230Ac cells were exposed to 40 mM ^{13}C-lactate and 5 mM CHC for 4 h, cell lysates showed a large ^{13}C-lactate peak in the ^{13}C spectrum (Fig 5B, top), and ^{13}C-lactate was still present after 24 h (Fig 5B, bottom). From previous observations, it is anticipated that all lactate metabolites should be exported at this time point (Fig 4G). The fact that a rather large ^{13}C-lactate peak was still detected after 24 h indicates that treatment with 5 mM CHC may be more effective at preventing lactate exportation than inhibiting uptake when extracellular lactate concentrations were high. Because CHC is a competitive inhibitor of MCT1, it is possible that lactate enters the cell when extracellular concentrations are high due to lactate outcompeting CHC. It should be noted that no ^{13}C-metabolites were present in the R3230Ac cell media treated with 40 mM ^{13}C-lactate + 5 mM CHC, indicating that 5 mM CHC prevented lactate catabolism even though it was taken up. Furthermore, with addition of 5 mM CHC, there were less ^{13}C-labeled metabolites present in the media of R3230Ac cells treated with 5 mM ^{13}C-lactate for 4 h, as expected with inhibition of lactate uptake at this lactate concentration (Fig 5C).

We next investigated the effects of low (0.1 mM) v. high (5 mM) CHC concentrations on lactate metabolism at a mid-range concentration (20 mM). The ^{13}C spectrum of the media only (blank) did not show evidence of large metabolite peaks, indicating that background noise was low (Fig S7A). Previously, we have shown that this concentration of ^{13}C-lactate will be taken up by R3230Ac cells (Fig 2B). In the ^{1}H and ^{13}C spectra of R3230Ac cells treated with low (Fig S7B&D) or high (Fig S7C&E) CHC in the absence of ^{13}C-lactate, no ^{13}C-lactate peaks were evident. Panels D-G in Figure 9 show ^{1}H spectra for R3230Ac cells after 4 h (Fig 5D&E) or 24 h (Fig 5F&G) exposure to 20 mM ^{13}C-lactate (-glucose) plus either 0.1 mM CHC (Fig 5D&F) or 5 mM CHC (Fig 5E&G). No ^{13}C-lactate was evident in the ^{1}H spectra of R3230Ac cell lysates after 4 h or 24 h incubation with 20 mM ^{13}C-lactate with low or high CHC (Fig 5D-G). Additionally, there was no evidence of ^{13}C-metabolites in any of the cell lysates (Fig 5D-G). We could not acquire ^{13}C spectra on these samples due to the low signal. Endogenous lactate ("L_{en}") was present in all cell lysates (Fig 5D-G). Glucose was not included in the media; therefore, glucose could not be the source of the endogenous lactate. Formation of endogenous lactate was derived from some other metabolite present, most likely glutamine or glycogen, as there have been reports of tumor cells with high glycogen content [66-70]. The presence of the endogenous lactate peak was evident after both 4 h and 24 h incubation, indicating that both low and high CHC partially inhibited endogenous lactate excretion (Fig 5D-G). Endogenous alanine ("A_{en}"), which was formed from the endogenous lactate, was present in cell lysates after 24 h regardless of the presence of high or low CHC (Fig 5F&G).

In addition to R3230Ac cell lysates, we collected cell media from these experiments (Fig 5H-K). In each of the ^{13}C spectra, an abundance of ^{13}C-lactate was seen in the cell media, indicating that both high and low CHC concentrations effectively inhibited a majority of ^{13}C-lactate uptake. Peak heights are very similar regardless of incubation time or CHC concentration; 0.1 mM CHC was as effective as 5 mM CHC for inhibiting lactate uptake. There was evidence of ^{13}C-glutamate generation (verified by HMQC, data not shown) and exportation into the media for each sample (Fig 5H-K). In the ^{1}H spectra of R3230Ac cell lysates, a large ^{13}C-glutamate peak was not apparent after 4 h or 24 h; however, there was evidence of a peak ~2.23 ppm, which corresponds to ^{13}C-glutamate (Fig 5D-G). This indicates that the small amount ^{13}C-lactate that was taken up in the presence of CHC was converted to ^{13}C-glutamate before the 4 h time point. This would suggest that pyruvate movement into mitochondria by the MPC was not completely inhibited by 5 mM CHC. The cell lysate samples do not have resolution comparable to the ^{13}C spectra, which is why the ^{13}C-glutamate peak is evident in the ^{13}C spectra of the media but not as apparent in the ^{1}H spectra of the cell lysates. Furthermore, the ^{1}H spectra of the R3230Ac cell media showed the presence of endogenous lactate in the media at relatively similar quantities (Fig S8A-D), which implies that either concentration of CHC provided incomplete inhibition of endogenous lactate exportation. The small peaks in the ^{1}H spectra of the cell media that may represent ^{13}C-glutamate are not much higher than background levels, which is why we generated ^{13}C plots (Fig 5H-K).

5 mM CHC significantly increased cell death in MCF7 and R3230Ac cell lines independent of the presence of exogenous lactate

MCT1 inhibitors have been given some attention as putative anti-cancer therapies [16,17,20]. We sought to characterize cell viability and death responses in MCF7 and R3230Ac cells to high (5 mM) or low (0.1 mM) CHC in the presence or absence of glucose ± high lactate (40 mM). If both the lower and higher CHC concentration showed significant cell death when lactate was supplemented, then lactate toxicity would be due to the inability of the cell to "detoxify" the lactate via biochemical pathways (generation of alanine and glutamate) or due to factors associated with prevention of lactate excretion. Of note, it has previously been shown that cell death is elicited by other MCT1 inhibitors via the inability of the cell to effectively regulate the lower pH_i that results from lactic acid accumulation from glycolysis [20]. If, however, cell death was elicited by another mechanism with high CHC, we would expect that the lower CHC concentration would not show any cell death. MCF7 cells were chosen as our human breast cancer model; MDA-MB-231 cells were deemed unfit for these experiments due to their lack of MCT1 expression. R3230Ac cells were also used for these studies to maintain consistency with our *in vivo* model and to test effects of CHC on an avid lactate-consuming cell line.

Fig 6A&E shows the percent of total MCF7 and R3230Ac cells that were viable (Annexin V–/7AAD-) after treatment with high (5 mM) or low (0.1 mM) CHC concentrations with or without glucose and/or 40 mM lactate. The control group represents cells in complete media without lactate or CHC treatment. In MCF7 cells, high CHC + glucose did not significantly change viability. Without glucose in the media, the percentage of viable cells dropped from 80% to 56% (#$p \leq 0.004$ compared to control, Fig 6A). This decrease in viable cells was significant compared to MCF7 cells treated with 40 mM lactate + glucose (‡‡$p < 0.01$, Fig S3B). High CHC + high lactate and no glucose resulted in 59% viability. This result was significant compared (*$p = 0.003$, Fig 6A) to all groups with no or low CHC, except for the no glucose, no lactate low CHC group. When a linear regression model was conducted for MCF7 cells, it was found that CHC concentration and glucose availability significantly influenced cell viability ($p < 0.0001$ and $p = 0.001$, respectively) but the presence of high lactate showed no significant changes in cell viability. All high CHC treatments in R3230Ac cells showed a significantly decreased percentage of live cells compared to all groups with no or low CHC (*$p < 0.008$; Fig 6E). These results show that cell viability

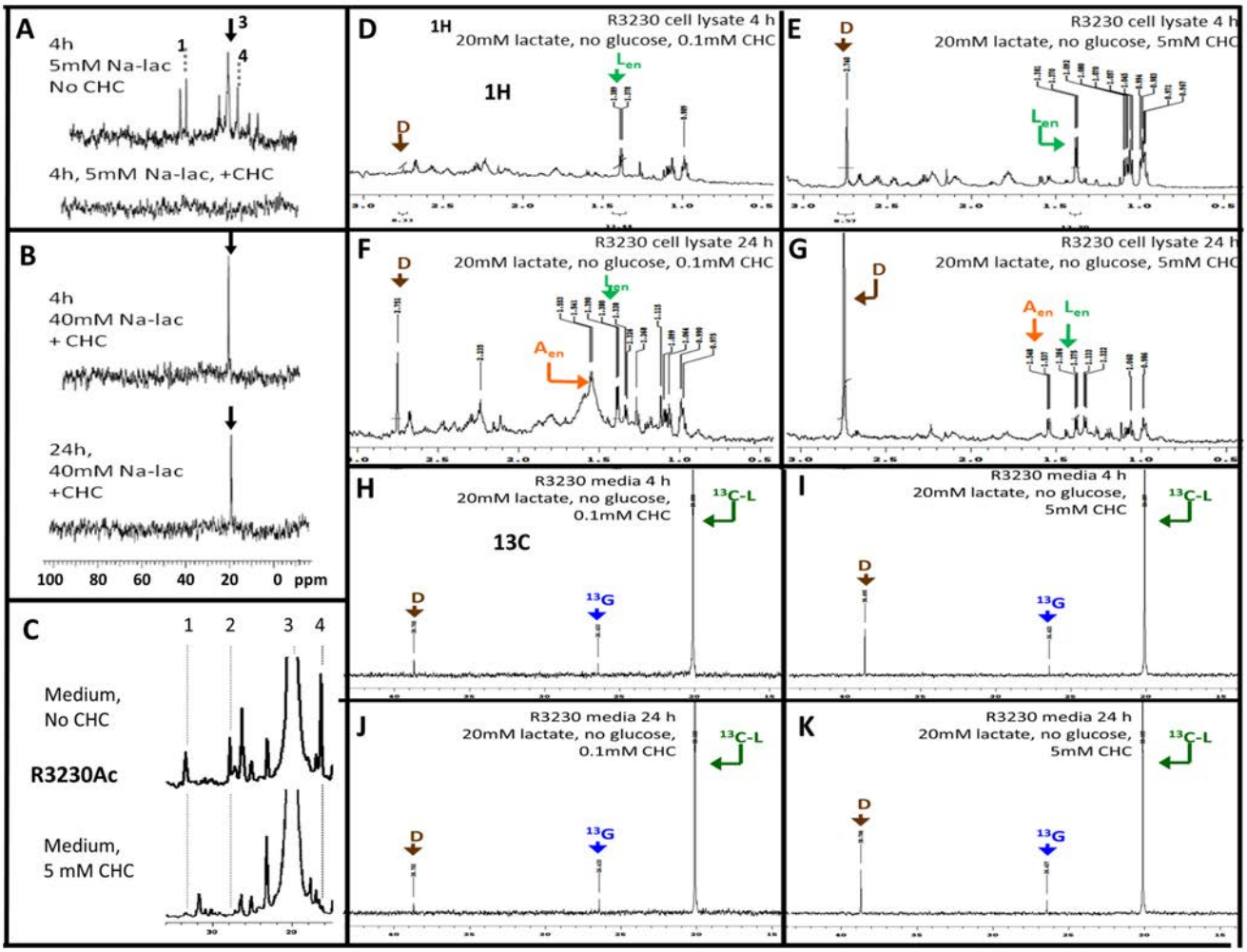

Figure 5. Inhibition of exogenous lactate uptake and endogenous lactate excretion with addition of CHC. All experiments represented were carried out in glucose-deprived conditions. ^{13}C spectra of R3230Ac cell lysates incubated for 4 h with 5 mM ^{13}C-lactate without CHC treatment shows peaks corresponding to lactate (''3''), alanine (''4'') and glutamate (''1'') (**A**, top). ^{13}C spectra of R3230Ac cell lysates incubated for 4 h with 5 mM ^{13}C-lactate with 5 mM CHC treatment show no peaks corresponding to lactate or metabolites (**A**, bottom). ^{13}C spectra of R3230Ac cell lysates incubated for 4 h and 24 h with 40 mM ^{13}C-lactate + 5 mM CHC shows a peak corresponding to lactate (arrow) but no other metabolites (**B**). ^{13}C spectra of R3230Ac cell media incubated with 5 mM ^{13}C-lactate for 4 h shows peaks corresponding to alanine and glutamate without CHC treatment (**C**, top); metabolite peaks are absent or smaller with 5 mM CHC (**C**, bottom). ^{1}H spectra of R3230Ac cell lysate with the following treatments: 20 mM ^{13}C-lactate + 0.1 mM CHC for 4 h (**D**) 20 mM ^{13}C-lactate + 5 mM CHC for 4 h (**E**), 20 mM ^{13}C-lactate + 0.1 mM CHC for 24 h (**F**), 20 mM ^{13}C-lactate + 5 mM CHC for 24 h (**G**). ^{13}C spectra of R3230Ac cell media with the following treatments: 20 mM ^{13}C-lactate + 0.1 mM CHC for 4 h (**H**) 20 mM ^{13}C-lactate + 5 mM CHC for 4 h (**I**), 20 mM ^{13}C-lactate + 0.1 mM CHC for 24 h (**J**), 20 mM ^{13}C-lactate + 5 mM CHC for 24 h (**K**).Endogenous lactate = green ''$\mathbf{L_{en}}$'', endogenous alanine = orange ''$\mathbf{A_{en}}$'', ^{13}C-lactate = dark green ''$\mathbf{^{13}C\text{-}L}$'', ^{13}C-glutamate = blue ''$\mathbf{^{13}G}$'', DMSO = brown ''**D**''
doi:10.1371/journal.pone.0075154.g005

with this assay is influenced more by CHC concentration and availability of glucose than the presence of lactate.

Also available from the data set is whether cells died via an apoptotic pathway (Annexin V+/7-AAD-), loss of membrane integrity (Annexin V–/7-AAD+) or marked for both (Annexin V+/7-AAD+) after CHC treatment. Apoptosis was significantly increased with high CHC in absence of glucose or lactate, but with those nutrients added back alone or together cells were protected from apoptosis (#$p < 0.05$; Fig 6B). R3230Ac cells showed a significant increase in the percentage of apoptotic cells with high CHC treatment compared to all no and low CHC treatments (*$p < 0.02$, Fig 6F).None of the treatments affected the loss of membrane integrity of MCF7 or R3230Ac cells (Fig 6C). The percentage of MCF7 cells marked for both apoptosis and loss of membrane integrity was significantly increased with all high CHC treatments (except the high CHC –glucose, -lactate group) compared to all no or low CHC groups (**$p < 0.05$, Fig 6D). There were no significant changes in the percentage of R3230Ac cells marked for both apoptosis and loss of membrane integrity in any treatment (Fig 6H).

These results show that R3230Ac cells primarily undergo apoptosis in response to high CHC and that MCF7 cells stain positive for both cell death pathways in response to high CHC. In all the statistical tests conducted, low CHC concentration was not significantly different from the untreated control or vehicle alone. The presence or absence of lactate showed no significance in the statistical models. In summary, the cell death responses elicited from 5 mM CHC are independent of the presence of exogenous lactate; therefore, our original hypothesis that CHC would elicit

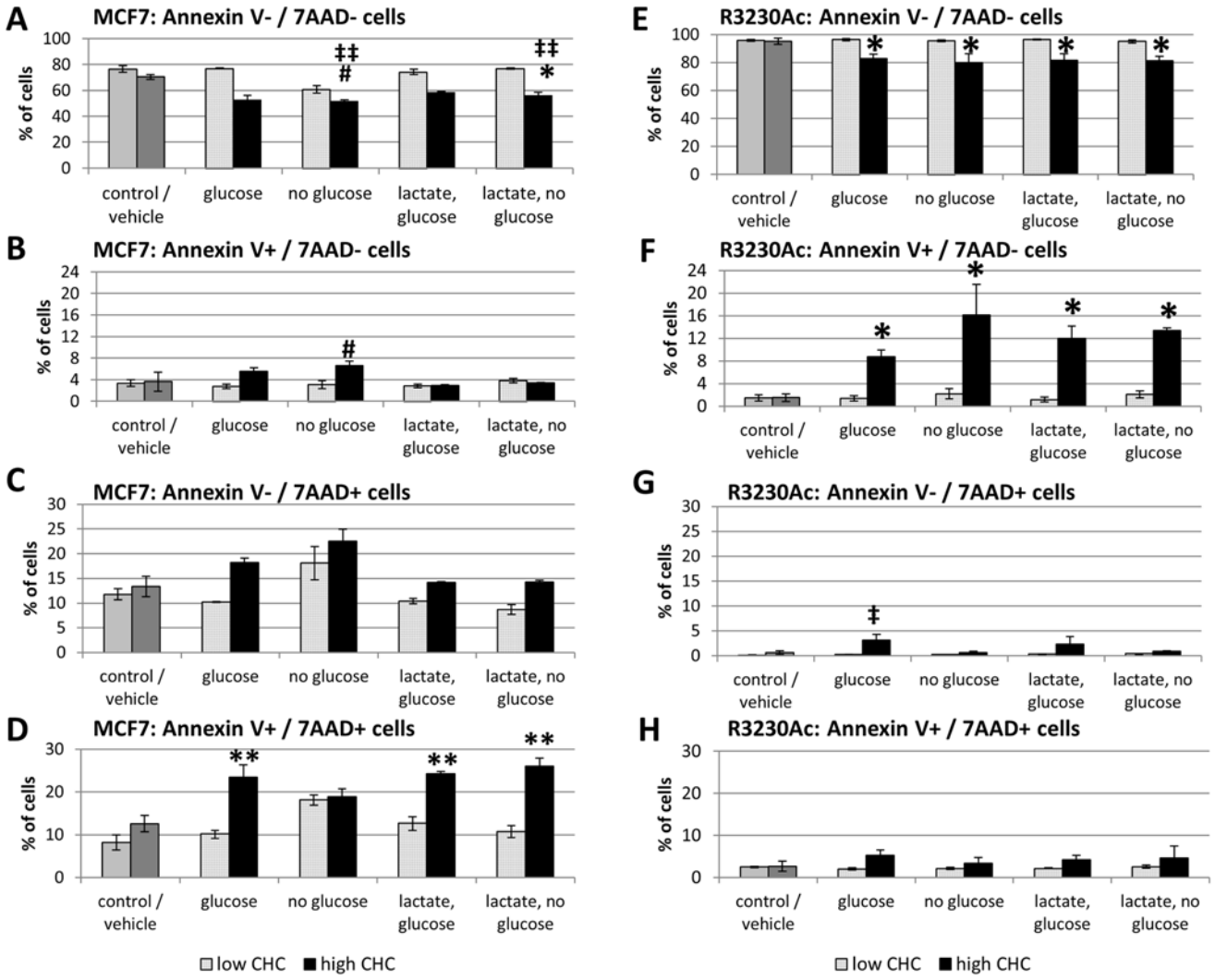

Figure 6. 24 h exposure to 5 mM CHC significantly decreases cell viability and increases cell death responses in MCF7 and R3230Ac cells independent of addition of high lactate. Cell viability as measured by Annexin V –/7-AAD – labeling (n = 3) in MCF and R3230Ac cells treated with high (5 mM) or low (0.1 mM) CHC with and without glucose (no lactate) and with 40 mM lactate (with and without glucose). Viable MCF7 cells show significant decreases with 5 mM CHC (A, #$p \leq 0.004$ compared to control (no CHC, no lactate + glucose), ‡‡$p < 0.01$ compared to 40 mM lactate-treated MCF7 cells, *$p = 0.003$ compared to all no CHC and low CHC groups). Percentage of apoptotic (Annexin V+/7-AAD-) MCF7 cells show significant increases with the –glucose-lactate+high CHC treatment and the +glucose+lactate+high CHC treatment (#$p < 0.05$) and between the –glucose–lactate+high CHC group and 40 mM lactate treatments without CHC (+ or – glucose) (†$p < 0.05$, B). Percentage of MCF7 cells with loss of membrane integrity (Annexin V–/7-AAD+) show no significant differences with CHC treatment (C). Percentage of MCF7 cells marked for both cell death pathways (Annexin V+/7-AAD+) show significant increases with 5 mM CHC compared to the no CHC and low CHC groups (**$p < 0.05$, D). Percentage of viable R3230Ac cells show significant decreases with 5 mM CHC compared all no CHC and low CHC groups (*$p < 0.008$, E). Percentage of apoptotic (Annexin V+/7-AAD-) R3230Ac cells show significant increases with 5 mM CHC compared to compared to no CHC and low CHC groups (*$p < 0.02$, F). Percentage of R3230Ac cells marked for loss of membrane integrity (Annexin V–/7-AAD+) show no significant differences except–glucose-lactate+high CHC treatment (‡$p < 0.05$, G). Percentage of R3230Ac cells marked for both cell death pathways (Annexin V+/7-AAD+) show no significant changes with any treatment (H). Results analyzed with One-Way ANOVA and Bonferroni/Dunn post-hoc tests.
doi:10.1371/journal.pone.0075154.g006

cell death in lactate-treated, glucose-deprived cells due to the inhibition of lactate uptake and utilization was incorrect.

Exogenous lactate is taken up but not catabolized in hypoxic R3230Ac cells

Figure 7C&D showed that lactate uptake occurs primarily in aerobic regions of R3230Ac tumors. It is known that hypoxic cells upregulate glycolysis, resulting in higher lactate production [71]. This glycolytically-derived lactate will then be exported from the cell, resulting in high lactate accumulation in hypoxic areas of the tumor [10]. Therefore we hypothesized that hypoxic cells would take up exogenous lactate, but would not be able to catabolize it. The ^{13}C spectra of glucose-deprived, ^{13}C-lactate-treated R3230Ac cells show uptake and utilization of ^{13}C-lactate, with many labeled metabolites present after 12 h. In glucose-deprived and hypoxic conditions, after 12 h incubation with 40 mM ^{13}C-lactate, the ^{13}C spectra of R3230Ac cell lysates show evidence of the lactate peak but no corresponding labeled metabolites. This indicates that although hypoxic cells can take up lactate, it is cannot be utilized for metabolite generation.

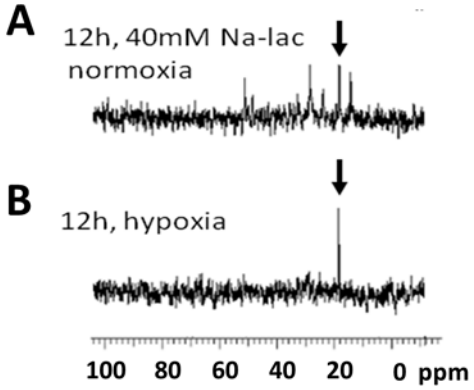

Figure 7. Hypoxic R3230Ac cells take up ^{13}C-lactate. Treatment with 40 mM ^{13}C-lactate in glucose-deprived, normoxic R3230Ac cancer cells result in lactate uptake and metabolism after 12 h (**A**). Under hypoxic conditions, evidence of lactate uptake (arrow) but no additional labeled metabolites can be seen in the cell lysates after 12 h (**B**). Arrow: ^{13}C-methyl lactate.
doi:10.1371/journal.pone.0075154.g007

Discussion

Our study shows that breast cancer cells tolerated and catabolized lactate at concentrations found in human breast cancer. Breast cancer cell lines showed different rates of lactate uptake and generation of similar catabolites (glutamate and alanine) *in vitro* and *in vivo*. *In vivo*, uptake of lactate occurred more quickly than uptake of glucose in tumor tissue, and this uptake coincided with perfused (rather than hypoxic areas) of the tumor. *In vitro*, hypoxic breast cancer cells did not show catabolism of lactate. Taken together, our study strongly supports one side of the metabolic symbiont model: the assertion that aerobic breast cancer cells can tolerate and metabolize lactate. Our autoradiography data provide further evidence that the metabolic symbiont model may operate in some solid tumors. Manipulation of lactate uptake and catabolism was accomplished with use of CHC, but higher concentrations of CHC killed breast cancer cells in a manner that was not dependent upon the presence of lactate. This suggests that cytotoxic activity of CHC is unpaired from lactate metabolism in our model.

In the past we have shown that lactate can be used as a substrate for aerobic cancer cells and that MCT1 and MCT4 expression correlate with the ability of certain cancer cell lines to consume lactate [17]. Here, we showed that cellular responses to exogenous lactate varied depending upon cell type and glucose availability, but, overall, at concentrations seen in human breast cancer, lactate was well-tolerated (Figs S1 & S2) and catabolized (Figs 3–5). Cell lines that consume more lactate (''high lactate-consumers'') showed less of a reliance on glucose for cell growth compared to cell lines that consumed less lactate (''low lactate-consumers'') (Fig 5, S5, 8). The R3230Ac tumors demonstrated a significantly higher kinetic uptake rate for lactate than for glucose (Fig 3) and showed no changes in cell survival with glucose-deprivation (Fig S1D & S2D), providing additional evidence for a high lactate-consuming phenotype.

In all of the experiments conducted, the concentration of glutamine was not altered, and therefore present at concentrations of the manufacturer's supplementation (4 mM). Glutamine has been shown to be an important metabolite for growth of cancer cell lines in culture [67]; therefore, we chose to not remove it. Previous reports indicate that the contribution of glutamine to lactate formation is approximately 7–13%, depending on the growth phase and other metabolites in the culture media [66]. While glutamine may contribute to a small amount of lactate formation [66], the major metabolite responsible for lactate formation is glucose. The significance of convergent pathways of glutamine and lactate metabolism may warrant future study, especially in tumor cells that may demonstrate less of a dependence on glucose as a primary substrate.

For lactate to act as an energy substrate, it needs to be converted to pyruvate, enter the mitochondria and go through oxidative phosphorylation. Through use of labeled lactate, it has been previously found that lactate completes the course of oxidative phosphorylation, as shown by generation of labeled CO_2 [56,72]. Likewise, we found that R3230Ac cells significantly increased oxygen consumption with increasing lactate concentrations (Fig 2E). Another strong indication of the use of labeled lactate as a substrate to enter the TCA cycle that we found in our study was the appearance of labeled glutamate in the cell lysates and media of all cell lines tested (Figs 5–8). The most straight-forward pathway for ^{13}C-glutamate formation is: ^{13}C-L-lactate $\leftrightarrow$ ^{13}C-pyruvate $\rightarrow$ $\rightarrow$ TCA cycle partial completion $\rightarrow$ ^{13}C- α – ketoglutarate $\rightarrow$ ^{13}C-glutamate. We also identified alanine peaks after adminstration of ^{13}C-L-lactate. Labeled alanine formation occurs through: ^{13}C-L-lactate $\leftrightarrow$ ^{13}C-pyruvate + glutamate $\leftrightarrow$ ^{13}C-alanine + α-ketoglutarate. Alanine and glutamate (whether labeled or endogenous) can participate in the reaction catalyzed by alanine aminotransferase (α -ketoglutarate + alanine $\leftrightarrow$glutamate + pyruvate). While this seems to only shift the balance of lactate catabolites, this reaction may serve to temporarily alleviate nitrogen stress in the cell by transferring it to glutamate. When alanine is formed in other organs, particularly in skeletal muscle, it can be shuttled to the liver to participate in the Alanine Cycle (similar to the Cori Cycle) [73]. Alanine generated in the tumor is unlikely to participate in the Alanine Cycle, as the diffusion of metabolites to a blood supply and transport is limited by vessel arrangement and efficiency, respectively [74]. The alanine generated may be used for anabolic purposes by the tumor, but it is also possible that alanine participates in futile metabolic cycles. The metabolic fate of these lactate catabolites would be an interesting avenue of further research, and future studies could determine whether inhibiting lactate catabolism pathways in tumors may provide another therapeutic option.

No prior reports have compared the consumption of lactate to that of glucose *in vivo*. We showed that the R3230Ac tumor consumes glucose and lactate simultaneously *in vivo*, converting lactate to alanine and glutamate. Our kinetic data support avid uptake of ^{14}C-lactate by the tumor *in vivo*, with uptake rate constants that are higher than that of glucose. These results suggest that lactate may be an important substrate for the R3230Ac tumor line. Second, we demonstrated that lactate was taken-up most preferentially in oxygenated tumor regions (Fig 4). In prior studies, we demonstrated that lactate accumulation was highest in perinecrotic hypoxic tumor regions of the R3230Ac tumor [10]. These results strongly suggest that at least part of the lactate that is produced by hypoxic tumor regions may diffuse down its own concentration gradient, toward better perfused aerobic cells, which can then take it up via the MCT transporters and utilize it. In other work by our group we have indeed found this to be the case [17], which leads to preferential death of hypoxic tumor cells, substantial growth delay and increased radiation response. Our *in vivo* results support this suggestion that there may be a cooperative relationship between different cells within the R3230Ac tumor. Recently, it has been reported that lactate uptake in endothelial cells contributes to increased angiogenesis and HIF-1α expression [64,75]. The ability of tumor stroma to consume lactate supports

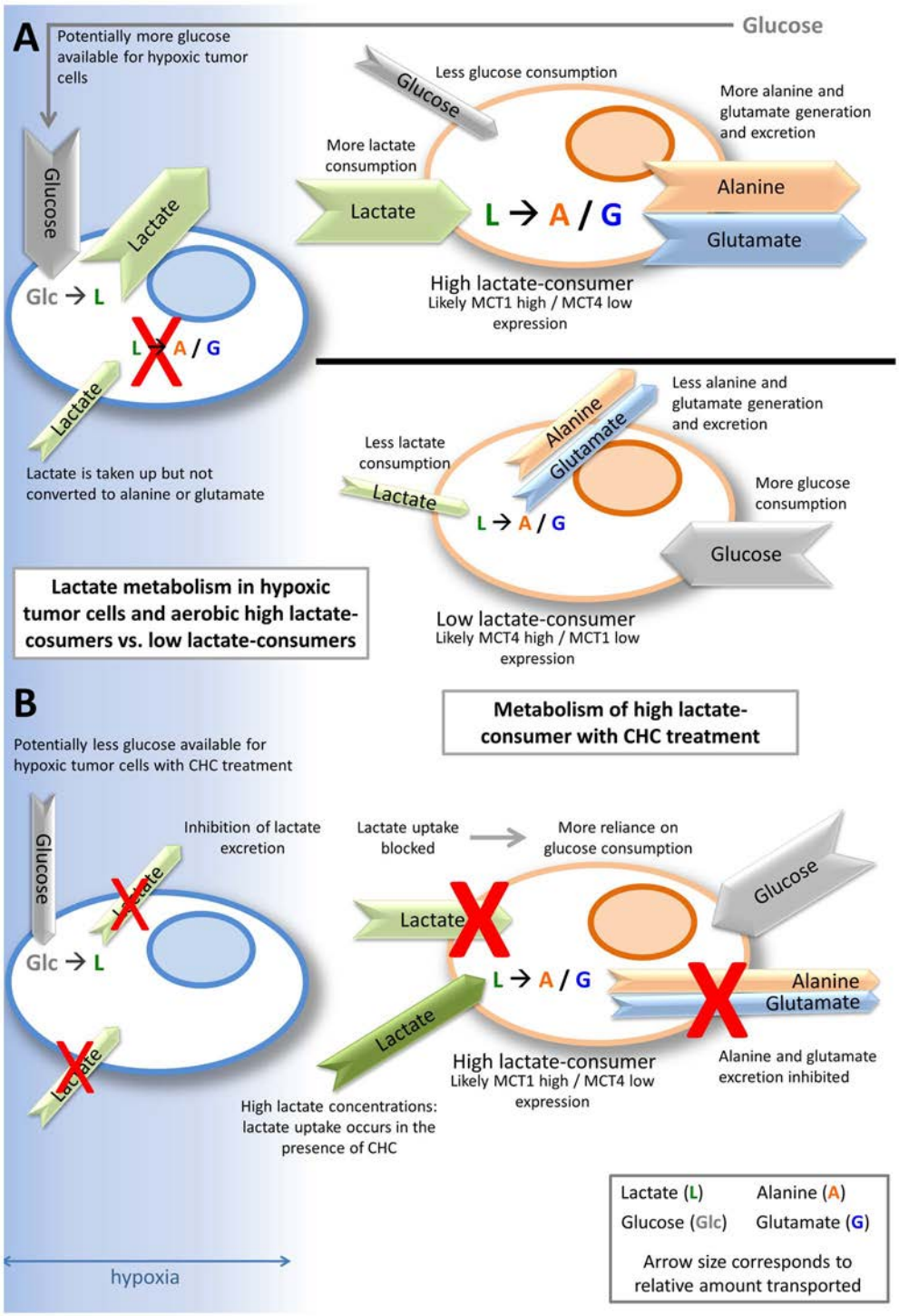

Figure 8. Summary diagram of lactate metabolism in high lactate-consumers vs. low lactate-consumers. The blue gradient represents oxygen diffusion. The cell on the left is hypoxic; the cells on the right are aerobic. Arrow colors correspond to substrates, and arrow size corresponds to relative amount. Hypoxic tumor cells take up glucose (gray "**Glc**") and produce lactate (dark green "**L**"), leading to higher concentrations of lactate. Lactate may be taken up by the hypoxic tumor cells, but it is not catabolized. Aerobic tumor cells that are high lactate-consumers and likely express high MCT1/low MCT4 can take up lactate and catabolize it to alanine (orange "**A**") and glutamate (blue "**G**"), which will be exported from the cell. With the aerobic high lactate-consumer cell consuming lactate, more glucose can potentially be spared for hypoxic tumor cell use, potentially conferring a survival advantage. Aerobic tumor cells that are low lactate-consumers and likely express low MCT1/high MCT4 take up less lactate than the high lactate-consumers, consequently producing and exporting less alanine and glutamate. Low lactate-consumers utilize more glucose, which will not allow glucose to reach the hypoxic tumor cells (**A**). One proposed strategy for starving hypoxic tumor cells of glucose in a high lactate-consuming tumor is to treat with a MCT1- inhibitor, like CHC. CHC prevents lactate uptake and catabolism in cells, forcing the aerobic high lactate-consumer to use glucose, which starves the hypoxic tumor cell of glucose. Lactate transport out of hypoxic cells is also inhibited, which would also lead to hypoxic cell death (**B**).
doi:10.1371/journal.pone.0075154.g008

tumor growth. Additionally, other groups have shown that tumor-associated fibroblasts undergo aerobic glycolysis, producing lactate, which can then be utilized by tumor cells; this has been termed the "Reverse Warburg Effect" [76–79]. *In vitro*, we observed production of both alanine and glutamate in R3230Ac cells as well as normal human breast epithelial cells and human breast cancer cell lines after administration of ^{13}C-lactate. The fact that lactate utilization was seen in human breast cancer as well warrants further investigation of their lactate-consuming ability *in vivo*, as the lactate-consuming phenotype of particular tumors may influence treatment strategies.

Therapeutically targeting lactate metabolism in tumor cells has been proposed [16,17,64,80] and is currently being evaluated in Phase I/II clinical trials [81]. Previously, inhibition of MCT1, specifically with CHC, was used to block lactate uptake in more oxidative cells, thereby starving their more hypoxic neighbors of glucose [17]. While these results are encouraging, it is well documented that CHC does not only inhibit lactate transport. MCTs transport many monocarboxylates. Though each subtype has a different affinity for particular monocarboxylates, the most widely-expressed and well-characterized subtypes (MCT1, 2 and 4) are capable of transporting lactate, pyruvate, butyrate and ketone bodies [14]. Inhibiting the transporter will theoretically prevent trafficking of each of these monocarboxylates. Diers *et al.* recently reported that 0.5 mM CHC treatment prevented pyruvate uptake and inhibited mitochondrial respiration in breast cancer cells [82]. At the CHC concentrations used in our study (0.1 and 5 mM), it is likely that pyruvate (in addition to lactate) transport was also impaired.

Despite the ability of 5 mM CHC to inhibit lactate catabolism and export at 40 mM concentrations (Fig 5B), we found that 40 mM lactate was not cytotoxic to MC7 or R3230Ac cells (Fig 6). High CHC elicited significant cell death independent of addition of exogenous lactate, indicating that off-target effects are responsible for cancer cell death at this concentration of CHC. These results suggest that CHC may not be the best therapeutic MCT1 inhibitor. Other MCT1 inhibitors have elicited cancer cell death via decreased pH_i with treatment [20]. It is important to also address the potential toxicity with MCT1 inhibition in normal tissue as well as in other diseases that show high lactate levels, such as meningitis or sepsis [83,84]. Encouragingly, in a recent study, we found that mice treated with CHC showed no morbidity [85].

Targeting tumor metabolism has been proposed as an anti-cancer therapy, specifically, MCT1 inhibition has received attention in recent years [16,17,20,64,80,81]. Our study supports the rationale that it is important to first know the metabolic phenotype of the individual tumor before administering metabolic intervention. With all breast cell lines tested, we saw tolerance of lactate at concentrations relevant to breast cancer. Our results demonstrate two different lactate-consuming phenotypes: high lactate-consumers (R3230Ac and MCF7) and low lactate-consumers (MDA-MB-231) (Fig 8). We showed that lactate consumption and glucose dependence differ between the lactate-consuming phenotypes and that catabolite generation from extracellular lactate was not equal in relative rates or amounts, with low lactate-consumers (MDA-MB-231 cells) showing smaller peaks of alanine and glutamate compared to high lactate-consumers (R3230Ac or MCF7 cells) (Fig 8). Inhibiting lactate uptake in aerobic R3230Ac cells may starve their hypoxic neighbors (metabolic symbiont); however, this model needs to be studied in more detail *in vivo* to assess its overall influence on tumor survival. Our studies also indicate that tumors that behave similar to MDA-MB-231 cells (lacking MCT1 expression and/or showing low lactate consumption) may not be a good candidate for manipulation of lactate pathways. Given these inherent differences, a single approach for metabolism manipulation is not appropriate; therapeutically targeting tumor metabolism would need to be tailored to particular metabolic phenotypes.

In clinical studies, it has been found that lactate accumulation is an indicator of shorter metastasis-free and overall patient survival [2,34,35,38,39,46]. A recent study measuring lactate accumulation and spatial distribution in prostate cancer compared the aggressive, anaplastic, fast-growing Dunning R3327-AT to the parental, well-differentiated, slow-growing Dunning R3327-H in animal models [86]. Similar to the findings in human solid tumors, the more aggressive AT tumor line showed significantly more lactate accumulation and necrosis, specifically in the tumor core [86]. Not surprisingly, the same conclusion from human and animal studies emerges: lactate accumulation is a reliable indicator of tumor aggressiveness, associated with fast growth and necrosis within a solid tumor [10,22,35,38,39,47,86]. The topic of lactate utilization is investigated comparatively less, and the importance of the lactate-consuming phenotype is currently unknown. Our study has investigated lactate uptake and catabolism in three breast cancer cell lines and two normal cell lines *in vitro* and in one breast tumor model *in vivo*. Comparing lactate consumption in benign and malignant tumor models is the next step in elucidating the importance of lactate consumption to tumor survival and/or aggressiveness.

Lactate accumulation and utilization are two sides of the same coin. The unanswered questions regarding the ability of the tumor to utilize lactate are: 1. Is it an indicator of a less aggressive tumor or is the ability to consume lactate a survival advantage? (Are these questions mutually exclusive?) 2. Can we effectively alter (and sustain the alteration of) the lactate-consuming phenotype of a tumor through manipulation of metabolic pathways? Recently there has been increasing interest in targeting lactate metabolism in tumors. A greater understanding of the complex and dynamic metabolic pathways that operate in tumors provide more avenues for tailored treatments.

Methods

Lactate, CHC and Cell Culture

Sodium L-lactate ($C_3H_5NaO_3$) was purchased from Sigma-Aldrich (St. Louis, MO, USA). All sodium lactate concentrations for cell treatments were made by diluting the powder in appropriate cell media. Solutions were discarded after 2 weeks. For NMR, sodium L-lacate-3-^{13}C solution (45–55% w/w in H_2O) 99 atom % ^{13}C was acquired from Isotec (Sigma, St. Louis, MO). Alpha-cyano-4-hydroxy-cinnamate (CHC) powder was acquired from Sigma (St. Louis, MO) and dissolved in DMSO to create 1 M and 100 mM stock solutions. The stock solution was passed through a 0.22 μm filter prior to dilution in treatment media to acquire concentrations equal to 0.1, 1, 2.5, 4, or 5 mM.

Cell lines used include MCF7 (ER+ human breast adenocarcinoma), MDA-MB-231 (triple negative human breast adenocarcinoma), HMEC (human mammary epithelial cells), and R3230Ac (rat mammary carcinoma. Cells were maintained in 37°C, 5%CO_2, 20% O_2 in a Forma Scientific (Marietta, OH) incubator. All cell lines were acquired through Duke University's Cell Culture Facility and from ATCC (Manassas, VA), except HMEC, which were acquired from Clonetics (Switzerland). HMEC cells were cultured in MEBM media from Lonza/Clonetics (Switzerland) with added supplements ("MEGM media", Single®Quots®: 2 mL BPE, 0.5 mL hEGF, 0.5 mL insulin, 0.5 mL hydrocortisone, 0.5 mL GA-1000). All other cell lines were cultured high glucose DMEM (Gibco) +10% FBS + 1% antibiotic/antimycotic. For

glucose deprivation experiments, DMEM without glucose or sodium pyruvate was used (Gibco) +10% FBS + 1% antibiotic/antimycotic. In all experiments, L-glutamine was present in DMEM media at the manufacturer's concentration; glutamine was never omitted or altered. Hypoxia experiments were carried out in the Invivo$_2$ 500 hypoxia chamber (Ruskinn Technology Ltd, Pencoed, Bridgend, UK). Gas mixtures were 0.5% O_2, 5% CO_2, and 94.5% N_2.

In vitro sodium lactate measurements in cell media

Unlabeled sodium lactate was measured in cell media with the commercially available first-generation (discontinued in favor of the second-generation) Lactate Pro measuring device, which has a reliable measuring range between 0.8 – 23 mM. Cells were plated at a known density and allowed to reach 60% confluency before the beginning of the experiment. At this time, the cell media was changed from high glucose DMEM (+ 10% FBS) to glucose-free DMEM (+ 10% FBS). Time zero was designated at the addition of 20 mM exogenous lactate. Lactate measurements were taken at times 0, 1, 2, 4, 8, 12, 24, 48, 72, 96 and 120 h. The media was not changed over the entire 5-day period. Lactate measurements were conducted as follows: 100 µL of cell media was placed on the Lactate Pro measuring strips that were then inserted into the Lactate Pro device. A standard curve of known lactate concentrations was performed, and the device was calibrated with a known lactate concentration prior to experimental measurements (SEM = ± 0.34 mM). At the end of the experiment, cells were counted. Five independent experiments were conducted. Overall mean lactate concentration decreases in the cell media and the amount of lactate consumed per cell were calculated. A linear regression analysis was conducted on the lactate measurements. Rate coefficients were determined after controlling for the time and batch effects.

Cell Growth in vitro in lactate media vs. glucose media

MCF7 and MDA-MB-231 cells were plated at equal densities and allowed to reach 60% confluency before the beginning of the experiment. At this time, the cell media was changed from high glucose DMEM (+ 10% FBS) to either glucose-free DMEM (+ 10% FBS) with supplemented 20 mM lactate or high-glucose DMEM (+10% FBS). Cells were allowed to grow for 5 days before being harvested and counted.

Cryosectioning, Bioluminescence and Image analysis

Collection of human tissue LABC biopsies was approved by Duke University Health System Institutional Review Board (IRB), and patient samples were de-identified before acquisition for cryosectioning. All patients provided written informed consent to participate in the study. The Duke University Institutional Review Board approved the protocol and the informed consent procedure.

Cryosectioning of human LABC biopsies was performed on the Leica CM1850 Cryostat (Leica, Wetzlar, Germany) at –30°C. Sections for immunohistochemistry were cut at 10 microns and mounted on Superfrost Plus Micro Slides (VWR, West Chester, PA), and sections for metabolite bioluminescence were cut at 20 microns and mounted on 22×40 micro cover glass (VWR) coverslips.

Bioluminescence techniques were carried out as previously described [10,36,37,87]. Briefly, 20 micron-thick frozen sections were exposed to a luciferase-bound LDH enzyme mixture and quickly placed in the dark under a light microscope camera. Luciferase signal was acquired for 10 seconds. Known lactate standards were run in parallel. All 16-bit images were imported to Image J for pixel grayscale intensity analysis; a standard curve was generated from the pixel values from the lactate standards. Lactate values were extrapolated from the standard curve. Three to four sections were measured per sample.

Protein extraction and Western Blots

Protein extraction was carried out on ice using complete RadioImmuno Precipitation Assay (RIPA) lysis buffer + 0.1% protease inhibitor cocktail (BioRad, Hercules, CA). Concentrations of total protein were measured with DC^{TM} Protein Assay from BioRad (Hercules, CA). For MCT1 Western blots, 15–50 ug per sample were loaded into wells. Proteins were separated by SDS-PAGE in a 12% gel (Bio-Rad, Hercules, CA), then transferred to a polyvinylidene fluoride (PDVF) membrane (Bio-Rad). Membranes were blocked for one hour in 5% non-fat, dry milk reconstituted in TBST. MCT1 rabbit anti-human IgG primary antibody (Millipore, Billerica, MA) and MCT4 rabbit (recognizes human, mouse and rat) IgG primary antibody (Santa Cruz Biotechnology, Dallas, TX, USA) were used, diluted 1:1000 in TBST and incubated in 4°C overnight. The secondary goat anti-rabbit IgG horseradish peroxidase-linked antibody (Jackson ImmunoResearch Labs, West Grove, PA) was diluted 1:2000 in TBST and incubated in room temperature for one hour. SuperSignal® West Pico Luminol/Enhancer Solution (Pierce, Rockford, IL) was used to detect bands before exposure to Kodak film (Rochester, NY). Pan-actin controls were run in accordance.

Measurement of ^{13}C lactate uptake using NMR: *in vitro studies*

Tissue culture dishes (15cm diameter) were plated at cell densities between 2 and 3×10^6 cells. After allowing 24 h for cells to attach, or after achieving 80% confluency, cells were washed twice with 1x DPBS and then treated with either high-glucose DMEM (untreated control), no glucose (and no pyruvate) DMEM + ^{12}C (unlabeled) lactate (unlabeled control) or 3-^{13}C-lactate (Isotec, Sigma, St. Louis, MO). Cells were exposed to 10–40 mM 3-^{13}C-lactate in normoxic or hypoxic conditions for 4, 12 or 24 h. At the end of the incubation period, 1 mL of media was collected and immediately frozen at –80°C. These media samples were used to acquire ^1H, ^{13}C and HMQC spectra of exported metabolites. Cells were washed twice with DPBS. For metabolite extraction, 1 mL of 0.9 M perchloric acid, diluted 1:10 in diH_2O, was added to each dish, and cells were scraped. The samples were centrifuged at 12,000 RPM for 10 minutes to pellet cell debris and precipitate. Supernatant was transferred to a fresh tube, and this was used for NMR on cell lysates.

For NMR readings, 600 µL total volume was used. For cell lysates, 450 µL of the perchloric acid cell lysate, 100 µL DPBS and 50 µL D_2O were added to the NMR tube. For media samples, 550 µL media and 50 uL D_2O were mixed. Tubes were capped and placed in the 500 MHz Varian Inova NMR spectrometer (Palo Alto, CA). The samples were measured with the High Resolution NMR Spectroscopy shared resource of the Duke Cancer Institute. VnmrJ Software (Varian) was used to acquire and analyze the spectra. All samples were tuned and shimmed before data acquisition. ^{13}C-NMR spectra were acquired at 125.7 MHz with a Varian 500 MHz spectrometer equipped with a 5 mm broad-brand probe. Specifications were: a 45° flip angle, 0.8 s interpulse delay, and a 1.334 s acquisition time. All proton spectra were measured at 500 MHz.

Annexin V/7-AAD staining

Cells were seeded in 6-well plates and allowed to reach 70% confluence before 24 h lactate treatment in high glucose

DMEM+10% FBS + 1% antibiotic/antimycotic or glucose-free and sodium pyruvate-free DMEM+10% FBS + 1% antibiotic/antimycotic. Lactate concentrations used were 0–40 mM. For MCF7 and R3230Ac cells, treatment groups also included high (5 mM) or low (0.1 mM) CHC concentrations in the context of available glucose or glucose-deprivation and with or without 40 mM lactate. After treatment, media and cells were collected and centrifuged. Cells were resuspended in PBS and centrifuged. Live (unfixed) cells were then resuspended in 100 µL of 1X Annexin Binding Buffer (BD Pharmigen, San Diego, CA) in a round-bottom polystyrene tube (BD Falcon^{TM}, Bedford, MA). 5 µL of PE-labeled Annexin V (BD Pharmigen, San Diego, CA) and 5 µL 7-AAD (BD Pharmigen, San Diego, CA) were added to each experimental tube. Samples were incubated in the dark for 15 minutes and tapped gently to mix. 300 µL of Annexin Binding Buffer was added to each tube. Tubes were covered with aluminum foil and transported to Duke Cancer Institute Flow Cytometry Shared Facility. All sample data for cell cycle were analyzed with BD Calibur Flow Cytometer (GMI, Ramsey, MN). 10,000 events were acquired and the percentage of total cells with positive staining was reported. Error bars represent ± SEM. Results were analyzed with One-Way ANOVA and post-hoc tests.

Animals

Female Fischer 344 rats (n = 9 for ^{14}C-glucose experiments, n = 3 for ^{14}C-lactate experiments) were implanted subcutaneously in dorsal mammary fat pad with 1–2 mm pieces of R3230Ac mammary carcinoma tissue extracted from a tumor from a donor animal. Experiments were conducted when tumors reached 1–2 cm in diameter. Prior to the start of the experiment rats were fasted for four hours [88]. Rats were anesthetized with isofluorane gas. Once anesthetized, the rat was placed on a heating pad (K-module, Baxter Healthcare, Valencia, CA) to maintain body temperature of 37°C. The heating pad and rat were contained within a light-tight box so that the light detected by the scintillation probes came only from interaction with the ^{14}C-electrons. The femoral artery and vein were cannulated for monitoring blood pressure with a Digital Manometer (Fiber optic Sensor Technologies Inc., Ann Arbor MI) and infusion of ^{14}C-glucose, ^{14}C-lactate or ^{13}C-lactate (*in vivo* NMR experiments).

This study was approved by Duke University's Institutional Animal Care and Use Committee (IACUC), and the experiments were carried out in strict adherence to their guidelines and recommendations. Duke University maintains an animal program that is registered with the USDA (Permit # 83), assured through the NIH/PHS (Permit # A3195-01), and accredited with AAALAC, International (Permit # 363). All surgery was performed under isofluorane anesthesia, and all efforts were made to minimize suffering.

^{14}C scintillation Probe Calibration

The purpose of these studies was to determine the kinetics of ^{14}C-labeled lactate and ^{14}C-labeled glucose uptake and excretion from tumor, compared with normal tissue. The detection device and scintillation probes were provided by Sicel Technologies Inc., Durham, NC. The apparatus consisted of fiber-optic scintillation probes connected to photomultiplier tubes (PMTs) and a computer. The electrons emitted by ^{14}C were detected by the fiber-optic probes, and this interaction of the electrons with the probe creates photons that are detected by the PMTs. In principle, the apparatus works like a scintillation counter. For each experiment two probes were used (tumor and SQ of the flank). Tumor dimensions were measured and the length of probe to be inserted into the tumor was determined (6–10 mm), based on tumor size. The length of probe inserted into the subcutaneous position was always 20 mm. Each individual probe was calibrated using a ^{14}C-lactate solution of known concentration (µCi/mL) with the probe being immersed in the solution at the same depth as the *in vivo* tumor measurement. This calibration was done to normalize for variability between probes and the insertion length of probe used in different tumors. Prior to the start of the probe calibration, the PMTs were turned on to check for light leakage into the device. If there was no light leakage measurements were recorded every two minutes for approximately three hours. After the calibration was finished, probes were cleaned with alcohol.

Pharmacokinetics of ^{14}C radioisotope *in vivo*

For each experiment, one probe was placed in the tumor and a second in SQ tissue. After the cover of the light-tight box was positioned a 45–60 minute probe stabilization period was allowed to elapse prior to injection of the ^{14}C-labeled substrate. During this time and for the rest of the experiment the rat was continually monitored. Blood pressure and heart rate were monitored using the Digital Manometer (Fiber optic Sensor Technologies Inc., Ann Arbor MI). Body temperature was measured using a rectal probe. Breathing rate and depth of anesthesia were monitored by observation via an infrared camera inside the box connected to a small television.

After stabilization, 100 µCi of ^{14}C-glucose (1 mCi/ml) or 50 µCi of ^{14}C-lactate (1 mCi/ml) was infused at a rate of 0.1 mL/minute and signals were collected for approximately three hours. Time zero was defined as the start of the infusion. Blood samples (300 µL –500 µL) were taken at 0, 4, 7, 10, 15, 25, 30, 60, 100, and 160 minutes from the artery cannula using heparinized syringes. The samples were centrifuged (40,000 RPM, 15 min) and the plasma removed and weighed. 7 mL of Ultima Gold scintillation cocktail (Perkin Elmer Life and Analytical Sciences Inc., Boston MA) was added to each vial. Samples were measured in a Packard Tri-Carb 1500 Liquid Scintillation Counter (Perkin Elmer Life and Analytical Sciences Inc., Boston MA). Counts per minute (CPM) were converted to Disintegrations per Minute (DPM) by the scintillation counter by using set of ^{14}C-standards at known concentrations. The scintillation counter uses the standards to create a quench curve allowing for the conversion of CPMs to DPMs. Concentration (µCi/g) for each sample was calculated by dividing the number of µCis in the plasma by plasma weight. The blood activity data were then normalized to dose/body weight.

Compartmental model

^{14}C-glucose and ^{14}C-lactate uptake data were analyzed using compartmental modeling. A 3-compartmental model was used for ^{14}C-glucose and ^{14}C-lactate data. The following parameters were defined in the model: C_p = glucose or lactate concentration in the blood compartment, C_i = glucose or lactate concentration in the tumor compartment, and C_s = glucose or lactate concentration in the subcutaneous compartment. Rates: k_0 = clearance by other tissues, k_1 = transfer rate of glucose or lactate from blood into tumor, k_2 = transfer rate out of tumor, k_3 = transfer rate into the subcutaneous tissue, and k_4 = transfer rate out of the subcutaneous tissue. The details of the model are described in the supplemental material (Fig S1).

^{13}C lactate NMR from extracted R3230Ac tumors

For *in vivo* NMR experiments, rats were handled in a similar manner. The femoral artery and vein were cannulated for monitoring blood pressure with Digital Manometer (Fiber optic Sensor Technologies Inc., Ann Arbor MI) and infusion of ^{13}C-

lactate, respectively. 1 mL of 100 mM ^{13}C-lactate was infused intravenously over 10 minutes. Time zero was considered to be the start of the infusion. At baseline, 15, 30, 45, 60 and 90 minutes rats were sacrificed and the tumor, liver and brain removed within 60 s and snap-frozen in liquid nitrogen. The frozen tissues were pulverized with a mortar and pestle under liquid nitrogen. 2 mL total of 0.9 M perchloric acid was added to the pulverized tissue. Once thawed at 4°C, the extract was homogenized and neutralized with KOH. Salt was removed by centrifugation and the supernatant was frozen and lyophilized. Each experiment was repeated three times.

The lyophilized samples were dissolved in 630 µL phosphate buffer and 70 µL (10%) deuterium. 15 µL of dioxane was added to each sample as an internal standard. ^{13}C-NMR spectra were acquired at 125.7 MHz with a Varian 500 MHz spectrometer equipped with a 5 mm broad-brand probe. A 45° flip angle, 0.8 s interpulse delay, and a 1.334 s acquisition time were used for all experiments. Standards of glucose, G6P, glutamate, lactate, and alanine at concentrations of 1 mM, 5 mM, and 10 mM with dioxane as an internal standard were also run. The standards were used to create standard curves, which were used to convert peak heights of the different metabolites in each spectrum to concentrations. Additionally the data were analyzed, comparing ratios of different metabolites within a spectrum. The ratios were obtained from peak heights of metabolites.

Autoradiography

^{14}C-lactate autoradiography was used to study the spatial distribution of lactate uptake. Athymic nude mice transplanted with R3230Ac tumors were infused with twoµCi of ^{14}C-lactate. The hypoxia marker drug, pimonidazole (60 mg/kg i.p.), was injected. Thirty minutes later, Hoechst-33342 was administered intravenously as a perfusion marker dye (10 mg/ml, 0.05 ml). Two minutes later, tissues were harvested and snap-frozen. A portion of the frozen tumor was cryosectioned at 14 µm thickness for autoradiography, Hoechst staining and pimonidazole staining.

Electronic autoradiography was performed with a storage phosphor system (Packard Bioscience, Downers Grove, IL). Sections were loaded onto a storage phosphor screen and exposed for 3 weeks. A slide with ^{14}C-standards was also placed on the screen for quantification. The screen was then processed and read in the phosphor system to visualize the distribution of ^{14}C-lactate. Intensity level obtained from the reader was converted to activity, based on the standard slides.

Immunohistochemistry staining

To co-localize the lactate uptake and oxygenation status in tumor, immunostaining of hypoxia with pimonidazole was performed on tumor sections. Tumor cryosections were fixed with paraformaldehyde (room temperature, 30 minutes), blocked, and then stained with mouse anti-pimonidazole antibody labeled with Alexa Fluor® 555 (excitation wavelength = 580 nm). Slides were imaged using a microscope equipped with automatic scanning stage for whole slide scan. Hoechst-33342 (excitation wavelength = 460 nm) images were also obtained by scanning slide with blue filter.

Autoradiography, hypoxia, and perfusion images were registered and overlaid to show the relationship between lactate uptake, hypoxia, and perfusion.

Measurement of oxygen consumption in confluent cells using a Seahorse XF24 extracellular flux analyzer

R3230Ac cells, cultured in high glucose DMEM with 10% serum and 1% antibiotics were washed, trypsinized, counted, and seeded in Seahorse XF24 cell culture plates at 60,000 cells per well in growth medium. According to the manufacturer's instructions, cells were allowed to adhere for 2 hours before growth medium was added to a total volume of 250 µL. Cells were allowed to grow overnight at 37°C, 5% CO_2. On the day of the experiment, cells were washed and mounted with warm XF assay medium, and incubated for 60 min at 37°C without CO_2 before starting the experiment. During the experiment, Na-Lac was added to each well at varying concentrations (diluted in water) by the automatic dispenser to equal a total volume of 75 µL. Three independent experiments were carried out in triplicate. Results are represented as percent of baseline respiration rate 4 minutes after addition of lactate.

Statistics

Student's T-test was used to evaluate mean lactate concentration differences between duplicate LABC biopsies from the same patient. Student's T-test was also used to evaluate differences in: 1. Oxygen consumption in lactate-treated cell in Figure 2, 2. Cell number between MCF7 and MDA-MB-231 cells after five days of lactate treatment in Figure 4, and 3. Cell number between glucose-free, lactate supplemented media and high-glucose, lactate-free media in Figure S5. A linear regression analysis was applied to cellular lactate consumption data in Figure 4. One-way analysis of variance (ANOVA) and Bonferroni/Dunn post-hoc tests were used to evaluate the main effects of lactate treatment on Annexin V/7-AAD staining for the cell lines tested. Cell viability statistics were analyzed with StatView software. All error bars on plots express ± SEM.

Supporting Information

Figure S1 24 h exposure to high lactate concentrations do not decrease cell viability or increase cell death responses when glucose is available *in vitro*. Cell viability as measured by Annexin V −/7-AAD – labeling (n = 3) in normal human mammary epithelial cells (HMEC) (**A**), MCF7 (**B**) MDA-MB-231 (**C**) and R3230Ac cells (**D**) show no significant changes 24 h after addition of exogenous sodium lactate (0−40 mM) in the context of available glucose. No significant changes in cell death responses (Annexin V +/7-AAD –, Annexin V −/7-AAD +, or Annexin V+/7-AAD +) (n = 3) were observed in HMEC (**E**), MCF7 (**F**) MDA-MB-231 (**G**) and R3230Ac cells (**H**) after addition of exogenous sodium lactate (0-40 mM) in the context of available glucose.
(TIF)

Figure S2 24 h exposure to high lactate concentrations (-glucose) significantly decrease breast cancer cell viability and increase cell death responses in human breast cancer cells but not normal breast or R3230Ac cells *in vitro*. Cell viability as measured by Annexin V −/7-AAD – labeling (n = 3) in normal human mammary epithelial cells (HMEC) (**A**) and R3230Ac cells (**D**) show no significant change after exposure to exogenous lactate for 24 h. MCF7 (**B**) and MDA-MB-231 cells (**C**) show a significant decrease in unstained cells after addition of 40 mM exogenous sodium lactate in the context of available glucose (One-Way ANOVA, Bonferroni/Dunn post-hoc test, # $p \leq 0.0006$ compared to untreated control and all other treatment groups). No significant changes in any cell death response were seen in HMEC (**E**) or R3230Ac cells (**H**) after lactate treatment in the context of glucose-deprivation. The percentage of cells with Annexin V+/7-AAD + labeling was significantly increased in MCF7 (**F**) and MDA-MB-231 (**G**) cells after addition of 40 mM sodium lactate with glucose deprivation

(n = 3, One-Way ANOVA, Bonferroni/Dunn post-hoc test, *p < 0.0001 compared untreated control and to all other treated groups).
(TIF)

Figure S3 MCT1 expression in breast cell lines. Total protein expression of MCT1 in MCF7, MDA-MB-231 and HMEC cells show MCT1 expression in MCF7 and HMEC but not MDA-MB-231 cells (**A**). Total protein expression of MCT4 in HMEC, MDA-MB-231, MCF7 and R3230Ac cells show abundant MCT4 expression in MDA-MB-231 cells, low MCT4 expression in HMEC and no detectable MCT4 expression in MCF7 or R3230Ac cells (**B**).
(TIF)

Figure S4 Compartmental model for ^{14}C-labeled glucose and lactate to analyze *in vivo* kinetic data. C_p = glucose or lactate in the blood/plasma compartment, C_i = glucose or lactate in the tumor compartment, C_s = glucose or lactate in the SQ compartment. k_0 = clearance by other tissues, k_1 = transfer rate into the tumor, k_2 = transfer rate out of the tumor, k_3 = transfer rate into the subcutaneous tissue, k_4 = transfer rate out of the subcutaneous tissue.
(TIF)

Figure S5 MCF7 and MDA-MB-231 cell growth in glucose-free, lactate-supplemented media vs. lactate-free, high-glucose media. MCF7 and MDA-MB-231 cells plated at equal densities and allowed to grow for 5 days in either glucose-free, 20 mM lactate-supplemented media (n = 6) or high-glucose media (n = 3). Five days after the media change, cells were harvested and counted. MCF7 cell counts showed no difference between media, but MDA-MB-231 cell counts were significantly higher in the high-glucose (no lactate) media than in the glucose-free, 20 mM lactate media (p = 0.005, Student's T-test).
(TIF)

Figure S6 Normal human cells take up lactate and export catabolites. HMQC plots of HMEC cell lysate (**A**) and media (**B**) after 4.5 h incubation with 10 mM ^{13}C-lactate, showing evidence of labeled lactate (dark green "**L**") and glutamate (blue "**G**") peaks. 1H spectra of HUVEC cell lysate (bottom) and media (top) after 24 h treatment with 5 mM ^{13}C-lactate (**C**). The lysate spectrum shows peaks corresponding to lactate, indicating uptake; the media spectrum shows evidence of labeled lactate, alanine and glutamate.
(TIF)

Figure S7 Control NMR spectra for R3230Ac cell media alone or treated with no lactate + high or low CHC. ^{13}C spectrum of glucose-free, pyruvate-free, +glutamine (+10% FBS) DMEM used for all *in vitro* NMR experiments show low background levels of ubiquitous metabolites (**A**). ^{1}H (**B&C**) or ^{13}C (**D&E**) spectra of R3230Ac cell lysates (**B&C**) or media (**D&E**) incubated for 4 h with no labeled lactate, no glucose + 0.1 mM CHC (**B&D**) or 5 mM CHC (**C&E**), showing no labeled lactate.
(TIF)

Figure S8 ^{1}H NMR spectra of R3230Ac cell media treated with ^{13}C-lactate + CHC show evidence of exportation of some endogenous lactate. ^{1}H spectra of R3230Ac cell media incubated with 20 mM ^{13}C-lactate and 0.1 mM (**A&C**) or 5 mM (**B&D**) of CHC for 4 h (**A&B**) or 24 h (**C&D**) show an abundance of ^{13}C-lactate and incomplete inhibition of endogenous lactate (green "$\mathbf{L_{en}}$") exportation.
(TIF)

Acknowledgments

Katie Clark and Alina Boico helped with cell viability assays. Neal Bhutiani helped conduct metabolic assays. Mike Cook PhD conducted flow cytometry for all Annexin V/7-AAD experiments. Ken Young provided support for hypoxia chamber experiments. Doug Weitzel PhD performed MCT4 Western blots. LABC sections were acquired from a breast oncologist, Kimberly Blackwell MD (DUMC). Analysis of LABC H&E sections for tumor regions conducted by Joseph Geradts MD and Laura Hale MD PhD. Greg Palmer PhD assisted with statistical analysis and Figure formatting. The ^{14}C scintillation probe was provided to us by Robert Black PhD of Sicel Technologies Inc.

Author Contributions

Conceived and designed the experiments: KMK PMS RR HY JTC TS MWD. Performed the experiments: KMK PMS AR RR HY TS. Analyzed the data: KMK PMS AR RR HY TS MWD. Contributed reagents/materials/analysis tools: AR HY SP MWD. Wrote the paper: KMK TS MWD. Provided intellectual input and consultation during the study and during assembly of the manuscript: PS CDL JTC SP.

References

1. Duh S-H, Cook JD (2005) LABORATORY REFERENCE RANGE VALUES. MD, USA: University of Maryland School of Medicine. APP17 APP17. 17 p.
2. Walenta S, Wetterling M, Lehrke M, Schwickert G, Sundfor K, et al. (2000) High lactate levels predict likelihood of metastases, tumor recurrence, and restricted patient survival in human cervical cancers. Cancer Res 60: 916–921.
3. Warburg O (1930) The metabolism of tumors. Arnold Constable London, UK.
4. Warburg OH, Dickens F, Kaiser-Wilhelm-Institut fuÎr Biologie. (1930) The Metabolism of tumours : investigations from the Kaiser Wilhelm Institute for Biology, Berlin-Dahlem. London: Constable. xxviii, 327 p., 325 leaves of plates p.
5. Warburg OH, Kaiser-Wilhelm-Institut fuÎr Biologie. (1926) Ãœber den Stoffwechsel der Tumoren : Arbeiten aus dem Kaiser Wilheim-Institut fÃ¼r Biologie, Berlin-Dahlem. Berlin: Julius Springer.263 p. p.
6. Hanahan D, Weinberg RA (2011) Hallmarks of cancer: the next generation. Cell 144: 646–674.
7. Gatenby RA, Gillies RJ (2004) Why do cancers have high aerobic glycolysis? Nat Rev Cancer 4: 891–899.
8. Gatenby RA, Smallbone K, Maini PK, Rose F, Averill J, et al. (2007) Cellular adaptations to hypoxia and acidosis during somatic evolution of breast cancer. Br J Cancer 97: 646–653.
9. Dang CV, Semenza GL (1999) Oncogenic alterations of metabolism. Trends Biochem Sci 24: 68–72.
10. Schroeder T, Yuan H, Viglianti BL, Peltz C, Asopa S, et al. (2005) Spatial heterogeneity and oxygen dependence of glucose consumption in R3230Ac and fibrosarcomas of the Fischer 344 rat. Cancer Res 65: 5163–5171.
11. Brizel DM, Scully SP, Harrelson JM, Layfield LJ, Bean JM, et al. (1996) Tumor oxygenation predicts for the likelihood of distant metastases in human soft tissue sarcoma. Cancer Res 56: 941–943.
12. Brizel DM, Sibley GS, Prosnitz LR, Scher RL, Dewhirst MW (1997) Tumor hypoxia adversely affects the prognosis of carcinoma of the head and neck. Int J Radiat Oncol Biol Phys 38: 285–289.
13. Chen JL, Lucas JE, Schroeder T, Mori S, Wu J, et al. (2008) The genomic analysis of lactic acidosis and acidosis response in human cancers. PLoS Genet 4: e1000293.
14. Halestrap AP, Meredith D (2004) The SLC16 gene family-from monocarboxylate transporters (MCTs) to aromatic amino acid transporters and beyond. Pflugers Arch 447: 619–628.
15. Halestrap AP, Price NT (1999) The proton-linked monocarboxylate transporter (MCT) family: structure, function and regulation. Biochem J 343 Pt 2: 281–299.
16. Kennedy KM, Dewhirst MW (2010) Tumor metabolism of lactate: the influence and therapeutic potential for MCT and CD147 regulation. Future Oncol 6: 127–148.
17. Sonveaux P, Vegran F, Schroeder T, Wergin MC, Verrax J, et al. (2008) Targeting lactate-fueled respiration selectively kills hypoxic tumor cells in mice. J Clin Invest 118: 3930–3942.
18. Hussien R, Brooks GA Mitochondrial and plasma membrane lactate transporter and lactate dehydrogenase isoform expression in breast cancer cell lines. Physiol Genomics 43: 255–264.
19. Manning Fox JE, Meredith D, Halestrap AP (2000) Characterisation of human monocarboxylate transporter 4 substantiates its role in lactic acid efflux from skeletal muscle. J Physiol 529 Pt 2: 285–293.

20. Fang J, Quinones QJ, Holman TL, Morowitz MJ, Wang Q, et al. (2006) The H+-linked monocarboxylate transporter (MCT1/SLC16A1): a potential therapeutic target for high-risk neuroblastoma. Mol Pharmacol 70: 2108–2115.
21. Peltz C, Schroeder T, Dewhirst MW (2005) Monitoring metabolite gradients in the blood, liver, and tumor after induced hyperglycemia in rats with R3230 flank tumors using microdialysis and bioluminescence imaging. Adv Exp Med Biol 566: 343–348.
22. Walenta S, Snyder S, Haroon ZA, Braun RD, Amin K, et al. (2001) Tissue gradients of energy metabolites mirror oxygen tension gradients in a rat mammary carcinoma model. Int J Radiat Oncol Biol Phys 51: 840–848.
23. Neve RM, Chin K, Fridlyand J, Yeh J, Baehner FL, et al. (2006) A collection of breast cancer cell lines for the study of functionally distinct cancer subtypes. Cancer Cell 10: 515–527.
24. Ibrahim E, Al-Gahmi AM, Zeenelin AA, Zekri JM, Elkhodary TR, et al. (2009) Basal vs. luminal A breast cancer subtypes: a matched case-control study using estrogen receptor, progesterone receptor, and HER-2 as surrogate markers. Med Oncol 26: 372–378.
25. Rouzier R, Perou CM, Symmans WF, Ibrahim N, Cristofanilli M, et al. (2005) Breast cancer molecular subtypes respond differently to preoperative chemotherapy. Clin Cancer Res 11: 5678–5685.
26. Asada K, Miyamoto K, Fukutomi T, Tsuda H, Yagi Y, et al. (2003) Reduced expression of GNA11 and silencing of MCT1 in human breast cancers. Oncology 64: 380–388.
27. Komarova EA, Zelnick CR, Chin D, Zeremski M, Gleiberman AS, et al. (1997) Intracellular localization of p53 tumor suppressor protein in gamma-irradiated cells is cell cycle regulated and determined by the nucleus. Cancer Res 57: 5217–5220.
28. Filyak OS, Stoika RS (2005) Comparative study of p53 expression in human carcinoma cell lines A549 and MCF7 under anticancer drug treatment. Ukr Biokhim Zh 77: 136–140.
29. Kellen JA, Mirakian A (1996) The effect of toremifene on the expression of genes in a rat mammary adenocarcinoma. In Vivo 10: 511–513.
30. Hui L, Zheng Y, Yan Y, Bargonetti J, Foster DA (2006) Mutant p53 in MDA-MB-231 breast cancer cells is stabilized by elevated phospholipase D activity and contributes to survival signals generated by phospholipase D. Oncogene 25: 7305–7310.
31. Katayose D, Gudas J, Nguyen H, Srivastava S, Cowan KH, et al. (1995) Cytotoxic effects of adenovirus-mediated wild-type p53 protein expression in normal and tumor mammary epithelial cells. Clin Cancer Res 1: 889–897.
32. Maddocks OD, Vousden KH (2011) Metabolic regulation by p53. J Mol Med (Berl) 89: 237–245.
33. Boidot R, Vegran F, Meulle A, Le Breton A, Dessy C, et al. Regulation of monocarboxylate transporter MCT1 expression by p53 mediates inward and outward lactate fluxes in tumors. Cancer Res 72: 939–948.
34. Brizel DM, Schroeder T, Scher RL, Walenta S, Clough RW, et al. (2001) Elevated tumor lactate concentrations predict for an increased risk of metastases in head-and-neck cancer. Int J Radiat Oncol Biol Phys 51: 349–353.
35. Walenta S, Chau TV, Schroeder T, Lehr HA, Kunz-Schughart LA, et al. (2003) Metabolic classification of human rectal adenocarcinomas: a novel guideline for clinical oncologists? J Cancer Res Clin Oncol 129: 321–326.
36. Mueller-Klieser W, Walenta S (1993) Geographical mapping of metabolites in biological tissue with quantitative bioluminescence and single photon imaging. Histochem J 25: 407–420.
37. Schwickert G, Walenta S, Mueller-Klieser W (1996) Mapping and quantification of biomolecules in tumor biopsies using bioluminescence. Experientia 52: 460–463.
38. Walenta S, Salameh A, Lyng H, Evensen JF, Mitze M, et al. (1997) Correlation of high lactate levels in head and neck tumors with incidence of metastasis. Am J Pathol 150: 409–415.
39. Walenta S, Schroeder T, Mueller-Klieser W (2004) Lactate in solid malignant tumors: potential basis of a metabolic classification in clinical oncology. Curr Med Chem 11: 2195–2204.
40. Yokota H, Guo J, Matoba M, Higashi K, Tonami H, et al. (2007) Lactate, choline, and creatine levels measured by vitro 1H-MRS as prognostic parameters in patients with non-small-cell lung cancer. J Magn Reson Imaging 25: 992–999.
41. Kumar V, Abbas AK, Fausto N (2005) Robbins and Cotran Pathological Basis of Disease. Philadelphia, PA: Elsevier Saunders.
42. Blackburn RV, Spitz DR, Liu X, Galoforo SS, Sim JE, et al. (1999) Metabolic oxidative stress activates signal transduction and gene expression during glucose deprivation in human tumor cells. Free Radic Biol Med 26: 419–430.
43. Ahmad IM, Aykin-Burns N, Sim JE, Walsh SA, Higashikubo R, et al. (2005) Mitochondrial O2*- and H2O2 mediate glucose deprivation-induced stress in human cancer cells. J Biol Chem 280: 4254–4263.
44. Simons AL, Mattson DM, Dornfeld K, Spitz DR (2009) Glucose deprivation-induced metabolic oxidative stress and cancer therapy. J Cancer Res Ther 5 Suppl 1: S2–6.
45. Spitz DR, Sim JE, Ridnour LA, Galoforo SS, Lee YJ (2000) Glucose deprivation-induced oxidative stress in human tumor cells. A fundamental defect in metabolism? Ann N Y Acad Sci 899: 349–362.
46. Schwickert G, Walenta S, Sundfor K, Rofstad EK, Mueller-Klieser W (1995) Correlation of high lactate levels in human cervical cancer with incidence of metastasis. Cancer Res 55: 4757–4759.
47. Walenta S, Mueller-Klieser WF (2004) Lactate: mirror and motor of tumor malignancy. Semin Radiat Oncol 14: 267–274.
48. Pinheiro C, Albergaria A, Paredes J, Sousa B, Dufloth R, et al. Monocarboxylate transporter 1 is up-regulated in basal-like breast carcinoma. Histopathology 56: 860–867.
49. Pinheiro C, Longatto-Filho A, Ferreira L, Pereira SM, Etlinger D, et al. (2008) Increasing expression of monocarboxylate transporters 1 and 4 along progression to invasive cervical carcinoma. Int J Gynecol Pathol 27: 568–574.
50. Pinheiro C, Longatto-Filho A, Scapulatempo C, Ferreira L, Martins S, et al. (2008) Increased expression of monocarboxylate transporters 1, 2, and 4 in colorectal carcinomas. Virchows Arch 452: 139–146.
51. Pinheiro C, Reis RM, Ricardo S, Longatto-Filho A, Schmitt F, et al. Expression of monocarboxylate transporters 1, 2, and 4 in human tumours and their association with CD147 and CD44. J Biomed Biotechnol 2010: 427694.
52. Dimmer KS, Friedrich B, Lang F, Deitmer JW, Broer S (2000) The low-affinity monocarboxylate transporter MCT4 is adapted to the export of lactate in highly glycolytic cells. Biochem J 350 Pt 1: 219–227.
53. Bonen A, Miskovic D, Tonouchi M, Lemieux K, Wilson MC, et al. (2000) Abundance and subcellular distribution of MCT1 and MCT4 in heart and fast-twitch skeletal muscles. Am J Physiol Endocrinol Metab 278: E1067–1077.
54. Ullah MS, Davies AJ, Halestrap AP (2006) The plasma membrane lactate transporter MCT4, but not MCT1, is up-regulated by hypoxia through a HIF-1alpha-dependent mechanism. J Biol Chem 281: 9030–9037.
55. Hilf R, Murant RS, Narayanan U, Gibson SL (1986) Relationship of mitochondrial function and cellular adenosine triphosphate levels to hematoporphyrin derivative-induced photosensitization in R3230AC mammary tumors. Cancer Res 46: 211–217.
56. Sauer LA, Dauchy RT (1994) Lactate release and uptake in hepatoma 7288CTC perfused in situ with L-[(U)-14C]lactate or D-[(U)-14C]glucose. Metabolism 43: 1488–1497.
57. Sauer LA, Dauchy RT (1986) In vivo lactate production and utilization by Jensen sarcoma and Morris hepatoma 7288CTC. Cancer Res 46: 689–693.
58. Guillaumond F, Leca J, Olivares O, Lavaut MN, Vidal N, et al. (2013) Strengthened glycolysis under hypoxia supports tumor symbiosis and hexosamine biosynthesis in pancreatic adenocarcinoma. Proc Natl Acad Sci U S A 110: 3919–3924.
59. Bouzier AK, Voisin P, Goodwin R, Canioni P, Merle M (1998) Glucose and lactate metabolism in C6 glioma cells: evidence for the preferential utilization of lactate for cell oxidative metabolism. Dev Neurosci 20: 331–338.
60. Bouzier-Sore AK, Canioni P, Merle M (2001) Effect of exogenous lactate on rat glioma metabolism. J Neurosci Res 65: 543–548.
61. Manning JE, Katz LM, Brownstein MR, Pearce LB, Gawryl MS, et al. (2000) Bovine hemoglobin-based oxygen carrier (HBOC-201) for resuscitation of uncontrolled, exsanguinating liver injury in swine. Carolina Resuscitation Research Group. Shock 13: 152–159.
62. Halestrap AP (2008) Inhibiting lactate oxidation in tumor cells. eLetters: The Journal of Clinical Investigation.
63. Halestrap AP (1975) The mitochondrial pyruvate carrier. Kinetics and specificity for substrates and inhibitors. Biochem J 148: 85–96.
64. Sonveaux P, Copetti T, De Saedeleer CJ, Vegran F, Verrax J, et al. (2012) Targeting the lactate transporter MCT1 in endothelial cells inhibits lactate-induced HIF-1 activation and tumor angiogenesis. PLoS ONE 7: e33418.
65. Kumar A, Kant S, Singh SM (2013) alpha-Cyano-4-hydroxycinnamate induces apoptosis in Dalton's lymphoma cells: role of altered cell survival-regulatory mechanisms. Anticancer Drugs 24: 158–171.
66. Zielke HR, Sumbilla CM, Sevdalian DA, Hawkins RL, Ozand PT (1980) Lactate: a major product of glutamine metabolism by human diploid fibroblasts. J Cell Physiol 104: 433–441.
67. Reitzer LJ, Wice BM, Kennell D (1979) Evidence that glutamine, not sugar, is the major energy source for cultured HeLa cells. J Biol Chem 254: 2669–2676.
68. Marin-Hernandez A, Gallardo-Perez JC, Rodriguez-Enriquez S, Encalada R, Moreno-Sanchez R, et al. (2011) Modeling cancer glycolysis. Biochim Biophys Acta 1807: 755–767.
69. Rasschaert J, Malaisse WJ (2001) Glycogen accumulation in cultured tumoral or normal pancreatic islet and acinar cells. Int J Mol Med 8: 63–65.
70. Favaro E, Bensaad K, Chong MG, Tennant DA, Ferguson DJ, et al. (2012) Glucose utilization via glycogen phosphorylase sustains proliferation and prevents premature senescence in cancer cells. Cell Metab 16: 751–764.
71. Porporato PE, Dhup S, Dadhich RK, Copetti T, Sonveaux P Anticancer targets in the glycolytic metabolism of tumors: a comprehensive review. Front Pharmacol 2: 49.
72. Herrero P, Dence CS, Coggan AR, Kisrieva-Ware Z, Eisenbeis P, et al. (2007) L-3-11C-lactate as a PET tracer of myocardial lactate metabolism: a feasibility study. J Nucl Med 48: 2046–2055.
73. Felig P, Pozefsky T, Marliss E, Cahill GF, Jr. (1970) Alanine: key role in gluconeogenesis. Science 167: 1003–1004.
74. Vaupel P (2004) Tumor microenvironmental physiology and its implications for radiation oncology. Semin Radiat Oncol 14: 198–206.
75. De Saedeleer CJ, Copetti T, Porporato PE, Verrax J, Feron O, et al. (2012) Lactate activates HIF-1 in oxidative but not in Warburg-phenotype human tumor cells. PLoS ONE 7: e46571.
76. Pavlides S, Tsirigos A, Vera I, Flomenberg N, Frank PG, et al. Transcriptional evidence for the "Reverse Warburg Effect" in human breast cancer tumor stroma and metastasis: similarities with oxidative stress, inflammation,

Alzheimer's disease, and "Neuron-Glia Metabolic Coupling". Aging (Albany NY) 2: 185–199.
77. Pavlides S, Vera I, Gandara R, Sneddon S, Pestell RG, et al. Warburg meets autophagy: cancer-associated fibroblasts accelerate tumor growth and metastasis via oxidative stress, mitophagy, and aerobic glycolysis. Antioxid Redox Signal 16: 1264–1284.
78. Pavlides S, Whitaker-Menezes D, Castello-Cros R, Flomenberg N, Witkiewicz AK, et al. (2009) The reverse Warburg effect: aerobic glycolysis in cancer associated fibroblasts and the tumor stroma. Cell Cycle 8: 3984–4001.
79. Bonuccelli G, Whitaker-Menezes D, Castello-Cros R, Pavlides S, Pestell RG, et al. The reverse Warburg effect: glycolysis inhibitors prevent the tumor promoting effects of caveolin-1 deficient cancer associated fibroblasts. Cell Cycle 9: 1960–1971.
80. Birsoy K, Wang T, Possemato R, Yilmaz OH, Koch CE, et al. (2013) MCT1-mediated transport of a toxic molecule is an effective strategy for targeting glycolytic tumors. Nat Genet 45: 104–108.
81. Dhup S, Dadhich RK, Porporato PE, Sonveaux P Multiple biological activities of lactic acid in cancer: influences on tumor growth, angiogenesis and metastasis. Curr Pharm Des 18: 1319–1330.
82. Diers AR, Broniowska KA, Chang CF, Hogg N Pyruvate fuels mitochondrial respiration and proliferation of breast cancer cells: effect of monocarboxylate transporter inhibition. Biochem J 444: 561–571.
83. Mikkelsen ME, Miltiades AN, Gaieski DF, Goyal M, Fuchs BD, et al. (2009) Serum lactate is associated with mortality in severe sepsis independent of organ failure and shock. Crit Care Med 37: 1670–1677.
84. Genton B, Berger JP (1990) Cerebrospinal fluid lactate in 78 cases of adult meningitis. Intensive Care Med 16: 196–200.
85. Kim HS, Masko EM, Poulton SL, Kennedy KM, Pizzo SV, et al. (2012) Carbohydrate restriction and lactate transporter inhibition in a mouse xenograft model of human prostate cancer. BJU Int 110: 1062–1069.
86. Yaligar J, Thakur SB, Bokacheva L, Carlin S, Thaler HT, et al. Lactate MRSI and DCE MRI as surrogate markers of prostate tumor aggressiveness. NMR Biomed 25: 113–122.
87. Oshida M, Uno K, Suzuki M, Nagashima T, Hashimoto H, et al. (1998) Predicting the prognoses of breast carcinoma patients with positron emission tomography using 2-deoxy-2-fluoro[18F]-D-glucose. Cancer 82: 2227–2234.
88. Richardson RA, Dewhirst MW (2003) The effect of nicotinamide & hyperoxic gases on blood glucose. Adv Exp Med Biol 510: 375–378.

The combination of theophylline and endothelin receptor antagonism improves exercise performance of rats under simulated high altitude

Daniel R. Radiloff, Yulin Zhao, Alina Boico, Chan Wu, Siqing Shan, Gregory Palmer, Karyn Hamilton, David Irwin, Gabi Hanna, Claude A. Piantadosi and Thies Schroeder

J Appl Physiol 113:1243-1252, 2012. First published 16 August 2012;
doi:10.1152/japplphysiol.01622.2011

Journal of Applied Physiology publishes original papers that deal with diverse areas of research in applied physiology, especially those papers emphasizing adaptive and integrative mechanisms. It is published 12 times a year (monthly) by the American Physiological Society, 9650 Rockville Pike, Bethesda MD 20814-3991. ISSN: 0363-6143, ESSN: 1522-1563. Visit our website at http://www.the-aps.org/.

J Appl Physiol 113: 1243–1252, 2012.
First published August 16, 2012; doi:10.1152/japplphysiol.01622.2011.

The combination of theophylline and endothelin receptor antagonism improves exercise performance of rats under simulated high altitude

Daniel R. Radiloff,[1] Yulin Zhao,[1] Alina Boico,[1] Chan Wu,[1] Siqing Shan,[1] Gregory Palmer,[1] Karyn Hamilton,[2] David Irwin,[3] Gabi Hanna,[1] Claude A. Piantadosi,[4] and Thies Schroeder[1]

[1]*Department of Radiation Oncology, Duke University Medical Center, Durham, North Carolina;* [2]*Department of Health and Exercise Science, Colorado State University, Fort Collins, Colorado;* [3]*Department of Cardiology, University of Colorado Denver, Aurora, Colorado; and* [4]*Division of Pulmonary Medicine, Department of Medicine, Duke University Medical Center, Durham, North Carolina*

Submitted 30 December 2011; accepted in final form 10 August 2012

Radiloff DR, Zhao Y, Boico A, Wu C, Shan S, Palmer G, Hamilton K, Irwin D, Hanna G, Piantadosi CA, Schroeder T. The combination of theophylline and endothelin receptor antagonism improves exercise performance of rats under simulated high altitude. *J Appl Physiol* 113: 1243–1252, 2012. First published August 16, 2012; doi:10.1152/japplphysiol.01622.2011.—Decreased physical performance is a well-known consequence of rapid ascent to high altitude. Hypoxic pulmonary vasoconstriction (HPV) potentially limits cardiac output and systemic blood flow, thus preventing successful adaptation to rapid ascent. We hypothesized that pharmacological enhancement of the heart rate with theophylline, combined with reversal of HPV via endothelin blockade, could increase exercise performance at high altitude. Female Sprague-Dawley rats were treated with combinations of *1*) theophylline, *2*) the endothelin receptor antagonists sitaxsentan/ambrisentan, and/or *3*) phosphodiesterase-5 inhibitor sildenafil and exposed to either a simulated high altitude (4,267 m) or 12% oxygen. Exercise capacity, peripheral blood flow, hemodynamics, and pulmonary leak were examined. Combination treatment with theophylline and endothelin blockade, but not with the respective single compounds, significantly prolonged run-to-fatigue time under simulated high altitude. No such efficacy was found when theophylline was combined with sildenafil. Neither theophylline nor sitaxsentan or their combination influenced breathing rates and hemoglobin oxygen saturation. Whereas under hypoxia, theophylline significantly increased muscular blood flow, and sitaxsentan increased tissue oxygenation, the combination improved both parameters but in a reduced manner. Under hypoxia, the combination treatment but not the single compounds significantly enhanced pulmonary arterial pressure compared with controls (13.1 ± 6.3 vs. 11.9 ± 5.2 mmHg), whereas mean arterial pressure remained unaffected. Pulmonary wet-to-dry weight ratios were unaffected by combination treatment. We conclude that concomitant dosing with a cardiac stimulant and endothelin antagonist can partially reverse loss of physical performance capacity under hypobaric hypoxia, independent from improving blood oxygen saturation.

blood pressure homeostasis; hypoxia; pulmonary vasoconstriction

ACUTE EXPOSURE TO ALTITUDES above 1,500 m decreases human physical performance capacity, and the primary factor contributing to this decrement is reduced oxygen availability due to decreased atmospheric pressure (22). Further complications arise from hypoxic pulmonary vasoconstriction (HPV) and peripheral hypoxic vasodilatation—the most plausible cause of orthostatic challenge at high altitudes (22, 36, 39, 48). Medications that have shown promise for treating high-altitude-induced performance loss include xanthene derivatives (23), corticoids (21), carbonic anhydrase inhibitors (32), beta adrenergic receptor blockers (49), and perhaps receiving the most attention, pulmonary vasodilators (29, 31, 39, 40).

The circulatory system responds paradoxically to acute high-altitude exposure. In the lung, alveolar hypoxia leads to pulmonary vasoconstriction, whereas systemic hypoxia induces vasodilatation in most other vascular beds in the body (1), making the ascent to high altitude a unique challenge to blood pressure homeostasis (9, 48). Whereas cardiac activity increases in response to exposure to high altitude, probably in response to systemic hypotension, there is evidence that the increased pulmonary vascular resistance resulting from HPV has the potential to limit the amount of blood that flows through the lung and can thus be transported to the periphery (39). On the other hand, endothelin receptor blockers have shown promise to block HPV (19, 39). We hypothesized that the concomitant application of a cardiostimulant drug, such as theophylline, and an endothelin receptor antagonist (ERA) would improve the mammalian physiological response to acute hypobaric hypoxia more effectively than either drug class alone, independent from blood oxygen content. Following our hypothesis, pharmacological support of the favorable adaptive responses to hypoxia—including cardiac stimulation—while simultaneously counteracting HPV, would lead to enhanced blood flow and enhanced oxygen delivery to hypoxic tissue, resulting in improved physical performance under diminished oxygen levels. To test this hypothesis, we treated rats with the cardiac stimulant theophylline, the endothelin-targeting pulmonary vasodilators sitaxsentan or ambrisentan, or a combination of theophylline with either sitaxsentan or ambrisentan; exposed them to acute hypobaric and normobaric hypoxia; and subsequently determined the running time to fatigue, voluntary running volume, hemodynamic and tissue oxygenation parameters, and pulmonary vascular leak. To test whether phosphodiesterase-5 (PDE5) inhibition can achieve the same effect as endothelin blockade, we also tested whether sildenafil, if combined with theophylline, would enhance hypobaric exercise performance of rats.

MATERIALS AND METHODS

Animals

All animal experiments were performed in accordance with Duke University and Colorado State University Institutional Animal Care and Use Committee-approved protocols. Sprague-Dawley rats, aged at 9–12 wk (200–250 g), were used for all experiments. Female rats were used for run-to-fatigue experiments, anesthetized studies, and pulmonary leak experiments. Male rats were used for voluntary running experiments.

Address for reprint requests and other correspondence: T. Schroeder, Dept. of Radiation Oncology, Duke Univ. Medical Center, Durham, NC 27710 (e-mail: thies.schroeder@duke.edu).

Drugs and Dosing Regimen

Rats were divided randomly into six groups with all dosing done intraperitoneally (ip): *1*) vehicle control; *2*) theophylline (15–30 mg/kg); *3*) ERAs (sitaxsentan at 1 mg/kg or ambrisentan at 0.1 mg/kg); *4*) the combination of theophylline and ERA; *5*) sildenafil (4.5 mg/kg); and *6*) the combination of theophylline and sildenafil. Theophylline was delivered in alkaline saline adjusted to pH 10, whereas sitaxsentan and ambrisentan were injected in a 0.9% NaCl solution (saline) ip. Sildenafil was dissolved in DMSO and coinjected with theophylline or alkaline saline (vehicle control).

Drug doses for theophylline, sitaxsentan, and ambrisentan were chosen to be within the range of equivalent doses that have been used previously in humans (14, 24, 26) as follows: *1*) sitaxsentan at 1 mg/kg in rats, ~11.3 mg/70 kg in humans; *2*) high-dose theophylline at 30 mg/kg in rats, ~338.7 mg/70 kg in humans; low-dose theophylline at 15 mg/kg in rats, ~169.4 mg/70 kg in humans; and *3*) ambrisentan at 0.1 mg/kg in rats, ~1.1 mg/70 kg in humans (48a). Sildenafil was dosed within the range of what has been used in rats and humans in the past (4.5 mg/kg in rats, ~51 g/70 kg in humans; recommended dose, 25–100 mg/day) (2, 33, 43). Theophylline and sildenafil were obtained from Sigma (St. Louis, MO). Sitaxsentan and ambrisentan were produced by the Duke University Small Molecule Synthesis Facility (Durham, NC).

Exercise Models

Run-to-fatigue measurements. Female Sprague-Dawley rats were used for the run-to-fatigue experiments because of the high risk of injury associated with male reproductive anatomy on a motorized wheel. To determine a maximal physical performance in rats exposed to simulated altitude, a run-to-fatigue protocol was developed. Rats were habituated to the motorized wheels (Lafayette Instrument, Lafayette, IN) for 10 min/day, starting at 3 m/min for 3 days, followed by 6 m/min for 7 days. This protocol was specifically established to provide the rats with sufficient time to become accustomed to running in the motorized wheels yet to avoid physical training effects. Rats were subjected to an altitude equivalent of 4,267 m (14,000 ft; barometric pressure, ~440 mmHg) in the Duke University hypobaric chamber, creating an equivalent of ~12% oxygen under hypobaric hypoxia. Running time to fatigue was determined by the following protocol: 10 min at 6 m/min, 80 min at 9 m/min, and 30 min at 12 m/min. The experiment was terminated after completion of this sequence to avoid injury associated with forced running over a long time. Preliminary experiments showed that this protocol was sufficient to induce fatigue under simulated high altitude in most of the untreated rats. Fatigue was determined by hind-limb sliding, skidding, and sideways movement or flipping in the wheel and verified by observation for locomotion after being placed on a level surface for 30 s. Fatigued animals showed lack of motivation for voluntary locomotion, often recovering lying on their bellies or on their sides. Any animal that showed signs of injury during the experiment was removed from the wheels immediately. The study protocol is outlined in Fig. 1*A*.

Two trials were carried out to test the efficacy of theophylline combined with ERAs in improving the exercise capacity of rats running at simulated high altitude. In the first trial, theophylline was combined with sitaxsentan and in the second trial, combined with ambrisentan. In a third trial, theophylline was combined with sildenafil.

Voluntary Physical Activity Measurements. To determine voluntary physical activity, male Sprague-Dawley rats were given free access to voluntary physical activity wheels (Mini Mitter/Philips Respironics, Bend, OR) for a minimum of 7 days, and activity was recorded with VitalView data acquisition software (Mini Mitter/Philips Respironics). Following acclimation to the activity wheels, rats were matched for baseline (normoxic) voluntary running volume, such that each pharmacological treatment group (or vehicle control group) had the same average normoxic running volume. Rats were then subjected to an altitude equivalent of 4,267 m for 48 h in the Colorado State University hypobaric chamber. Study drugs were injected immediately before ascent to simulated altitude and once again 24 h later while maintaining the 4,267 altitude equivalent. Voluntary physical activity (running distance) was measured continuously during the 48-h hypobaric hypoxic exposure. Two studies were carried out to test the effects of combined dosing with theophylline/sitaxsentan and theophylline/ambrisentan on the voluntary physical activity in rats exposed to simulated high altitude. The outline of the study schedule is given in Fig. 1*B*.

Hemodynamic Measurements and Breathing Rate

Rats were anesthetized with ketamine/xylazine (80 mg/kg; 8 mg/kg), and body temperature was maintained with a water-circulating heating pad. Animals were placed on their backs, and indwelling catheters were placed in the carotid polyethylene catheter (PE-50) artery for blood pressure measurements as described previously (30). Blood pressures were recorded with an APT300 arterial pressure transducer (Hugo Sachs Elektronik, Germany) interfaced with LabChart software through an ADI bridge amplifier and PowerLab module (ADInstruments, Australia). A pulse oximetry foot clip was applied to the left hind limb of the animal (MouseOx, Starr Life Sciences, Oakmont, PA) to record arterial hemoglobin oxygen saturation (HbO_2) and heart rate. The experimental protocol consisted of 15 min at normoxia (21% oxygen, 79% nitrogen), followed by drug injection and after 15 more minutes, by inspired hypoxia (12%, balance nitrogen) for at least 30 more minutes. Breathing rate was measured by counting chest movements over successive time periods: directly before drug injection (minutes 10–15), directly before onset of hypoxia (minutes 25–30), and under hypoxia (minutes 50–55).

Muscular Blood Flow and Tissue Oxygen Partial Pressure

To enable proper probe placement, the skin was removed from the hind limb to expose the surface of the vastus lateralis muscle. For tissue oxygen partial pressure (pO_2) measurements, a needle-encased optical pO_2 probe (Oxford Optronix, Oxford, UK) was placed in the hind-limb muscle, and data were acquired with LabChart interfaced with the PowerLab module. Acceptability of needle placement of the pO_2 needle was tested by subjecting the rat to an initial hypoxic episode of 15 min of breathing a 12% oxygen gas mixture (hypoxia), followed by 10 min of breathing room air before dosing with drugs or controls (Fig. 1*D*). The measurement was accepted when inspired hypoxia was inducing a change in tissue pO_2. A laser Doppler analyzer probe (OxyFlow, Oxford Optronix) was placed perpendicular to the surface directly onto the muscle to record peripheral blood flow. Flow values are arbitrary [blood perfusion units (BPU)] and are normalized to the baseline at time of injection.

Pulmonary Vascular Leak Measurements

After injection of study drugs, animals were exposed to a simulated altitude of 4,267 m and were either subjected to the run-to-fatigue protocol or remained unchallenged on nonmoving wheels for 120 min. Immediately after return to normobaria, animals were killed, and lungs were removed and weighed on an analytical scale. Lungs were subsequently transferred to an oven and dried at 37°C until a stable weight was achieved. As a separate sea-level control group, wet-to-dry weights were obtained from one set of unexercised animals, which remained under normobaric conditions ($n = 10$, all groups).

Data Analysis and Statistics

Run-to-fatigue data were analyzed using Kaplan-Meier plotting and log rank testing of differences among groups. Except for breathing rates, differences in hemodynamic/tissue oxygenation parameters among treatment groups were analyzed from averaged individual

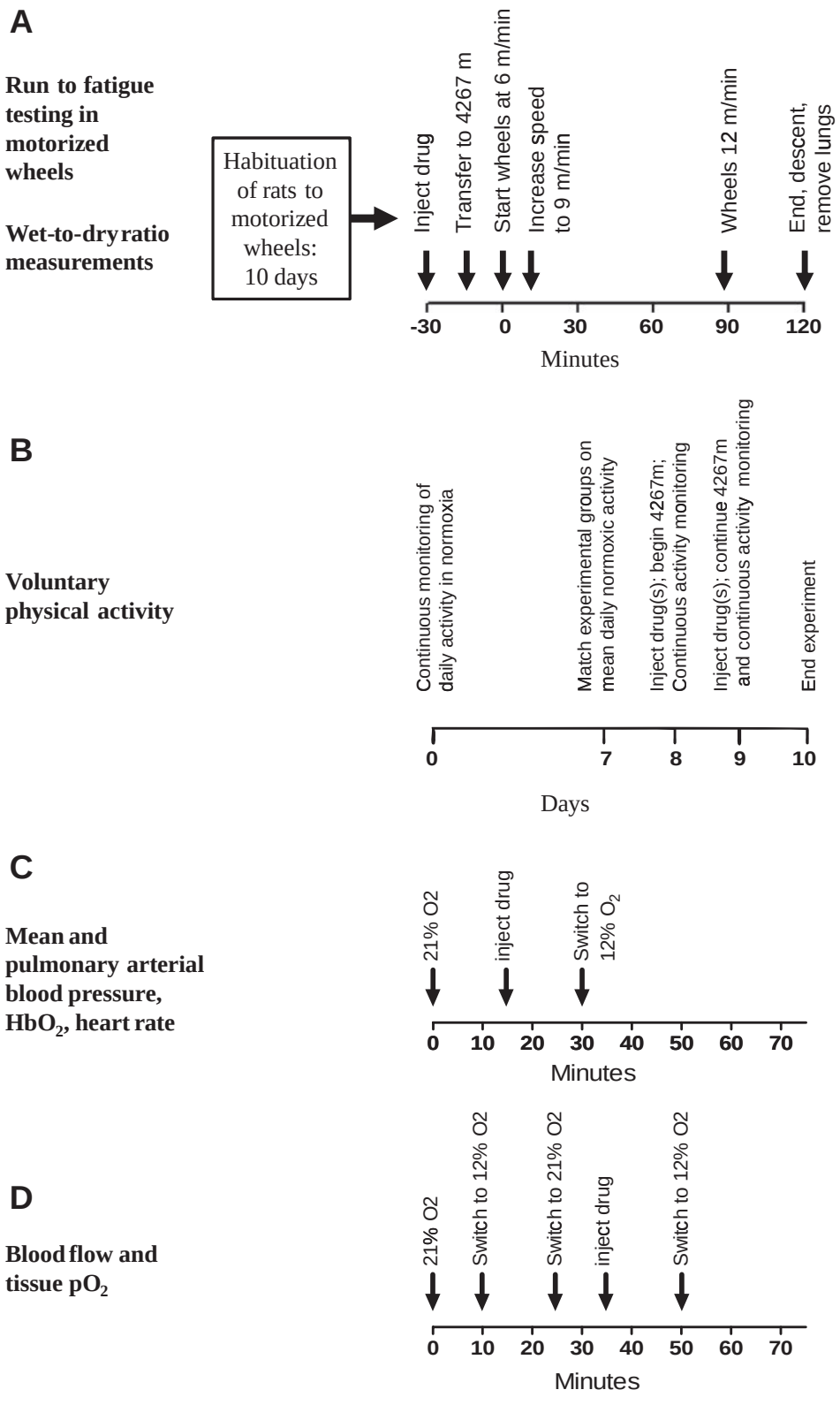

Fig. 1. Experimental design of (*A*) run-to-fatigue tests, wet-to-dry weight measurements on rat lungs; (*B*) voluntary physical activity, (*C*) hemodynamic studies; and (*D*) blood flow and tissue oxygen partial pressure (pO_2).

measurements during 5 min before injection, during 5 min before onset of hypoxia, and between 30 and 40 min postinjection (under hypoxia) using the *t*-test. Changes in hemodynamic parameters compared with the individual baseline were measured using the paired *t*-test throughout. Differences among treatment groups in wet-to-dry ratios (WDR) of lungs were analyzed with the use of the *t*-test. Data are expressed as mean ± SE unless otherwise indicated. All analyses were done using GraphPad Prism software (GraphPad Software, La Jolla, CA). Statistical tests were corrected for multiple comparisons using the false discovery rate method (8). This approach controls the false discovery rate, as opposed to the family error rate, and was applied to all *P* values within a given endpoint (e.g., all intra- and

intergroup tests for changes in heart rate). The false discovery rate threshold was set at 0.05. For all tests, the raw *P* values are reported but are described as significant only if they meet this false discovery threshold.

RESULTS

Run to Fatigue

In the theophylline/sitaxsentan trial, the median run-to-fatigue time in the control group was 97 min. No median run-to-fatigue time could be identified in the other treatment groups, because more than one-half of the animals were still running when the experiments were terminated (Fig. 2*A*). The group treated with the combination of theophylline and sitaxsentan ran significantly longer than the control (log rank test, $P < 0.005$), whereas the groups treated with theophylline or sitaxsentan individually did not (log rank, $P = 0.0829$ and 0.1864, respectively). In the theophylline/ambrisentan trial, the median run-to-fatigue time in the control group was 52.5 min, theophylline alone was 113 min [comparison with control (log rank, $P = 0.083$)], and ambrisentan alone was 93 min. In the combination group, more than one-half of the animals were still running when the experiment was terminated (Fig. 2*B*). The only treatment that significantly increased running time was the combination of theophylline and ambrisentan (log rank, $P < 0.005$), whereas treatment with the single drugs did not increase the run-to-fatigue time (log rank theophylline, $P = 0.0527$; ambrisentan, $P = 0.3997$; Fig. 2, *A* and *B*). In the theophylline/sildenafil trial, mean run time in controls was 40 min, theophylline was 115 min, and sildenafil was 79 min, and the mean run-to-fatigue time after combination treatment remained undefined because more than one-half of the animals were still running at the end of the experiment. None of the treatment groups ran longer than controls.

Voluntary physical activity. Acute exposure to simulated altitude decreased voluntary running volume by ~60–90%

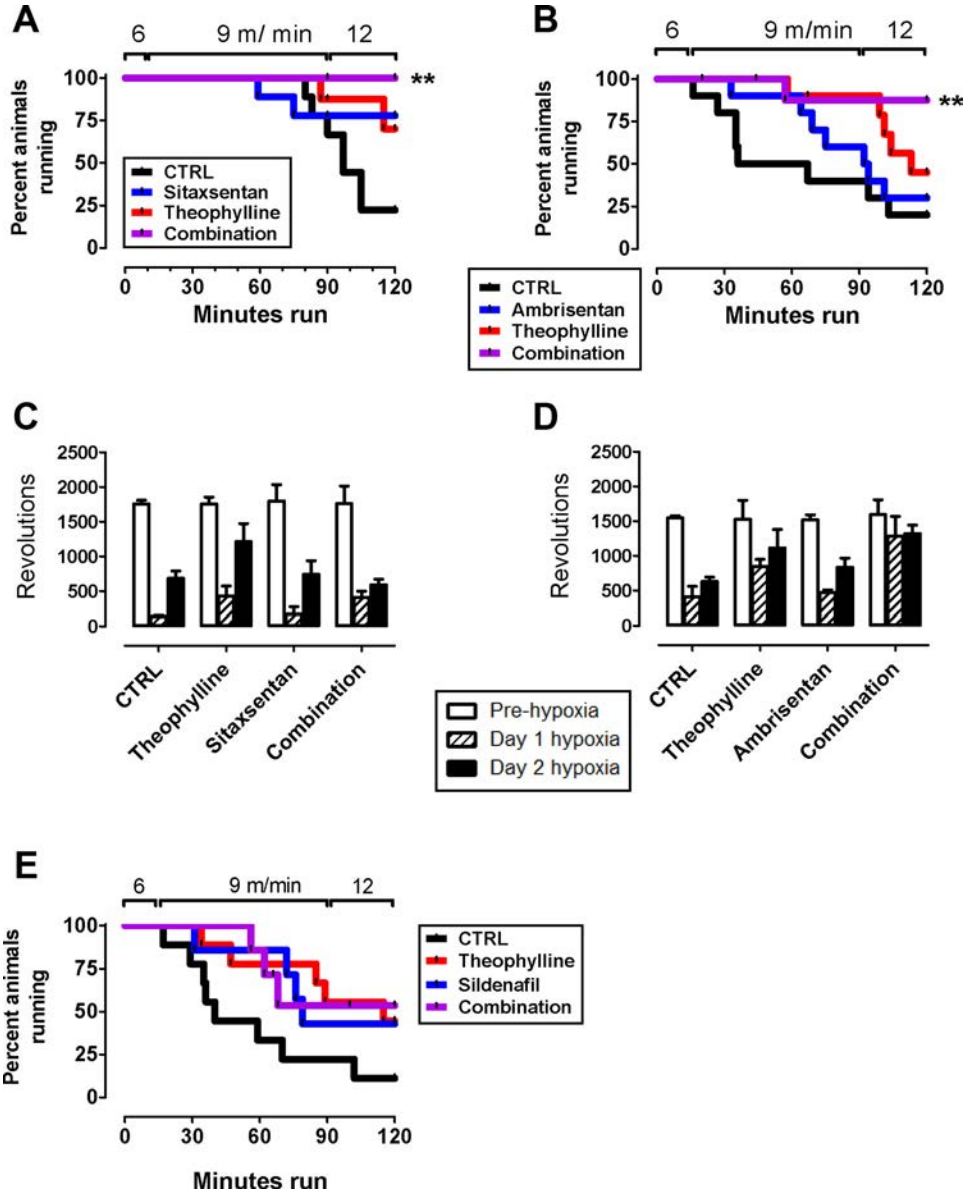

Fig. 2. Run to fatigue and voluntary physical activity under simulated high altitude. Asterisks indicate significant difference to control (CTRL). *A*: run-to-fatigue testing theophylline at 30 mg/kg and sitaxsentan at 1 mg/kg. Vehicle control was saline pH = 10. Log rank tests showed no significant differences in time run to exhaustion in control vs. theophylline or sitaxsentan alone but a significant difference when the drugs were combined; $n = 9$, except theophylline ($n = 8$). *B*: run-to-fatigue testing of theophylline at 15 mg/kg and ambrisentan at 0.1 mg/kg. Log rank tests: no significant difference between control and theophylline or ambrisentan alone but significant improvement in run to fatigue when combined; $n = 10$/group. *C* and *D*: voluntary physical activity (running wheel revolutions) of rats under simulated altitude over 48 h after dosing with theophylline at 30 mg/kg and sitaxsentan at 1 mg/kg or ambrisentan at 0.1 mg/kg; $n = 4$/group. *E*: time-to-fatigue testing with theophylline at 15 mg/kg and sildenafil at 4.5 mg/kg. No significant difference in the run-to-fatigue time compared with control was found in any of the groups; $n = 9$ (control and theophylline); $n = 7$ (sildenafil and combination).

(Fig. 2, *C* and *D*). None of the treatments increased voluntary running volume after onset of hypoxia (Fig. 2, *C* and *D*).

Peripheral Blood Flow, Blood Gases, and Hemodynamics

Peripheral blood flow. Theophylline significantly increased peripheral blood flow during hypoxia compared with control (*t*-test, $P = 0.0005$). The observed average increase after combination treatment was not significant. Sitaxsentan alone had no effect on blood flow in the hypoxic muscle (Fig. 3*A*).

Hemoglobin saturation. Average hemoglobin saturation values at the time of injection in all groups were 90.0 ± 18.0%. Hypoxia alone induced the expected significant decrease in HbO_2 in all treatment groups to an average of 70.4 ± 21.6% (Fig. 3*B*; paired *t*-test comparing preinjection and hypoxia: $P < 0.005$ in all groups). Injection of pH-adjusted saline increased HbO_2 in control groups from 93.1 ± 3.7 to 95.6 ± 2.5% (paired *t*-test, $P = 0.0009$). Neither of the single drugs nor their combination altered HbO_2 under hypoxia compared with controls.

Tissue pO_2. Hypoxia decreased hind-muscle pO_2 in the control group from an average of 25.9 ± 11.1 mmHg to 15.4 ± 8.8 mmHg. pO_2 did not decrease significantly in any of the other treatment groups. The observed increase of muscular pO_2 following combination treatment compared with controls was not significant. Only sitaxsentan treatment led to a tissue pO_2 that was higher than control treatment (*t*-test, $P = 0.0063$; Fig. 3*C*). Control treatment with injection of alkaline saline induced an increase in hemoglobin saturation by 93.1 ± 3.7 to 95.6 ± 2.5% HbO_2 (paired *t*-test, $P = 0.0009$).

Breathing rate. Average respiration rate was 41.7 ± 11.6 breaths/min before injection. Breathing rate increased in all treatment groups after onset of hypoxia to 56.4 ± 16.6 (paired *t*-test, $P < 0.05$ in all groups). No differences were found among any of the treatment groups for any of the time points (Fig. 3*D*).

Heart rate. Average preinjection heart rates in all groups were 242.2 ± 27.7 beats/min. Theophylline injection increased heart rate significantly from 241.8 ± 25.7 to 271.0 ± 33.0 beats/min (paired *t*-test, $P < 0.01$). Under hypoxia, the heart rate decreased in control-treated animals from 246.4 ± 26.1 to 227.6 ± 32.0 beats/min (paired *t*-test, $P < 0.001$) and in the sitaxsentan-treated animals from 245.6 ± 30.5 to 231.7 ± 33.6 beats/min (paired *t*-test, $P < 0.001$) but remained unaffected in theophylline- and combination-treated rats (Fig. 4*A*).

Blood pressures. Average mean arterial blood pressure (MAP) in all groups was 79.7 ± 11.4 mmHg preinjection. No changes of MAP were seen following any of the treatments (Fig. 4*B*). Average pulmonary arterial pressure (PAP) preinjection was 13.5 ± 5.3 mmHg, which was slightly increased to 14.2 ± 7.7 in all groups after onset of hypoxia; however, this was not significant. No changes were observed in response to any of the treatments, except in the combination group, where hypoxia increased PAP from 11.8 ± 5.4 mmHg postinjection to 13.1 ± 6.3 mmHg (paired *t*-test, $P = 0.0023$).

Pulmonary Wet-to-Dry Weight

WDR were 4.86 ± 0.09 in normoxic resting rats and 4.90 ± 0.09 in hypoxic resting rats. Adding exercise reduced WDR under hypobaric hypoxia (4.80 ± 0.09; *t*-test, $P < 0.05$). Treatment of exercising rats with theophylline did not change WDR compared with controls (4.77 ± 0.10). Treatment of exercising rats with sitaxsentan increased WDR compared with exercising controls (4.92 ± 0.05; *t*-test $P < 0.005$). The treatment of exercising rats with the drug combination, however, reduced WDR back to control levels (4.77 ± 0.09; comparison with sitaxsentan only; *t*-test, $P = 0.0002$; Fig. 4*D*).

DISCUSSION

In rats exposed to a simulated, moderately high altitude of 4,267 m or 12% inspired oxygen and treated with theophylline, sitaxsentan, ambrisentan, or the respective combination, the combinational treatments significantly improved maximal exercise performance, whereas the single treatments did not. Sildenafil, when combined with theophylline, did not produce any such synergism. Whereas none of the treatments impacted

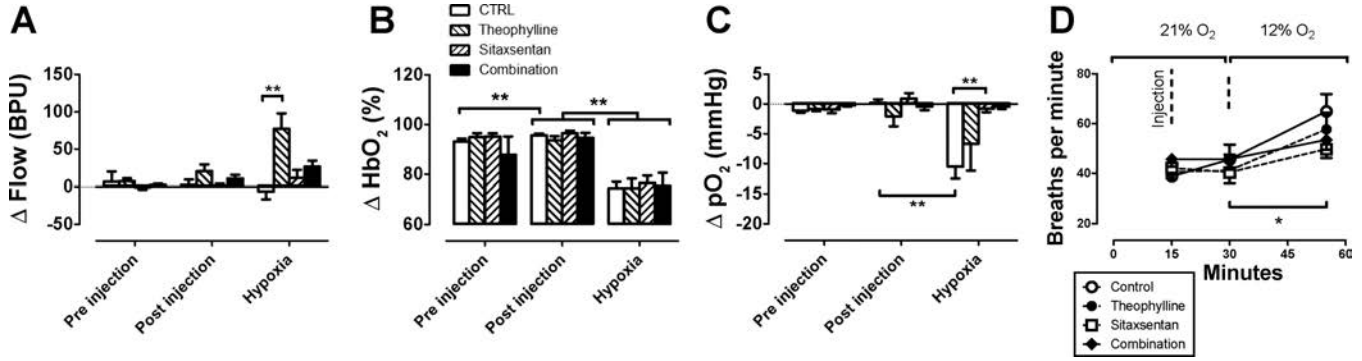

Fig. 3. The effects theophylline and sitaxsentan treatment on blood flow, oxygen transport, and tissue oxygenation in anesthetized, hypoxic rats. Asterisks indicate a significantly different physiological response compared with another treatment group or with the respective baseline (*$P < 0.05$; **$P < 0.01$). *A*: increased blood flow during hypoxia compared with control treatment was observed in theophylline-treated animals (*t*-test, $P = 0.0005$); $n = 10$ (control); $n = 8$ (theophylline); $n = 5$ (sitaxsentan); and $n = 6$ (combination). BPU, blood perfusion units. *B*: hypoxia induced a significant decrease of HbO_2 in all groups compared with baseline (paired *t*-test, $P < 0.005$ in all groups). None of the treatments significantly affected hemoglobin saturation under hypoxia compared with controls; $n = 10$ (control); $n = 8$ (theophylline); and $n = 9$ (sitaxsentan and combination). *C*: inspired hypoxia decreased tissue pO_2 in the hind-limb muscle of control animals by ~10 mmHg compared with baseline (paired *t*-test, $P = 0.0003$). Treatment with sitaxsentan reversed the hypoxia-induced change in tissue pO_2 reflected by a significant difference to control-treated animals under hypoxia (*t*-test, $P = 0.0063$, control: $n = 9$; all other groups: $n = 4$). *D*: in all groups, respiration rate increased significantly after onset of hypoxia (paired *t*-test, $P < 0.05$). No difference could be found among any of the groups for any given time point; $n = 11$ (control); $n = 9$ (theophylline and combination); and $n = 10$ (sitaxsentan).

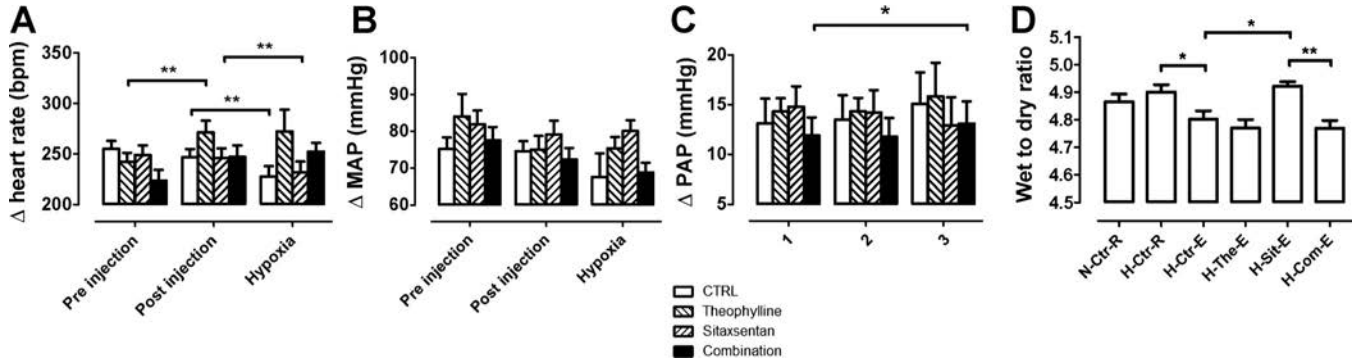

Fig. 4. The effects of theophylline and sitaxsentan treatment on cardiac activity and blood pressure in anesthetized rats exposed to hypoxia. Asterisks indicate significant differences (*$P < 0.05$; **$P < 0.01$). *A*: control- and sitaxsentan-treated animals experienced a significant decrease in heart rate after onset of hypoxia (paired *t*-test, $P < 0.05$ and $P < 0.001$), whereas the heart rate of theophylline- and combination-treated rats was unaffected by hypoxia. Theophylline alone, however, caused a significant increase in heart rate after injection compared with its baseline (paired *t*-test, $P = 0.0042$). No other differences were found among treatment groups at any given time point; $n = 8$–11/group. bpm, beats/min. *B*: no changes in mean arterial pressure (MAP) were observed among any of the groups or following any of the treatments; $n = 8$–11/group. *C*: pulmonary arterial pressure (PAP) increased significantly after onset of hypoxia in the combination group (paired *t*-test, $P < 0.05$). No other group showed any significant difference to controls or compared with each other; $n = 8$–11/group. *D*: wet-to-dry lung weight ratio after treatment with theophylline and sitaxsentan in exercising or nonexercising rats under hypoxia. Exposure time to altitude was 2.5 h; $n = 10$/group. N-Ctr-R, normoxia control rest; H-Ctr-R, hypoxia control rest; H-Ctr-E, hypoxia control exercise; H-The-E, hypoxia theophylline exercise; H-Sit-E, hypoxia sitaxsentan exercise; H-Com-E, hypoxia combination treatment exercise.

HbO_2, breathing rates, or mean MAP, theophylline alone significantly enhanced muscular blood flow under hypoxia, whereas sitaxsentan significantly improved muscular tissue pO_2. The combination treatment produced an intermediate effect in both muscular blood flow and tissue oxygenation. Whereas the combination of theophylline and sitaxsentan increased PAP significantly, pulmonary fluid content was unaffected in exercising hypoxic rats after combination treatment. Our results support the initial hypothesis that concomitant dosing with a cardiac stimulant and endothelin blockade can partially reverse loss of physical performance capacity under hypobaric hypoxia.

Theoretically, two main physiological strategies exist to improve oxygen transport from the lung to peripheral organs: improving blood oxygen loading or increasing blood flow (36). The increased breathing rate in response to hypoxia (also observed in this study) and the increased hematocrit in response to long-term hypoxic exposure are examples of the first strategy (35). Regarding the second mechanism of increased blood flow, it is known that (hypobaric) hypoxia itself increases the heart rate (36); however, in light of the potentially limiting effect of HPV on blood flow through the lung, it can be debated whether pharmaceutical targeting of HPV can improve exercise capacity at altitude (17, 37–39). As part of the criticism, it has been reasoned that a primary effect of pulmonary vasodilator treatment, such as with sildenafil, is the improvement of oxygen loading of the blood rather than the reduction in cardiac afterload and that respective human trials were inconclusive as to the importance of HPV on limiting performance at high altitude (3, 4). The obvious importance of the cardiac activity in the adaptation to high altitude, however, raises the question of whether this mechanism can be pharmacologically used and enhanced to improve adaptation to high altitude. The drugs used to test our original hypothesis were theophylline as a cardiac stimulant, or positive inotrope, and the endothelin receptor blockers sitaxsentan and ambrisentan as pulmonary vasodilators.

Theophylline

Theophylline is a methylxanthene drug with pleiotropic effects including nonselective PDE and adenosine receptor inhibition (6, 18). Theophylline has chronotropic activity, predominantly mediated by its nonselective and competitive adenosine receptor antagonism subtypes $A_1/A_2/A_3$. Theophylline also relaxes pulmonary smooth muscle via its nonspecific inhibitory effects on PDEs (in particular, PDE3 and -4), which contributed to its long-term use as an antiasthma medication (15). Of note, PDE3 inhibition also leads to increases in heart rate and stroke volume (44). Theophylline has been downgraded as an antiasthma medication recently because of its unwanted side-effects on the heart, blood ionic balance, blood pressure, and nervous system, as well as its nauseating effect (10). Theophylline has a narrow therapeutic index with optimal plasma concentrations in humans between 10 and 20 μg/ml (=55–110 mM) (7). Injection of 10 mg/kg ip of theophylline in rats already produces peak plasma concentrations of >25 μg/ml (27). The inhibition of both PDEs and the adenosine receptors is expected at a plasma level of 20 μg/ml (7), and consequently, both adenosine receptor antagonism and PDE3 and -4 inhibition were present in our experiments. Caffeine, structurally similar to theophylline, has shown efficacy in enhancing human performance at both sea level (28) and under hypobaric hypoxia (23). Treatment with theophylline alone has increased heart rates in anesthetized rats in our trials, and whereas hypoxia reduced heart rate in anesthetized control- and sitaxsentan-treated rats, heart rates in the theophylline group remained elevated under hypoxia (Fig. 4*A*). Although muscular blood flow was enhanced significantly when animals were treated with theophylline alone, this increase did not lead to a significant improvement of tissue oxygenation (Fig. 3, *A* and *C*). One possible explanation for our observation is that theophylline monotherapy may result in increased blood flow through the muscle compared with controls, but parts of this flow bypasses the capillary beds by being shunted to the postcapillary, venous compartment.

ERAs

Sitaxsentan and ambrisentan are both subtype A-specific antagonists of circulating endothelin that were originally designed to treat pulmonary arterial hypertension in human patients (11). Sitaxsentan has been shown to reduce HPV and to improve exercise capacity in humans at high altitude (39). Sitaxsentan has never been approved by the U.S. Food and Drug Administration (FDA) in the United States following concerns of liver toxicity and has recently been taken off the market in Europe (42). Ambrisentan has a more benign safety profile than sitaxsentan and is currently approved by the FDA for human use (24, 34, 42). The observation that endothelin blockade via sitaxsentan alone was sufficient to reverse tissue hypoxia (Fig. 3*C*), yet did not augment tissue blood flow, might be explained by its direct dilating effect on peripheral arterioles and by the reduced demand for cardiac output in the anesthetized animal.

Run to Fatigue and Voluntary Running

Our most important observation was that the combination of theophylline and endothelin blockade consistently enhanced run-to-fatigue time at altitude compared with the single compounds. These results, together with the absence of alterations to respiratory rates or blood oxygenation levels in any of the groups, support our initial hypothesis that it is possible to counteract tissue hypoxia and performance loss under hypobaric hypoxia by pharmaceutically improving blood flow rate, accomplished by counteracting endothelin-mediated vasoconstriction and accelerating heart rate (37). The absence of a significant increase in PAP in control animals after onset of hypoxia (Fig. 4*C*) and the absence of increased pulmonary fluid content after onset of exercise and theophylline treatment (Fig. 4*D*) illustrate that HPV was only weakly expressed in our model and might not be limiting to blood flow through the lung under these conditions. It is therefore possible that the observed beneficial effect of ERAs is due to extrapulmonary mechanisms. It is known that the vasoconstrictive activity of endothelin-1 affects not only the pulmonary but also all other peripheral vasculature (12). Importantly, endothelin blockade was only effective in our exercise models when combined with theophylline. The observation that combining sildenafil (as opposed to ambrisentan or sitaxsentan) with theophylline did not lead to any additional benefit over the single compounds argues for the importance of targeting endothelin to achieve the observed synergism. The voluntary running data suggest that both theophylline alone and combined with endothelin receptor blockade may have the potential to increase adaptation to high altitude over a period of ~1 day; however, further experimentation needs to be conducted to definitively conclude this.

Pulmonary WDR

Heavy exercise in conjunction with acute exposure to hypoxia at altitude has the potential to increase pulmonary leak, as both exercise and hypoxia increase heart rate, leading to increased hydrostatic pressure on the pulmonary vasculature (16). The fact that exercise reduced, rather than increased, vascular fluid content is therefore surprising. However, the redistribution of blood flow in response to high altitude and exercise in rats is different from the human situation, at least in part, due to differences in size and posture. We also initially expected that treatment with theophylline of rats undergoing the run-to-fatigue protocol in hypobaric hypoxia would further augment pulmonary extracellular fluid content reflected by an increase of lung weight WDR. The observation that theophylline alone did not increase vascular leak might be explained by the known vasodilatory effects of theophylline and its reported ability to reduce HPV (5). Sitaxsentan, however, had the opposite effect, increasing the fraction of blood present in the pulmonary vasculature, which is reflected by the increased lung weight WDR after sitaxsentan treatment (Fig. 4*D*). The overall ratios obtained in our study are similar to those found in other rodent studies (41). Whereas the highest increase of ratios in our study were from 4.8 in controls to 5.0 in the sitaxsentan-treated group, representing an increase of 4%, other studies in rats, including pulmonary edema and reperfusion injury models, demonstrate increases of >66% compared with controls (41). Even the significant increase in WDR after sitaxsentan treatment, therefore, is unlikely to represent a pathophysiological state. Specifically, the observation that PAP increased after combination treatment with theophylline and that sitaxsentan is not reflected by increases in WDR indicates that neither of the treatments sufficiently increases the pressure burden on the pulmonary vasculature enough to cause significant extravasation of fluid. The absence of any aggravating effect of simulated altitude, with and without exercise, on the pulmonary fluid content of the rats and the lack of a reducing effect of sitaxsentan on WDR support the conclusion that at least parts of the beneficial effect of endothelin blockade might be extrapulmonary in nature.

Heart rates measured in anesthetized rats were ~30% lower than values reported in the literature (50). A further significant reduction of heart rates occurred after onset of hypoxia in control- and sitaxsentan-treated animals. This discrepancy is probably due to the effect of ketamine anesthesia. Whereas conscious mammals, including humans and rats, react to inspired hypoxia with an increase in heart rate, hypoxia—in conjunction with ketamine anesthesia—generally appears to reverse this reaction (13, 36, 47).

Blood Pressures

The overall baseline values found for MAP are in accordance with what has been reported elsewhere (13). It has been shown that inspired hypoxia leads to a drop in MAP, which was present but nonsignificant in our study. Theophylline-induced hypotension was nonsignificant in our study (45). Overall, PAP values are, however, lower than those reported before in male-anesthetized and awake Sprague-Dawley rats of similar age and weight (~19 mmHg). Furthermore, the increase in PAP after onset of hypoxia was smaller than in comparable studies. In our study, an increase of 112.82% [from 15.6 ± 3.7 to 17.6 ± 5.7 mmHg after fraction of inspired oxygen (FiO_2) of 12%] was observed in control-treated animals, whereas other studies reported an increase of 131.58% in male rats exposed to 10% FiO_2 (19.0 ± 1 to 25.0 ± 1 mmHg) (30). This potential discrepancy may be due to the female

gender of the animals, as it has been reported that female mammals show weaker vasoconstrictive and ventilatory responses to hypoxia (25, 46, 51). It is plausible that all changes to PAP, which were observed in this study, are due to increased cardiac output following the treatment.

HbO_2 and Breathing Rates

As expected, reduced FiO_2 induced a decrease of HbO_2 and an increase in breathing rates. In support of our initial hypothesis, no increases in hemoglobin saturation or breathing rates were found after any of the treatments, indicating that the performance-enhancing effect of the combination treatment was not due to increased oxygen content of the blood. The small increase of HbO_2 observed after ip injection of control treatment (alkaline saline) might be caused by the Bohr effect, which would favor release of oxygen from hemoglobin under acidic conditions and retention during alkalosis.

Rationale for Modified Experimental Protocol for Tissue pO_2 and Blood Flow Measurements

The protocol that was used to measure tissue oxygenation and muscular blood flow, which has been done on the same set of animals, was slightly different from the one used for the other hemodynamic data, as outlined in Fig. 1. To account for the known sensitivity of the pO_2 needle-probe measurements to differences in sensor placement, a pretreatment hypoxic episode was introduced into this cohort, which served to verify that the needle was sensitive to tissue pO_2 changes in response to inspired hypoxia. As a result of this calibration, three out of 24 measurements were removed from analysis, where due to poor needle placement, the initial hypoxic episode did not cause any change in tissue pO_2. A comparison of the relative margin of changes in tissue pO_2 during the post-treatment hypoxic cycle with those changes during initial hypoxia in the same animals confirmed the findings with absolute pO_2 values in each treatment group, supporting the validity of the measurements (data not shown).

Tissue pO_2

Interestingly, the onset of inspired hypoxia caused a significant drop in tissue pO_2 in control animals, whereas each of the treatments appeared to prevent such a drop. Only treatment with sitaxsentan led to a significantly increased pO_2 under hypoxia compared with control treatment. It is plausible that both increased blood flow, as observed with theophylline treatment, and vasodilatation of pulmonary and peripheral arterioles via endothelin blockade can independently contribute to improved oxygen delivery to the capillary bed. The particular efficacy of sitaxsentan could be due to the special situation of the anesthetized animal, where due to reduced requirements toward homeostasis of blood pressure and blood flow in the resting state, pulmonary and other peripheral arteriolar vasodilatation could be sufficient to allow improved oxygen transport to tissues.

Muscular Blood Flow

It is important for understanding the muscular blood flow data to recognize that laser doppler values (arbitrary BPU) have no dimension and should always be read in relation to a baseline value; therefore, all values have been normalized to the measurement at the time of injection. Because theophylline itself appears to be able to counteract pulmonary vasoconstriction in rats (5), it is possible that a blood flow-enhancing effect through the lung could be caused by this drug alone. Interestingly, the addition of sitaxsentan appeared to partially blunt the flow-enhancing effect of theophylline alone in the muscle. This observation can be explained by vasodilatory effects of endothelin receptor blockade in peripheral tissues. Endothelin blockade may cause vasodilatation of arterioles, thus reducing shunting and diverting more blood to the capillary beds. This would lead to improved delivery of oxygen and nutrients to the parenchymal tissues but at the same time, reduce overall blood flow velocity through the respective organ. It is known that the vasoconstrictive activity of endothelin-1 affects not only the pulmonary but also all other peripheral vasculature (12); however, little is known about the influence of sitaxsentan or ambrisentan on muscular vascular resistance and oxygen transport.

Potential Synergism Between Theophylline and Endothelin Receptor Blockers

The combination of theophylline and sitaxsentan did improve tissue oxygenation and tissue blood flow to a lesser extent than the respective single drugs. The synergism observed in our exercise trials could therefore have arisen from the ability of endothelin blockers to reduce shunting by dilating arterioles and to redirect theophylline-enhanced blood flow toward the tissue capillary systems, resulting in improved oxygen delivery to the peripheral capillary beds.

The combination of pharmaceutical-driven cardiac stimulation and vasodilatation is a novel, physiological concept in treating high-altitude-induced decreases in physical performance and potentially other altitude-related illnesses. Our data suggest that cardiac stimulants, such as xanthene derivatives, might be used for this purpose and may have greater therapeutic potential when delivered in combination with endothelin receptor blockers.

ACKNOWLEDGMENTS

We thank the staff of the Duke Center for Hyperbaric Medicine and Environmental Physiology, especially Albert Boso, Eric Schinazi, Michael Natoli, Aaron Walker, and Dr. Richard Moon for technical assistance in the hypobaric chamber and Craig Marshall for his help with the wet-to-dry measurements of rat lungs. We also acknowledge Laurie Biela, Natalie Rea, and Daniel Warro at Colorado State University for their assistance with the voluntary activity experiments, as well as the Duke University Small Molecule Synthesis Facility, in particular, Dr. David Gooden, for producing sitaxsentan and ambrisentan. We also thank Drs. Terry Opgenorth and Joseph DeAngelo for intellectual input on this project.

GRANTS

Support for this research was provided by the U.S. Defense Advanced Research Projects Agency (DARPA) Prime Award Number N66001-10-C-2134.

DISCLOSURES

No conflicts of interest, financial or otherwise, are declared by the author(s).

AUTHOR CONTRIBUTIONS

Author contributions: D.R.R., Y.Z., S.S., G.P., K.H., D.I., G.H., C.A.P., and T.S. conception and design of research; D.R.R., Y.Z., A.B., C.W., S.S., K.H., D.I., and T.S. performed experiments; D.R.R., A.B., C.W., G.P., K.H., D.I.,

and T.S. analyzed data; D.R.R., Y.Z., A.B., C.W., S.S., G.P., K.H., D.I., G.H., C.A.P., and T.S. interpreted results of experiments; D.R.R., K.H., and T.S. prepared figures; D.R.R. and T.S. drafted manuscript; D.R.R., S.S., G.P., K.H., D.I., C.A.P., and T.S. edited and revised manuscript; D.R.R., Y.Z., A.B., C.W., S.S., G.P., K.H., D.I., G.H., C.A.P., and T.S. approved final version of manuscript.

REFERENCES

1. **Allen BW, Piantadosi CA.** How do red blood cells cause hypoxic vasodilation? The SNO-hemoglobin paradigm. *Am J Physiol Heart Circ Physiol* 291: H1507–H1512, 2006.
2. **Andersen ML, Bignotto M, Tufik S.** Effect of sildenafil (Viagra) on the genital reflexes of paradoxical sleep-deprived male rats. *Braz J Med Biol Res* 40: 1473–1480, 2007.
3. **Anholm JD, Foster GP.** Con: hypoxic pulmonary vasoconstriction is not a limiting factor of exercise at high altitude. *High Alt Med Biol* 12: 313–317, 2011.
4. **Anholm JD, Foster GP.** Con: rebuttal. *High Alt Med Biol* 12: 321, 2011.
5. **Arisaka Y, Sato S, Kato S, Yuki H, Takahashi H, Tomoike H.** Effect of theophylline on hypoxic pulmonary vasoconstriction in awake rats. *Tohoku J Exp Med* 182: 231–239, 1997.
6. **Arnaud MJ.** Pharmacokinetics and metabolism of natural methylxanthines in animal and man. *Handb Exp Pharmacol* 200: 33–91, 2011.
7. **Barnes PJ.** Theophylline in chronic obstructive pulmonary disease: new horizons. *Proc Am Thorac Soc* 2: 334–339, 2005.
8. **Benjamini Y, Hochberg Y.** Controlling the false discovery rate: a practical and powerful approach to multiple testing. *J R Stat Soc B (Stat Methodol)* 57: 289–300, 1995.
9. **Blaber AP, Hartley T, Pretorius PJ.** Effect of acute exposure to 3660 m altitude on orthostatic responses and tolerance. *J Appl Physiol* 95: 591–601, 2003.
10. **Boison D.** Methylxanthines, seizures, and excitotoxicity. *Handb Exp Pharmacol* 200: 251–266, 2011.
11. **Boniface S, Reynaud-Gaubert M.** Endothelin receptor antagonists—their role in pulmonary medicine. *Rev Mal Respir* 28: e94–e107, 2011.
12. **Bussey CT, Kolka CM, Rattigan S, Richards SM.** Adiponectin opposes endothelin-1-mediated vasoconstriction in the perfused rat hindlimb. *Am J Physiol Heart Circ Physiol* 301: H79–H86, 2011.
13. **Cummings J, Kaplan JL, Gao E, Clas D, Dalsey WC, de Garavilla L.** Antagonism of the cardiodepressant effects of adenosine during acute hypoxia. *Acad Emerg Med* 7: 618–624, 2000.
14. **de Bisschop C, Martinot JB, Leurquin-Sterk G, Faoro V, Guenard H, Naeije R.** Improvement in lung diffusion by endothelin A receptor blockade at high altitude. *J Appl Physiol* 112: 20–25, 2012.
15. **Dennis RJ, Solarte I, Rodrigo G.** Asthma in adults. *Clin Evid (Online)* 2011: 1512, 2011.
16. **Eldridge MW, Braun RK, Yoneda KY, Walby WF.** Effects of altitude and exercise on pulmonary capillary integrity: evidence for subclinical high-altitude pulmonary edema. *J Appl Physiol* 100: 972–980, 2006.
17. **Erzurum SC, Ghosh S, Janocha AJ, Xu W, Bauer S, Bryan NS, Tejero J, Hemann C, Hille R, Stuehr DJ, Feelisch M, Beall CM.** Higher blood flow and circulating NO products offset high-altitude hypoxia among Tibetans. *Proc Natl Acad Sci USA* 104: 17593–17598, 2007.
18. **Essayan DM.** Cyclic nucleotide phosphodiesterases. *J Allergy Clin Immunol* 108: 671–680, 2001.
19. **Faoro V, Boldingh S, Moreels M, Martinez S, Lamotte M, Unger P, Brimioulle S, Huez S, Naeije R.** Bosentan decreases pulmonary vascular resistance and improves exercise capacity in acute hypoxia. *Chest* 135: 1215–1222, 2009.
21. **Fischler M, Maggiorini M, Dorschner L, Debrunner J, Bernheim A, Kiencke S, Mairbaurl H, Bloch KE, Naeije R, Brunner-La Rocca HP.** Dexamethasone but not tadalafil improves exercise capacity in adults prone to high-altitude pulmonary edema. *Am J Respir Crit Care Med* 180: 346–352, 2009.
22. **Fulco CS, Rock PB, Cymerman A.** Maximal and submaximal exercise performance at altitude. *Aviat Space Environ Med* 69: 793–801, 1998.
23. **Fulco CS, Rock PB, Trad LA, Rose MS, Forte VA Jr, Young PM, Cymerman A.** Effect of caffeine on submaximal exercise performance at altitude. *Aviat Space Environ Med* 65: 539–545, 1994.
24. **Galie N, Badesch D, Oudiz R, Simonneau G, McGoon MD, Keogh AM, Frost AE, Zwicke D, Naeije R, Shapiro S, Olschewski H, Rubin LJ.** Ambrisentan therapy for pulmonary arterial hypertension. *J Am Coll Cardiol* 46: 529–535, 2005.
25. **Gassmann M, Tissot van Patot M, Soliz J.** The neuronal control of hypoxic ventilation: erythropoietin and sexual dimorphism. *Ann N Y Acad Sci* 1177: 151–161, 2009.
26. **Gillum JG, Sesler JM, Bruzzese VL, Israel DS, Polk RE.** Induction of theophylline clearance by rifampin and rifabutin in healthy male volunteers. *Antimicrob Agents Chemother* 40: 1866–1869, 1996.
27. **Gomita Y, Furuno K, Eto K, Okazaki M, Suemaru K, Araki Y.** Effect of cigarette smoking on theophylline pharmacokinetics in rats. *J Pharm Pharmacol* 43: 621–624, 1991.
28. **Greer F, Friars D, Graham TE.** Comparison of caffeine and theophylline ingestion: exercise metabolism and endurance. *J Appl Physiol* 89: 1837–1844, 2000.
29. **Hsu AR, Barnholt KE, Grundmann NK, Lin JH, McCallum SW, Friedlander AL.** Sildenafil improves cardiac output and exercise performance during acute hypoxia, but not normoxia. *J Appl Physiol* 100: 2031–2040, 2006.
30. **Irwin DC, Foreman B, Morris K, White M, Sullivan T, Jacobs R, Monnet E, Hackett T, TissotvanPatot MC, Hamilton KL, Gotshall RW.** Polymerized bovine hemoglobin decreases oxygen delivery during normoxia and acute hypoxia in the rat. *Am J Physiol Heart Circ Physiol* 295: H1090–H1099, 2008.
31. **Kressler J, Stoutenberg M, Roos BA, Friedlander AL, Perry AC, Signorile JF, Jacobs KA.** Sildenafil does not improve steady state cardiovascular hemodynamics, peak power, or 15-km time trial cycling performance at simulated moderate or high altitudes in men and women. *Eur J Appl Physiol* 111: 3031–3040, 2011.
32. **Lafleur JE, Bartniczuk D, Collier A, Griffin N, Swenson ER.** Acetazolamide and exercise hypoxia. *Int J Sports Med* 31: 372–376, 2010.
33. **Loran OB, Stroberg P, Lee SW, Park NC, Kim SW, Tseng LJ, Collins S, Stecher VJ.** Sildenafil citrate 100 mg starting dose in men with erectile dysfunction in an international, double-blind, placebo-controlled study: effect on the sexual experience and reducing feelings of anxiety about the next intercourse attempt. *J Sex Med* 6: 2826–2835, 2009.
34. **McGoon MD, Frost AE, Oudiz RJ, Badesch DB, Galie N, Olschewski H, McLaughlin VV, Gerber MJ, Dufton C, Despain DJ, Rubin LJ.** Ambrisentan therapy in patients with pulmonary arterial hypertension who discontinued bosentan or sitaxsentan due to liver function test abnormalities. *Chest* 135: 122–129, 2009.
35. **Muza SR.** Military applications of hypoxic training for high-altitude operations. *Med Sci Sports Exerc* 39: 1625–1631, 2007.
36. **Naeije R.** Physiological adaptation of the cardiovascular system to high altitude. *Prog Cardiovasc Dis* 52: 456–466, 2010.
37. **Naeije R.** Pro: hypoxic pulmonary vasoconstriction is a limiting factor of exercise at high altitude. *High Alt Med Biol* 12: 309–312, 2011.
38. **Naeije R.** Pro: rebuttal. *High Alt Med Biol* 12: 319, 2011.
39. **Naeije R, Huez S, Lamotte M, Retailleau K, Neupane S, Abramowicz D, Faoro V.** Pulmonary artery pressure limits exercise capacity at high altitude. *Eur Respir J* 36: 1049–1055, 2010.
40. **Olfert IM, Loeckinger A, Treml B, Faulhaber M, Flatz M, Burtscher M, Truebsbach S, Kleinsasser A.** Sildenafil and bosentan improve arterial oxygenation during acute hypoxic exercise: a controlled laboratory trial. *Wilderness Environ Med* 22: 211–221, 2011.
41. **Parker JC, Townsley MI.** Evaluation of lung injury in rats and mice. *Am J Physiol Lung Cell Mol Physiol* 286: L231–L246, 2004.
42. **Safdar Z.** Effect of transition from sitaxsentan to ambrisentan in pulmonary arterial hypertension. *Vasc Health Risk Manag* 7: 119–124, 2011.
43. **Sanna F, Succu S, Boi A, Melis MR, Argiolas A.** Phosphodiesterase type 5 inhibitors facilitate noncontact erections in male rats: site of action in the brain and mechanism of action. *J Sex Med* 6: 2680–2689, 2009.
44. **Schror K.** The pharmacology of cilostazol. *Diabetes Obes Metab* 4, *Suppl* 2: S14–S19, 2002.
45. **Skinner MH.** Adverse reactions and interactions with theophylline. *Drug Saf* 5: 275–285, 1990.
46. **Smith AM, Jones RD, Channer KS.** The influence of sex hormones on pulmonary vascular reactivity: possible vasodilator therapies for the treatment of pulmonary hypertension. *Curr Vasc Pharmacol* 4: 9–15, 2006.
47. **Sugimura M, Hanamoto H, Boku A, Morimoto Y, Taki K, Kudo C, Niwa H.** Influence of acute hypoxia combined with nitrous oxide on cardiovascular variability in conscious hypertensive rats. *Auton Neurosci* 156: 73–81, 2010.
48. **Thomas KN, Burgess KR, Basnyat R, Lucas SJ, Cotter JD, Fan JL, Peebles KC, Lucas RA, Ainslie PN.** Initial orthostatic hypotension at high altitude. *High Alt Med Biol* 11: 163–167, 2010.

48a. **U.S. Department of Health and Human Services, Food and Drug Administration, Center for Drug Evaluation and Research (CDER).** *Guidance for Industry, Estimating the Maximum Safe Starting Dose in Initial Clinical Trials for Therapeutics in Adult Healthy Volunteers*. Rockville, MD: U.S. Food and Drug Administration, 2005, p. 1–30.

49. **Valentini M, Revera M, Bilo G, Caldara G, Savia G, Styczkiewicz K, Parati S, Gregorini F, Faini A, Branzi G, Malfatto G, Magri D, Agostoni P, Parati G.** Effects of beta-blockade on exercise performance at high altitude: a randomized, placebo-controlled trial comparing the efficacy of nebivolol versus carvedilol in healthy subjects. *Cardiovasc Ther* 30: 240–248, 2012.

50. **Walker BR.** Role of vasopressin in the cardiovascular response to hypoxia in the conscious rat. *Am J Physiol Heart Circ Physiol* 251: H1316–H1323, 1986.

51. **Wetzel RC, Sylvester JT.** Gender differences in hypoxic vascular response of isolated sheep lungs. *J Appl Physiol* 55: 100–104, 1983.

One-stop-shop tumor imaging: buy hypoxia, get lactate free

Ashley A. Manzoor,[1,2] Thies Schroeder,[1] and Mark W. Dewhirst[1]

[1]Department of Radiation Oncology and [2]Medical Physics Program, Duke University, Durham, North Carolina, USA.

The ability to noninvasively assess physiological changes in solid tumors is desired for its diagnostic and therapeutic potential. In this issue of *JCI*, Matsumoto and colleagues reveal their development and use of a novel imaging approach, combining pulsed electron paramagnetic resonance imaging (EPRI) with conventional MRI to image squamous cell carcinoma tumor–bearing mice (see the related article beginning on page 1965). This method provides coregistered images of oxygenation and blood volume/flow with the underlying anatomy and concentrations of metabolites such as lactate and choline. This technique, combining functional and anatomic imaging, shows immediate preclinical applicability in monitoring factors that control tumor hypoxia and metabolism and may have future clinical potential for monitoring tumor response to treatment.

It has been known for well over two decades that tumor angiogenesis results in blood vessels that are structurally and functionally abnormal, contributing to inefficient tumor perfusion and hypoxia (1, 2). Hypoxia has an impact on patient survival for a wide range of solid tumors and is associated with poor prognosis following radiation, chemotherapy, and surgery (3–5). Interest in the hypoxic status of tumors has further increased with the discovery that hypoxia regulates dozens of genes that alter cellular behavior and result in a more malignant tumor phenotype (6). However, in spite of the known importance of hypoxia in tumor pathophysiology, there has yet to be identified a method that can noninvasively and repeatedly measure partial pressure of oxygen (oxygenation; pO_2) of tumors with precision. Additionally, the multifaceted causality of tumor hypoxia has not been addressed; both metabolic rate and perfusion can influence hypoxia, but to date there has not been an integrated method that can assess these multiple physiologic parameters.

An important milestone in multimodal imaging is achieved

The study by Matsumoto and colleagues in this issue of the *JCI* represents the pièce de résistance of multiparametric tumor imaging (7). They have demonstrated the ability to obtain noninvasive, accurate measurements of tissue pO_2 in a live animal with an integrated imaging platform that provides overlay of acquired oxygen maps with further anatomic, physiologic, and metabolic information. This work is truly groundbreaking, and if implemented on a wider basis, it could revolutionize the way in which we study and understand the principles controlling tumor hypoxia at the preclinical level. Although implementing this technique in the clinical environment will be challenging, successful translation of this research method into clinical use would create a true paradigm shift in how technology is used in diagnostic and therapeutic oncology.

The current study (7) describes a novel platform that uses pulsed electron paramagnetic resonance imaging (EPRI), a method fundamentally similar to MRI that utilizes an injected oxygen-sensitive chemical probe to obtain 3D maps of tissue pO_2. The authors combine EPRI with MRI by exploiting the common radio frequency of 300 MHz between EPRI and MRI signals at their magnetic field strengths of 10 mT and 7 T, respectively. This elegant design allows for serial monitoring and multiparametric analysis of the tumor environment, merging the refined oxygen-imaging ability of EPRI with the multitude of powerful parameters available through MRI and magnetic resonance spectroscopy (MRS).

The method outlined by Matsumoto et al. (7) offers a unique capacity for hypoxia imaging by providing 3D images of absolute tissue pO_2 with a resolution of 3–4 mmHg. No other hypoxia imaging modality can currently match this ability (Table 1). While polarographic electrodes and optical methods are also capable of assessing absolute oxygen content in mmHg, they are severely limited in their imaging capability (8); polarography, the current gold standard for measuring tissue pO_2, is invasive and provides only point or line measurements, and optical methods have limited penetration depths in the order of millimeters to centimeters. PET imaging of oxygen-dependent hypoxia marker compounds is the most commonly used clinical method for determining tumor hypoxia, with a variety of available fluorinated (^{18}F) nitroimidazoles and chelated copper compounds. These radioactive tracers are bioreduced and consequently trapped inside cells with low oxygen tension (8–10). However, PET imaging provides only a relative measure of hypoxia and is influenced by the cellular uptake and retention of the radiotracers. This is in contrast to the pulsed EPRI system, which provides quantitative information on hypoxic intensity, enabling severely hypoxic (<1 mmHg) tumor regions to be discriminated from mildly hypoxic (approximately 10 mmHg) tumor regions, at a spatial resolution far superior to that of PET.

Competing MRI methods of imaging hypoxia such as blood oxygen level–dependent (BOLD) and dynamic contrast–enhanced (DCE) MRI also have limitations, particularly when compared with this novel method. BOLD MRI provides a measure of relative hemoglobin oxygen saturation, but confounding influences of blood flow, arterial saturation, microvessel density, hematocrit, and oxygen consumption complicate interpretation of the BOLD signal and limit the ability to infer tissue pO_2 (8, 9, 11). DCE MRI has also been used to infer differences in tumor pO_2, but the parameters of perfusion,

Nonstandard abbreviations used: BOLD, blood oxygen level dependent; DCE, dynamic contrast enhanced; EPRI, electron paramagnetic resonance imaging; IMRT, intensity-modulated radiation therapy; MRS, magnetic resonance spectroscopy; PFC, perfluorocarbon; pO_2, partial pressure of oxygen (oxygenation).

Conflict of interest: The authors have declared that no conflict of interest exists.

Citation for this article: *J. Clin. Invest.* **118**:1616–1619 (2008). doi:10.1172/JCI35543.

Table 1
Comparison of common hypoxia imaging modalities

Parameter	Combined EPRI/MRI	PFC ^{19}F MRS	BOLD	PET[A]	Eppendorf electrode
Noninvasive[B]	Yes; i.v.	Yes; i.v. or intratumoral contrast	Yes	Yes; i.v.	No
Measures absolute pO_2	Yes	Yes	No	No	Yes
Affected by other factors	No	No	Yes	No	No
Good spatial resolution	Yes	No	Yes	No	No
Temporal repeatability	Yes	Yes	Yes	Frequency depends on isotope half-life	Challenging due to invasive nature
Sensitive below 20 mmHg	Yes	Yes	Yes	Yes	Yes
Precision in mmHg	3–4 mmHg	1–3 mmHg	NA	NA	1 mmHg

[A]Fluorinated (^{18}F) nitroimidazoles and chelated copper compounds (8–10). [B]i.v. delivery of contrast is not considered invasive in this context.

permeability, and extracellular volume fraction obtained from this method are only tangentially related to hypoxia; studies have reported weak correlates between these endpoints and the hypoxic status of tumors (12, 13). Perfluorocarbon (PFC) ^{19}F MRS provides the most comparable imaging capabilities, as PFCs acquire absolute pO_2 with a resolution of 1–3 mmHg (14). However, the main disadvantage of PFC MRI/MRS is its spatial resolution, which is inferior to that of pulsed EPRI.

While EPRI shows great promise for hypoxia imaging, until now it has been limited by its lack of ability to provide anatomical information. In this issue, Matsumoto et al. (7) demonstrate that they have overcome this limitation and provide a further adjunct to the anatomical information by incorporating multiple magnetic resonance parameters. The authors obtained magnetic resonance angiograms, apparent diffusion coefficient (ADC) maps, and arterial spin-labeling, corresponding to parameters of blood volume, cellularity/necrosis, and blood flow, respectively. This approach is particularly significant as the multiparametric possibilities are not limited to the analysis conducted in this experiment; BOLD or DCE MRI could be performed as easily as the ADC or arterial spin-labeling methods.

A comprehensive view of the tumor microenvironment requires metabolic information

From the overlaid functional and anatomical images obtained, Matsumoto et al. (7) selected regions of interest within the tumors and performed proton MRS to measure levels of metabolites such as lactate and choline. This is the first report of an imaging modality providing metabolic information simultaneously with pO_2 values, furthering the elegance of this study. Yet, from this laudatory introduction arises a note of caution: imaging technology is only as valuable as its validation and interpretation. Matsumoto et al. conclude that their findings, showing high levels of lactate at normal pO_2 levels, support the predominance of aerobic glycolysis in normoxic regions of tumor, also known as the *Warburg effect* (15). However, the role of lactate in tumor metabolism has much greater complexity than acknowledged with these conclusions. Without additional information to aid and support interpretation of the imaging results, it is difficult to claim that the images provide evidence for the Warburg effect.

Tumor metabolism is a dynamic process of nutrient delivery and breakdown, which influences the tissue concentration of its substrates and products in a complicated manner. It has been well described that cancer cells, as most other cells, compensate for hypoxia by increasing their rate of glycolysis, a phenomenon known as the *Pasteur effect* (16). While the Pasteur effect in cancer cells was first described in the early 1930s, in part by Otto Warburg himself, it has never been found that lactate production decreases with hypoxia (16–18). Moreover, regions of chronic severe hypoxia in experimental tumors usually surround a necrotic core, which functions as a sink to accumulate lactate (Figure 1). Considering these factors, a situation in which lactate levels are lower in hypoxic as compared with normoxic tumor areas is highly unlikely, even if individual cancer types exhibit a strong Warburg effect. A possible explanation is that short-term changes in hypoxia, also known as *fluctuating hypoxia*, lead to metabolite concentrations that do not represent the current pO_2 state of the tissue. In this scenario, the EPRI takes a "snapshot" of the oxygen status of the tumor, which may not be representative of the tumor over time. The authors themselves illustrate this influence by the fluctuations of EPRI pO_2 values with carbogen breathing. As fluctuating hypoxia tends to be perfusion dominated, this would coincide with an area that has higher blood volume. Another explanation is that local tissue hypoglycemia could be restricting lactate production in tumors. However, such a lack of substrate will most likely lead to cell death shortly thereafter. In short, the authors' finding of lactate being higher in normoxic than hypoxic tissue is unexpected and necessitates further explanation. This is particularly important when a novel method is used to measure these parameters. We would therefore like to underscore that imaging modalities, while powerful methods to provide insight into the tumor environment, are only as valuable as their validation and interpretation.

Potential for clinical translation

On a final note, Matsumoto et al. (7) highlight the clinical implications of this combined imaging modality, particularly with respect to utilizing this method for dose contouring with intensity-modulated radiation therapy (IMRT). IMRT, also referred to as *dose painting*, is a technique used in radiation oncology in which the dose can be contoured to subvolumes within the tumor (19). For instance, a subvolume of a hypoxic area within the tumor could be targeted with higher radiation dose through IMRT. From a clinical perspective, the results of Matsumoto and colleagues are quite profound. They imply that a single diagnostic test could provide insight into tumor pO_2 status, necrosis, metabolism, and perfusion, all with anatomic overlay. However, the clinical benefit and ease of implementation remains unknown. While

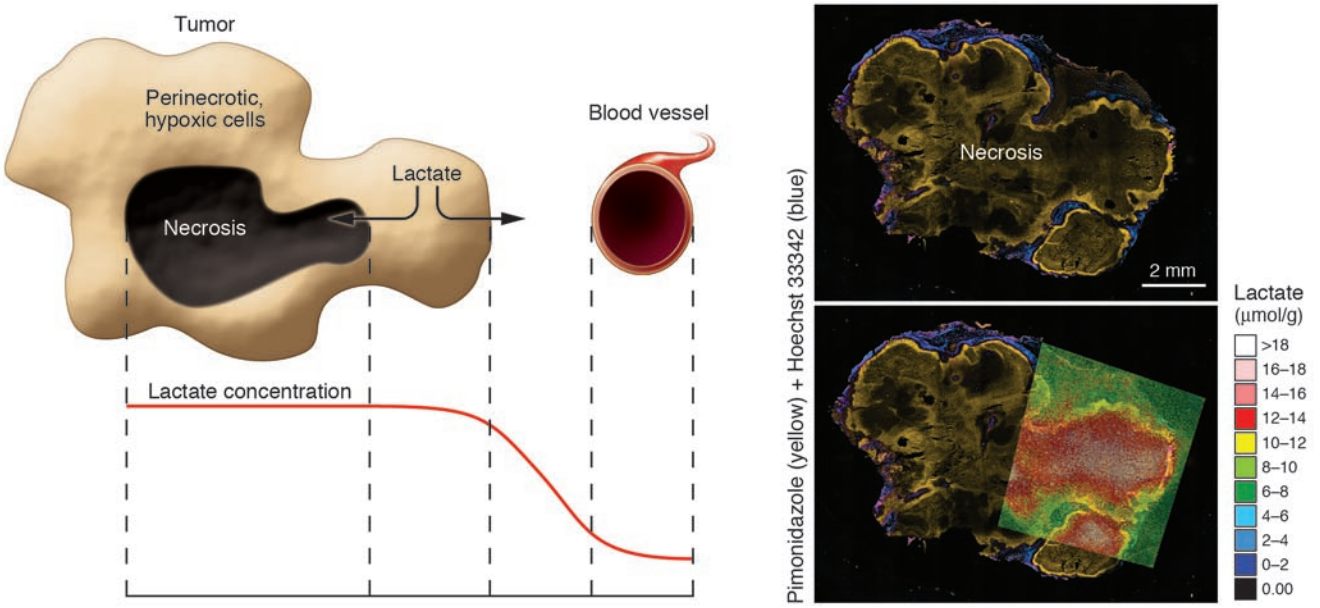

Figure 1
Mechanisms underlying increased lactate concentrations in hypoxic and necrotic versus normoxic, well-perfused tumor areas. Necrosis occurs within the hypoxic core of the (experimental) tumor. Lactate produced by perinecrotic, hypoxic cells is cleared through the microvasculature. Lacking a route of drainage, lactate accumulates in the necrotic cavity. In addition, hypoxia leads to an increase in baseline lactate production rate via the Pasteur effect (16). Consequently, the concentration of lactate in hypoxic tumor areas is determined by oncogenic/hypoxic lactate production, lactate backflow from necrosis, and other factors, such as vascular efficiency and substrate availability. The right panel illustrates these principles in a human cervical carcinoma (SiHa) xenografted in a mouse. The administered hypoxia marker pimonidazole (yellow) labels hypoxic cells, whereas external Hoechst 33342 (blue) marks better-perfused and oxygenated parts of the tumor. Lactate was determined from cryoslices using quantitative bioluminescence microscopy. The images were color encoded and coregistered with the pimonidazole/Hoechst image.

there are studies illustrating the feasibility of performing hypoxia-guided IMRT (20, 21), of including hypoxia information in dose optimization algorithms (22), and of modeling tumor control probability (23, 24), there are currently no clinical data to support that a patient benefit exists. The majority of the current literature has failed to account for changes in hypoxic regions over the course of treatment that may render an original treatment plan ineffective or even more toxic. Sovik et al. have incorporated fluctuating hypoxic regions into their planning and have shown that a maximum tumor control probability would require IMRT replanning twice weekly (25). The clinical utility of the combined EPRI/MRI modality in IMRT dose painting will be uncertain until clinical trials assessing patient outcome and cost-benefit analyses are performed.

Currently, this combined modality requires a 7-T MRI machine. There are only about twenty 7-T or higher field strength MRI machines in use around the world, and those in clinical use are for research purposes (26). Theysohn et al. recently reported that 7-T magnets require scan times approximately twice as long as 1.5-T machines and that 7-T machines also elicit a broader range of complaints from patients. However, they also concluded that, in general, the complaints were not serious and that 7-T imaging was well tolerated by the majority of patients. Further data collection will be necessary to better determine the effects and acceptance of 7-T clinical MRI machines. As a possible alternative, future designs may attempt to find a common resonance at a more clinically useful field strength.

Despite some clinical challenges, this combined pulsed EPRI/MRI technique is relatively limitless in its preclinical applications, and the ability to noninvasively and repeatedly measure multiple tumor parameters will be an exceedingly powerful tool for assessing and refining our knowledge of the tumor environment. For example, the ability to assess multiple tumor parameters concomitantly will heighten the elegance of studies in transgenic mice or in spontaneous tumor models (27). The repeatability and noninvasive nature of this technique will be important for following tumor development and assessing therapeutic response. Successful translation into the clinic will provide clinicians with a greater understanding of how patients respond to therapy, and the metabolic and hypoxic information obtained could be used to decide treatment options in a patient- and tumor physiology–specific manner. In clinical trials, this method would aid in determining treatment schedules based on physiologic response.

In summary, the elegant method of combining pulsed EPRI with MRI/MRS provides a powerful tool to perform multiparametric analysis of tumor physiology, metabolism, and anatomy. It is clear that this method will be exceedingly valuable preclinically to better understand important interrelationships between perfusion, pO_2, and metabolism. Eventual implementation of this technique into the clinic would translate this potential into patient benefit. Furthermore, even though this method has been initially highlighted in oncology, the imaging technique could be applied to many other diseases that involve hypoxia, such as ischemic heart disease, stroke, and inflammatory diseases.

Acknowledgments

Our thanks to Benjamin L. Viglianti, Andrew N. Fontanella, and Kelly Kennedy for their thoughtful discussions regarding this commentary. We also thank Chamali Wickramasekara for technical help and the creativity of Isabel Cardenas-Navia. This work was supported by NIH/NCI grants CA40355 and CA42745.

Address correspondence to: Mark W. Dewhirst, Duke University Medical Center, Box 3455, Room 201 MSRB Research Drive, Durham, North Carolina, USA. Phone: (919) 684-4180; Fax: (919) 684-8718; E-mail: dewhi001@mc.duke.edu.

1. Folkman, J. 1974. Tumor angiogenesis. *Adv. Cancer Res.* **19**:331–358.
2. Secomb, T.W., Hsu, R., Dewhirst, M.W., Klitzman, B., and Gross, J.F. 1993. Analysis of oxygen transport to tumor tissue by microvascular networks. *Int. J. Radiat. Oncol. Biol. Phys.* **25**:481–489.
3. Nordsmark, M., et al. 2005. Prognostic value of tumor oxygenation in 397 head and neck tumors after primary radiation therapy. An international multi-center study. *Radiother. Oncol.* **77**:18–24.
4. Hockel, M., et al. 1996. Association between tumor hypoxia and malignant progression in advanced cancer of the uterine cervix. *Cancer Res.* **56**:4509–4515.
5. Hockel, M., et al. 1998. Tumor hypoxia in pelvic recurrences of cervical cancer. *Int. J. Cancer.* **79**:365–369.
6. Vaupel, P., and Harrison, L. 2004. Tumor hypoxia: causative factors, compensatory mechanisms, and cellular response. *Oncologist.* **9**(Suppl. 5):4–9.
7. Matsumoto, S., et al. 2008. Low-field paramagnetic resonance imaging of tumor oxygenation and glycolytic activity in mice. *J. Clin. Invest.* **118**:1965–1973.
8. Manzoor, A., Yuan, H., Palmer, G., Viglianti, B., and Dewhirst, M. 2008. Imaging hypoxia. In *Molecular imaging: principles and practice*. R. Weissleder, et al., editors. B.C. Decker. Hamilton, Ontario, Canada. In press.
9. Padhani, A.R., Krohn, K.A., Lewis, J.S., and Alber, M. 2007. Imaging oxygenation of human tumours. *Eur. Radiol.* **17**:861–872.
10. Lewis, J.S., and Welch, M.J. 2001. PET imaging of hypoxia. *Q J Nucl. Med.* **45**:183–188.
11. Neeman, M., Dafni, H., Bukhari, O., Braun, R.D., and Dewhirst, M.W. 2001. In vivo BOLD contrast MRI mapping of subcutaneous vascular function and maturation: validation by intravital microscopy. *Magn. Reson. Med.* **45**:887–898.
12. Cooper, R.A., et al. 2000. Tumour oxygenation levels correlate with dynamic contrast-enhanced magnetic resonance imaging parameters in carcinoma of the cervix. *Radiother. Oncol.* **57**:53–59.
13. Lyng, H., et al. 2001. Assessment of tumor oxygenation in human cervical carcinoma by use of dynamic Gd-DTPA-enhanced MR imaging. *J. Magn. Reson. Imaging.* **14**:750–756.
14. Zhao, D., Jiang, L., and Mason, R.P. 2004. Measuring changes in tumor oxygenation. *Methods Enzymol.* **386**:378–418.
15. Gatenby, R.A., and Gillies, R.J. 2004. Why do cancers have high aerobic glycolysis? *Nat. Rev. Cancer.* **4**:891–899.
16. Schroeder, T., et al. 2005. Spatial heterogeneity and oxygen dependence of glucose consumption in R3230Ac and fibrosarcomas of the Fischer 344 rat. *Cancer Res.* **65**:5163–5171.
17. Zu, X.L., and Guppy, M. 2004. Cancer metabolism: facts, fantasy, and fiction. *Biochem. Biophys. Res. Commun.* **313**:459–465.
18. Robey, I.F., Lien, A.D., Welsh, S.J., Baggett, B.K., and Gillies, R.J. 2005. Hypoxia-inducible factor-1alpha and the glycolytic phenotype in tumors. *Neoplasia.* **7**:324–330.
19. Ling, C.C., et al. 2000. Towards multidimensional radiotherapy (MD-CRT): biological imaging and biological conformality. *Int. J. Radiat. Oncol. Biol. Phys.* **47**:551–560.
20. Chao, K.S., et al. 2001. A novel approach to overcome hypoxic tumor resistance: Cu-ATSM-guided intensity-modulated radiation therapy. *Int. J. Radiat. Oncol. Biol. Phys.* **49**:1171–1182.
21. Lee, N.Y., et al. 2008. Fluorine-18-labeled fluoromisonidazole positron emission and computed tomography-guided intensity-modulated radiotherapy for head and neck cancer: a feasibility study. *Int. J. Radiat. Oncol. Biol. Phys.* **70**:2–13.
22. Alber, M., Paulsen, F., Eschmann, S.M., and Machulla, H.J. 2003. On biologically conformal boost dose optimization. *Phys. Med. Biol.* **48**:N31–N35.
23. Malinen, E., Sovik, A., Hristov, D., Bruland, O.S., and Olsen, D.R. 2006. Adapting radiotherapy to hypoxic tumours. *Phys. Med. Biol.* **51**:4903–4921.
24. Thorwarth, D., Eschmann, S.M., Paulsen, F., and Alber, M. 2007. Hypoxia dose painting by numbers: a planning study. *Int. J. Radiat. Oncol. Biol. Phys.* **68**:291–300.
25. Sovik, A., et al. 2007. Radiotherapy adapted to spatial and temporal variability in tumor hypoxia. *Int. J. Radiat. Oncol. Biol. Phys.* **68**:1496–1504.
26. Theysohn, J.M., et al. 2007. Subjective acceptance of 7 Tesla MRI for human imaging. *MAGMA*. doi:10.1007/s10334-007-0095-x.
27. Kirsch, D.G., et al. 2007. A spatially and temporally restricted mouse model of soft tissue sarcoma. *Nat. Med.* **13**:992–997.

Linking adiponectin to proteinuria

Rexford S. Ahima

Department of Medicine, Division of Endocrinology, Diabetes, and Metabolism, University of Pennsylvania School of Medicine, Philadelphia, Pennsylvania, USA.

Obesity predisposes toward renal disease independently of diabetes and hypertension. In this issue of the *JCI*, Sharma and colleagues assessed the role of adiponectin, an adipose-derived hormone, in the pathogenesis of albuminuria (see the related article beginning on page 1645). Obese African Americans had reduced adiponectin levels associated with albuminuria. Adiponectin deficiency in mice induced oxidative stress, fusion of podocyte foot processes in the kidney glomerulus, and urinary albumin excretion. Adiponectin treatment reversed these abnormalities, likely through activation of AMPK. The benefits of adiponectin were observed in diabetic and nondiabetic mice. These findings suggest that adiponectin is a biomarker for kidney disease and may be targeted for prevention and treatment.

Nonstandard abbreviations used: AdipoR, adiponectin receptor; AICAR, 5-aminoimidazole-4-carboxamide-1-β-D-ribonucleoside; HMW, high molecular weight; Nox, NADPH oxidase; ZO-1, zonula occludens–1.

Conflict of interest: R.S. Ahima has received research support from Biomeasure/Ipsen Inc. and served on scientific advisory boards of Biomeasure/Ipsen Inc. and Ethicon Endo-Surgery (Johnson & Johnson).

Citation for this article: *J. Clin. Invest.* **118**:1619–1622 (2008). doi:10.1172/JCI35655.

Obesity and kidney disease

The obesity epidemic has been linked to rising incidences of type 2 diabetes, cardiovascular disease, nonalcoholic fatty liver disease, sleep apnea, and cancer (1). Studies also indicate that obesity increases the risk of kidney disease independently of diabetes and hypertension (2, 3). Renal blood flow and glomerular filtration rate are elevated in obesity and are related to increased levels of the protein albumin in the urine (albuminuria) (4). Epidemiological studies suggest that microalbuminuria, defined as a urine albumin/creatinine ratio of 30–300 μg/mg, increases cardiovascular morbidity (5). Furthermore, an albumin/creatinine ratio considered to be within the normal range (10–30 μg/mg) is associated with higher cardiovascular risk (6). Insulin resistance, oxidative stress, and inflammation have all been implicated in albuminuria and declining kidney function, but the underlying mechanisms are unclear (4).

Hypoadiponectinemia is related to albuminuria

In the current issue of the *JCI*, Sharma et al. describe a role of adiponectin in the pathogenesis of albuminuria (7). Adiponectin is

Targeting lactate-fueled respiration selectively kills hypoxic tumor cells in mice

Pierre Sonveaux,[1,2] Frédérique Végran,[1] Thies Schroeder,[2] Melanie C. Wergin,[2] Julien Verrax,[1] Zahid N. Rabbani,[2] Christophe J. De Saedeleer,[1] Kelly M. Kennedy,[2] Caroline Diepart,[3] Bénédicte F. Jordan,[3] Michael J. Kelley,[4] Bernard Gallez,[3] Miriam L. Wahl,[5] Olivier Feron,[1] and Mark W. Dewhirst[2,5]

[1]Unit of Pharmacology & Therapeutics, Université catholique de Louvain, Brussels, Belgium. [2]Department of Radiation Oncology, Duke University Medical Center, Durham, North Carolina, USA. [3]Unit of Biomedical Magnetic Resonance, Université catholique de Louvain, Brussels, Belgium. [4]Department of Hematology & Medical Oncology and [5]Department of Pathology, Duke University Medical Center, Durham, North Carolina, USA.

Tumors contain oxygenated and hypoxic regions, so the tumor cell population is heterogeneous. Hypoxic tumor cells primarily use glucose for glycolytic energy production and release lactic acid, creating a lactate gradient that mirrors the oxygen gradient in the tumor. By contrast, oxygenated tumor cells have been thought to primarily use glucose for oxidative energy production. Although lactate is generally considered a waste product, we now show that it is a prominent substrate that fuels the oxidative metabolism of oxygenated tumor cells. There is therefore a symbiosis in which glycolytic and oxidative tumor cells mutually regulate their access to energy metabolites. We identified monocarboxylate transporter 1 (MCT1) as the prominent path for lactate uptake by a human cervix squamous carcinoma cell line that preferentially utilized lactate for oxidative metabolism. Inhibiting MCT1 with α-cyano-4-hydroxycinnamate (CHC) or siRNA in these cells induced a switch from lactate-fueled respiration to glycolysis. A similar switch from lactate-fueled respiration to glycolysis by oxygenated tumor cells in both a mouse model of lung carcinoma and xenotransplanted human colorectal adenocarcinoma cells was observed after administration of CHC. This retarded tumor growth, as the hypoxic/glycolytic tumor cells died from glucose starvation, and rendered the remaining cells sensitive to irradiation. As MCT1 was found to be expressed by an array of primary human tumors, we suggest that MCT1 inhibition has clinical antitumor potential.

Introduction

Glycolysis is a cascade of reactions that reduce glucose to pyruvic acid. In eukaryotic cells, the glycolytic flux is modulated by several allosteric effectors, including ATP, which create negative feedback when oxygen is abundant (the Pasteur effect) and allow mitochondria to further oxidize pyruvate to CO_2, H_2O, and energy catabolites (1). Fine-tuning of this metabolic control is essential for maintenance of adequate cell energy production throughout a range of physiological tissue oxygenation levels. In tumors and in wounds, however, oxygen availability is limited (2, 3). Hypoxia selects cells to undergo a fundamental metabolic adaptation, the "glycolytic switch," by which glycolysis is uncoupled from respiration and becomes the primary source of cell ATP production (4). The glycolytic switch formally proceeds through downregulation of the Pasteur effect. Although this response is transient in essence, pioneering studies revealed that some tumor cells remain glycolytic even when oxygen availability is restored (5). Persistence of aerobic glycolysis, the Warburg effect, is a characteristic of cancer cells and a hallmark of advanced cancers (6). It involves stable genetic and epigenetic changes that are still incompletely understood.

Glycolysis provides only 2 ATP molecules for each glucose, whereas respiration provides 38 ATP molecules. Interestingly however, bioenergetic measurements have shown that global ATP concentration and adenylate energy charge change only marginally in tumors compared with normal tissues (7–9). Strong evidence also indicates that the glycolytic phenotype of cancer cells is a crucial component of malignancy that confers a significant growth advantage (10). Our study focused on the nature of this advantage and on its relevance as a therapeutic target. We found that lactate, the end-product of glycolysis, is the keystone of an exquisite symbiosis in which glycolytic and oxidative tumor cells mutually regulate their access to energy metabolites. We also identified monocarboxylate transporter 1 (MCT1) as the gatekeeper of this metabolic symbiosis: using 3 different tumor models, we validated MCT1 inhibition as what we believe to be a new, efficient anticancer treatment alone and in combination with radiotherapy. The efficacy and safety profile of MCT1 inhibition in experimental tumors and the expression of MCT1 in a variety of primary human tumors strongly support the clinical amenability of this therapeutic strategy.

Results

Metabolic characterization of glycolytic and oxidative tumor cell lines. In culture media, phenol red exhibits a gradual color transition from red to yellow over the pH range 8.0 to 6.6. Interestingly, we observed that, when cultured in fresh medium at confluence, some tumor cell lines failed to induce the color shift. Absence of change was typically observed with SiHa human cervix squamous carcinoma cells, whereas WiDr human colorectal adenocarcinoma cells induced the color transition (Figure 1A, inset). Extracellular pH measurements confirmed that WiDr cell cultures gradually

Nonstandard abbreviations used: CHC, α-cyano-4-hydroxycinnamate; EF5, 2-(2-nitro-1H-imidazol-1-yl)-*N*-(2,2,3,3,3-pentafluoropropyl) acetamide; EPR, electron paramagnetic resonance; LLc, Lewis lung carcinoma; MCT, monocarboxylate transporter; ρ0, mitochondrial DNA–depleted (cells); TLT, transplantable liver tumor.

Conflict of interest: The authors have declared that no conflict of interest exists.

Citation for this article: *J. Clin. Invest.* doi:10.1172/JCI36843.

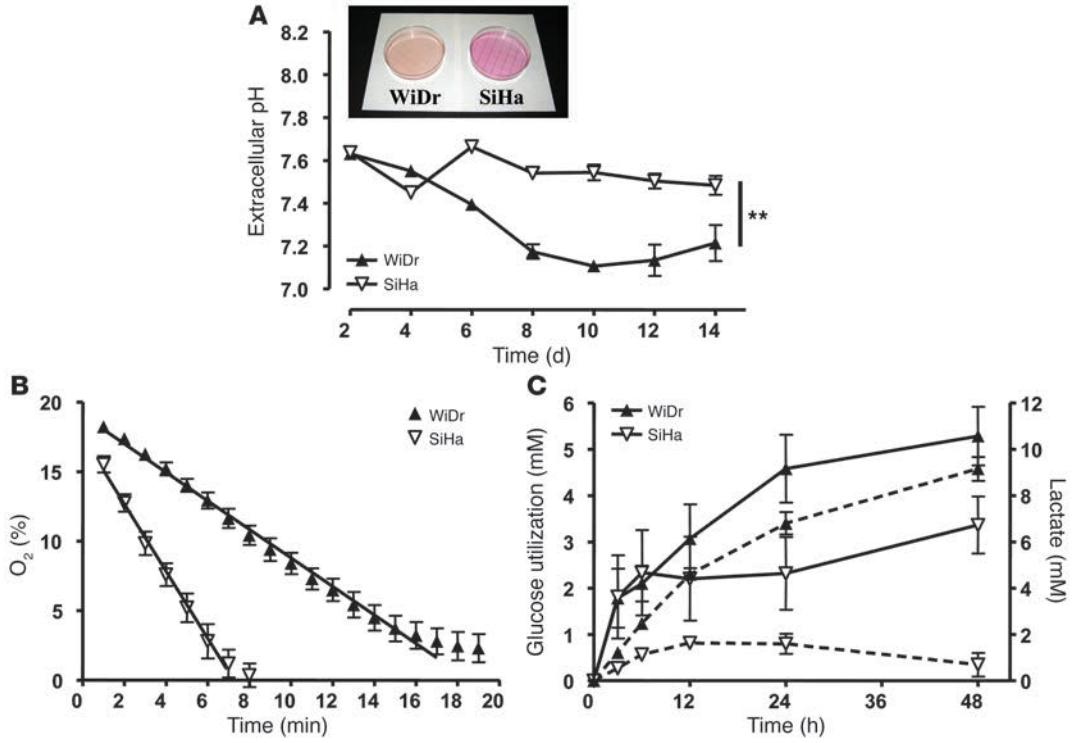

Figure 1

Metabolic characterization of oxidative SiHa and glycolytic WiDr tumor cell lines. (**A**) pH of cell culture supernatants after reaching cell confluence on day 0 was measured with a pH meter. Inset shows typical dishes containing confluent WiDr and SiHa cells in phenol red–containing medium. $^{**}P = 0.0013$ (2-way ANOVA; $n = 3$). (**B**) An equal amount (2×10^7 cells/ml) of viable SiHa and WiDr cells were placed in a sealed tube containing an EPR oxygen sensor. EPR measurements revealed a significant difference ($P < 0.0001$) in the rate of oxygen consumption between SiHa and WiDr tumor cells (Student's *t* test; $n = 5–9$). (**C**) At time 0, confluent cells received fresh medium containing glucose and FBS. Glucose utilization (solid lines, left *y* axis) and lactate concentration in the cell supernatant (dotted lines, right *y* axis) were determined enzymatically. Note the different scales of the left and right *y* axes. $n = 4$. Error bars represent the SEM and are sometimes smaller than symbols.

became more acidic, whereas SiHa cell cultures did not acidify (Figure 1A). We therefore suspected that the 2 cell lines had a different metabolic behavior in vitro.

In sealed tubes, cells consume available oxygen at a rate dictated by their oxidative capacity (11), which can be measured using electron paramagnetic resonance (EPR). Using this technique, we observed that WiDr cells had a lower rate of oxygen consumption than did SiHa cells (Figure 1B and Table 1), suggesting that medium acidification by WiDr cells was not due to accumulation of CO_2 from respiration. Rather, glucose and lactate measurements revealed that, with adequate oxygen supply, WiDr cells exhibited predominantly a glycolytic metabolism (Warburg phenotype), as they released 2 lactate molecules for each glucose consumed (Figure 1C). Curve fitting ($R^2 = 0.97$) indicated that export of lactate used a saturable pathway. In contrast, SiHa cells exhibited an oxidative metabolism characterized by lower glucose utilization and limited lactate release. The bell-shaped aspect of the lactate concentration curve in SiHa cell medium suggested that these cells could take up and perhaps metabolize lactate.

Lactate fuels tumor cell respiration preferentially to glucose. Existence of a lactate consumption pathway was tested in vitro as cells received exogenous lactate. Sodium lactate was used at a concentration of 10 mM to match lactate release achieved by WiDr cells in vitro; this concentration also corresponds to the range of lactate detected in tumors (9). In the presence of glucose and lactate, oxidative SiHa cells switched from glucose to lactate uptake and thus imported consistently less glucose than in the absence of lactate (Figure 2A). The average rate of glucose utilization was significantly lower in the presence of lactate (0.29 ± 0.06 mM/d) than in its absence (1.68 ± 0.31 mM/d; $P = 0.0016$, Student's *t* test; $n = 4–5$). Profoundly contrasting with SiHa cells, lactate production by WiDr cells was insensitive to exogenous lactate. The glycolytic stoichiometry was lost, which further documented the saturable nature of this pathway. When glucose was removed, lactate only marginally entered WiDr cells (which eventually died) but was massively cleared by SiHa cells (Figure 2B). Furthermore, induction of mitochondrial dysfunction in mitochondrial DNA–depleted (ρ0) SiHa cells caused a switch from lactate oxidation to glycolysis (Figure 2C), which indicated that the normal fate of lactate is to fuel the TCA cycle in these cells. Compared with wild-type cells, ρ0 WiDr cells showed increased glucose uptake despite unchanged lactate release (Figure 2D).

We then showed that exogenous lactate could efficiently replace glucose to fuel SiHa cell respiration (Figure 2E and Table 1), whereas respiration was dramatically reduced in the absence of both glucose and lactate. The respiration rate of WiDr cells, which was already low in the presence of glucose (see Figure 1B), decreased sharply upon glucose removal (Figure 2F). Interestingly, exogenous lactate rescued part of WiDr cell respiration, providing evidence that lactate can also fuel the marginal oxidative metabolism of dominantly Warburg phenotype tumor cells. We verified

Table 1
Lactate fuels tumor cell respiration in an MCT1-dependent manner

Tumor cell type	Glucose + FBS	Exogenous sodium lactate	MCT1 inhibition	Respiration rate (slope ± SEM)	*P*	*n*
SiHa	+	–	–	–2.41 ± 0.16	NA	5
	–	–	–	–0.96 ± 0.02	$<10^{-4}$ [A]	4
	–	+	–	–2.29 ± 0.08	0.50[A]	6
	+	–	+ (CHC)	–2.12 ± 0.09	0.13[A]	6
	–	+	+ (CHC)	–0.27 ± 0.01	$<10^{-4}$ [A]	5
	–	+	– (Sham transfection)	–2.42 ± 0.13	NA	3
	–	+	– (Scrambled siRNA)	–2.49 ± 0.07	0.65[B]	3
	–	+	+ (MCT1 siRNA)	–1.79 ± 0.05	0.0004[B]	4
	–	+	– (shRNA empty vector)	–4.09 ± 0.21	NA	4
	–	+	+ (MCT1 shRNA)	–2.83 ± 0.07	0.0002[B]	6
WiDr	+	–	–	–1.07 ± 0.04	NA	9
	–	–	–	–0.34 ± 0.03	$<10^{-4}$ [A]	7
	–	+	–	–0.62 ± 0.02	$<10^{-4}$ [A]	4
	+	–	+ (CHC)	–0.92 ± 0.02	0.04[A]	4
	–	+	+ (CHC)	–0.19 ± 0.01	$<10^{-4}$ [A]	4

[A]Compared with cells in medium containing only glucose and FBS. [B]Compared with control transfection.

the existence of lactate-fueled respiration in vivo using NMR. Thirty minutes after [^{13}C]lactate delivery to tumor-bearing mice, we consistently detected its TCA metabolite [^{13}C]glutamate in SiHa and WiDr tumors (data not shown).

MCT1 gates lactate-fueled ATP production in tumor cells. In nonmalignant tissues, the lactate anion can shuttle between intracellular and extracellular compartments through MCTs that function as passive lactate-proton symporters (12). Among known isoforms, MCT4 has been detected at the plasma membrane of glycolytic muscle fibers, where it facilitates lactate export (13), and MCT1 at the plasma membrane of oxidative fibers, where it mediates lactate uptake during intensive training or supramaximal exercise (14–16). Here, we found that oxidative SiHa tumor cells, like oxidative muscle fibers, constitutively expressed *MCT1* mRNA at a higher relative level compared with glycolytic WiDr cells (Figure 3A). In SiHa cells, *MCT1* was more actively transcribed than *MCT4* (Figure 3B), whereas MCT4 was preferentially expressed in WiDr cells (data not shown). The plasma membrane expression of MCT1 in SiHa cells contrasted with the scattered cytosolic, almost undetectable expression of MCT4 (Figure 3C), suggesting that lactate uptake by these cells primarily depends on MCT1. To confirm MCT involvement in lactate uptake, we measured changes in intracellular pH in response to acute lactate exposure. A small but significant decrease in intracellular pH was observed in SiHa cells exposed to exogenous lactate (Figure 3D), indicating activation of a lactate-proton symporter. In contrast, intracellular pH remained unchanged in WiDr cells after lactate treatment.

Immunostaining of SiHa and WiDr tumor biopsies revealed localization of MCT1 at the vascularized tumor periphery and around blood vessels (Figure 3E). This similar pattern of expression indicated that, although the metabolic phenotype of SiHa and WiDr cells diverge in vitro, local pO_2 and MCT1 expression may vary in vivo according to the oxidative capacity of tumor cells. We further documented that SiHa tumors contained 2 viable tumor cell subpopulations defined by differential pO_2 and MCT1 expression. A first subset of cells, located in the well-vascularized (positive CD31 staining) and oxygenated (negative HIF-1α and pimonidazole stainings) tumor margin, expressed MCT1 (Figure 3F). The other subpopulation was hypoxic (positive for HIF-1α and pimonidazole), poorly vascularized, and did not express MCT1. MCT1 expression and hypoxia were also mutually exclusive in WiDr tumors (Figure 3F).

Existence of distinct tumor cell phenotypes indicated that exogenous lactate and MCT1 could play important functions in tumors. It was verified using α-cyano-4-hydroxycinnamate (CHC), a drug known to reversibly inhibit MCT1 with approximately 10-fold selectivity compared with other MCTs (17). MCT1 inhibition induced a switch from lactate to glucose utilization by SiHa cells (Figure 4A). In fact, upon MCT1 inhibition, oxygenated cells became entirely glycolytic, consuming glucose abundantly and releasing lactate stoichiometrically, thereby recapitulating the Warburg phenotype. Importantly, when lactate was the sole energy source, MCT1 inhibition blocked both lactate uptake (Figure 4B) and SiHa cell respiration (Figure 4C and Table 1) and induced tumor cell death. CHC also prevented partial rescue of respiration by lactate in glucose-deprived WiDr cells (Figure 4D), which is in agreement with previous studies documenting lactate uptake by glycolytic tumor cells when cultured in the absence of glucose (18, 19). Of note, CHC did not affect either SiHa or WiDr cell respiration in the presence of glucose, indicating that the mitochondrial function is independent of MCT1 in these cells (20). Methylpyruvate, a membrane-permeable form of pyruvate (21), almost totally rescued the respiration of SiHa cells in the presence of lactate and CHC (Figure 4E). SiHa respiration rates (slope ± SEM) were –2.81 ± 0.16 in the presence of lactate alone (n = 8), –0.01 ± 0.01 for lactate plus CHC (n = 4), and –1.56 ± 0.06 in the presence of lactate, CHC, and methylpyruvate (n = 8). Moreover, we found that a significant reduction in MCT1 expression (>90%, obtained after transfection with a specific siRNA or a specific shRNA) was associated with a decreased rate of lactate-fueled SiHa cell respiration (Table 1). Although full protein extinction was not achieved in our experimental conditions (and probably accounts for residual respiration), this observation confirms the prominent role of MCT1 compared with other MCT isoforms in mediating lactate uptake to fuel oxidative tumor cell respiration.

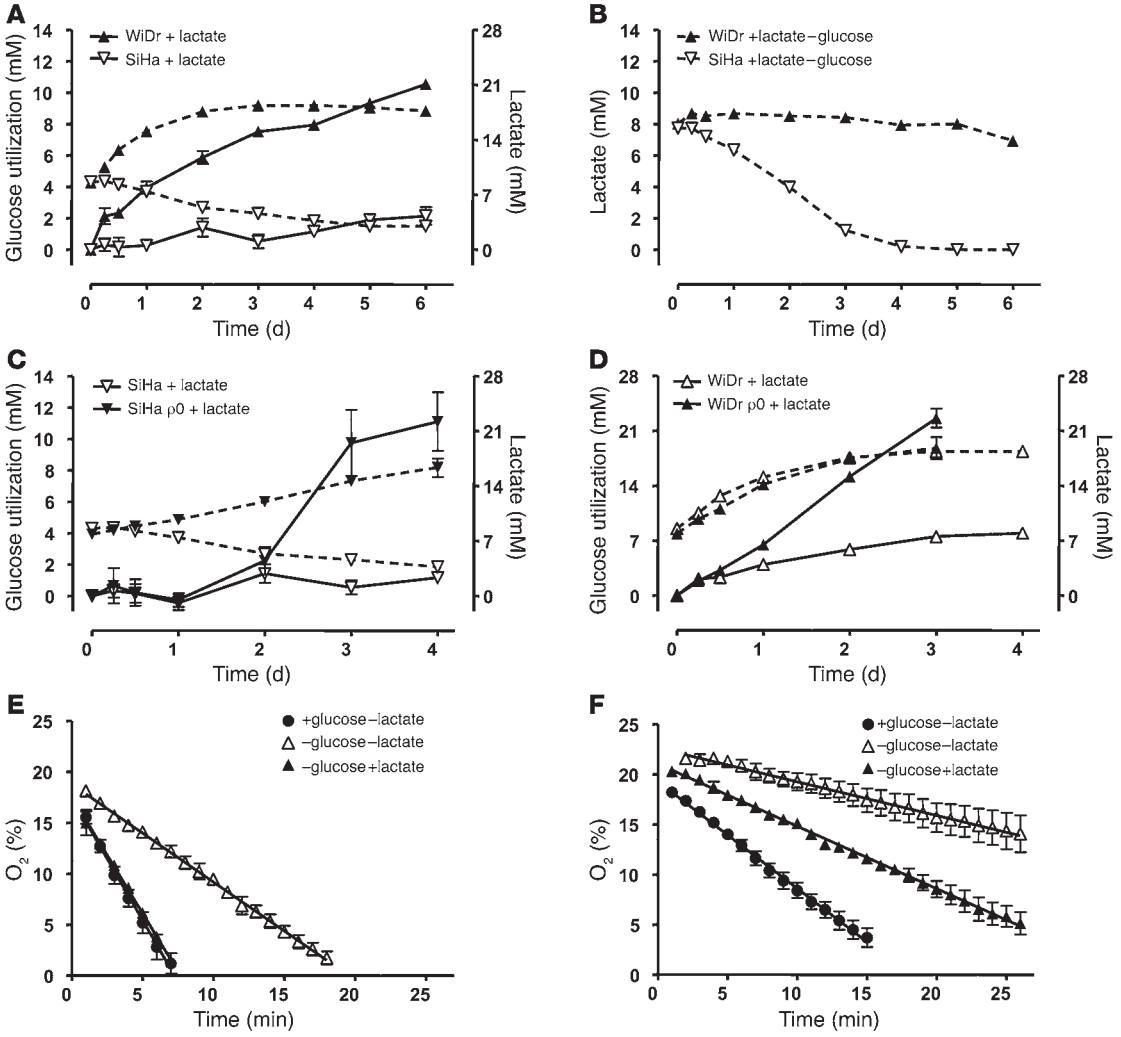

Figure 2

Lactate is a substrate for oxidative tumor cell metabolism. (**A** and **B**) Enzymatic assays were used to determine glucose utilization (solid lines) and lactate concentration in the supernatant of confluent cells (dotted lines). Note the different scales of the left and right *y* axes in **A**. At time 0, cells received fresh medium containing glucose, FBS, and sodium lactate (**A**) or medium containing sodium lactate but no glucose and FBS (**B**). $n = 4–5$. (**C** and **D**) ρ0 SiHa and WiDr cells were produced by a chronic treatment with low-dose ethidium bromide. Then, cells were cultured in fresh medium containing glucose, FBS, and sodium lactate from time 0. Glucose utilization (solid lines, left *y* axes) and lactate concentration in the supernatant of confluent cells (dotted lines, right *y* axes) were assayed enzymatically to compare the metabolic activity of wild-type versus ρ0 SiHa cells (**C**) and wild-type versus ρ0 WiDr cells (**D**). Note the different scales of the left and right *y* axes. $n = 3–5$. (**E** and **F**) EPR measurements of tumor cells oxygen consumption by SiHa cells (**E**) and WiDr cells (**F**) in the indicated experimental culture media. Statistical analyses are presented in Table 1. Error bars represent the SEM and are sometimes smaller than symbols.

From the bioenergetic standpoint, lactate oxidation would be futile if not yielding ATP production. We therefore measured intracellular ATP and found that replacement of glucose by lactate almost entirely preserved ATP stores in SiHa cells (Figure 5A). In the presence of glucose, CHC did not poison mitochondria (see Figure 4C) and, accordingly, only marginally influenced glucose-fueled ATP production by SiHa cells. However, when lactate was the sole energy source, MCT1 inhibition caused rapid ATP breakdown and cell death. These responses were even faster than in the absence of both glucose and lactate. In WiDr cells deprived of glucose, the decrease in ATP was not rescued by lactate (Figure 5B). Interestingly, however, MCT1 inhibition partially reduced glucose-fueled ATP synthesis, which, together with our other results, indicates that WiDr cells may recycle part of their own lactate production to produce energy oxidatively. To formally demonstrate its role in controlling lactate respiration, we silenced MCT1 with a specific shRNA or a specific siRNA in SiHa cells. RT-PCR confirmed a 94.5% ± 1.5% and a 92.3% ± 2.6% transcript reduction, respectively. While MCT1 silencing did not affect cell survival in glucose-containing media (with or without lactate), it induced cell death when lactate was the only source of energy (Figure 5C). In the latter situation, cells were rescued by the addition of methylpyruvate, which confirms that MCT1 inhibition did not have an impact on the mitochondrial function of these cells (see also Figure 4, C and E). Importantly, MCT1 silencing was as efficient as complete removal of all energy substrates to induce SiHa tumor cell death, demon-

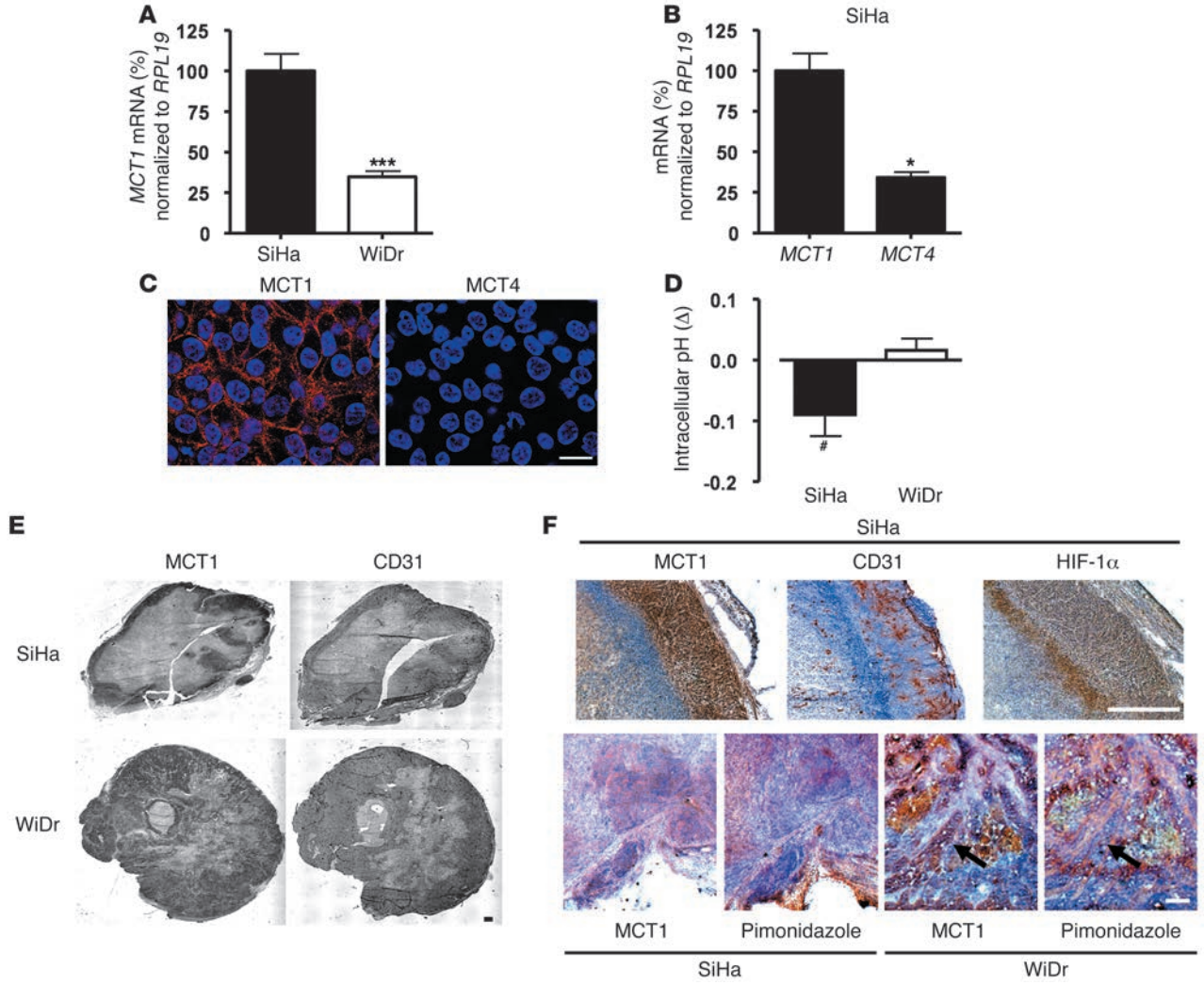

Figure 3

Oxidative tumor cells prominently express MCT1. (**A**) qRT-PCR analysis showing higher *MCT1* mRNA expression in oxidative SiHa tumor cells compared with glycolytic WiDr tumor cells. ***P = 0.0002 (Student's t test; n = 8–13). (**B**) qRT-PCR analysis also showed that oxidative SiHa cells expressed higher levels of *MCT1* compared with *MCT4* mRNA. *P = 0.0116 (Student's t test; n = 3–13). (**C**) MCT1, but not MCT4, is expressed at the plasma membrane of oxidative SiHa tumor cells. Representative confocal pictures show fluorescent staining of MCT1 (red), MCT4 (red), and nuclei (blue) in cultured cells. (**D**) SiHa and WiDr cells were loaded with the intracellular pH sensor C.SNARF1-AM. Intracellular pH was determined from fluorescence emission before and after addition of sodium lactate to the cell culture medium maintained at pH 7.3. Columns represent the difference (Δ) between the intracellular pH measured in the presence of exogenous lactate and the intracellular pH measured in the absence of exogenous lactate. #P = 0.0393 (Student's t test; n = 4). (**E** and **F**) Immunohistological analyses of tumor biopsies revealed that MCT1 is expressed in both SiHa and WiDr tumors in vivo and that MCT1 expression and hypoxia are mutually exclusive. (**E**) Representative pictures of whole SiHa and WiDr tumor sections. (**F**) Representative pictures are shown with H&E counterstaining. Arrows indicate typical mutually exclusive MCT1 and pimonidazole stainings in WiDr tumors. Scale bars: 20 μm (**C**), 0.5 mm (**E** and **F**). Error bars represent SEM.

strating the absolute requirement of MCT1 over other transporters to fuel tumor cell respiration with lactate. Survival of sham-transfected and wild-type SiHa cells were not different from each other in all media tested. In contrast, MCT1 silencing did not modulate WiDr cell death that occurred independently of exogenous lactate upon glucose removal (Supplemental Figure 1; supplemental material available online with this article; doi:10.1172/JCI36843DS1).

MCT1 inhibition exerts antitumor effects. To test the in vivo relevance and the therapeutic amenability of the lactate pathway that we identified, we sought to determine the antitumor potential of MCT1 inhibition. We used daily CHC delivery as a treatment protocol: no overt systemic toxicity was observed at this drug regimen (Supplemental Figure 2). We first selected 2 experimental mouse models based on MCT1 expression. In the first model, Lewis lung carcinoma (LLc) cells expressed MCT1 at the plasma membrane (Figure 6A). Intramuscular injection of these cells generated aggressive malignancies in the hindlimbs of syngeneic mice (Figure 6B). In this model, chronic MCT1 blockade induced sustained tumor growth retardation. Analysis of size-matched LLc tumors at the end of treatments revealed extensive central necrosis after MCT1 inhibition (Figure 6C). In the second model, hepatocarcinoma (transplantable liver tumor [TLT]) cells did not express MCT1

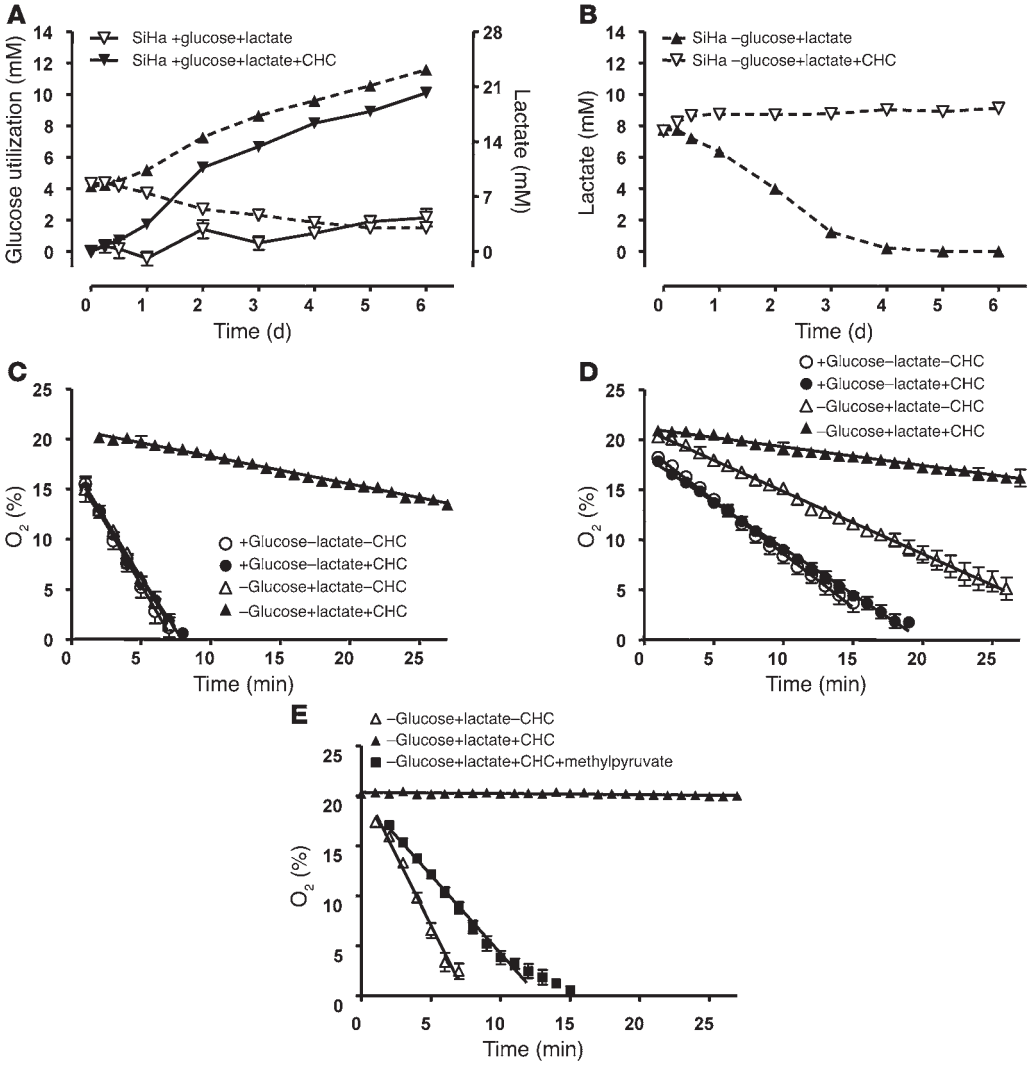

Figure 4

MCT1 inhibition blocks lactate-fueled tumor cell respiration. (**A** and **B**) Enzymatic assays were used to determine glucose utilization (solid lines) and lactate concentration (dotted lines) in the supernatant of confluent cells. Note the different scales of the *y* axes in **A**. At time 0, cells received fresh medium containing glucose, FBS, and sodium lactate (**A**) or medium containing sodium lactate but no glucose and FBS (**B**). The MCT1 inhibitor CHC was added where indicated. $n = 4–5$. (**C**–**E**) EPR measurements of tumor cell oxygen consumption by SiHa (**C** and **E**) and WiDr cells (**D**) in the indicated experimental culture media. Statistical analyses of **C** and **D** are presented in Table 1. Error bars represent the SEM and are sometimes smaller than symbols.

at the plasma membrane (Figure 6D). The corresponding tumors were also totally insensitive to daily CHC (Figure 6E), confirming that the antitumor efficacy of MCT1 inhibition is restricted to tumor cells expressing MCT1 at the plasma membrane. These data also allow us to exclude a major contribution of host cells to the response to the MCT1 inhibitor (22) and off-target effects. It is well known that SiHa cells do not reproducibly generate tumors in vivo. To extend our paradigm to human tumors, we therefore chose to use WiDr tumors, in which oxygenated tumor cells consistently expressed MCT1 in vivo (see Figure 3, E and F). MCT1 was also found at the plasma membrane of WiDr cells in vitro (Figure 6F). As in the LLc model, chronic MCT1 inhibition sustainably delayed WiDr tumor growth (Figure 6G), mostly because of the extension of a necrotic area at the center of the tumor (as determined on size-matched treated and untreated tumors; Figure 6H). Compared with vehicle, MCT1 inhibition also dramatically reduced hypoxia at the tumor periphery. Increased tumor oxygenation was particularly evident around arterioles (where the hypoxic front had completely disappeared) and at the tumor-muscle interface. CHC-treated tumors also showed a lower density of hypoxic islets in the viable tumor cell compartment. This relief of tumor hypoxia very likely results from decreased tumor cell oxygen consumption upon MCT1 inhibition (see Figure 4D). These data also reveal that microenvironmental influences can stimulate MCT1-mediated lactate consumption, which is otherwise nonexistent in vitro. A model of tumor metabolic symbiosis underscoring the outcomes of anti-MCT1 strategy is presented in Figure 7.

MCT1 inhibition radiosensitizes tumors. To confirm and exploit increased tumor pO_2 resulting from the metabolic switch to glycolysis in oxidative cells, we combined MCT1 inhibition and

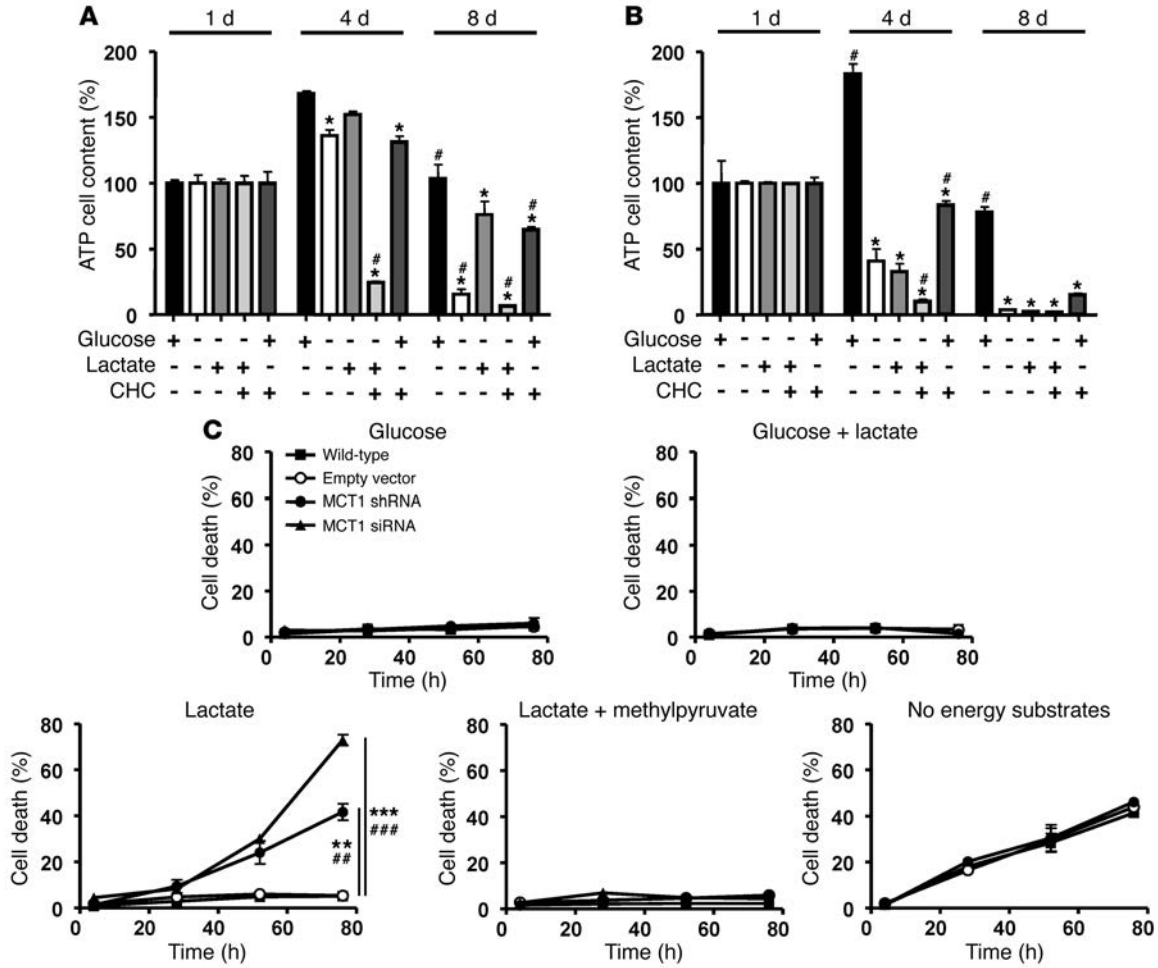

Figure 5

MCT1 inhibition prevents lactate-fueled ATP production and the survival of oxidative tumor cells. (**A** and **B**) ATP content was determined over time in SiHa (**A**) and WiDr (**B**) cells using a bioluminescence assay. Cells were cultured in the indicated media. $^{*}P < 0.05$ compared with medium containing only glucose. $^{\#}P < 0.05$ compared with medium containing only lactate (Student's *t* test; $n = 4$). (**C**) SiHa cells were transfected with a specific MCT1 shRNA or siRNA or a control vector, or were left untreated. After a 24-hour recovery period, cells were cultured in the indicated media from time 0. Cell death was determined over time using a NucleoCounter. Slope comparison: $^{**}P = 0.0014$ and $^{***}P = 0.0003$ compared with wild-type cells; $^{\#\#}P = 0.0013$ and $^{\#\#\#}P = 0.0003$ compared with control vector transfection (Student's *t* test; $n = 3$–7). Error bars represent the SEM and are sometimes smaller than symbols.

radiotherapy to treat LLc tumors in mice. As single therapeutic modalities, MCT1 inhibition or a 6-Gy irradiation induced similar effects on tumor growth, with a small advantage for MCT1 inhibition (Figure 8, A and B). Importantly, the overall benefit of combined treatment on tumor growth retardation (growth delay of 13.5 ± 0.9 days) was significantly increased compared with calculated additive effects (+10.5 ± 0.8 days; $P = 0.0424$, Student's *t* test). These data underscore the therapeutic impact of targeting MCT1-driven symbiosis between hypoxic and oxygenated tumor cell subpopulations.

MCT1 is expressed in an array of human tumors. We concluded our study by evaluating MCT1 distribution in a range of human tumors of different origins. In addition to WiDr colorectal adenocarcinoma and SiHa cervix squamous cell carcinoma, MCT1 was detected in human squamous cell carcinoma (FaDu) and human breast adenocarcinoma (MCF-7) cell lines (Figure 9A). Muscle and heart were used as positive controls (12), and the human breast cancer cell line MDA-MB-231, in which MCT1 is silenced by gene methylation (23), was used as a negative control. MCT1 plasma membrane expression was present in 4 of 6 tumor cell lines tested, including WiDr, FaDu, SiHa, and human prostate cancer PC-3 (Figure 9B). It was absent in MDA-MB-231 cells. In MCF-7 cells, clustered cytoplasmic localization suggested mitochondrial expression of the transporter (20). MCT1 was also present in biopsies of primary human colon, breast, head and neck, and lung cancers (Figure 9, C and D). In human colon cancer, we detected strong MCT1 expression in 78% (7 of 9) of independent biopsies (data not shown). Of note, as in our experimental models (see Figure 3F), MCT1 expression and hypoxia (2-[2-nitro-1H-imidazol-1-yl]-*N*-[2,2,3,3,3-pentafluoropropyl] acetamide [EF5] staining) were mutually exclusive in primary human lung tumors (Figure 9D). In the clinical context, MCT1 expression is thus also in line with its function of facilitator of lactate respiration.

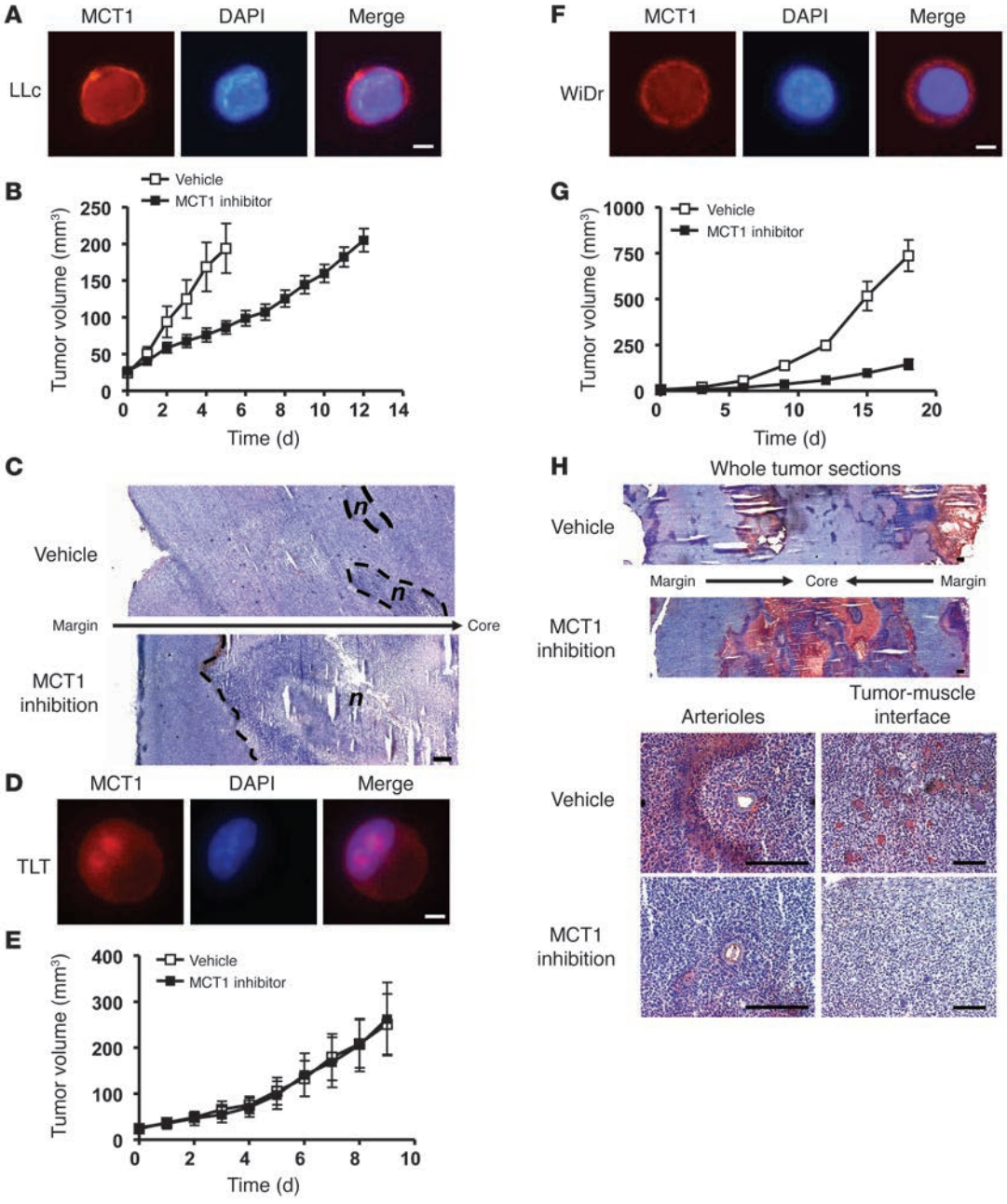

Figure 6

MCT1 inhibition delays tumor growth, induces tumor core necrosis, and decreases tumor hypoxia. (**A**) MCT1 is expressed at the plasma membrane of mouse LLc cells. Representative pictures show fluorescent staining of MCT1 (red) and nuclei (blue) in cultured cells. (**B**) From day 0, LLc tumor growth was determined in groups of mice treated with daily CHC (25 μmol in 200 μl i.p.) or vehicle. *n* = 11–17. (**C**) Representative H&E staining of biopsies of size-matched tumors after treatments. Dashed lines delineate necrosis (n). (**D**) MCT1 is not expressed at the plasma membrane of mouse TLT cells. Representative pictures show fluorescent staining of MCT1 (red) and nuclei (blue) in cultured cells. (**E**) Similar analysis was performed as in **B**, but using TLT cells. *n* = 6. (**F**) Similar analysis was performed as in **A**, but using WiDr human colorectal adenocarcinoma cells. (**G**) Similar analysis was performed as in **B**, but using WiDr cells in athymic Balb/C mice. *n* = 9–15. (**H**) Representative histological pictures of pimonidazole staining of WiDr tumor biopsies at the end of the tumor growth delay assay are shown with H&E counterstaining. Top: Analysis of whole tumor sections revealed extensive necrosis at the core of tumors from an animal treated with the MCT1 inhibitor. Bottom: MCT1 inhibition decreased tumor hypoxia around arterioles and at the tumor-muscle interface at the tumor periphery. Scale bars: 20 μm (**A**, **D**, and **F**); 200 μm (**C** and **H**). Error bars represent SEM.

Discussion

Lactic acid (negative logarithm of the acid ionization constant [pK_a] 3.86) is almost fully dissociated in biological fluids. Although important roles have been ascribed to protons in tumor progression (24), the biological contribution of lactate has been largely ignored. Interestingly, however, lactate accumulation in human tumors was shown to be associated with metastasis, tumor recurrence, and poor survival (25–27). Our study identifies lactate as a prominent fuel for the oxi-

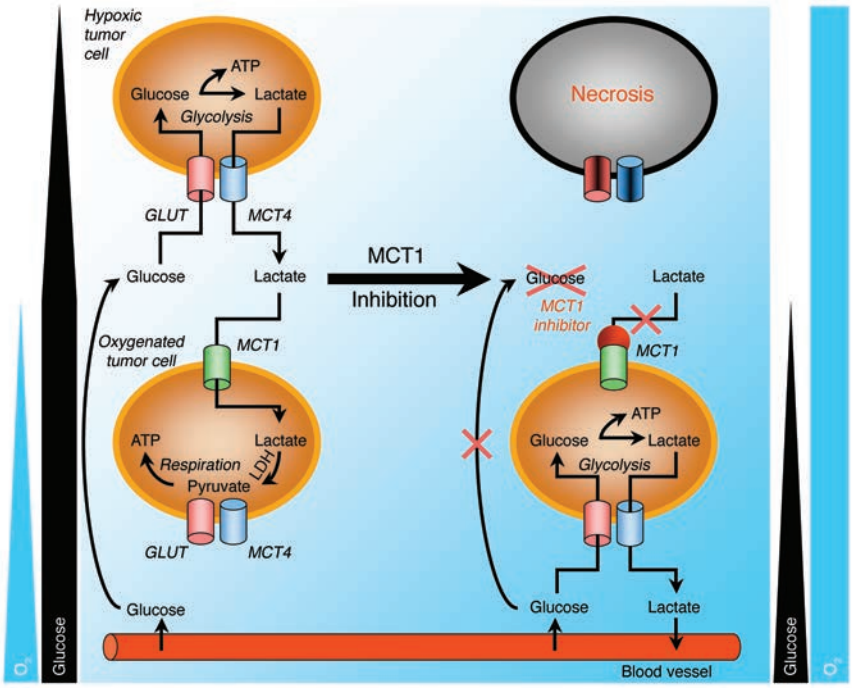

Figure 7
Model for therapeutic targeting of lactate-based metabolic symbiosis in tumors. Hypoxic tumor cells depend on glucose and glycolysis to produce energy. Lactate, the end-product of glycolysis, diffuses along its concentration gradient toward blood vessels. By contrast, oxygenated tumor cells import lactate (a process mediated by MCT1 located at the cell plasma membrane) and oxidize it to produce energy. In the respiration process, lactate is a substrate preferred to glucose. As a consequence, glucose freely diffuses through the oxygenated tumor cell sheath to fuel glycolysis of distant, hypoxic tumor cells. This metabolic symbiosis can be disrupted by MCT1 inhibition. Upon MCT1 inhibition, oxidative tumor cells switch from lactate oxidation to glycolysis, thereby preventing adequate glucose delivery to glycolytic cells, which die from glucose starvation. This glycolytic switch is associated with a decrease in oxygen consumption of surviving tumor cells, which is responsible for increased tumor pO_2. MCT1 inhibition is thus a potent antitumor strategy that indirectly eradicates hypoxic/glycolytic tumor cells. GLUT, glucose transporter.

dative metabolism of oxygenated tumor cells and MCT1 as a crucial component of a metabolic symbiosis based on lactate exchange in tumors. Accordingly, using 3 different tumor models, we document that MCT1 inhibition exerts profound antitumor effects alone or in combination with radiotherapy, provided that tumor cells express MCT1, as we found in an array of primary human tumors.

Oxidative preference of tumor cells for lactate over glucose was evidenced in the current study, supporting the concept of a tumor metabolic symbiont. Lactate, released as the end-product of glycolysis in the hypoxic tumor cell compartment, prominently fuels the oxidative metabolism of the oxygenated tumor cell subpopulation, thereby sparing glucose for glycolytic cells. That lactate can substitute glucose for oxidation has also been observed in ischemic brain recovery (28). The mechanism set forward involves a competition between lactate and glucose metabolism for the intracellular NAD^+ pool. Existence of this feedback could provide several advantages to oxidative tumor cells. First, oxidation of lactate to pyruvate by lactate dehydrogenase (LDH) involves the sustained production of reducing equivalents that could buffer tumor oxidative stress (29) and activate prosurvival pathways (30). Second, lactate oxidation does not require the initial energy input that drives ATP production from glucose. Third, respiration of lactate yields 18 ATP per lactate molecule and spares energy normally intended for housekeeping glycolytic enzymes. Lactate oxidation is thus more concise and more effective than glucose in the tumor cell energy metabolism under aerobic conditions.

Shuttling of lactate between hypoxic and oxygenated sites in tumors is reminiscent of muscle physiology (12, 13). Indeed, during intense or supramaximal exercise, fast-twitch glycolytic fibers (white muscle) produce and release lactic acid (16). Extracellular lactate is then removed by oxidation in slow-twitch fibers (red muscle), which recycle it as a respiratory fuel (14–16). These activities are mediated by MCTs, among which MCT1–MCT4 are known to passively convey lactate across cell membranes (12, 13). MCT4 is a low-affinity lactate transporter (K_m = 22 mM), which is adapted to the release of lactate from glycolytic cells such as white muscle fibers (31). It is hypoxia inducible (32). Conversely, MCT1 has a higher affinity for lactate (K_m = 3.5–10 mM) and is predominantly found at the plasma membrane of oxidative muscle fibers, where it promotes lactate influx and oxidation (13, 16, 32). While MCT4 is part of the arsenal of proton extruders in glycolytic tumor cells (33), we here formally demonstrate that MCT1 is the foremost facilitator of lactate uptake by oxidative tumor cells. MCT1 silencing was sufficient to inhibit lactate-fueled respiration and survival of tumor cells as efficiently as complete metabolite energy starvation. The oxygen dependence of MCT1 expression accounts for its distribution in oxygenated tumor areas and brings its expression in line with its function as a mediator of lactate oxidation. Similar to angiogenesis, which is physiological in essence, the lactate exchange system of the exercising muscle is thus usurped by cancer cells.

Using a pharmacological inhibitor and silencing RNAs, we have documented antitumor effects of MCT1 inhibition without overt toxicity in 3 different models of animal and human tumors (see also Supplemental Data). Although it targets oxygenated cells close to drug-supplying blood vessels, MCT1 inhibition indirectly induces necrosis of distant hypoxic tumor cells known to be resistant to conventional antitumor treatments and responsible for tumor relapse (34) (see Figure 7). Hypoxic cell death by virtue of glucose starvation originates from a switch from lactate oxidation to glycolysis (and avid glucose uptake) in oxygenated tumor cells, which can logically be attributed to the inhibition of cell respiration by glucose ("Crabtree effect") (35). The same metabolic switch accounts for reduced oxygen consumption by surviving tumor cells and, thereby, tumor radiosensitization after MCT1 inhibition.

That the lactate-MCT1 pathway is the keystone for metabolic symbiosis in tumors sheds a new light on previous reports. First, the energy substrate nature of lactate provides what we believe is an unprecedented explanation for its autocrine growth factor activity, which has been authenticated in vitro (36) and for its bidirectional transport in different cell types according to the

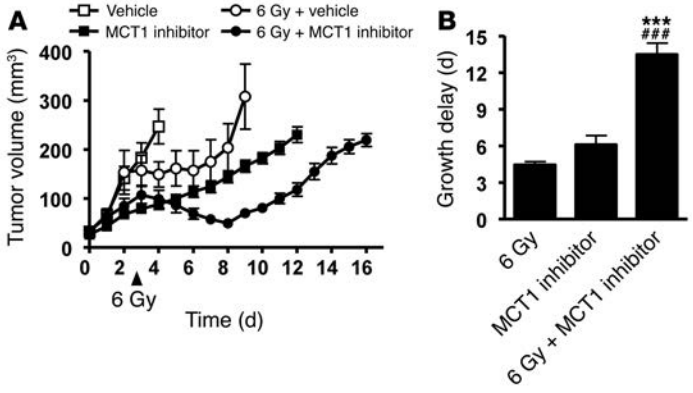

Figure 8
MCT1 inhibition radiosensitizes tumors. LLc tumor–bearing mice were treated with CHC (daily doses of 25 μmol in 200 μl i.p.) or vehicle (200 μl) from day 0, local radiotherapy (1 dose of 6 Gy) on day 3, or combined treatments. (**A**) Tumor volume was determined daily. (**B**) Treatment efficacy was compared after determination of tumor growth delays. ***$P < 0.001$ compared with 6 Gy; ###$P < 0.001$ compared with MCT1 inhibitor alone (1-way ANOVA; $n = 6–12$). Error bars represent the SEM and are sometimes smaller than symbols.

experimental conditions (18, 19, 37). Second, our study extends to tumor cells a mechanism that has previously been described as a process exploited by stromal cells to buffer products of the anaerobic metabolism of cancer cells (22). Of note, potential interference with the capacity of stromal cells to take up lactate did not appear to be part of the antitumor effects that we observed: the expression of MCT1 by tumor cells was the key factor in anticipating a therapeutic response (i.e., tumors generated from MCT1-negative TLT cells were insensitive to the treatment). Conversely, as shown in the WiDr model, the relative expression or activity of MCT1 in vitro had no prognostic value for therapeutic gain in vivo, most probably because the onset of metabolic symbiosis is under the control of microenvironmental influences. Finally, a number of reports have attributed to MCT1 a role in lactate efflux in tumor cells with active aerobic glycolysis (33, 38–41). These studies showed further evidence of lethal intracellular acidification upon MCT1 inhibition in vitro. Our observations that in vivo MCT1 expression and hypoxia are mutually exclusive indicates that this form of death could only marginally account for the antitumor effects of MCT1 inhibition. Our results strongly suggest that there are no significant off-target effects of CHC on lactate export (that would equally kill Warburg phenotype cells at the tumor periphery) or on metabolite trafficking in the mitochondrion.

MCT1 is expressed in a variety of human cancer cell lines and in primary human tumors, including breast, head and neck, and lung cancers (Figure 9, C and D) as well as neuroblastoma (40), brain (42), and colon (ref. 22, ref. 43, and Figure 9C) cancers. Broad MCT1 distribution among human cancers opens promising therapeutic perspectives for the development and clinical evaluation of pharmacological MCT1 inhibitors. Our study demonstrates the need for a careful selection of patients with a plasma membrane expression of MCT1 as well as the benefit of combining MCT1 inhibition with conventional anticancer therapies, particularly radiotherapy.

Methods

Cells. WiDr human colorectal adenocarcinoma, SiHa human cervix squamous cell carcinoma, LLc mouse carcinoma, TLT mouse hepatocarcinoma (44), FaDu human squamous cell carcinoma, MDA-MB-231 human breast cancer, MCF-7 human breast adenocarcinoma, and PC-3 human prostate cancer cells were routinely cultured in DMEM containing 4,500 mg/l glucose with 10% FBS. For some metabolic assays, cells were cultured in DMEM without glucose or FBS (Krackeler Scientific). ρ0 cells were produced as previously described (45). Sodium lactate (10 mM), methylpyruvate (10 mM), and CHC (5 mM in cell cultures) were from Sigma-Aldrich. All media were buffered at pH 7.3, supplemented with 1% penicillin-streptomycin, and were pyruvate free and glutamine free. To minimize artifactual variations due to unequal growth rates and cell sizes, all assays were performed on confluent cells in fresh medium.

In vivo experiments. Tumor cells (10^6 in 100 μl saline) were injected intramuscularly in the rear leg of mice: SiHa or WiDr cells in female athymic Balb/C mice (NIH), LLc cells in syngeneic C57BL/6J mice (Elevage Janvier), and TLT cells in syngeneic Rj:NMRI mice (Elevage Janvier). Tumor growth delays were carried out as previously described (46). Vehicle or CHC (25 μmol in 200 μl; ref. 47) was injected i.p. each day. For NMR, 50 μl of a 100 mM solution of [3-^{13}C]lactate (Sigma-Aldrich) in saline were infused i.v. to tumor-bearing mice. For the determination of hypoxia, tumor-bearing mice received an i.p. injection of 70 mg/kg pimonidazole (Chemicon) before sacrifice. Where indicated, tumors in anesthetized mice (ketamine/xylazine) were irradiated using the RT-250 device (Philips) following an established protocol (48). Mouse care and experimental procedures were approved by Duke Institutional Animal Care and Use Committee and by Université catholique de Louvain authorities according to national animal care regulations.

pH and metabolite measurements. Extracellular pH was measured with a pH meter. Intracellular pH was measured at extracellular pH 7.3 using the pH sensor 5-(and-6)-carboxy-seminaphthorhodafluor-acetoxymethylester (C.SNARF1-AM; Invitrogen), as previously described (33). Lactate and glucose concentrations were measured on deproteinized supernatant samples using a CMA600 microdialysis analyzer.

Oxygen consumption assay. Determination of cell oxygen consumption was carried out using EPR as previously reported (49). Briefly, 2×10^7 viable cells/ml were sealed in glass capillary tubes in the presence of 0.2 mM of the O_2 sensor 4-oxo-2,2,6,6-tetramethylpiperidine-D-^{15}N-1-oxyl (CDN isotopes) and with CHC where indicated. Cells were maintained at 37°C during recording on a Bruker EMX EPR spectrometer operating at 9 GHz.

NMR. Tumors were collected 30 minutes after [3-^{13}C]lactate delivery to mice, weighted, washed with cold PBS, and extracted with cold 0.9 M perchloric acid. Tumor extracts were neutralized and lyophilized. ^{13}C NMR analysis was carried out with a 500-MHz Varian Inova spectrometer operating at 125.7 MHz, with 45° pulse and 0.8-second repetition time in a 5-mm tunable broadband probe. Dioxane was used as an internal standard.

Quantitative RT-PCR and western blotting. We used previously reported protocols for SYBR Green quantitative PCR (50) and western blotting (51). hMCT1 primers were sense, 5′-GTGGCTCAGCTCCGTATTGT-3′, antisense, 5′-GAGCCGACCTAAAAGTGGTG-3′. hMCT4 primers were sense, 5′-CAGTTCGAGGTGCTCATGG-3′, antisense, 5′-ATGTAGACGTGGGTCGCATC-3′. Housekeeping control human ribosomal protein L19 (hRPL19) primers were sense, 5′-CAAGCGGATTCTCATGGAACA-3′,

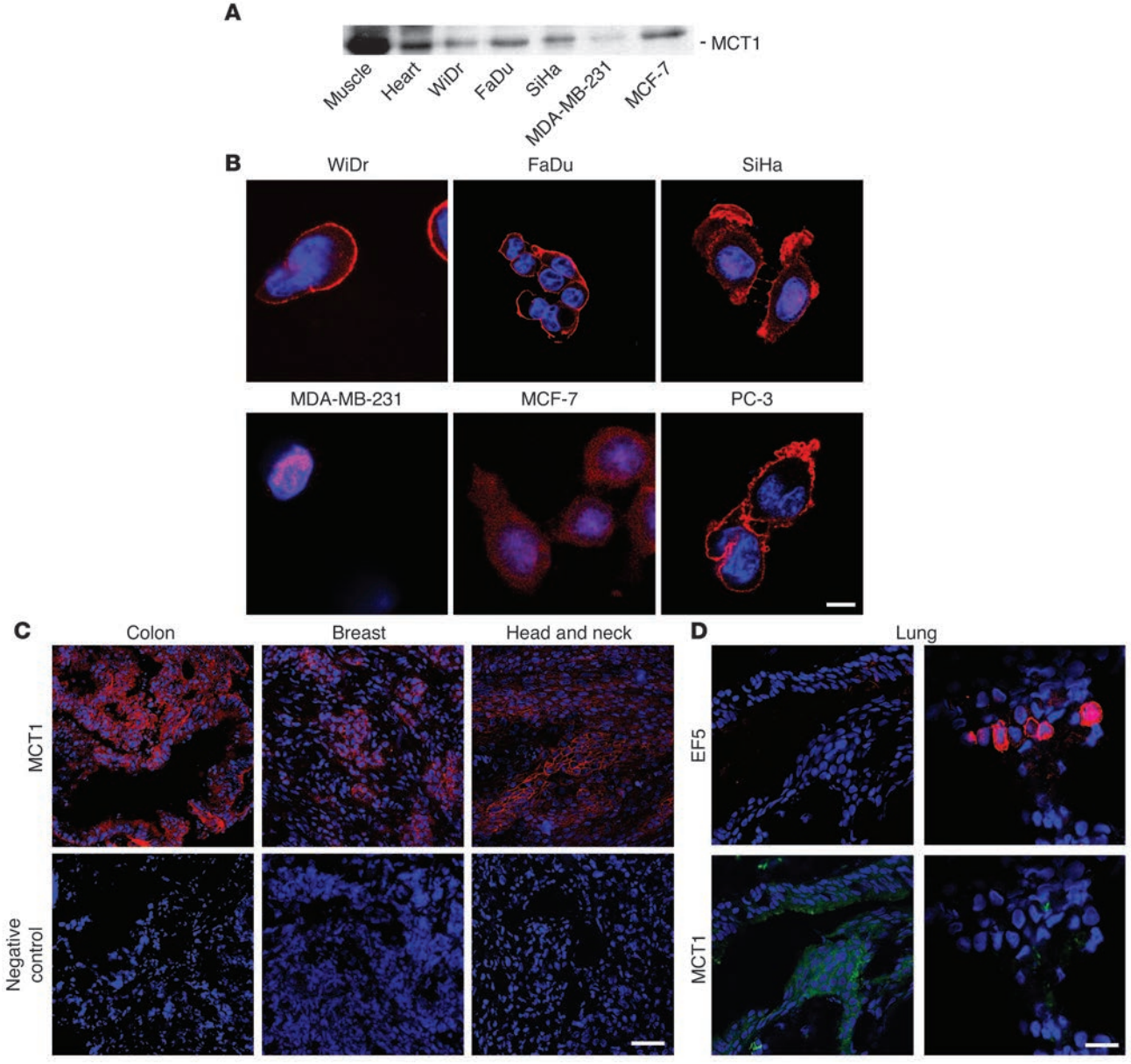

Figure 9
MCT1 is expressed in a variety of different human tumor cell lines and primary human tumor biopsies. (**A** and **B**) MCT1 was detected by western blot (**A**) and confocal microscopy (**B**) in human tumor cell lines and control tissues. Note the plasma membrane expression of the lactate transporter in WiDr, FaDu, SiHa, and PC-3 cancer cells. (**C**) MCT1 (red) and nuclei (blue) were detected using immunofluorescence in biopsies of primary human colon, breast, and head and neck human cancers. (**D**) MCT1 and hypoxia were detected in cryoslices of a primary human lung cancer. The patient had received EF5 before tumor biopsy. Representative confocal microscopy pictures revealed that the staining of MCT1 (green) and of the hypoxia marker EF5 (red) did not overlap. Scale bars: 20 μm (**B**); 100 μm (**C** and **D**).

antisense, 5′-TGGTCAGCCAGGAGCTTCTT-3′. For western blots, primary anti-MCT1 and anti-MCT4 antibodies were from Chemicon, and the antibody against β-actin was from Sigma-Aldrich.

Immunohistochemistry. Tumor cryoslices from mouse biopsies were permeabilized with 0.1% Triton X-100, stained using the VECTASTAIN ABC kit (Vector Laboratories) according to the manufacturer's protocol, developed using NovaRED solution (Vector Laboratories), and counterstained with Harris's hematoxylin. Primary human tumor cryoslices from a tissue bank constituted under approval of the Duke University Institutional Review Board were permeabilized with 0.1% Triton X-100 and stained with the primary antibody indicated in Figure 9, C and D. Primary antibodies were rat monoclonal against CD31 (BD Biosciences — Pharmingen) and rabbit polyclonals against MCT1 or MCT4 (both from Chemicon), HIF-1α (Santa Cruz Biotechnology Inc.), pimonidazole (gift from James Raleigh, University of North Carolina at Chapel Hill, Chapel Hill, North Carolina, USA), and EF5 (gift from Cameron Koch, University of Pennsylvania, Philadelphia, Pennsylvania, USA). Secondary antibodies were Alexa Fluor 594 or Alexa Fluor 488, where appropriate. Slices were counterstained with Hoechst and Prolong Gold antifade reagent with DAPI (Invitrogen). Omission of the primary antibody was used as staining control.

For immunofluorescence, 10^4 cells/ml were seeded to adhere for 24 hours in Lab-Tek multichamber slides (VWR) and then cultured for 24 hours in the indicated experimental medium. Cells were rinsed 3 times for 3 minutes each time in HBSS, fixed for 20 minutes in 4% paraformaldehyde in PBS, washed 3 times for 3 minutes each time in PBS, and permeabilized with 0.3% triton in PBS for 10 minutes. After washing (3 times for 3 minutes each time in PBS), cells were blocked for 30 minutes with 5% PBS/BSA. Antigen labeling was then performed using the primary antibodies indicated in Figure 3C; Figure 6, A, D, and F; and Figure 9B in 1% PBS/BSA. The secondary anti-rabbit antibody coupled to TRITC was from Jackson ImmunoResearch Laboratories Inc. Cell nuclei were stained with VECTASHIELD mounting medium containing DAPI (Vector Laboratories). Omission of primary antibodies was used as staining control.

ATP assay. On day 0, tumor cells (10^5 in 200 μl of medium as indicated in Figure 5, A and B) were seeded in 96-well plates. ATP cell content was determined over time using the ATP Bioluminescent Somatic Cell Assay kit (Sigma-Aldrich) according to the manufacturer's recommendations. The conversion of luciferin to oxoluciferin in the presence of ATP generated a fluorescent signal proportional to intracellular ATP that was measured with an IVIS50 Imaging System (Xenogen Corp.).

MCT1 silencing. Where indicated, cells were transfected with siRNAs as previously reported (50) or with a shRNA according to the manufacturer's protocol (Invitrogen). Human MCT1-specific siRNA targeted AAGAGGCTGACTTTTCCAAAT sequence, a scrambled siRNA (AACTCGCTGAG-ATTTCGTTAT) served to control specificity, and sham-transfected cells were used as a negative control. The sequence of the MCT1 shRNA was as follows: top, 5′-CACCGCAGTATCCTGGTGAATAAATCGAAATTTATTCACCAGGATACTGC-3′; bottom, 5′-AAAAGCAGTATCCTGGTGAATAAATTTCGATTTATTCACCAGGATACTGC-3′. Transfection of the vector pcDNA 1.2/V5-GW/lacZ served as a negative control. Cells were allowed to recover for 24 hours in DMEM containing 4,500 mg/l glucose and 10% FBS. Exposure to experimental media was set as time 0 for cell survival assays. Prior to O_2 consumption measurements, cells were cultured for 6 hours in the appropriate experimental medium.

Cell death assay. Cell death was quantified using the NucleoCounter device from ChemoMetec according to the manufacturer's recommendations.

Statistics. Results are expressed as mean ± SEM. Student's *t* test, 1-way ANOVA (Tukey's post-hoc test), and 2-way ANOVA were used where indicated. For oxygen consumption and cell death assays, the slopes of individual linear regression lines were compared. $P < 0.05$ was considered statistically significant in all experiments.

Acknowledgments

This work was supported by grants from the NIH (CA40355 to M.W. Dewhirst, CA91565 to M.J. Kelley, and CA56690 to M.L. Wahl), by the Fonds de la Recherche Scientifique — Fonds National de la Recherche Scientifique (F.R.S.-FNRS), by an Action de Recherche Concertée grant (ARC 04/09-317) from the Communauté Française de Belgique (to O. Feron), by the NEOANGIO research program from the Région Wallonne de Belgique (to O. Feron), and by the J. Maisin and St. Luc Foundations (to O. Feron). M.W. Dewhirst is the Gustavo S. Montana Professor of Radiation Oncology at Duke University. O. Feron is a Senior Research Associate of the F.R.S.-FNRS. P. Sonveaux and B.F. Jordan are F.R.S.-FNRS Research Associates. For this study, P. Sonveaux was also supported by the Belgian American Educational Foundation (BAEF) and by the Fonds Spéciaux de la Recherche (Université catholique de Louvain).

Received for publication July 18, 2008, and accepted in revised form October 15, 2008.

Address correspondence to: Pierre Sonveaux, Université catholique de Louvain, 52 Avenue E. Mounier, B-1200 Brussels, Belgium. Phone: 32-2-764-52-67; Fax: 32-2-764-52-69; E-mail: pierre.sonveaux@uclouvain.be.

Olivier Feron and Mark W. Dewhirst are co–senior authors.

1. Wu, R., and Racker, E. 1959. Regulatory mechanisms in carbohydrate metabolism. IV. Pasteur effect and Crabtree effect in ascites tumor cells. *J. Biol. Chem.* **234**:1036–1041.
2. Dewhirst, M.W. 1998. Concepts of oxygen transport at the microcirculatory level. *Semin. Radiat. Oncol.* **8**:143–150.
3. Dewhirst, M.W. 2003. Mechanisms underlying hypoxia development in tumors. *Adv. Exp. Med. Biol.* **510**:51–56.
4. Dang, C.V., and Semenza, G.L. 1999. Oncogenic alterations of metabolism. *Trends Biochem. Sci.* **24**:68–72.
5. Warburg, O. 1930. *The metabolism of tumors*. Constable. London, United Kingdom. 327 pp.
6. Semenza, G.L., et al. 2001. 'The metabolism of tumours':70 years later. *Novartis Found. Symp.* **240**:251–260.
7. Vaupel, P.W. 1994. Blood flow, oxygenation, tissue pH distribution, and bioenergetic status of tumors. Lecture 23. Ernst Schering Research Foundation. Berlin, Germany. 79 pp.
8. Vaupel, P. 1996. Is there a critical tissue oxygen tension for bioenergetic status and cellular pH regulation in solid tumors? *Experientia.* **52**:464–468.
9. Walenta, S., et al. 2001. Tissue gradients of energy metabolites mirror oxygen tension gradients in a rat mammary carcinoma model. *Int. J. Radiat. Oncol. Biol. Phys.* **51**:840–848.
10. Kim, J.W., and Dang, C.V. 2006. Cancer's molecular sweet tooth and the Warburg effect. *Cancer Res.* **66**:8927–8930.
11. James, P.E., Jackson, S.K., Grinberg, O.Y., and Swartz, H.M. 1995. The effects of endotoxin on oxygen consumption of various cell types in vitro: an EPR oximetry study. *Free Radic. Biol. Med.* **18**:641–647.
12. Halestrap, A.P., and Meredith, D. 2004. The SLC16 gene family-from monocarboxylate transporters (MCTs) to aromatic amino acid transporters and beyond. *Pflugers Arch.* **447**:619–628.
13. Halestrap, A.P., and Price, N.T. 1999. The proton-linked monocarboxylate transporter (MCT) family: structure, function and regulation. *Biochem. J.* **343**:281–299.
14. Baker, S.K., McCullagh, K.J., and Bonen, A. 1998. Training intensity-dependent and tissue-specific increases in lactate uptake and MCT-1 in heart and muscle. *J. Appl. Physiol.* **84**:987–994.
15. Bonen, A., et al. 1998. Short-term training increases human muscle MCT1 and femoral venous lactate in relation to muscle lactate. *Am. J. Physiol.* **274**:E102–E107.
16. Dubouchaud, H., Butterfield, G.E., Wolfel, E.E., Bergman, B.C., and Brooks, G.A. 2000. Endurance training, expression, and physiology of LDH, MCT1, and MCT4 in human skeletal muscle. *Am. J. Physiol. Endocrinol. Metab.* **278**:E571–E579.
17. Manning Fox, J.E., Meredith, D., and Halestrap, A.P. 2000. Characterisation of human monocarboxylate transporter 4 substantiates its role in lactic acid efflux from skeletal muscle. *J. Physiol.* **529**:285–293.
18. Spencer, T.L., and Lehninger, A.L. 1976. L-lactate transport in Ehrlich ascites-tumour cells. *Biochem. J.* **154**:405–414.
19. Cheeti, S., Warrier, B.K., and Lee, C.H. 2006. The role of monocarboxylate transporters in uptake of lactic acid in HeLa cells. *Int. J. Pharm.* **325**:48–54.
20. Hashimoto, T., Hussien, R., and Brooks, G.A. 2006. Colocalization of MCT1, CD147, and LDH in mitochondrial inner membrane of L6 muscle cells: evidence of a mitochondrial lactate oxidation complex. *Am. J. Physiol. Endocrinol. Metab.* **290**:E1237–E1244.
21. Jijakli, H., et al. 1996. Insulinotropic action of methyl pyruvate: enzymic and metabolic aspects. *Arch. Biochem. Biophys.* **335**:245–257.
22. Koukourakis, M.I., Giatromanolaki, A., Harris, A.L., and Sivridis, E. 2006. Comparison of metabolic pathways between cancer cells and stromal cells in colorectal carcinomas: a metabolic survival role for tumor-associated stroma. *Cancer Res.* **66**:632–637.
23. Asada, K., et al. 2003. Reduced expression of GNA11 and silencing of MCT1 in human breast cancers. *Oncology.* **64**:380–388.
24. Stubbs, M., McSheehy, P.M., Griffiths, J.R., and Bashford, C.L. 2000. Causes and consequences of tumour acidity and implications for treatment. *Mol. Med. Today.* **6**:15–19.
25. Brizel, D.M., et al. 2001. Elevated tumor lactate concentrations predict for an increased risk of metastases in head-and-neck cancer. *Int. J. Radiat. Oncol. Biol. Phys.* **51**:349–353.
26. Walenta, S., et al. 1997. Correlation of high lactate levels in head and neck tumors with incidence of metastasis. *Am. J. Pathol.* **150**:409–415.
27. Walenta, S., et al. 2000. High lactate levels predict likelihood of metastases, tumor recurrence, and

restricted patient survival in human cervical cancers. *Cancer Res.* **60**:916–921.
28. Tanaka, M., et al. 2004. Role of lactate in the brain energy metabolism: revealed by Bioradiography. *Neurosci. Res.* **48**:13–20.
29. Lee, Y.J., Kang, I.J., Bunger, R., and Kang, Y.H. 2003. Mechanisms of pyruvate inhibition of oxidant-induced apoptosis in human endothelial cells. *Microvasc. Res.* **66**:91–101.
30. Pelicano, H., et al. 2006. Mitochondrial respiration defects in cancer cells cause activation of Akt survival pathway through a redox-mediated mechanism. *J. Cell Biol.* **175**:913–923.
31. Dimmer, K.S., Friedrich, B., Lang, F., Deitmer, J.W., and Broer, S. 2000. The low-affinity monocarboxylate transporter MCT4 is adapted to the export of lactate in highly glycolytic cells. *Biochem. J.* **350**:219–227.
32. Ullah, M.S., Davies, A.J., and Halestrap, A.P. 2006. The plasma membrane lactate transporter MCT4, but not MCT1, is up-regulated by hypoxia through a HIF-1alpha-dependent mechanism. *J. Biol. Chem.* **281**:9030–9037.
33. Wahl, M.L., et al. 2002. Regulation of intracellular pH in human melanoma: potential therapeutic implications. *Mol. Cancer Ther.* **1**:617–628.
34. Brown, J.M., and Wilson, W.R. 2004. Exploiting tumour hypoxia in cancer treatment. *Nat. Rev. Cancer.* **4**:437–447.
35. Crabtree, H.G. 1929. Observations on the carbohydrate metabolism of tumours. *Biochem. J.* **23**:536–545.
36. Pike, S.E., Markey, S.P., Ijames, C., Jones, K.D., and Tosato, G. 1991. The role of lactic acid in autocrine B-cell growth stimulation. *Proc. Natl. Acad. Sci. U. S. A.* **88**:11081–11085.
37. Wang, Q., Lu, Y., and Morris, M.E. 2007. Monocarboxylate transporter (MCT) mediates the transport of gamma-hydroxybutyrate in human kidney HK-2 cells. *Pharm. Res.* **24**:1067–1078.
38. Belt, J.A., Thomas, J.A., Buchsbaum, R.N., and Racker, E. 1979. Inhibition of lactate transport and glycolysis in Ehrlich ascites tumor cells by bioflavonoids. *Biochemistry.* **18**:3506–3511.
39. Coss, R.A., Storck, C.W., Daskalakis, C., Berd, D., and Wahl, M.L. 2003. Intracellular acidification abrogates the heat shock response and compromises survival of human melanoma cells. *Mol. Cancer Ther.* **2**:383–388.
40. Fang, J., et al. 2006. The H+-linked monocarboxylate transporter (MCT1/SLC16A1): a potential therapeutic target for high-risk neuroblastoma. *Mol. Pharmacol.* **70**:2108–2115.
41. Mathupala, S.P., Parajuli, P., and Sloan, A.E. 2004. Silencing of monocarboxylate transporters via small interfering ribonucleic acid inhibits glycolysis and induces cell death in malignant glioma: an in vitro study. *Neurosurgery.* **55**:1410–1419.
42. Froberg, M.K., et al. 2001. Expression of monocarboxylate transporter MCT1 in normal and neoplastic human CNS tissues. *Neuroreport.* **12**:761–765.
43. Pinheiro, C., et al. 2008. Increased expression of monocarboxylate transporters 1, 2, and 4 in colorectal carcinomas. *Virchows Arch.* **452**:139–146.
44. Taper, H.S., Woolley, G.W., Teller, M.N., and Lardis, M.P. 1966. A new transplantable mouse liver tumor of spontaneous origin. *Cancer Res.* **26**:143–148.
45. King, M.P., and Attardi, G. 1989. Human cells lacking mtDNA: repopulation with exogenous mitochondria by complementation. *Science.* **246**:500–503.
46. Sonveaux, P., et al. 2003. Irradiation-induced angiogenesis through the up-regulation of the nitric oxide pathway: implications for tumor radiotherapy. *Cancer Res.* **63**:1012–1019.
47. Del Prete, E., Lutz, T.A., and Scharrer, E. 2004. Inhibition of glucose oxidation by alpha-cyano-4-hydroxycinnamic acid stimulates feeding in rats. *Physiol. Behav.* **80**:489–498.
48. Martinive, P., et al. 2006. Preconditioning of the tumor vasculature and tumor cells by intermittent hypoxia: implications for anticancer therapies. *Cancer Res.* **66**:11736–11744.
49. Sonveaux, P., et al. 2002. Modulation of the tumor vasculature functionality by ionizing radiation accounts for tumor radiosensitization and promotes gene delivery. *FASEB J.* **16**:1979–1981.
50. Bouzin, C., Brouet, A., De Vriese, J., DeWever, J., and Feron, O. 2007. Effects of vascular endothelial growth factor on the lymphocyte-endothelium interactions: identification of caveolin-1 and nitric oxide as control points of endothelial cell anergy. *J. Immunol.* **178**:1505–1511.
51. Feron, O., et al. 1996. Endothelial nitric oxide synthase targeting to caveolae. Specific interactions with caveolin isoforms in cardiac myocytes and endothelial cells. *J. Biol. Chem.* **271**:22810–22814.